

**School of Engineering & Science
Department of Civil & Construction Engineering**

**The Behaviour of Axially Loaded
Cold-formed Steel Back-to-back C-channel Built-up Columns**

Tina Ting Chui Huon

**This thesis is presented for the Degree of
Doctor of Philosophy
of
Curtin University**

September 2013

Volume I

DECLARATION

To the best of my knowledge and belief this thesis contains no material previously published by any other person except where due acknowledgment has been made.

This thesis contains no material which has been accepted for the award of any other degree or diploma in any university.

Signature:

.....

Date:

.....

PUBLICATIONS

T.C.H. Ting¹, and H.H. Lau², 2011. “Compression Test on Built-up Back-to-back Channel Stub Columns”, *Advanced Materials Research Vols. 201-203* (2011) pp 2900-2903. (Available online since 2011/Feb/21 at www.scientific.net)

T.C.H. Ting¹, H.H. Lau², 2012. “Effects of the Plate Slenderness Ratio on Built-up Back-to-back Channel Stub Columns” 1st (ASEA-SEC), Perth, Australia.

T.C.H. Ting¹, H.H. Lau², 2011. “A Numerical Investigation on Cold-formed Steel Built-up Back-to-back Channel Stub Columns” 7th International Conference on Steel & Aluminium (ICSAS), Kuching, Sarawak, Malaysia.

T.C.H. Ting¹, H.H. Lau², 2011. “Compression Tests on Cold-formed Steel Built-up Back-to-back Channel Stub Columns” 2nd International Conference on Manufacturing Science and Engineering (ICMSE), Guilin, China.

T.C.H. Ting¹, H.H. Lau², M.C. Law³, 2010. “Compression Tests on Cold-formed Steel Lipped C-Channel Columns – Short Column” World Engineering Congress 2010 Conference on Building & Infrastructural Technology (WEC), Kuching, Sarawak, Malaysia.

H.H. Lau¹, T.C.H. Ting¹, F.E. Tang, C.C. Mei, 2010. “Applications Of Cold-Formed Steel Built-Up Sections In Building Construction” 3rd International Symposium on Cold-formed Metal Structures (ISCMS), Hong Kong, China.

H.H. Lau¹, T.C.H. Ting², 2009. “Load Carrying Capacity of High Strength Cold-Formed Steel Built-Up Box Sections” 4th International Conference on Steel & Composite Structures (ICSCS), Sydney, Australia.

H.H. Lau¹, T.C.H. Ting¹, 2009. “An Investigation of the Compressive Strength of Cold-Formed Steel Built-up I Sections” 6th International Conference on Advances in Steel Structures (ICASS), Hong Kong, China.

The Behaviour of Axially Loaded Cold-formed Steel Back-to-back C-channel Built-up Columns

ABSTRACT

Cold-formed steel structural elements have been widely used in the construction industry and have emerged as a preferred economical solution for single-storey commercial and industrial buildings. Cold formed steel built-up sections are commonly used as compression elements to carry larger loads when a single section is insufficient. However, the built-up sections exhibit some unique buckling behaviours which the current codes do not have comprehensive provisions. The only provision is clause C4.5 of the 2001 edition of American Iron and Steel Institute (AISI) North American Specifications on cold formed steel design which was adopted from research and recommendations for hot-rolled steel built-up members connected with bolts or welds. This is ambiguous as the behaviour of hot rolled steel is different from cold formed steel. In addition, very few studies have been carried out to study cold formed steel built-up sections such as back-to-back C-channel column without a gap, back-to-back C-channel column with a gap, battened, and laced columns. There is also no comprehensive analytical approach to the design of cold-formed steel built up sections. Thus, the aim of this research is to investigate the behaviours of axially loaded cold formed steel back-to-back C-channel built-up columns through design calculations, finite element studies, and experimental studies.

The experimental studies involved tensile coupon tests, mortar tests and column compression tests. A total of 138 specimens with two sizes of lipped C-channel column, back-to-back C-channel built-up column with and without a gap with lengths of 300mm, 500mm, 1000mm, and 2000mm were tested. Tests were carried out on stub columns with fix end conditions, whereas the short, intermediate and slender columns were tested with pinned-end conditions.

The finite element analyses in this research were conducted using the commercial programme LUSAS, version 14.4. The two key criteria in modelling built-up columns are the screw connection and the surface contact. The finite element results were compared with the results and buckling behaviour of the columns obtained from the

experimental study. The model for the back-to-back built-up columns with a gap was also used for a parametric study on the effects of intermediate connectors.

The ultimate loads obtained from the experimental and finite element studies were also compared with those obtained from design calculations. The design calculations were obtained from two well-known methods: the Effective Width Method (EWM) and the Direct Strength Method (DSM). Based on the EWM and the DSM, a modified design method known as Thickness Reduction Method (TReM) was proposed for the design of back-to-back built-up columns with and without a gap.

Results show that the strength of the back-to-back C-channel built-up column with a gap is higher than the back-to-back C-channel built up column without a gap for specimens with smaller cross sections e.g. BU75. However, for the specimens with larger cross sections e.g. the BU90, the capacity for all the tested back-to-back C-channel built-up columns with a gap decreased slightly due to the shift of the failure axis. In both cases, the restraint at the mid-length for both the back-to-back C-channel built-up columns with and without a gap is critical regardless of the number of fasteners along the length of the built-up column. When compared to finite element models, the strength and behaviour of the C-channel, back-to-back C-channel built-up columns with and without a gap correlate well.

The current design methods, EWM and DSM, are conservative in predicting the capacity of cold-formed steel plain back-to-back C-channel built-up columns, especially when the fastener spacing is beyond the spacing requirements from clause C4.5 of the AISI Specifications 2001 Edition. The modified slenderness ratio from clause C4.5 is more conservative for longer columns than the shorter back-to-back C-channel built-up columns. The proposed design method, TReM, is able to predict the capacity of back-to-back C-channel built-up column with and without a gap well.

ACKNOWLEDGEMENT

First of all, I would like to extend my deepest appreciation to **Dr. Lau Hieng Ho**, my supervisor, for his patience in clearing my cluttered thoughts, for his time in going through my work, and his persistency in providing help and guidance throughout my study period.

I would also like to express my gratitude to **Dr. Law Ming Chiat**, my associate supervisor, for providing useful knowledge in programming and modelling, and for inspiring me in doing research work.

I am also grateful to **Mr. Mei Chee Chiang** from **Ecosteel Sdn. Bhd., Kuching**, the cold-formed steel company, for sponsoring all my test specimens, and for providing me with advices throughout my research studies.

I would also like to acknowledge the following individuals:

- Dennis Sek from Astasoft Sdn. Bhd., for providing technical support and assisting me in using the finite element analysis software – LUSAS;
- Serina Ann Doss from Curtin University, for proofreading;
- Dr. Tang Fu Ee from Curtin University, for giving comments and suggestions;
- Professor Marcus Lee from Curtin University for giving comments and suggestions;
- Michael Ding from Curtin University for assisting in laboratory work; and
- George Edmund from Curtin University, for assisting in laboratory work.

I am also thankful to my friends, Mr. Johnny Chu Kam Vai, Mr. Kwong Kok Zee, Mr. Kenneth Jee Kok Yew, Mr. Desmond Ling Yii Dao, and Mr. Yong Kian Lik who assisted me in various aspects; and my course mates, Miss Sharon Yee Jia Huey, Miss Bridgid Chin Lai Fui and Miss Valerie Jong Siaw Wee, who have helped me through giving support, and encouragement.

Special thanks to **Mr. Ng Boon Yuh**, for being there to support and offer light moments during stressful periods, for taking time to listen to all the complaints, for

cheering me up when I was down and for countless other reasons which make you a huge part of this piece of work.

Most importantly, thank you **to my family**, who have been my source of strength and support to proceed whenever I faced difficulties throughout the course of study.

TABLE OF CONTENTS

DECLARATION	v
PUBLICATIONS	vi
ABSTRACT	vii
ACKNOWLEDGEMENT	ix
TABLE OF CONTENTS	xi
LIST OF FIGURES	xv
LIST OF TABLES	xxii
LIST OF NOTATIONS	xxiv
1 Introduction	1
1.1 Background	1
1.1.1 Cold Formed Steel	1
1.1.2 Development of Cold-formed Steel Built-up Members	2
1.1.3 Applications in the Local Construction Industry	5
1.1.4 Design of Cold-formed Steel Structures	10
1.2 Objectives	12
1.3 Scope of Work	13
1.4 Thesis Outline	13
2 Literature Review	17
2.1 Introduction	17
2.2 Design of Cold-formed Steel Columns	17
2.2.1 Current Design Methods	17
2.2.2 Limitations of Direct Strength Method (DSM)	20
2.3 Shift of Effective Centroid	23
2.4 Built-up Column	26
2.4.1 Modified Slenderness Ratio	27
2.4.2 Intermediate Fasteners	30
2.5 Built-up Column with a Gap	32
2.6 Computational Modelling	37
2.6.1 Element Type	38
2.6.2 Surface Contact	39
2.6.3 Intermediate Fasteners	39

2.7	Conclusions	42
3	Experimental Investigation	43
3.1	Introduction	43
3.2	Materials Properties	43
3.3	Specimen Design	45
3.3.1	Labelling	46
3.3.2	Dimensional Limits	46
3.3.3	Member Slenderness Ratio	47
3.3.4	Modified Slenderness Ratio	50
3.4	Initial Imperfection	56
3.5	Test Setup	58
3.5.1	Fixed End for Stub Columns	58
3.5.2	Pinned End for All Other Columns	61
3.6	Mortar Test	67
3.7	Conclusions	69
4	Test Results & Observations	70
4.1	Introduction	70
4.2	Ultimate Load	70
4.2.1	C-channel Columns	70
4.2.2	Plain Back-to-back C-channel Built-up Columns	71
4.2.3	Back-to-back C-channel Built-up Columns with a Gap	74
4.3	Improved Test Results	77
4.4	Specimen Behaviour	83
4.4.1	C-channel Columns	86
4.4.2	Plain Back-to-back C-channel Built-up Columns	92
4.4.3	Back-to-back C-channel Built-up Columns with a Gap	98
4.5	Comparison of Back-to-back C-channel Built-up Columns with and without a Gap	103
4.5.1	Effects of Fasteners Spacing	108
4.6	Conclusions	109
5	Finite Element Modelling	111
5.1	Introduction	111
5.2	Finite Element Model	111
5.2.1	Non-linear Analysis	112

5.2.2	Element Type	113
5.2.3	Convergence Study	114
5.2.4	Surface Contact	116
5.2.5	Intermediate Fasteners	117
5.2.6	Boundary Conditions	118
5.2.7	Imperfections	119
5.2.8	Loading	120
5.3	Modelling Procedure	121
5.4	Conclusions	121
6	Finite Element Analysis	123
6.1	Introduction	123
6.2	Ultimate Strength	123
6.2.1	C-channel Columns	124
6.2.2	Plain Back-to-back C-channel Built-up Columns	128
6.2.3	Back-to-back C-channel Built-up Columns with a Gap	137
6.3	Deformation	143
6.3.1	C-channel Columns	144
6.3.2	Plain Back-to-back C-channel Built-up Columns	148
6.3.3	Back-to-back C-channel Built-up Columns with a Gap	153
6.4	Parametric Study on the Effects of Intermediate Fasteners	157
6.5	Conclusions	163
7	Current Design Methods	164
7.1	Introduction	164
7.2	C-channel Columns	164
7.2.1	Design Procedures	165
7.3	Plain Back-to-back C-channel Built-up Columns	168
7.3.1	Section Properties	168
7.3.2	Current Design Methods	169
7.3.3	CUFSM	170
7.3.4	Design Procedures	172
7.4	Evaluation of the Current Design Methods	174
7.4.1	C-channel Columns	174
7.4.2	Plain Back-to-back C-channel Built-up Columns	177
7.5	Conclusions	194

8	Proposed Design Method	195
8.1	Introduction	195
8.2	Design Approach	195
8.3	Thickness Reduction Method (TReM)	197
8.3.1	Design Procedures	201
8.4	Evaluation of the Thickness Reduction Method (TReM)	202
8.4.1	Plain Back-to-back C-channel Built-up Columns	202
8.4.2	Back-to-back C-channel Built-up Columns with a Gap	212
8.5	Conclusions	218
9	Conclusions	219
9.1	Introduction	219
9.2	Conclusions	220
9.3	Recommendations & Future Works	221
	References	223

LIST OF FIGURES

Figure 1.1:	Built-up Sections	2
Figure 1.2:	Built-up Columns in this Research	3
Figure 1.3:	Simplified Truss Connection (Mei et. al 2009)	4
Figure 1.4:	Multi-purpose Hall in Curtin University Sarawak Malaysia	5
Figure 1.5:	Exposed Roof Structure	6
Figure 1.6:	Sarawak International Medical Centre, Samarahan, Sarawak	7
Figure 1.7:	Roof Structure of Sarawak International Medical Centre, Samarahan, Sarawak	8
Figure 1.8:	Built-up Wall Frame of MBO Cinema, Kuching, Sarawak, Malaysia	9
Figure 1.9:	Connections	10
Figure 2.1:	CUFSM Models for Buckling Stress Determination (Chen & Young 2008, 727-737)	22
Figure 2.2:	Stress Redistribution of C-channel under Uniform Compression with Effective Width Representation (Young 2006, 128)	24
Figure 2.3:	Locally Buckled Pin-ended Channel Column (Young 2006, 129)	24
Figure 2.4:	Stress Redistribution of Doubly Symmetric Cross Section under Uniform Compression (Young 2006, 130)	25
Figure 2.5:	Cross Section of Built-up Column with a Gap in Johnston (1971)	33
Figure 2.6:	Buckling modes of Built-up Columns with a Gap proposed by Johnston (1971)	34
Figure 2.7:	Models for Built-up Column with a Gap in Rondal & Niazi (1990)	35
Figure 2.8:	Finite Element Model of Connection in Butterworth (1999, 1-14)	40
Figure 2.9:	Finite Element Model of Connection in Chin (2008, 1-81)	40
Figure 3.1:	Shape & Dimensions of Tensile Coupon in accordance to AS1391-2007 (Standards Australia 2007, 26)	44

Figure 3.2:	Stress Strain Curves from Tensile Coupon Tests	45
Figure 3.3:	Dimensions of the Specimen Cross Sections	45
Figure 3.4:	Specimens Label	46
Figure 3.5:	CUFSM Results	49
Figure 3.6:	Specimens within the Limitations from clause C4.5 of AISI Specification with $s/L < 0.25$	53
Figure 3.7:	Specimens Slightly Exceed the Limitations from clause C4.5 of AISI Specification at $0.25 < s/L < 0.50$	54
Figure 3.8:	Specimens Exceed the Limitations from clause C4.5 of AISI Specification at $s/L > 0.50$	55
Figure 3.9:	Measuring Initial Imperfection	57
Figure 3.10:	Imperfection Measurements	57
Figure 3.11:	Imperfections at Flanges for BU75S50L300-1	58
Figure 3.12:	Test Setup for Stub Column Compression Test	61
Figure 3.13:	Stub Column Test Setup	61
Figure 3.14:	Test Setup for Intermediate Column Compression Test	66
Figure 3.15:	Setting Time by Penetration Test using Vicat Needle	68
Figure 3.16:	Graph of Penetration of Vicat Needle versus Time	68
Figure 3.17:	Mortar Test Cubes	69
Figure 4.1:	Failure Modes of C90L300-1	71
Figure 4.2:	Mortar Failure	73
Figure 4.3:	Failure of Pinned-end when Testing BU90S225L1000-3	73
Figure 4.4:	Specimens from BU90 Test Series Failed in Both x and y-axis	74
Figure 4.5:	Back-to-back Channels Stub Columns with a Gap Failed at Ends	76
Figure 4.6:	GBU90S100L500-4 Failed with a Mixed Failure in x and y-axis	76
Figure 4.7:	GBU90S225L1000-2 Failed at End	76
Figure 4.8:	Failure modes of GBU90S900L1000-2	77

Figure 4.9:	Position of LVDT for Shortening	78
Figure 4.10:	LVDT measuring beam deflection	78
Figure 4.11:	LVDT measuring plate deflection	79
Figure 4.12:	Test Results Before and After Additional Work for C90L1000-2	79
Figure 4.13:	Graph of Load versus Shortening for C75L300-3	80
Figure 4.14:	Graph of Load versus Shortening for C90L500-3	80
Figure 4.15:	Graph of Load versus Shortening for BU75S50L300-3	81
Figure 4.16:	Graph of Load versus Shortening for BU75S50L300-3	81
Figure 4.17:	Graph of Load versus Deformation for GBU75S50L300-2	82
Figure 4.18:	Graph of Load versus Deformation for GBU75S100L500-1	82
Figure 4.19:	Graph of Load versus Deformation for C75L300-3	84
Figure 4.20:	Graph of Load versus Deformation for C90L500-3	84
Figure 4.21:	Graph of Load versus Deformation for C75L1000-2	85
Figure 4.22:	Graph of Load versus Deformation for C75L2000-3	86
Figure 4.23:	Failure Modes of Tested L300 C-channel Columns	87
Figure 4.24:	Failure Modes of Tested C90L500 C-channel Columns	88
Figure 4.25:	Failure Modes of Tested C75L500 C-channel Columns	89
Figure 4.26:	Failure Modes of Tested C75L1000 C-channel Columns	89
Figure 4.27:	Failure Modes of Tested C90L1000 C-channel Columns	90
Figure 4.28:	Failure Modes of Tested C75L2000 C-channel Columns	91
Figure 4.29:	Failure Modes of Tested S50L300 Built-up Columns	92
Figure 4.30:	Failure Modes of Tested S100L300 Built-up Columns	92
Figure 4.31:	Failure Modes of Tested S200L300 Built-up Columns	93
Figure 4.32:	Failure of Tested BU75L500 Built-up Columns	93
Figure 4.33:	Failure Modes of Tested BU90L500 Built-up Columns	94
Figure 4.34:	Failure Modes of Tested BU90S225L1000 Built-up Columns	94

Figure 4.35:	Failure Modes of Tested BU90S450L1000 Built-up Columns	95
Figure 4.36:	Failure Modes at Mid-Length of Tested BU75L1000 Built-up Columns	96
Figure 4.37:	Failure Modes of Tested BU75L1000 Built-up Columns	96
Figure 4.38:	Failure Modes of Tested BU75L2000 Built-up Columns	97
Figure 4.39:	Failure Modes of Tested S50L300 Built-up Columns with a Gap	98
Figure 4.40:	Failure Modes of Tested S200L300 Built-up Columns with a Gap	99
Figure 4.41:	Failure Modes of Tested S100L500 Built-up Columns with a Gap	99
Figure 4.42:	Failure Modes of Tested S400L500 Built-up Columns with a Gap	100
Figure 4.43:	Failure Modes of Tested S225L1000 Built-up Columns with a Gap	101
Figure 4.44:	Failure Modes of Tested S900L1000 Built-up Columns with a Gap	102
Figure 4.45:	Failure Modes of Tested GBU75L2000 Built-up Columns with a Gap	103
Figure 4.46:	Comparison on Test Results for BU75 and GBU75 at $s/L < 0.25$	105
Figure 4.47:	Comparison on Test Results for BU75 and GBU75 at $s/L > 0.50$	106
Figure 4.48:	Comparison on Test Results for BU90 and GBU90 at $s/L < 0.25$	107
Figure 4.49:	Comparison on Test Results for BU90 and GBU90 at $s/L > 0.50$	107
Figure 5.1:	Linear 4-node Quadrilateral Thick Shell Element (FEA 2012)	113
Figure 5.2:	Examples of LUSAS Model at Different Mesh Configurations	114
Figure 5.3:	Surface Contact Analysis using Slideline	117
Figure 5.4:	Simplified Screw Connections	117
Figure 5.5:	Fixed End Condition in LUSAS	118
Figure 5.6:	Pinned End Condition in LUSAS	119
Figure 5.7:	Deformed Shape (Scaled to 0.1) from Linear Buckling Analysis	119
Figure 5.8:	Loading in LUSAS	120
Figure 5.9:	Modelling Procedures using LUSAS version 14.4	121

Figure 5.10:	Typical Finite Element Models	122
Figure 6.1:	Graph of FE and Test Results for C-channel Columns	126
Figure 6.2:	Comparison between FE and Test Results for C75	127
Figure 6.3:	Comparison between FE and Test Results for C90	128
Figure 6.4:	Graph of FE & Test Results for BU Test Series	129
Figure 6.5:	Graph of FE & Test Results for BU75 at $s/L < 0.25$	131
Figure 6.6:	Graph of FE and Test Results for BU75 at $0.25 < s/L < 0.50$	132
Figure 6.7:	Graph of FE & Test Results for BU75 at $s/L > 0.50$	132
Figure 6.8:	Graph of FE & Test Results for BU90 at $s/L < 0.25$	135
Figure 6.9:	Graph of FE & Test Results for BU90 at $0.25 < s/L < 0.50$	136
Figure 6.10:	Graph of FE & Test Results for BU90 at $s/L > 0.50$	136
Figure 6.11:	Graph of FE & Test Results for Back-to-back C-channel Built-up Columns with a Gap	137
Figure 6.12:	Graph of FE & Test Results for GBU75 at $s/L < 0.25$	139
Figure 6.13:	Graph of FE & Test Results for GBU75 at $s/L > 0.50$	140
Figure 6.14:	Graph of FE & Test Results for GBU90 at $s/L < 0.25$	142
Figure 6.15:	Graph of FE & Test Results for GBU90 at $s/L > 0.50$	142
Figure 6.16:	A sample of Test Results Before and After Remedial Work (C90L1000-2)	143
Figure 6.17:	Failure Modes of FE and Tested C75L300 and C90L300 C-channel (C) Stub Columns	144
Figure 6.18:	Failure Modes of FE and Tested C90L500 C-channel (C) Short Columns	145
Figure 6.19:	Failure Modes of FE and Tested C75L500, C75L1000 and C90L1000 C-channel (C) Intermediate Columns	146
Figure 6.20:	Failure Modes of FE and Tested C75L2000 C-channel (C) Slender Columns	147

Figure 6.21:	Failure Modes of FE and Tested BU75L300 and BU90L300 Plain Back-to-back C-channel Built-up (BU) Stub Columns	148
Figure 6.22:	Failure Modes of FE and Tested BU75L500, BU90L500 and BU90L1000 Plain Back-to-back C-channel Built-up (BU) Short Columns	150
Figure 6.23:	Failure Modes of FE and Tested BU75L1000 Plain Back-to-back C-channel Built-up (BU) Columns	151
Figure 6.24:	Failure Modes of FE and Tested BU75L2000 Plain Back-to-back C-channel Built-up (BU) Slender Columns	152
Figure 6.25:	Failure Modes of FE and Tested GBU75L300 and GBU90L300 Back-to-back C-channel Built-up (GBU) Stub Columns with a Gap	153
Figure 6.26:	Failure Modes of FE and Tested GBU75L500 and GBU90L500 Back-to-back C-channel Built-up (GBU) Columns with a Gap	154
Figure 6.27:	Failure Modes of FE and Tested GBU75L1000 and GBU90L1000 Back-to-back C-channel Built-up (GBU) Columns with a Gap	155
Figure 6.28:	Failure Modes of FE and Tested GBU75L2000 Back-to-back C-channel Built-up (GBU) Columns with a Gap	156
Figure 6.29:	Fastener Spacing for Back-to-back C-channel Built-up Columns with a Gap with $0.25 < s/L < 0.50$	158
Figure 6.30:	Load versus Member Slenderness Ratio for GBU75	159
Figure 6.31:	Load versus Member Slenderness Ratio for GBU90	159
Figure 6.32:	Failure Modes of FE GBU75 Back-to-back C-channel Built-up Columns with a Gap	161
Figure 6.33:	Failure Modes of FE GBU90 Back-to-back C-channel Built-up Columns with a Gap	162
Figure 7.1:	Design Procedures of the C-channel Columns using EWM	165
Figure 7.2:	Design Procedures of the C-channel Columns using DSM I	166
Figure 7.3:	Design Procedures of the C-channel Columns using DSM II	167
Figure 7.4:	Notations for Plain Back-to-back C-channel Built-up Sections	168

Figure 7.5:	Design Procedures of the Plain Back-to-back C-channel Built-up Columns using EWM	172
Figure 7.6:	Design Procedures of the Plain Back-to-back C-channel Built-up Columns using DSM I	173
Figure 7.7:	Design Procedures of the Plain Back-to-back C-channel Built-up Columns using DSM II	174
Figure 7.8:	Comparison of Test and Design Calculated Results for BU75 with Three Intermediate Fasteners at $s/L < 0.25$	179
Figure 7.9:	Comparison of Test and Design Calculated Results for BU75 with One Intermediate Fastener at $0.25 < s/L < 0.50$	180
Figure 7.10:	Comparison of Test and Design Calculated Results for BU75 with No Intermediate Fastener at $s/L > 0.50$	180
Figure 7.11:	Comparison of Test & Design Calculated Results for BU90 with Fastener Spacing at $s/L < 0.25$	183
Figure 7.12:	Comparison of Test & Design Calculated Results for BU90 with Fastener Spacing at $0.25 < s/L < 0.50$	183
Figure 7.13:	Comparison of Test & Design Calculated Results for BU90 with Fastener Spacing at $s/L > 0.50$	184
Figure 8.1:	CUFSM Result for Back-to-back C-channel Built-up Column (AISI 2006, 54)	196
Figure 8.2:	Notations for Back-to-back C-channel Built-up Section with a Gap	197
Figure 8.3:	CUFSM Model for the Analysis of GBU Columns	198
Figure 8.4:	Design Procedure using TReM	201
Figure 8.5:	Comparison of Proposed Method with Test Results for BU	211
Figure 8.6:	Comparison of Proposed Method with FE Results for BU	212
Figure 8.7:	Comparison of Proposed Method with Test Results for GBU	216
Figure 8.8:	Comparison of Proposed Method with FE Results for GBU	217

LIST OF TABLES

Table 1.1:	Characteristics of Cold-formed and Hot-rolled Steel	2
Table 3.1:	Tensile Coupon Test Results	44
Table 3.2:	DSM and EWM Dimensional Limits	47
Table 3.3:	Lengths to achieve the required slenderness ratio	47
Table 3.4:	Chosen Specimen Length	49
Table 3.5:	Fastener Spacing in Accordance with the AISI Specifications	51
Table 3.6:	Categories of Test Specimens	56
Table 3.7:	Measured Specimen Dimensions for Stub Columns from C75, BU75 and GBU75 Test Series	59
Table 3.8:	Measured Specimen Dimensions for Stub Column from C90, BU90 and GBU90 Test Series	60
Table 3.9:	Measured Dimensions for C75 Specimen $L_1=500\text{mm}$	62
Table 3.10:	Measured Dimensions for C90 Specimen $L_1=500\text{mm}$	63
Table 3.11:	Measured Dimensions for C75 Specimens $L_1=1000\text{mm}$	64
Table 3.12:	Measured Dimensions for C90 Specimens $L_1=1000\text{mm}$	64
Table 3.13:	Measured Dimensions for C75 Specimens $L_1=2000\text{mm}$	65
Table 3.14:	Compressive Strength of Test Cubes at Different Duration	69
Table 4.1:	Test Results of C-channel Columns	71
Table 4.2:	Test Results of Plain Back-to-back C-channel Built-up Columns	72
Table 4.3:	Test Results of Back-to-back C-channel Built-up Columns with a Gap (GBU)	75
Table 4.4:	Comparison of the Ultimate Loads of Back-to-back C-channel Built-up Columns with and without a Gap	104
Table 5.1:	Finite Element Results for C75L300 at Different Mesh Size	115
Table 5.2:	Finite Element Results for C75L500 at Different Mesh Size	115

Table 5.3:	Finite Element Results for C75L1000 at Different Mesh Size	115
Table 5.4:	Finite Element Results for C75L2000 at Different Mesh Size	115
Table 6.1:	Comparison of Test Results and FE for C-channel Columns	124
Table 6.2:	Comparison between FE Results & Test Results for BU75	130
Table 6.3:	Comparison between FE & Test Results for BU90	134
Table 6.4:	Comparison between FE & Test Results for GBU75	138
Table 6.5:	Comparison between FE & Test Results for GBU90	141
Table 7.1:	Comparison of Test & Design Results for C-channel C75 Stub Columns	175
Table 7.2:	Comparison of Test & Design Results for Pin-ended C-channel Columns from C75 and C90 Test Series	176
Table 7.3:	Comparison of Test & Design Results for BU75 With & Without Modified Slenderness Ratio	177
Table 7.4:	Comparison of Test & Design Results for BU90 With & Without Modified Slenderness Ratio	182
Table 7.5:	Comparison of Test & Finite Element Results to Design Calculated Results for BU75 Stub Columns	186
Table 7.6:	Comparison of Test & Finite Element Results to Design Calculated Results for BU75 Columns	189
Table 7.7:	Comparison of Test & Finite Element Results to Design Calculated Results for BU90 Columns	191
Table 8.1:	Comparison of Test and FE Results with TReM for BU75	203
Table 8.2:	Comparison of Test and FE Results with TReM for BU90	208
Table 8.3:	Comparison of Test and FE Results with TReM for GBU75	213
Table 8.4:	Comparison of Test and FE Results with TReM for GBU90	215

LIST OF NOTATIONS

The following are symbols used throughout this thesis.

A'	Measured web width
A_{bu}	Cross sectional area of built-up section
A_c	Cross sectional area of C-channel section
A_e	Effective cross sectional area
A_f	Cross sectional area of flange
A_g	Gross cross-sectional area
a	Clear width of web
\bar{a}	Center-to-center width of web
B'	Measured flange width
b	Clear width of flange
\bar{b}	Center-to-center width of flange
b_{corner}	Corner length
b_{flange}	Effective flange width
b_{lip}	Effective lip width
b_t	Total effective width
b_{web}	Effective web width
C'	Measured lip width
c	Clear width of lip
\bar{c}	Center-to-center width of lip
C_b	Bending coefficient dependent on moment gradient
C_{my}	Moment gradient factor
C_s	Coefficient for lateral-torsional buckling
C_{wc}	Warping constant for C-channel
C_{wBU}	Warping constant for built-up sections
C_{wf}	Warping constant for flange

E	Modulus of elasticity of steel (20000MPa)
e_s	Shift of centroid with respect to centroidal axes of effective section determined at stress level F_{ne}
F_c	Critical buckling stress
F_{cr}	Critical elastic buckling stress
F_e	Elastic buckling stress calculated as the minimum of elastic flexural, torsional and torsional-flexural buckling stresses
F_y	Yield stress
F_{ne}	Nominal buckling stress (denoted as F_n in AISI design codes)
f_{crd}	Critical elastic distortional buckling stress
f_{cre}	Critical elastic flexural buckling stress
f_{crl}	Critical elastic local buckling stress
G	Shear modulus of steel (78000MPa)
h_x	Distance from centroid of flange to shear centre of flange in x-axis
h_y	Distance from centroid of flange to shear centre of flange in y-axis
I_a	Adequate moment of inertia of stiffener, so that each component element will behave as a stiffened element
I_s	Moment of inertia of full section of stiffener about its own centroidal axis parallel to element to be stiffened. For edge stiffeners, the round corner between stiffener and element to be stiffened shall not be considered as part of the stiffener
I_{xBU}	Moment of inertia about x-axis for a full unreduced built-up section
I_{xC}	Moment of inertia about x-axis for a full unreduced C-channel section
I_{xf}	Moment of inertia of flange in x-axis
I_{xyf}	Product of the moment of inertia of flange
I_{yBU}	Moment of inertia about y-axis for a full unreduced built-up section
I_{yC}	Moment of inertia about y-axis for a full unreduced C-channel section
I_{yf}	Moment of inertia of flange in y-axis

J_C	Torsional constant for C-channel section
J_{BU}	Torsional constant for built-up section
J_f	St. Venant torsion constant of flange
j	Section property for torsional-flexural buckling
K_x	Effective length factor for bending about x axis (1 = simply supported, 0.5 = fixed end)
K_y	Effective length factor for bending about y axis (1 = simply supported, 0.5 = fixed end)
K_t	Effective length factor for torsion (1 = simply supported, 0.5 = fixed end)
k_{web}	Plate buckling coefficient for web
k_{flange}	Plate buckling coefficient for flange
k_{lip}	Plate local buckling coefficient for lip
k_ϕ	Rotational stiffness/ laterally unbraced length of member ($k_{\phi f}, k_{\phi g}$ for flange and $k_{\phi we}, k_{\phi wg}$ for web)
L	Unbraced length between the inner concrete bases of the stub column. Unbraced length between the centre of rotation of the pinned-end assemblies.
L_{cr}	Critical length
L_l	Unbraced length of member for bending about x and y axis
L_t	Unbraced length of member for twisting
L_x	Unbraced length of compression member for bending about x-axis
L_y	Unbraced length of compression member for bending about y-axis
M_{crl}	Critical local buckling flexural strength
M_{crd}	Critical distortional buckling flexural strength
M_{nx}, M_{ny}	Nominal flexural strengths about centroidal axes determined in accordance with clause C3.1 of the AISI Specifications
M_{ux}, M_{uy}	Required flexural strengths with respect to centroidal axes of effective section determined for required compressive axial strength alone

M_{ne}	Minimum of global buckling nominal flexural strength
M_{nl}	Local buckling nominal flexural strength
M_{nd}	Distortional buckling nominal flexural strength
M_{cre}	Elastic critical lateral-torsional buckling stress
M_y	Full nominal strength (yield moment)
M_{crd} / M_y	Distortional buckling load ratio determined as the second minima from the CUFSM curve
M_{cre} / M_y	Global buckling load ratio
M_{crl} / M_y	Local buckling load ratio determined as the first minima from the CUFSM curve
n	Number of tests
P_{crd}	Critical elastic distortional buckling load
P_{cre}	Critical elastic global buckling load
P_{crl}	Critical elastic local buckling load
P_{DSMI}	Axial design strength prediction by Direct Strength Method by manual calculation (DSMI)
P_{DSMII}	Axial design strength prediction by Direct Strength Method by CUFSM (DSMII)
P_{EWM}	Axial design strength prediction by Effective Width Method (EWM)
P_e	Effective compressive strength
P_{Ex}, P_{Ey}	Elastic buckling strengths
P_n	Nominal axial compression strength
P_{nd}	Nominal axial strength for distortional buckling
P_{ne}	Nominal axial strength for global buckling
P_{nl}	Nominal axial strength for local buckling
P_{Test}	Experimental compressive strength
P_u	Required compressive axial strength
P_y	Yield load
P_{crd} / P_y	Distortional buckling load ratio determined as the second minima

	from the CUFSM curve
P_{cre} / P_y	Global buckling load ratio
P_{crl} / P_y	Local buckling load ratio determined as the first minima from the CUFSM curve
R	Radii at corners
R_l	Reduction factor $R_l = \frac{I_s}{I_a} \leq 1$
r	Radii at corner center to center
r_o	Radius of gyration of full unreduced cross section about axis of buckling
r_{xBU}	Radius of gyration about x-axis for built-up section
r_{xC}	Radius of gyration about x-axis for C-channel section
r_{yBU}	Radius of gyration about y-axis for built-up section
r_{yC}	Radius of gyration about y-axis for C-channel section
S	$1.28 \sqrt{\frac{E}{f}}$ used in the determination of k_{flange}
s	Fastener spacing along the length of the built-up column
S_c	Elastic section modulus of effective section relative to extreme compression fiber at F_c
S_e	Elastic section modulus of effective section relative to extreme compression or tension fiber at F_y
S_f	Elastic section modulus of full unreduced section relative to extreme compression fiber
S_g	Gross section modulus to the extreme compression fiber
t	Material's thickness
u	Centre-to-centre corner length
w	Gap between two individual C-channels of a built-up section
x_c	Distance between centroid and web center line
x_{ic}	Distance between centroid and outside of web of a C-channel section
x_o	Distance from flange/ web junction to the centroid of the flange

Greeks Symbols

α	Constant for stiffened lipped section (Taken as 1.0)
α_x, α_y	$\alpha_x = 1 - \frac{P_u}{P_{Ex}} > 0, \alpha_y = 1 - \frac{P_u}{P_{Ey}} > 0$
β	Coefficient
ϕ_b	Resistance factor for bending strength
ϕ_c	Resistance factor for concentrically loaded compression member
ψ	Load combination factor
λ	Slenderness factor (0.673)
λ_c	Slenderness factor (1.5)
λ_l	Slenderness factor (0.776)
λ_d	Slenderness factor (0.561)
ρ	Effective width reduction factor
π	Pi
θ	Angle between flange and lip
σ_t	$\frac{1}{Ar_o^2} \left[GJ + \frac{\pi^2 EC_w}{(K_t L_t)^2} \right]$
σ_{ex}	$\frac{\pi^2 E}{\left(\frac{K_x L_x}{r_x} \right)^2}$
u	Poisson's ratio (0.3 for steel)

1 Introduction

1.1 Background

1.1.1 Cold Formed Steel

Cold-formed steel members are structural steel products that are made by bending a flat sheet of steel at room temperature into a shape that will support more load than the flat sheet itself (Hancock, Murray, and Ellifritt 2001, 1). The most widely used fabrication technique is cold roll forming. This technique uses 6 to 15 pairs of rollers to progressively form the desired cross section from rolled-up steel stripes. It is economical especially when large quantities of a particular shape are needed. Alternatively, press braking is used when low production volume and varied shapes are required. The press braking process is economical as the number of machinery and tools required for the process are less. Due to low machinery requirement and ease of fabrication, the cross-sections of cold-formed steel are easily varied to suit construction needs. This results in a variety of joint configurations which make standardisation difficult. Unlike cold-formed steel, the production of traditional hot-rolled steel requires higher cost thus cross sections are standardised.

The characteristics of cold-formed steel are different from hot-rolled steel due to the fabrication process. The yield stress of cold-formed steel is much higher than that of the conventional hot-rolled steel because the cold-forming process induces residual stresses which increase the yield stress. It is important for design standards to cater for these characteristics because they differentiate cold-formed steel from hot-rolled steel. Table 1.1 shows a comparison between the characteristics of cold-formed steel and hot-rolled steel compiled according to several sources such as Allen (2006, 29), and Hancock, Murray, and Ellifritt (2001, 2-3).

Table 1.1: Characteristics of Cold-formed and Hot-rolled Steel

Characteristic	Cold Formed Steel	Hot Rolled Steel
Yield Stress (MPa)	280 – 550	250 - 480
Thickness (mm)	1.2 – 3.0	5.0 – 40.0
Buckling Mode	Local Global Distortional	Global Distortional
Cross Section	Simple section Complex section	Simple section
Manufacturing Temperature	Ambient temperature	Elevated temperature

1.1.2 Development of Cold-formed Steel Built-up Members

Being thin and light weight, cold formed steel performs very differently compared to conventional hot-rolled steel. The characteristics of cold-formed steel make it high in strength but low in stiffness and thus can be easily deformed. The construction industry did not have enough confidence to largely utilise cold formed steel members until the 1940s when more understanding was developed. Since then, cold formed steel became popular and is very much used. Later, individual columns were no longer sufficient to fulfil construction needs. In order to utilize it as load bearing members, designers came up with many methods to strengthen the individual column. One of the many methods is by connecting two single columns to form a built-up column. The need to carry larger loads prompted the development of built-up sections and it is now one of the more widely used sections.

Built-up columns composed of two or more structural members connected together mechanically by using intermediate fasteners such as self-drilling screws, as shown in Figure 1.1 similar to those from Yu and LaBoube (2010, 2).

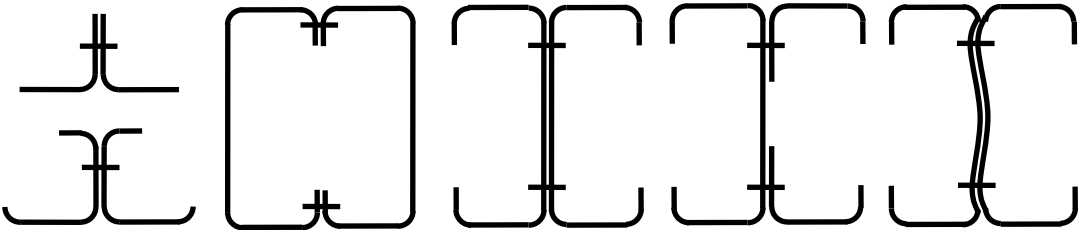


Figure 1.1: Built-up Sections

Structural viability and installation requirements in current construction projects make built-up columns high in demand for many low and medium-rise residential and

commercial buildings. These built-up columns are categorised as open sections and closed sections.

This research investigated two types of built-up sections known as plain back-to-back C-channel built-up sections (without a gap) and back-to-back C-channel built-up sections with a gap, as shown in Figure 1.2.

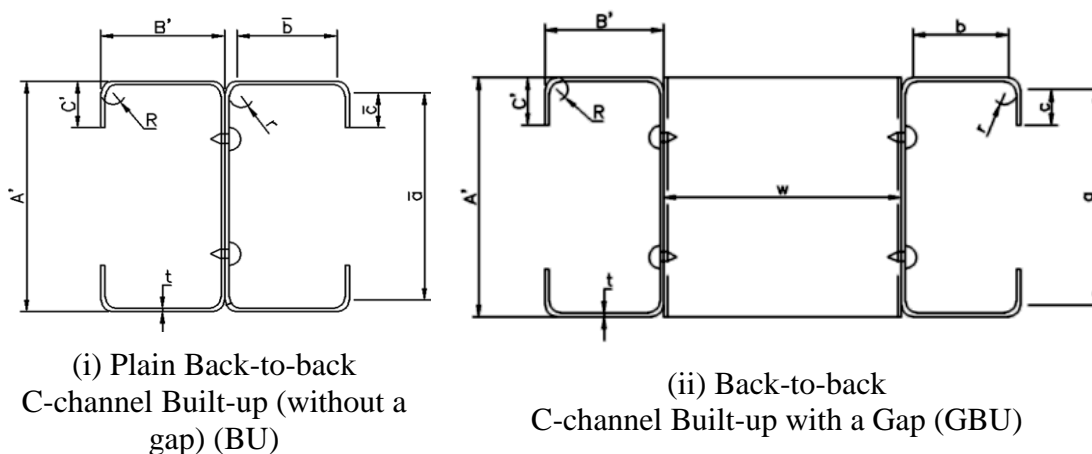


Figure 1.2: Built-up Columns in this Research

Back-to-back C-channel built-up columns are formed by connecting two identical C-channels at the webs with self-drilling screws at regular intervals along the length. The plain back-to-back C-channel built-up columns are without a gap, whereas the ones with a gap have short C-channels as intermediate fasteners between the individual C-channels.

These built-up columns have improved lateral stiffness when two individual C-channels are connected together thus preventing the structural member from wobbling during lifting and installation. Moreover, when connected to form trusses, the connection detailing of the web members to the chord members are simplified with the use of built-up columns as shown in Figure 1.3. With the enhanced strength given by built-up sections, less materials are required thus making the structure lighter.



Figure 1.3: Simplified Truss Connection (Mei et. al 2009)

The advantages of built-up members in steel structures are also evident from AISI (1997, 1). The study showed that:

- (a) built-up members are protected against web crippling because the two individual C-channels stiffen and support each other at concentrated loads, thus resulting in higher strength,
- (b) for thin and deep sections, the two individual C-channels in built-up members stiffened and supported each other against high shear loads, and
- (c) built-up members have coinciding centroid and shear centre, thus increasing torsional stability.

These characteristics of built-up members offer advantages to the construction industry, particularly in large span and heavily loaded situation. Built-up columns thus become one of the popular cold formed steel members in the present construction industry. As the application of built-up members increase, understanding the behaviour of built-up member becomes essential because individual members in a built-up member may act either separately or integrally. This uncertainty causes difficulty in accurately predicting their behaviour and strength accurately. Further

study is essential in order to understand their characteristics and behaviour, and to develop design methods for strength predictions.

1.1.3 Applications in the Local Construction Industry

Many fabricators and designers face challenges to improve strength, deflection, lateral stability, and constructability of structures when dealing with local projects in Malaysia. One solution is to increase the member sizes. However, this leads to other on-site difficulties such as space limitation and practicality in installation. Therefore, built-up members are gaining popularity in structural projects. Here are a few examples from Mei et. al (2009, 857-864).

1.1.3.1 Exposed Aesthetic Roof Truss

It is commonly perceived that cold formed steel structures cannot be left as exposed structures, as they are often hidden behind ceilings or claddings. However, the roof truss in the new multi-purpose hall in Curtin University, Sarawak Campus has been designed as an exposed aesthetic roof structure as shown in Figure 1.4.

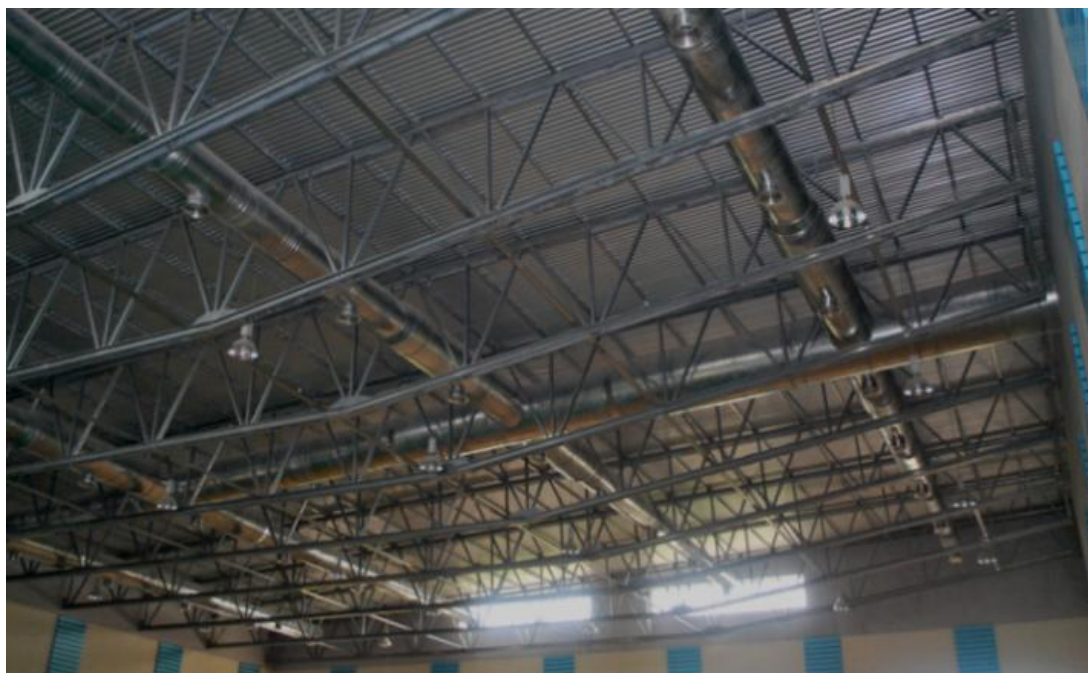


Figure 1.4: Multi-purpose Hall in Curtin University Sarawak Malaysia

The back-to-back C-channel built up member used are 150mm in width and 2.5mm in thickness for the top and the bottom chords. These back-to-back C-channel built-up members with a gap are to accommodate the internal web members of 100mm in width

and 1.6mm in thickness as shown in Figure 1.5. The trusses support a roof system and span 32.5m with a three degree pitch.



(a) Built-up Trusses



(b) Back-to-back C-channel Built-up

Figure 1.5: Exposed Roof Structure

1.1.3.2 Curved Roof Structure

Back-to-back C-channel built-ups are used to form trusses that curve and span as required while maintaining a smaller depth and lighter weight. The Sarawak International Medical Centre at Kota Samarahan, Sarawak utilizes a curved roof structure to span across a length of 9.0m, as shown in Figure 1.6 and Figure 1.7.



Figure 1.6: Sarawak International Medical Centre, Samarahan, Sarawak



(a) Curved Roof Structure



(b) Back-to-back C-channel built-up forming Curved Roof

**Figure 1.7: Roof Structure of Sarawak International Medical Centre,
Samarahan, Sarawak**

1.1.3.3 Wall Frame Structures

Wall frame structures were constructed for MBO cinema's viewing halls at The Spring Shopping Mall, Kuching, Sarawak. The back-to-back C-channel built-up members are formed by C-channels with 200mm width and 2.5 mm thickness. They are spaced at 400mm centre-to-centre. They span 15m vertically and are bolted to mild steel angle at their ends. Two cold formed steel built up frames were constructed side by side in the adjacent viewing halls as shown in Figure 1.8.



(a) Double Frames



(b) Wall Panel

Figure 1.8: Built-up Wall Frame of MBO Cinema, Kuching, Sarawak, Malaysia

Each frame carries the wall cladding, which consists of 3 layers of 12mm gypsum boards, independently. The gypsum boards were fastened directly onto the built-up frames and act as lateral restraint to the critical flanges to provide sound insulation as shown in Figure 1.9.



(a) End connections



(b) Connected to Gypsum board

Figure 1.9: Connections

1.1.4 Design of Cold-formed Steel Structures

The first cold-formed steel standard was developed by the American Iron and Steel Institute (AISI) in 1946 (AISI 2002b, 9). This design standard was largely based on the study done by Professor George Winter and his team at Cornell University between 1939 and 1946 on beams, studs, roof decks and connections. Currently, there are many

international standards for the design of cold-formed steel structures such as Standard Australia (SA) AS4600, British Standard BS5950-Part 5, the Eurocode 3 Part 1.3 other than the AISI specifications. These design standards use the Effective Width Method (EWM) and the Direct Strength Method (DSM).

The EWM is an elemental method since it considers each element of a cross section individually in its calculation. According to North American Specification (Hancock, Murray, and Ellifritt 2001, 375), it was first proposed by Von Karman (1932) and calibrated for cold-formed members by Winter (1947). This method uses a reduced area i.e. effective area, which involves tedious calculations, to account for the post-buckling effect of cold-formed steel members. The EWM column design covers four types of elements, namely:

- (i) uniformly compressed stiffened elements,
- (ii) uniformly compressed stiffened elements with an edge stiffener,
- (iii) uniformly compressed unstiffened elements, and
- (iv) uniformly compressed elements with multiple intermediate stiffeners.

Therefore the type of elements affects the effective width (b_{eff}) calculation. The effective area is calculated by multiplying the effective width of each element by its thickness, i.e. $A_e = b_{eff} t$. The design strength of cold-formed steel is then obtained by the product of the effective area (A_e), and the nominal compressive stress (F_{ne}) of the cold-formed steel.

An alternative design method, the DSM was later proposed and developed. This method uses elastic buckling solutions and also takes into consideration the interaction between the individual elements in cross-section. The determination of elastic buckling solutions can be done through manual calculation or software analysis such as CUFSM and THINWALL. Both design methods are used to determine the critical buckling strengths for local buckling (P_{crl}), distortional buckling (P_{crd}) and overall buckling (P_{cre}). These critical buckling strengths are required to determine the nominal buckling strengths for local buckling (P_{nl}), distortional buckling (P_{nd}), and

overall buckling (P_{ne}). The least of the three nominal buckling strength is taken as the design strength (P_n), i.e. $P_n = \min(P_{nt}, P_{nd}, P_{ne})$.

1.1.4.1 Design of Built-up Columns

The strength of back-to-back C-channel built-up columns is mainly governed by the fastener spacing, the slenderness, and the gap between the C-channels. However, there are no comprehensive guidelines on the design of complex cross sections such as built-up section in the design standards. Designers conveniently adopt a conservative approach due to knowledge gap in the design of built-up columns by assuming that the built-up columns perform similarly to two individual columns. This conservative approach can make the built-up columns design uneconomical.

The current design standards are insufficient to cover these governing factors. The only provision available for built-up columns is the modified slenderness ratio from clause C4.5 of the North American Specification (AISI 2002c, 83). The modified slenderness ratio was not originally designed for cold-formed steel columns. It was adopted from the studies on hot rolled built-up columns connected with bolts and welds. A conservative requirement on the maximum fastener spacing is given to allow the use of other fasteners such as screws in cold-formed steel design. Further refinement on the requirement of fastener spacing is possible as cold-formed steel is higher in strength and different in failure modes compared to hot-rolled steel.

1.2 Objectives

The aim of this research is to investigate the behaviour of the back-to-back C-channel built-up columns with and without a gap. The detailed objectives are outlined below:

- (a) predict the design strength of cold formed steel built-up columns using the EWM and the DSM from the North American Specifications (NAS) for Cold-Formed Steel (CFS) structures 2001 edition published by American Iron and Steel Institute (AISI);
- (b) study experimentally the behaviour of axially loaded cold-formed steel built-up columns and propose design recommendation;
- (c) model the cold-formed steel built-up columns using finite element analysis software, LUSAS version 14.4; and

- (d) study the fastener spacing requirement and the provision for built-up columns documented in clause C4.5 of the AISI North American Specification (NAS) 2001 edition.

1.3 Scope of Work

In assessing the behaviour of built-up columns, this research examines the parameters that are associated with the structure performance. These include the fastener spacing, cross-section of the column, and column length. The scope of work undertaken to study these parameters involved experimental investigation, finite element modelling, and design evaluation. The following provides a general overview of the work involved in achieving the aim and objectives defined in the previous section.

Experimental analysis was conducted on cold-formed steel C-channel columns, plain back-to-back C-channel built-up columns and back-to-back C-channel built-up columns with a gap. The experimental investigation involved specimens tested at various lengths and fastener spacing to investigate the current design provisions. The fastener spacing was designed to cover spacing within and beyond the spacing requirement of clause C4.5 of the AISI North American Specifications (NAS) 2001 edition. The cross sections of the test specimens were designed so that one cross-section was dimensioned to satisfy the dimensional limits of both EWM and DSM; while the other does not. The length of the columns was determined using the member slenderness ratio (KL/r) and assisted by finite strip software, CUFSM.

Based on the AISI North American Specifications (NAS) 2001 edition, two well-known cold formed steel design methods EWM and DSM were used for the design evaluation in this research.

As for finite element modelling, LUSAS version 14.4 was used. The models serve to evaluate the test results and observations from the experimental investigation. These models were then be used to generate more data on back-to-back C-channel built-up columns with a gap.

1.4 Thesis Outline

This thesis documents a research study on the behaviour of axially loaded cold-formed steel back-to-back C-channel built-up columns with two volumes.

The first volume contains 9 chapters of the thesis.

Chapter 2 documents a review of the available literature related to the study.

Chapter 3 describes an experimental programme on cold-formed steel C-channel, plain back-to-back C-channel built-up columns and back-to-back C-channel built-up columns with a gap with various lengths and screw spacings. The test specimens include two types of cross sections with 75mm and 90mm web width.

Chapter 4 presents and discusses all the test results and observations.

Chapter 5 presents the finite element modelling procedure on cold-formed steel C-channel, and back-to-back C-channel built-up columns with and without a gap. Description on modelling of surface contacts, and screw connections of the finite element model is presented.

Chapter 6 presents and discusses all the finite element results for cold-formed steel C-channel, back-to-back C-channel built-up columns with and without a gap. A parametric study on back-to-back C-channel built-up columns with a gap is also presented.

Chapter 7 details the current design methods available for the design of the sections under investigation. This chapter also compiles and discusses all the design results and compares with the test and finite element results.

Chapter 8 presents a proposed design approach known as the Thickness Reduction Method (TReM) for the design of back-to-back C-channel built-up columns with a gap. The applicability of TReM was evaluated on both the back-to-back C-channel built-up columns with and without a gap.

Chapter 9 concludes this thesis with findings, recommendations and future works.

The second volume contains all the appendices.

Appendix A contains Tensile Coupon Test results.

Appendix B contains the imperfection results for C-channel stub, short, intermediate and slender columns.

Appendix C contains the imperfection results for plain back-to-back C-channel built-up stub, short, intermediate and slender columns.

Appendix D contains the imperfection results for back-to-back C-channel built-up stub, short, intermediate and slender columns with a gap.

Appendix E contains C-channel column test results. Graphs are presented in load versus shortening curve and load versus deformation curve from test results and finite element results for all test specimens Photographs for all tested specimens from laboratory testing are included as well.

Appendix F contains plain back-to-back C-channel built-up column test results. Graphs are presented in load versus shortening curve and load versus deformation curve from test results and finite element results for all test specimens Photographs for all tested specimens from laboratory testing are included as well.

Appendix G contains back-to-back C-channel built-up column with a gap test results. Graphs are presented in load versus shortening curve and load versus deformation curve from test results and finite element results for all test specimens Photographs for all tested specimens from laboratory testing are included as well.

Appendix H contains design methods and design spreadsheets for C-channel, plain back-to-back C-channel built-up, and back-to-back C-channel built-up column with a gap. Sample spreadsheets include Effective Width Method (EWM), Direct Strength Method by manual calculation (DSMI), Direct Strength Method by finite strip analysis (DSMII) and modified design method known as Thickness Reduction Method (TReM).

2 Literature Review

2.1 Introduction

This chapter reviews the literature on the development of cold formed steel built-up members including design methods, experimental investigations, and finite element studies. Literature related to the current design methods and the associated limitations for general cold-formed steel columns are reviewed.

More specifically, relevant literatures on C-channel columns and built-up columns are reviewed. The shift of effective centroid is reviewed for C-channel columns. Relevant literature that covers the design methods and the behaviour are assessed for built-up columns. Further reviews specific to built-up column with a gap are also presented. Finally, the literatures on computational modelling on cold-formed steel are reviewed.

2.2 Design of Cold-formed Steel Columns

2.2.1 Current Design Methods

Current design methods outlined in the design standards for cold-formed steel cover the Effective Width Method (EWM) and Direct Strength Method (DSM). EWM involves tedious calculation to obtain the effective area, the interaction between the elements of the cross-section is not accounted for, and the distortional buckling is not considered. The DSM was proposed and developed to overcome the limitations of the EWM. This method uses elastic buckling solutions and also takes into consideration the interaction between cross-sectional elements.

Some researchers have compared the EWM and the DSM and found that the DSM predicts the strength and behaviour better especially at longer column lengths.

Young and Rasmussen (1998a, 140 – 148) tested on fixed and pinned end lipped C-channel columns. The test programme comprised of two series of lipped C-channel columns with two different flange widths of 36mm and 48mm at a nominal thickness of 1.5mm, a nominal web width of 96mm and a nominal lip width of 12mm. The length of these columns ranged from 280mm to 3000mm. Based on the test results from Young and Rasmussen (1998a, 140 – 148), Young and Yan (2002, 728-736)

presented a design and numerical investigation of singly symmetric C-channel columns. The results of lipped C-channel columns with 6.0mm thickness calculated using the EWM are conservative for the long columns but unconservative for the shortest columns. Moreover, they also noted that the EWM is unconservative for long columns at 1.5mm thickness, and short columns at 6mm thickness.

Besides C-channel columns, Young (2005, 1390-1396) investigated cold-formed steel lipped angle concentrically loaded fix-ended columns at various lengths. He tested three test series with lipped angle columns with thicknesses 1.2mm, 1.5mm and 1.9mm and lengths between 250mm to 3500mm. He compared the test results with the design calculated results obtained from the EWM. The comparison showed that the results calculated using the EWM are conservative for the long lipped angle columns but unconservative for the shortest columns. The comparison of test results and design calculations showed similar conclusions to the study carried out on C-channel columns in Young's previous publications.

More investigation was conducted by Young and Yan (2002, 737-745) on both the EWM and the DSM. Young and Yan tested fixed-ended channel columns with complex stiffeners at length ranging from 500mm to 3500mm. The experimental programme consisted of four series with different thicknesses and flange widths. The four series are 1.5mm and 1.9mm thickness each with 80mm and 120mm flange width. They concluded that the design strengths predicted by the EWM of AISI specification are generally not conservative for the channel columns with complex stiffeners. The failure modes predicted are generally in agreement with the failure modes observed in the tests for long columns, but not for short and intermediate columns. Young and Yan (2004, 1756-1763) recalculated the design calculated results in Young and Yan (2002, 737-745) using the DSM. Same as the EWM, the failure modes predicted by the DSM was accurate in the tests for long columns, but not for short and intermediate columns. Comparison also shows that the DSM provides good agreement with the column strength obtained from the tests.

The DSM is generally more accurate compared to the EWM because the EWM is not sensitive to buckling interaction, which is a common buckling mode in long columns.

Unlike the EWM, the DSM covers the failure modes resulted from the interaction between local and overall buckling, interaction between distortional and overall buckling, as well as distortional buckling alone.

Schafer (2002, 289-299) proposed several design approaches for the performance of the EWM and the DSM. Among all the proposed design approaches, he concluded that the DSM which considered the interaction with global buckling strength in the calculation for distortional buckling was most accurate for column design. His DSM approach considers all the buckling modes in a consistent manner and does not require tedious effective width calculations. Schafer evaluated existing and proposed methods for the design of cold-formed steel columns using experimental data gathered from several studies on unperforated lipped channel and zed columns with 90° edge stiffeners tested in a pin-ended configuration. The geometry of the tested sections covered a wide variety of dimensions. The comparison between the design calculations by the DSM and the test results shows that local and global interaction is well established, local and distortional interaction is not significant, but distortional and global interaction is uncertain. Nevertheless, he proposed to include this interaction in the design of columns.

Later, Schafer (2008, 766-778) reviewed the development and current progress of the DSM for cold-formed steel member design for beams and columns. He stated that the EWM is unconservative for a C-channel column design when the web slenderness is high. Moreover, according to his review, the reliability of the DSM was as good as, or even better than, the reliability of the EWM. The reason for this is that the EWM does not account for distortional buckling limit states unlike the DSM.

Kwon, Kim and Hancock (2009, 278-289) tested simple lipped channels and lipped channels with intermediate stiffeners in the flanges and web fabricated from high strength steel plate of thickness 0.6 and 0.8 mm at fix-ended conditions. They tested a total of 28 stub and intermediate columns under axial compression with lengths of 400mm to 1200mm. From their study they found that there is a clear interaction between local and distortional buckling for intermediate length columns, and interaction between local buckling and flexural buckling for long columns. Further, in

their study they have found that the DSM is conservative in predicting the design strength of test specimens failing in local buckling and flexural buckling interaction.

The study by Dos Santos, Barista and Camotim (2012, 19-34) on lipped C-channels undergoing local-distortional-global buckling modes also showed important findings regarding the behaviour of pin-ended columns. They presented a set of 12 column tests with various cross section geometries. Their study shows that intermediate length columns are susceptible to buckling modes interaction. They concluded that local deformations have no effect on the post-buckling strength of lipped C-Channels. Thus the failure mode of their columns involves a combination of symmetric distortional and global deformations where the global deformation seems more prominent.

These studies show that buckling interaction is apparent in the behaviour of cold-formed steel columns. Therefore, the DSM which takes buckling interaction into account is a viable alternative design method for cold-formed steel member design. Despite the advantages, there are major limitations to the DSM, which includes the provisions for shear, web crippling, and strength increase due to cold-work forming, and there is limited pre-qualified members.

2.2.2 Limitations of Direct Strength Method (DSM)

The DSM is further limited by the finite strip method implemented by Cornell University Finite Strip Method (CUFSM) for the elastic buckling load determination. One major limitation of the finite strip method is that, it does not allow varying cross section and load along the length. Therefore elastic buckling determination for complex cross-section using CUFSM which is not constant along the length has to rely on assumptions.

Megnounif, Djafour, Belarbi and Kerdal (2007, 443-460) proposed a design procedure for predicting the ultimate strength of cold-formed steel built-up columns based on the effective width approach from the Eurocode and the DSM. In their study, they proposed several design approaches. Their proposal for the EWM included:

- (i) EWM with buckling factor 4.0 and 0.43, and
- (ii) EWM with the buckling factor calculated from buckling stresses obtained from a

proposed compound spline finite strip method.

For the DSM, design alternatives included:

- (i) DSM with the local buckling strength obtained from the classical element method,
- (ii) DSM with the local buckling strength calculated by hand,
- (iii) DSM with a proposed equation for distortional buckling strength, and
- (iv) DSM with the buckling strength calculated from buckling stresses obtained from a proposed compound spline finite strip method.

They stated that whether implemented as a classic hand method or spline finite strip method, the DSM provides significantly different prediction as compared to their experimental data. Thus, the accuracy of the DSM requires further investigation.

Macdonald, Heiyantuduwa and Rhodes (2008, 1047-1053) stated that the DSM was initially developed with the idea that the initial buckling strength for any cross-section is easily achievable by numerical means. This approach was initially applied in the analysis of simple cross sections such as the C-channel, where the ultimate strength was empirically related to the critical load using a simple power law based on test results. Further, they said that the result was only approximate for sections other than simple cross sections, which the method was developed for.

Macdonald, Heiyantuduwa and Rhodes stated that the finite strip method analytically evaluates the deformation pattern of a structure in one direction. It is essentially a simplified version of the finite element method. Therefore, the finite strip method is only suitable for determining critical loads of structural members of constant cross-section. Hence, further investigation is required to allow its use on built-up members with cross sections not constant along the length such as back-to-back C-channel built-up columns with and without a gap. Since the basis of the CUFSM is the finite strip method, there is a need to improve the analysis of back-to-back C-channel built-up columns with and without a gap using the CUFSM.

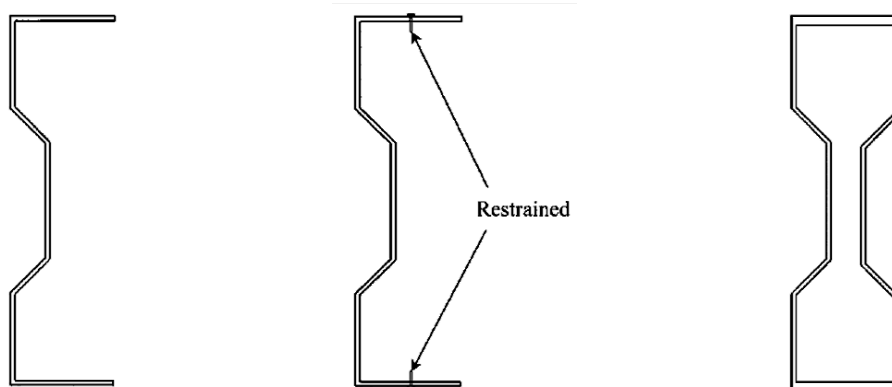
The DSM design guide proposed two possible models to analyse the critical elastic buckling strengths (AISI 2006, 54-55) of built-up columns using the CUFSM,. They are:

- (i) modelling the built-up section as a rigidly connected I-section, and
- (ii) modelling the built-up section as an individual C-channel and taking the required values as twice of the C-channel.

From these models, model (i) gives the upper limit of the calculated elastic buckling strengths whereas model (ii) gives the lower limit of the calculated elastic buckling strengths. Thus, there is still room for improvement on modelling built-up columns using the CUFSM.

Further investigation on the applicability of built-up columns using the finite strip method was studied by Young and Chen (2008, 727-737) using CUFSM. In their study, they used three models as shown in Figure 2.1 with:

- (i) modelling as twice an individual section,
- (ii) modelling as twice an individual section with restraint provided at the screw locations, and
- (iii) modelling as a thicker section with two times the thickness for elements where the screws occur.



(a) Single Section (b) Single Restrained Section (c) Double Section

Figure 2.1: CUFSM Models for Buckling Stress Determination (Chen & Young 2008, 727-737)

The results showed that model (i) yielded conservative column strength prediction, while model (ii) and (iii) resulted in unconservative column strength prediction. It shows that modelling built-up column as twice an individual column with restraint and as a thicker cross section with twice the thickness at elements with screw are both unconservative. This is because both (ii) and (iii) models are more rigidly connected than an actual built-up column which is only connected at discrete locations along the length of the column. These models do not predict the strength of built-up columns

well because the CUFSM is only capable of predicting specimens with constant cross section along the length. Thus, the proposed models by Young and Chen (2008, 727-737) were only approximations. It is apparent that there is a need for further investigation.

The approximation method was later improved by Zhang and Young (2012, 1-11). They introduced contact thickness to account for the thickness of the element in contact. In their study, contact thickness in calculating the design strength of back-to-back C-channel built-up column with edge and web stiffeners was evaluated using the CUFSM. They calculated the elastic buckling strengths for the cross section based on different cross section assumptions. They found that the CUFSM is applicable for the strength calculation of built-up column with web and edge stiffeners. They pointed out that the design strength obtained by considering the built up column as rigidly connected with a contact area of 1.2 times the web thickness of a single element is generally conservative and reliable. However, this finding of 1.2 times the web thickness was developed through arbitrary assumptions in the design. Thus, may not be applicable for other built-up columns. Moreover, the cross sections used in the design evaluation were also limited. Therefore, the proposed method in built-up column design needs to be further evaluated. The importance of determining the contact thickness for the CUFSM model is once again shown. Thus, further study is required to determine elastic buckling strengths of built-up sections with appropriate web contact thickness using the CUFSM.

2.3 Shift of Effective Centroid

One of the key factors affecting the strength and behaviour of compression members is the support conditions at the ends of the column. The effect of support conditions is especially important for singly symmetric columns such as C-channel columns. This is because uniformly compressed pin-ended singly symmetric column such as C-channel column undergoes a shift in the line of action of the internal force when the column buckles locally.

According to Young (2006, 119-132), Rhodes and Harvey (1977) explained that the shift of effective centroid is caused by the asymmetric redistribution of longitudinal

stress due to local buckling deformation. This leads to an eccentricity of the applied load in pin-ended C-channel columns as shown in Figure 2.2. Hence, local buckling of pin-ended C-channel columns induces overall bending, as shown in Figure 2.3.

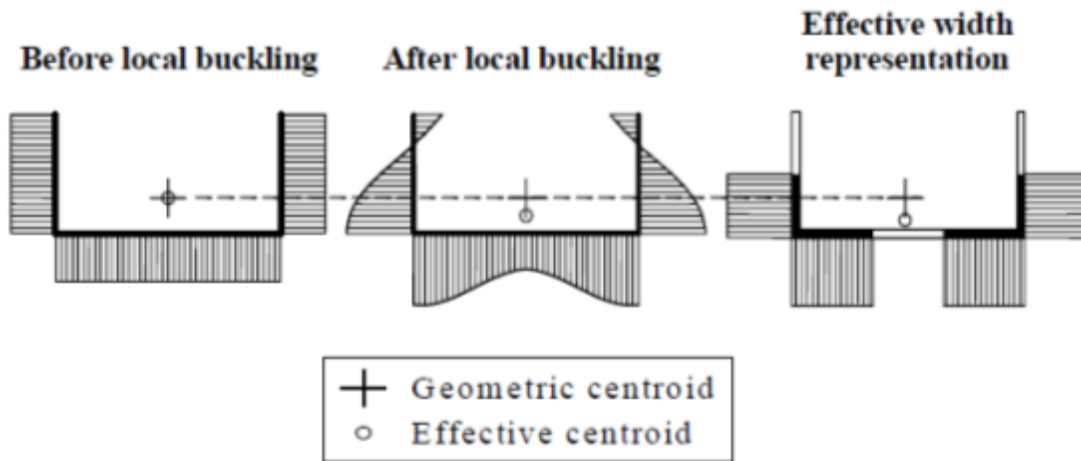


Figure 2.2: Stress Redistribution of C-channel under Uniform Compression with Effective Width Representation (Young 2006, 128)

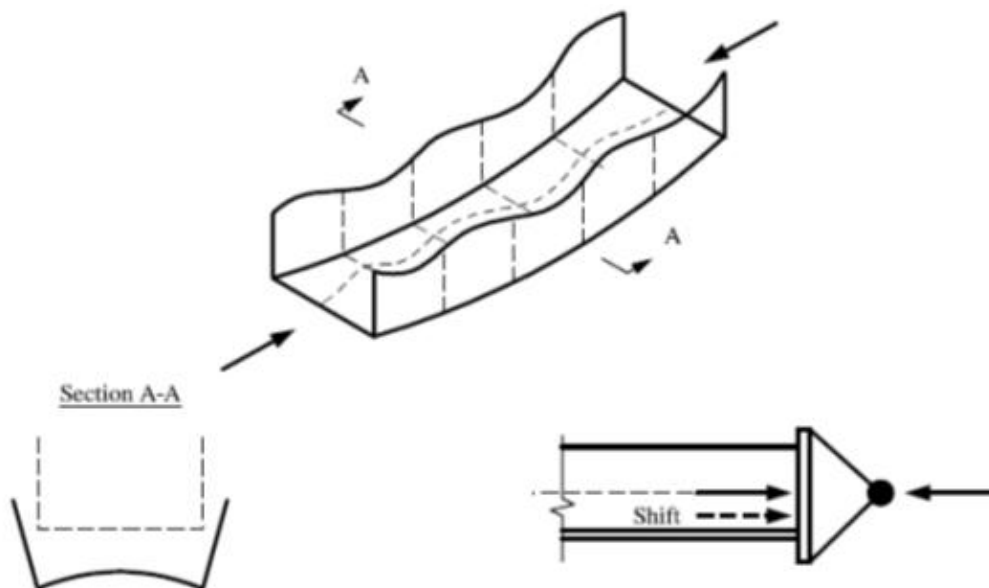


Figure 2.3: Locally Buckled Pin-ended Channel Column (Young 2006, 129)

The shift of the centroid, however, does not occur in doubly symmetric columns, which include the back-to-back C-channel columns investigated in this study. In locally buckled doubly symmetric columns, the redistribution of longitudinal stress does not cause a shift in the line of action of the internal force because the cross section is symmetrical as shown in Figure 2.4.

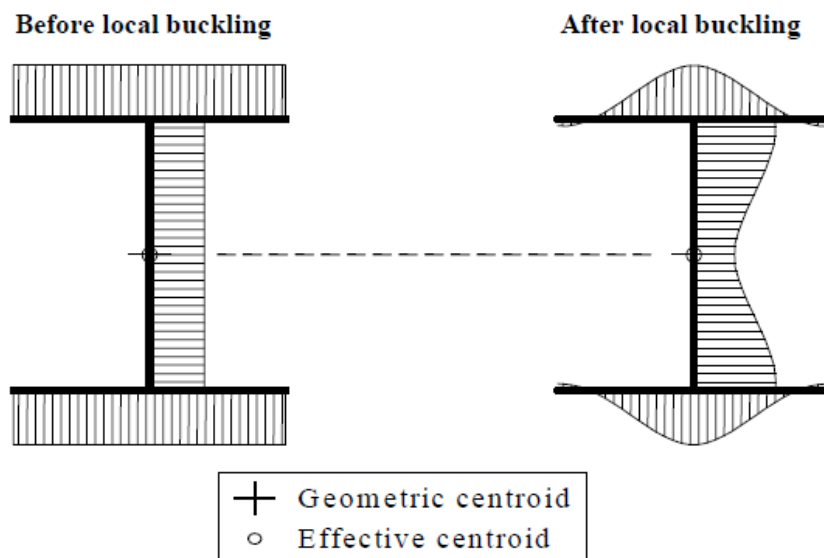


Figure 2.4: Stress Redistribution of Doubly Symmetric Cross Section under Uniform Compression (Young 2006, 130)

Since it is apparent that shift of effective centroid occurs in singly symmetric pin-ended columns, it is important for the design methods to be able to cater for the shift. Young and Rasmussen (1998c, 131-139) evaluated the design of singly symmetrical C-channel columns at pin and fix-ended support condition. The test programme in their study comprised two series of plain C-channel columns with two different flange widths of 36mm and 48mm at a nominal thickness of 1.5mm, a nominal web width of 96mm and a nominal lip width of 12mm. The length of these columns ranged from 280mm to 3000mm. Their experimental testing shows that the shift in the line of action of the internal force caused by local buckling does not induce overall bending in fixed-ended channel columns. Therefore, it was recommended to design fixed-ended singly symmetric columns using column equations using an effective length of one-half of the column length. However, beam-column equations were recommended for pin-ended C-channel columns because local buckling induced overall bending in pin-ended C-channel columns. Comparison of experimental results and design calculation using beam-column equations shows that it is conservative for both test series. This is due to the overestimated values of the shift of the effective centroid of the applied force, and also due to the underestimated values of the bending capacity.

The effect of shift of effective centroid was also evaluated by Yiu and Peköz (2000, 13-22) in their study on the design of cold-formed steel plain channels on flat-ended and pin-ended columns. Based on the experimental investigations and finite element studies by several researchers, their study evaluated the design procedures on:

- (i) minor axis bending with stiffened element in tension,
- (ii) minor axis bending with stiffened element in compression,
- (iii) major axis bending with unstiffened elements in uniform compression,
- (iv) flat-ended columns,
- (v) pin-ended columns, and
- (vi) beam-columns.

They demonstrated that the design methods should differ depending on the end support condition. They proposed using the column equations to design fix-ended columns and beam-column equations to design pin-ended columns. When using beam-column equations, they determined the eccentricity of the load on the basis of the location of the load and the average deflections of the beam column instead of the maximum deflections as in Young and Rasmussen (1998c, 131-139). They also proposed an improved plate buckling coefficient, k , for the beam-column equations.

From these studies, it is apparent that fix-ended C-channel columns are better designed with column equations while pin-ended C-channel columns are better designed with beam-column equations due to shift of effective centroid. However, the shift of effective centroid is not of concern for doubly symmetrical built-up columns.

2.4 Built-up Column

The gaining popularity in the use of built-up columns leads to complex design problems. The complexity is due to the unique buckling characteristic of built-up columns under load, either buckling as one single member or two individual members. In order to account for the unique buckling behaviours, a specific provision for the design of built-up columns was introduced in clause C4.5 of the American Iron and Steel Institute (AISI) North American Specification (NAS) 2001 edition for the Design of Cold Formed Steel Structural Members (AISI 2002c, 83). The AISI

specifications highlighted in clause C4.5 the two important criteria for the design of built up columns:

- (i) the modified slenderness ratio, and
- (ii) the minimum fastener requirement.

The modified slenderness ratio was introduced to take into account the effects of shear forces induced between the fasteners on the buckling stress (AISI 2002c, 83). Whereas, the fastener requirement is to account for loose or ineffective fastener thus preventing the flexural buckling of individual shapes between intermediate fasteners.

2.4.1 Modified Slenderness Ratio

According to the Commentary on the AISI North American Specifications (AISI 2002b, 98-99) the modified slenderness ratio is used in other steel standards including the hot rolled-steel design standard such as the American Iron and Steel Construction (AISC) specification.

Study on the modified slenderness ratio for built-up column began as early as 1952, when Bleich (1952) proposed an analytical criterion to modify the overall slenderness ratio of battened columns (Aslani and Goel 1991, 159). However, the proposed equation was limited to hot-rolled battened columns with hinged-end conditions only. The slenderness modification became of great interest when it was first introduced in the design standards for hot-rolled steel in the 1986's AISC Specification (Whittle and Ramseyer 2009, 190). This showed that studies performed on hot-rolled built-up members are the foundation of the design for cold formed steel built-up members. It was the study on hot-rolled members that led to the addition of the slenderness modification equation into the design standards. Therefore, relevant literatures related to hot-rolled steel's modified slenderness ratio are important for the design of cold-formed steel built-up members.

Temple and Elmahdy (1996, 1295-1304) carried out an experimental program on welded hot-rolled built-up battened columns consisting of double channels arranged in a toe-to-toe manner to form a box-like section. The number of intermediate fasteners was varied from 1 to the number of intermediate fasteners required to satisfy clause 19.1.16 of the CSA-S16.1-M89, a national standard of Canada. In addition to these

intermediate fasteners, end fasteners were used. They found that the buckling load for x-axis buckling is not affected by the number of intermediate fasteners. For y-axis buckling, the equivalent slenderness ratio is sufficient to predict the buckling load. The test results show that the requirements of Clause 19.1.16 of S16.1-M89 result in more intermediate fasteners than are required.

Later, more study on modified slenderness ratio was conducted using other hot-rolled steel design standards. Lue, Yen and Liu (2006, 1325-1332) conducted experimental study to verify the AISC-LRFD slenderness ratio formulas on hot-rolled steel for snug-tight bolted built-up columns and welded built-up columns. They tested a total of 12 built-up columns divided into four groups with bolts or welds. The design codes being considered in their investigation include the American Code (AISC-LRFD), Australian Code (AS4100), and Canadian Code (CSA S16-01). Comparison of the experimental results and design calculation showed that the use of slenderness ratio formulas in AS4100 yields more conservative results compared to the LRFD and the CSA.

Liu, Lue and Lin (2009, 237-248) further investigated the hot-rolled built-up columns with various slenderness ratios or provisions used in the American code (AISC-ASD and AISC-LRFD), Australian code (AS4100), and Canadian code (CSA S16-01). They found that the effect of fastener spacing on the strength of built-up columns formed is apparent. Their study pointed out that the greater the fasteners spacing, the lower the strength of the built-up column. They also found that the requirement in the design standard where the component slenderness ratio does not exceed three-fourth times the governing slenderness ratio for built-up columns, seems justified. Overall their study concluded that the modified slenderness ratio for hot-rolled built-up column calculations is reasonably applicable.

These studies show that the modified slenderness ratio is applicable when designing hot-rolled built-up columns. This is as expected as the modified slenderness ratio is adopted from study on hot rolled steel. However, the characteristics of hot rolled steel are considerably different than those of the cold formed steel. Several researchers have

investigated the reliability of modified slenderness ratio in the design of cold-formed steel built-up columns.

Stone and LaBoube (2005, 1805-1817) conducted tests on built-up studs of varying material thickness to study the use of modified slenderness ratio. In their study, they tested a total of 32 back-to-back C-channel built-up studs with self-drilling screws spaced at a set interval within the column length of 2.1m. As a result of the investigation, they concluded that the modified slenderness ratio is very conservative for the design of built up columns with thick sheets while it is on average conservative for built up columns with thin sheets. Although varying screw spacing was used, it was not the main focus of their study. There was a lack of investigation on the effects of varying screw spacing with varying column length despite the fact that these are important parameters affecting the design of built-up columns.

In Whittle and Ramseyer (2009, 190-201), the design methods for built-up columns was studied using built-up closed section based on thickness, geometry, column length, and location/ number of intermediate weld attachments. They tested 155 built-up columns with fastener spacing that did and did not meet the provision stated in the design standard. They suggested that when the built-up column fastener spacing provisions were followed, the modified slenderness ratio was conservative for built-up columns with shorter widths, longer length and thicker sections. Their study concluded that the average design strength calculated using the modified slenderness ratio is very conservative.

The conservativeness of modified slenderness ratio was also identified by Brueggen and Ramseyer (2005) through small C-channels in open- and closed-sections with intermediate, welded stitch attachments (Whittle and Ramseyer 2009, 190). Different cross section sizes were studied and it was found that the modified slenderness ratio is on average conservative for compact cross sections but potentially unconservative for members with slender elements. This is because columns with different cross section elements slenderness tend to behave differently.

The effects of cross section elements slenderness on the ultimate strength and the behaviour of a built-up stub column were also shown in Gao et al. (2009, 918 – 924). The main focus of their study was not on modified slenderness ratio; however, their study shows important findings on built-up stub columns. They found that the ultimate strength of stub columns with square cross sections (smaller web-flange ratio) was always much larger than that of columns with rectangular cross sections (larger web-flange ratio). The failure mode changed from material strength failure to buckling failure as the web-flange ratio becomes larger. However, the variation was not obvious for columns with small width-thickness ratio. Their investigation shows that the slenderness of the plate elements affects the effectiveness of the cross section of the column, and hence also affects its overall strength and behaviour. When designing stub columns, the overall slenderness ratio (L_e/r) of the column has little effect on the design strength of the cross section. The cross section plays a more important role instead. They also found that the design strength predicted using the current AISI provisions provides results that are exceedingly conservative compared to actual test results for stub columns.

These studies show that the modified slenderness ratio may not be completely applicable for cold-formed steel built-up columns. Thus, the current design requirements on the modified slenderness ratio for built-up columns need to be further evaluated. Important parameters to the investigation include the spacing of intermediate fasteners and the slenderness of the column's cross section.

2.4.2 Intermediate Fasteners

Intermediate fasteners are important components of a built-up column. In addition to reducing the effective length, intermediate fasteners maintain the spacing between the individual columns, carry shear and moment that company bending of the built-up column and also provide some torsional restraint to the individual columns. The design standard specifies the requirement for intermediate fasteners where the maximum slenderness ratio should not exceed one-half times of the individual columns of a built-up column, i.e.

$$s/r_y \leq 0.5(KL/r)_o$$

This requirement restricted the maximum allowable screw spacing, which resulted in more intermediate fasteners required for a built-up column. This is uneconomical because lesser number of intermediate fasteners is actually required for the built-up column. Thus, further studies were conducted by researchers to investigate the fastener spacing requirement.

Aslani and Goel (1991, 159-168) verified the use of modified slenderness ratio in designing built-up members analytically and experimentally by varying overall and individual slenderness ratios. The overall slenderness ratio is modified by using the LRFD empirical, Bleich's approximate analytical, and the proposed analytical equation. The proposed analytical equations are verified with test results from the authors' previous publications by comparing the calculated buckling load. Only specimens with individual slenderness ratio greater than 50 were included in the comparison. They concluded that predicted strength using modified slenderness ratio reduced significantly when shear flexibility is involved. Due to large intermediate fasteners spacing, shear flexibility occurred and caused the individual components of the built-up member to separate.

Tang and Ma (2005, 523-528) studied the behaviour of bolted cold-formed back-to-back C-channel built-up columns using the finite element programme ANSYS version 6.1. They modelled C-channel with 350mm height, 100mm width, 20mm lipped, and 3mm thickness at member length of 2000mm with simply supported at the ends. They found that the strength of built-up columns decreases when the bolts spacing in the longitudinal direction was larger than half of the span length. The strength of built-up columns was twice of the single C-channel columns when the bolts on the built-up column were fully effective. When the effective width of webs was less than $\frac{2}{3}$ times web height, local buckling may occur before the overall buckling of the built-up column, and the local buckling strength was deeply influenced by the bolt spacing in vertical direction. They concluded that built-up columns connected with bolts symmetrical in vertical direction at bolt spacing 0.35 times the height of the cross section were more effective. The strength of built-up column is very much influenced by the intermediate fasteners between the C-channels.

Reyes and Guzman (2011, 929-935) studied the behaviour of cold-formed built-up box members connected by means of welds. They focused on the effect of member thickness and fastener spacing on the behaviour of closed built-up members. They tested a total of 48 test specimens, all with a length of 900 mm. The specimens had fastener spacings of 100 mm, 300 mm, 600 mm, and 900 mm. Their study concluded that in test specimens consisting of thicker elements, the use of modified slenderness ratio to calculate the design strength is not necessary. Further, they pointed out, that the effect of fastener spacing on the strength of built-up members was not apparent for test specimens with a fastener spacing of less than 600mm apart. Their study showed that for built-up members, there was a trend towards greater ultimate strength as fastener spacing reduces. However, the same effect diminishes when the fasteners are spaced too near to each other.

These studies show that the purpose of limiting the slenderness ratio of the individual columns of a built-up column is to avoid coupled instabilities. Thus, it is apparent that the intermediate fasteners is important to built-up columns, however, the maximum allowable spacing suggested by the design standard may be restrictive and conservative. Therefore, further study on the intermediate fasteners' requirement is required.

2.5 Built-up Column with a Gap

Built-up column with a gap is similar to the usual built-up columns but has greater lateral stiffness than individual columns due to larger cross section. Current design codes do not provide comprehensive methods to design such columns with complex cross section. Due to this, designers usually resort to conservative assumptions in designing built up columns with a gap. It is common to design it by assuming that the column acts as two individual columns without modifying the slenderness ratio. However this approach may not reflect the true behaviour of the built-up column with a gap.

Georgieva, Schueremans and Pyl (2011, 125-134) studied on complex built up columns composed from Z-sections. Eight full-scale tests on 4.45m long cold-formed steel built-up columns are performed and out of plane displacements and strains at 6

locations per member are recorded. Their study made several assumptions to design the double-Z built-up columns because it is difficult to determine cross section properties for complex cross sections. They pointed out that strength predictions using the North American Specification and the Eurocodes yielded conservative results compared to the actual test results. The beneficial effect of connecting two Z-sections together is not reflected in the strength prediction according to current design standards. Furthermore, they pointed out that the design of built-up columns relies heavily on the column's cross sectional properties which cannot be accurately derived, such as the warping constant and the torsional constants. Therefore the strength prediction relies heavily on the assumptions made. This is also true for built-up column with a gap because the column's cross section is complex and is not constant along the length of the column. Thus, it is difficult to calculate its section properties.

The first attempt to propose calculations for section properties of built-up columns with a gap was done by Johnston (1971, 1465-1479) in his study on the behaviour and design of back-to-back C-channel built-up columns with a gap. The notations of the back-to-back C-channel built-up columns with a gap are shown in Figure 2.5.

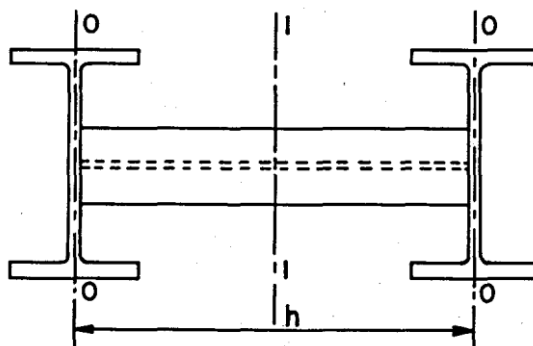


Figure 2.5: Cross Section of Built-up Column with a Gap in Johnston (1971)

His study showed that if the built-up columns with a gap are assumed to act as an integral, the cross sectional area could be assumed as the sum of the two individual columns that make up the built-up columns with a gap.

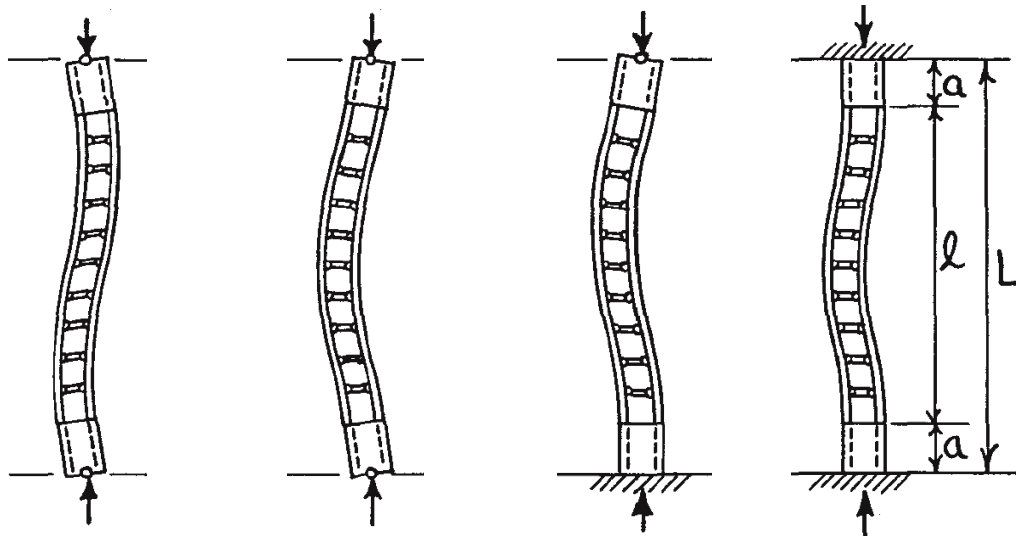
$$A = 2A_o$$

With that, the following equation is used to calculate the second moment of inertia of the member with gap about the l-l axis.

$$I = \frac{A_o h^2}{2} + 2I_o$$

Johnston also showed that there are four buckling modes for built-up columns with a gap with end ties depending on the end connections. As shown in Figure 2.6, the buckling modes are:

- (a) Pinned- pinned end – center reversal of curvature,
- (b) Pinned- pinned end – semi-fixed shape,
- (c) Fixed-pinned end, and
- (d) Fixed-fixed end.



(a) pinned-pinned (b) pinned- pinned (c) fixed-pinned (d) fixed- fixed

Figure 2.6: Buckling modes of Built-up Columns with a Gap proposed by Johnston (1971)

From these buckling modes, Johnston developed a series of equations to calculate the strength of a built-up column with a gap with end ties. However, it is important to note that his designs were for hot rolled steel members. Although the design equations were primarily designed for hot-rolled built up column with a gap with end ties, it is the groundwork for the study of behaviour and design methods for cold-formed steel built-up column with a gap.

Specifically for pin-ended built-up columns with a gap, Johnston stated that there are two possible buckling modes, with mode 1 as the reversal of curvature and mode 2 as the semi-fixed shape shown in Figure 2.6 (a) and (b) respectively. In mode (a) buckling, there is no differential change in length between the two individual columns that form the built-up column with a gap. In mode (b) buckling, the shortening is greater on the concave side than on the convex side. There is an added internal resisting moment due to the direct forces in the components that is added to the

bending moments induced in the components themselves. The critical loads for mode (b) buckling may be less than those for mode (a) when the ratio of the moment of inertia for the built-up column with a gap to the moment of inertia for the individual columns, $I_{GBU} / I_{Individual}$ is relatively small and the ratio of fastener spacing to overall column length, s/L is large. Thus, it is expected that mode (b) buckling is of higher possibility for specimens with large fastener spacing. For specimens with the same geometry and under the same test conditions, specimens with mode (a) buckling are potentially higher in ultimate strength compared to specimens with mode (b) buckling.

Johnston also pointed out that the predominant factor for the determination of the behaviour and the strength of a back-to-back C-channel built-up column with a gap was the end ties. He demonstrated that for built up columns with a gap where the individual C-channels were connected by plates with pinned connections there was no transfer of shear forces between the individual C-channels. Therefore, for the built up columns with a gap without end ties, the strength of the column is simply the sum of the strength of the individual C-channels. In order to ensure that the columns act as an integral, it is important to provide end ties.

Based on the buckling modes and equations proposed by Johnston (1971, 1465-1479), Rondal and Niazi (1990, 329-335) conducted a study on back-to-back C-channel built-up columns with a gap with batten plates or short C-channels as intermediate fasteners using the models as illustrated in Figure 2.7 for analysis.

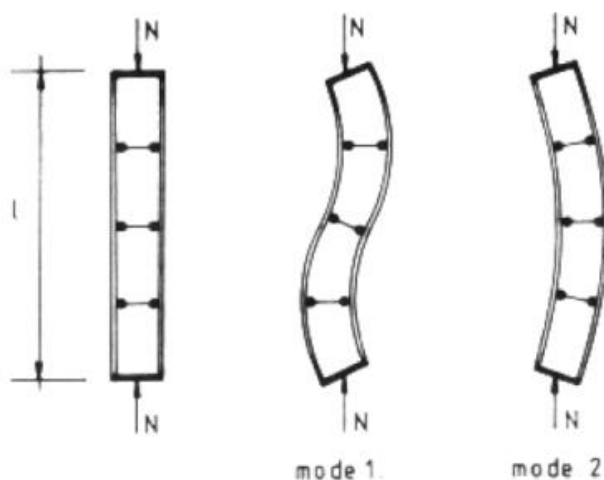


Figure 2.7: Models for Built-up Column with a Gap in Rondal & Niazi (1990)

In their study, built-up columns with a gap made up of two different sizes of C-channels at 3m and 4m were considered. The intermediate connectors of the built-up columns with a gap were spaced at 970mm with four batten plates and 1300mm with three batten plates. Their experimental and finite element investigations show that the ultimate strengths of the built-up columns with a gap were insensitive to the mode of buckling. Therefore it is expected that as long as the built-up columns with a gap have sufficient short C-channel fasteners to ensure that the individual C-channels do not separate, their ultimate strengths are expected to be very similar.

From these studies, intermediate fasteners are of important influence to the behaviour of built-up columns with a gap. They also show that behaviour of built-up columns with a gap with batten plates or short C-channels as intermediate fasteners are similar but different in terms of the rigidity of the intermediate connectors. Thus, studies on both types of column are reviewed.

Dubina, Zaharia and Ungureanu (2002, 179-186) studied the behaviour of built-up columns made of back-to-back lipped channels, bolted together by short C-channels. They compared and evaluated the existing Eurocode 3 provisions with Rondal and Niazi (1990; 1993) via experimental and numerical results for battened cold-formed columns. In their research, they combined Eurocode 3 with findings from Rondal and Niazi and proposed a design method for built-up columns with a gap. They also used ANSYS to model the built-up columns with a gap. The built-up columns with a gap were made up of two types of C-channels with intermediate connectors spaced with three or four batten plates. They pointed out that the behaviour of back-to-back C-channel built-up column with a gap connected by battens and by short C-channels is essentially the same. The major difference between the two is the rigidity of the connection between the individual C-channels of the back-to-back C-channel built up column with a gap. The short C-channel connection is less rigid and is reasonable to be considered as a pinned connection. Their research showed that the number of intermediate fasteners does not have an influence on the ultimate strength when sufficient number of intermediate fasteners is provided. Identical deformed shapes at the level of ultimate load were obtained for model with three and four intermediate fasteners.

Salem et al. (2004, 117-125) presented an analytical approach to monitor the behaviour of built-up struts composed of C-channels connected together with batten plates. The battened details, end conditions, and bolt size cover a wide range of cases and also satisfy the AISI, AISC and Euro Code requirements. However, the spacing between the batten plates is extended beyond the limit defined in the design standards, to test the behaviour and strength of slender battened columns governed by the spacing. Their results showed that the corresponding ultimate strength decreases as the distance between the two longitudinal C-channels increases, for columns with the same number of intermediate fasteners and member slenderness ratio. Salem et al. also proved that increasing the number of intermediate fasteners enhanced the ultimate strength of columns.

It is apparent that the predominant parameters affecting the capacity of a back-to-back C-channel built-up column with a gap are:

- (i) gap between the individual C-channels, and
- (ii) spacing and stiffness of intermediate fasteners.

More experimental data is required to provide further insight into these parameters.

2.6 Computational Modelling

Finite element modelling had successfully been used in the past to predict the behaviour of cold-formed steel structures. The finite element method does not require constructing or pre-fabricating and testing a structure. This not only saves time but also reduces the testing cost. There are many finite element software, such as ANSYS, ABAQUS, LUSAS, etc available commercial in the market.

To date, limited research has been conducted in the area of built-up members (Whittle and Ramseyer 2007, 190; Lue, Yen, and Liu 2006, 1325; Liu, Lue and Lin 2009, 237). Even fewer studies have been carried out to model cold formed steel built-up columns using finite element analysis. Thus, all the relevant literatures related to finite element computational modelling are reviewed. The literature review in this section covers the concept and techniques applicable to model a built-up column, particularly in terms of element type, surface contact, and connection model.

2.6.1 Element Type

Cold-formed steel members are generally made out of thin sheets. In finite element modelling, thin sheets are well replicated by shell type elements. Shell type element as surface element requires only the centreline dimensions and the thickness as inputs. The shell type element requires much less memory and run time compared to other element types such as a three-dimensional element model.

Young and Yan (2000, 281-305) conducted investigations into the strength and the behaviour of cold-formed lipped channel columns using finite element analysis. In their research, a finite element model was developed to investigate the behaviour and strengths of cold-formed plain and lipped channel columns compressed between fixed-ends and pinned-ends using ABAQUS version 5.8. The ultimate loads and failure modes obtained were verified against the column tests conducted by Young and Rasmussen (1998c, 131-139; 1998b, 140-148). The numerical simulation consisted of two stages. In the first stage, an eigenvalue elastic buckling analysis was performed on a "perfect" geometry to establish probable buckling modes of the column. In the second stage, a non-linear analysis was carried out by incorporating both geometric and material non-linearities using the modified Riks method to obtain the ultimate load and failure modes of the column. In their research, the finite element results were generally in good agreement with the test results. Thus, the shell elements are suitable to simulate the behaviour of thin cold-formed steel sheets.

The benefits of using shell type elements were also demonstrated in Zaharia and Dubina (2005, 61-68). They conducted a numerical study on the stability of cold-formed built-up columns connected with bolted short C-channels using ANSYS. In their study, a thin shell element known as SHELL43 was used to model their columns. Their finite element results were compared with 12 existing experimental results obtained from Rondal and Niazi (1991, 329-335). Comparison of their finite element results and experimental results shows good correlation using element type SHELL43 to model the built-up columns.

2.6.2 Surface Contact

Another important aspect in modelling built-up columns is the surface contact. In the context of back-to-back C-channel built-up columns, the surface contact is required on the web surfaces of the individual C-channels. This is to ensure that the individual C-channels recognise the presence of each other during the finite element analysis.

Becque and Rasmussen (2009, 1349-1356) conducted a numerical investigation using ABAQUS on the interaction of local and overall buckling of stainless steel back-to-back unlippped C-channels columns. In their finite element models, surface-to-surface type contact was defined between the outside surfaces of the webs of the two unlippped C-channels. The interface of these surfaces was modelled as frictionless. This finite element model was subsequently used in parametric studies which covered the practical ranges of overall slenderness between 0.25 and 2.0, and cross-sectional slenderness between 1.0 and 2.4. Their finite element results were compared with the experimental data from the authors' previous publication. The finite element model predicts the behaviour and strength of the test specimens well. They stated that any contact between surfaces has to be explicitly defined to ensure the built-up columns act as an integral unit.

Barrios, Angelo, and Goncalves (2005, 413-422) also demonstrated the importance of surface contact. They conducted a finite element analysis on shot peening using LUSAS. In their research, the surface contact feature was applied between the shot and the plate. The contact surface pair was modelled using the slideline function in the LUSAS software. This slideline function consists of two slideline surfaces called master and slave surfaces. Their finite element model was verified using a series of experimental results obtained from several researchers. Comparison of finite element results and experimental results shows that the surface contact can be successfully modelled using slideline function in LUSAS.

2.6.3 Intermediate Fasteners

One of the important parameters in modelling built-up column is the intermediate fastener. For plain back-to-back C-channel built-up columns, intermediate fasteners are the screw connections; whereas, for back-to-back C-channel built-up columns with

a gap, the intermediate fasteners are the short C-channels. The main function of intermediate fasteners is to hold the individual C-channels together so that the built-up columns act as an integral unit. Therefore, the intermediate fasteners are important to keep the individual C-channels together throughout the analysis.

Butterworth (1999, 1-14) modelled the extension of end plates from column flange connected using bolt connection. In his research, M20 grade 8.8 bolts with tensile stress area of 245mm^2 were used. The bolt holes were modelled as square cut-outs in the end plate and column flange. The bolts were modelled using three dimensional bar element known as BRS2 elements for the bolt shank; whereas, the head and nut were modelled using three dimensional solid element known as HX8M elements shown in Figure 2.8. Comparison of the finite element results and the test results showed good correlation.

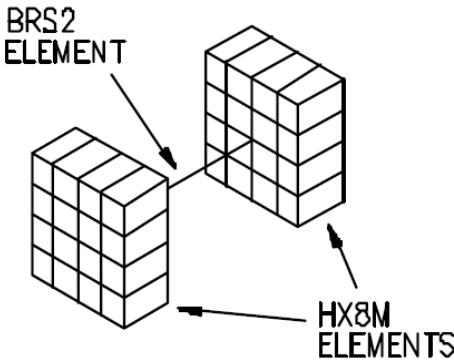


Figure 2.8: Finite Element Model of Connection in Butterworth (1999, 1-14)

Chin (2008, 1-81) studied beam to column bolted connections using LUSAS. He improved the bolt model from Tan (2006) by incorporating the bolt model from Butterworth (1999, 1-14). Instead of a simplified bolt model, he used a detailed bolt model using volume geometry shown in Figure 2.9.

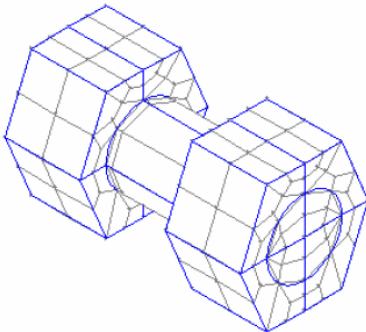


Figure 2.9: Finite Element Model of Connection in Chin (2008, 1-81)

Actual dimensions of the test specimens from Tahir et al. (2004) and Hussin (2001) were used to model the bolts. Finite element results obtained from the detailed bolt model were compared with the experimental results from Tahir et al. (2004) and Hussin (2001), and the finite element results from Tan (2006). Comparisons on failure modes, maximum resistance moment and the shape of moment-rotation, $M - \Phi$ curves show that the detailed bolt model predicts the strength and behaviour of the test specimens well.

The benefits of modelling intermediate fasteners using simplified model were also highlighted in the Becque and Rasmussen (2009, 1349-1356) research. They conducted numerical investigation on stainless steel back-to-back un-lipped C-channel built-up columns using ABAQUS. The finite element model was verified against an experimental program of 24 back-to-back stainless steel columns failing by interaction of local and overall flexural buckling from authors' experimental investigation. The model was subsequently used in parametric studies, where the overall and cross-sectional slenderness values were varied within practical limits. In their research, the physical connections between the two individual C-channels were not explicitly modelled. They explained that when the individual C-channels are bolted together in the actual experiment, a finite sliding of the two web surface relative to each other takes place at the location of the bolt hole or even that a small gap forms between the surfaces when the bolts are insufficiently tightened. Thus, not explicitly modeling the connectors would result in a more realistic solution than when the degrees of freedom of corresponding nodes on the two surfaces were totally coupled. They further explained that by not modeling the connectors, no additional constraints were imposed on the local buckling pattern or on the relative sliding of the surfaces. Comparison of finite element results and experimental results shows that although the intermediate fasteners were not explicitly modelled, there was good agreement in the prediction of strength and behaviour of the built-up columns.

It is apparent that modelling using simplified connection model is just as good as modelling using a detailed connection model. The behaviour of the built-up columns can be modelled without modelling the intermediate fasteners in detail.

2.7 Conclusions

The DSM is a viable alternative design method to the EWM for cold-formed steel member design. The CUFSM is commonly used to determine the elastic buckling solutions for the DSM. However, the CUFSM does not allow varying cross section along the length. Therefore assumptions are required in elastic buckling determination for complex section such as built-up columns which cross section of which is not constant along the length. Thus, there is a need to simplify and improve the analysis of plain and back-to-back C-channel built-up columns with a gap using the CUFSM.

The support at the ends of the column is one of the key factors affecting the strength and behaviour of compression members. The support condition for singly symmetric columns such as C-channel columns is critical because pinned-end condition causes shift of effective centroid. Due to this shift of effective centroid, pin-ended C-channel columns are better designed with beam-column equations while fix-ended C-channel columns are better designed with column equations.

The design provision for cold formed steel built-up members is adopted from the research studies performed on hot-rolled built-up members. However, the characteristics of hot rolled steel are considerably different than the cold formed steel. Moreover, the design provision restricted the maximum allowable screw spacing, which resulted in more intermediate fasteners required for a built-up column. Thus, lesser number of intermediate fasteners is possible for economical built-up column design.

Current design codes do not provide comprehensive methods to design complex cross section. The design of complex section such as built-up columns depends on the column cross sectional properties. However, some cross sectional properties such as the warping constant and the torsional constants cannot be accurately derived. Therefore assumptions were made for design calculations.

3 Experimental Investigation

3.1 Introduction

This chapter presents the experimental investigation on cold-formed C-channels, plain and back-to-back C-channel built-up columns with a gap consist of stub, short, intermediate and slender columns. This experimental investigation covers testing on C-channels and back-to-back built-up columns fabricated from cold-formed steel C-channels. These specimens are designed with various member slenderness ratios, and screw spacing to study the behaviour of the built-up columns. There are two types of cross sectional dimensions for this experimental investigation, differentiated by their web width of 75mm and 90mm.

The test specimens were brake-pressed from aluminium/zinc-coated grade G550 structural steel sheets of 1.2mm thickness. Dimensions of the test specimens were selected with reference to the dimensional limits proposed by the AISI specification. The cross-sections were then analysed by the CUFSM to determine suitable lengths that fall within the categories of stub, short, intermediate and slender columns. A total of 138 specimens with two sizes of lipped C-channels column, back-to-back C-channel built-up column with and without a gap at lengths of 300mm, 500mm, 1000mm, and 2000mm were tested. Tests were carried out on stub columns with the fixed end condition, whereas the short, intermediate and slender columns were tested with the pinned end condition.

3.2 Materials Properties

The material properties of the specimens were determined by tensile coupon tests. The coupons were wire cut from the centre of the web plate from specimens of the same batches as the column test specimens. This is to ensure that the results represent the material properties of the column test specimens. The coupon dimensions conformed to the Standard Australia (SA) AS1391 (2007, 29) for the tensile testing of metals using 12.5mm wide coupons with a gauge length 50mm.

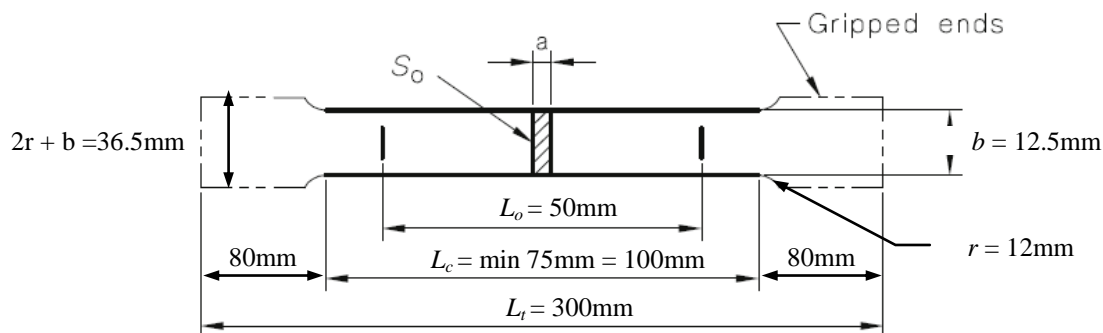


Figure 3.1: Shape & Dimensions of Tensile Coupon in accordance to AS1391-2007 (Standards Australia 2007, 26)

A data acquisition system was used to record the loads and the readings of strain from strain gauges at regular intervals during the tests. Six tensile coupons were tested with three from each cross-section batches. The tensile coupons from cross section with 75mm web width and 90mm web width are labelled as TC75 and TC90 respectively to represent each test specimen batch. The test results are shown in Table 3.1. The test result for coupon TC75-1 was discarded because the coupon broke outside of the 50mm gauge length, thus the elongation of the coupon was not recorded. Results from TC90-2 with a Young's modulus of 207.04GPa and a yield stress of 560MPa were used for design calculations later. The stress-strain curve from this coupon presented in Figure 3.2 was also used for material modelling in the finite element analysis described in Chapter 5. TC90-2 was chosen because this coupon provided result closest to the averaged results for all coupons.

Table 3.1: Tensile Coupon Test Results

Specimen	Young's Modulus	Yield Stress	Ultimate Stress
	E (GPa)	F _y (MPa)	F _u (MPa)
TC75-2	208.77	560.0	591.21
TC75-3	206.61	562.0	599.64
TC90-1	196.08	535.0	567.49
TC90-2	207.04	560.0	589.02
TC90-3	210.08	570.5	621.56
Average	205.72	557.5	593.78

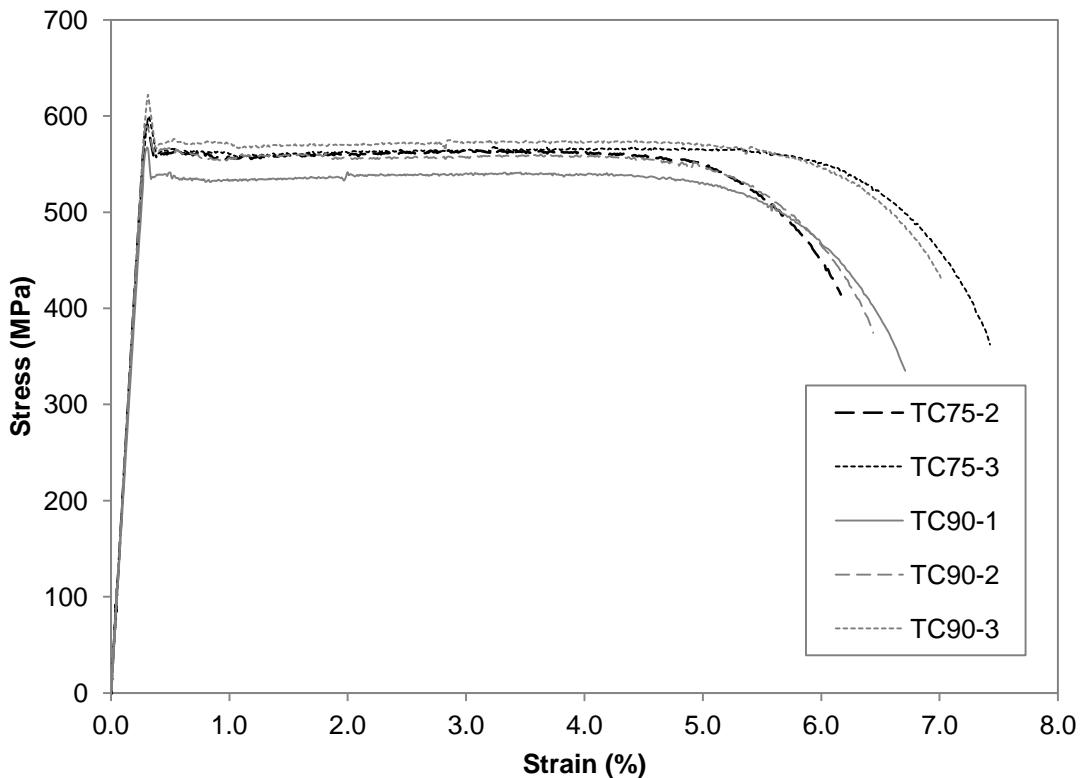


Figure 3.2: Stress Strain Curves from Tensile Coupon Tests

3.3 Specimen Design

The nominal cross-sectional dimensions for the test specimens in this experimental investigation are presented in Figure 3.3.

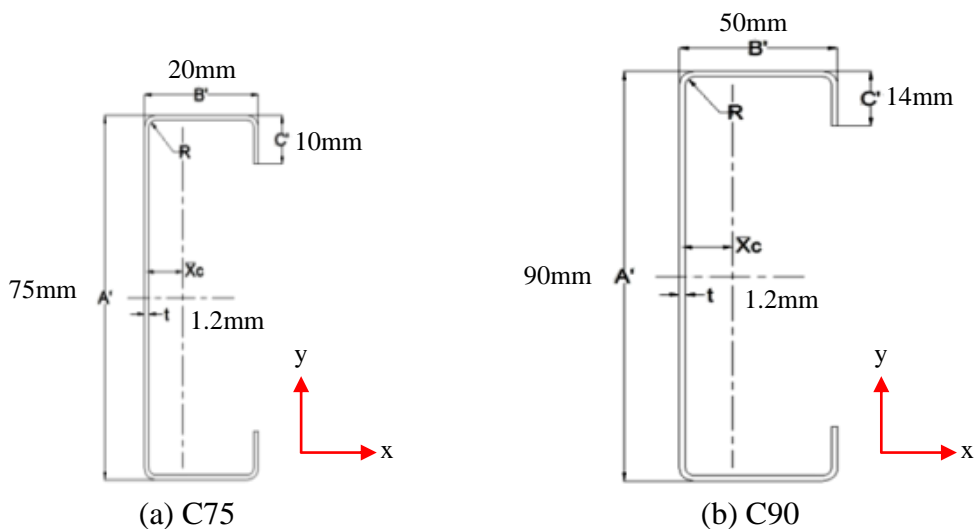


Figure 3.3: Dimensions of the Specimen Cross Sections

A total number of 24 specimens of C-channel columns, 66 specimens of plain back-to-back C-channel built-up columns, and 48 specimens of back-to-back built-up

columns with a gap were tested. They consist of four column lengths i.e. 300mm, 500mm, 1000mm and 2000mm designed with different fastener spacings. Each column length covers different fastener spacings as follows:

- (a) column length of 300mm with 50mm, 100mm, and 200mm fastener spacings,
- (b) column length of 500mm with 100mm, 200mm, and 400mm fastener spacings,
- (c) column length of 1000mm with 225mm, 450mm and 900mm fastener spacings, and
- (d) column length of 2000mm with 475mm, 950mm, and 1900mm fastener spacings.

3.3.1 Labelling

The test specimens were labelled such that the type of section, screw spacing, nominal length of specimen and specimen number were expressed by the label. The type of section is denoted as C for C-channels column, BU for plain back-to-back C-channel built-up column (without a gap) and GBU for back-to-back C-channel built-up with a gap. Two types of cross sectional dimensions tested are differentiated by their web width with 75 and 90 in the label. The intermediate fastener spacing is denoted as S with spacing. The column length is stated last in the label as L together with the nominal column length. Figure 3.4 shows a sample of the labels used.

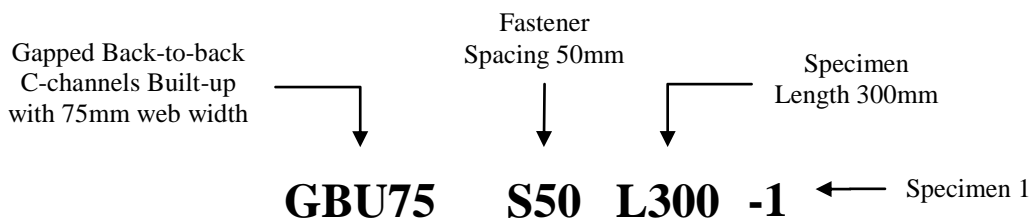


Figure 3.4: Specimens Label

3.3.2 Dimensional Limits

The cross sections of the test specimens were determined in accordance with clause B1 of the North American Specification (NAS) (AISI 2002c, 45-47) and clause 1.1.1.1 from the Direct Strength Method (DSM) Design Guide (AISI 2005, Appendix 1-5). The criteria in the design standards were intended to provide limiting conditions to the cold-formed steel design. From the design standards, the web has a relatively large width to thickness ratio. This is to provide a sufficient means for load transfer into the web. The limitation for the flange is because a thin flange with a large width to

thickness ratio is flexible and is prone to damages during transportation, handling and erection. As for the lip, it has one edge supported by flange and the other is free, thus the limiting width to thickness ratio is much lesser than for web and flange element. The dimensional limits for the test specimens are shown in Table 3.2. C75 was designed beyond the dimensional limits while C90 was designed within the dimensional limits.

Table 3.2: DSM and EWM Dimensional Limits

No.	EWM Requirements	DSM Requirements	C75	C90
1.	$A'/t < 260$	$34 < A'/t < 472$	62.5	75.0
2.	$B'/t < 60$	$18 < B'/t < 159$	# 16.7	41.7
3.	-	$4 < C'/t < 33$	8.3	11.7
4.	-	$0.7 < A'/B' < 5$	3.8	1.8
5.	$C'/B' < 0.8$	$0.05 < C'/B' < 0.41$	# 0.5	0.3
6.	-	90 degree	90.0	90.0
7.	-	$340 < E/F_y < 1020$	363.6	363.6

beyond the limit

*Note: Refer to Figure 3.3 and Table 3.1 for symbols.

3.3.3 Member Slenderness Ratio

The member slenderness ratio (KL/r_y) was used to categorise columns into stub, short, intermediate and slender. It can be separately defined with K as the coefficient for end condition, L as the column length, and r_y as the radius of gyration in the y-axis. Table 3.3 shows the lengths required to meet the respective member slenderness ratio.

Table 3.3: Lengths to achieve the required slenderness ratio

Cross-section	Radius of Gyration		Effective Length (L_e)								
			Stub			Short $50r_y/K$		Intermediate $100r_y/K$		Slender $200r_y/K$	
	r_{yC}	r_{yBU}	$< 20r_{yC}$	$< 20r_{yBU}$	$> 3A'$	C	BU	C	BU	C	BU
	mm	mm	mm	mm	mm	mm	mm	mm	mm	mm	mm
C75	7.4	9.4	147	189	225	368	472	735	943	1470	1886
C90	18.93	25.97	378.6	519.4	270	946.5	1298.5	1893	2597	3786	5194

According to the AISI Manual (2002a, VI-19), the stub column length shall not exceed twenty times the minimum radius of gyration, i.e. $20r_y$ and these columns shall be tested at fix-ended condition. The length of the stub columns was designed to be short enough to eliminate the overall buckling effects of the column but long enough to retain the residual stresses. However, the column length of $20r_y$ for C75 i.e. 147mm is too restrictive and inadequately short to be used as C90 stub column length. In this case, the column length limitation of more than three times of the web width i.e. $L > 3A'$ is to be complied. Thus, the column length of 300mm is chosen for both C75 and C90 stub columns. This column length of 300mm appears to be suitable to accommodate both C75 and C90 to allow the local buckling mode to occur along the length of the stub column.

The maximum length of 2000mm was chosen for the slender columns due to limitations in the test machine and the press braking machine. The cross section is limited, in order to achieve $KL/r_y > 200$ with 2000mm column length.

For short and intermediate columns, the lengths were determined using CUFSM and the member slenderness limits of $KL/r_y < 50$ and $KL/r_y < 100$. The CUFSM results on the load ratio against the half-wavelength for both C75 and C90 are plotted in Figure 3.5.

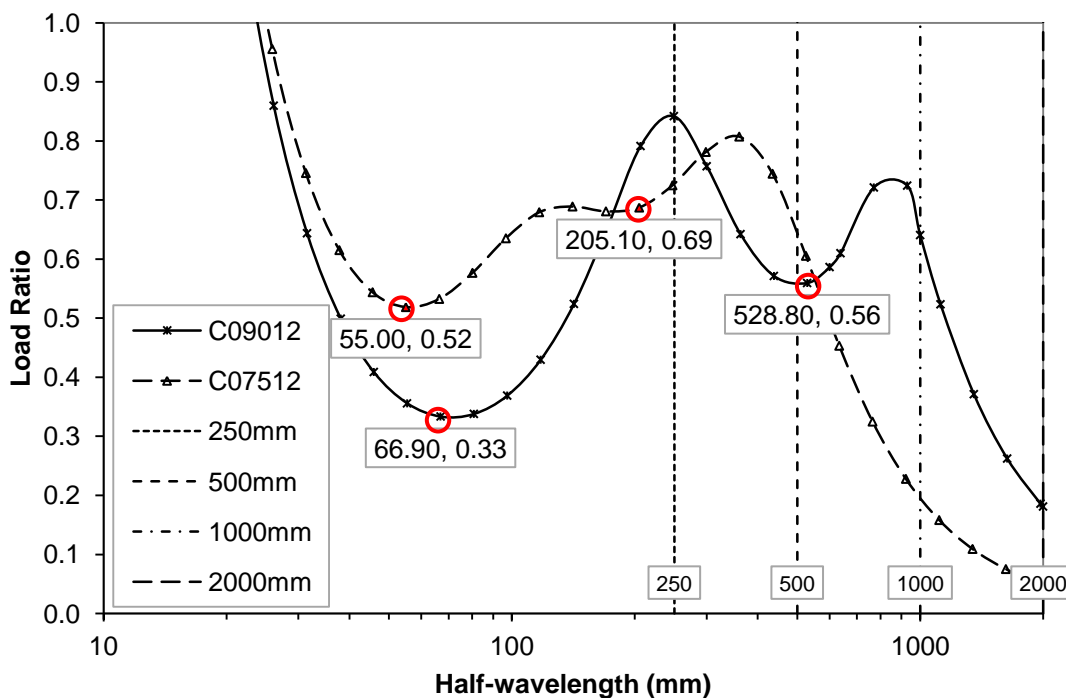


Figure 3.5: CUFSM Results

The two minima of the curves indicated two critical buckling modes with local buckling at the first minima and distortional buckling at the second minima. Based on the results of the finite strip analysis, the lengths of 500mm, 1000mm and 2000mm were chosen. These lengths also satisfy the required member slenderness ratio. The chosen length of the columns are summarised in Table 3.4.

Table 3.4: Chosen Specimen Length

Category	$\frac{KL}{r_y}$	Required Length (Limit)				Chosen Length					
		C		BU		C		BU		GBU	
		75	90	75	90	75	90	75	90	75	90
Stub	$< 20r_y$ $> 3A'$	225	270	225	270	300	300	300	300	300	300
Short	< 50 (50)	368	947	472	1299	-	500	500	500 1000	500 1000 2000	500 1000
Intermediate	50 – 200 (100)	735	1893	943	2597	500 1000	1000	1000	-	-	-
Slender	> 200 (200)	1470	3786	1886	5194	2000	-	2000	-	-	-

3.3.4 Modified Slenderness Ratio

The effects of fasteners' spacing along the length of the columns were investigated in accordance with the modified slenderness ratio in clause C4.5 of the AISI specifications. The fasteners in this research refer to the screws in a plain back-to-back C-channel built-up column; whereas in a back-to-back C-channel built-up column with a gap, they refer to the short C-channel connectors.

The fasteners' spacing within and beyond the conservative spacing requirement stated in the clause C4.5 of the AISI specifications (2002c, 83) were investigated. The conservative spacing requirement is expressed as:

$$s/r_y \leq 0.5(KL/r_y)_o$$

where s is the fastener spacing, r_y is the minimum radius of gyration, and $(KL/r_y)_o$ is the overall member slenderness ratio of a built-up section.

This conservative spacing requirement was proposed to prevent the flexural buckling of individual C-channels between intermediate fasteners and to account for the possibility of any one of the fasteners becoming loose or ineffective.

The chosen fasteners spacings are shown in Table 3.5.

Table 3.5: Fastener Spacing in Accordance with the AISI Specifications

Cross-section	Length	Minimum Radius of Gyration		Member Slenderness			Maximum Allowable Spacing	Chosen Spacing		
	L	r_{yC}	r_{yBU}	KL/r_{yC}	KL/r_{yBU}	Category	C4.5 Modified Slenderness Ratio $s/r_{yC} < 0.5 (KL/r_y)_o$	Within C4.5	Slightly Exceed C4.5	Exceed C4.5
							$s < (KL/r_y)_o (r_{yC}/2)$	$s/L < 0.25$	$0.25 < s/L < 0.50$	$s/L > 0.50$
C75	300	7.35	9.43	20.41	15.91	Stub	58.46	50.	100	200
	500	7.35	9.43	68.03	53.02	Short	194.86	100	200	400
	1000	7.35	9.43	136.05	106.04	Intermediate	389.71	225	450	900
	2000	7.35	9.43	272.11	212.09	Slender	779.43	475	950	1900
C90	300	18.93	25.97	7.92	5.78	Stub	54.67	50	100	200
	500	18.93	25.97	26.41	19.25	Short	182.23	100	200	400
	1000	18.93	25.97	52.83	38.51	Short	364.46	225	450	900

*Note: K = 0.5 for $L_1 = 300$ mm specimens; K = 1.0 for $L_1 = 500, 1000,$ and 2000 mm specimens

In the plain back-to-back C-channel built-up columns design, the specimens are categorised as follows:

- (i) Spacing less than 0.25 of the overall length e.g. BU75S50L300;
- (ii) Spacing between 0.25 and 0.50 of the overall length e.g. BU75S100L300; and
- (iii) Spacing more than 0.50 of the overall length e.g. BU75S200L300.

Similarly, for back-to-back C-channel built-up columns with a gap, the specimens are categorised as follows:

- (i) Spacing less than 0.25 of the overall length e.g. GBU75S50L300;
- (ii) Spacing more than 0.50 of the overall length e.g. GBU75S200L300.

The two individual C-channels for both built-up columns with and without a gap were fastened together through their webs with screws at 50 mm from the end and the centre-to-centre spacing of the screws were varied according to the length of the columns, whereas the transverse spacing of the screws was 40mm , as shown in Figures 3.6 to 3.8.

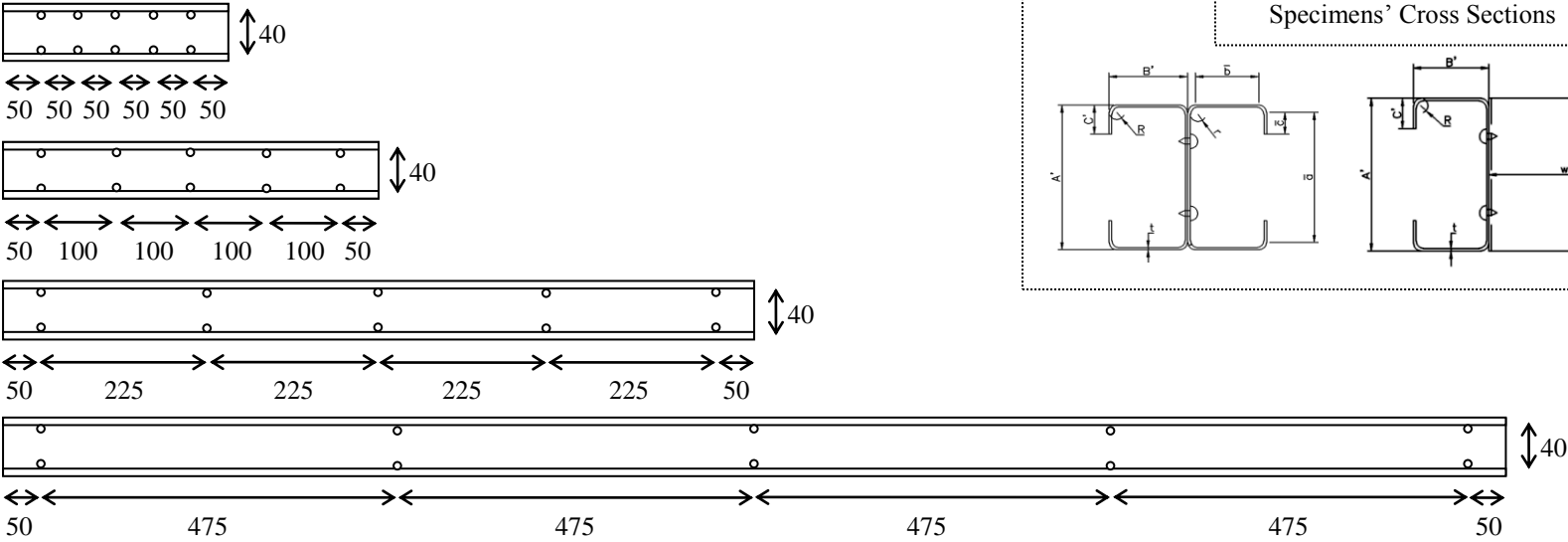


Figure 3.6: Specimens within the Limitations from clause C4.5 of AISI Specification with $s/L < 0.25$

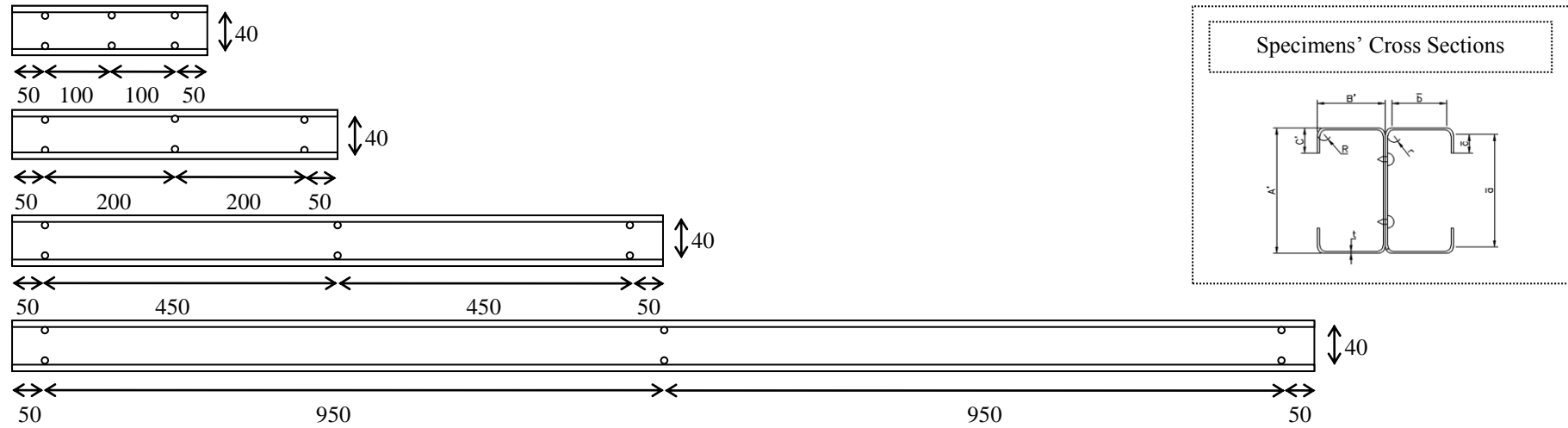


Figure 3.7: Specimens Slightly Exceed the Limitations from clause C4.5 of AISI Specification at $0.25 < s/L < 0.50$

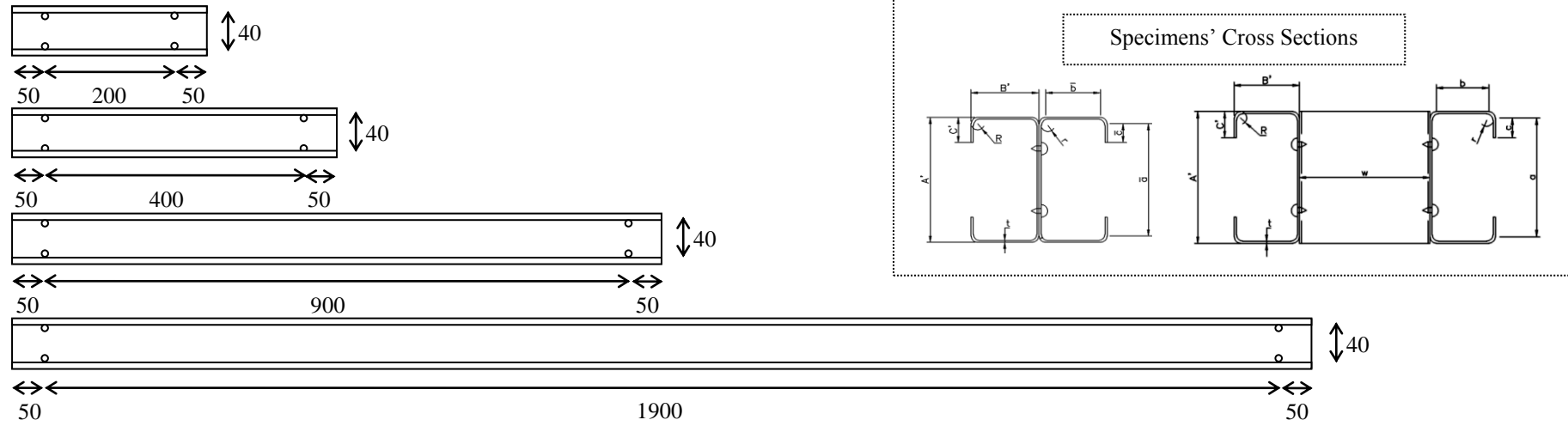


Figure 3.8: Specimens Exceed the Limitations from clause C4.5 of AISI Specification at $s/L > 0.50$

Table 3.6 tabulates all the test specimens designed for this research.

Table 3.6: Categories of Test Specimens

L (mm)	C75	C90	BU75	BU90	GBU75	GBU90
300	L300	L300	S50L300	S50L300	S50L300	S50L300
			S100L300	S100L300	-	-
			S200L300	S200L300	S200L300	S200L300
500	L500	L500	S100L500	S100L500	S100L500	S100L500
			S200L500	S200L500	-	-
			S400L500	S400L500	S400L500	S400L500
1000	L1000	L1000	S225L1000	S225L1000	S225L1000	S225L1000
			S450L1000	S450L1000	-	-
			S900L1000	S900L1000	S900L1000	S900L1000
2000	L2000	L2000	S475L2000	S475L2000	S475L2000	S475L2000
			S950L2000	S950L2000	-	-
			S1900L2000	S1900L2000	S1900L2000	S1900L2000

In this research, the plain back-to-back C-channel built-up column specimens with the $s/L < 0.25$ have five fastener locations, $0.25 < s/L < 0.50$ contain three fastener locations, while $s/L > 0.50$ contain only two fastener locations. However, the back-to-back C-channel built-up columns with a gap were only tested at $s/L < 0.25$ with five fastener locations, and $s/L > 0.50$ with only two fastener locations. The back-to-back C-channel built-up columns with a gap with $0.25 < s/L < 0.50$ are simulated with finite element modelling and the results are reported in Chapter 6.

3.4 Initial Imperfection

Buckling behaviour is sensitive to the presence of imperfections, thus it is important to measure the magnitude and shape of the imperfections of the test specimens. The required apparatus include a LVDT with 0.01mm accuracy and a data logger connected to a laptop. The test specimen was fixed at one end using a G-clamp while the LVDT travelled along the length of the specimen as shown in Figure 3.9.

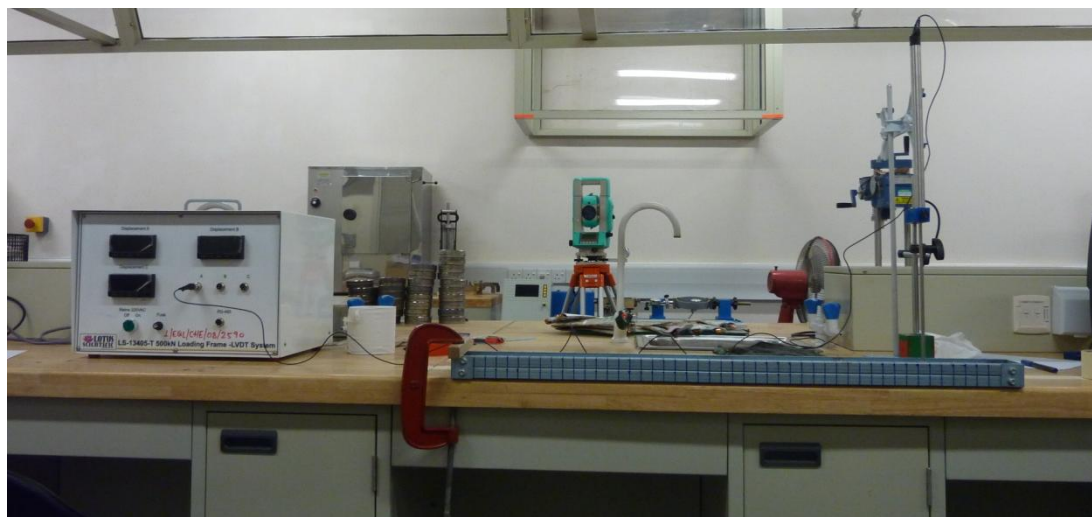


Figure 3.9: Measuring Initial Imperfection

Gridlines of 20mm spacings were hand drawn on every test specimens. The LVDT records the readings at every 20mm along the length of the test specimens at the centre of the web, the centre of the flanges, and the edge of the lips as shown in Figure 3.10.

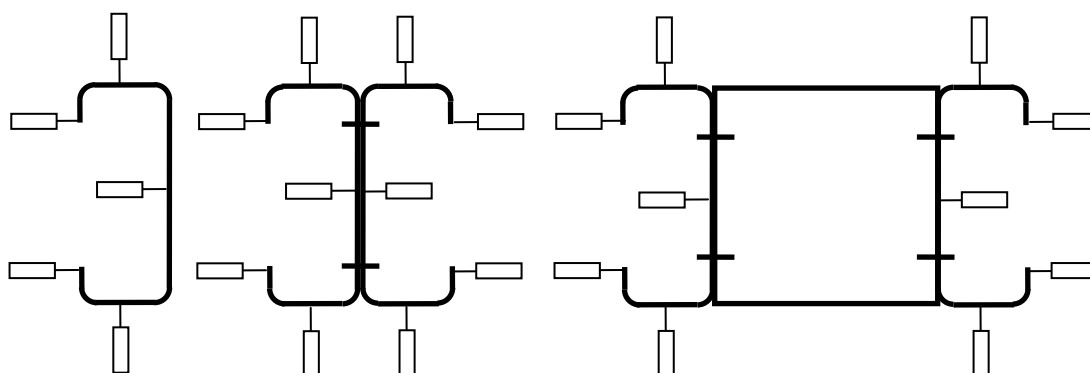


Figure 3.10: Imperfection Measurements

The imperfections recorded provided information about the initial shape of the column. These imperfections influence the overall buckling, local buckling of the web and the distortional buckling of the flange. A typical plot of the imperfections versus length is shown in Figure 3.11. Imperfection measurements for other specimens are documented in Appendix A.

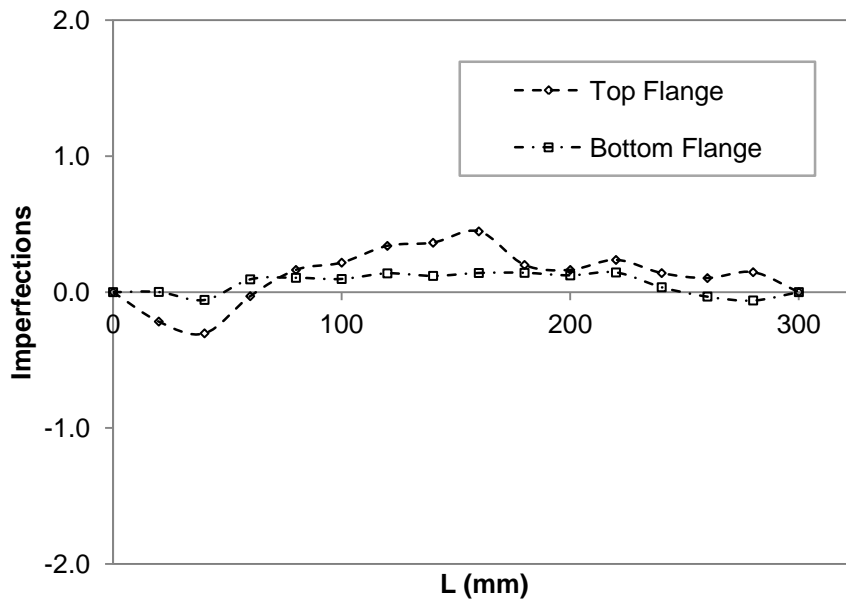


Figure 3.11: Imperfections at Flanges for BU75S50L300-1

The data collected revealed that the maximum imperfections of the test specimens for specimens with the length of 300 mm, 500 mm, 1000 mm and 2000 mm were 0.2 mm, 0.2 mm, 0.4 mm, and 0.6 mm respectively. These maximum geometrical imperfections for each length were used in the finite element modelling.

3.5 Test Setup

The specimens were tested at fix-end and pin-end conditions. The stub columns were tested at fix-ended condition to fulfil the stub column test requirement in accordance with clause 7 of the AISI Manual (2002a, VI-19). All other columns were tested at pin-ended condition.

3.5.1 Fixed End for Stub Columns

A total of 45 stub columns were tested. The tests included 8 C-channel specimens, 21 plain back-to-back C-channel built-up specimens and 16 back-to-back C-channel built-up specimens with a gap. The fix-ended stub columns were casted to end plates using high strength mortar and are tested on fixed ends. Dimensions of the stub column specimens are tabulated in Table 3.7 and Table 3.8.

Table 3.7: Measured Specimen Dimensions for Stub Columns from C75, BU75 and GBU75 Test Series

Specimen	Length	Spacing	Web	Flange	Lip	Radius	Thickness
	L (mm)	s (mm)	A' (mm)	B' (mm)	C' (mm)	r (mm)	t (mm)
C75L300-1	267	-	75.73	19.66	10.34	1.5	1.2
C75L300-2	271	-	75.56	19.70	10.31	1.5	1.2
C75L300-3	270	-	75.41	19.63	10.35	1.5	1.2
C75L300-4	267	-	75.76	19.64	10.30	1.5	1.2
BU75S50L300-1	273	50	73.14	19.81	11.13	1.5	1.2
BU75S50L300-2	280	50	73.06	19.82	11.20	1.5	1.2
BU75S50L300-3	270	50.92	72.71	19.47	10.82	1.5	1.2
BU75S100L300-2	267	99.68	73.12	19.76	11.20	1.5	1.2
BU75S100L300-3	273	100.22	73.10	19.88	11.19	1.5	1.2
BU75S100L300-4	273	99.5	73.57	19.71	11.16	1.5	1.2
BU75S200L300-1	266.5	200	73.67	19.82	11.22	1.5	1.2
BU75S200L300-2	266	199.5	73.62	19.85	11.18	1.5	1.2
BU75S200L300-3	268	200	72.88	19.95	11.16	1.5	1.2
GBU75S50L300-2	271	50	73.17	19.83	11.16	1.5	1.2
GBU75S50L300-3	270	50.07	73.61	19.85	11.11	1.5	1.2
GBU75S50L300-4	268	50.19	73.57	19.78	11.13	1.5	1.2
GBU75S200L300-1	268	201	73.55	19.74	11.11	1.5	1.2
GBU75S200L300-2	271	200	73.59	19.74	11.15	1.5	1.2
GBU75S200L300-4	263	199	72.29	18.48	10.56	1.5	1.2

Table 3.8: Measured Specimen Dimensions for Stub Column from C90, BU90 and GBU90 Test Series

Specimen	Length	Spacing	Web	Flange	Lip	Radius	Thickness
	L (mm)	s (mm)	A' (mm)	B' (mm)	C' (mm)	r (mm)	t (mm)
C90L300-2	270.0	-	90.42	49.87	14.43	1.5	1.2
C90L300-3	275.0	-	90.54	49.92	14.50	1.5	1.2
C90L300-4	267.0	-	90.63	49.84	14.49	1.5	1.2
BU90S50L300-1	277.0	50	91.31	49.81	14.56	1.5	1.2
BU90S50L300-2	272.0	49.78	91.78	49.70	14.54	1.5	1.2
BU90S50L300-3	261.0	50	92.88	49.44	14.52	1.5	1.2
BU90S100L300-3	262.0	99.9	90.84	49.69	14.58	1.5	1.2
BU90S100L300-4	268.0	100	90.63	49.54	14.58	1.5	1.2
BU90S200L300-1	273.5	201	90.69	49.42	14.55	1.5	1.2
BU90S200L300-2	269.5	199	90.66	49.43	14.63	1.5	1.2
BU90S200L300-4	280.5	199	89.51	48.33	14.00	1.5	1.2
GBU90S50L300-3	265.0	50	92.15	49.53	14.46	1.5	1.2
GBU90S50L300-4	270.0	50.25	90.68	49.56	14.57	1.5	1.2
GBU90S200L300-2	258.0	200	90.68	49.63	14.58	1.5	1.2
GBU90S200L300-3	270.0	200	90.7	49.51	14.57	1.5	1.2
GBU90S200L300-4	262.0	199	90.69	49.51	14.63	1.5	1.2

The test setup is shown in Figure 3.12. The ends of the specimens were concreted into 25mm thick moulds to ensure that the specimens stayed in position throughout the testing. The external load cell was positioned at the base and two LVDTs were positioned at the web, and a third positioned at the top. All these external measurement devices were connected to an external data logger for data collection. Load was applied axially to the specimens via a 600kN capacity GOTECH, GT-7001-LC60 Universal Testing Machine (UTM). The loading rate was kept below 25kg/cm²/s for all the test specimens.

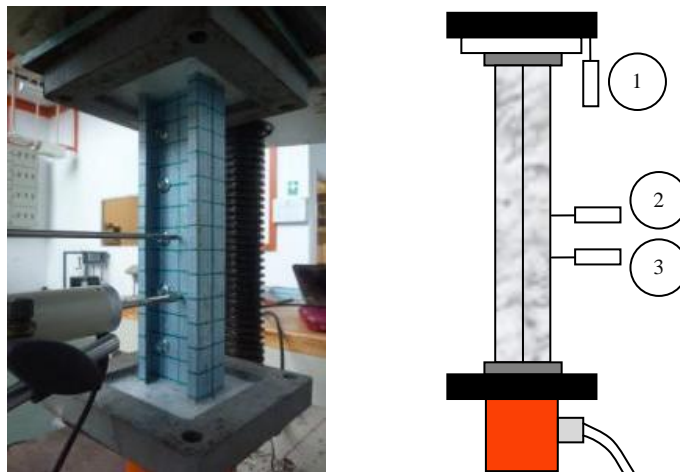


Figure 3.12: Test Setup for Stub Column Compression Test

During the setting up, the centroid was drawn at the bottom bearing of the testing machine to indicate the loading point. The specimens were then placed at their centroid at the marked loading point on the bottom bearing as shown in Figure 3.13 (a). The load cell at the top was then lowered until it touched the top end plate of the specimen. Spirit Level was used for a rough check on the straightness of the specimen as shown in Figure 3.13 (b). The built-up column specimen was centred and aligned in the test rig so that the load would be concentrically applied through the centroid of the test specimens.



(a) Specimens Positioned at Centroid



(b) Level used to examine straightness of the specimens

Figure 3.13: Stub Column Test Setup

3.5.2 Pinned End for All Other Columns

A total of 16 C-channel columns, 45 plain back-to-back C-channels columns, and 32 back-to-back C-channels columns with a gap at length of 500mm, 1000mm and 2000mm were tested between pinned end conditions. Pinned end conditions were

achieved by means of fabricated hinge assemblies at the top and bottom ends. The distance between the centre of the pin and the top surface of the hinge assembly was 65mm. Thus the effective length of the test specimens was the sum of the specimen length, L and the distance from the specimen end plates to the top surface of the hinge assembly i.e. 130mm. Additional 50mm length was added to the physical length for specimens when 25mm end plates were positioned at top and bottom end before the hinge assemblies. In this case, the distance from the top surface of the hinge assembly to the specimen end plate was measured to be 180mm. Dimensions of the specimens are tabulated in Tables 3.9 to 3.13.

Table 3.9: Measured Dimensions for C75 Specimen $L_1=500\text{mm}$

Specimen	Length	Spacing	Web	Flange	Lip	Radius	Thickness
	L (mm)	s (mm)	A' (mm)	B' (mm)	C' (mm)	r (mm)	t (mm)
C75L500-2	679.0	-	77.15	19.52	10.39	1.5	1.2
C75L500-3	681.0	-	76.99	19.57	10.48	1.5	1.2
C75L500-4	678.0	-	77.12	19.61	10.48	1.5	1.2
BU75S100L500-1	655.0	100.0	73.61	19.79	11.23	1.5	1.2
BU75S100L500-2	679.0	100.0	73.56	19.73	11.23	1.5	1.2
BU75S100L500-3	680.0	100.5	73.55	19.67	11.20	1.5	1.2
BU75S200L500-1	653.0	195.0	73.45	19.53	11.30	1.5	1.2
BU75S200L500-2	678.0	195.0	73.64	19.59	11.32	1.5	1.2
BU75S200L500-3	680.0	200.5	73.35	19.68	11.31	1.5	1.2
BU75S400L500-1	678.0	400.0	73.57	19.68	11.31	1.5	1.2
BU75S400L500-2	679.0	401.0	73.51	19.66	11.30	1.5	1.2
BU75S400L500-3	680.0	399.0	73.51	19.74	11.30	1.5	1.2
GBU75S100L500-1	678.0	100.2	73.57	19.84	11.25	1.5	1.2
GBU75S100L500-2	679.0	100.0	73.58	19.92	11.20	1.5	1.2
GBU75S100L500-3	681.0	100.0	73.50	19.83	11.26	1.5	1.2
GBU75S400L500-1	679.0	399.0	73.55	19.86	11.24	1.5	1.2
GBU75S400L500-2	680.0	400.0	73.54	19.75	11.12	1.5	1.2
GBU75S400L500-3	680.0	400.0	73.58	19.86	11.30	1.5	1.2

Table 3.10: Measured Dimensions for C90 Specimen $L_1=500\text{mm}$

Specimen	Length	Spacing	Web	Flange	Lip	Radius	Thickness
	L (mm)	s (mm)	A' (mm)	B' (mm)	C' (mm)	r (mm)	t (mm)
C90L500-1	678.0	-	91.43	49.31	14.55	1.5	1.2
C90L500-2	679.0	-	88.80	50.55	14.58	1.5	1.2
C90L500-3	680.0	-	89.62	49.77	14.66	1.5	1.2
BU90S100L500-1	656.0	100.5	90.57	49.46	14.62	1.5	1.2
BU90S100L500-2	678.0	100.5	90.56	49.38	14.62	1.5	1.2
BU90S200L500-1	653.0	199.5	90.40	49.33	14.67	1.5	1.2
BU90S200L500-2	678.0	199.5	90.42	49.26	14.66	1.5	1.2
BU90S200L500-3	680.0	200.5	90.37	49.34	14.59	1.5	1.2
BU90S400L500-1	678.0	400.0	90.59	49.43	14.65	1.5	1.2
BU90S400L500-2	678.0	399.0	90.39	49.39	14.67	1.5	1.2
GBU90S100L500-1	680.0	100.5	90.54	49.40	14.64	1.5	1.2
GBU90S100L500-2	680.0	100.5	90.63	49.42	14.57	1.5	1.2
GBU90S100L500-3	680.0	100.3	88.85	49.42	15.46	1.5	1.2
GBU90S400L500-1	680.0	400.0	90.47	49.46	13.37	1.5	1.2
GBU90S400L500-2	680.0	400.0	90.49	49.47	14.62	1.5	1.2
GBU90S400L500-3	680.0	400.0	90.33	49.45	14.66	1.5	1.2
GBU90S400L500-4	680.0	401.0	90.55	49.40	14.58	1.5	1.2

Table 3.11: Measured Dimensions for C75 Specimens $L_1=1000\text{mm}$

Specimen	Length	Spacing	Web	Flange	Lip	Radius	Thickness
	L (mm)	s (mm)	A' (mm)	B' (mm)	C' (mm)	r (mm)	t (mm)
C75L1000-1	1130	-	76.10	19.85	10.38	1.5	1.2
C75L1000-2	1130	-	75.79	19.93	10.45	1.5	1.2
BU75S225L1000-1	1133	225.3	75.27	20.24	10.37	1.5	1.2
BU75S225L1000-2	1131	225.3	75.74	19.87	10.41	1.5	1.2
BU75S450L1000-1	1131	447.0	75.80	19.93	10.44	1.5	1.2
BU75S450L1000-2	1133	450.0	75.62	19.85	10.35	1.5	1.2
BU75S450L1000-3	1182	450.0	75.91	19.79	10.29	1.5	1.2
BU75S900L1000-1	1131	900.0	75.97	19.92	10.31	1.5	1.2
BU75S900L1000-2	1133	900.0	76.30	19.76	9.11	1.5	1.2
BU75S900L1000-3	1183	901.0	75.91	19.79	10.33	1.5	1.2
GBU75S225L1000-1	1131	225.0	76.06	19.81	10.37	1.5	1.2
GBU75S225L1000-2	1132	225.0	76.16	20.31	10.41	1.5	1.2
GBU75S225L1000-3	1183	224.8	75.81	19.83	10.38	1.5	1.2
GBU75S900L1000-1	1133	900.0	75.86	19.79	10.38	1.5	1.2
GBU75S900L1000-2	1132	897.5	76.02	19.85	10.25	1.5	1.2
GBU75S900L1000-3	1182	900.0	76.00	19.80	10.30	1.5	1.2

Table 3.12: Measured Dimensions for C90 Specimens $L_1=1000\text{mm}$

Specimen	Length	Spacing	Web	Flange	Lip	Radius	Thickness
	L (mm)	s (mm)	A' (mm)	B' (mm)	C' (mm)	r (mm)	t (mm)
C90L1000-1	1133	-	90.65	49.73	14.36	1.5	1.2
C90L1000-2	1133	-	90.78	49.69	14.28	1.5	1.2
C90L1000-3	1180	-	90.67	49.70	14.26	1.5	1.2
BU90S225L1000-1	1182	225.0	90.82	49.63	14.38	1.5	1.2
BU90S225L1000-2	1132	225.0	90.64	49.64	14.34	1.5	1.2
BU90S450L1000-2	1130	450.0	90.56	49.72	14.39	1.5	1.2
BU90S450L1000-3	1182	448.0	90.43	49.66	14.43	1.5	1.2
BU90S900L1000-1	1131	897.0	90.48	49.58	14.35	1.5	1.2
BU90S900L1000-2	1182	899.0	90.95	49.32	14.43	1.5	1.2
GBU90S225L1000-1	1133	225.3	90.52	49.66	14.40	1.5	1.2
GBU90S225L1000-3	1183	224.8	89.75	48.47	13.67	1.5	1.2
GBU90S900L1000-1	1132	892.0	90.60	49.64	14.39	1.5	1.2
GBU90S900L1000-3	1183	900.0	90.55	49.69	14.35	1.5	1.2

Table 3.13: Measured Dimensions for C75 Specimens $L_1=2000\text{mm}$

Specimen	Length	Spacing	Web	Flange	Lip	Radius	Thickness
	L (mm)	s (mm)	A' (mm)	B' (mm)	C' (mm)	r (mm)	t (mm)
C75L2000-1	2181	-	74.05	20.25	10.77	1.5	1.2
C75L2000-2	2180	-	73.95	20.25	10.77	1.5	1.2
C75L2000-3	2186	-	73.99	20.36	10.73	1.5	1.2
BU75S475L2000-2	2184	474.5	73.94	20.34	10.68	1.5	1.2
BU75S475L2000-3	2183	462.0	73.90	20.22	10.77	1.5	1.2
BU75S950L2000-2	2184	949.5	73.93	20.32	10.76	1.5	1.2
BU75S950L2000-3	2184	950.0	73.91	20.24	10.77	1.5	1.2
BU75S1900L2000-2	2183	1900.0	73.88	20.28	10.86	1.5	1.2
BU75S1900L2000-3	2184	1901.0	73.86	20.39	10.74	1.5	1.2
GBU75S475L2000-1	2183	474.3	73.61	20.32	10.75	1.5	1.2
GBU75S475L2000-2	2183	474.5	73.96	20.28	10.61	1.5	1.2
GBU75S475L2000-3	2184	474.8	73.87	20.35	10.84	1.5	1.2
GBU75S1900L2000-1	2183	1901.0	73.81	20.30	10.77	1.5	1.2
GBU75S1900L2000-2	2183	1907.0	73.94	20.37	10.70	1.5	1.2
GBU75S1900L2000-3	2184	1902.0	73.98	20.35	10.76	1.5	1.2

All test specimens were also cast into 25mm steel moulds at the top and bottom end using high strength mortar. The cast specimens were then locked to the pinned end assemblies as illustrated in Figure 3.14. The pinned-end assembly at the bottom end was not secured to the strong floor. Thus, during the loading process, movement at the bottom end was possible. It is important to note that there were frictions in the fabricated pinned-end assemblies during the compression test although grease was applied to the hinge. Maintenance was conducted constantly to ensure that the pinned-end assemblies performed as pin end.

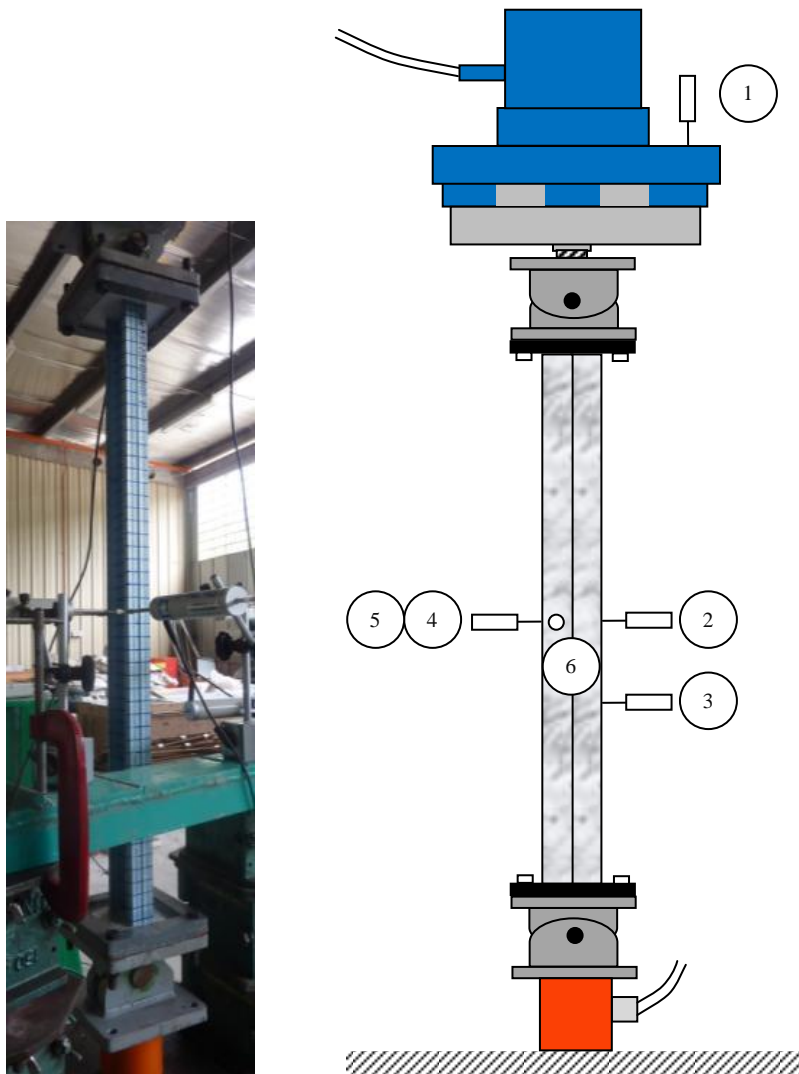


Figure 3.14: Test Setup for Intermediate Column Compression Test

All pinned-end tests were conducted using 500kN hydraulic loading system. A pre-load was applied to the specimen to ensure that the endplates were fully in contact with the specimen. The loading rate was kept relatively low for all specimens. The ultimate strength of the test specimens is defined as the maximum load achieved.

External load cell were positioned at the bottom and a total of 6 LVDTs (Linear Variable Displacement Transducers) were used to monitor the specimen displacements. All these external measurement devices were connected to external data logger for data collection. The LVDTs were positioned as shown in Figure 3.14. These LVDTs were positioned as such that LVDT 1 was at top to monitor the axial shortening of the specimen, LVDT 2 at web to monitor the displacement at mid-length, LVDT 3 at web to assist in determination of the occurrence of local

buckling, LVDT 4 and LVDT 5 at lip to detect twisting, and LVDT 6 at flange to pick up distortional buckling. All these readings are tabulated in the Appendices.

3.6 Mortar Test

As mentioned in section 3.5, all test specimens were cast into steel moulds by using high strength mortar. The purpose of this high strength mortar is to hold the specimens in position at 90 degree to the end plates. The specimens were first cast into mortar at top ends. When the mortar hardened, the specimen was turned around and the bottom ends were cast. The cast specimens were left to cure so that sufficient strength was gained before the compression test was conducted. Experiments to determine the setting time and compressive strength gain over time were conducted on the high strength mortar.

The initial setting time determines the time required for the mortar to achieve 25mm penetration. This provides the information on the duration required for the mortar paste to harden. The casting of the top end needs to be completed before initial setting time. The final setting time determines the duration required for the mortar paste to gain sufficient strength to resist penetration from the needle and does not leave a complete circular impression in the paste surface. This provides an estimate on when the mortar starts to develop initial strength and stiffness. Thus, the cast specimens were tested after the final setting time was reached. The setting time of the high strength mortar was determined by Vicat Needle in accordance with ASTM C191-08 (ASTM 2008, 1-8). Sampling of mortar comprises portions taken from different points in the batch as shown in Figure 3.15. The resistance of mortar to penetration by the Vicat needle was measured at regular intervals. Figure 3.16 shows the results obtained at each interval. Figure 3.16 shows that the initial setting time was reached at 3.7 hours when penetration of 25mm was achieved, whereas, the final setting time was achieved at approximately 11 hours when the Vicat needle failed to penetrate the paste.



Figure 3.15: Setting Time by Penetration Test using Vicat Needle

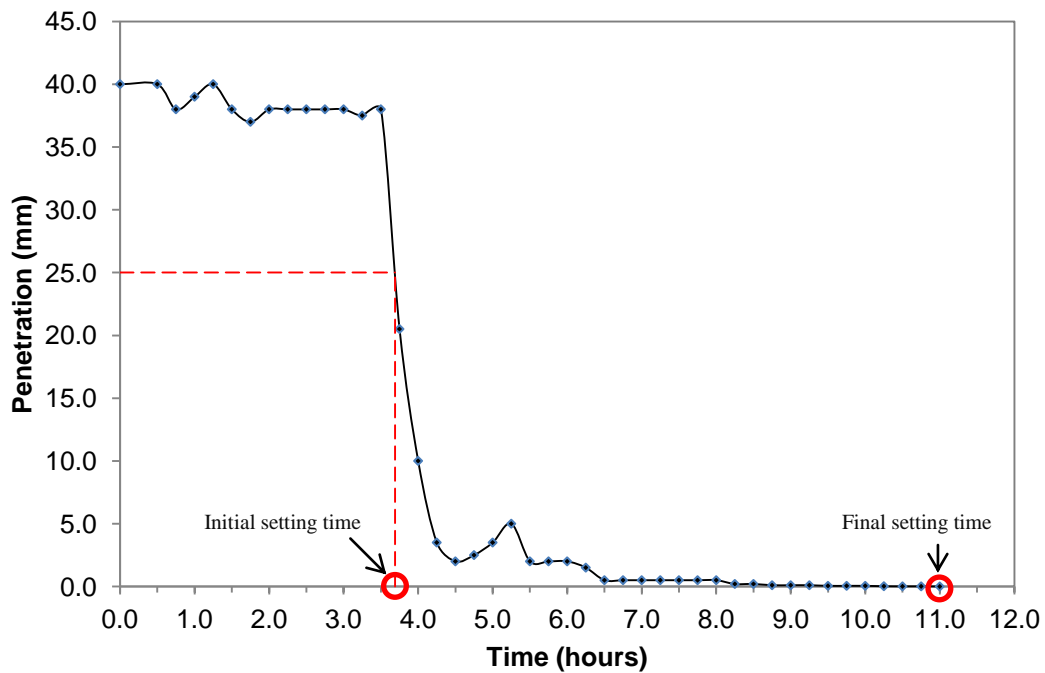


Figure 3.16: Graph of Penetration of Vicat Needle versus Time

A compression test was also conducted to understand the early strength gain of the high strength mortar. The result from this test determined the duration required for the mortar to gain sufficient strength before the cast test specimens was tested. Compressive strength of 50 mm cubic mortars shown in Figure 3.17 was determined at 12, 24, 48, and 72 hours. The tests were conducted in accordance with ASTM C109/C109M-01 (ASTM 2008) using a universal testing machine. Results from these tests showed that average strength gained after 12 hours was low with 6kN only. The

strength of the mortar increased greatly within the next 12 hours and achieved 54kN as shown in Table 3.14. Thus, in order to provide sufficient strength for column compression test, the mortar needed to be cured for more than 12 hours.



Figure 3.17: Mortar Test Cubes

Table 3.14: Compressive Strength of Test Cubes at Different Duration

Duration (hours)	Compressive Strength (kN)			
	Cube 1	Cube 2	Cube 3	Average
12	5.58	4.58	7.22	5.79
24	55.19	48.17	56.99	53.45
48	81.87	87.60	88.58	86.02
72	96.98	74.59	94.69	88.75

With results from the mortar test, casting and testing schedule was determined. The top end was cast and left to set for at least 12 hours, and then the specimen was turned over for the bottom end to be cast. The bottom end was then left to cure for approximately 24 hours before the cast specimens were tested.

3.7 Conclusions

This chapter documents the testing programme to investigate the influence of fastener spacing to back-to-back C-channel built-up columns with and without a gap. The specimen dimensions, intermediate fastener details, and end conditions were determined to cover a series of conditions within and beyond the design standard requirements.

4 Test Results & Observations

4.1 Introduction

This chapter presents the test results and test observations on the behaviour of C-channel, plain back-to-back C-channel built-up, and back-to-back C-channel built-up columns with a gap. A total of 138 test specimens were tested in the structural laboratory at Curtin University Sarawak Malaysia. These test specimens include 24 numbers of C-channels, 66 numbers of plain back-to-back C-channel built-up columns, and 48 numbers of back-to-back C-channel built-up columns with a gap. The test specimens were tested at fixed end condition for stub columns, and at pinned end condition for short, intermediate and slender columns as per detailed in Chapter 3. A complete documentation of the test results is in the Appendix E, F and G for C-channel columns, plain back-to-back C-channel built-up columns (without a gap), and back-to-back C-channel built-up columns with a gap respectively.

4.2 Ultimate Load

The ultimate strength of the test specimens is defined as the maximum load achieved. These ultimate strengths are documented in terms of load versus deformation curves in the Appendix E, F and G for C-channel columns, plain back-to-back C-channel built-up columns (without a gap), and back-to-back C-channel built-up columns with a gap respectively. These test results are later compared with the finite element results in Chapter 6 and with the calculated results presented in Chapter 8.

4.2.1 C-channel Columns

Table 4.1 presents the ultimate loads achieved during compression tests of C-channel columns.

Table 4.1: Test Results of C-channel Columns

Specimen	Stub		Short	Intermediate			Slender
	C75L300	C90L300	C90L500	C75L500	C75L1000	C90L1000	C75L2000
1	60.63	Discard	82.84	Discard	15.80	84.95	7.49
2	58.24	83.70	81.20	52.07	16.38	86.94	6.79
3	59.91	86.12	78.04	53.01	Discard	70.79	9.83
4	55.70	86.70	-	40.13	-	-	-
Mean	58.62	85.51	80.69	48.40	16.09	80.89	8.04

From Table 4.1, results for the test specimen of C90L300-1, C75L500-1, C75L500-4 and C75L1000-3 were discarded. Result for C90L300-1 was discarded because there was concentrated loading caused by the specimen's uneven end. Thus, local buckling failure occurred at a slope on the web of the specimen as shown in Figure 4.1. Results of C75L500-1 and C75L500-4 were outliers. Whereas for C75L1000-3, the pinned-end assemblies were faulty where rotation only occurred after the ultimate load had been achieved. The specimen acted as fix-ended condition rather than pin-ended condition.

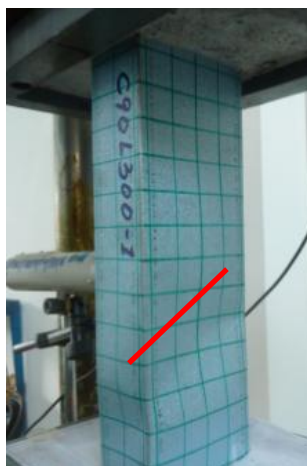


Figure 4.1: Failure Modes of C90L300-1

4.2.2 Plain Back-to-back C-channel Built-up Columns

Table 4.2 presents the ultimate loads achieved during the compression test of plain back-to-back C-channel built-up column. The plain back-to-back C-channel built-up columns specimens were divided into three types of spacing proportionate to the overall length as follows:

- (i) Spacing less than 0.25 of the overall length e.g. BU75S50L300;
- (ii) Spacing between 0.25 and 0.50 of the overall length e.g. BU75S100L300; and

(iii) Spacing more than 0.50 of the overall length e.g. BU75S200L300.

Table 4.2: Test Results of Plain Back-to-back C-channel Built-up Columns

	$s/L < 0.25$	$0.25 < s/L < 0.50$	$s/L > 0.50$	$s/L < 0.25$	$0.25 < s/L < 0.50$	$s/L > 0.50$
Specimen No.	Stub			Stub		
	BU75S50 L300	BU75S100 L300	BU75S200 L300	BU90S50 L300	BU90S100 L300	BU90S200 L300
1	120.66	Discard	122.51	172.49	Discard	170.25
2	118.87	117.48	119.12	171.61	Discard	177.50
3	118.65	122.74	113.14	167.56	171.18	Discard
4	-	115.37	-	-	173.87	171.88
Mean	113.93	118.53	118.26	170.55	172.53	173.21
Specimen No.	Short			Short		
	BU75S100 L500	BU75S200 L500	BU75S400 L500	BU90S100 L500	BU90S200 L500	BU90S400 L500
1	82.96	86.21	74.77	165.01	170.48	170.01
2	Discard	88.93	80.56	163.22	173.17	151.41
3	74.07	93.61	87.64	Discard	151.53	Discard
Mean	78.52	89.58	80.99	164.12	165.06	160.71
Specimen No.	Intermediate			Short		
	BU75S225 L1000	BU75S450 L1000	BU75S900 L1000	BU90S225 L1000	BU90S450 L1000	BU90S900 L1000
1	47.04	50.43	39.90	167.81	Discard	164.86
2	46.28	45.02	33.70	151.76	175.18	150.94
3	Discard	41.77	31.48	Discard	161.12	Discard
Mean	46.66	45.74	35.10	159.79	168.15	157.90
Specimen No.	Slender					
	BU75S475 L2000	BU75S950 L2000	BU75S1900 L2000			
1	Discard	Discard	Discard			
2	15.33	13.22	12.12			
3	12.87	12.99	13.11			
Mean	14.10	13.11	12.62			

As seen in Table 4.2, BU75S100L300-1, BU90S200L300-3, BU75S100L500-2, BU90S100L500-3, BU90S400L500-3, BU75S225L1000-3, BU75S475L2000-1, BU75S950L2000-1, and BU75S1900L2000-1 were all discarded because they were outliers. BU90S100L300-1 and BU90S100L300-2 were discarded due to mortar

failure prior to specimen failure as shown in Figure 4.2. The strength and behaviour of the specimens were much different in these cases.



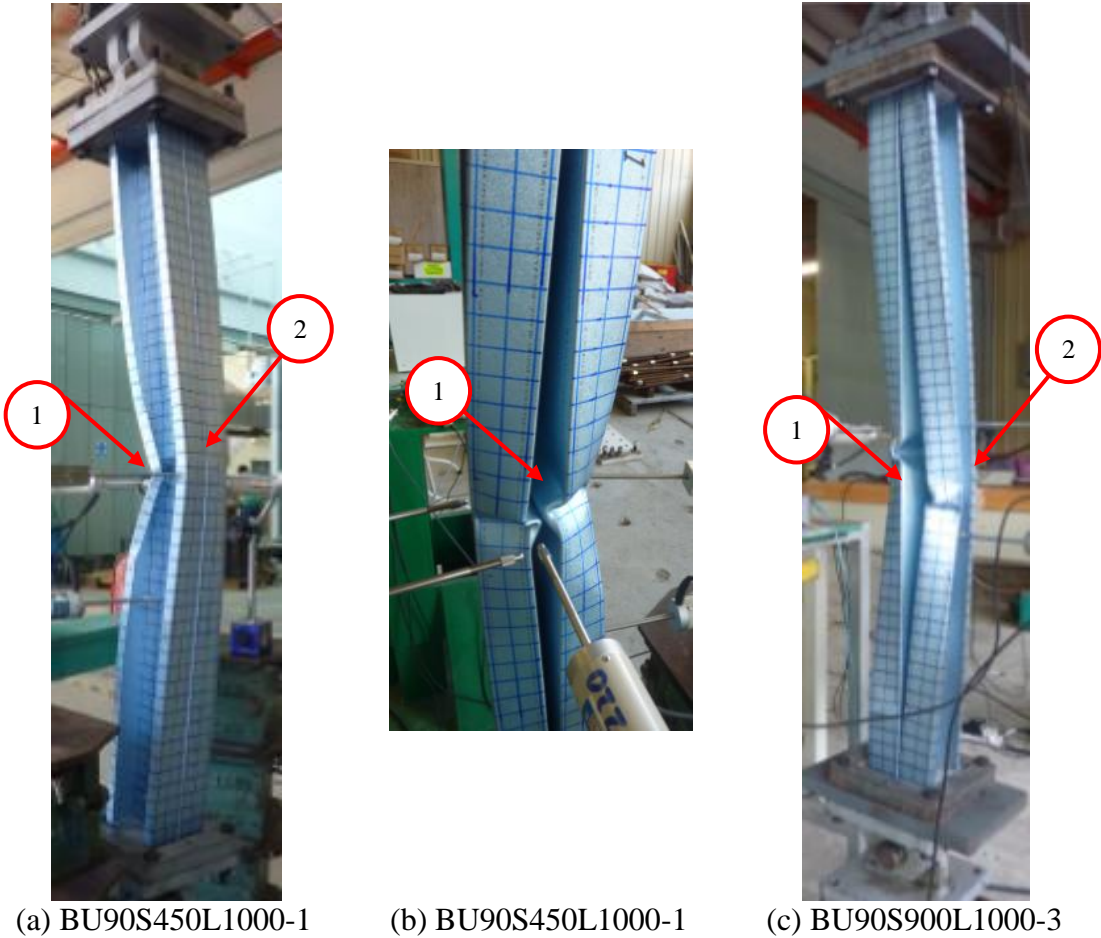
Figure 4.2: Mortar Failure

BU90S225L1000-3 was discarded because the specimen failed in the wrong direction and caused the pinned-end assembly to wedge as shown in Figure 4.3.



Figure 4.3: Failure of Pinned-end when Testing BU90S225L1000-3

BU90S450L1000-1 and BU90S900L1000-3 were discarded because they failed in separate ways with a mix of curvature in both x and y-axis as shown in Figure 4.4. It was observed that the individual C-channels in these test specimens moved separately with the C-channels prying apart on one side as shown by (1) in Figure 4.4. However, on the other side, the intermediate fastener at mid-height held the C-channels together, preventing them from buckling separately as shown by (2) in Figure 4.4.



* (1) denotes C-channels prying apart
* (2) denotes C-channels held together by fasteners

Figure 4.4: Specimens from BU90 Test Series Failed in Both x and y-axis

4.2.3 Back-to-back C-channel Built-up Columns with a Gap

Table 4.3 shows the ultimate loads of back-to-back C-channel built-up column with a gap for the compression test.

Table 4.3: Test Results of Back-to-back C-channel Built-up Columns with a Gap (GBU)

	s/L < 0.25	s/L > 0.50	s/L < 0.25	s/L > 0.50
Specimen No.	Stub		Stub	
	GBU75S50L300	GBU75S200L300	GBU90S50L300	GBU90S200L300
1	Discard	105.19	Discard	Discard
2	112.09	107.06	Discard	145.56
3	110.57	Discard	147.66	161.47
4	128.94	112.09	164.40	149.42
Mean	117.20	108.11	156.03	152.15
Specimen No.	Short		Short	
	GBU75S100L500	GBU75S400L500	GBU90S100L500	GBU90S400L500
1	101.68	106.12	161.82	150.82
2	98.05	100.04	159.01	149.65
3	105.78	113.61	160.65	171.65
4	-	-	Discard	174.93
Mean	101.84	106.59	160.49	161.76
Specimen No.	Short		Short	
	GBU75S225L1000	GBU75S900L1000	GBU90S225L1000	GBU90S900L1000
1	86.62	73.36	143.33	152.58
2	85.63	64.12	Discard	Discard
3	72.19	69.74	146.14	141.70
Mean	81.48	69.07	144.74	147.14
Specimen No.	Short			
	GBU75S475L2000	GBU75S1900L2000		
1	29.25	27.97		
2	29.14	27.73		
3	29.37	24.81		
Mean	29.25	26.84		

As seen in Table 4.3, results of GBU75S50L300-1 and GBU75S200L300-3 were considered as outliers. In addition, the GBU90S50L300-1, GBU90S50L300-2 and GBU90S200L300-1 results were discarded because they failed at the column end as shown in Figure 4.5. These specimens failed at the column end because the mortar cement failed prematurely as the specimens punched through the mortar cement as shown in Figure 4.5.

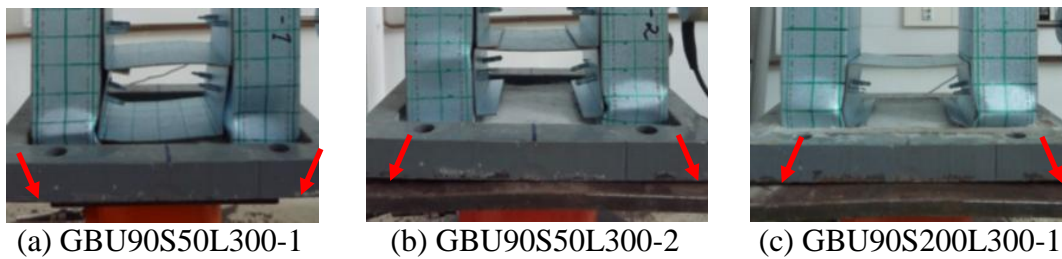


Figure 4.5: Back-to-back Channels Stub Columns with a Gap Failed at Ends

The GBU90S100L500-4 result was discarded because this specimen failed in a combination of buckling in both x and y-axis as shown in Figure 4.6.



Figure 4.6: GBU90S100L500-4 Failed with a Mixed Failure in x and y-axis

The GBU90S225L1000-2 result was discarded due to mortar failure at the end of the specimen as shown in Figure 4.7.



Figure 4.7: GBU90S225L1000-2 Failed at End

The GBU90S900L1000-2 result was discarded because the specimen failed with torsion in the individual C-channels as shown in Figure 4.8.



Figure 4.8: Failure modes of GBU90S900L1000-2

4.3 Improved Test Results

Additional work is carried out to rectify the measurements obtained from LVDT measuring the shortening of the test specimen. This is because the position of the LVDT was not isolated from the movement of the loading frame during the testing process as shown in Figure 4.9.

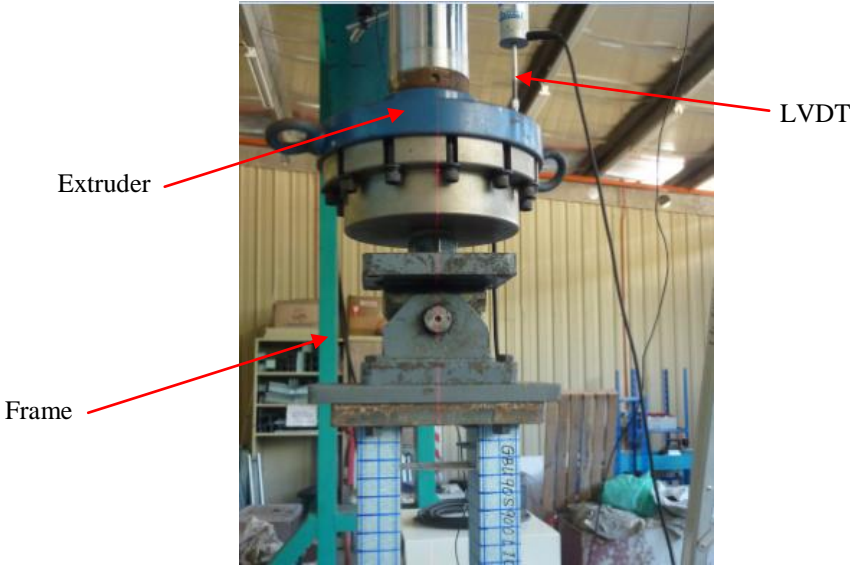


Figure 4.9: Position of LVDT for Shortening

The beam of the loading frame deflected upwards (hogging) when the load was applied through the extruder. The hogging of the beam caused the measured shortening of the columns to be greater than the actual shortening. Therefore, additional work was carried out to verify the actual shortening of the column by identifying the deflections of the beam through an isolated LVDT as shown in Figure 4.10. Therefore the actual shortening was calculated by subtracting the measured shortening with the measured beam deflection.



Figure 4.10: LVDT measuring beam deflection

For specimens at 500mm length, additional work is carried out to verify the actual shortenings that were further extended. This extension is due to the steel prop used for supporting the specimens to appropriate height for testing as shown in Figure 4.11.



Figure 4.11: LVDT measuring plate deflection

The top plate of the steel prop deflected during the testing causing axial displacement at the bottom of the specimens. Therefore, another isolated LVDT was introduced to measure the plate deflection of the prop. A sample of test results before and after rectification is as shown in Figure 4.12.

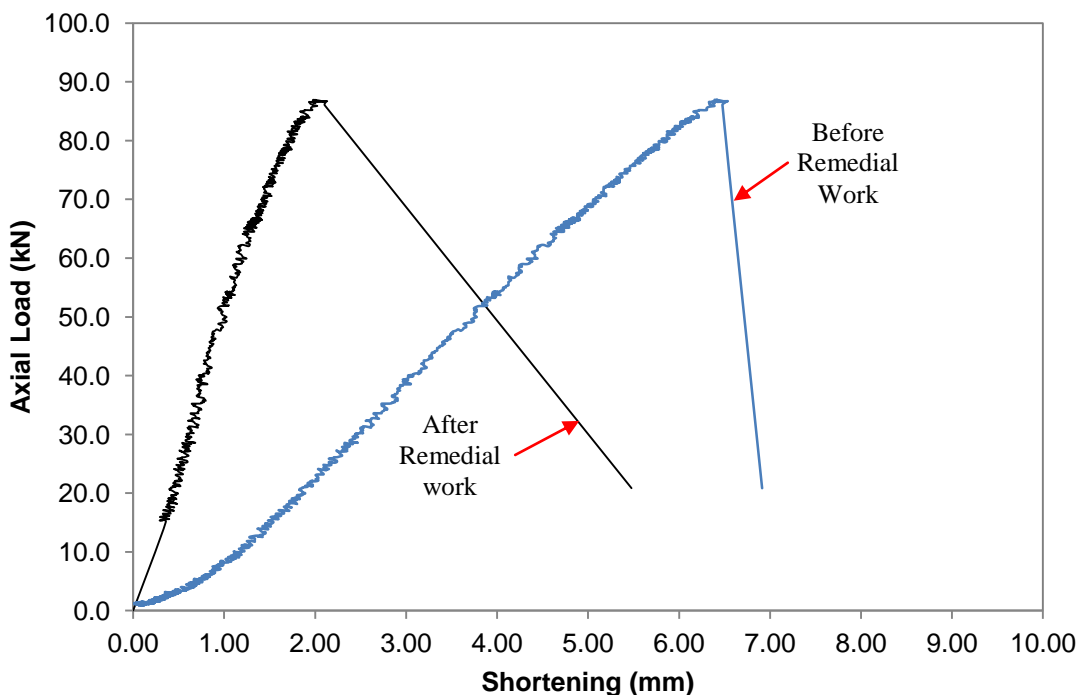


Figure 4.12: Test Results Before and After Additional Work for C90L1000-2

The rectified graphs of load applied versus shortening after are shown in Figures 4.13 to 4.18. The graphs of load applied versus shortening for all other columns are presented in Appendix E, F and G for C-channel columns, plain built-up columns and built-up columns with a gap respectively.

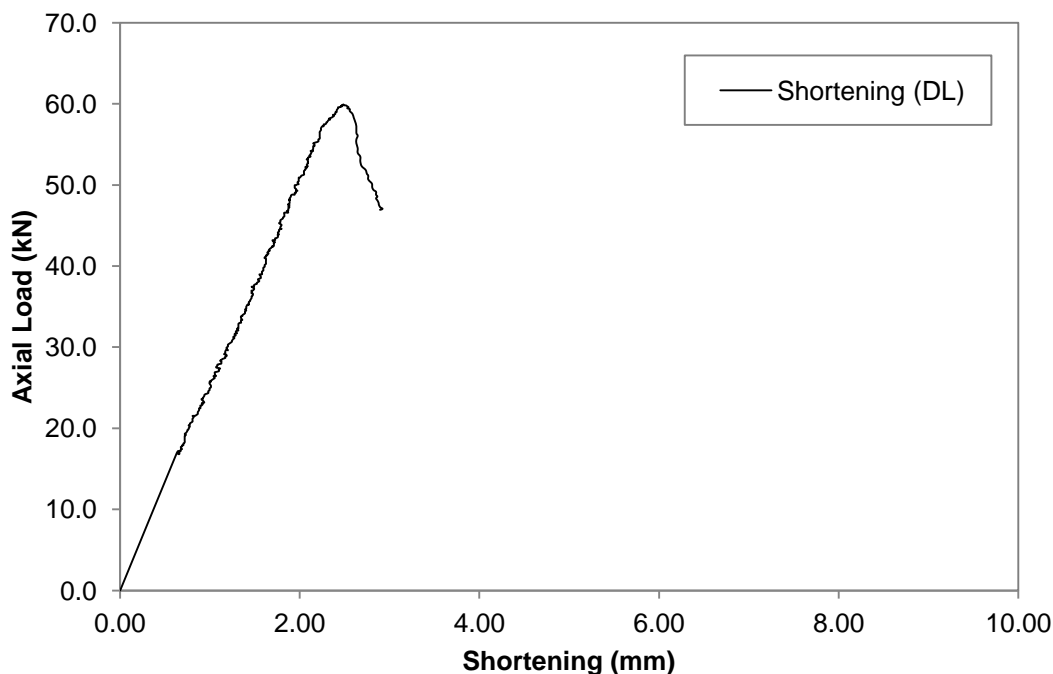


Figure 4.13: Graph of Load versus Shortening for C75L300-3

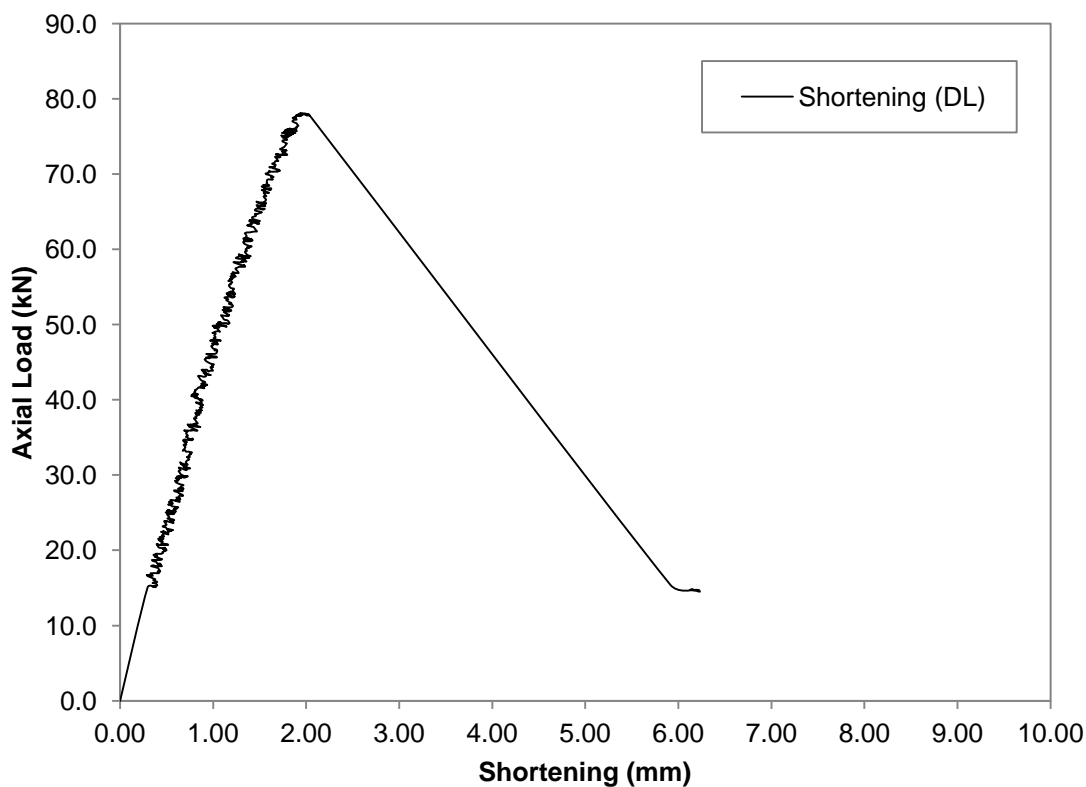


Figure 4.14: Graph of Load versus Shortening for C90L500-3

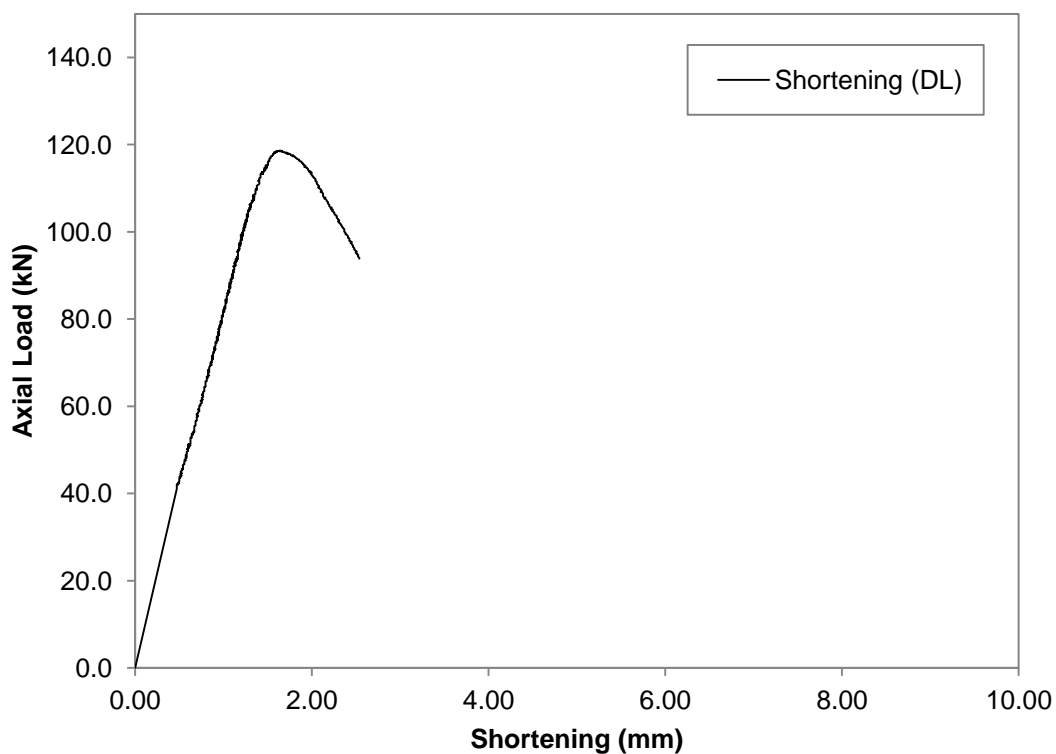


Figure 4.15: Graph of Load versus Shortening for BU75S50L300-3

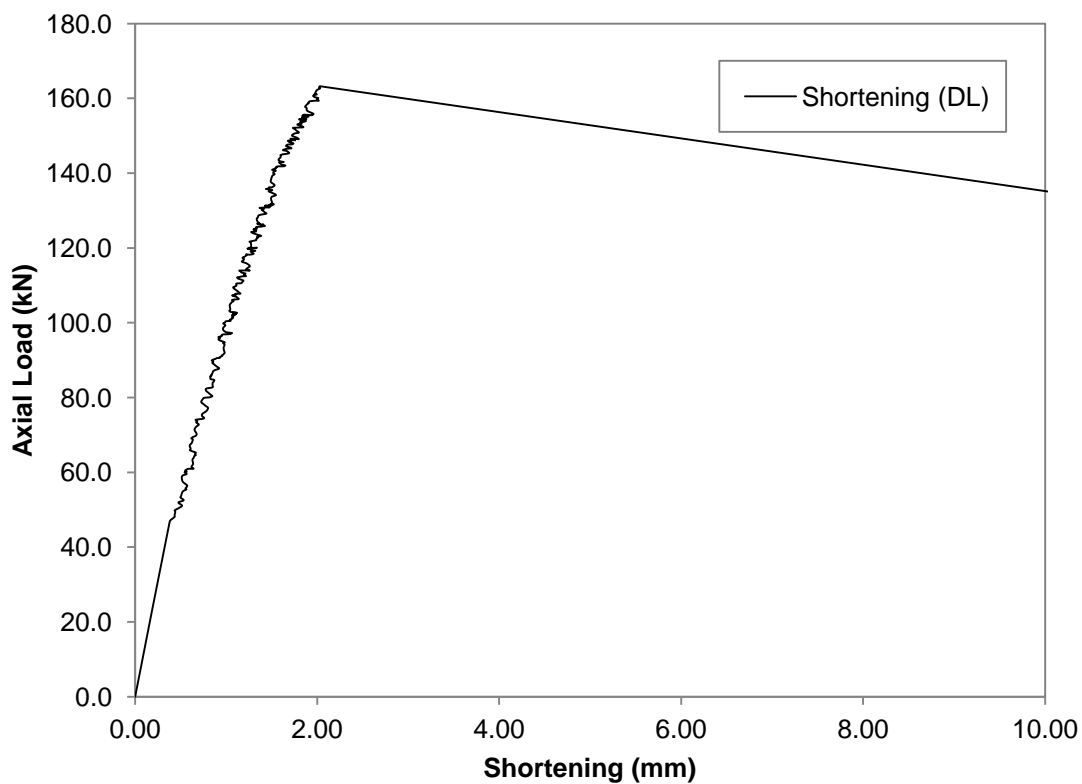


Figure 4.16: Graph of Load versus Shortening for BU75S50L300-3

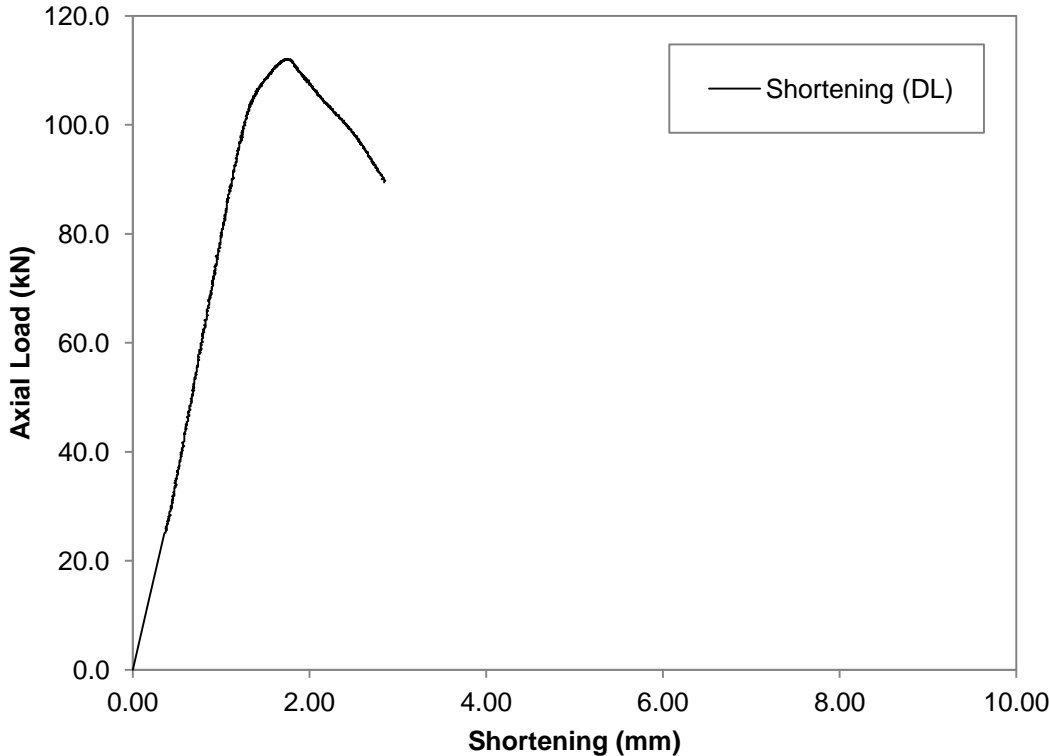


Figure 4.17: Graph of Load versus Deformation for GBU75S50L300-2

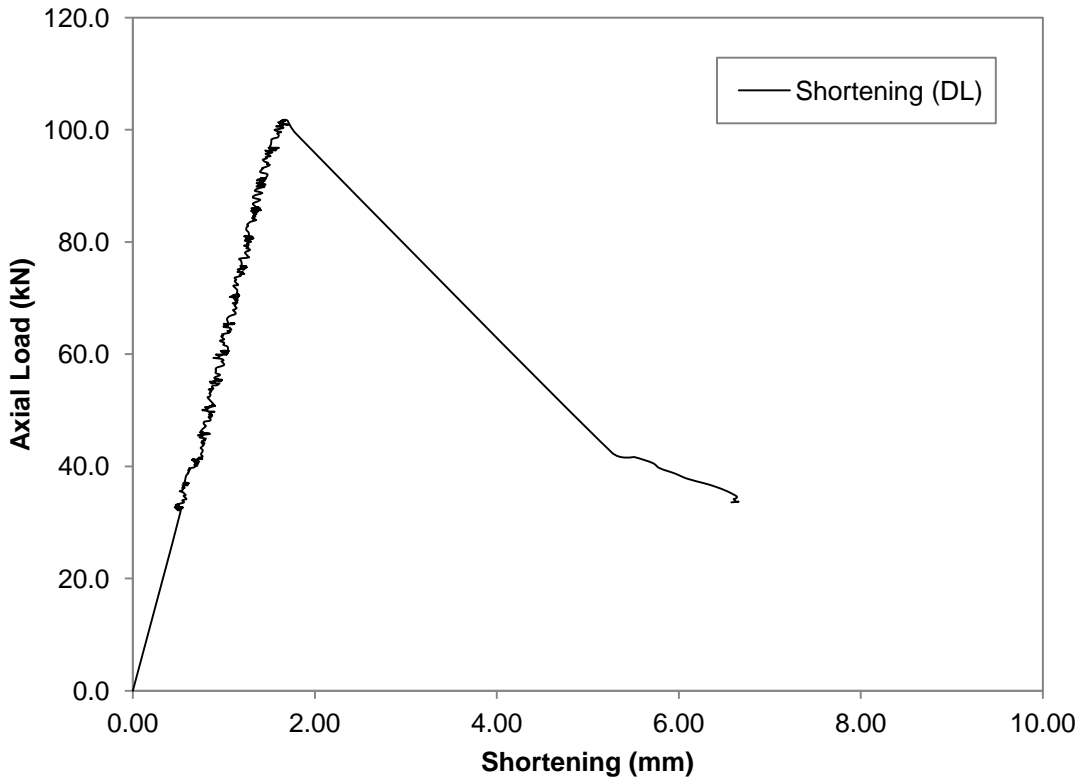


Figure 4.18: Graph of Load versus Deformation for GBU75S100L500-1

From the load versus shortening curves, the graphs show that the columns remained elastic and proportionate at the beginning. The initial gradient of the curve at elastic stage for '90' test series was steeper than the '75' test series. For the '90' test series, the strength of the column decreased rapidly upon reaching the ultimate load and sudden failure occurred soon after that. The large individual C-channels provided a stiffening effect to the web. Thus, the failure of the column was generally due to plastic deformation near to the end of the columns. For the '75' test series with smaller flange, the smooth transition curve at ultimate load showed that sudden failure was not observed during testing. This is because the web of the '75' test series was not stiffened enough. Deformation was visible even before reaching the ultimate load.

4.4 Specimen Behaviour

The behaviour of the test specimens were observed throughout the testing. Deformation readings were obtained by LVDTs positioned at various designated locations as described in Chapter 3. It was noted that no conclusive data for load buckling could be derived from the LVDTs readings for most of the test specimens. It was difficult to accurately identify the buckling loading from visual observation and from using the static LVDT. Thus, the buckling load was not further analysed to identify the buckling load. Common observations on the behaviour of the test columns during the laboratory testing were documented as follows.

Figure 4.19 shows a sample of deformation readings for the C75L300-3 test specimen obtained from the LVDTs positioned at mid-length and at one-third length from the bottom end of the fix-ended column. The onset of local buckling can be clearly shown in the load against deformation graph occurred at a load of approximately 20kN.

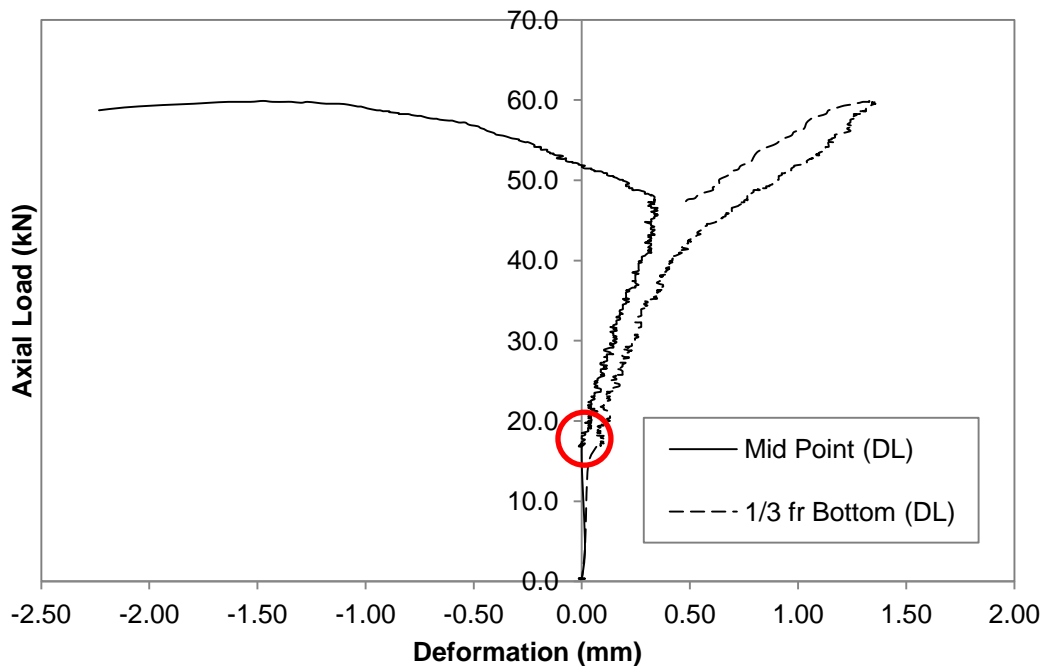


Figure 4.19: Graph of Load versus Deformation for C75L300-3

Similarly, Figure 4.20 shows another sample of deformation readings for C90L500-3 test specimen obtained from the LVDTs positioned at web, flange and lips of the pin-ended short column. In this case, the start of local buckling occurred at approximately 40kN as shown clearly in the load against deformation graph.

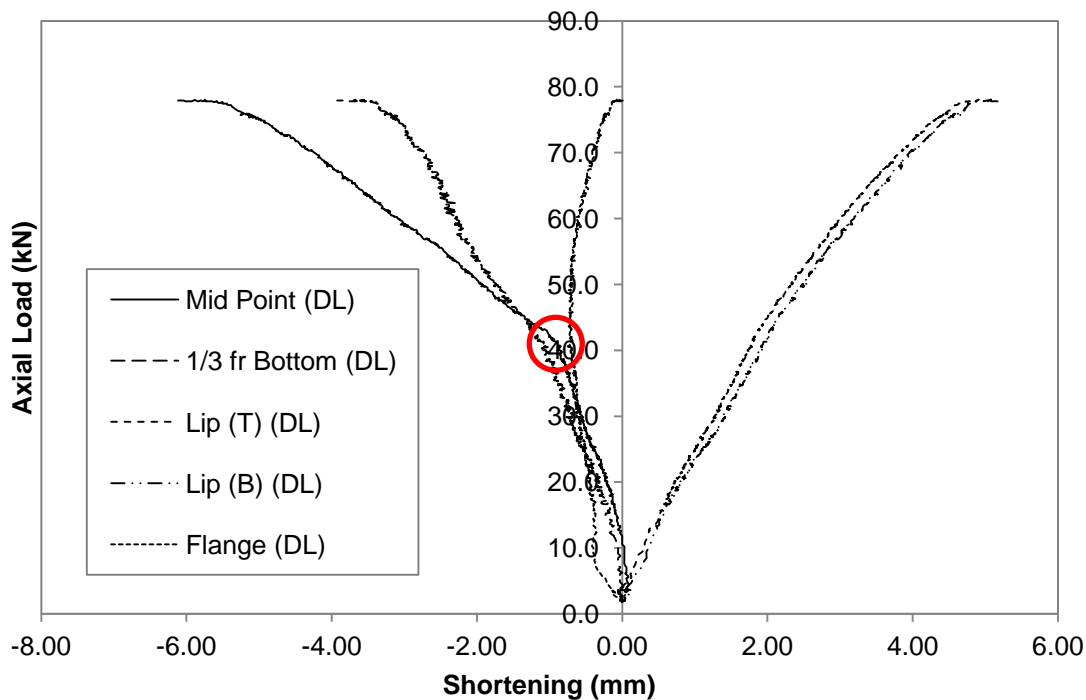


Figure 4.20: Graph of Load versus Deformation for C90L500-3

Both graphs show that the local buckling started when the load against deformation curve for deformation at mid-length and one-third length moved in different directions. This separation was due to the wave-like local buckling failure mode.

Furthermore, distortional buckling could be identified from the load against deformation graph when the deformation readings from all the LVDTs at flanges and lips increased rapidly. However, it was difficult to pinpoint the first appearance of distortional buckling from the load against deformation graph due to the drawback of the static positioning of the LVDTs in the test setup.

Figure 4.21 and Figure 4.22 show deformation readings for the C75L1000-2 and C75L2000-3 test specimen obtained from the LVDTs positioned at web, flange, and lips of the intermediate and slender pinned-end columns. From the same graphs, gradual changes in global cross-section of the specimens showed the occurrence of global buckling.

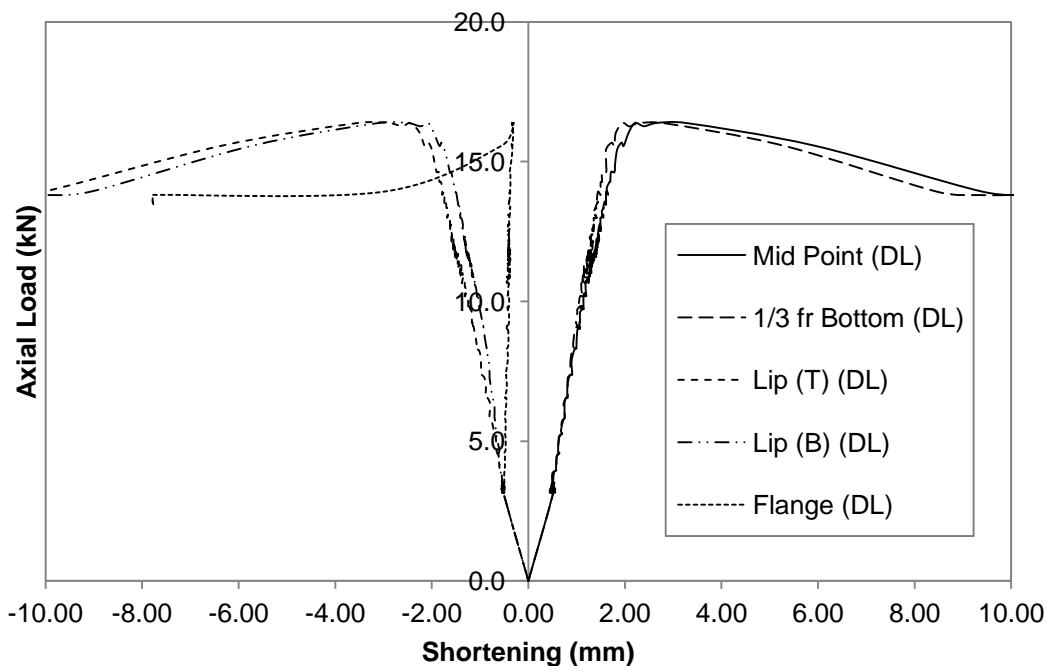


Figure 4.21: Graph of Load versus Deformation for C75L1000-2

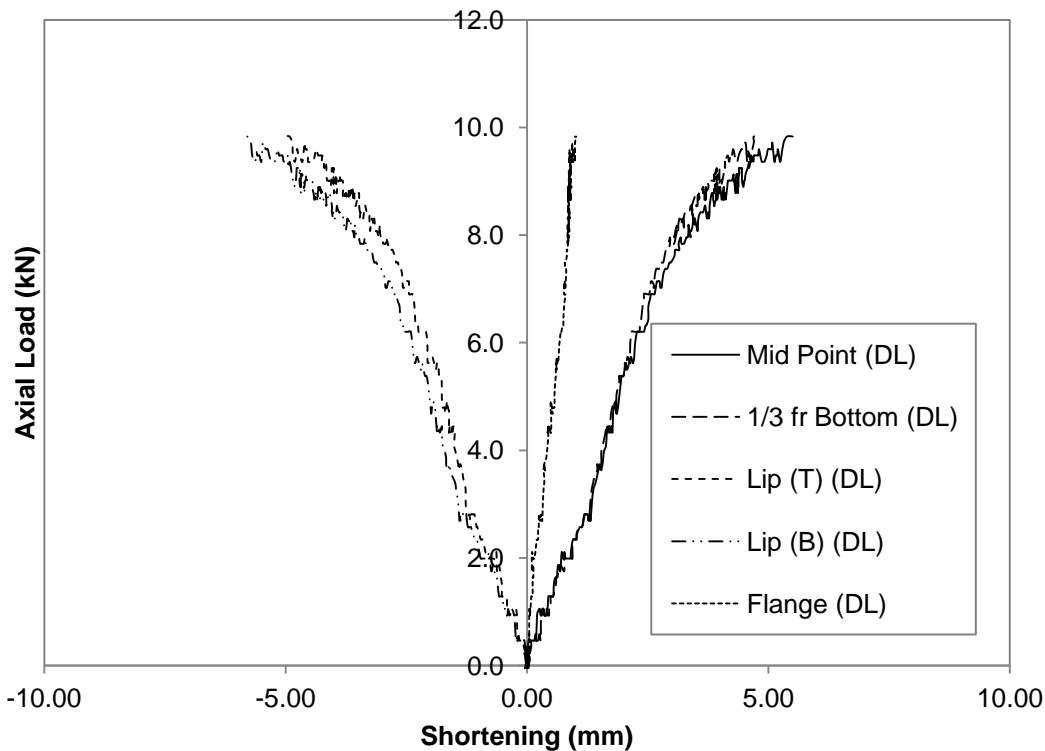


Figure 4.22: Graph of Load versus Deformation for C75L2000-3

4.4.1 C-channel Columns

4.4.1.1 Stub Column Tests

At the elastic stage, the C-channel stub columns experienced local buckling at web as the applied load increased. The effect of local buckling at mid-length increased when the column reached ultimate strength. Distortional buckling was also visible upon reaching the ultimate load. Deflection in web and flanges continued to increase, accompanied by a sudden drop in load carrying capacity when the specimen failed. The maximum deformation occurred on the web of most stub column specimens as shown in Figure 4.23.

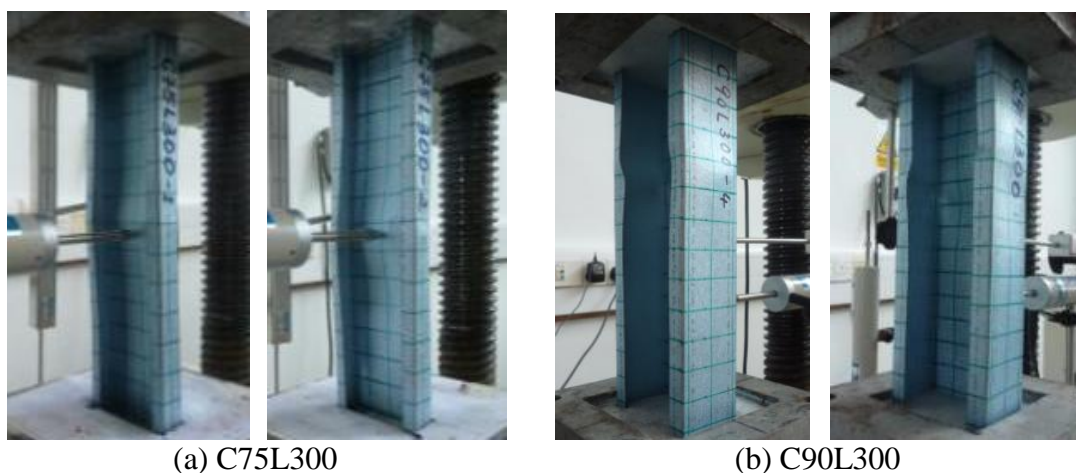


Figure 4.23: Failure Modes of Tested L300 C-channel Columns

For the C75L300 test specimens with 75mm flange width, the permanent effect of local buckling was visible near mid-length as shown in Figure 4.23(a) because these specimens have smaller flange and are less effective. Therefore, the specimens failed with the flanges and the lips curved in and the flanges moved inwards at the mid-length.

Whereas, the results for the C90L300 with 90mm web width showed the permanent effect of local buckling is visible near to the end of the specimens as shown in Figure 4.23(b). This failure occurred with plastic deformation mainly near to the top or the bottom end of the column because the cross section with smaller web to flange ratio (A'/B') was stiffer and thus more effective in resisting the applied load. This gave the specimens higher capacity to resist the applied load.

4.4.1.2 Short Column Tests

The ultimate strength and behaviour of singly symmetric pin-ended columns were sensitive to the location of the applied load. The overall bending caused a shift in the effective centroid of the singly symmetric pin-ended column. In the short C-channel column test in this research, the effective centroid shifted away from the web. Thus, the concentrically applied load became eccentric. Due to this shift, specimens were observed to bend towards the lips and resulted in lower column strengths. Generally, the concentrically loaded C-channel columns failed in local and flexural buckling modes. The local buckling eventually localised near the mid-length of the column as shown in Figure 4.24. However, some specimens showed buckling away from mid-length as shown in Figure 4.24 (c) due to initial imperfections of the test specimens.

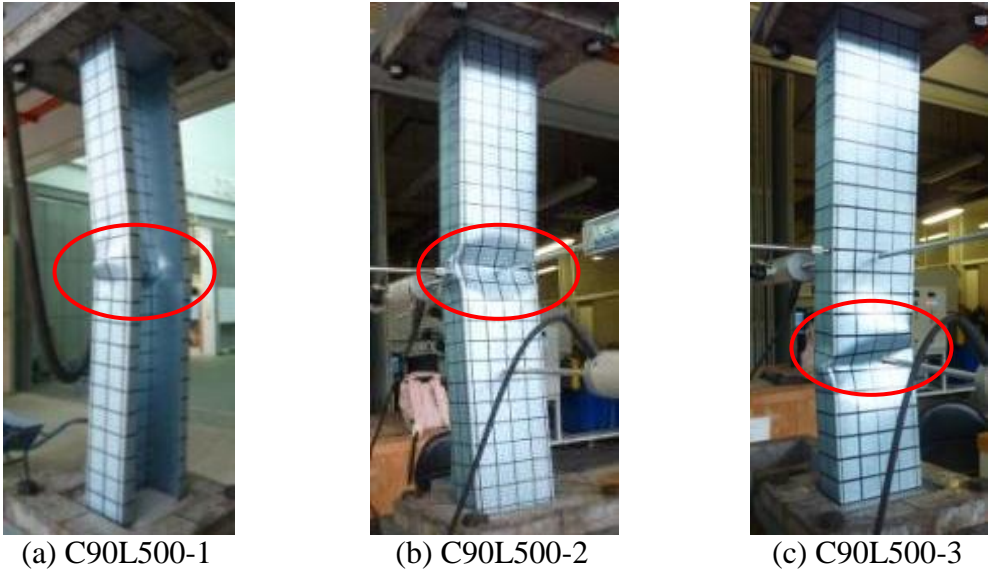


Figure 4.24: Failure Modes of Tested C90L500 C-channel Columns

4.4.1.3 Intermediate Column Tests

Intermediate column such as the C75L500 and C75L1000 test specimens failed with large deformation at mid-length as shown in Figure 4.25 and Figure 4.26.

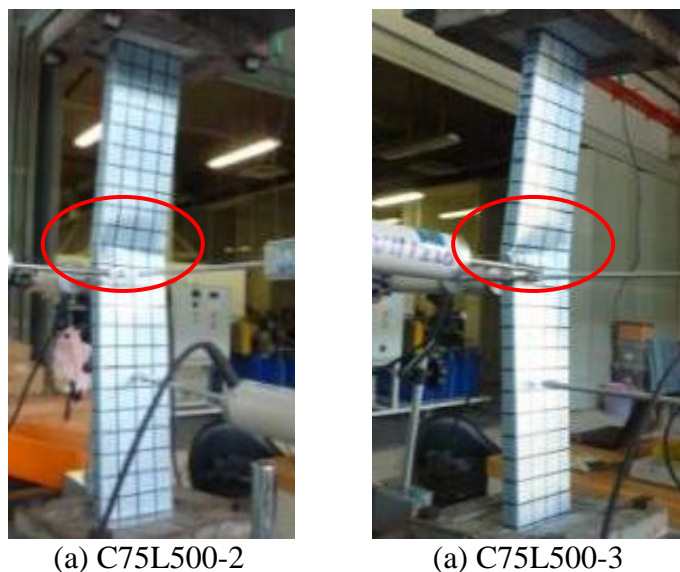


Figure 4.25: Failure Modes of Tested C75L500 C-channel Columns

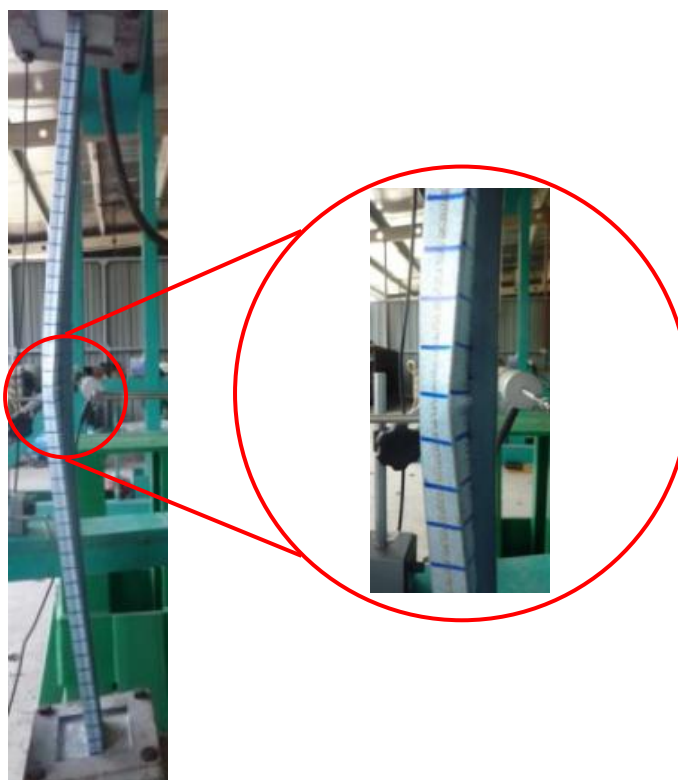


Figure 4.26: Failure Modes of Tested C75L1000 C-channel Columns

The C75L1000 test specimens failed towards the web because the C75 test series have smaller flanges. The failure of the C75L1000 test specimens was also affected by

twisting at mid-length due to the imperfection of cross section geometry as shown in Figure 4.26.

Comparing the buckling behaviours of the C75L1000 and C90L1000 test specimens, the results showed that the C90L1000 test specimens with larger width–thickness ratio (B'/t) buckled in the opposite direction from the C75L1000 test specimens. The C90L1000 test specimens buckled towards the lips as shown in Figure 4.27.

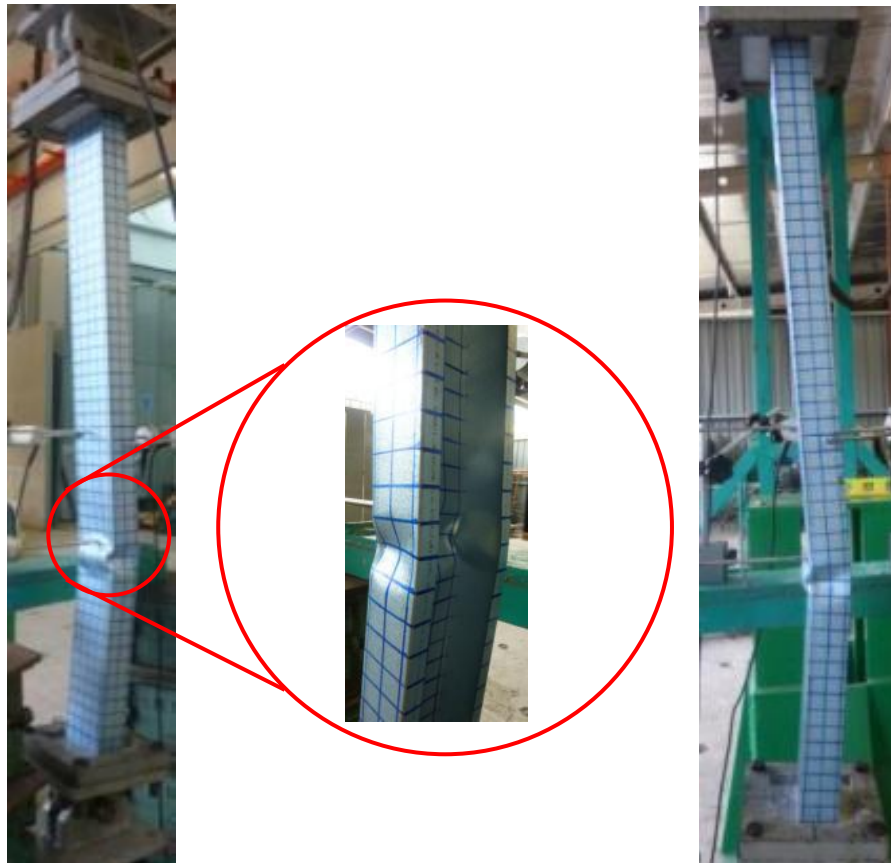


Figure 4.27: Failure Modes of Tested C90L1000 C-channel Columns

4.4.1.4 Slender Column Tests

Slender columns from the C75L2000 test specimens buckled in the flexural buckling mode as shown in Figure 4.28. The local buckling mode was not observed in the slender columns. The slender columns from the C75L2000 test specimens buckled gradually as the load increased. The buckled shape started to form almost immediately after the axial load was applied. The failed shape of the C-channel columns showed that the C75L2000-1 and C75L2000-3 buckled in the direction towards the web while the C75L2000-2 failed towards the lips as shown in Figure 4.28. Both failed shape of C75L2000 test specimens achieved similar ultimate loads. The difference of these failed shapes of C75L2000 test specimens reflects the difficulties associated with the positioning of the specimen concentrically in the test rig.



(a) C75L2000-1
(towards the web)

(b) C75L2000-2
(towards the lips)

(c) C75L2000-3
(towards the web)

Figure 4.28: Failure Modes of Tested C75L2000 C-channel Columns

4.4.2 Plain Back-to-back C-channel Built-up Columns

4.4.2.1 Stub Column Tests

The most common buckling mode of the built-up stub column is local buckling. Built-up stub columns buckled either as an integral column or with the individual C-channels buckle separately. The built-up stub columns with 3 intermediate fasteners at 50mm spacing buckled in an angular buckling shape as shown in Figure 4.29. This buckled shape formed a “hinge” near the fastener location of the column when the deformation increased. The individual C-channels also buckled together laterally as an integral built-up column.

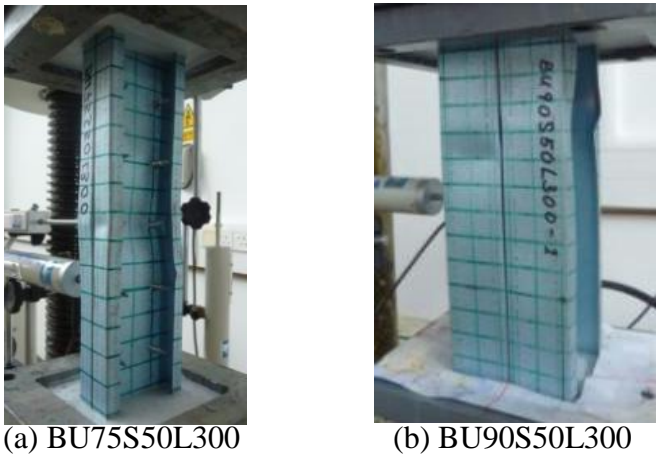


Figure 4.29: Failure Modes of Tested S50L300 Built-up Columns

The failure modes for both the BU75S100L500 and BU90S100L500 test specimens are similar to the BU75S50L500 and BU90S50L500 test specimens. However, the individual C-channels tended to buckle separately between the intermediate fasteners as shown in Figure 4.30.

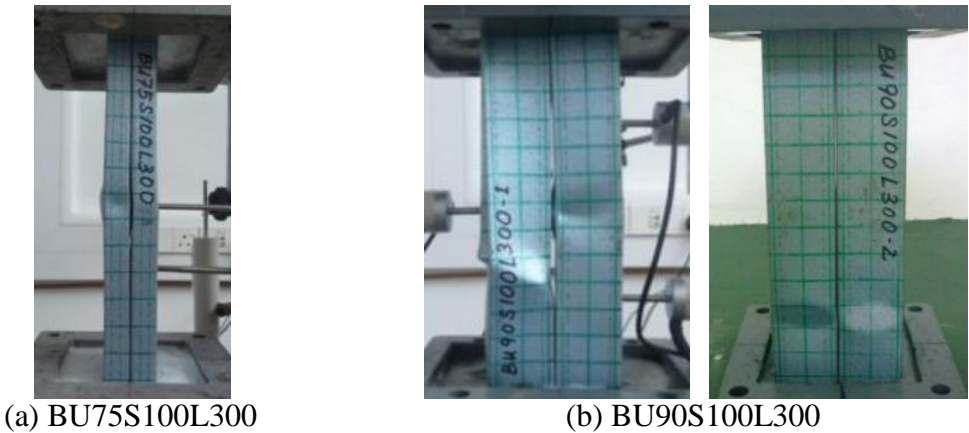


Figure 4.30: Failure Modes of Tested S100L300 Built-up Columns

However, the individual C-channels pry apart at mid-length for both the BU75S200L300 and BU90S200L300 test specimens due to the lack of fasteners along the length of the column as shown in Figure 4.31.

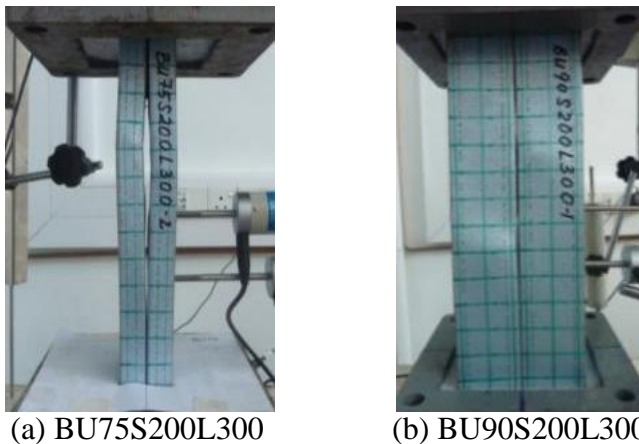


Figure 4.31: Failure Modes of Tested S200L300 Built-up Columns

4.4.2.2 Short Column Tests

The BU75L500 test specimens showed local buckling waves at web during the initial stage of the testing. The magnitude of the displacement slowly increased as the specimens continued to carry load until the ultimate load was achieved. After the ultimate load, deformation localised near the mid-length on the compression side of the specimens. It was observed that for the BU75L500 test specimens global buckling dominated the final and total deformation as shown in Figure 4.32.



Figure 4.32: Failure of Tested BU75L500 Built-up Columns

The behaviour of the BU90L500 test specimens was different from the BU75L500 test specimens. All the BU90 test series at 500mm column length failed with crushing failure near to the top or bottom end of the built-up columns. Figure 4.33 shows the crushing failure for all the BU90 built-up short columns.

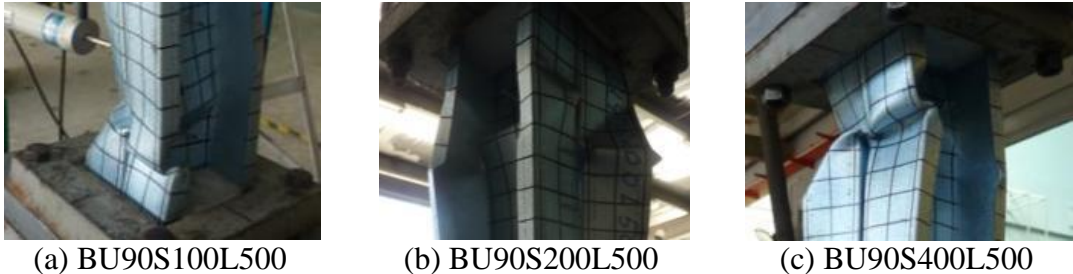


Figure 4.33: Failure Modes of Tested BU90L500 Built-up Columns

The BU90L1000 test specimens at 1000mm column length experienced sudden failures. During the testing, the test specimens of the BU90 test series showed little deformation as shown in the graph of load against deformation in Appendix F. Upon reaching failure, the specimens buckled suddenly and instantaneously into distortional and flexural modes as shown in Figure 4.34.



Figure 4.34: Failure Modes of Tested BU90S225L1000 Built-up Columns

The BU90S450L1000 test specimens showed crushing failure near the bottom end of the specimens as shown in Figure 4.35. The intermediate fasteners prevented the individual C-channels from separation and ensured that the columns act as integral built-up columns.

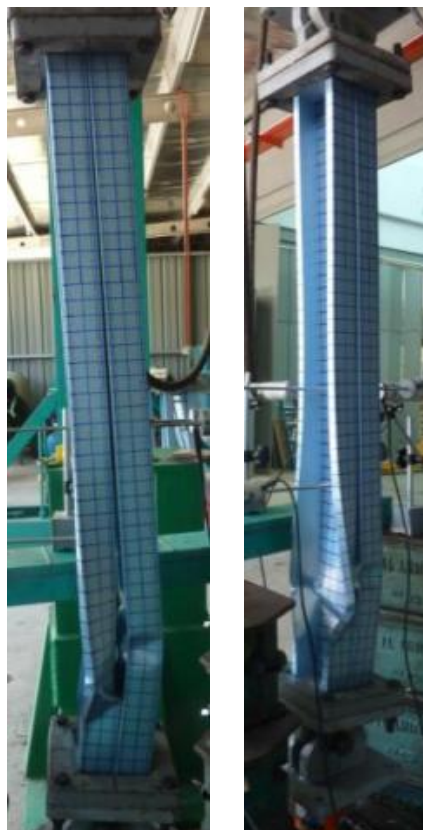


Figure 4.35: Failure Modes of Tested BU90S450L1000 Built-up Columns

Flexural-torsional buckling was observed in some of the BU90L1000 test specimens during testing as the test setup was unable to provide sufficient restraint. This flexural-torsional buckling mode was predicted by the design analysis when the design strength of the column was calculated as pin-ended condition in all directions. However, the test setup was designed to allow rotation only about the y-axis. Since the pinned assembly was not fixed to the floor, when the applied load was large enough, the pinned assembly moved allowing the flexural-torsional buckling to occur during testing.

4.4.2.3 Intermediate Column Tests

The BU75L1000 test specimens showed local buckling waves at web during the initial stage of the testing. The magnitude of displacement slowly increased as the specimens continued to carry load until ultimate load was achieved. After the ultimate load, deformation localised near the mid-length on the compression side of the specimens as shown in Figure 4.36. It was observed that for intermediate columns global buckling dominated the final and total deformation as shown in Figure 4.37.



Figure 4.36: Failure Modes at Mid-Length of Tested BU75L1000 Built-up Columns



(a) 225mm



(b) 450mm



(c) 900mm

Figure 4.37: Failure Modes of Tested BU75L1000 Built-up Columns

4.4.2.4 Slender Column Tests

Local and distortional buckling was not observed during the testing of slender columns for the BU75L2000 test specimens. Global buckling was noticeable immediately with a large curved deformation at mid-length as shown in Figure 4.38. The deformation magnitude increased slowly as the specimens continued to carry load. After the ultimate load has reached, localised deformation was visible near the mid-length of the compression side of the specimens.



Figure 4.38: Failure Modes of Tested BU75L2000 Built-up Columns

4.4.3 Back-to-back C-channel Built-up Columns with a Gap

4.4.3.1 Stub Column Test ($L_t=300\text{mm}$)

A total of 16 stub columns with two different fastener spacing were tested. GBU75S50L300 and GBU90S50L300 test specimens with three intermediate fasteners at 50mm spacing failed as an integral column with plastic deformation near to the bottom end of the specimens as shown in Figure 4.39. The failure modes of the GBU75L300 test specimens were different from the BU75L300 test specimens because the short C-channels in the GBU75L300 test specimens provided sufficient restraints to prevent buckling failure at mid-length of the column. For the GBU90L300 test specimens, plastic deformation appeared near to the top or bottom of the specimens. Both the GBU75L300 and GBU90L300 test specimens failed with localised failure at the end of the columns.

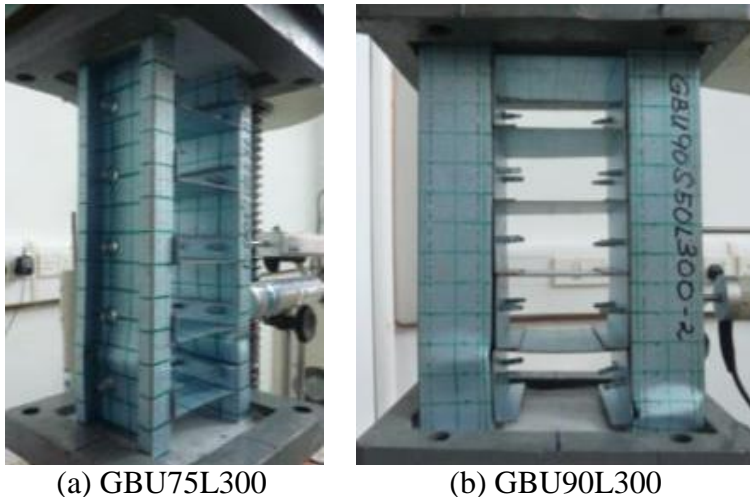


Figure 4.39: Failure Modes of Tested S50L300 Built-up Columns with a Gap

Both the GBU75S200L300 and GBU90S200L300 specimens with no intermediate fastener buckled separately where the individual C-channels of these GBU columns deformed at mid-length as shown in Figure 4.40. The individual C-channels in the GBU75S200L300 test specimens failed separately like an O-shape due to the lack of fasteners along the length of the column. This behaviour was not obvious in the GBU90S200L300 test specimens as the individual C-channels are stockier thus strengthened the columns.

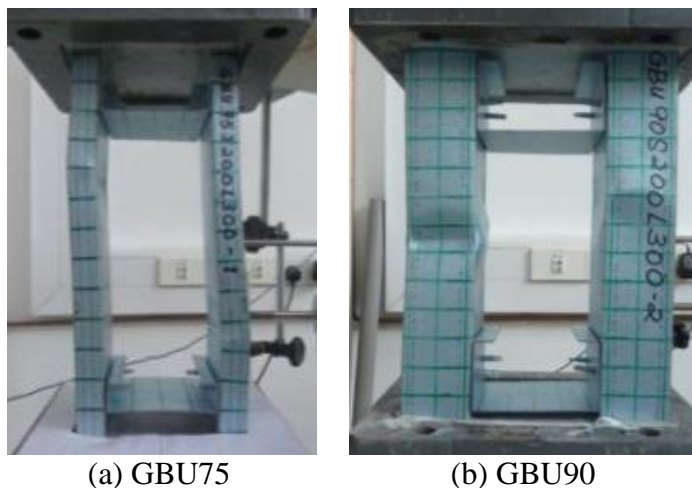
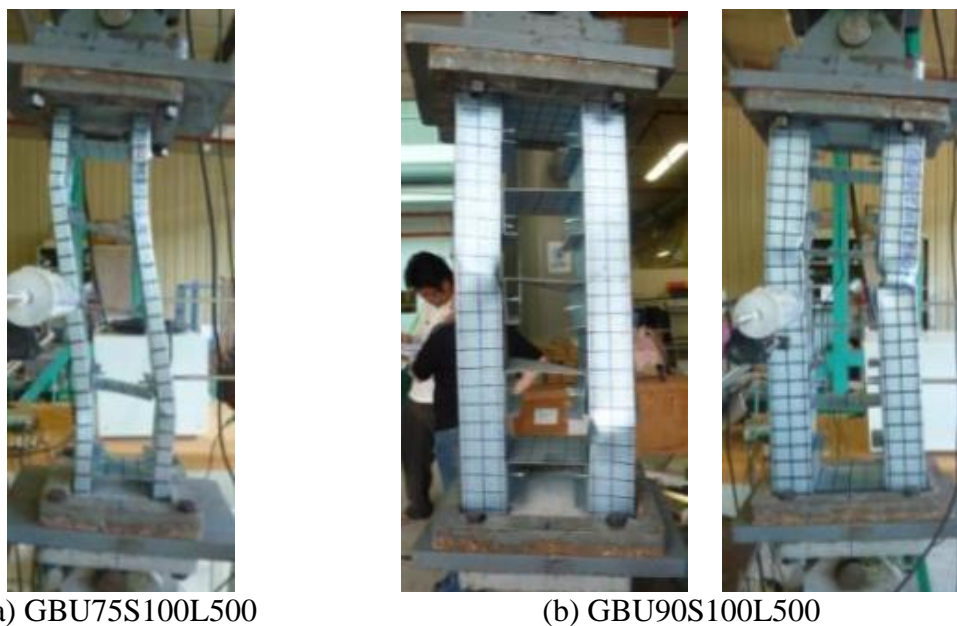


Figure 4.40: Failure Modes of Tested S200L300 Built-up Columns with a Gap
4.4.3.2 Short Column Test ($L_t=500mm$)

The GBU75S100L500 test specimens with three intermediate fasteners at 100mm spacing buckled in a reverse curvature forming an S-shape as the intermediate fasteners prevented differential change in the segment length of the individual C-channels. This resulted in a hinge-like angular buckling shape at about one-third length or near to both ends of the columns. However, the GBU90S100L500 test specimens buckled in a single curvature due to the rigidity of the column as compared to the GBU75L500 test specimens. The large flanges in the GBU90S100L500 test specimens provided higher stiffness to the column thus the S-shape buckling failure was not observed.



(a) GBU75S100L500 (b) GBU90S100L500
Figure 4.41: Failure Modes of Tested S100L500 Built-up Columns with a Gap

The GBU75S400L500 and GBU90S400L500 test specimens with no intermediate fasteners buckled with the individual C-channels separated at mid-length forming an O-shape due to the lack of fasteners along the length of the column. As there were no intermediate fasteners to hold the individual C-channels together, the deformation occurred at mid-length. The O-shaped failure mode was not observed in the GBU90S400L500 test specimens whereas in some cases, a K-shape deformation was observed as shown in Figure 4.42. The formation of K-shape was due to eccentric loading in the test setup for the pinned-end condition, unequal C-channel dimension and initial imperfections between the two individual C-channels of the GBU column.



Figure 4.42: Failure Modes of Tested S400L500 Built-up Columns with a Gap

4.4.3.3 Short Column Test ($L_c=1000mm$)

Behaviours of GBU test specimens with 1000mm column length were similar to those of GBU test specimens with 500mm column length in section 4.4.3.2 but the GBU test specimens with 1000mm column length revealed clearer deformed shape. The GBU75S225L1000 test specimens buckled in a reverse curvature forming an S-shape similar to the GBU75S100L500 test specimens as shown in Figure 4.43(a). On the other hand, the GBU90S225L1000 test specimens buckled in a single curvature similar to the GBU90S100L500 test specimens as shown in Figure 4.43(b).



Figure 4.43: Failure Modes of Tested S225L1000 Built-up Columns with a Gap

The GBU75S900L1000 and GBU90S900L1000 test specimens with no intermediate fasteners buckled separately with the individual C-channels prying apart at mid-length forming an O-shape due to the lack of fasteners along the length of the column as shown in Figure 4.44. The individual C-channels in the GBU75S900L1000 test specimens failed with visible deformation at mid-length. The GBU90S900L1000 test specimens buckled with an O-shaped similar to the GBU90S400L500 test specimens in section 4.4.3.2. This buckling was less obvious in the GBU90S900L1000 test specimens compared to the GBU75S900L1000 test specimens whereas in some other cases, the K-shape buckling was observed in both the GBU75S900L1000 and GBU90S900L1000 test specimens as shown in Figure 4.44.



Figure 4.44: Failure Modes of Tested S900L1000 Built-up Columns with a Gap

4.4.3.4 Short Column Test ($L_I=2000\text{mm}$)

Similar buckling behaviour of the GBU column with 2000mm column length was observed. Again, the intermediate fasteners prevented differential change in the segment length of the individual C-channels for the GBU75S475L2000 test specimens, thus the two individual columns buckled in a reverse curvature forming an S-shape. However, the S-shape was less obvious in some specimens due to mortar failure at the column end and friction in the pinned-end assemblies as shown in Figure 4.45. The GBU75S1900L2000 test specimens failed separately with the individual C-channels buckling laterally in the same direction and forming a buckled K-shape. The individual C-channels which are eccentrically loaded failed with different curvatures due to the eccentricity in the test setup for the pinned-end condition, unequal C-channel dimension and initial imperfections between the two individual C-channels of the GBU column.



(a) GBU75S475L2000

(b) GBU75S1900L2000

Figure 4.45: Failure Modes of Tested GBU75L2000 Built-up Columns with a Gap

4.5 Comparison of Back-to-back C-channel Built-up Columns with and without a Gap

Table 4.4 shows the results of the comparison between back-to-back C-channel built-up columns with and without a gap.

Table 4.4: Comparison of the Ultimate Loads of Back-to-back C-channel Built-up Columns with and without a Gap

Specimen	Smallest Spacing			Largest Spacing		
	$P_{n \text{ Test BU}}$	$P_{n \text{ Test GBU}}$	Variation	$P_{n \text{ Test BU}}$	$P_{n \text{ Test GBU}}$	Variation
	kN	kN	%	kN	kN	%
75L300-1	120.66	N/A		122.51	105.19	
75L300-2	118.87	112.09		119.12	107.06	
75L300-3	118.65	110.57		113.14	N/A	
75L300-4	N/A	128.94		N/A	112.09	
Mean	119.39	117.20	-1.84%	118.26	108.11	-8.58%
75L500-1	82.96	101.68		74.77	106.12	
75L500-2	N/A	98.05		80.56	100.04	
75L500-3	74.07	105.78		87.64	113.61	
Mean	78.52	101.84	29.70%	80.99	106.59	31.61%
75L1000-1	47.04	86.62		39.90	73.36	
75L1000-2	46.28	85.63		33.70	64.12	
75L1000-3	N/A	72.19		31.71	69.74	
Mean	46.66	81.48	74.62%	35.10	69.07	96.77%
75L2000-1	N/A	29.25		N/A	27.97	
75L2000-2	15.33	29.14		12.12	27.73	
75L2000-3	12.87	29.37		13.11	24.81	
Mean	14.10	29.25	107.47%	12.62	26.84	112.74%
90L300-1	172.49	N/A		170.25	N/A	
90L300-2	171.61	N/A		177.50	145.56	
90L300-3	167.56	147.66		N/A	161.47	
90L300-4	N/A	164.40		171.88	149.42	
Mean	170.55	156.03	-8.52%	173.21	152.15	-12.16%
90L500-1	165.01	161.82		170.01	150.82	
90L500-2	163.22	159.01		151.41	149.65	
90L500-3	N/A	160.65		N/A	171.65	
90L500-4		N/A			N/A	
Mean	164.12	160.49	-2.21%	160.71	157.37	-2.08%
90L1000-1	167.81	143.33		164.86	152.58	
90L1000-2	151.76	N/A		150.94	N/A	
90L1000-3	N/A	146.14		N/A	141.70	
90L1000-4		N/A			N/A	
Mean	159.79	144.74	-9.42%	157.90	147.14	-6.81%

Comparison shows that the GBU75 test series have higher strength compared to the BU75 test series. The strength increased from 30% to 80% and to 110% for the column length of 500mm, 1000mm and 2000mm respectively as the GBU75 test specimens became stiffer compared to the BU75 test specimens. In the case of the BU90 and GBU90 test specimens with stockier cross section, comparison showed that the strength reduced from 2% to 8% as the column length increased from 500mm to 1000mm. In the case of the GBU90 test series, the moment of inertia about the y-axis was larger than the x-axis; thus the weak axis was the x-axis.

Figure 4.46 shows the comparison of test results for the BU75 and GBU75 at spacing within the code requirements at $s/L < 0.25$; while Figure 4.47 shows the comparison of test results for the BU75 and GBU75 at spacing exceeding the code requirements at $s/L > 0.50$.

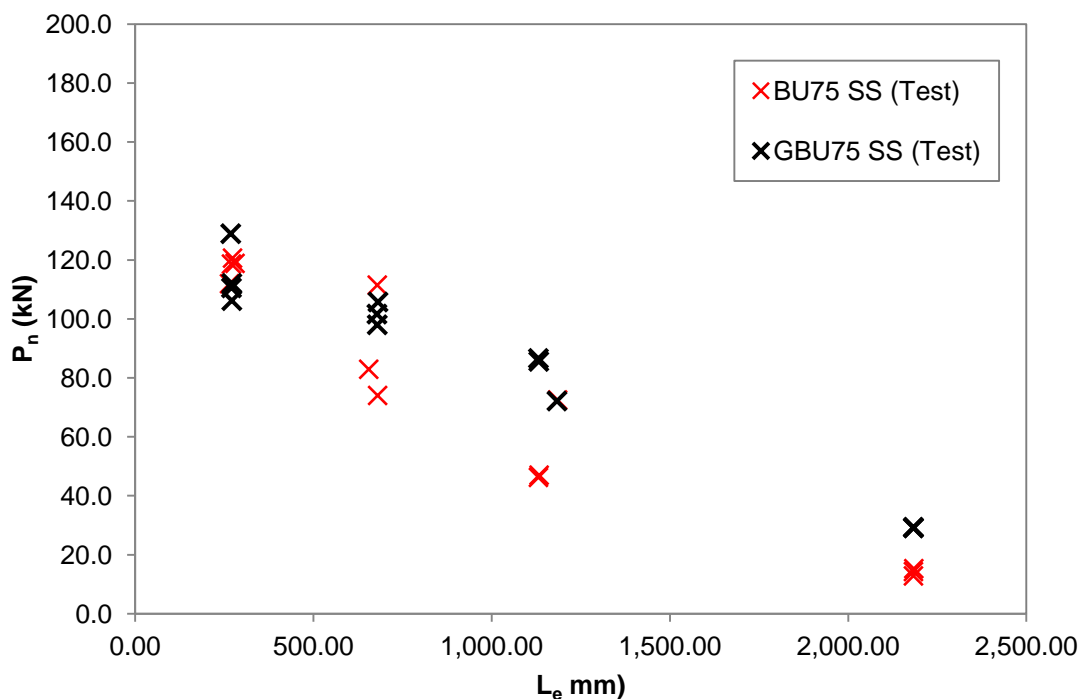


Figure 4.46: Comparison on Test Results for BU75 and GBU75 at $s/L < 0.25$

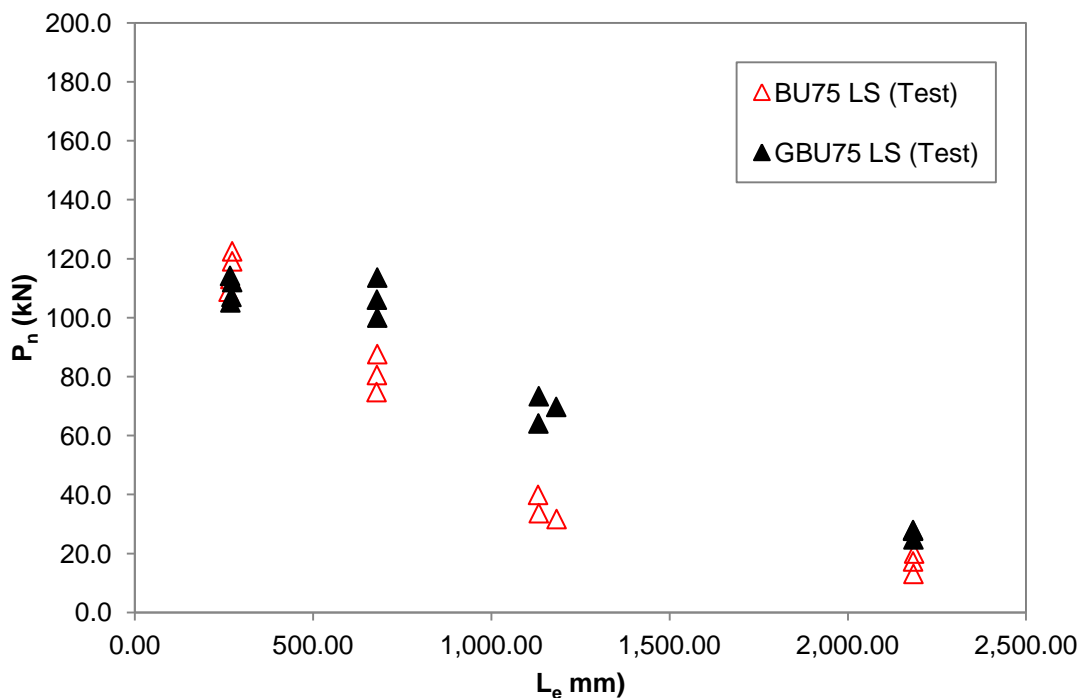


Figure 4.47: Comparison on Test Results for BU75 and GBU75 at $s/L > 0.50$

Both graphs show that the ultimate strengths achieved by the GBU75 test series are higher than the BU75 test series. As explained, test specimens from the GBU75 test series have larger second moment of inertia about the y-axis compared to test specimens from the BU75 test series. The increase in moment of inertia provided better stability and higher stiffness thus the ultimate strength of the column also increased. However, introducing the gap for the BU75 stub columns did not show similar result as the failure of stub columns is governed by yielding rather than buckling. The individual C-channels in the stub columns of BU75 test series are stiffer than the individual C-channels in the stub columns of GBU75 test series because the webs of BU75 test series are fully in contact.

On the other hand, specimens of the GBU90 test series have lower strength compared to specimens of the BU90 test series. Figure 4.48 shows the comparison of test results for the BU90 and GBU90 at spacing within the code requirements at $s/L < 0.25$; while Figure 4.49 shows the comparison on test results for the BU90 and GBU90 at spacing exceeding the code requirements at $s/L > 0.50$.

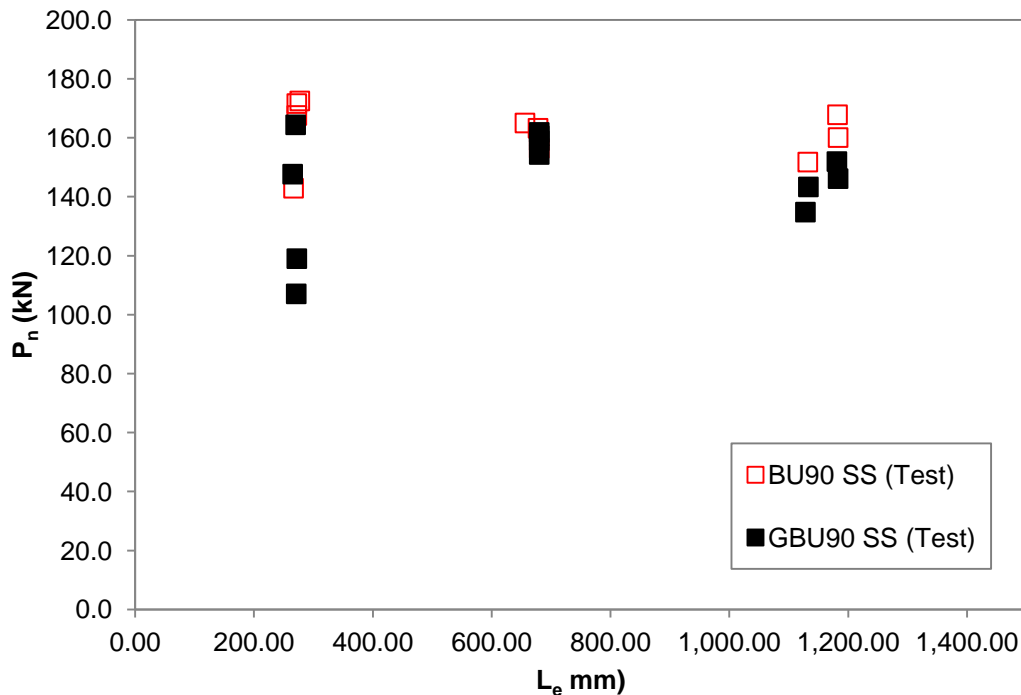


Figure 4.48: Comparison on Test Results for BU90 and GBU90 at $s/L < 0.25$

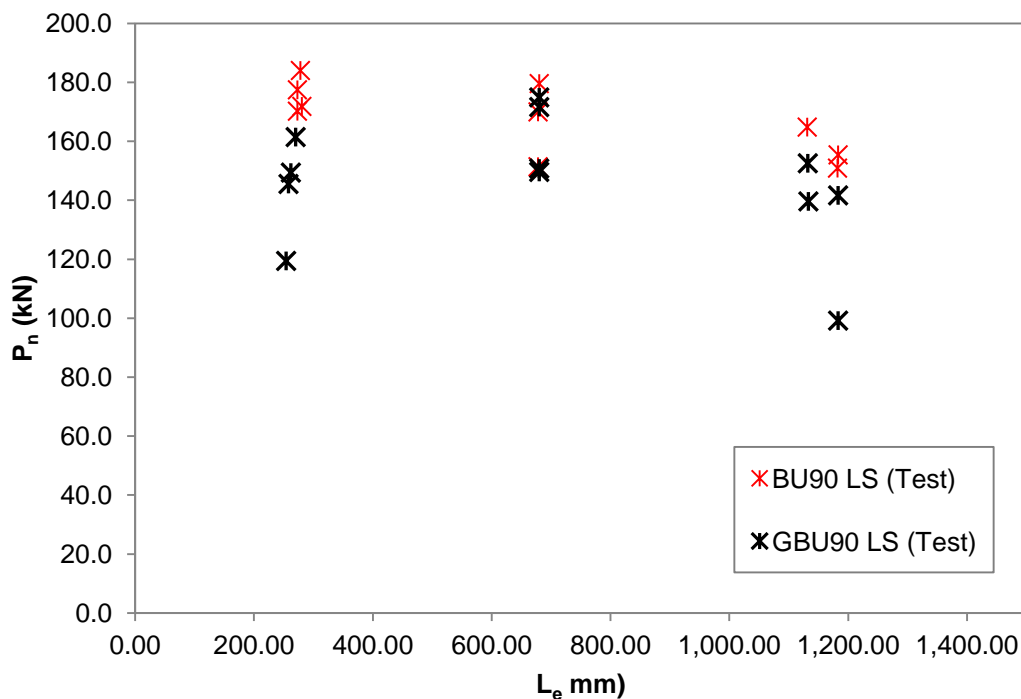


Figure 4.49: Comparison on Test Results for BU90 and GBU90 at $s/L > 0.50$

The BU90 column was equally strong in both x and y axes when there is no gap. However, the overall width of the cross section about y-axis increased when the gap was introduced. Thus, y-axis became the stronger axis rather than the x-axis. This

changed the failure mode from flexural-torsional buckling as in BU90 specimens to global buckling about the weaker axis as in GBU90 specimens. Although the experimental setup limited the test specimens to fail only about the y-axis, the test specimens tended to rotate the fabricated pinned-end assemblies towards x-axis when the axial load was applied. Thus, the specimens finally buckled in a combination of x and y-axes. It is important to note that when the test specimens of the GBU90 test series failed about the x-axis, the gap and intermediate fasteners were no longer effective in strengthening the columns. Therefore, the test results of GBU90 test series showed a decrease in strength when compared to the test results of the BU90 test series.

4.5.1 Effects of Fasteners Spacing

As the number of intermediate fasteners reduced, there were fewer restraints in a built-up column. This prevented the built-up column to act as an integral and affected the stability of the column. The effects became apparent when the fasteners spacing was beyond the AISI Specifications spacing requirements. The individual C-channels behaved individually rather than as an integral column. These columns were more susceptible to distortional and global buckling.

Moreover, results indicated that the back-to-back C-channel built-up columns with three intermediate fasteners ($s/L < 0.25$) and one intermediate fasteners ($0.25 < s/L < 0.50$) consistently achieved higher strength than built-up columns with no intermediate fasteners ($s/L > 0.50$). There was a slight reduction of built-up column strength for columns with no intermediate fasteners ($s/L > 0.50$). This further shows that when the fastener spacing is spaced beyond the AISI Specifications, the fasteners spacing does not have significant influence on the built-up column's ultimate strength.

However, the optimum fasteners spacing is difficult to assess from the results, as both the back-to-back C-channel built-up columns with three intermediate fasteners ($s/L < 0.25$) and columns with one intermediate fastener ($0.25 < s/L < 0.50$) provided the maximum ultimate strength of the columns in the compression tests.

Results show that the specimens with fastener spacing within the AISI specifications requirements (i.e. $(s/L < 0.25)$) and slightly more than the AISI specifications requirements (i.e. $(0.25 < s/L < 0.50)$) resulted in similar ultimate strength and deformed shapes for specimens with similar dimension. This indicated that an upper capacity was reached with three intermediate fasteners along the length of the built-up column. Thus, it is important to have intermediate fasteners at mid-length where maximum deflection occurs to ensure that the built-up column act as an integral unit.

4.6 Conclusions

Compression tests were conducted on C-channel columns, plain back-to-back C-channel built-up columns and back-to-back C-channel built-up columns with a gap. For stub column test, 6 C-channel specimens, 23 built-up back-to-back channels specimens and 12 built-up back-to-back channels specimens with a gap were tested at fixed end condition. A total of 15 C-channel columns, 54 back-to-back channels columns, and 30 back-to-back channels columns with a gap at short, intermediate and slender column with length of 500mm, 1000mm and 2000mm respectively were tested at pinned-end condition.

Generally, failures of the axially loaded C-channel and plain back-to-back C-channel built-up columns are governed by local buckling for stub columns, local and distortional buckling for short columns, distortional and global buckling for intermediate columns and global buckling for slender columns. As for back-to-back C-channel built-up columns with a gap, they generally failed with “S” shape or “O” shape depending on the spacing of the intermediate fasteners. It was also demonstrated by specimens with 75mm web width that columns with very slender element are inefficient in terms of strength and are prone to stability problems. Flexural-torsional buckling was observed in some of the specimens in the BU90 test series during testing due to out of plumb, imperfections of the column and frictions generated by pinned-end assemblies.

Results of the built-up column with and without a gap show that the strength of built-up columns reduced with increased fastener spacing. Comparisons also show that the ultimate strength of the GBU75 test series was higher than the BU75 test series.

The strength increment was higher as the column length increased. However, columns of the GBU90 test series achieved lower ultimate strength compared to columns of the BU90 test series due to the shift of buckling axis.

When the fastener spacing was beyond the spacing requirement of clause C4.5 of the AISI Specifications 2001 edition, the effects of fastener spacing were apparent for both back-to-back C-channel built-up columns with and without a gap. The individual C-channels behaved separately rather than as an integral column at larger spacing. These columns with larger spacing became more susceptible to distortional and global buckling effects. Therefore, it is important to have fasteners at mid-length where maximum deflection occurs to ensure that the built-up column act as an integral unit.

5 Finite Element Modelling

5.1 Introduction

This chapter explains the development of finite element model to simulate the test specimens in the compression tests carried out in the laboratory. In this research, LUSAS version 14.4 was used in the finite element analysis of cold-formed steel columns. All the results from the finite element analysis were compiled in load-deflection curves, deflected shapes, and ultimate strengths as documented in Appendix E, F, and G for C-channel column, plain back-to-back built-up column (without a gap), and back-to-back built-up column with a gap respectively.

Three different finite element models were developed to simulate C-channel columns, plain back-to-back C-channel built-up columns (without a gap), and back-to-back C-channel built-up columns with a gap. A total of 117 finite element analyses were carried out using these models to cover 22 C-channel columns, 53 plain back-to-back C-channel built-up columns (without a gap), and 42 back-to-back C-channel built-up columns with a gap for differences in cross sections. These analyses evaluated the stub columns at fixed end condition; and short, intermediate and slender columns at pinned end condition.

The finite element results were compared to the experimental results in Chapter 6 of this thesis. Results from the finite element models provided alternative solutions and improvements to the laboratory investigation as there are many constraints in the laboratory investigations. The finite element models were also essential for future parametric study in this research.

5.2 Finite Element Model

Finite element modelling of cold-formed steel members can be complicated because the finite element models are sensitive to input parameters and have a relatively high degree of nonlinearity. The finite element results are influenced by element selection, mesh discretization, boundary conditions, type of loading, geometric imperfections, residual stresses and material properties.

5.2.1 Non-linear Analysis

Geometric nonlinearity and material nonlinearity are two common nonlinearities in structural analysis. This research covers both nonlinearities in geometry and materials. LUSAS deals with nonlinearities using incremental-iterative method. In this method, a linear prediction of the nonlinear response is made within each load increment. At the same time, iterative corrections are performed to restore equilibrium by eliminating the residual or out of balance forces (FEA 2012).

5.2.1.1 Geometric Nonlinearity

The geometric nonlinearity is due to continuous and significant change in deformation of the cold-formed steel columns during loading. A Lagrangian approach is preferred in structural problems where it is required to monitor the path of a particular particle through space (FEA 2012). The geometric nonlinearity formulation, i.e. Total Lagrangian, available in LUSAS is chosen for this research because it is the most robust formulation and is capable of catering substantial load increments.

The geometric non linearity is represented with Total Lagrangian formulation in terms of the nonlinear strain-displacement relationship. The Total Lagrangian finite element formulation for a continuum is derived using the Second Piola-Kirchhoff stress tensor and the Green-Lagrange strain tensor based on the principle of virtual work. The stress measure that conjugate the Green's strain tensor is the second Piola-Kirchhoff stress tensor, S_2 , or its vector equivalent, S (Crisfield, 1991, 118-119). Using the Green's strain, the finite element formulation from a virtual work expression is given by:

$$V = V_i - V_e = \int S^T \delta E_v dV_o - V_e = \int S_2 : \delta E_{v_2} dV_o - V_e \quad \text{Eq. 5-1}$$

where V is the virtual work, S is the second Piola-Kirchhoff stress, and E is the Green-Lagrange strain.

The changes in the second Piola-Kirchhoff stress, δS is assumed to relate to the changes in Green's strain, δE via:

$$\delta S = C_{i2} \delta E, \quad \delta S_2 = C_{i4} \delta E_2 \quad \text{Eq. 5-2}$$

where the first form involves a matrix or second order constitutive tensor, C_2 , while the second form involves a fourth order constitutive tensor C_4 .

Hence, Eq. 5-1 becomes:

$$\delta V = \int (\delta E_{v_2} : C_{t_4} : \delta E_2 + S : \delta D_v^T \delta D) dV_o = \int (\delta E^T C_{t_2} \delta E + S^T \delta(\delta E_{v_2})) dV_o \quad \text{Eq. 5-3}$$

5.2.1.2 Material Nonlinearity

The material nonlinearity is due to the plastic behaviour of cold-formed steel. The elasto-plastic models used for the material nonlinearity in this research is von Mises plastic model which is available in LUSAS. The von Mises plastic model was chosen because it is widely accepted for modelling ductile materials as it exhibits little volumetric plastic strain (FEA 2012). The criterion is based on considerations of distortional strain energy. The yield function is defined as:

$$F(\sigma \cdot \kappa) = \bar{\sigma} - \kappa(\bar{e}^p) = 0 \quad \text{Eq. 5-4}$$

where the equivalent, generalised of effective stress is defined as:

$$\bar{\sigma} = \sqrt{3}(J_2)^{\frac{1}{2}} \quad \text{Eq. 5-5}$$

where κ is the state variable dependent upon equivalent plastic strain \bar{e}^p and J_2 is the second stress invariant.

The von Mises yield criterion is defined by hardening curve using the coordinate data from the actual stress strain curve. This actual stress strain curve was plotted based on the tensile coupon test results as documented in Section 3.2.

5.2.2 Element Type

Shell type elements were selected for simulations because cold-formed steel members are made from thin steel sheets. This element type accounts for finite membrane strains and arbitrarily large rotations. Therefore, it is suitable for large-strain analyses and geometrically non-linear analyses as required by this research. The finite element model was created using a linear 4-node quadrilateral thick shell element (QTS4) as shown in Figure 5.1.

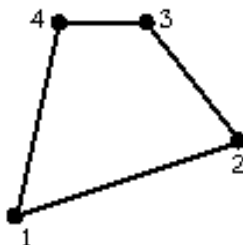


Figure 5.1: Linear 4-node Quadrilateral Thick Shell Element (FEA 2012)

QTS4 is a stiffened shell structure that accommodates curved geometry which allows curves at the corners of the steel column. QTS4 formulation accounts for membrane,

shear and flexural deformations. This element uses three translational and three rotational degrees of freedom at each node. QTS4 being quadratic elements allow greater flexibility in meshing the LUSAS model of curved (at corner) and straight elements. QTS4 also ensures that logical results are obtained using Total Lagrangian formulation. Most importantly, QTS4 is one of the few elements that allow the use of slideline function which is critical for surface contact analysis.

5.2.3 Convergence Study

The finite element analysis result is influenced by the element size of the finite element model. Finer mesh improves solution accuracy at the expense of higher computing time. In order to choose an optimum mesh size, convergence study was carried out on C-channel column specimens C07512 at stub, short, intermediate and slender conditions. Imperfections were not included in the model for the convergence study. Four different mesh configurations of (i) 2mm by 2mm, (ii) 5mm by 5mm, (iii) 10mm by 10mm and (iv) 15mm by 15mm were used. The mesh configurations are illustrated in Figure 5.2 below.

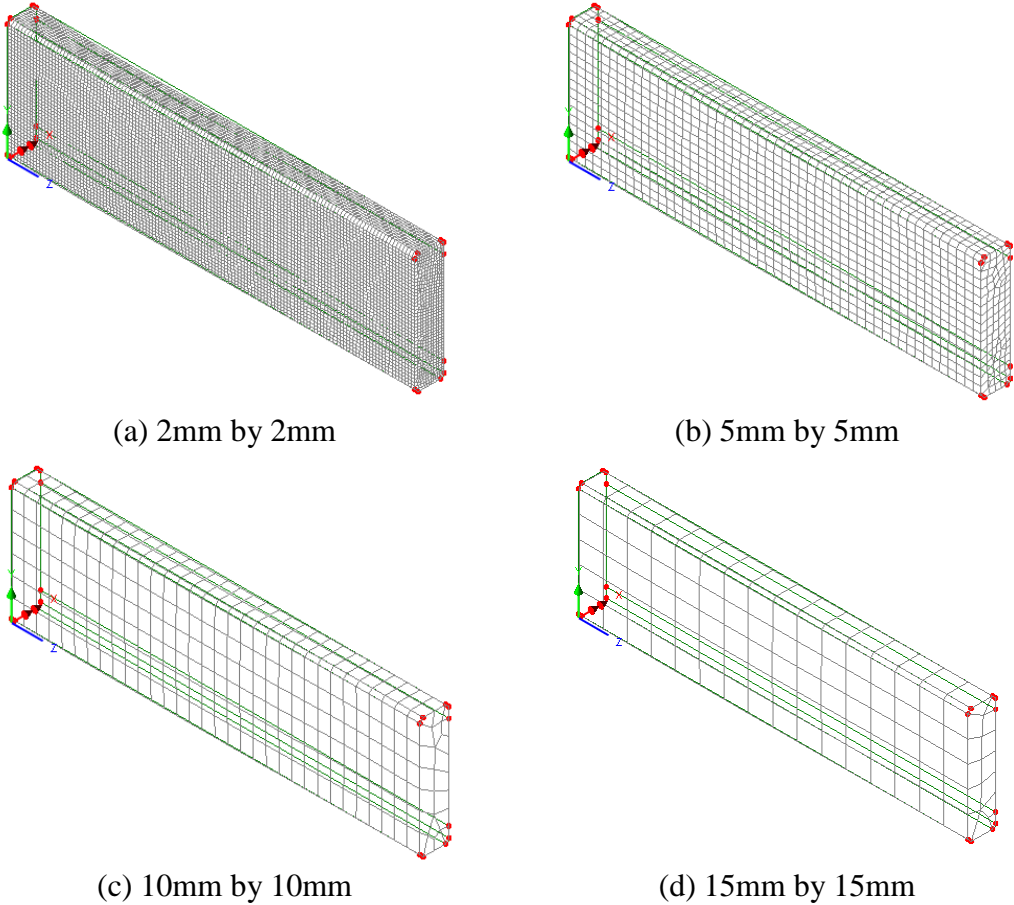


Figure 5.2: Examples of LUSAS Model at Different Mesh Configurations

Tables 5.1 to 5.4 show the results from the convergence study. The study shows that as the number of elements increases, differences between the results from different mesh sizes are small. In this research, a 6% difference was targeted. Thus, 5mm by 5mm mesh size was chosen for the finite element analysis of stub columns; while, 15mm by 15mm mesh size was appropriate for the finite element analysis of all other columns.

Element Size (mm)	Number of Elements	Ultimate Load (kN)	% Difference (2x2 as Reference)
15x15	208	50.69	14.6%
10x10	425	48.13	8.8%
5x5	1550	45.58	3.1%
2x2	8875	44.23	-

Table 5.1: Finite Element Results for C75L300 at Different Mesh Size

Element Size (mm)	Number of Elements	Ultimate Load (kN)	% Difference (2x2 as Reference)
15x15	600	41.09	6.1%
10x10	1020	40.47	4.5%
5x5	3720	39.50	2.0%
2x2	21300	38.74	-

Table 5.2: Finite Element Results for C75L500 at Different Mesh Size

Element Size (mm)	Number of Elements	Ultimate Load (kN)	% Difference (2x2 as Reference)
15x15	990	15.88	2.1%
10x10	1700	15.81	1.6%
5x5	6200	15.63	0.4%
2x2	35500	15.56	-

Table 5.3: Finite Element Results for C75L1000 at Different Mesh Size

Element Size (mm)	Number of Elements	Axial Load (kN)	% Difference (2x2 as Reference)
15x15	1995	5.39	6.1%
10x10	3400	5.24	3.1%
5x5	12400	5.14	1.2%
2x2	71000	5.08	-

Table 5.4: Finite Element Results for C75L2000 at Different Mesh Size

5.2.4 Surface Contact

The web of the individual C-channels of built-up columns were in contact when fastened together in a back-to-back manner. The surface-to-surface contact between the outside surfaces of the two webs needs to be defined in the finite element model so that the individual C-channels interact with each other during the loading process.

LUSAS offers a unique slideline function to model the surface contact behaviour between two or more bodies. The contact problem is equivalent to an inequality constrained minimisation. The minimisation of the total potential energy of the system, Φ is subject to the inequality constraint: $g_N \geq 0$, where g_N is the normal penetration of a node N. A node is in contact if g_N is negative and out of contact if g_N is greater than or equal to zero. The problem is solved by minimising the incorporation of the constraint into the function, thus, converting the constrained minimisation into one which is unconstrained. The minimisation is done using the Newton Raphson method.

It is beneficial to model the surface contact behaviour using slideline function because no prior knowledge of the exact surface contact is required. The ability of the slideline function to model surface contact was demonstrated in Butterworth (1999, 1-14) on the extension of end plates from column flange. In his numerical study, tied slidelines were used to model the interface between the end plate and the column flange. His finite element model was verified with five full scale tests which were conducted using the self-straining frame. His finite element results predicted the strength and the behaviour of the end plate and the column flange well.

In this research, the surface-to-surface contact of the built-up columns is defined between the outside surfaces of the webs of the two individual C-channels. One of the web surfaces is defined as a master surface while the other as a slave surface as shown in Figure 5.3.

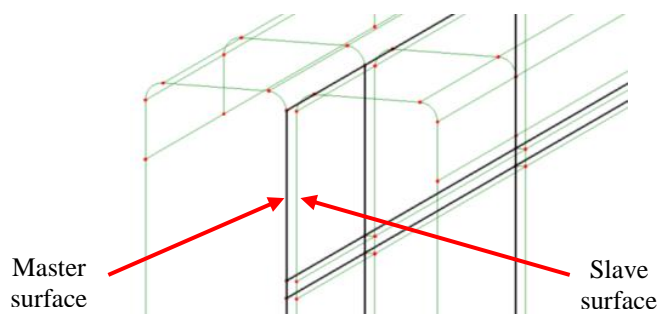


Figure 5.3: Surface Contact Analysis using Slideline

5.2.5 Intermediate Fasteners

It was assumed that the individual C-channels in a built-up column were in contact at locations connected by screws. The screw connections were not explicitly modelled in this research. Instead, a simplified model of a 2mm thin strip was used to connect two lipped C-channels together as shown in Figure 5.4 to ensure that the channels remained in contact with each other at discrete points over the entire load history.

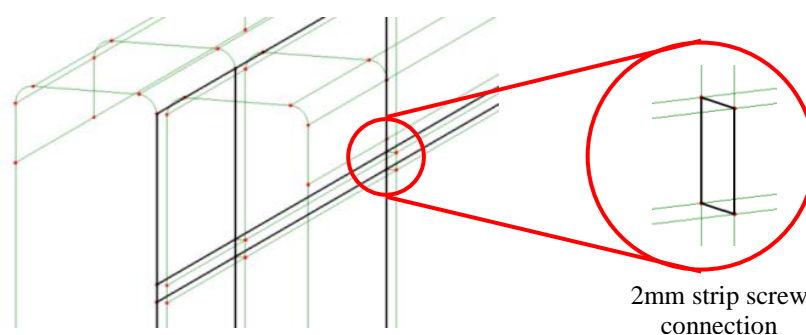


Figure 5.4: Simplified Screw Connections

Screw connections were modelled using 2mm thin strip elements. The locations where these elements are introduced as intermediate fasteners were determined using “sweep” function in LUSAS. This “sweep” function was used to offset the existing cross section to the location of the screw connections. For back-to-back C-channel built-up models with a gap, the distance of the sweep depended on the fasteners spacing along the length of the column.

An additional step was carried out to duplicate the intermediate connectors, known as short C-channels in this research, along the length of the column for back-to-back C-channel built-up column with a gap. After the duplication of these short C-channels,

these 2mm thin strips are then used to connect the short C-channels and the two individual C-channel columns together.

5.2.6 Boundary Conditions

The boundary conditions used in the model represented the end conditions in the experimental tests. Stub columns were tested at fixed-end conditions, while all other columns were tested using the fabricated pinned-end assemblies. In the finite element models, the end conditions were modelled as either pure fixed or pure pinned.

For fixed end condition, the boundary condition was applied to both ends of the stub columns as shown in Figure 5.5. The fixed end boundary conditions at the end of the stub column were fixed against all degrees of freedom, except for the vertical displacement where the axial load is applied. This allowed the stub column to shorten in the direction of the applied load.

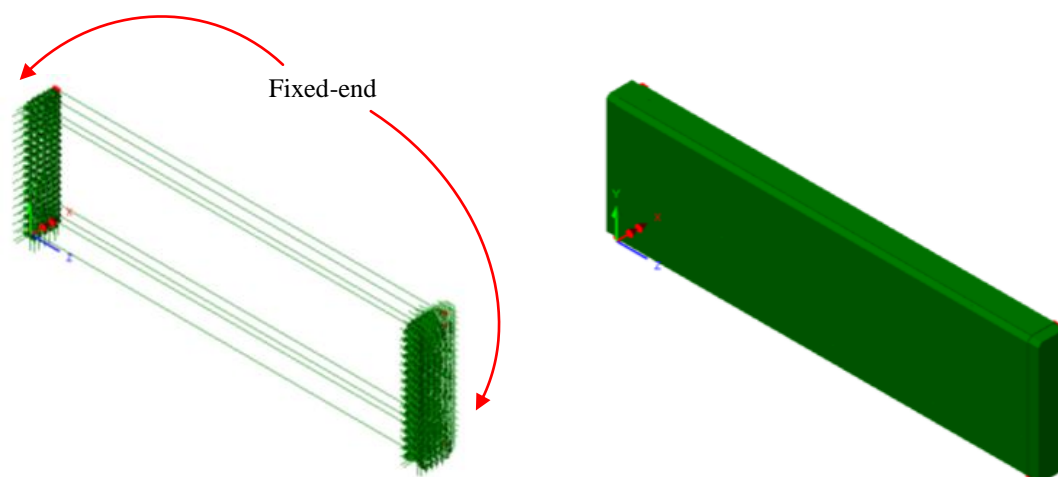


Figure 5.5: Fixed End Condition in LUSAS

Pinned end conditions were achieved by means of fabricated hinge assemblies at top and bottom ends in the experimental test. The distance between the centre of the pin and the top surface of the hinge assembly was 65mm. The effective length of the test specimens is the sum of the specimen length, L and the distance from the specimen end plates to the top surface of the hinge assembly. Therefore, a simplified model which included the 65mm depth as shown in Figure 5.6 was modelled instead of modelling the hinge assemblies. In the experiment, specimens were allowed to rotate in the weak axis i.e. y -axis only. Thus, a rotation axis across the weak axis at the centroid of the specimen's cross section was created to simulate the pinned end boundary condition.

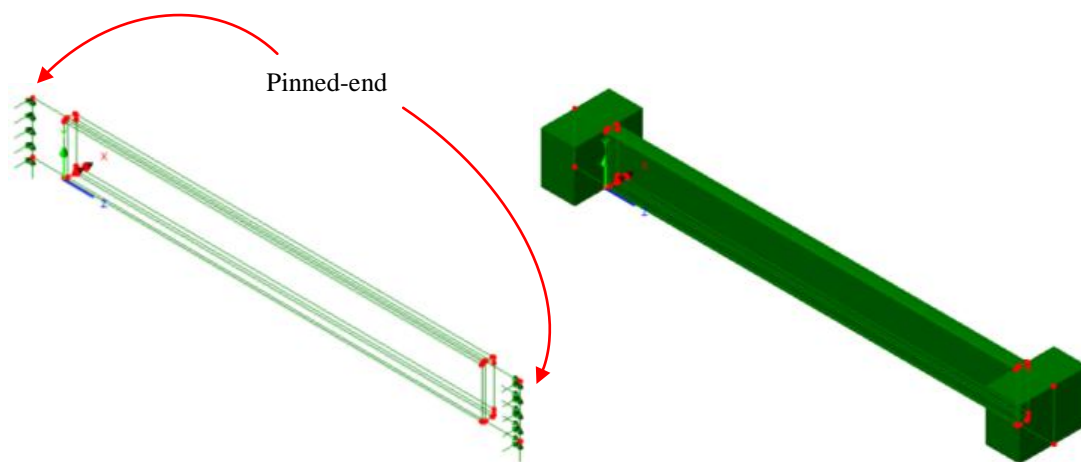


Figure 5.6: Pinned End Condition in LUSAS

5.2.7 Imperfections

The actual imperfections of the test specimens were simplified by using equivalent geometrical imperfections for the finite element models. The initial deformed shape was obtained from the linear buckling analysis of a perfect model to model the initial imperfections of the test specimens. The nonlinear buckling analysis was then performed on this initially deformed shape. Both linear and non-linear analysis model must use the same attributes such as mesh, dimensions and etc. to ensure that the deformed shape from linear analysis could be analysed in the non-linear analysis. The imperfections from the linear deformed shape were required to be scaled to the maximum imperfections measured from the test specimens. The factored deformed shape was then used as the initial mesh for nonlinear buckling analysis. Figure 5.7 shows the deformed shape of the column from linear analysis.

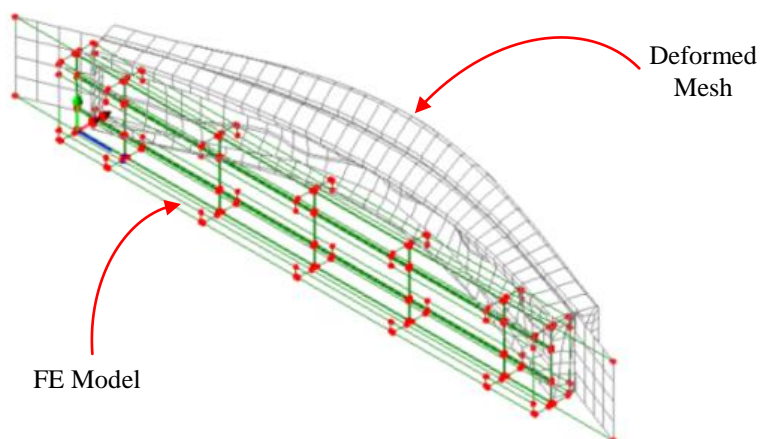
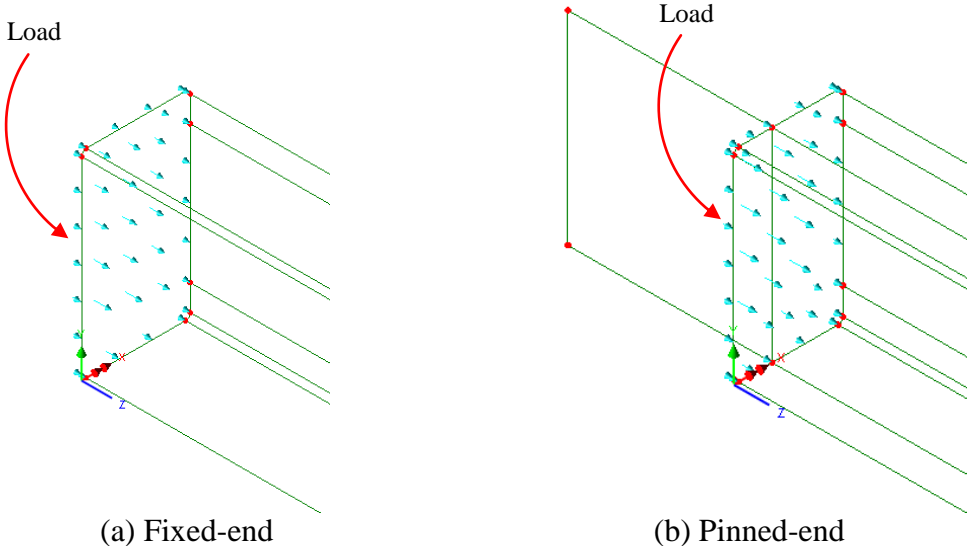


Figure 5.7: Deformed Shape (Scaled to 0.1) from Linear Buckling Analysis

5.2.8 Loading

The load was applied at the top end of the specimen where displacements in the direction of the applied load were allowed. Automated increment of 1kN is applied uniformly through the centroid of the column's cross section as shown in Figure 5.8.



*Note: The green arrows indicate the applied load.

Figure 5.8: Loading in LUSAS

5.3 Modelling Procedure

Figure 5.9 shows the summary of the processes in the finite element modelling using LUSAS version 14.4.

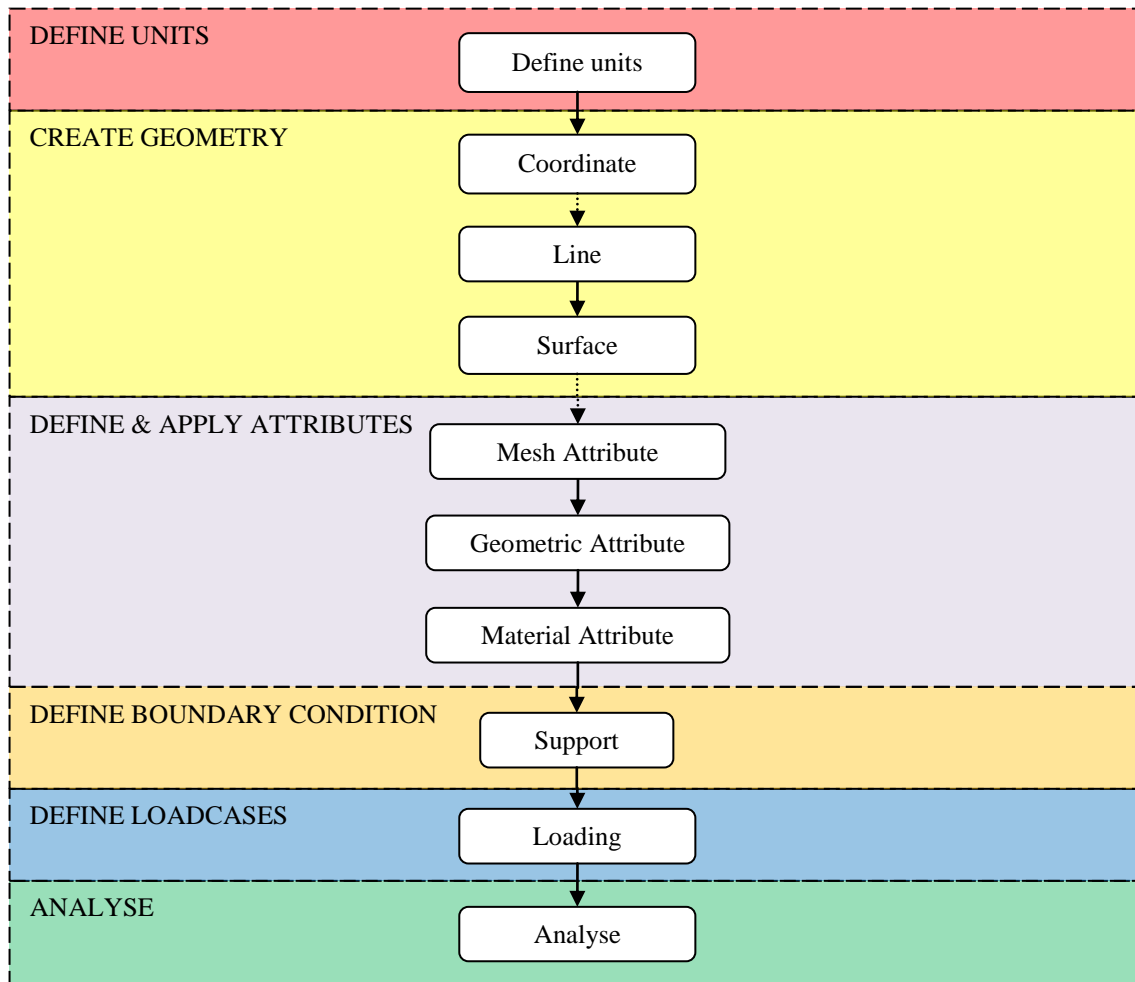


Figure 5.9: Modelling Procedures using LUSAS version 14.4

5.4 Conclusions

A total of 117 C-channel and built-up columns were successfully modelled at stub, short, intermediate and slender lengths. These columns were modelled using the actual material properties. The essential aspects in modelling built-up columns were the modelling of surface contact and screw connections. In terms of surface contact, QTS4 shell elements were used to enable the slideline function for surface contact analysis. Simplified 2mm strips were used to model the screw connections in built-up columns. The typical finite element models of the three types of columns used in this research are shown in Figure 5.10.

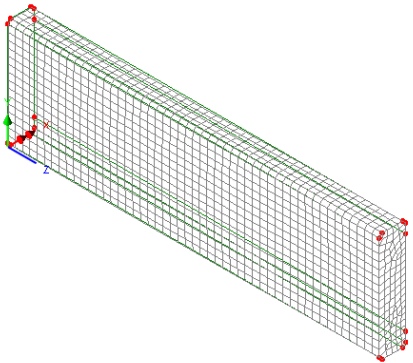
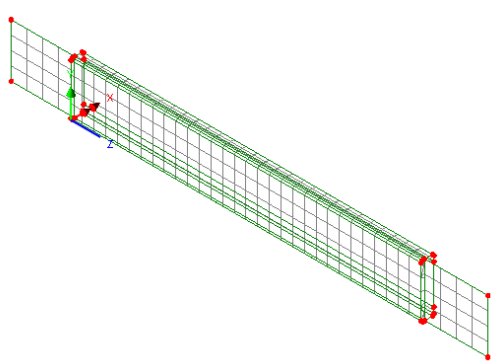
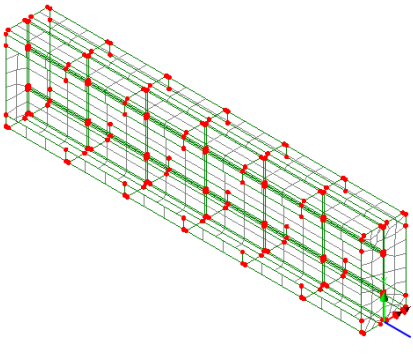
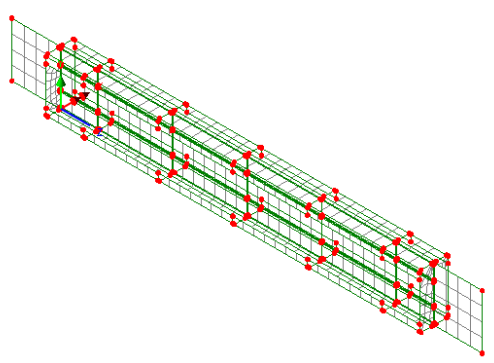
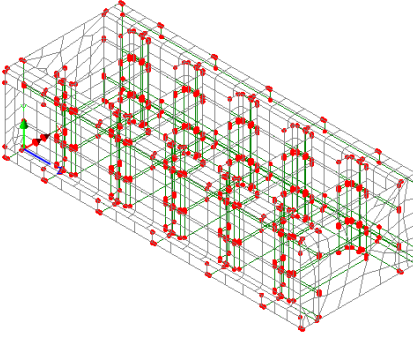
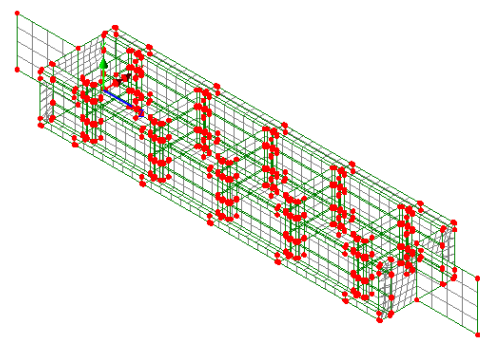
Type	Fixed-end	Pinned-end
C		
BU		
GBU		

Figure 5.10: Typical Finite Element Models

6 Finite Element Analysis

6.1 Introduction

A comparison of the results from the finite element modelling against the laboratory test results is presented here. The sections compared include: C-channel section, plain back-to-back C-channel built-up section (without a gap) and back-to-back C-channel built-up section with a gap. The finite element results are obtained from analysing the finite element models using LUSAS version 14.4 as shown in Chapter 5, whereas the test results are from experimental investigation as shown in Chapter 3 and reported in Chapter 4.

The C-channel model was evaluated with the results from 22 numbers of tested C-channel columns, where 8 specimens were tested with fixed end condition and 14 specimens were tested with the pinned end condition. The plain back-to-back C-channel built-up model (without a gap) was also evaluated with the test results from 52 numbers of specimens with 17 specimens at fixed end condition and 35 specimens at pinned end condition. As for back-to-back C-channel built-up model with a gap, it was evaluated with test results from 40 numbers of specimens with 11 specimens at fixed end condition and 29 specimens at pinned end condition.

The results from finite element analysis and experimental investigation were evaluated by comparing the failure modes, the graph of load against shortening, and the graph of load against deformation at several locations such as mid-height, one-third from bottom, and flange and lips at mid-height. The finite element models are modelled based on average measured dimension and the dimensions are assumed to be constant along the cross section.

6.2 Ultimate Strength

The ultimate strength of the test specimens is defined as the maximum load achieved under the axial compression load in this research. These ultimate strengths can be determined from the graph of load against deformation. All the graphs of load against deformation for test and finite element results are documented in the Appendices.

6.2.1 C-channel Columns

C-channel model were evaluated by the test results of 22 numbers C-channel columns. All the experimental results and finite element results are compared and documented in Appendix E.

Table 6.1 summarises the comparison between the ultimate strength obtained from experimental analysis and from the finite element analysis with the LUSAS model.

Table 6.1: Comparison of Test Results and FE for C-channel Columns

Specimen	P_{test} (kN)	P_{FE} (kN)	$\frac{P_{test}}{P_{FE}}$	Specimen	P_{test} (kN)	P_{FE} (kN)	$\frac{P_{test}}{P_{FE}}$
C75L300-1	60.63	50.66	1.20	C90L300-1	Discard		
C75L300-2	58.24	50.79	1.15	C90L300-2	83.70	88.91	0.94
C75L300-3	59.91	50.75	1.18	C90L300-3	86.12	88.23	0.98
C75L300-4	55.70	50.85	1.10	C90L300-4	86.70	88.21	0.98
Mean			1.15	Mean			0.97
C75L500-1	Discard			C90L500-1	82.84	83.89	0.99
C75L500-2	52.07	43.65	1.19	C90L500-2	81.20	86.12	0.94
C75L500-3	53.01	41.24	1.29	C90L500-3	78.04	85.69	0.91
C75L500-4	40.13	43.81	0.92	-			
Mean			1.13	Mean			0.95
C75L1000-1	15.80	10.89	1.45	C90L1000-1	84.95	99.67	0.85
C75L1000-2	16.38	10.89	1.50	C90L1000-2	86.94	99.50	0.87
C75L1000-3	Discard			C90L1000-3	70.79	101.37	0.70
Mean			1.48	Mean			0.81
C75L2000-1	7.49	4.56	1.64				
C75L2000-2	6.79	4.46	1.52				
C75L2000-3	9.83	4.49	2.19				
Mean			1.78				

*Overall Mean = 1.15,

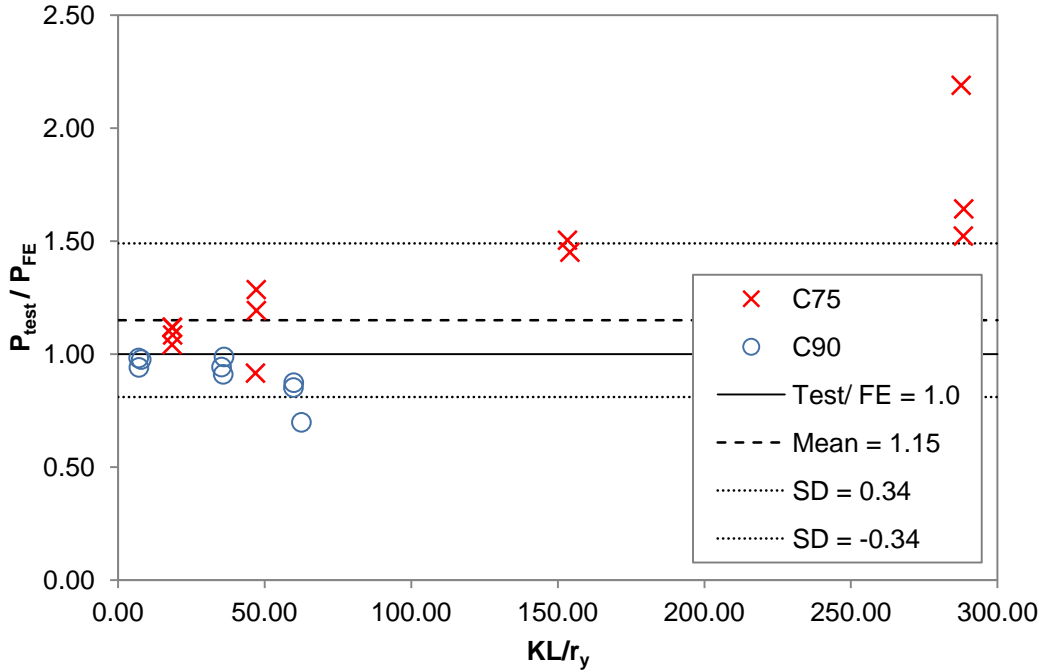
*Overall Population Standard Deviation = 0.34

The results show that the C75 finite element model predicts the capacity of the columns conservatively compared to the test results with the P_{test}/P_{FE} ratio greater than 1.0. Comparison shows that the P_{test}/P_{FE} ratios are higher for longer columns compared to shorter columns of the C75 test series. The P_{test}/P_{FE} ratio is 1.15, 1.13, 1.48, and 1.78 for the C75L300, C75L500, C75L1000, and C75L2000 respectively. The finite element model is conservative in predicting the column strength of the C75 test series. However, in the finite element model, the end conditions were modelled as pure pinned which is of a higher degree of freedom compared to the actual condition in the testing. Therefore, the finite element results are lower than the test results for the C75 test series.

On the other hand, the C90 test series results are less conservative compared to the results from the C75 test series with the P_{test}/P_{FE} ratio lesser than 1.0. The P_{test}/P_{FE} ratio of the C90 test series is 0.97, 0.95, and 0.87 for the C90L300, C90L500, and C90L1000 respectively. The finite element model is unconservative in predicting the column strength of the C90 test series because the inefficiency of the bottom pinned-end assembly caused the test specimens from the C90 test series to fail earlier than expected during testing.

Overall, this finite element model conservatively predicted the C-channel columns of the C75 and C90 test series with an average P_{test}/P_{FE} ratio of 1.15 and a standard deviation of 0.34.

The comparison of the ultimate strength obtained from experimental investigation and finite element model is also presented in Figure 6.1.

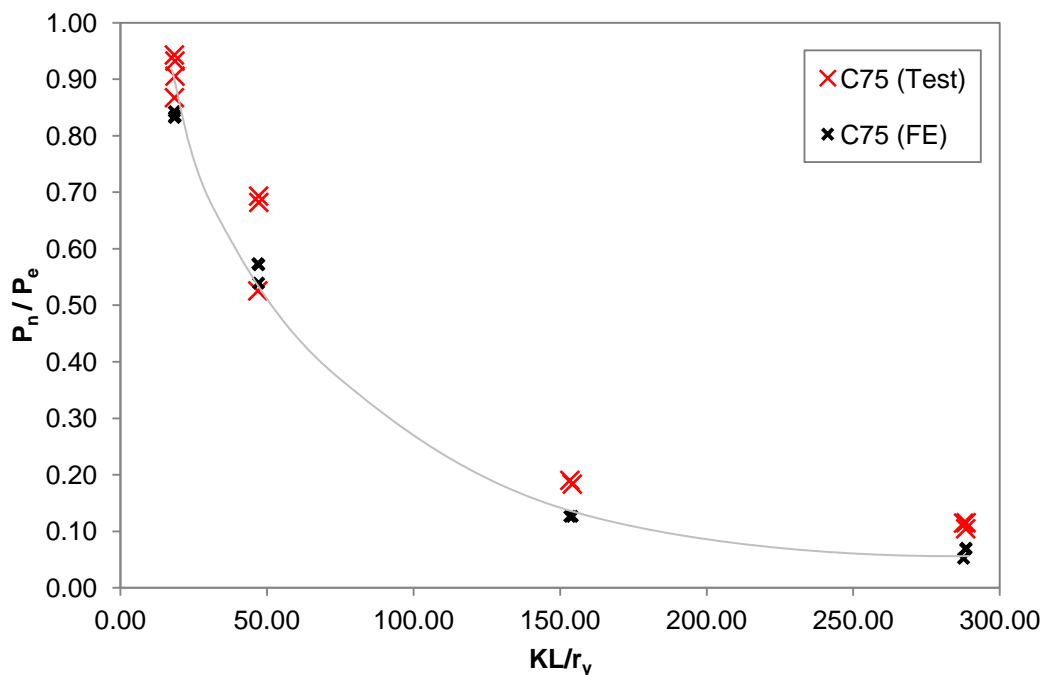


*Note: K = 0.5 for fix, 1.0 for pin, r_y (nominal) = 7 for C75, 19 for C90

Figure 6.1: Graph of FE and Test Results for C-channel Columns

It can be seen that the distribution of the P_{test}/P_{FE} ratio falls within the standard deviation except for the slender columns as the friction in the pinned-end assemblies caused the C75L2000 slender columns to behave more like a fixed-end column. The pinned-end assemblies were unable to rotate due to this high resistance. Moreover the C75L2000 slender columns failed at a low ultimate load and were unable to overcome the friction resistance. Thus, the rotation only occurred after ultimate load was reached when visible global buckling was observed.

Figure 6.2 shows the comparison of the ultimate strength against member slenderness ratio for the C75 test series. The ultimate strength, P_n was normalised by dividing it with the effective strength, P_e . The effective strength, P_e was obtained by the product of yield stress and the effective area calculated using the equations from the AISI specifications, i.e. $F_y A_e$.

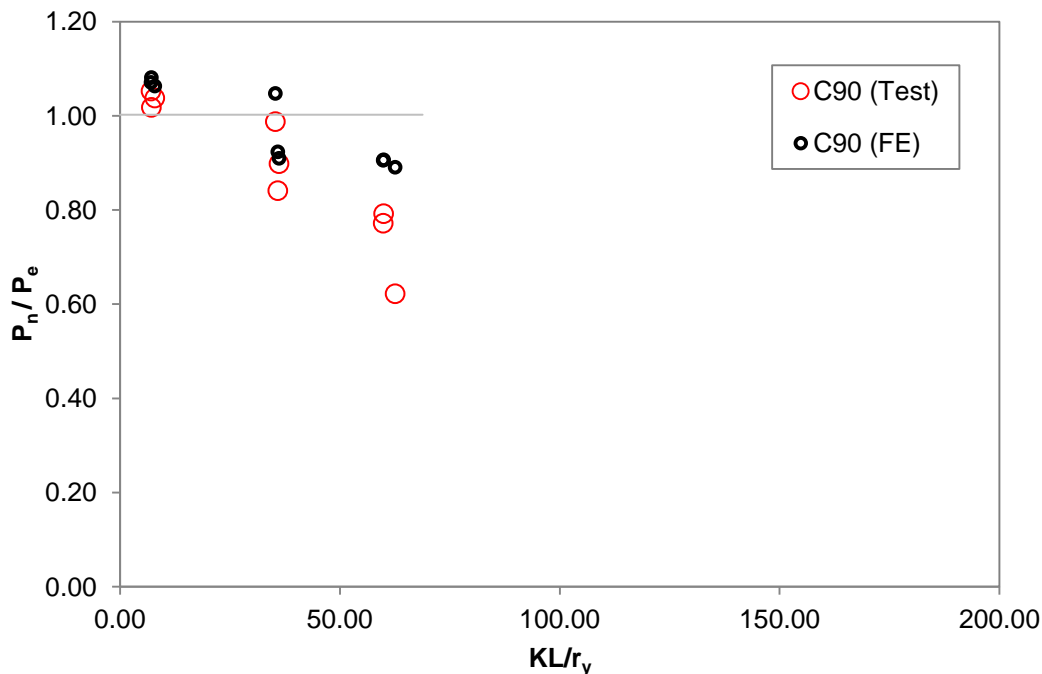


*Note: K = 0.5 for fix, 1.0 for pin, r_y (nominal) = 7 for C75

Figure 6.2: Comparison between FE and Test Results for C75

The graph shows that the finite element results are lesser than the experimental results thus is generally conservative. Moreover, the ultimate strength reduced as the column length increased with the P_y/P_e ratio close to 1.0 at stub column length.

Similarly, the graph of the ultimate strength against member slenderness ratio for the C90 test series is plotted in Figure 6.3.



*Note: K = 0.5 for fix, 1.0 for pin, r_y (nominal) = 19 for C90

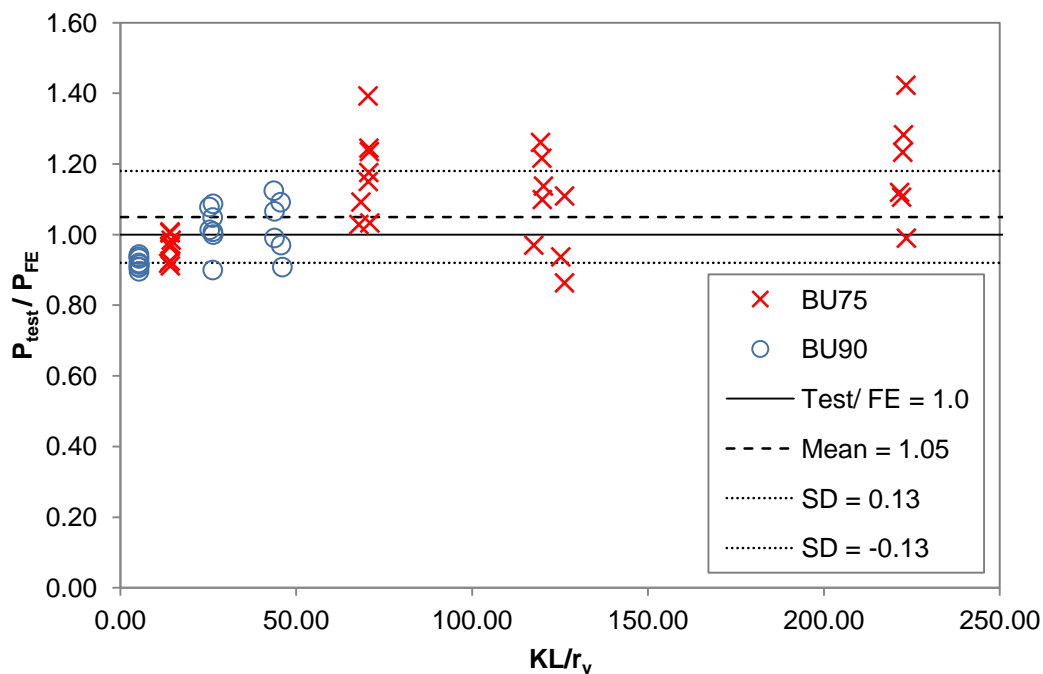
Figure 6.3: Comparison between FE and Test Results for C90

The graph shows that the finite element results are generally higher than the test results for the C90 test series. Similarly, the ultimate strength of the C75 test series reduced as the column length increased. However, the strength reduction was not as significant as the C75 test series because the column lengths were relatively short. Due to the short column length, the P_y/P_e ratios are generally close to 1.0. The P_y/P_e ratios are greater than 1.0 at stub column length because the effective area, A_e was conservatively estimated using the equations from the AISI specifications.

6.2.2 Plain Back-to-back C-channel Built-up Columns

Plain back-to-back C-channel built-up column models were evaluated by the test results of 52 numbers of plain back-to-back C-channel built-up columns. All the experimental results and finite element results were compared and documented in Appendix F.

The comparison of the ultimate strength of the plain back-to-back C-channel built-up columns obtained from experimental investigation and finite element model are presented in Figure 6.4.



*Note: K = 0.5 for fix, 1.0 for pin, r_y (nominal) = 9 for BU75, 26 for BU90

Figure 6.4: Graph of FE & Test Results for BU Test Series

The graph shows that in most cases, the finite element results correlate well with the test results. The graph also shows that predictions are more conservative for slender columns compared to predictions for shorter columns.

Table 6.2 tabulates the comparison of the ultimate strengths for the BU75 plain back-to-back C-channel built-up columns from the experimental investigation and also from the finite element analysis of the LUSAS model.

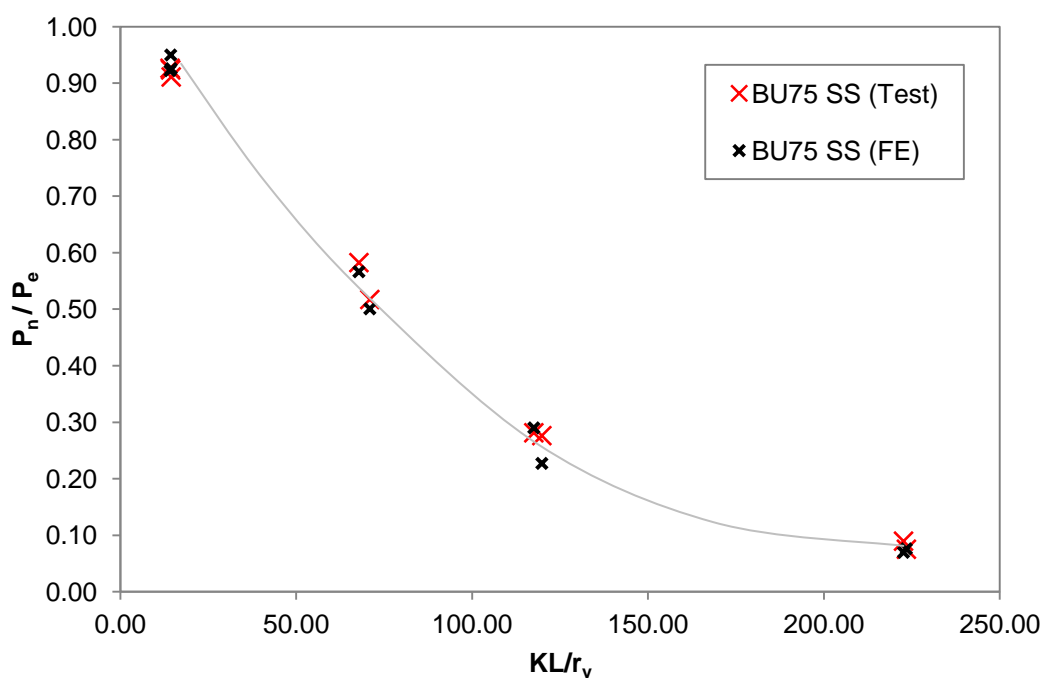
Table 6.2: Comparison between FE Results & Test Results for BU75

Specimen No.	s/L < 0.25			Specimen No.	0.25 < s/L < 0.50			Specimen No.	s/L > 0.50		
	P _{test} (kN)	P _{FE} (kN)	$\frac{P_{test}}{P_{FE}}$		P _{test} (kN)	P _{FE} (kN)	$\frac{P_{test}}{P_{FE}}$		P _{test} (kN)	P _{FE} (kN)	$\frac{P_{test}}{P_{FE}}$
BU75S50L300-1	120.66	120.13	1.05	BU75S100L300-1	Discard			BU75S200L300-1	122.51	121.56	1.01
BU75S50L300-2	118.87	126.74	0.94	BU75S100L300-2	117.48	127.00	0.93	BU75S200L300-2	119.12	123.23	0.97
BU75S50L300-3	118.65	122.04	0.97	BU75S100L300-3	122.74	127.03	0.97	BU75S200L300-3	113.14	123.17	0.92
-				BU75S100L300-4	115.37	126.58	0.91	-			
Mean			0.99	Mean			0.93	Mean			0.96
BU75S100L500-1	82.96	80.66	1.03	BU75S200L500-1	86.21	78.93	1.09	BU75S400L500-1	74.77	65.01	1.15
BU75S100L500-2	Discard			BU75S200L500-2	88.93	72.01	1.23	BU75S400L500-2	80.56	64.72	1.24
BU75S100L500-3	74.07	71.70	1.03	BU75S200L500-3	93.61	79.62	1.18	BU75S400L500-3	87.64	62.94	1.39
Mean			1.03	Mean			1.17	Mean			1.26
BU75S225L1000-1	47.04	48.49	0.97	BU75S450L1000-1	50.43	39.99	1.26	BU75S900L1000-1	39.90	36.60	1.10
BU75S225L1000-2	46.28	38.05	1.22	BU75S450L1000-2	45.02	39.58	1.14	BU75S900L1000-2	33.70	35.97	0.94
BU75S225L1000-3	Discard			BU75S450L1000-3	41.77	37.65	1.11	BU75S900L1000-3	31.48	36.46	0.87
Mean			1.10	Mean			1.17	Mean			0.97
BU75S475L2000-1	Discard			BU75S950L2000-1	Discard			BU75S1900L2000-1	Discard		
BU75S475L2000-2	15.33	11.95	1.28	BU75S950L2000-2	13.22	10.72	1.23	BU75S1900L2000-2	12.12	10.96	1.11
BU75S475L2000-3	12.87	13.00	0.99	BU75S950L2000-3	12.99	9.13	1.42	BU75S1900L2000-3	13.11	11.71	1.12
Mean			1.14	Mean			1.33	Mean			1.12

*(BU75) Overall mean = 1.09; *Population standard deviation = 0.14

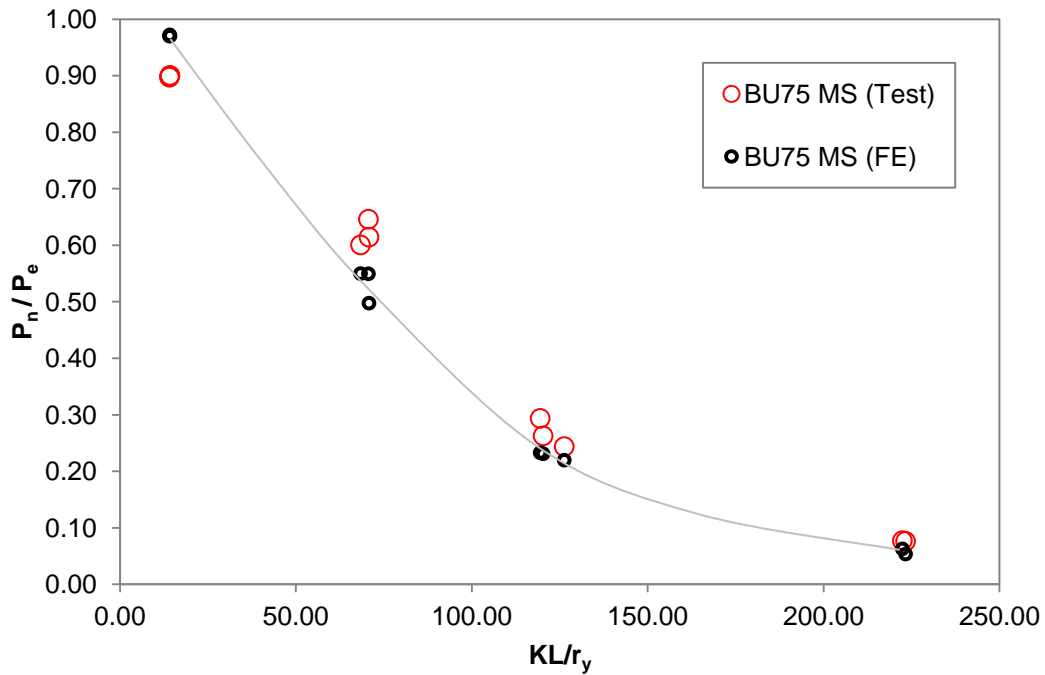
The averaged P_{test}/P_{FE} ratio is 1.09 with a standard deviation of 0.14 for the BU75 test series. The P_{test}/P_{FE} ratios of the BU75 test series are generally lower than 1.0 at shorter columns compared to slender columns regardless of the fastener spacing. This shows that the finite element model of BU75 test series is unconservative in predicting the stub column strength as the finite element model has fix-ended condition with less degree of freedom compared to the fix-ended condition in the actual testing. However, the finite element results are lower for all other pinned-end columns because in the actual testing there are frictions resistance in the pinned-end assemblies.

Figures 6.5, 6.6, and 6.7 present the load against member slenderness ratio for the BU75 with fastener spacing at $s/L < 0.25$, $0.25 < s/L < 0.50$, and $s/L > 0.50$ respectively. The graphs compare the ultimate strength predicted by the finite element model with the test results for plain back-to-back C-channel built-up columns at different spacing.



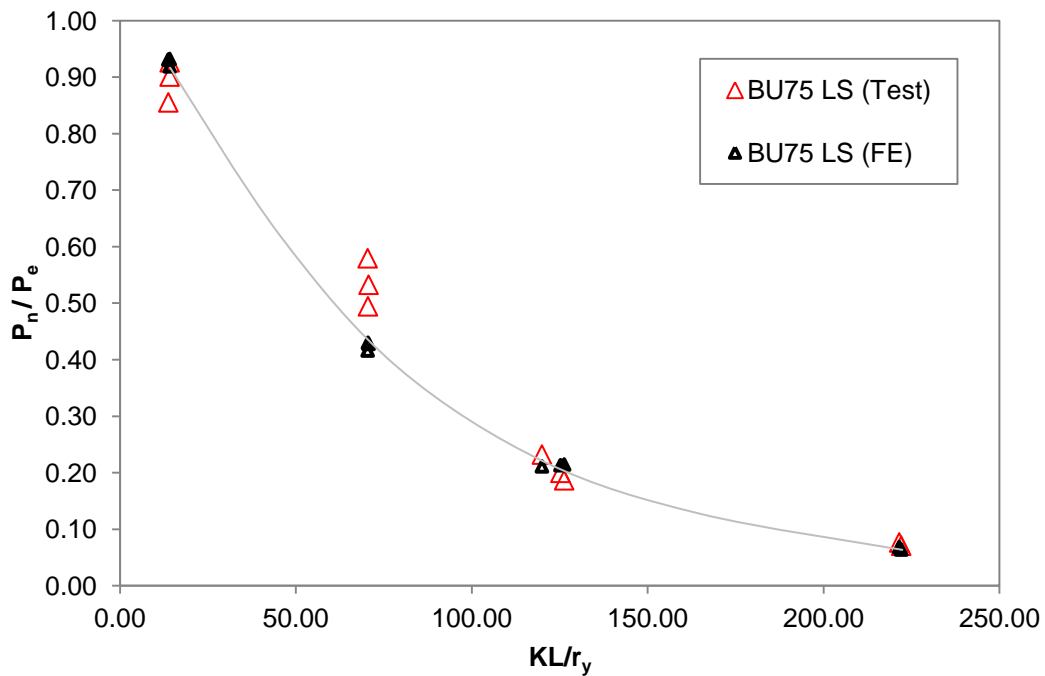
*Note: $K = 0.5$ for fix, 1.0 for pin, r_y (nominal) = 9.43 for BU75

Figure 6.5: Graph of FE & Test Results for BU75 at $s/L < 0.25$



*Note: K = 0.5 for fix, 1.0 for pin, r_y (nominal) = 9.43 for BU75

Figure 6.6: Graph of FE and Test Results for BU75 at 0.25 < s/L < 0.50



*Note: K = 0.5 for fix, 1.0 for pin, r_y (nominal) = 9.43 for BU75

Figure 6.7: Graph of FE & Test Results for BU75 at s/L > 0.50

All the graphs show that, the P_n/P_e ratios are close to 1.0 for stub column length and gradually decrease for longer column length, similar to the C75 test series in section 6.2.1. Generally, the finite element results for stub columns from the BU75 test series is greater than test results, while the finite element results for all other columns from the BU75 test series are lower than test results. This is because the actual end condition of the stub columns was not fully fixed and the actual end condition of all other columns was not fully pinned. This makes it difficult to replicate the actual end condition in the finite element model.

Table 6.3 summarises the comparison for the ultimate strength of the BU90 plain back-to-back C-channel built-up columns from experimental investigation and from the finite element analysis of the LUSAS model.

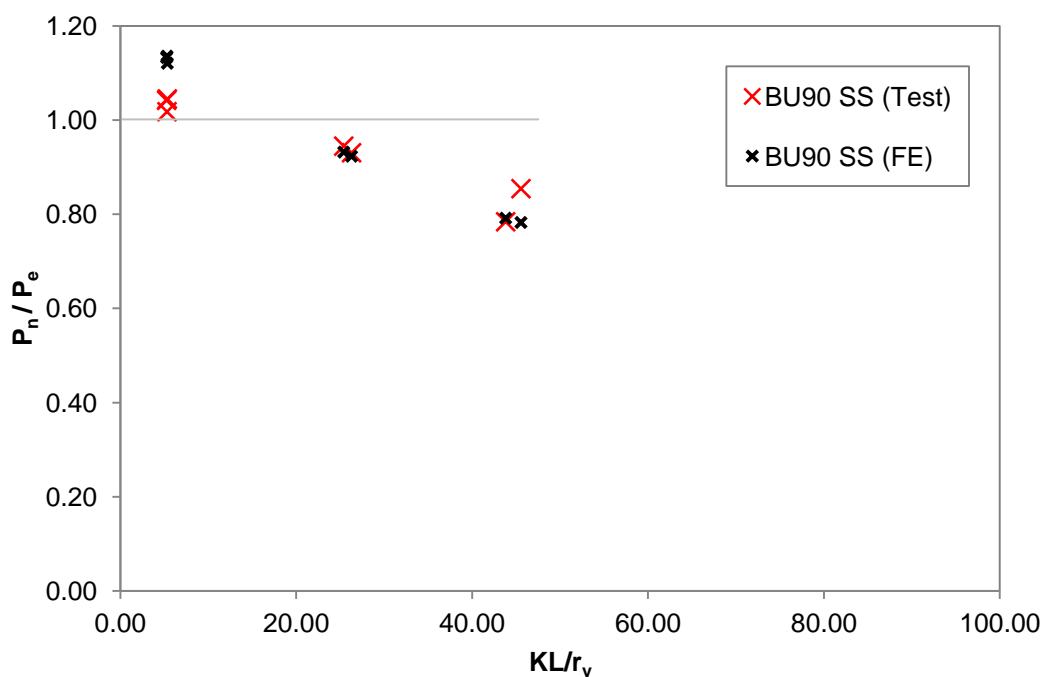
Table 6.3: Comparison between FE & Test Results for BU90

Specimen	s/L < 0.25			Specimen	0.25 < s/L < 0.50			Specimen	s/L > 0.50		
	P _{test} (kN)	P _{FE} (kN)	$\frac{P_{test}}{P_{FE}}$		P _{test} (kN)	P _{FE} (kN)	$\frac{P_{test}}{P_{FE}}$		P _{test} (kN)	P _{FE} (kN)	$\frac{P_{test}}{P_{FE}}$
BU90S50L300-1	172.49	185.00	0.93	BU90S100L300-1	Discard			BU90S200L300-1	170.25	187.72	0.91
BU90S50L300-2	171.61	186.58	0.92	BU90S100L300-2	Discard			BU90S200L300-2	177.50	188.12	0.94
BU90S50L300-3	167.56	187.00	0.90	BU90S100L300-3	171.18	188.44	0.91	BU90S200L300-3	Discard		
-				BU90S100L300-4	173.87	185.52	0.94	BU90S200L300-4	171.88	187.81	0.92
Mean			0.92	Mean			0.92	Mean			0.92
BU90S100L500-1	165.01	162.81	1.01	BU90S200L500-1	170.48	158.13	1.08	BU90S400L500-1	170.01	162.16	1.05
BU90S100L500-2	163.22	161.92	1.01	BU90S200L500-2	173.17	159.29	1.09	BU90S400L500-2	151.41	168.28	0.90
BU90S100L500-3	Discard			BU90S200L500-3	151.53	151.53	1.00	BU90S400L500-3	Discard		
Mean			1.01	Mean			1.06	Mean			0.98
BU90S225L1000-1	167.81	153.71	1.09	BU90S450L1000-1	Discard			BU90S900L1000-1	164.86	154.68	1.07
BU90S225L1000-2	151.76	153.23	0.99	BU90S450L1000-2	175.18	155.82	1.12	BU90S900L1000-2	150.94	166.23	0.91
BU90S225L1000-3	Discard			BU90S450L1000-3	161.12	166.05	0.97	BU90S900L1000-3	Discard		
-				BU90S450L1000-4	Discard			-			
Mean			1.04	Mean			1.05	Mean			0.99

*(BU90) Overall mean = 0.98; *Population standard deviation = 0.07

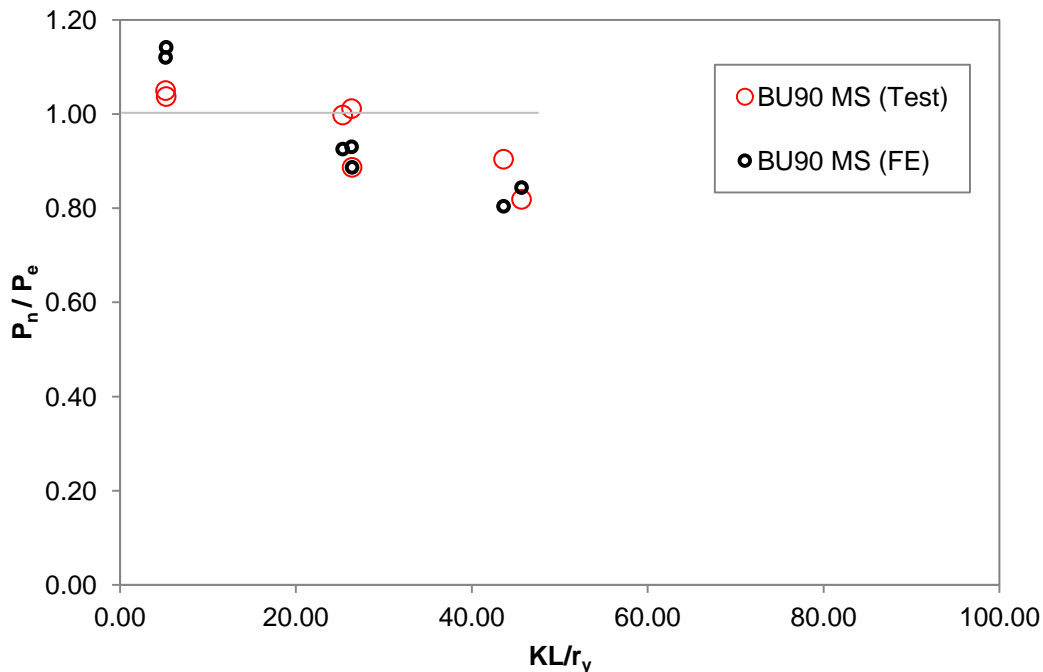
Comparison shows that the averaged P_{test}/P_{FE} ratio is 0.98 with a standard deviation of 0.07 for the BU90 test series. The P_{test}/P_{FE} ratios of BU90 test series are greater for longer columns compared to shorter columns similar to the BU75 test series. However, the P_{test}/P_{FE} ratios are closer to the test results compared to the BU75 test series. The finite element model of BU90 test series is unconservative in predicting stub column strength but conservative in predicting all other pinned-end column strength as it is difficult to model the actual end conditions during the compression tests. Furthermore, the P_{test}/P_{FE} ratios for columns with fastener spacing at $s/L > 0.50$ are lower compared to the other columns because there is no intermediate fastener along the length of these $s/L > 0.50$ built-up columns. The individual C-channels in these columns have higher tendency to buckle separately thus resulting in lower ultimate strength.

Figures 6.8, 6.9, and 6.10 present the load against member slenderness ratio for BU90 at fastener spacing $s/L < 0.25$, $0.25 < s/L < 0.50$, and $s/L > 0.50$ respectively. The graphs compare the ultimate strength predicted by the finite element model with the test results for the BU90 built-up columns at different spacing.



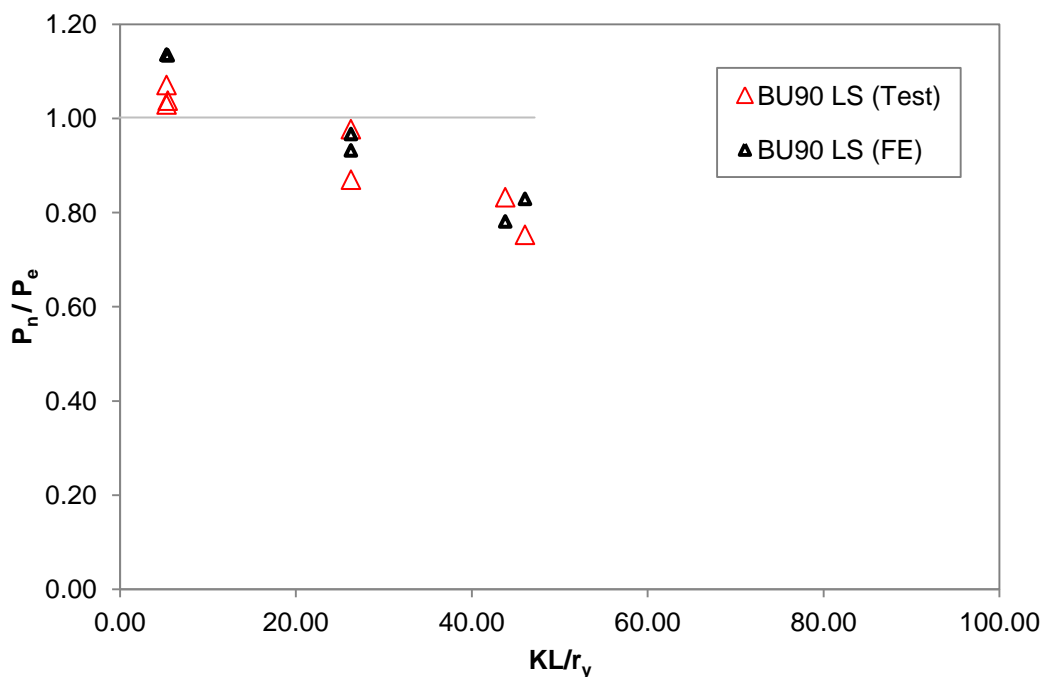
*Note: K = 0.5 for fix, 1.0 for pin, r_y (nominal) = 26 for BU90)

Figure 6.8: Graph of FE & Test Results for BU90 at $s/L < 0.25$



*Note: K = 0.5 for fix, 1.0 for pin, r_y (nominal) = 26 for BU90

Figure 6.9: Graph of FE & Test Results for BU90 at 0.25 < s/L < 0.50



*Note: K = 0.5 for fix, 1.0 for pin, r_y (nominal) = 26 for BU90

Figure 6.10: Graph of FE & Test Results for BU90 at s/L > 0.50

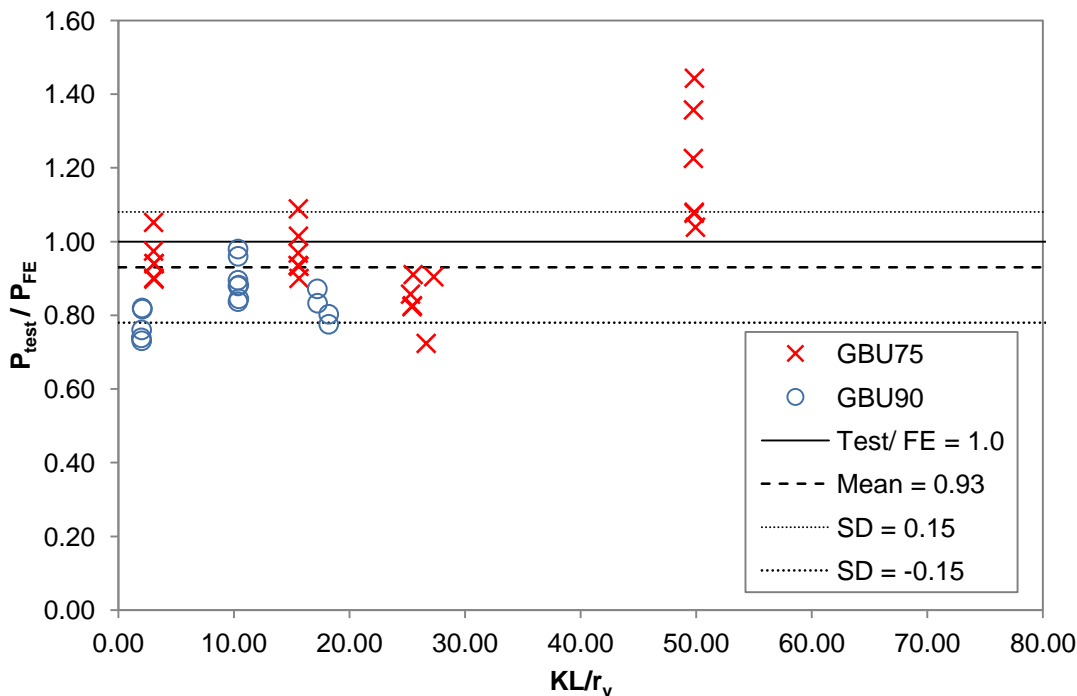
All the graphs show that the finite element results are greater than the test results for the BU90 test series as the finite element model for the BU90 failed about the y-axis

only. However, the test specimens from the BU90 test series buckled in a combination of x and y-axes. It is also noted that the variation of the ultimate strength was minimal because the tested columns are generally at shorter lengths. Furthermore, due to the short column length, the P_n/P_e ratios are generally close to 1.0. However, for stub column the P_n/P_e ratios are greater than 1.0 due to the conservative estimate on the effective area, A_e using equations from the AISI specifications when calculating the effective compressive strength, P_e .

6.2.3 Back-to-back C-channel Built-up Columns with a Gap

Back-to-back C-channel built-up column with a gap model was evaluated by 40 numbers of back-to-back C-channel built-up columns with a gap test results. All the test results and finite element results are compared and documented in Appendix G.

Figure 6.11 plots the test to finite element results ratio against the overall member slenderness for 40 numbers of back-to-back C-channel built-up columns with a gap.



*Note: K = 0.5 for fix, 1.0 for pin, r_y (nominal) = 44 for GBU75, and 66 for GBU90

Figure 6.11: Graph of FE & Test Results for Back-to-back C-channel Built-up Columns with a Gap

This graph shows that in most cases, the finite element results correlate well with the test results. The graph shows that the P_{test}/P_{FE} ratios generally fall within the standard deviation except for the GBU75L2000 as the longer back-to-back C-channel built-up columns with a gap with a lower ultimate strength tend to be affected by friction resistance in the pin-ended assemblies.

Table 6.4 compares the finite element results with the test results of the GBU75 back-to-back C-channel built-up columns with a gap at different spacing.

Table 6.4: Comparison between FE & Test Results for GBU75

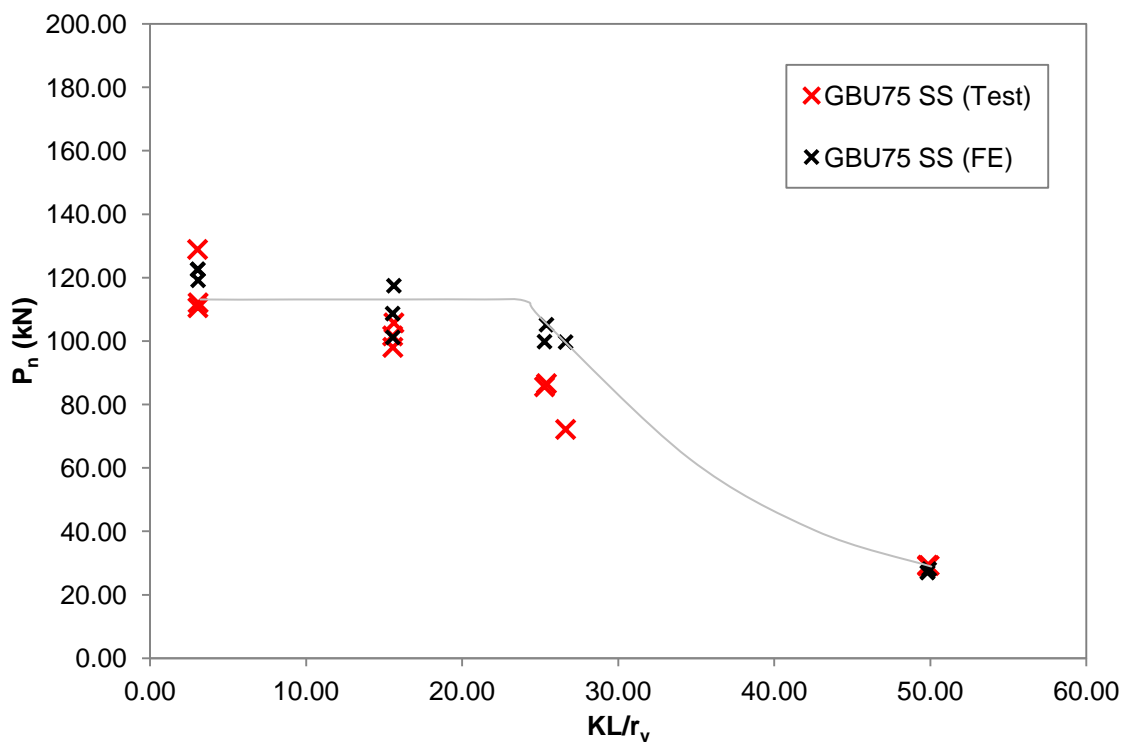
Specimen No.	P_{test} (kN)	P_{FE} (kN)	$\frac{P_{test}}{P_{FE}}$	Specimen No.	P_{test} (kN)	P_{FE} (kN)	$\frac{P_{test}}{P_{FE}}$
GBU75S50L300-1	Discard			GBU75S200L300-1	105.19	120.06	0.88
GBU75S50L300-2	112.09	125.46	0.89	GBU75S200L300-2	107.06	121.49	0.88
GBU75S50L300-3	110.57	126.60	0.87	GBU75S200L300-3	Discard		
GBU75S50L300-4	128.94	122.44	1.05	GBU75S200L300-4	112.09	119.93	0.93
Mean			0.94	Mean			0.90
GBU75S100L500-1	101.68	108.71	0.94	GBU75S400L500-1	106.12	97.45	1.09
GBU75S100L500-2	98.05	101.18	0.97	GBU75S400L500-2	100.04	107.23	0.93
GBU75S100L500-3	105.78	117.50	0.90	GBU75S400L500-3	113.61	111.97	1.01
Mean			0.94	Mean			1.01
GBU75S225L1000-1	86.62	105.20	0.82	GBU75S900L1000-1	73.36	80.57	0.91
GBU75S225L1000-2	85.63	99.86	0.86	GBU75S900L1000-2	64.12	77.60	0.83
GBU75S225L1000-3	72.19	99.73	0.72	GBU75S900L1000-3	69.74	77.09	0.90
Mean			0.80	Mean			0.88
GBU75S475L2000-1	29.25	28.15	1.04	GBU75S1900L2000-1	27.97	19.38	1.44
GBU75S475L2000-2	29.14	27.06	1.08	GBU75S1900L2000-2	27.73	20.43	1.36
GBU75S475L2000-3	29.37	27.20	1.08	GBU75S1900L2000-3	24.81	20.24	1.23
Mean			1.07	Mean			1.34

*(GBU75) Overall mean = 0.99; *Population standard deviation = 0.16

Comparison shows that the finite element result is generally less conservative compared to the test results of the GBU75 test series because it was difficult to ensure concentric loading in the test setup thus caused premature failure in the columns. All the P_{test}/P_{FE} ratios are lesser than 1.0 except for the GBU75L2000 test specimens.

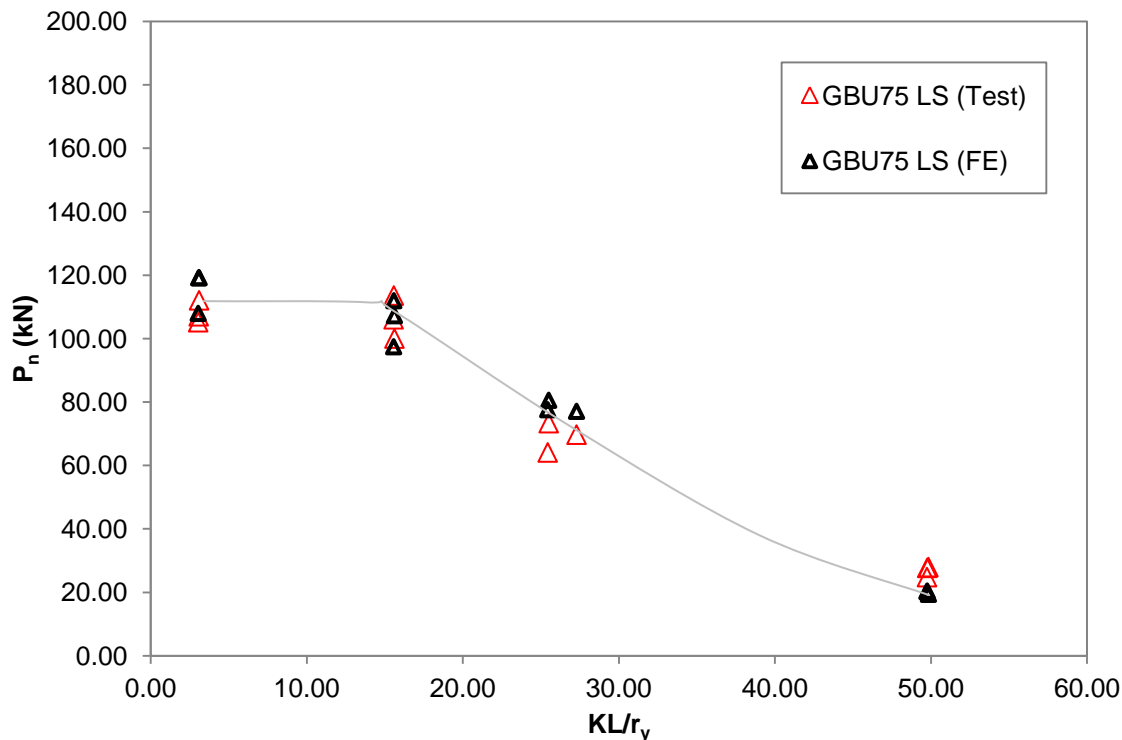
The GBU75L2000 test specimens produce greater P_{test}/P_{FE} ratios because the ultimate load of the GBU75L2000 slender columns is relatively lower. The friction resistance in the pinned-end assemblies affect the rotation of the pinned-end.

Figure 6.12 and Figure 6.13 present the load against member slenderness ratio for the GBU75 with three intermediate fasteners at $s/L < 0.25$ and one intermediate fastener at $s/L > 0.50$. Unlike the graphs in sections 6.2.1 and 6.2.2, the ultimate strength of back-to-back C-channel built-up columns with a gap is not normalised with the effective compressive strength since there is currently no design guidelines for the determination of effective area of such column. The graphs compare the ultimate strength predicted by the finite element model with the test results of the GBU75 back-to-back C-channel built-up columns with a gap at different spacing. The finite element results are averaged and indicated by a straight line on the graphs.



*Note: K = 0.5 for fix, 1.0 for pin, r_y (nominal) = 44 for GBU75

Figure 6.12: Graph of FE & Test Results for GBU75 at $s/L < 0.25$



*Note: K = 0.5 for fix, 1.0 for pin, r_y (nominal) = 44 for GBU75

Figure 6.13: Graph of FE & Test Results for GBU75 at $s/L > 0.50$

Significant strength reduction occurred when column length is beyond 1000mm for GBU75 with three intermediate fasteners; whereas, for the GBU75 with no intermediate fastener, significant strength reduction occurred when column length is beyond 500mm. This is because there are no intermediate fasteners along the column length to hold the individual C-channels together at large fastener spacing. These columns with large fastener spacing tend to become unstable and resulted in premature failure.

Table 6.5 compares the ultimate load for the finite element model of each stub, short, intermediate and slender back-to-back C-channel built-up column with a gap at different spacing with the test results.

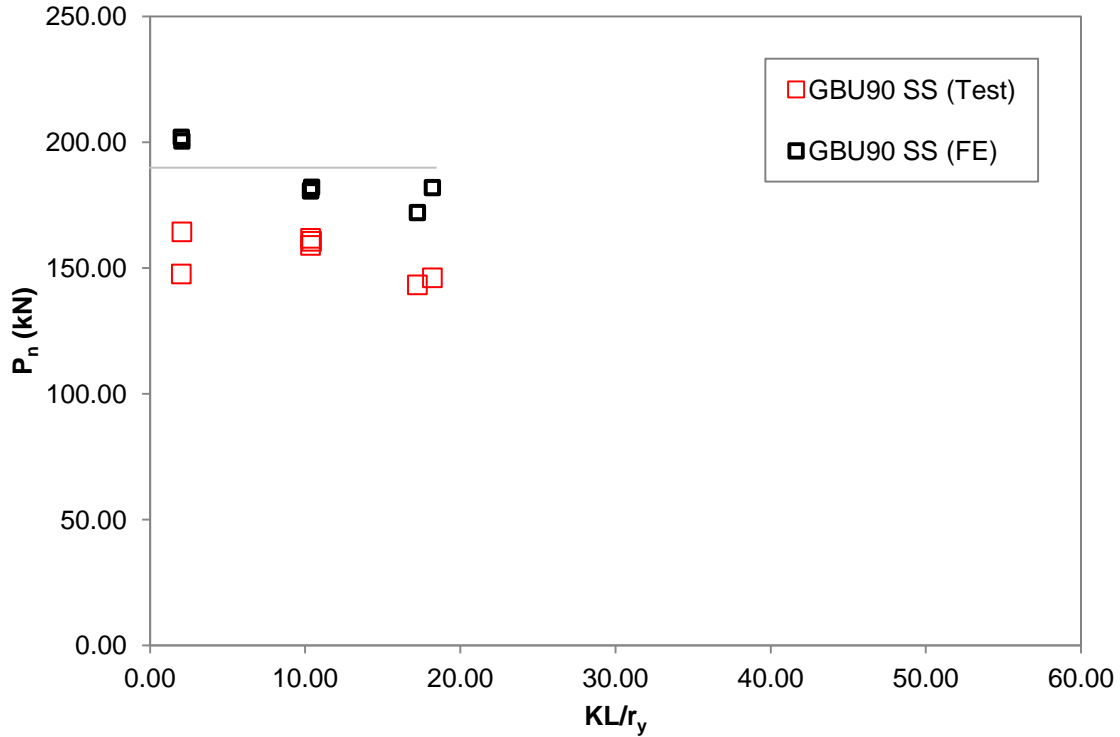
Table 6.5: Comparison between FE & Test Results for GBU90

Specimen	P_{test} (kN)	P_{FE} (kN)	$\frac{P_{test}}{P_{FE}}$	Specimen	P_{test} (kN)	P_{FE} (kN)	$\frac{P_{test}}{P_{FE}}$
GBU90S50L300-1	Discard			GBU90S200L300-1	Discard		
GBU90S50L300-2	Discard			GBU90S200L300-2	145.56	189.43	0.77
GBU90S50L300-3	147.66	190.23	0.78	GBU90S200L300-3	161.47	188.61	0.86
GBU90S50L300-4	164.40	189.63	0.87	GBU90S200L300-4	149.42	189.36	0.79
Mean			0.82	Mean			0.80
GBU90S100L500-1	161.82	180.76	0.90	GBU90S400L500-1	150.82	178.53	0.84
GBU90S100L500-2	159.01	180.74	0.88	GBU90S400L500-2	149.65	178.75	0.84
GBU90S100L500-3	160.65	182.14	0.88	GBU90S400L500-3	171.65	178.77	0.96
-				GBU90S400L500-4	174.93	178.53	0.98
Mean			0.89	Mean			0.91
GBU90S225L1000-1	143.33	172.07	0.83	GBU90S900L1000-1	152.58	175.00	0.87
GBU90S225L1000-2	Discard			GBU90S900L1000-2	Discard		
GBU90S225L1000-3	146.14	182.00	0.80	GBU90S900L1000-3	141.70	182.65	0.78
Mean			0.82	Mean			0.83

*(GBU90) Overall mean = 0.85; *Population standard deviation = 0.06

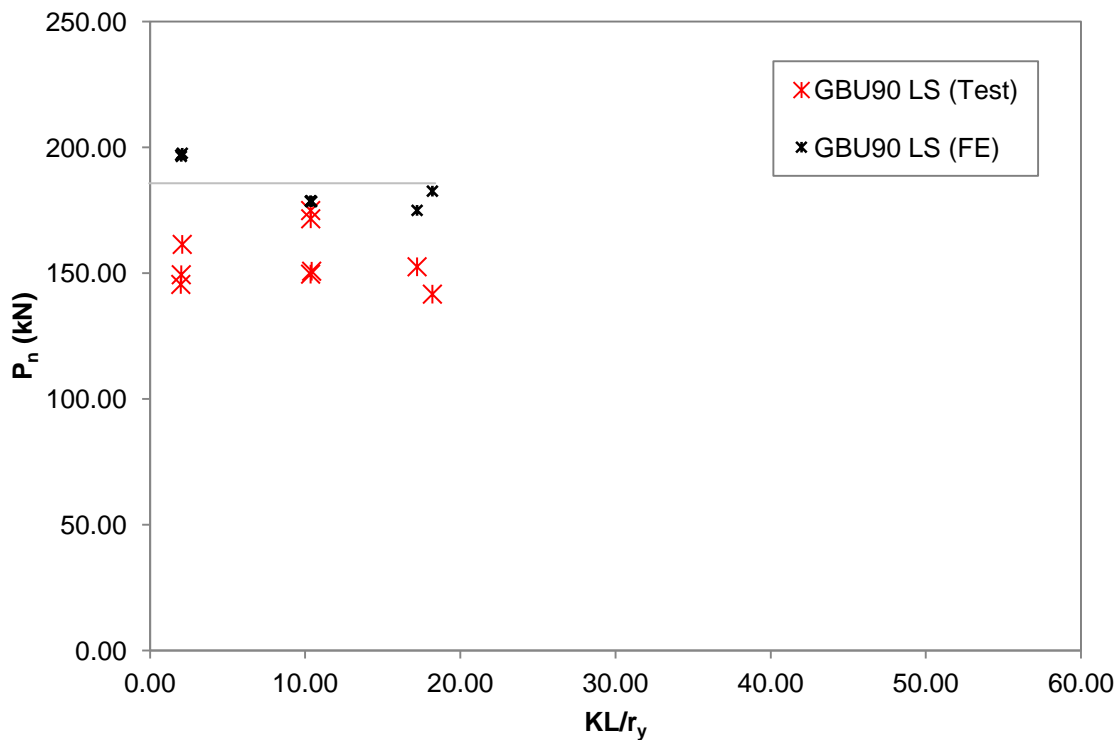
The $\frac{P_{test}}{P_{FE}}$ ratios of the GBU90 test series are less conservative with an average of 0.85 and a standard deviation of 0.06. The behaviour of back-to-back C-channel built-up column with a gap is different from C-channel and plain back-to-back C-channel built-up column because back-to-back C-channel built-up column with a gap has larger cross sections especially for the GBU90 test series. The larger cross section provides higher stability to the columns and thus greater ultimate strength. Comparison shows that the test results are generally lower compared to the finite element results because the end conditions of the finite element model rotate only about the y-axis although the test specimens tend to fail in the weaker x-axis.

Figure 6.14 and Figure 6.15 present the ultimate strength against member slenderness ratio for the GBU90 with $s/L < 0.25$ and $s/L > 0.50$. The graphs compare the ultimate strength predicted by the finite element model of each stub, short, intermediate and slender specimen at different spacing with the test results. The finite element results are averaged and indicated by a straight line on the graphs.



*Note: K = 0.5 for fix, 1.0 for pin, r_y (nominal) = 66 for GBU90

Figure 6.14: Graph of FE & Test Results for GBU90 at $s/L < 0.25$



*Note: K = 0.5 for fix, 1.0 for pin, r_y (nominal) = 66 for GBU90

Figure 6.15: Graph of FE & Test Results for GBU90 at $s/L > 0.50$

Unlike the GBU75 test series, difference between the ultimate strength of columns with different fastener spacing was not significant in the GBU90 test series as the specimens are too short to show the effects of fastener spacing.

6.3 Deformation

The specimen deformations are measured by the LVDTs positioned at web, mid and one-third length of the column in the experimental setup. These experimental deformations are compared with the finite element results for all C-channel, plain and back-to-back C-channel built-up columns with a gap as shown by the graphs in Appendix E, F, and G respectively. A sample of the comparison between test and finite element results is shown in Figure 6.16.

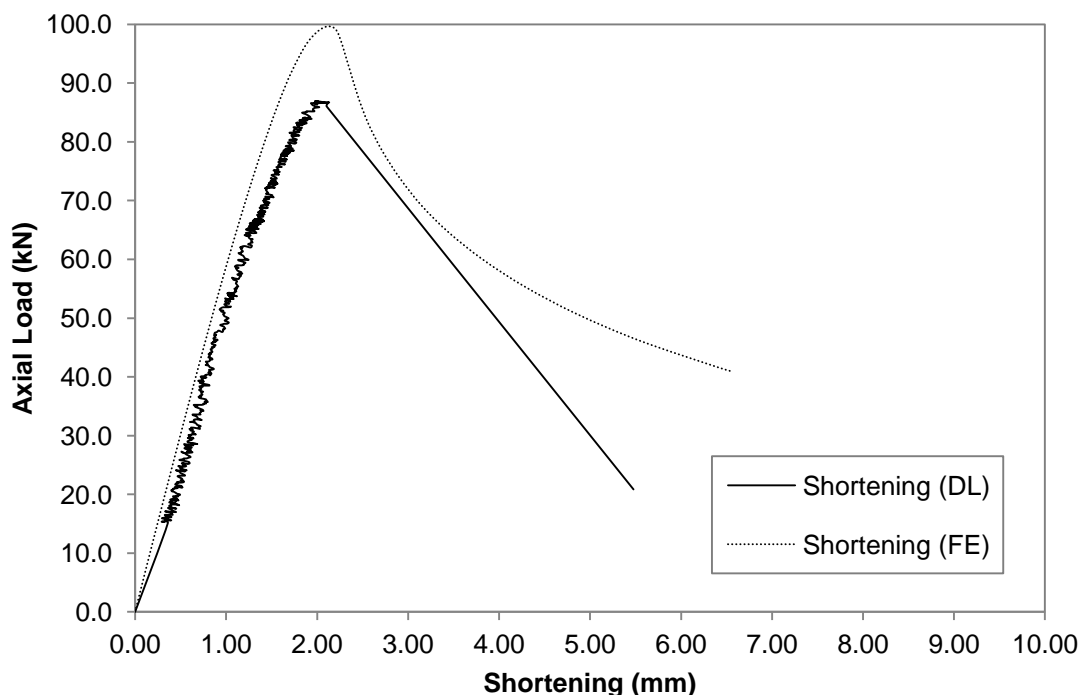


Figure 6.16: A sample of Test Results Before and After Remedial Work (C90L1000-2)

The comparison shows good correlation between the finite element results and test results before the failure of the specimens. However, after the specimen failed in a sudden manner, the deformation of the web, flange and lip obtained from the finite element analysis differs with the test results. This is because the sudden displacement of the column caused the LVDTs to be displaced. Thus, the readings obtained by the LVDTs are no longer measuring the initial deformation of the web, flange, and lip.

6.3.1 C-channel Columns

Figures 6.17 to 6.20 show the failure modes of a number of C-channels at various lengths as observed in the experiment compared to their corresponding finite element models. The finite element models are modelled based on average measured dimension and the dimensions are assumed to be constant along the cross section.

Figure 6.17 shows the failure modes of the finite element model and tested specimen of C-channel stub columns.

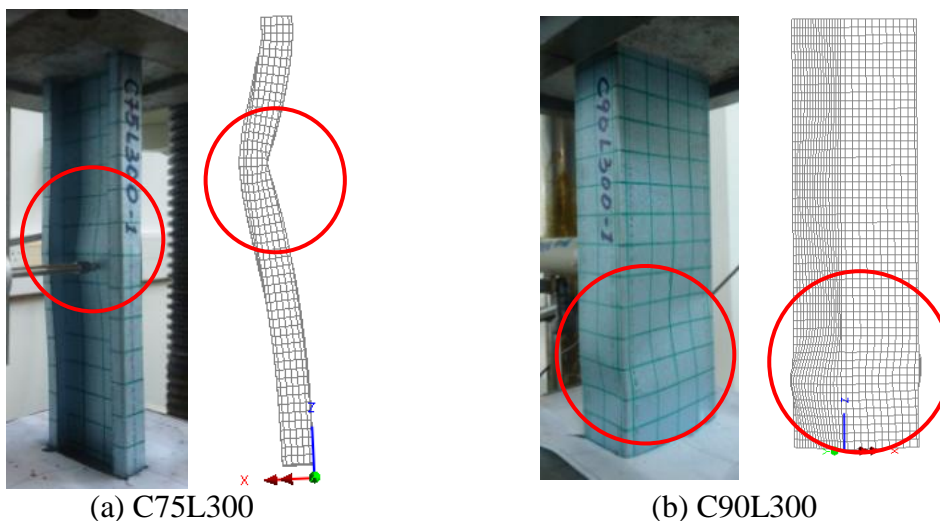


Figure 6.17: Failure Modes of FE and Tested C75L300 and C90L300 C-channel (C) Stub Columns

The finite element model predicted that the C75L300 stub columns failed with maximum deflection at one-third length. However, the local buckling localised at mid-length in the tested specimen. This is because the finite element model is modelled with fixed-end condition, whereas the test setup is setup in fixed end condition. The fixed-end finite element model has less degree of freedom compared to the fixed end column in the test setup. For C90L300 stub columns, they are predicted to fail near the end of the column with a yield line straight across the web. However, in the tested specimen, the yield line was at a slope due to uneven cross section as explained previously in section 4.2.1.

Figure 6.18 shows the failure modes of the finite element model and tested specimen of C-channel short columns.

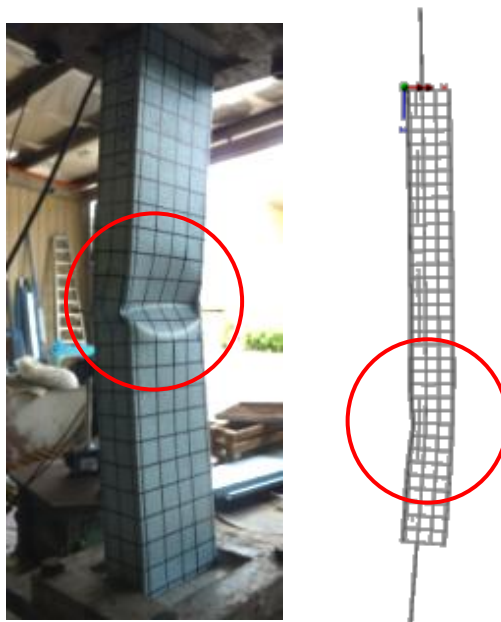
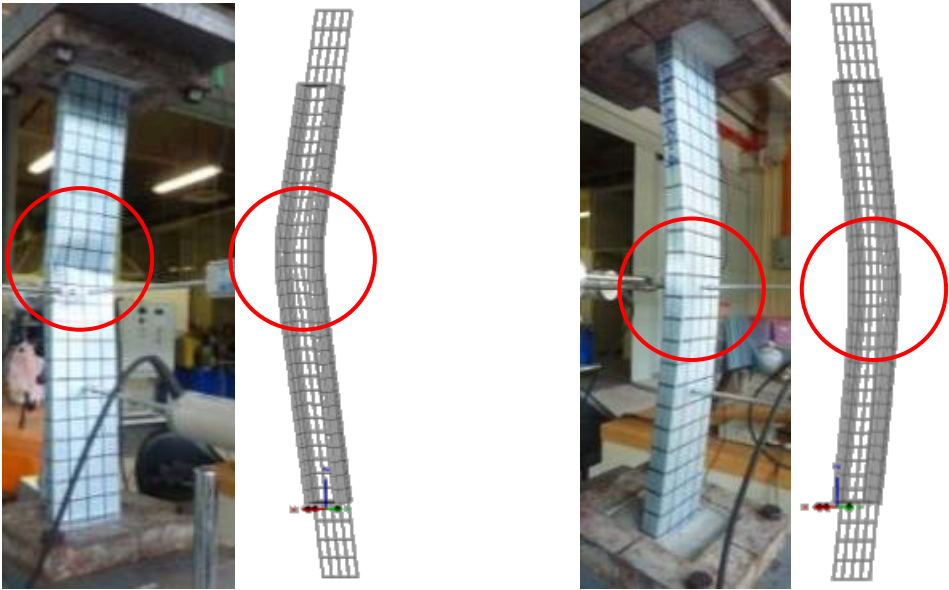


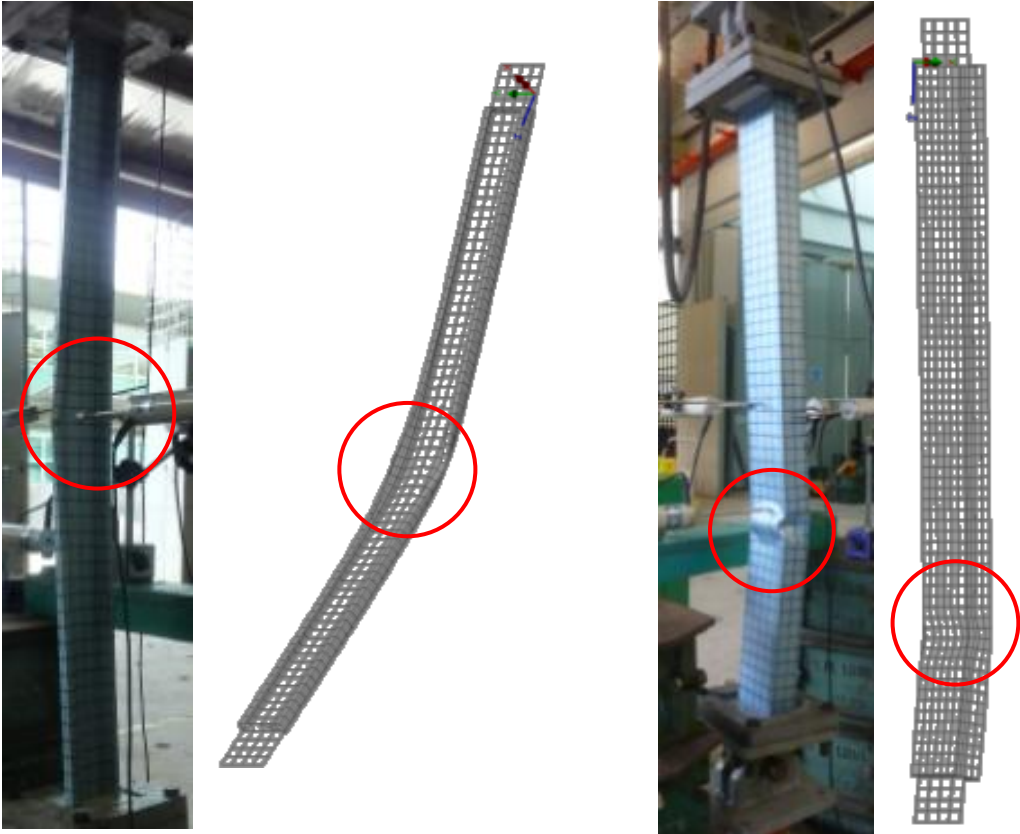
Figure 6.18: Failure Modes of FE and Tested C90L500 C-channel (C) Short Columns

The finite element model predicted that the C90L500 failed at about one-third length of the columns. However, in the tested specimens, failure is near to mid-length of the columns due to the eccentric loading during testing.

The failure modes of the finite element model and tested specimen of C-channel intermediate columns are as shown in Figure 6.19.



(a) C75L500



(b) C75L1000

(c) C90L1000

Figure 6.19: Failure Modes of FE and Tested C75L500, C75L1000 and C90L1000 C-channel (C) Intermediate Columns

For the C75L500 and C75L1000, both the finite element model and tested specimen show global buckling with maximum deflection at mid-length. For the C90L1000,

both the finite element model and tested specimen show failure at one-third length of the columns.

The failure modes of the finite element model and tested specimen of C-channel slender columns are as shown in Figure 6.20.

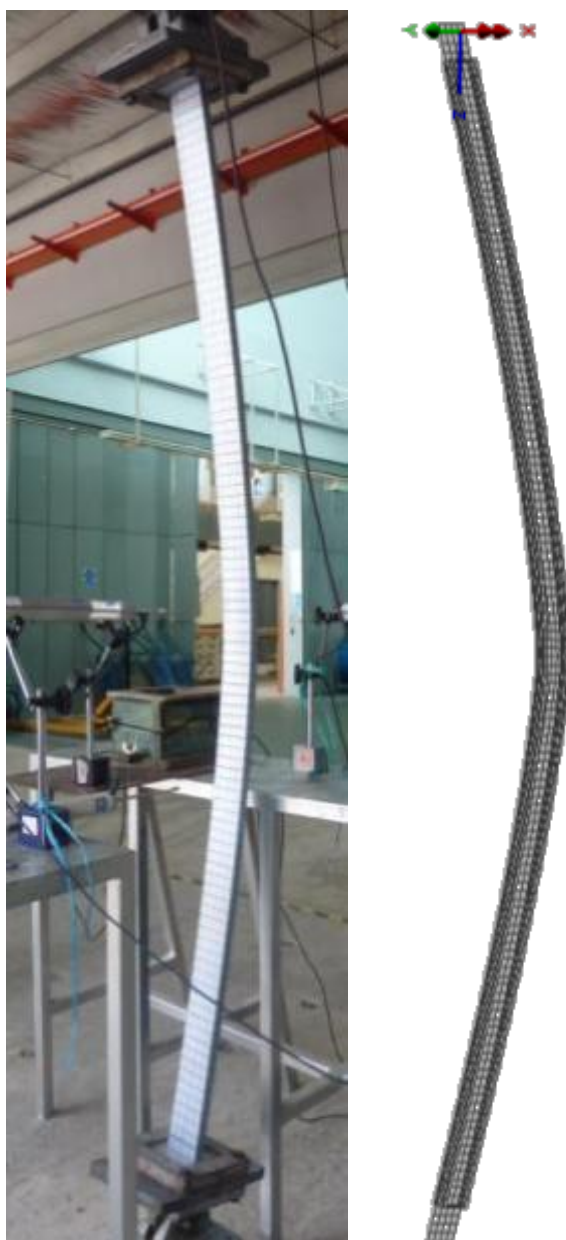


Figure 6.20: Failure Modes of FE and Tested C75L2000 C-channel (C) Slender Columns

The finite element model predicted the global buckling failure observed during the compression test of the C75L2000 C-channel slender columns. The finite element

results show that the C75L2000 C-channel slender columns buckle with maximum deflection at mid-length.

6.3.2 Plain Back-to-back C-channel Built-up Columns

Figures 6.21 to 6.24 show the failure modes of a number of plain back-to-back C-channel built-up columns at various lengths as observed in the experiment compared to their corresponding finite element models. All plain back-to-back C-channel built-up column behaviours predicted by the finite element models are verified against the experimentally recorded behaviour in Appendix F.

Figure 6.21 shows the failure modes of the finite element model and tested specimen of plain back-to-back C-channel built-up stub columns.

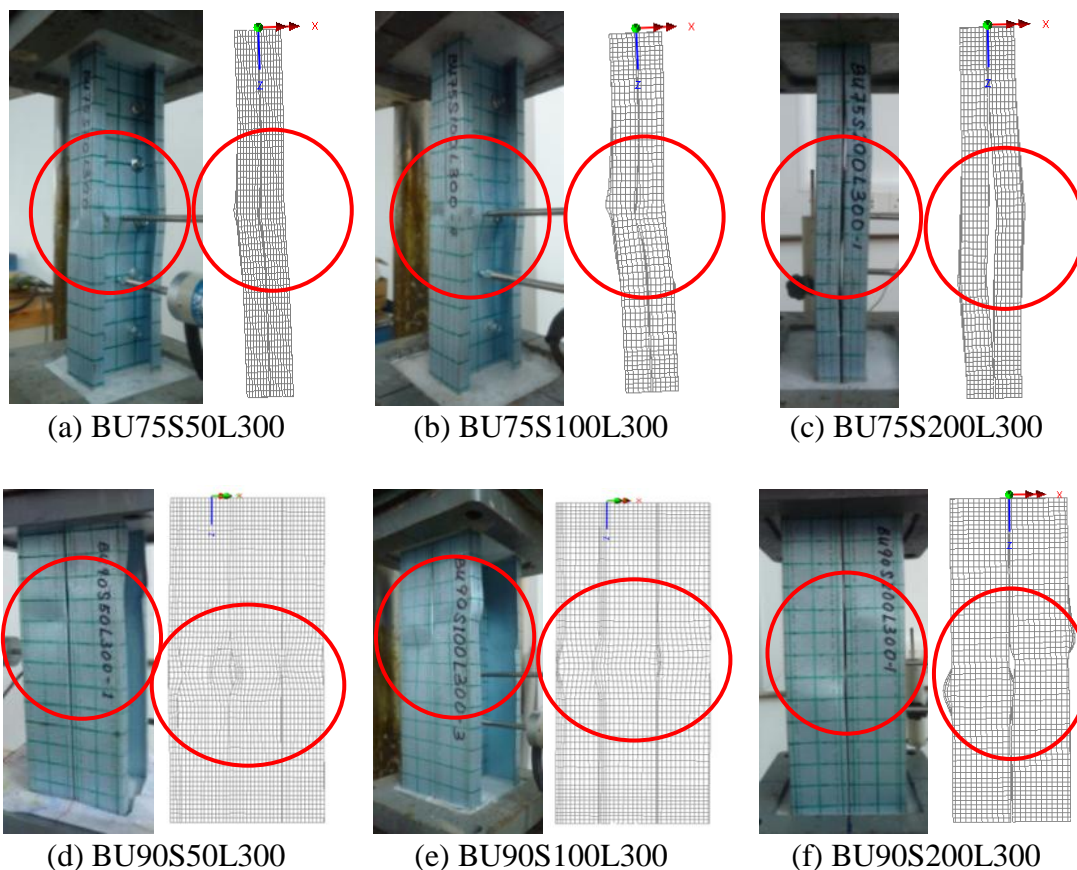


Figure 6.21: Failure Modes of FE and Tested BU75L300 and BU90L300 Plain Back-to-back C-channel Built-up (BU) Stub Columns

The finite element model predicted that the BU75S50L300 and BU75S100L300 buckle in a similar manner with maximum deflection at mid-length. The tested

specimens of the BU75S50L300 and BU75S100L300 also show this similar behaviour. For the BU90S50L300 and BU90S100L300, the finite element model predicted failure at mid-length with a yield line straight across the web; however, the yield line on the test specimens is slightly shifted on the individual C-channels. The BU75S200L300 and BU90S200L300 finite element model show different buckling failure that the individual C-channel buckled separately. This is also shown in most of the tested specimens of the BU75S200L300 and BU90S200L300.

Figure 6.22 shows the failure modes of the finite element model and tested specimen of plain back-to-back C-channel built-up short columns.

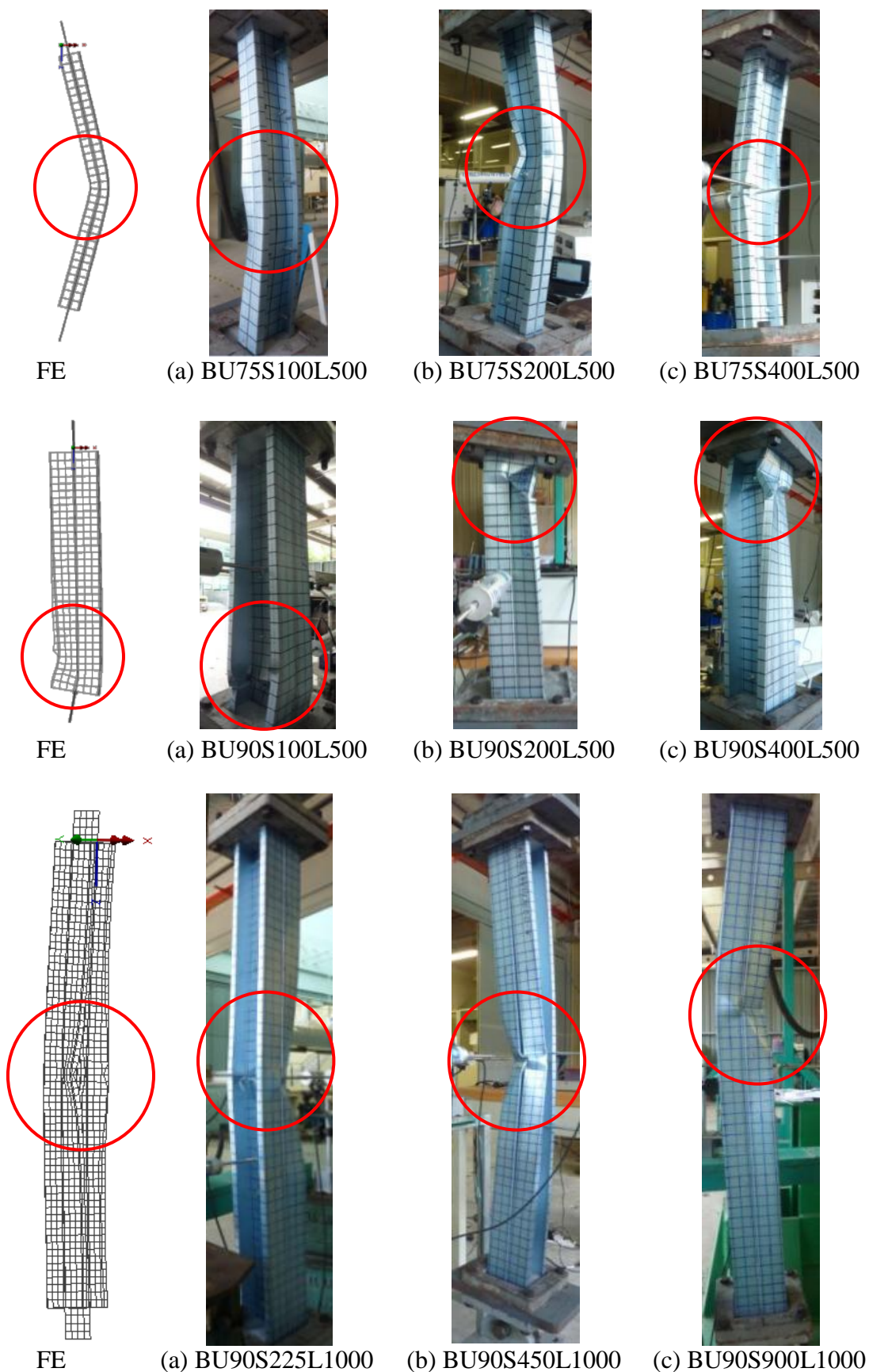


Figure 6.22: Failure Modes of FE and Tested BU75L500, BU90L500 and BU90L1000 Plain Back-to-back C-channel Built-up (BU) Short Columns

The finite element model for built-up short columns shows similar failure modes regardless of the fastener spacing. The finite element model for the BU75L500 and BU90L1000 shows maximum deflection at mid-length. Similar behaviour was observed during the testing. For the BU90L500, the finite element model shows yielding failure at the bottom end of the column. The test specimens show similar yielding failure but it may also occur at the top or bottom end of the column.

Figure 6.23 shows the failure modes of the finite element model and tested specimen of plain back-to-back C-channel built-up intermediate columns.

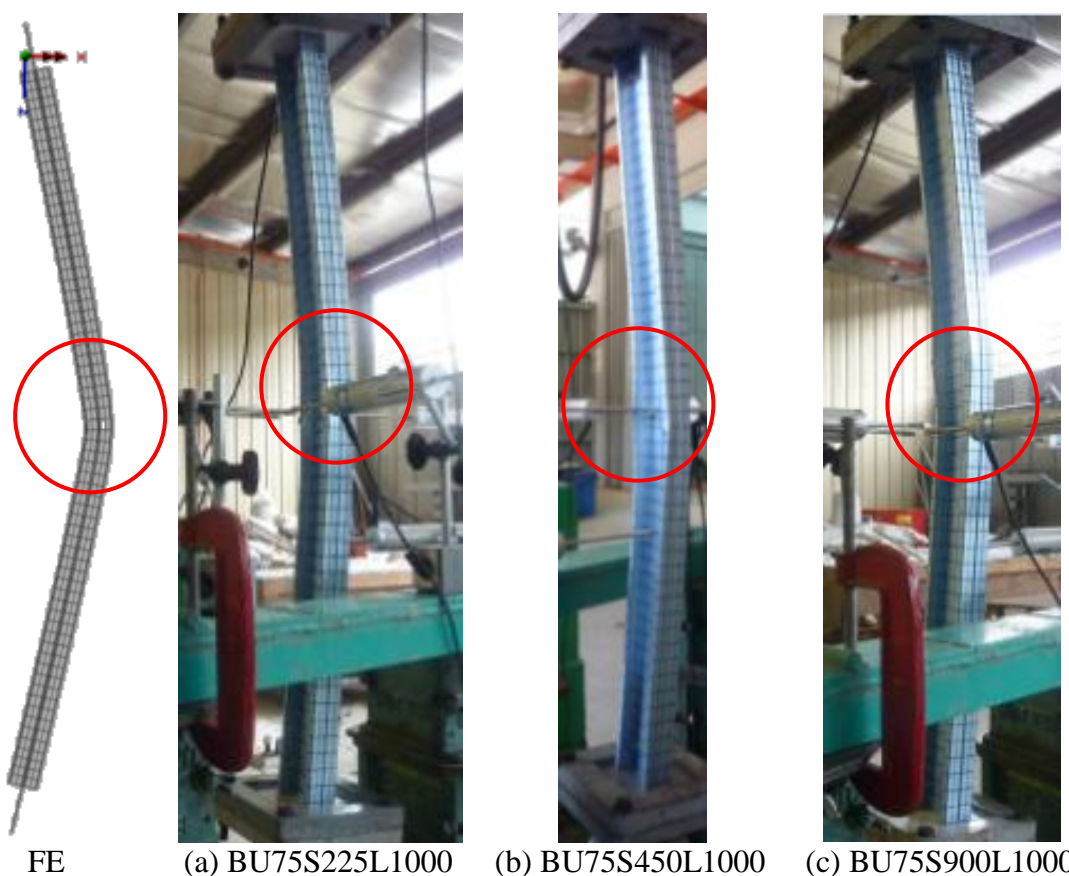
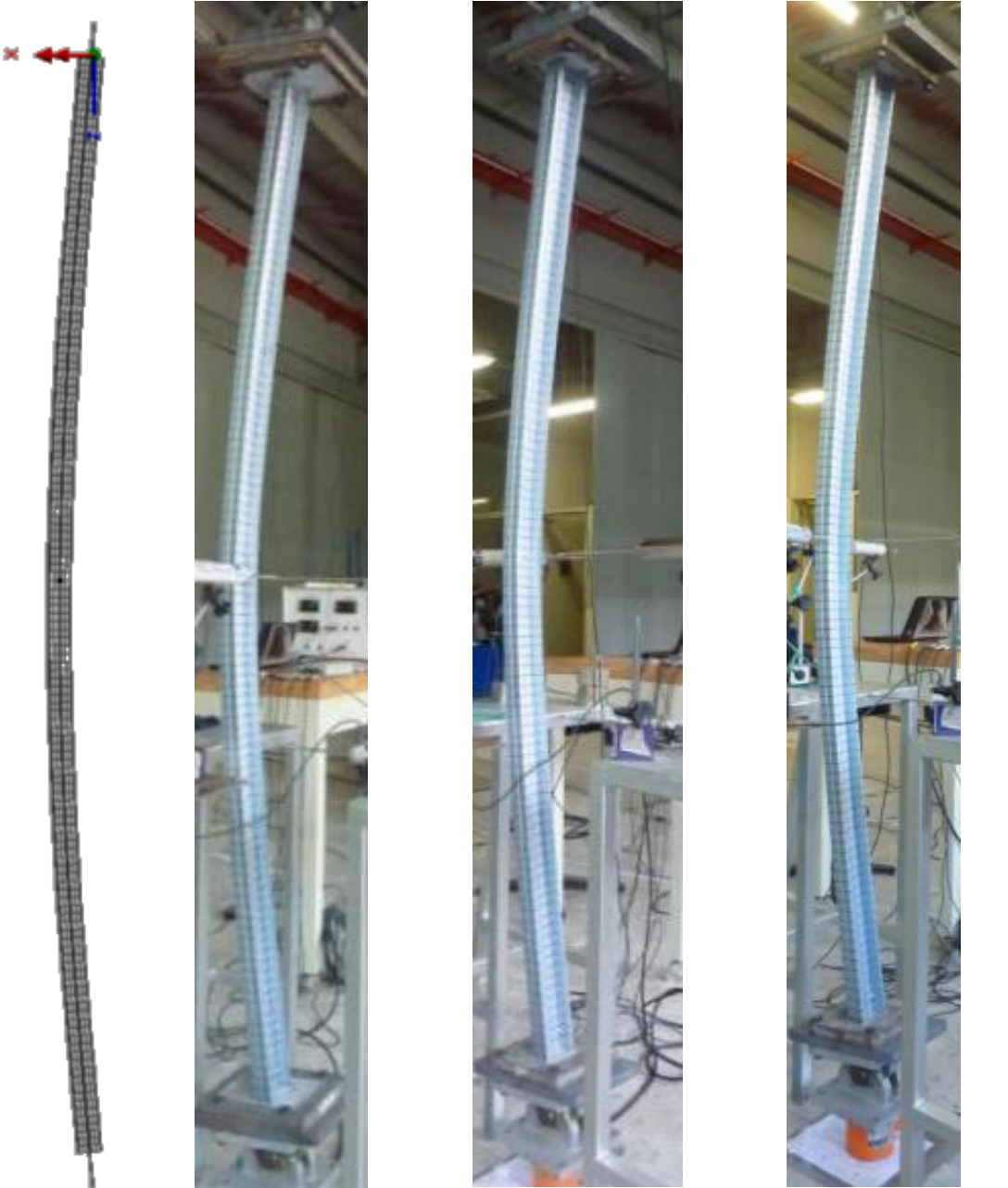


Figure 6.23: Failure Modes of FE and Tested BU75L1000 Plain Back-to-back C-channel Built-up (BU) Columns

Similar to some of the short columns, the BU75L1000 finite element model deformed with maximum deflection at mid-length. All BU75L1000 test specimens showed similar failure modes regardless of the fastener spacing.

Figure 6.24 shows the failure modes of the finite element model and tested specimen of plain back-to-back C-channel built-up slender columns.



FE (a) BU75S475L2000 (b) BU75S950L2000 (c) BU75S1900L2000
Figure 6.24: Failure Modes of FE and Tested BU75L2000 Plain Back-to-back C-channel Built-up (BU) Slender Columns

Similar to some of the short columns and the intermediate columns, the BU75L2000 finite element model deformed with maximum deflection at mid-length. All BU75L2000 test specimens showed similar failure modes regardless of the fastener spacing.

6.3.3 Back-to-back C-channel Built-up Columns with a Gap

Figures 6.25 to 6.28 show the failure modes of a number of back-to-back C-channel built-up columns with a gap at various lengths as observed in the experiment compared to their corresponding finite element models. All back-to-back C-channel built-up columns with a gap behave as predicted by the finite element model. These behaviours are verified against the experimentally recorded behaviour as presented in Appendix G.

Figure 6.25 shows the failure modes of the finite element model and tested specimen of back-to-back C-channel built-up stub columns with a gap.

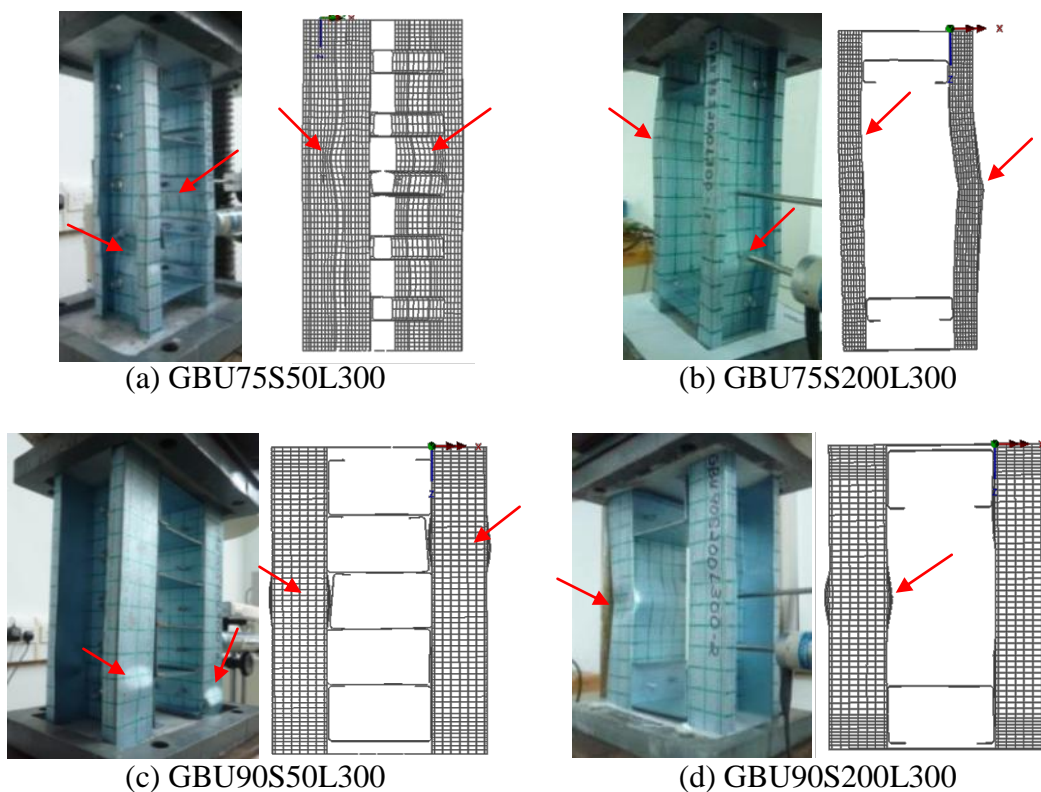


Figure 6.25: Failure Modes of FE and Tested GBU75L300 and GBU90L300 Back-to-back C-channel Built-up (GBU) Stub Columns with a Gap

The GBU75S50L300 model with three intermediate fasteners predicted buckling between the fasteners with the yield line at similar height on the individual C-channels. The tested specimen showed similar failures. However the yield line is at slightly different height due to the end conditions with higher degree of freedom. The GBU90S50L300 model also with three intermediate fasteners showed yield line at around one-third height with slightly different location. The tested specimens showed

similar failed shape but the yield line is closer to the column end. For specimens with no intermediate connectors, both finite element model and tested specimen of GBU75S200L300 and GBU90S200L300 showed that the individual C-channels buckled separately forming an O-shape.

Figure 6.26 shows the failure modes of the finite element model and tested specimen of back-to-back C-channel built-up 500mm columns with a gap.

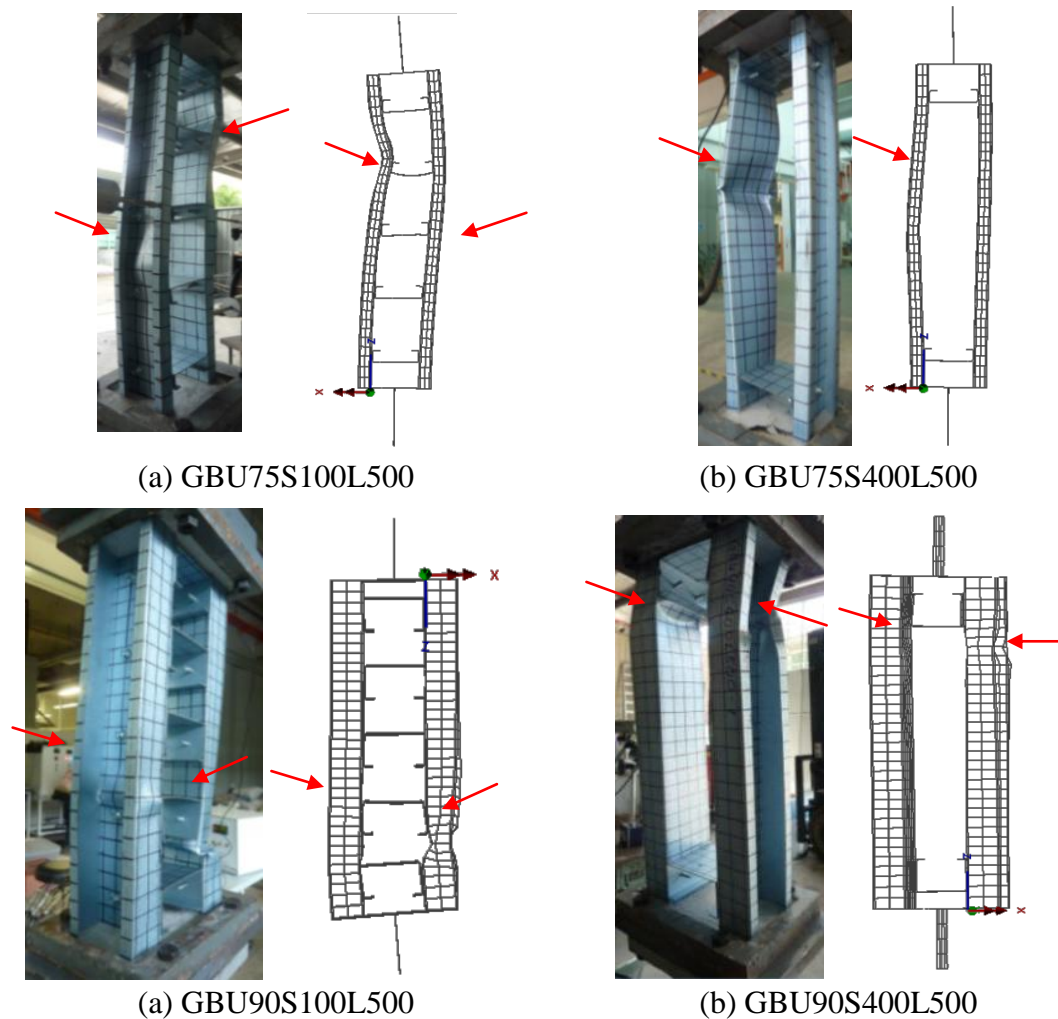


Figure 6.26: Failure Modes of FE and Tested GBU75L500 and GBU90L500 Back-to-back C-channel Built-up (GBU) Columns with a Gap

Similar to back-to-back C-channel built-up stub columns with a gap, both finite element model and tested specimen of the GBU75S100L500 buckled between intermediate fasteners forming an S-shape; while the GBU75S400L500 showed that the individual C-channels buckled separately forming an O-shape. For GBU90L500, the yield line was generally near to the column end.

Figure 6.27 shows the failure modes of the finite element model and tested specimen of back-to-back C-channel built-up 1000mm columns with a gap.

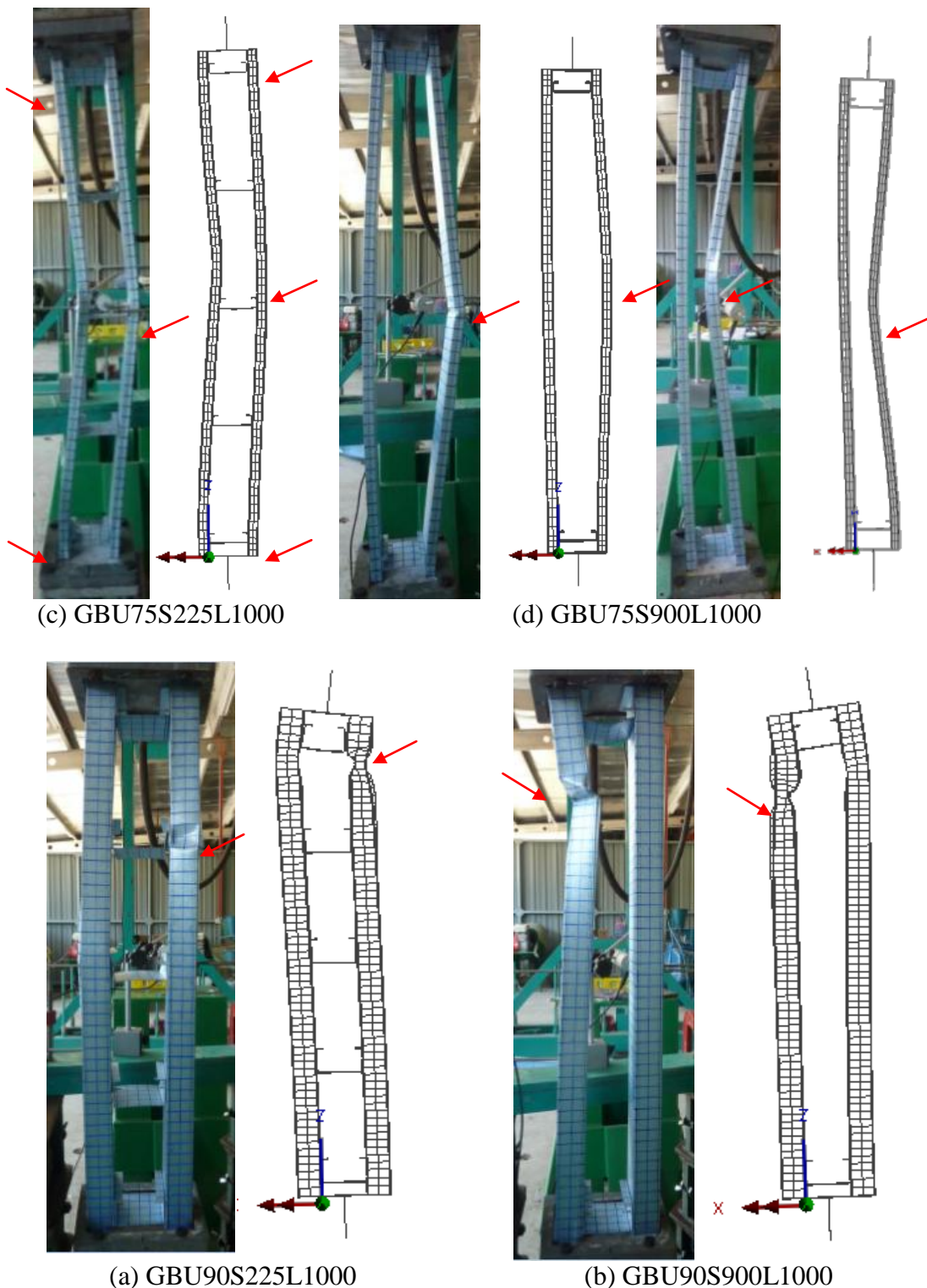


Figure 6.27: Failure Modes of FE and Tested GBU75L1000 and GBU90L1000 Back-to-back C-channel Built-up (GBU) Columns with a Gap

The finite element model also predicted the S-shape for the GBU75S225L1000 tested specimen and the O-shape or K-shape for the GBU75S900L1000 tested specimen. The

buckling shape of the back-to-back C-channel built-up columns with 1000mm column length is more obvious compared to the back-to-back C-channel built-up columns with a gap with 500mm column length. As for the GBU90S225L1000 specimens, the finite element model predicted failure at columns ends. A similar pattern was observed for the GBU90S900L1000 tested specimens.

Figure 6.28 shows the failure modes of the finite element model and tested specimen of back-to-back C-channel built-up 2000mm columns with a gap.

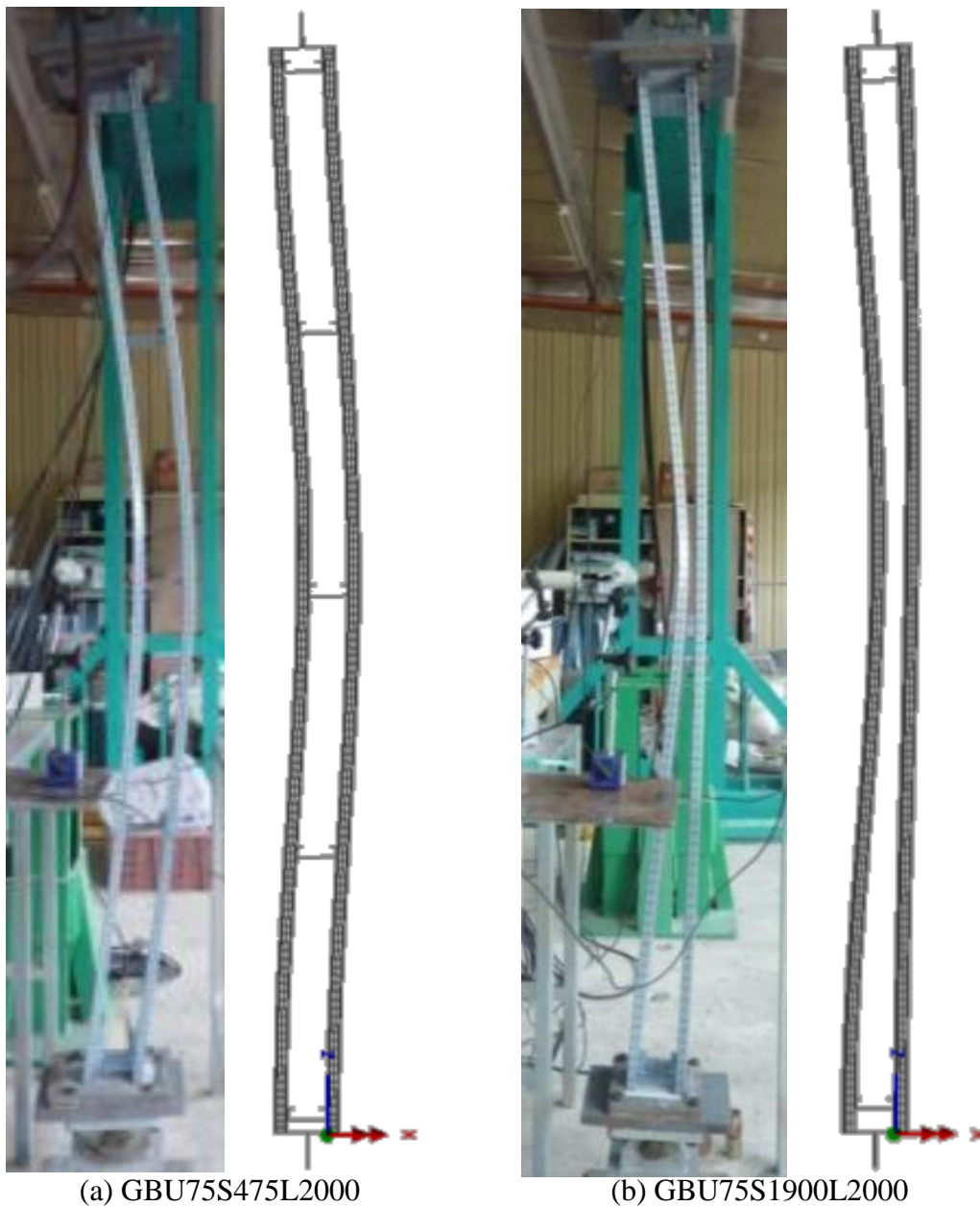


Figure 6.28: Failure Modes of FE and Tested GBU75L2000 Back-to-back C-channel Built-up (GBU) Columns with a Gap

The finite element model predicted similar S-shape and K-shape buckling failure with even more obvious buckled shape compared to the GBU75 back-to-back C-channel built-up columns with a gap with 500mm and 1000mm column length.

6.4 Parametric Study on the Effects of Intermediate Fasteners

The finite element model is used to study the effects of intermediate fasteners for back-to-back C-channel built-up columns with a gap. As mentioned in Chapter 3, back-to-back C-channel built-up columns with a gap with $s/L < 0.25$ have three intermediate fasteners, while $s/L > 0.50$ contains no intermediate fasteners. However, back-to-back C-channel built-up columns with a gap with $0.25 < s/L < 0.50$ were not designed and tested. Therefore, this parametric study is conducted to study the effects of intermediate fasteners for columns with $0.25 < s/L < 0.50$ which contain only one intermediate fastener as shown in Figure 6.29.

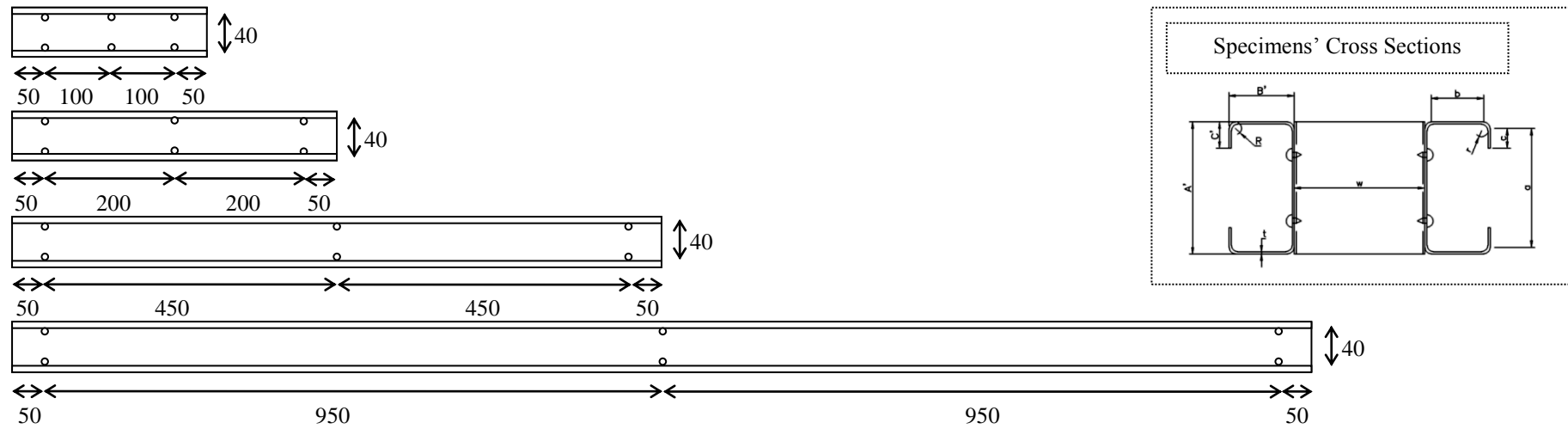


Figure 6.29: Fastener Spacing for Back-to-back C-channel Built-up Columns with a Gap with $0.25 < s/L < 0.50$

The finite element results from the parametric study are as shown in Figure 6.30 and Figure 6.31. All finite element and test results for the GBU75 built-up columns with a gap are included. The different intermediate fastener spacing are denoted as: (i) SS for $s/L < 0.25$, (ii) MS for $0.25 < s/L < 0.50$, and (c) LS for $s/L > 0.50$.

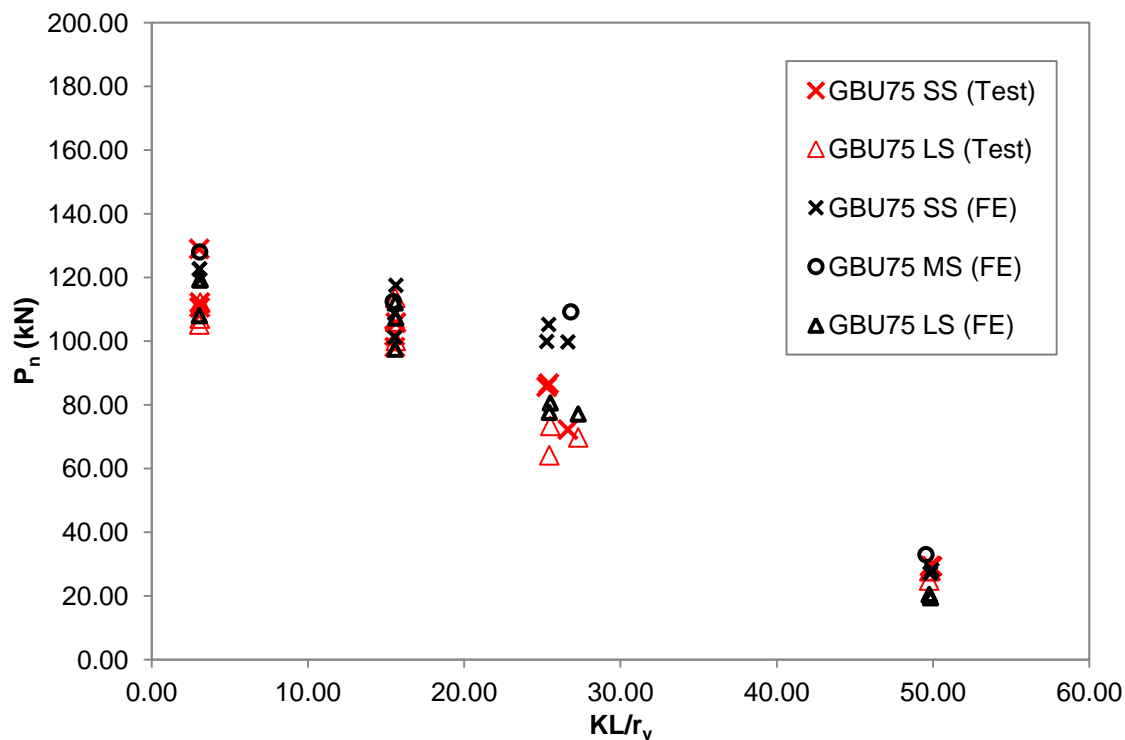


Figure 6.30: Load versus Member Slenderness Ratio for GBU75

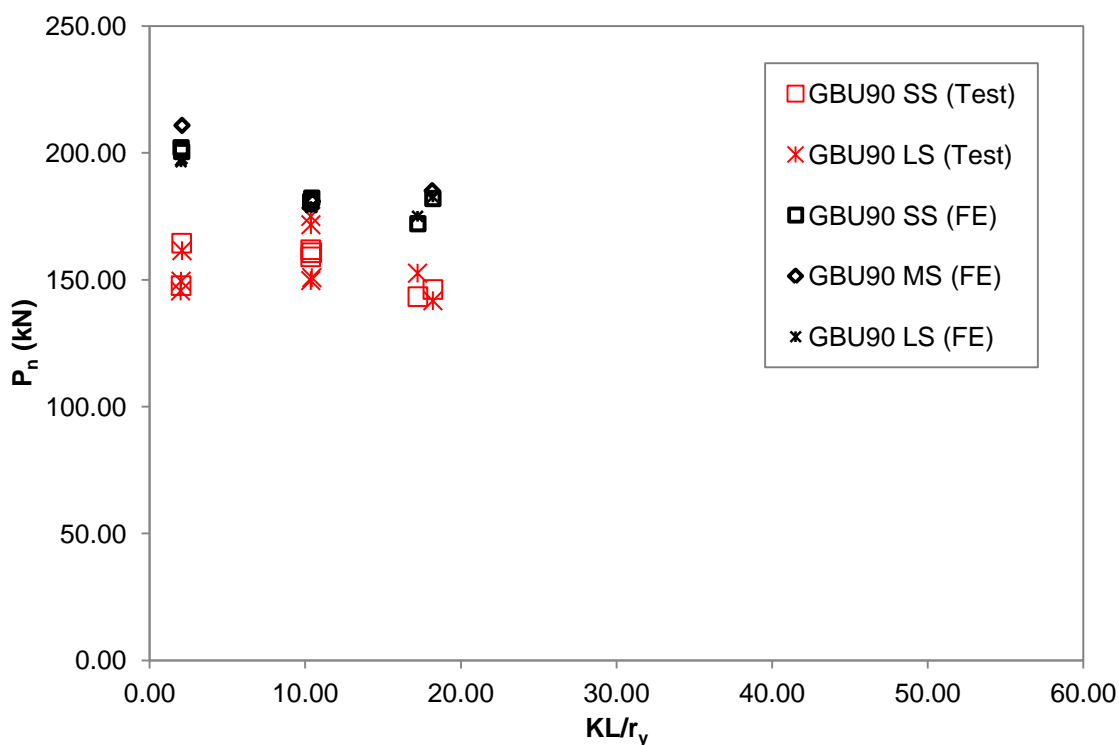


Figure 6.31: Load versus Member Slenderness Ratio for GBU90

All the finite element results show that back-to-back C-channel built-up columns with a gap with one and three intermediate fasteners have higher capacity compared to columns without intermediate fasteners. Columns with intermediate fasteners provide better cross-section stability and provide high torsional restraint. When the intermediate fasteners are spaced beyond the spacing requirement, there are no intermediate fasteners to hold the two individual C-channels together as a built-up column. Thus, the built-up column acted separately and caused the reduction of built-up column strength.

From the parametric study results, the back-to-back C-channel built-up columns with a gap with $s/L < 0.25$ and $0.25 < s/L < 0.50$ spacing consistently achieved higher strength than columns with $s/L > 0.50$ spacing. The intermediate spacing used for columns with $0.25 < s/L < 0.50$ spacing are very close to the spacing requirement of the AISI Specifications, thus the parametric results show the maximum strength is also achieved. Even for columns with $s/L > 0.50$, the built-up column strength reduction is minimal compared to columns with $s/L < 0.25$ and columns with $0.25 < s/L < 0.50$. The fasteners spacing does not have significant influence on the ultimate strength for columns with three and one intermediate fasteners. Therefore, it is important to have fasteners at mid-length where the maximum deflection occurs to ensure that the built-up column acts as an integral column and achieves maximum capacity.

The deformed shapes for the back-to-back C-channel built-up columns with a gap are shown in Figure 6.32 and Figure 6.33.

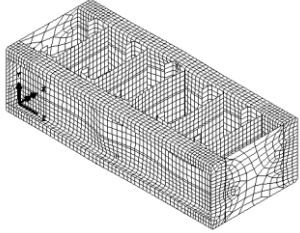
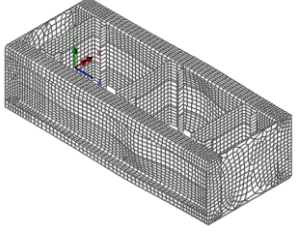
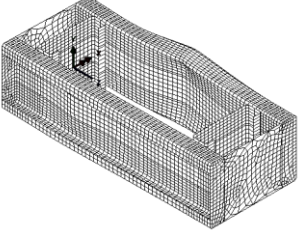
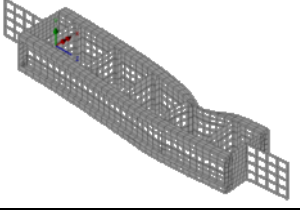
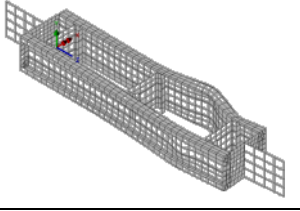
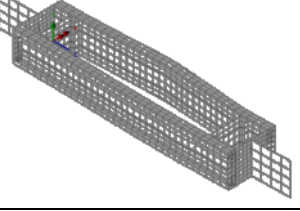
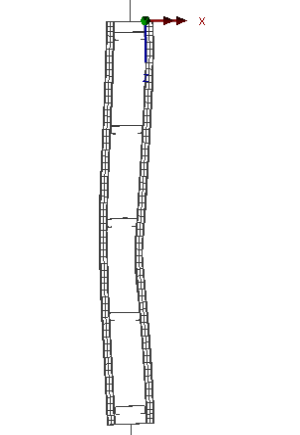
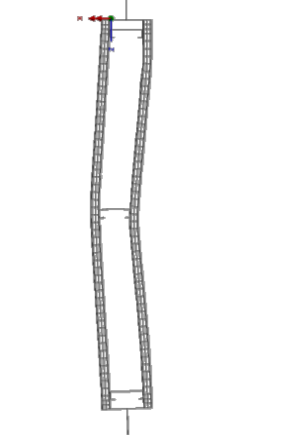
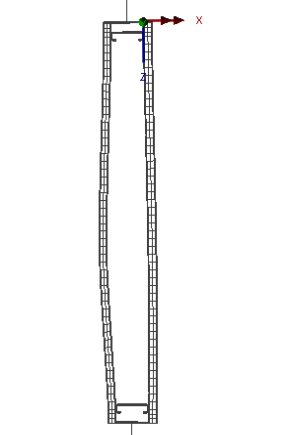
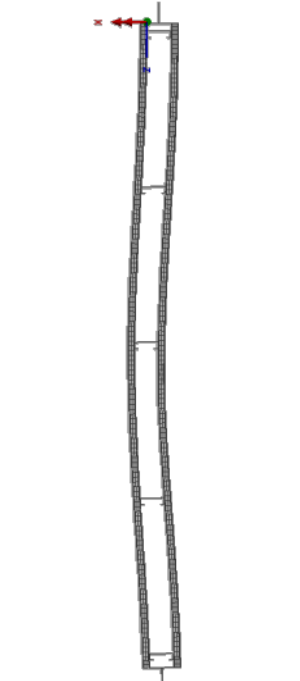
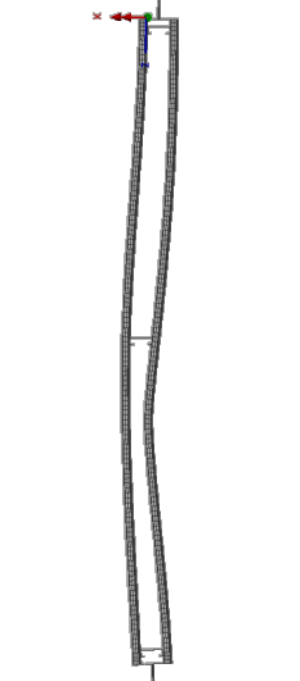
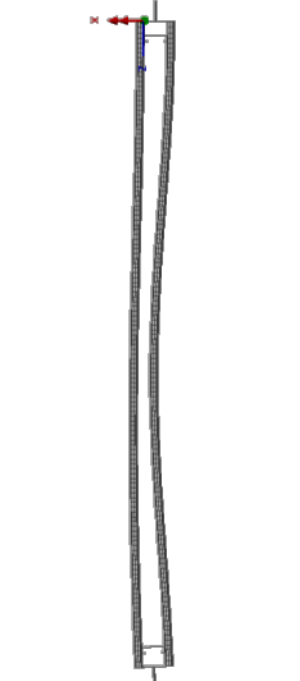
Length	(a) $s/L < 0.25$	(b) $0.25 < s/L < 0.50$	(c) $s/L < 0.50$
300mm			
500mm			
1000mm			
2000mm			

Figure 6.32: Failure Modes of FE GBU75 Back-to-back C-channel Built-up Columns with a Gap

The finite element model of the GBU75 back-to-back built-up columns with a gap predicted that columns with three intermediate fasteners and one intermediate fastener resulted in similar failed shape as shown in Figure 6.32. The stub columns showed yield line between the intermediate fasteners at similar height on the individual C-channels; whereas all other columns failed with an S-shape. Different from these S-shape failed columns, the finite element model predicted that the GBU75 back-to-back built-up columns with a gap with no intermediate fasteners failed with an O-shape or K-shape.

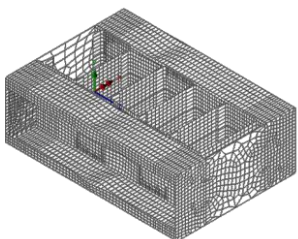
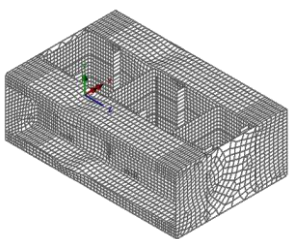
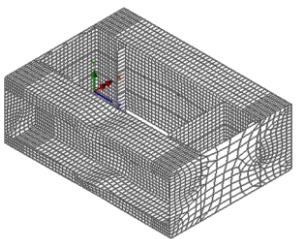
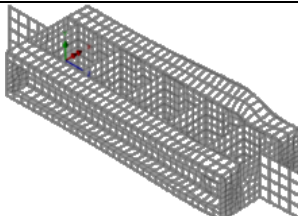
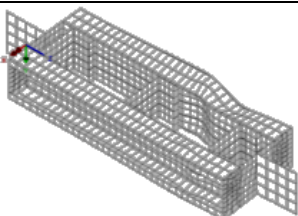
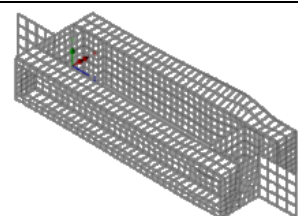
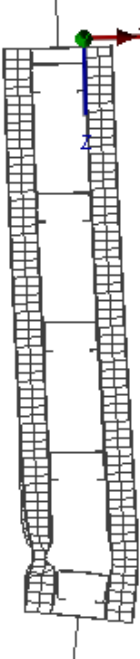
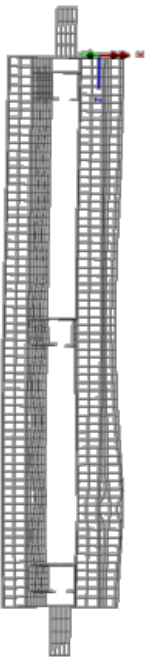
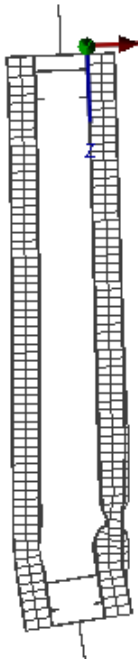
Column Length	(a) $s/L < 0.25$	(b) $0.25 < s/L < 0.50$	(c) $s/L < 0.50$
300mm			
500mm			
1000mm			

Figure 6.33: Failure Modes of FE GBU90 Back-to-back C-channel Built-up Columns with a Gap

On the other hand, the GBU90 back-to-back C-channel built-up columns with a gap showed failure at the ends of all the columns as shown in Figure 6.33.

6.5 Conclusions

Evaluation of the finite element models using the experimental results shows that the proposed finite element models predicted the capacity, the failure modes, and the deformations of the cold-formed steel C-channel columns well. Generally the experimental results show higher ultimate strength compared to the finite element results. However, this is not the case for back-to-back C-channel built-up columns with a gap due to the constraints in experimental investigation as discussed in this chapter.

A parametric study on the effects of fasteners spacing on back-to-back C-channel built-up column with a gap was conducted on columns with fastener spacing $0.25 < s/L < 0.50$ since it was not included in the test specimens. The results from the parametric study indicated that the back-to-back C-channel built-up column with a gap with fastener spacing within the AISI requirements consistently achieved higher ultimate strength than built-up columns with fastener spacing beyond the AISI requirements. Parametric study results also show that the number of intermediate fasteners does not significantly influence the ultimate strength for columns with three and one intermediate fasteners. Therefore, an intermediate fastener at mid-length is vital to ensure the built-up columns act as an integral column and achieve maximum strength.

7 Current Design Methods

7.1 Introduction

This chapter evaluates the current design methods for cold-formed steel C-channel columns, and plain built-up back-to-back channels columns. In this research, design standards from American Iron and Steel Institute (AISI) are used for the design of cold-formed steel C-channel and built-up columns. The current American Iron and Steel Institute (AISI) design standards for cold-formed steel are based on the Effective Width Method (EWM). The Direct Strength Method (DSM) was recently included in the design standards for cold-formed steel structures in the Appendix of the North American Specifications (NAS) for Cold-formed Steel Structural Members (2004).

Based on the EWM and the recent DSM, three design approaches i.e. EWM, DSM I and DSM II are exploited for the design of C-channel columns and plain back-to-back C-channel built-up columns (without a gap). The difference between DSM I and DSM II is in the determination of the elastic buckling loads, whereas, the elastic buckling loads are manually calculated in the DSM I, and in the DSM II, Finite Strip Analysis software (CUFSM) is used to determine the elastic buckling loads.

The three design approaches were compared with the test results for C-channel and plain back-to-back C-channel built-up columns (without a gap). The design of plain back-to-back C-channel built-up columns (without a gap) was evaluated with respect to the modified slenderness ratio to assess the appropriateness of the design method using modified slenderness ratio. Test results were compared to design calculated results with and without the modified slenderness ratio. Detailed design equations and sample design spreadsheets are attached in Appendix H.

7.2 C-channel Columns

Singly symmetric columns like C-channel columns experience a shift of effective centroid under axial load. The shift causes an additional moment to the column, thus, the strength of the column is better estimated as a beam-column rather than a column. The detailed beam-column design is documented in Appendix H.

7.2.1 Design Procedures

7.2.1.1 Effective Width Method (EWM)

Figure 7.1 shows the summary of the processes in the determination of the design strength of a C-channel column according to the EWM. Appendix H contains the details for calculating the C-channel columns in this thesis.

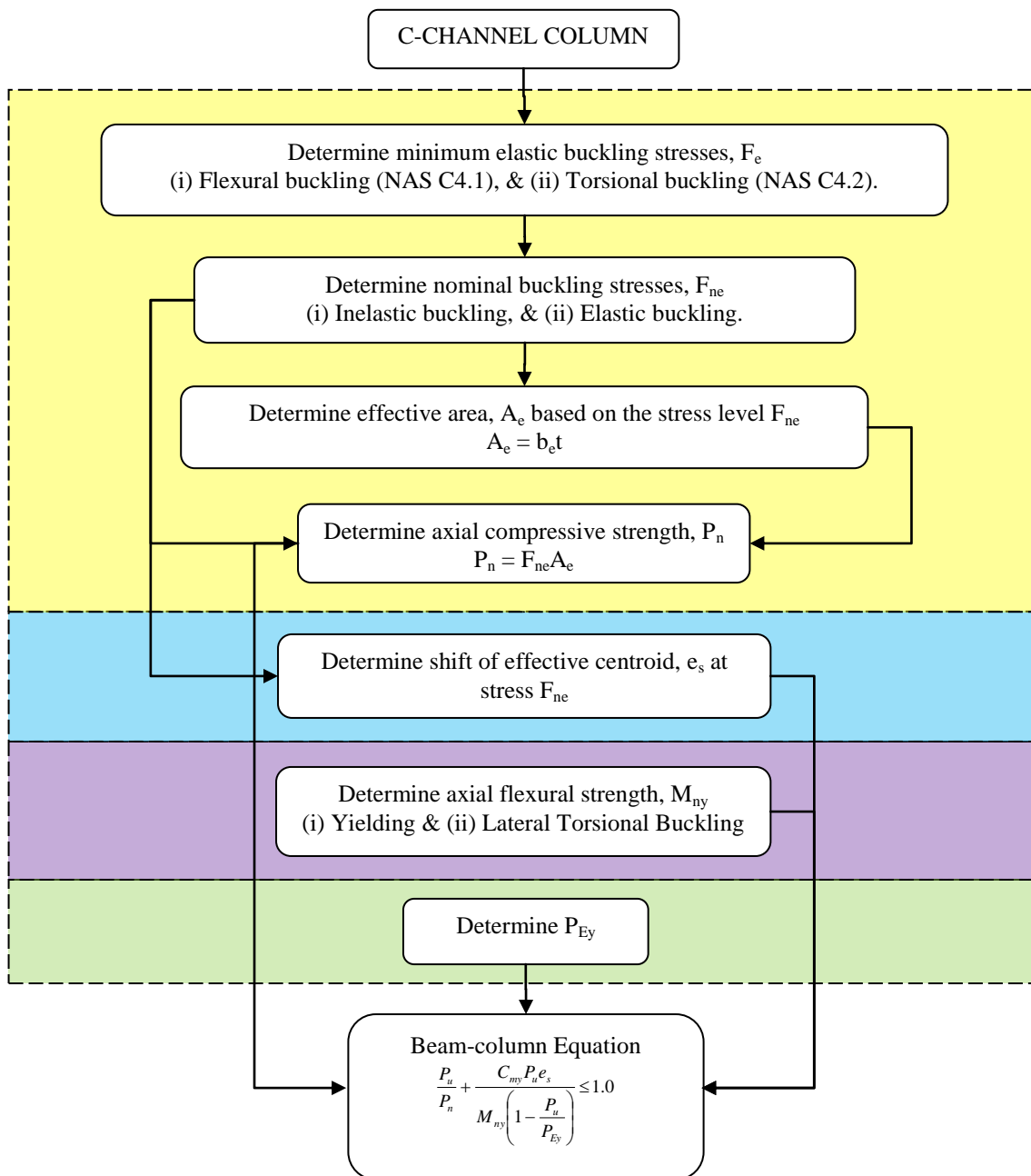


Figure 7.1: Design Procedures of the C-channel Columns using EWM

7.2.1.2 Direct Strength Method by Manual Calculation (DSM I)

Figure 7.2 shows the summary of the processes in the determination of the design strength of a C-channel column according to the DSM I. Appendix H contains the details for calculating the C-channel columns in this thesis.

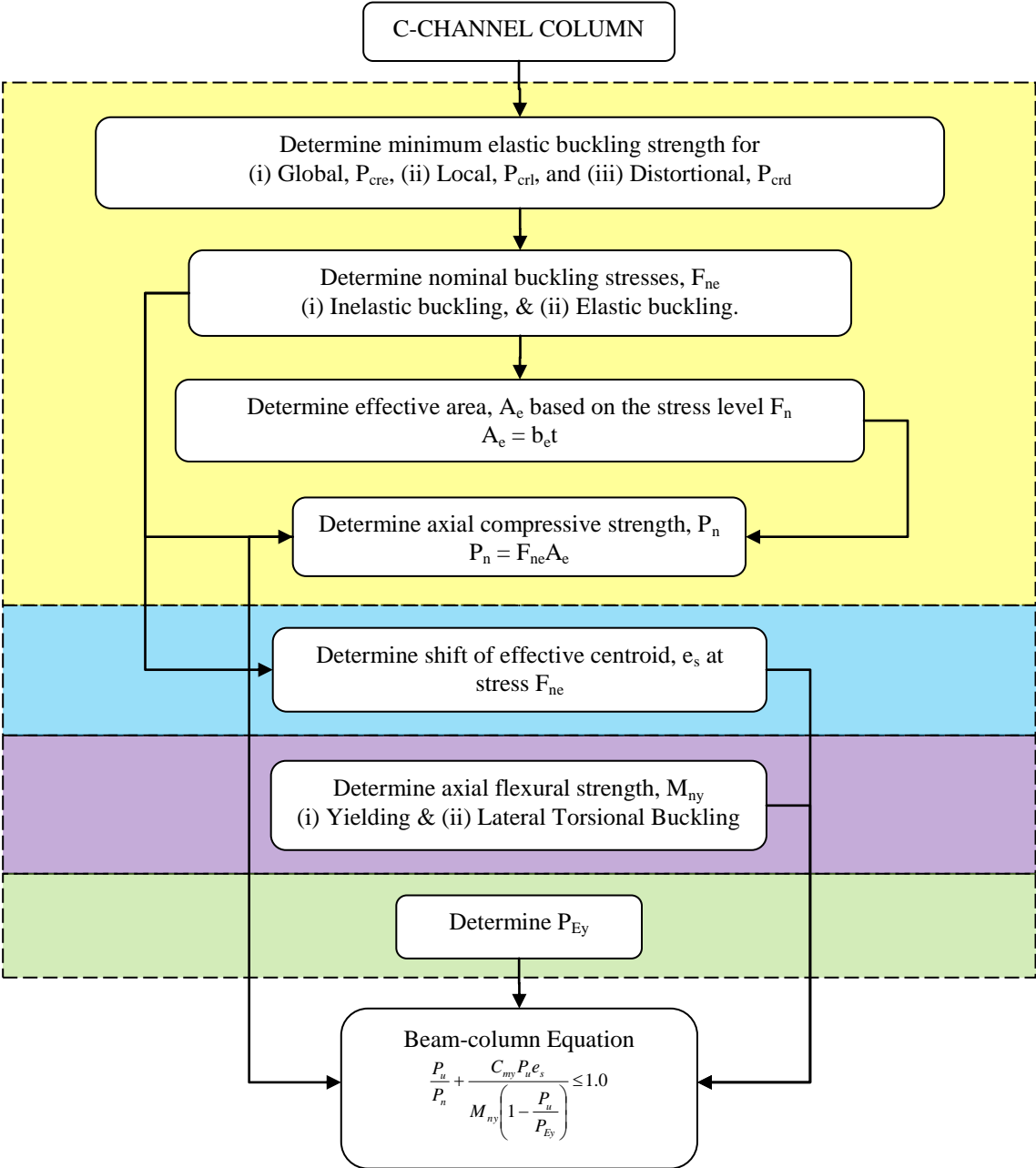


Figure 7.2: Design Procedures of the C-channel Columns using DSM I

7.2.1.3 Direct Strength Method by CUFSM (DSM II)

Figure 7.3 shows the summary of the processes in the determination of the design strength of a C-channel column according to the DSM II. Appendix H contains the details for calculating the C-channel columns in this thesis.

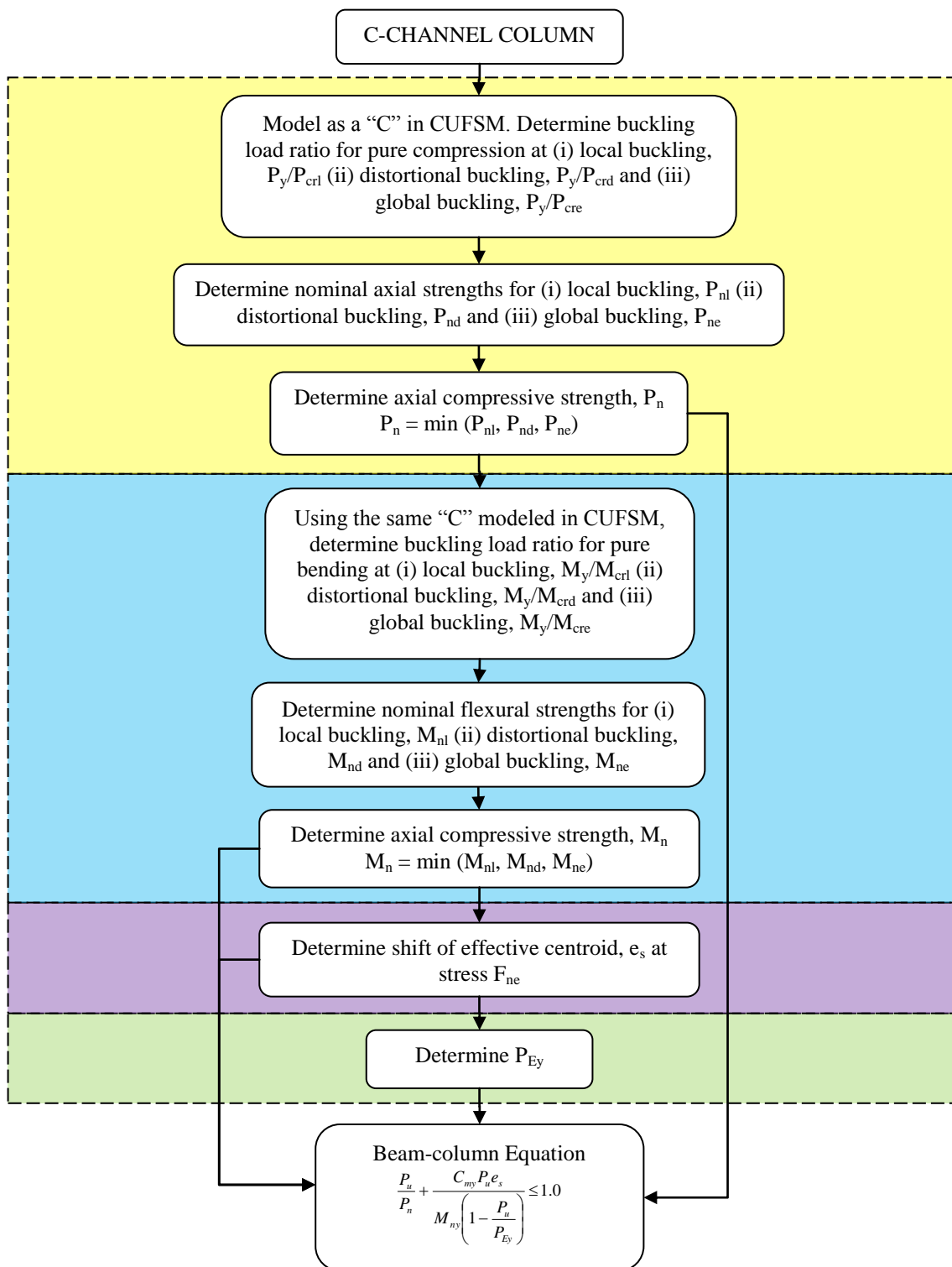


Figure 7.3: Design Procedures of the C-channel Columns using DSM II

7.3 Plain Back-to-back C-channel Built-up Columns

Design of a plain back-to-back C-channel built-up column is similar to a C-channel column except certain changes to the sectional properties and design formulae.

7.3.1 Section Properties

A back-to-back C-channel built-up section is basically made up of two C-channel sections. Thus, most of the sectional properties are regarded as twice of a C-channel. The equations required for a plain back-to-back C-channel built-up column are shown below. Figure 7.4 shows the notations used in this research.

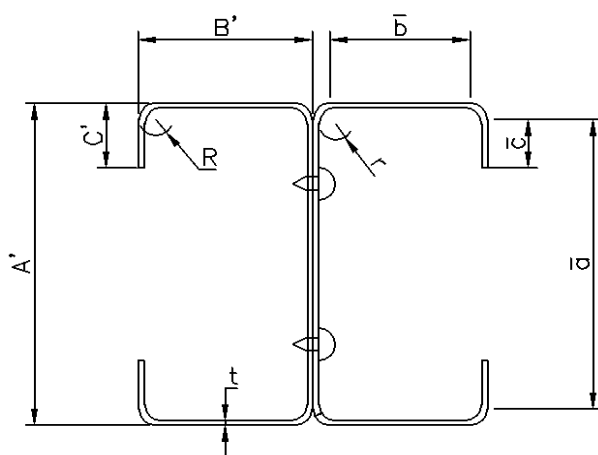


Figure 7.4: Notations for Plain Back-to-back C-channel Built-up Sections

Cross sectional area

$$A_{bu} = 2A_c \quad \text{Eq. 7-1}$$

Second Moment of Inertia for Plain Back-to-back Built-up

$$I_{xbu} = 2I_{xc} \quad \text{Eq. 7-2}$$

$$I_{ybu} = 2(I_{yc} + A_c x_{ib}^2) \quad \text{Eq. 7-3}$$

Radius of gyration

$$r_{xb} = \sqrt{\frac{I_{xb}}{A_b}} \quad \text{Eq. 7-4}$$

$$r_{yb} = \sqrt{\frac{I_{yb}}{A_b}} \quad \text{Eq. 7-5}$$

$$r_o = \sqrt{r_{xb}^2 + r_{yb}^2} \quad \text{Eq. 7-6}$$

Torsional Constant

$$J = \frac{2t^3}{3} [a + 2b + 2u + \alpha(2c + 2u)] \quad \text{Eq. 7-7}$$

Warping Constant

$$C_{wBU} = 2C_{wC} \quad \text{Eq. 7-8}$$

7.3.2 Current Design Methods

A plain built-up column requires different considerations compared to a C-channel column. A plain back-to-back C-channel built-up column reduces shear rigidity due to the screw connection at discrete locations along the length of the column. In the design standards, the only provision taking the screw spacing into consideration is the modified slenderness ratio from Clause C4.5 of the AISI Specifications 2001 Edition. The modified slenderness ratio is important to accommodate two major influences, i.e. the overall slenderness and the local slenderness between the screws, to the compressive strength of a plain back-to-back C-channel built-up column. This combined influence is considered in the design by replacing the slenderness ratio with the modified slenderness ratio when calculating the flexural buckling stress. Elastic Buckling Stress, F_e is calculated as follows:

Flexural Buckling

$$F_e = \frac{\pi^2 E}{(KL/r)_m^2}$$

where

$$\left(\frac{KL}{r}\right)_m = \sqrt{\left(\frac{KL}{r}\right)_o^2 + \left(\frac{s}{r_{yc}}\right)^2} \quad \text{Eq. 7-9}$$

It is important to note that this equation only applies when built-up column buckles in the weak axis with fasteners. This equation is required because shear forces is produced in the fasteners between the individual C-channels due to relative deformations.

According to clause C4.5 of the AISI Specification 2001 Edition, the fastener spacing is limited such that the slenderness of the individual column is less than or equal to 0.5 times of the governing slenderness ratio of the built-up column as shown below:

$$\left(\frac{s}{r_y}\right)_C \leq 0.5 \left(\frac{KL}{r_y}\right)_{BU} \quad \text{Eq. 7-10}$$

This is to account for any of the fasteners becoming ineffective. The requirement is conservative mainly because it is adopted from the hot rolled steel design provisions. Thus one of the objectives of this research is to investigate the use of modified slenderness ratio for screw spacing beyond the limit.

In terms of torsional buckling stress, equation for doubly symmetric section is used.

Torsional Buckling

Doubly Symmetric Sections

$$F_e = \sigma_1 = \frac{1}{A_{bu} r_o^2} \left[GJ + \frac{\pi^2 EC_w}{(K_t L_t)^2} \right] \quad \text{Eq. 7-11}$$

Moreover, the effective area of a plain back-to-back built up section is twice of the effective area of a C-channel section, i.e.

$$A_{eb} = 2A_{ec} \quad \text{Eq. 7-12}$$

7.3.3 CUFSM

The Direct Strength Method (DSM) Design Guide (AISI 2006, 54-55) provides two ways to model the built-up columns in the CUFSM. One of the methods is to analyse the built-up section as a C-channel. The result for built-up section is simply twice of the C-channel. This is a conservative estimation thus provide a lower bound model. The other alternative is to model as a back-to-back built-up column with ideal fasteners connecting the web together. The CUFSM assumes the cross section to be constant along its length. Thus, this assumption provides an upper bound model because the connection is assumed to be continuous rather than spaced along the length of the column. In this research, the lower bound model is used since it is more conservative compared to the upper bound model.

In the lower bound model, the buckling stresses for local and distortional buckling for a C-channel are not different from two C-channels connecting together (AISI 2006, 55). P_{crl} and P_{crd} for built-up column is twice of a C-channel column. Thus,

$$P_{crl,BU} = 2P_{crl,C} \quad \text{Eq. 7-13}$$

$$P_{crd,BU} = 2P_{crd,C} \quad \text{Eq. 7-14}$$

In addition, the area of a plain back-to-back C-channel built-up is also twice of a C-channel. Thus, the nominal strength of a plain back-to-back C-channel built-up column is as follows:

$$P_{yb} = (2A_{gc})F_y = 2P_{yc} \quad \text{Eq. 7-15}$$

By rearranging the previous equations, the local and distortional buckling load ratio derived for a plain back-to-back C-channel built-up column is not different from C-channel column. Therefore, the buckling load ratio for local buckling and distortional buckling of plain back-to-back C-channel built-up column can be obtained directly from the CUFSM curve for C-channel column.

$$\frac{2P_{yc}}{2P_{crl}} = \left(\frac{P_y}{P_{crl}} \right)_{channel} \quad \text{Eq. 7-16}$$

$$\frac{2P_{yc}}{2P_{crd}} = \left(\frac{P_y}{P_{crd}} \right)_{channel} \quad \text{Eq. 7-17}$$

Since the local and distortional buckling load ratio for plain back-to-back C-channel built-up column are similar to C-channel column, analysis for plain back-to-back C-channel built-up column in the CUFSM is similar to analysis for a C-channel column.

However, the global buckling load ratio for plain back-to-back C-channel built-up columns could not be identified from the CUFSM curve for C-channel columns because the built-up columns have greater flexural strength in the weak axis than C-channel columns. Therefore, the DSM with hand calculation (i.e. same as the DSM I) is preferred compared to the CUFSM in the determination of the global buckling solution.

7.3.4 Design Procedures

7.3.4.1 Effective Width Method (EWM)

Figure 7.5 shows the summary of the processes in the determination of the design strength of a plain back-to-back C-channel built-up column according to the EWM.

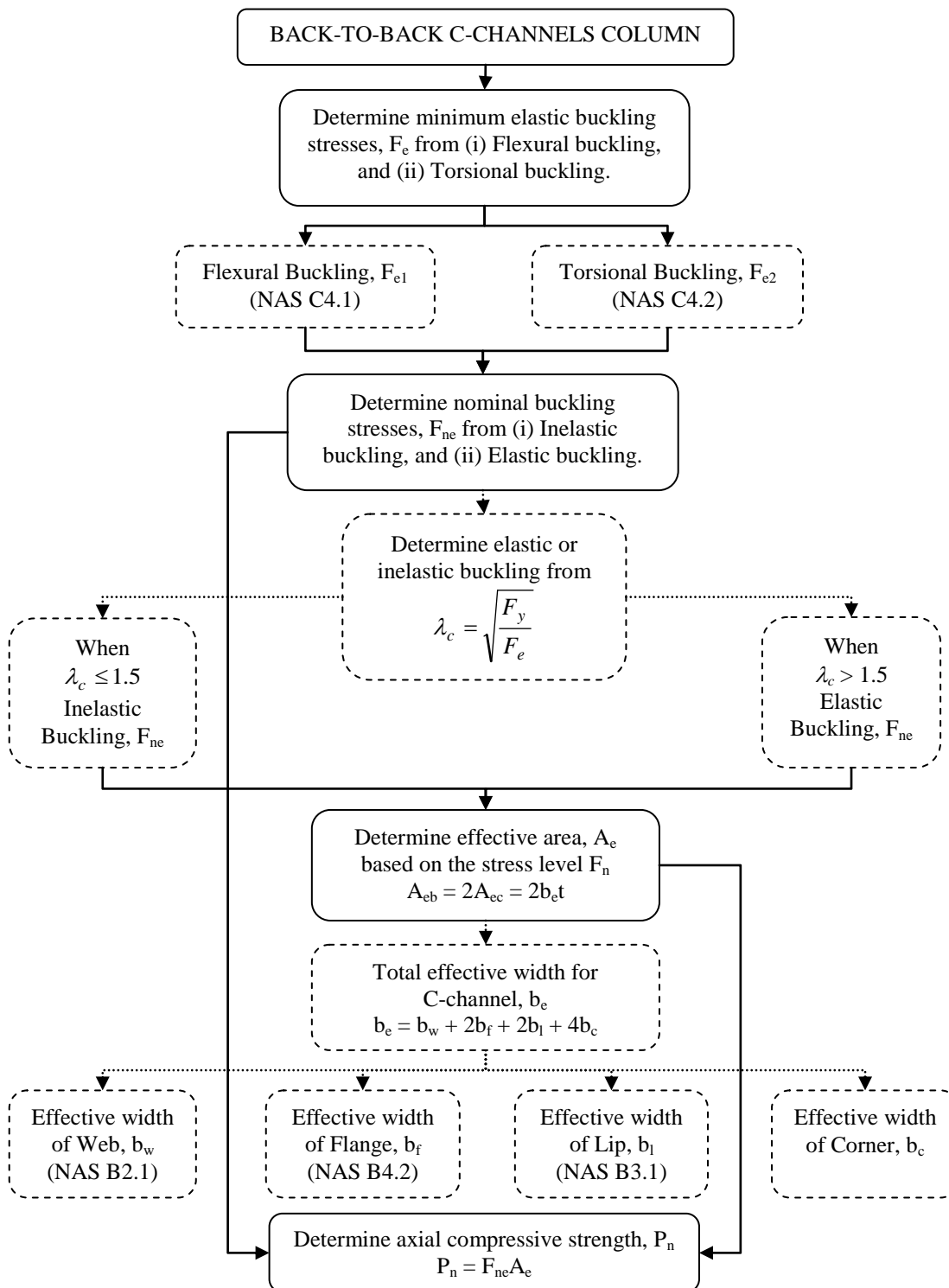


Figure 7.5: Design Procedures of the Plain Back-to-back C-channel Built-up Columns using EWM

7.3.4.2 Direct Strength Method by Manual Calculation (DSM I)

Figure 7.6 shows the summary of the processes in the determination of the design strength of a plain back-to-back C-channel built-up column according to the DSM I.

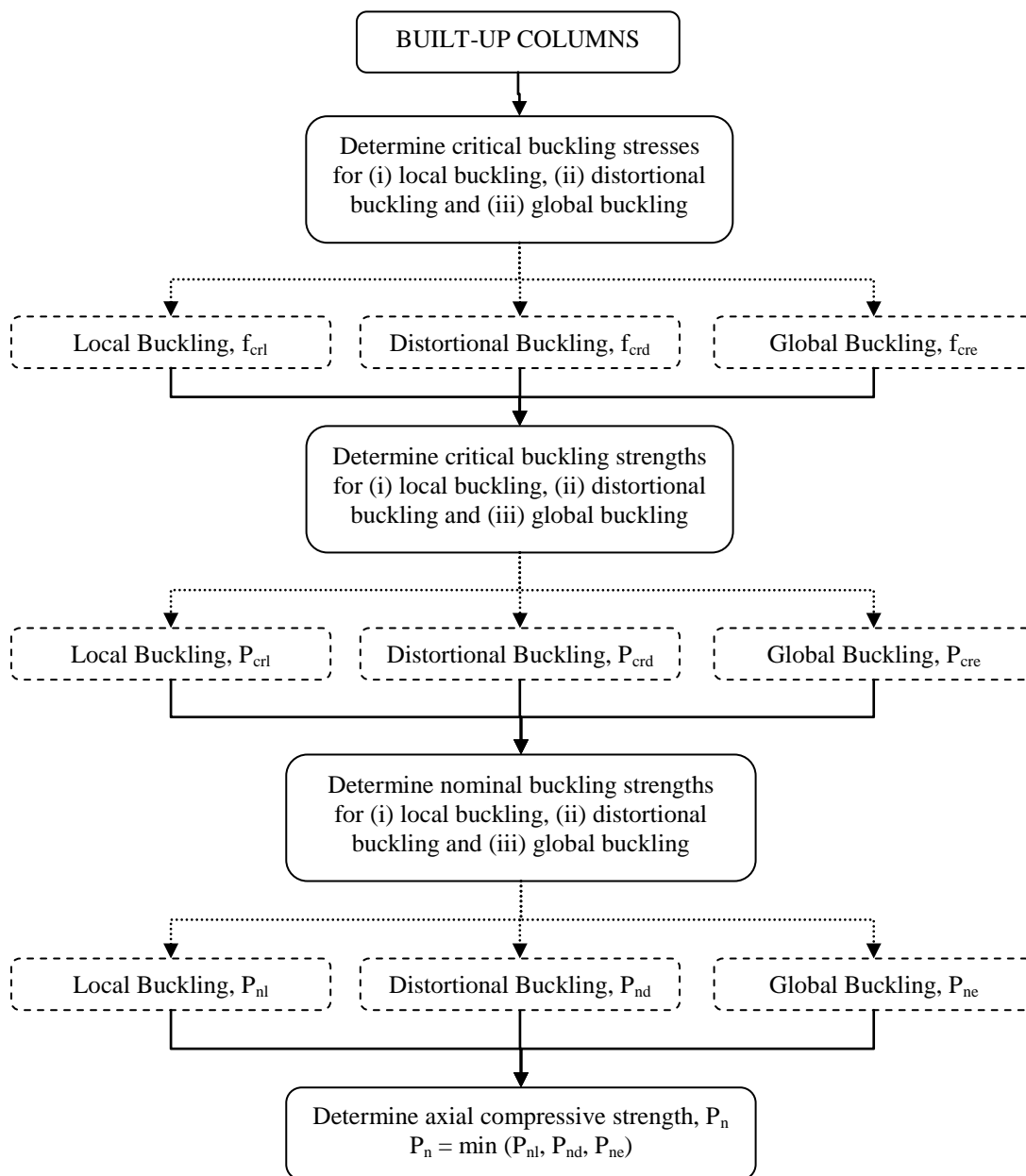


Figure 7.6: Design Procedures of the Plain Back-to-back C-channel Built-up Columns using DSM I

7.3.4.3 Direct Strength Method by CUFSM (DSM II)

Figure 7.7 shows the summary of the processes in the determination of determining the design strength of a plain back-to-back C-channel built-up column according to the DSM II.

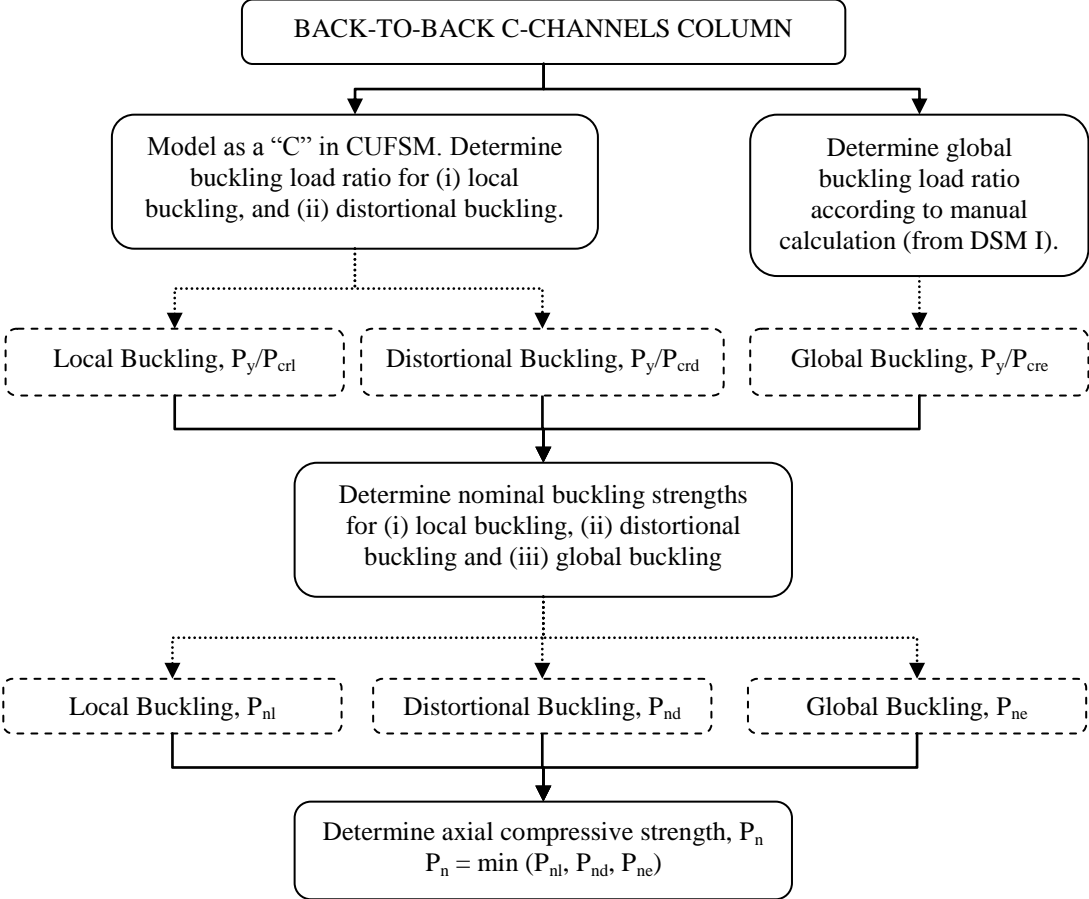


Figure 7.7: Design Procedures of the Plain Back-to-back C-channel Built-up Columns using DSM II

7.4 Evaluation of the Current Design Methods

7.4.1 C-channel Columns

Table 7.1 shows the comparison of test results and design calculated results for the stub column test specimens of the C75 and C90 test series. The ratios of the test result to the design calculated result of the EWM, DSM I and DSM II are also included in Table 7.1.

Table 7.1: Comparison of Test & Design Results for C-channel C75 Stub Columns

Specimen	P_{test} (kN)	P_{EWM} (kN)	P_{DSMI} (kN)	P_{DSMII} (kN)	$\frac{P_{test}}{P_{EWM}}$	$\frac{P_{test}}{P_{DSMI}}$	$\frac{P_{test}}{P_{DSMII}}$
C75L300-1	60.63	62.82	56.79	58.18	0.97	1.07	1.04
C75L300-2	58.24	61.81	55.88	57.29	0.94	1.04	1.02
C75L300-3	59.91	61.77	55.88	57.28	0.97	1.07	1.05
C75L300-4	55.70	61.78	55.86	57.24	0.90	1.00	0.97
Mean					0.94	1.04	1.02
C90L300-2	83.70	81.41	78.29	83.58	1.03	1.07	1.00
C90L300-3	86.12	82.76	79.45	84.25	1.04	1.08	1.02
C90L300-4	86.70	82.87	79.53	84.84	1.05	1.09	1.02
Mean					1.04	1.08	1.02
Overall Mean					0.98	1.06	1.02
Population Standard Deviation					0.05	0.03	0.02

It is shown in Table 7.1 that the EWM and the DSM conservatively predict the design strength of C75L300 and C90L300 stub column specimens. Among all the design methods, DSM is the most conservative design method for stub column. When comparing the two DSMs, the DSMI is more conservative compared to the DSMII because the DSMI uses classical hand calculated solution while the DSMII uses finite strip analysis for the determination of elastic buckling solutions. Classical hand calculated solutions are tedious for more complex buckling modes, such as distortional buckling and the method may ignore critical mechanical features such as inter-element equilibrium and compatibility (Schafer and Ádány 2006, 2). This is less accurate compared to finite strip analysis which provides a means to examine all the possible instabilities for a cold-formed steel column under longitudinal stresses. This shows that the analysis in the DSMII is more thorough compared to the DSMI.

Table 7.2 shows the comparison of test results and design calculation for the short, intermediate and slender column test specimens of the C75 and C90 test series. The ratios of the test result to the design calculated results of the EWM, DSMI and DSMII are also included in Table 7.2.

Table 7.2: Comparison of Test & Design Results for Pin-ended C-channel Columns from C75 and C90 Test Series

Specimen	P_{test} (kN)	P_{EWM} (kN)	P_{DSMI} (kN)	P_{DSMII} (kN)	$\frac{P_{test}}{P_{EWM}}$	$\frac{P_{test}}{P_{DSMI}}$	$\frac{P_{test}}{P_{DSMII}}$
C75L500-2	52.07	24.78	27.32	26.08	2.10	1.91	2.00
C75L500-3	53.01	24.90	27.43	26.10	2.13	1.93	2.03
C75L500-4	40.13	25.08	27.67	26.61	1.60	1.45	1.51
Mean					1.94	1.76	1.85
C75L1000-1	15.80	11.59	11.59	11.33	1.36	1.36	1.39
C75L1000-2	16.38	11.73	11.73	11.33	1.40	1.40	1.45
Mean					1.38	1.38	1.42
C75L2000-1	7.49	3.30	3.30	3.31	2.27	2.27	2.26
C75L2000-2	6.79	3.30	3.30	3.31	2.06	2.06	2.05
C75L2000-3	9.83	3.32	3.32	3.31	2.96	2.96	2.97
Mean					2.43	2.43	2.43
C90L500-1	82.84	62.13	62.59	49.01	1.33	1.32	1.69
C90L500-2	81.20	60.52	62.49	48.60	1.34	1.30	1.67
C90L500-3	78.04	61.63	62.57	48.94	1.27	1.25	1.59
Mean					1.31	1.29	1.65
C90L1000-1	84.95	50.46	47.44	47.34	1.68	1.79	1.79
C90L1000-2	86.94	50.41	47.40	47.40	1.72	1.83	1.83
C90L1000-3	70.79	46.69	44.39	43.61	1.52	1.59	1.62
Mean					1.64	1.74	1.75
Overall Mean					1.77	1.74	1.85
Population Standard Deviation					0.46	0.46	0.40

Table 7.2 shows that design strength calculated using beam-column equations due to shift of effective centroid for all design methods are conservative compared to the experimental results of the C-channel columns. Generally, the DSMII is the most conservative while the EWM predictions are the closest to the experimental results. However, the EWM predictions tend to be more conservative for longer columns. The experimental results for these pin-ended C-channel columns were relatively high due to frictions in the pinned-end assemblies during the testing. Due to relatively small variation of geometry among the C75L2000 specimens, the averaged ratios of test result to design calculation are similar.

7.4.2 Plain Back-to-back C-channel Built-up Columns

7.4.2.1 Modified Slenderness Ratio, $(KL/r)_m$

Clause C4.5 of the AISI Specifications 2001 Edition (AISI 2002c, 83) specifies that for columns composed of two individual columns in contact, the slenderness ratio needs to be replaced with a modified slenderness ratio. The modified slenderness ratio is used to account for the effect of fastener spacing on the design strength of the built-up column. Therefore, the plain back-to-back C-channel built-up column test specimens are designed with varying fastener spacing. These test specimens include fastener spacing that is within and beyond the AISI Specifications requirements as mentioned in Chapter 3. The design calculations with and without the modified slenderness ratio are carried out and compared with the experimental results.

Table 7.3 shows the comparison of design calculated results using modified and unmodified slenderness ratio to test results for the BU75 test series at various fastener spacing.

Table 7.3: Comparison of Test & Design Results for BU75 With & Without Modified Slenderness Ratio

Specimen	P_{test} (kN)	Modified Slenderness Ratio			Unmodified Slenderness Ratio		
		P_{EWM} (kN)	P_{DSMI} (kN)	P_{DSMII} (kN)	P_{EWM} (kN)	P_{DSMI} (kN)	P_{DSMII} (kN)
BU75S50L300-1	120.66	126.68	114.32	114.39	127.02	114.56	114.39
BU75S50L300-2	118.87	126.77	114.40	114.39	127.10	114.63	114.39
BU75S50L300-3	118.65	124.84	113.25	112.77	125.20	113.51	112.77
Mean	119.39	126.10	113.99	113.85	126.44	114.23	113.85
BU75S100L300-2	117.48	125.10	113.23	112.96	127.07	114.62	112.96
BU75S100L300-3	122.74	125.41	113.41	113.26	127.38	114.80	113.26
BU75S100L300-4	115.37	124.89	113.01	113.46	126.87	114.41	113.46
Mean	118.53	125.13	113.22	113.23	127.11	114.61	113.23
BU75S200L300-1	122.51	119.05	108.80	109.38	127.36	114.69	115.31
BU75S200L300-2	119.12	119.09	108.82	109.36	127.33	114.67	115.24
BU75S200L300-3	113.14	119.36	109.12	108.99	127.57	114.94	114.80
Mean	118.26	119.17	108.91	109.24	127.42	114.77	115.12

(contd.)

BU75S100L500-1	82.96	82.37	81.21	82.17	83.80	82.33	83.32
BU75S100L500-3	74.07	78.83	78.41	79.27	80.22	79.53	80.40
Mean	78.52	80.60	79.81	80.72	82.01	80.93	81.86
BU75S200L500-1	86.21	77.49	77.36	78.11	82.82	81.64	82.44
BU75S200L500-2	88.93	75.21	75.49	76.36	80.37	79.65	80.57
BU75S200L500-3	93.61	75.26	75.56	76.26	80.68	79.92	80.67
Mean	89.58	75.99	76.14	76.91	81.29	80.40	81.23
BU75S400L500-1	74.77	61.30	63.91	64.60	80.86	80.04	80.94
BU75S400L500-2	80.56	60.99	63.65	64.31	80.61	79.85	80.70
BU75S400L500-3	87.64	61.56	64.13	64.80	80.96	80.11	80.98
Mean	80.99	61.28	63.90	64.57	80.81	80.00	80.87
BU75S225L1000-1	47.04	36.34	37.41	37.41	38.34	39.86	39.86
BU75S225L1000-2	46.28	35.05	35.94	35.94	36.98	38.30	38.30
Mean	46.66	35.70	36.68	36.68	37.66	39.08	39.08
BU75S450L1000-1	50.43	30.67	30.73	30.73	37.27	38.66	38.66
BU75S450L1000-2	45.02	30.09	30.09	30.09	36.67	37.92	37.92
BU75S450L1000-3	41.77	27.81	27.81	27.81	33.77	34.44	34.44
Mean	45.74	29.52	29.54	29.54	35.90	37.01	37.01
BU75S900L1000-1	39.90	18.74	18.74	18.74	36.93	38.29	38.29
BU75S900L1000-2	33.70	17.04	17.04	17.04	33.61	34.44	34.44
BU75S900L1000-3	31.48	17.63	17.63	17.63	33.80	34.47	34.47
Mean	35.03	17.80	17.80	17.80	34.78	35.73	35.73
BU75S475L2000-2	15.33	10.27	10.27	10.27	11.08	11.08	11.08
BU75S475L2000-3	12.87	10.22	10.22	10.22	10.99	10.99	10.99
Mean	14.10	10.25	10.25	10.25	11.04	11.04	11.04
BU75S950L2000-2	13.22	8.43	8.43	8.43	11.11	11.11	11.11
BU75S950L2000-3	12.99	8.36	8.36	8.36	11.00	11.00	11.00
Mean	13.11	8.40	8.40	8.40	11.06	11.06	11.06
BU75S1900L2000-2	12.12	4.90	4.90	4.90	11.13	11.13	11.13
BU75S1900L2000-3	13.11	4.93	4.93	4.93	11.19	11.19	11.19
Mean	12.62	4.92	4.92	4.92	11.16	11.16	11.16

Table 7.3 shows that most of the average design calculated results based on the modified slenderness ratio were more conservative than the average design calculated results based on the unmodified slenderness ratio. The design calculated results based on the unmodified slenderness ratio did not show much variation at different screw spacing. However, the design calculated results with modified slenderness ratio predicted otherwise, where the results decreased with the increased screw spacing. This phenomenon was shown in the experimental results but was not as significant as predicted by the design calculation with modified slenderness ratio.

Results are also presented in Figures 7.8, 7.9, and 7.10 for $s/L < 0.25$ denoted as SS, for $0.25 < s/L < 0.50$ denoted as MS and for $s/L > 0.50$ denoted as LS respectively. In these graphs, the test results are represented by larger markers without line while the design calculated results are represented by a full line for the results calculated using modified slenderness ratio and a dotted line for the results calculated using unmodified slenderness ratio. The design methods include the EWM, the DSMI and the DSMII.

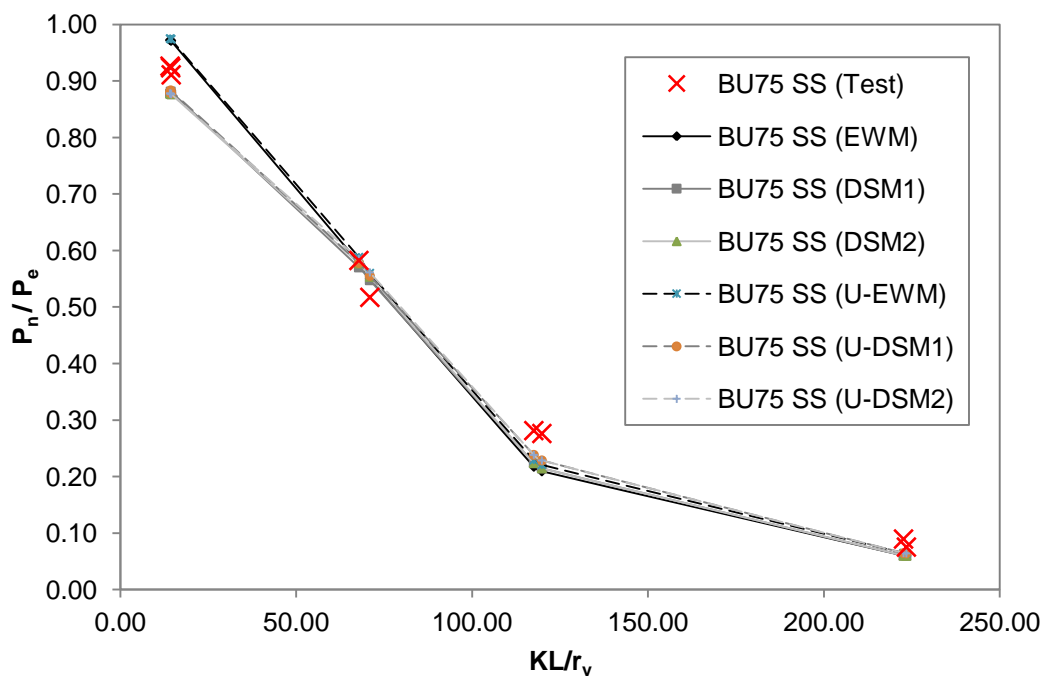


Figure 7.8: Comparison of Test and Design Calculated Results for BU75 with Three Intermediate Fasteners at $s/L < 0.25$

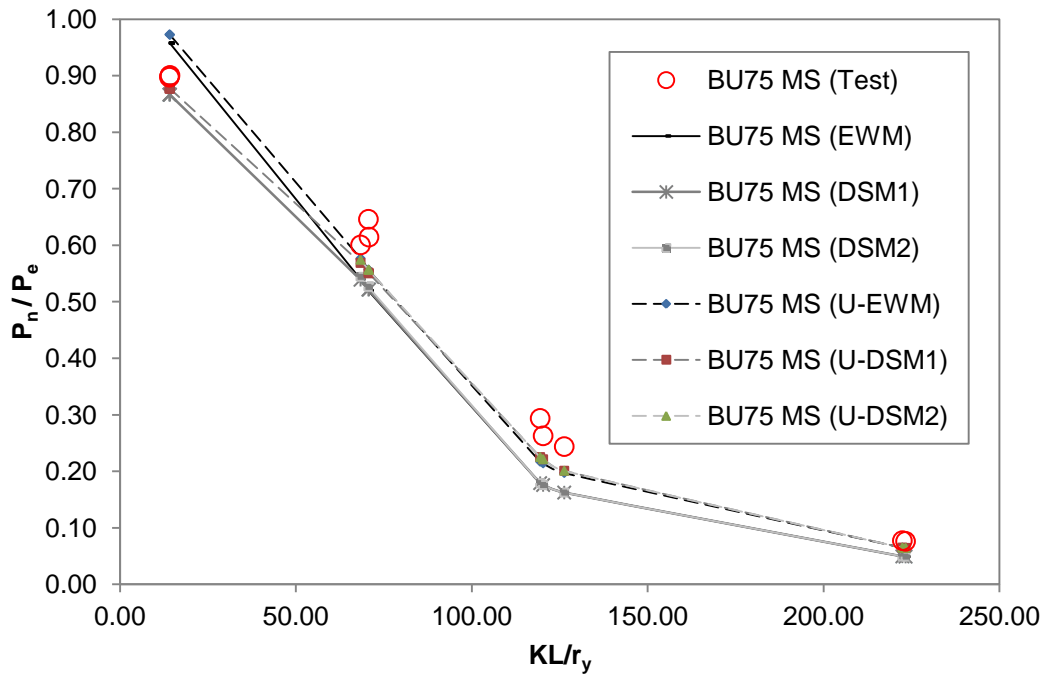


Figure 7.9: Comparison of Test and Design Calculated Results for BU75 with One Intermediate Fastener at $0.25 < s/L < 0.50$

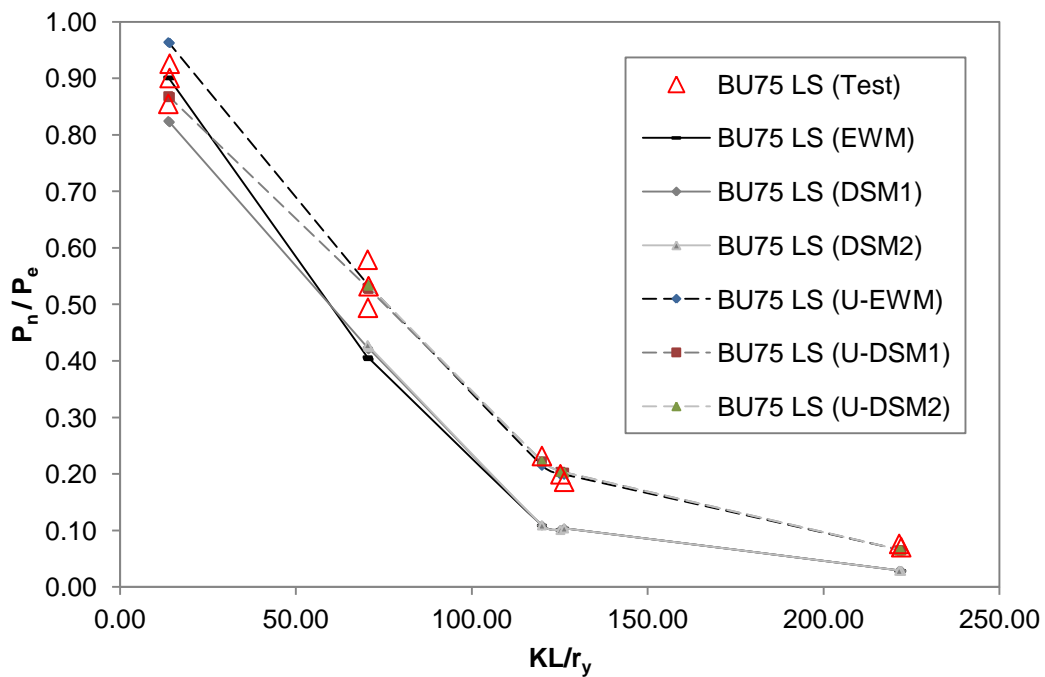


Figure 7.10: Comparison of Test and Design Calculated Results for BU75 with No Intermediate Fastener at $s/L > 0.50$

The averaged design calculated results with modified slenderness ratio were lower than the averaged design strength calculated with unmodified slenderness ratio for plain back-to-back C-channel built-up columns with screw spacing within the code requirement. Comparison of the graphs shows that the design calculation with unmodified slenderness ratio is closer to the strength of the tested columns at large fastener spacing such as $0.25 < s/L < 0.50$ and $s/L > 0.50$. The design calculated results show significant strength reduction as the fastener spacing increased. However, the test results show only slight strength reduction. The difference between the design strength and test results is even more apparent for slender columns. This shows that the use of modified slenderness ratio is conservative for longer columns especially when the fastener spacing is beyond the code requirement of clause C4.5 of the AISI Specification 2001 edition.

Similarly, Table 7.4 shows the comparison of design calculation with modified and unmodified slenderness ratio to test results for the BU90 test series at various fastener spacing.

Table 7.4 shows that the average design calculation based on the modified slenderness ratio was more conservative than the average design calculation based on the unmodified slenderness ratio. The design calculation based on both modified and unmodified slenderness ratio shows similar results for columns with different fastener spacing because all the columns from the BU90 test series are relatively short.

Table 7.4: Comparison of Test & Design Results for BU90 With & Without Modified Slenderness Ratio

Specimen	P _{test} (kN)	Modified Slenderness Ratio			Unmodified Slenderness Ratio		
		P _{EWM} (kN)	P _{DSMI} (kN)	P _{DSMII} (kN)	P _{EWM} (kN)	P _{DSMI} (kN)	P _{DSMII} (kN)
BU90S50L300-1	172.49	164.05	156.66	166.83	164.05	156.67	166.83
BU90S50L300-2	171.61	163.73	156.36	166.47	163.73	156.36	166.47
BU90S50L300-3	167.56	163.64	155.64	165.61	163.64	155.64	165.61
Mean	170.55	163.81	156.22	166.30	163.81	156.22	166.30
BU90S100L300-3	171.18	163.83	156.71	166.91	163.85	156.73	166.91
BU90S100L300-4	173.87	163.78	156.62	166.80	163.81	156.64	166.80
Mean	172.53	163.81	156.67	166.86	163.83	156.69	166.86
BU90S200L300-1	170.25	162.66	155.41	165.77	163.61	156.41	166.84
BU90S200L300-2	177.50	163.08	155.58	165.92	164.01	156.55	166.96
BU90S200L300-4	171.88	162.95	155.62	166.05	163.86	156.57	167.08
Mean	173.21	162.90	155.54	165.91	163.83	156.51	166.96
BU90S100L500-1	165.01	151.37	143.41	148.77	151.37	143.41	148.77
BU90S100L500-2	163.22	150.47	142.42	147.73	150.47	142.42	147.73
Mean	164.12	150.92	142.92	148.25	150.92	142.92	148.25
BU90S200L500-1	170.48	151.66	143.5	149.37	151.66	143.5	149.37
BU90S200L500-2	173.17	150.6	142.37	148.19	150.6	142.37	148.19
BU90S200L500-3	151.53	150.18	142.27	148.06	150.18	142.27	148.06
Mean	165.06	150.81	142.71	148.54	150.81	142.71	148.54
BU90S400L500-1	170.01	150.66	142.54	148.59	150.66	142.54	148.59
BU90S400L500-2	151.41	150.72	142.57	148.41	150.72	142.57	148.41
Mean	160.71	150.69	142.56	148.50	150.69	142.56	148.50
BU90S225L1000-1	167.81	124.67	117.28	121.61	124.67	117.28	121.61
BU90S225L1000-2	151.76	127.09	119.71	124.13	127.09	119.71	124.31
Mean	159.79	125.88	118.50	122.87	125.88	118.50	122.96
BU90S450L1000-2	175.18	127.57	120.08	124.53	127.57	120.08	124.53
BU90S450L1000-4	161.12	124.73	117.19	121.51	124.73	117.19	121.51
Mean	168.15	126.07	118.61	123.09	126.15	118.64	123.02
BU90S900L1000-1	164.86	122.43	115.16	119.39	127.12	119.72	124.14
BU90S900L1000-2	150.94	120.72	112.93	117.03	124.52	116.60	120.85
Mean	157.90	121.58	114.05	118.21	125.82	118.16	122.50

Results are also presented in Figures 7.11, 7.12, and 7.13. In these graphs, the markers and notations used are the same as the previous series of graphs for the BU75 test series.

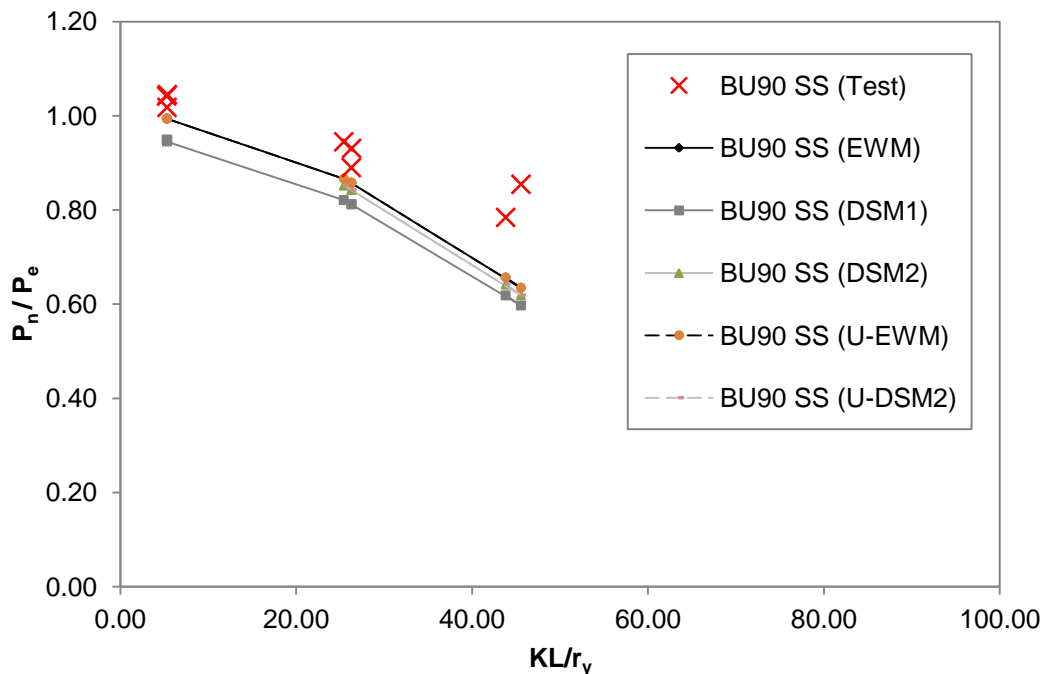


Figure 7.11: Comparison of Test & Design Calculated Results for BU90 with Fastener Spacing at $s/L < 0.25$

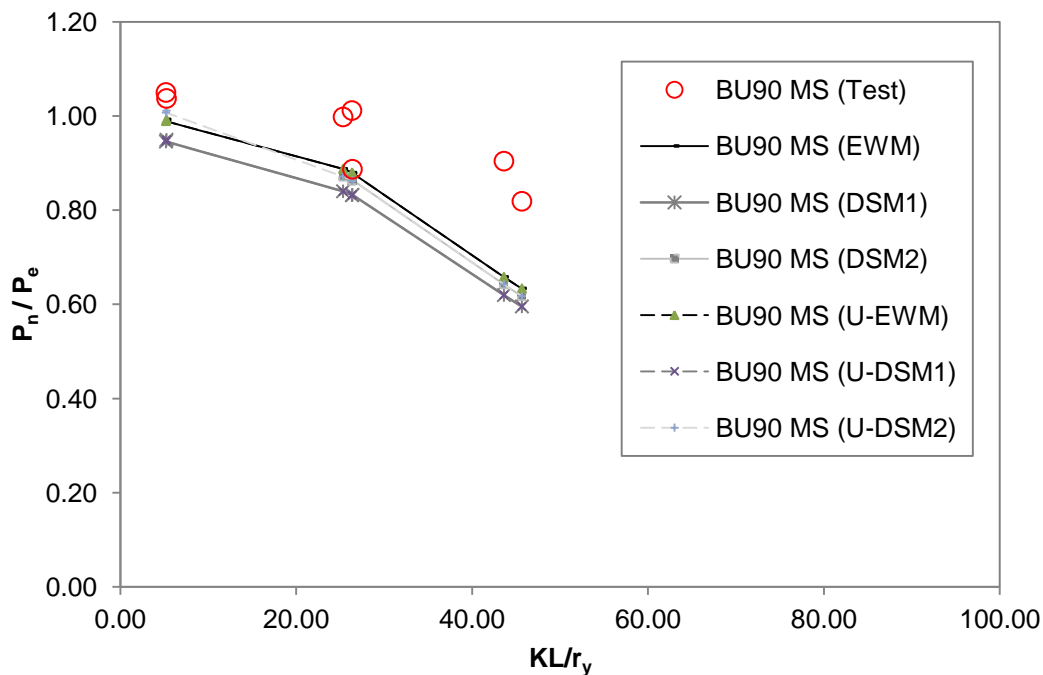


Figure 7.12: Comparison of Test & Design Calculated Results for BU90 with Fastener Spacing at $0.25 < s/L < 0.50$

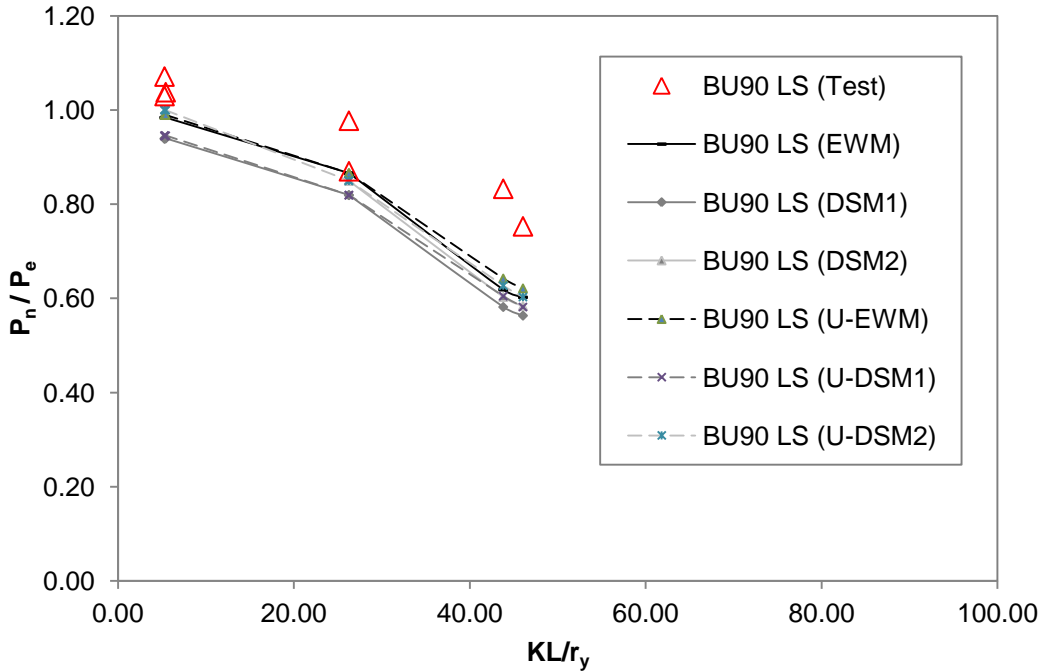


Figure 7.13: Comparison of Test & Design Calculated Results for BU90 with Fastener Spacing at $s/L > 0.50$

Figures 7.11 to 7.13 show that the AISI Specifications predicted the design strength of the plain back-to-back C-channel built-up columns well when the screw spacing is within the AISI Specifications. When the screw spacing increased beyond the requirement of the AISI Specifications, the design strength of the plain back-to-back C-channel built-up columns was underestimated.

Similar to the BU75 test series, the design calculation with modified and unmodified slenderness ratio are both conservative in predicting the experimental results of the BU90 test series. The difference between experimental and design calculated results was similar for all screw spacing because the BU90 test series are relatively short with an overall slenderness ratio (KL/r_y) of less than 50. This is too short for the effects of the screw spacing to be significant. However, similar to BU75 test series, comparison shows larger difference between design calculation and test results for specimens with greater length. Thus, the design calculated results based on the modified slenderness ratio were more conservative for longer columns than shorter columns.

Furthermore, the averaged design calculation with the unmodified slenderness ratio was closer to the experimental results than the design calculation with modified

slenderness ratio. The test results show that increment of the screw spacing beyond the requirement of clause C4.5 did not significantly reduce the strength of the plain back-to-back C-channel built-up columns.

In general, the flexural buckling stress is greatly affected by the overall slenderness of the cross section as shown by the flexural buckling stress equation for built-up columns below:

$$F_e = \frac{\pi^2 E}{(KL/r)^2} = \frac{\pi^2 E}{(KL/r)_m^2}$$

The greater the slenderness the lower the predicted flexural buckling stresses.

For plain back-to-back C-channel built-up columns, the overall slenderness ratio is replaced by the modified slenderness ratio which is greater than the original unmodified slenderness ratio. Thus for cross sections with larger fastener spacing, the slenderness modification greatly increased the slenderness ratio which reduced the elastic flexural buckling stress, F_e and later reduced the design strength prediction, P_n as well. Thus, capacity of the plain back-to-back C-channel built-up columns at larger spacing is better predicted with the unmodified method, as the design strength calculated is less conservative.

The design calculated result predicts that plain back-to-back C-channel built-up columns of the same length became prone to buckling as the screw spacing increased thus causing the column to reduce in strength at an earlier stage. The slenderness ratio modification accounts for the reduction in shear rigidity which is a significant issue in larger spacing as the restraints reduced. This is shown in the test results but the effect was not as significant as predicted by the design calculations. Observations from the compression test also show that it is important to have fasteners at mid-length where deflection is the greatest to ensure that the column acted as an integral unit. This fastener spacing is close or within the fastener spacing requirement of the clause C4.5 of the AISI Specifications 2001 Edition. Thus, modified slenderness ratio is used for further analysis in this research.

7.4.2.2 Current Design Methods

Table 7.5 shows the ratios of test and finite element results to calculated results for the EWM, DMSI, and DSMII for the BU75S50L300 and BU90S50L300 stub column specimens.

Table 7.5: Comparison of Test & Finite Element Results to Design Calculated Results for BU75 Stub Columns

Specimen	P_{test} (kN)	P_{FE} (kN)	P_{EWM} (kN)	P_{DSMI} (kN)	P_{DSMII} (kN)	$\frac{P_{test}}{P_{EWM}}$	$\frac{P_{test}}{P_{DSMI}}$	$\frac{P_{test}}{P_{DSMII}}$	$\frac{P_{FE}}{P_{EWM}}$	$\frac{P_{FE}}{P_{DSMI}}$	$\frac{P_{FE}}{P_{DSMII}}$
BU75S50L300-1	120.66	120.13	126.68	114.32	114.39	0.95	1.06	1.05	0.95	1.05	1.05
BU75S50L300-2	118.87	126.74	126.77	114.40	114.39	0.94	1.04	1.04	1.00	1.11	1.11
BU75S50L300-3	118.65	122.04	124.84	113.25	112.77	0.95	1.05	1.05	0.98	1.08	1.08
Mean						0.95	1.05	1.05	0.98	1.08	1.08
BU75S100L300-1	Discard										
BU75S100L300-2	117.48	127.00	125.10	113.23	112.96	0.94	1.04	1.04	1.02	1.12	1.12
BU75S100L300-3	122.74	127.03	125.41	113.41	113.26	0.98	1.08	1.08	1.01	1.12	1.12
BU75S100L300-4	115.37	126.58	124.89	113.01	113.46	0.92	1.02	1.02	1.01	1.12	1.12
Mean						0.95	1.05	1.05	1.01	1.12	1.12
BU75S200L300-1	122.51	121.56	119.05	108.80	109.38	1.03	1.13	1.12	1.02	1.12	1.11
BU75S200L300-2	119.12	123.23	119.09	108.82	109.36	1.00	1.09	1.09	1.03	1.13	1.13
BU75S200L300-3	113.14	123.17	119.36	109.12	108.99	0.95	1.04	1.04	1.03	1.13	1.13
Mean						0.99	1.09	1.08	1.03	1.13	1.12

(contd.)

Specimen	P_{test} (kN)	P_{FE} (kN)	P_{EWM} (kN)	P_{DSMI} (kN)	P_{DSMII} (kN)	$\frac{P_{test}}{P_{EWM}}$	$\frac{P_{test}}{P_{DSMI}}$	$\frac{P_{test}}{P_{DSMII}}$	$\frac{P_{FE}}{P_{EWM}}$	$\frac{P_{FE}}{P_{DSMI}}$	$\frac{P_{FE}}{P_{DSMII}}$
BU90S50L300-1	172.49	185.00	164.05	156.66	166.83	1.05	1.10	1.03	1.13	1.18	1.11
BU90S50L300-2	171.61	186.58	163.73	156.36	166.47	1.05	1.10	1.03	1.14	1.19	1.12
BU90S50L300-3	167.56	187.00	163.64	155.64	165.61	1.02	1.08	1.01	1.14	1.20	1.13
Mean						1.04	1.09	1.03	1.14	1.19	1.12
BU90S100L300-1	Discard										
BU90S100L300-2	Discard										
BU90S100L300-3	171.18	188.44	163.83	156.71	166.91	1.04	1.09	1.03	1.15	1.20	1.13
BU90S100L300-4	173.87	185.52	163.78	156.62	166.80	1.06	1.11	1.04	1.13	1.18	1.11
Mean						1.05	1.10	1.03	1.14	1.19	1.12
BU90S200L300-1	170.25	187.72	162.66	155.41	165.48	1.05	1.10	1.03	1.15	1.21	1.13
BU90S200L300-2	177.50	188.12	163.08	155.58	165.67	1.09	1.14	1.07	1.15	1.21	1.14
BU90S200L300-3	Discard										
BU90S200L300-4	171.88	187.81	162.95	155.62	165.53	1.05	1.10	1.04	1.15	1.21	1.13
Mean						1.06	1.11	1.05	1.15	1.21	1.13
Overall Mean						1.01	1.08	1.05	1.07	1.15	1.12
Population Standard Deviation						0.05	0.03	0.03	0.07	0.05	0.02

Results show that prediction by the EWM is unconservative. The prediction by the DSMI is always more conservative compared to the DSMII because the DSMI uses classical hand solutions while the DSMII uses finite strip analysis. Classical hand solutions are cumbersome for more complex buckling modes, such as distortional buckling and may ignore critical mechanical features such as inter-element equilibrium and compatibility (Schafer and Ádány 2006, 2). This is less accurate compared to finite strip analysis which examines all possible instabilities in a cold-formed steel member under longitudinal stresses. Generally, all design approaches conservatively predict the capacity of the plain back-to-back C-channel built-up column with the DSMI as the most conservative.

The results are different for the BU90 test series compared to the BU75 test series because the BU90 test series are compact section with large flange which are equally strong on both axis, making them very stable on their own. Large moment is required to induce rotation at the ends.

Comparing the DSMI approach and the DSMII approach for the BU75 test series, there is similar observation whereby the prediction by the DSMI is always more conservative. This is because the classical plate buckling model of the DSMI and the finite strip analysis of the DSMII are both susceptible towards change in dimensions. Results show that the EWM is very accurate for stub columns as both methods are capable of predicting the capacity of test specimen to about 5% accuracy for the stub column test series of test specimens.

Table 7.6 and Table 7.7 show the ratios of test result to design calculated result for the EWM, DSMI, and DSMII for the short, intermediate and slender test specimens from the BU75 and BU90 test series respectively.

Table 7.6: Comparison of Test & Finite Element Results to Design Calculated Results for BU75 Columns

Specimen	P_{test} (kN)	P_{FE} (kN)	P_{EWM} (kN)	P_{DSMI} (kN)	P_{DSMII} (kN)	$\frac{P_{test}}{P_{EWM}}$	$\frac{P_{test}}{P_{DSMI}}$	$\frac{P_{test}}{P_{DSMII}}$	$\frac{P_{FE}}{P_{EWM}}$	$\frac{P_{FE}}{P_{DSMI}}$	$\frac{P_{FE}}{P_{DSMII}}$
BU75S100L500-1	82.96	80.66	82.37	81.21	82.17	1.01	1.02	1.01	0.98	0.99	0.98
BU75S100L500-3	74.07	71.70	78.83	78.41	79.27	0.94	0.94	0.93	0.91	0.91	0.90
Mean						0.97	0.98	0.97	0.94	0.95	0.94
BU75S200L500-1	86.21	78.93	77.49	77.36	78.11	1.11	1.11	1.10	1.02	1.02	1.01
BU75S200L500-2	88.93	73.01	75.21	75.49	76.36	1.18	1.18	1.16	0.97	0.97	0.96
BU75S200L500-3	93.61	79.62	75.26	75.56	76.26	1.24	1.24	1.23	1.06	1.05	1.04
Mean						1.18	1.18	1.17	1.02	1.01	1.00
BU75S400L500-1	74.77	65.01	61.30	63.91	64.60	1.22	1.17	1.16	1.06	1.02	1.01
BU75S400L500-2	80.56	64.72	60.99	63.65	64.31	1.32	1.27	1.25	1.06	1.02	1.01
BU75S400L500-3	87.64	62.94	61.56	64.13	64.80	1.42	1.37	1.35	1.02	0.98	0.97
Mean						1.32	1.27	1.25	1.05	1.01	0.99
BU75S225L1000-1	47.04	48.49	36.34	37.41	37.41	1.29	1.26	1.26	1.33	1.30	1.30
BU75S225L1000-2	46.28	38.05	35.05	35.94	35.94	1.32	1.29	1.29	1.09	1.06	1.06
Mean						1.31	1.27	1.27	1.21	1.18	1.18
BU75S450L1000-1	50.43	39.99	30.67	30.73	30.73	1.64	1.64	1.64	1.30	1.30	1.30
BU75S450L1000-2	45.02	39.58	30.09	30.09	30.09	1.50	1.50	1.50	1.32	1.32	1.32
BU75S450L1000-3	41.77	37.65	27.81	27.81	27.81	1.50	1.50	1.50	1.35	1.35	1.35
Mean						1.55	1.55	1.55	1.32	1.32	1.32

(contd.)

Specimen	P_{test} (kN)	P_{FE} (kN)	P_{EWM} (kN)	P_{DSMI} (kN)	P_{DSMII} (kN)	$\frac{P_{test}}{P_{EWM}}$	$\frac{P_{test}}{P_{DSMI}}$	$\frac{P_{test}}{P_{DSMII}}$	$\frac{P_{FE}}{P_{EWM}}$	$\frac{P_{FE}}{P_{DSMI}}$	$\frac{P_{FE}}{P_{DSMII}}$
BU75S900L1000-1	39.90	36.60	18.74	18.74	18.74	2.13	2.13	2.13	1.95	1.95	1.95
BU75S900L1000-2	33.70	35.97	17.04	17.04	17.04	1.98	1.98	1.98	2.11	2.11	2.11
BU75S900L1000-3	31.48	36.46	17.63	17.63	17.63	1.79	1.80	1.80	2.07	2.07	2.07
Mean						1.96	1.96	1.96	2.04	2.04	2.04
BU75S475L2000-2	15.33	11.95	10.27	10.27	10.27	1.49	1.49	1.49	1.16	1.16	1.16
BU75S475L2000-3	12.87	13.00	10.22	10.22	10.22	1.26	1.26	1.26	1.27	1.27	1.27
Mean						1.38	1.38	1.38	1.22	1.22	1.22
BU75S950L2000-2	13.22	10.72	8.43	8.43	8.43	1.57	1.57	1.57	1.27	1.27	1.27
BU75S950L2000-3	12.99	9.13	8.36	8.36	8.36	1.55	1.55	1.55	1.09	1.09	1.09
Mean						1.56	1.56	1.56	1.18	1.18	1.18
BU75S1900L2000-2	12.12	10.96	4.90	4.90	4.90	2.47	2.47	2.47	2.24	2.24	2.24
BU75S1900L2000-3	13.11	11.71	4.93	4.93	4.93	2.66	2.66	2.66	2.38	2.38	2.38
Mean						2.57	2.57	2.57	2.31	2.31	2.31
Overall Mean						1.53	1.52	1.51	1.36	1.36	1.35
Population Standard Deviation						0.43	0.44	0.44	0.45	0.45	0.46

Table 7.7: Comparison of Test & Finite Element Results to Design Calculated Results for BU90 Columns

Specimen	P_{test} (kN)	P_{FE} (kN)	P_{EWM} (kN)	P_{DSMI} (kN)	P_{DSMII} (kN)	$\frac{P_{test}}{P_{EWM}}$	$\frac{P_{test}}{P_{DSMI}}$	$\frac{P_{test}}{P_{DSMII}}$	$\frac{P_{FE}}{P_{EWM}}$	$\frac{P_{FE}}{P_{DSMI}}$	$\frac{P_{FE}}{P_{DSMII}}$
BU90S100L500-1	165.01	162.81	151.37	143.41	148.77	1.09	1.15	1.11	1.08	1.14	1.09
BU90S100L500-2	163.22	161.92	150.47	142.42	147.73	1.08	1.15	1.10	1.08	1.14	1.10
Mean						1.09	1.15	1.11	1.08	1.14	1.10
BU90S200L500-1	170.48	158.13	151.66	143.50	149.37	1.12	1.19	1.14	1.04	1.10	1.06
BU90S200L500-2	173.17	159.29	150.60	142.37	148.19	1.15	1.22	1.17	1.06	1.12	1.07
BU90S200L500-3	151.53	151.53	150.18	142.27	148.06	1.01	1.07	1.02	1.01	1.07	1.02
Mean						1.09	1.16	1.11	1.04	1.10	1.05
BU90S400L500-1	170.01	162.16	150.66	142.54	148.59	1.13	1.19	1.14	1.08	1.14	1.09
BU90S400L500-2	151.41	168.28	150.72	142.57	148.41	1.00	1.06	1.02	1.12	1.18	1.13
Mean						1.07	1.13	1.08	1.10	1.16	1.11

(contd.)

Specimen	P_{test} (kN)	P_{FE} (kN)	P_{EWM} (kN)	P_{DSMI} (kN)	P_{DSMII} (kN)	$\frac{P_{test}}{P_{EWM}}$	$\frac{P_{test}}{P_{DSMI}}$	$\frac{P_{test}}{P_{DSMII}}$	$\frac{P_{FE}}{P_{EWM}}$	$\frac{P_{FE}}{P_{DSMI}}$	$\frac{P_{FE}}{P_{DSMII}}$
BU90S225L1000-1	167.81	153.71	124.67	117.28	121.61	1.35	1.43	1.38	1.23	1.31	1.26
BU90S225L1000-2	151.76	153.23	127.09	119.71	124.13	1.19	1.27	1.22	1.21	1.28	1.23
Mean						1.27	1.35	1.30	1.22	1.30	1.25
BU90S450L1000-2	175.18	155.82	127.57	120.08	124.53	1.37	1.46	1.41	1.22	1.30	1.25
BU90S450L1000-3	161.12	166.05	124.73	117.19	121.51	1.29	1.37	1.33	1.33	1.42	1.37
Mean						1.33	1.42	1.37	1.28	1.36	1.31
BU90S900L1000-1	164.86	154.68	122.43	115.16	119.39	1.35	1.43	1.38	1.26	1.34	1.30
BU90S900L1000-2	150.94	166.23	120.72	112.93	117.03	1.25	1.34	1.29	1.38	1.47	1.42
Mean						1.30	1.38	1.34	1.32	1.41	1.36
Overall Mean						1.18	1.26	1.21	1.16	1.23	1.18
Population Standard Deviation						0.12	0.13	0.13	0.11	0.13	0.12

Result shows that all design approaches conservatively predicts the capacity of the plain built-up short columns. The design approaches EWM, DSMI, and DSMII are conservative and get more conservative when the spacing increased. For fastener spacing within the code requirement, all design approaches are conservative in predicting the column strength. The design calculated results are even more conservative for specimens with fastener spacing beyond the code requirement.

Comparison shows that the EWM is the most conservative because the EWM considers plate buckling in isolation but in actual fact, the plates interact with one another. One advantage of the EWM is that it takes into account the effects of cold forming processes by introducing the concept of effective area. It is assumed that the effective area of a built-up column is twice of a single C-Channel. However, the webs of built-up sections are only screwed together at certain fastener spacing. This may not have resulted in the same effectiveness of two single C-Channels as assumed.

The design calculated results by the DSMI and DSMII are generally lower than the results calculated using the EWM. This is because the DSM considers the effects of all possible buckling modes for cold formed steel including local buckling, distortional buckling and global buckling. The elastic buckling solutions is used for the entire cross section rather than individual elements as calculated by the EWM. The DSM also predicts the local buckling behaviour using elastic local buckling stress of the whole column with an appropriate strength design curve for local instability. Besides, it also takes into consideration the flange/web and flange/lip interaction. This enables better representation of the actual condition.

Comparing the DSMI approach and the DSMII approach, prediction by the DSMI is always more conservative. This is because the DSMI uses classical plate buckling model while the DSMII uses finite strip analysis. Consideration in classical plate buckling model focuses on the cross section. This is less accurate compared to finite strip analysis which accounts for the whole column using strip by strip method.

Comparison of all the design approaches indicates that all results for slender columns are similar because the governing failure for slender columns is global buckling. In all the design approaches, global buckling is accounted for by the same flexural buckling equation. For other failure modes like local buckling and distortional buckling, the EWM takes into account of the effectiveness of the cross section, whereas the DSM takes into account of the interaction between the elements. However, for slender columns, the effects of failure modes other than global buckling are minimal. Thus, similar results are obtained from all design approaches as expected.

7.5 Conclusions

The design of cold-formed steel columns in this research is based on the currently available American Iron and Steel Institute (AISI) design standards. The design standards introduced two well-known design methods known as the EWM and the DSM. In this research, the design strength of the C-channel and plain back-to-back C-channel built-up columns are calculated using the EWM, the DSM I, and the DSM II. Beam-column design is used for singly symmetrical C-channel columns due to shift of effective centroid; whereas, the modified slenderness ratio in accordance to clause C4.5 of AISI specifications is used for built-up columns.

Comparison of the test and finite element results to the design calculated results shows that the predictions using beam-column equations are generally conservative for the C-channel columns. For built-up columns, the design calculation with modified slenderness ratio predicts that column of the same length became more prone to buckling as the spacing increases. This was demonstrated by the test and finite element results but the effect was not as significant as predicted by the design calculation. Therefore, if the modified slenderness ratio is omitted, the design calculation overestimated the test specimen strength for columns with fastener spacing within the code requirement but better estimated the test specimen strength for columns with fastener spacing beyond the code requirement. This is because the modification accounts for reduction in shear rigidity which is a significant issue in columns with large fastener spacing due to reduction in restraint. Observations from the compression test also show that it is important to have fasteners at mid-length where deflection is the greatest to ensure that the column acted as an integral unit. The modified slenderness ratio is required in calculating the capacity of plain back-to-back C-channel built-up columns.

8 Proposed Design Method

8.1 Introduction

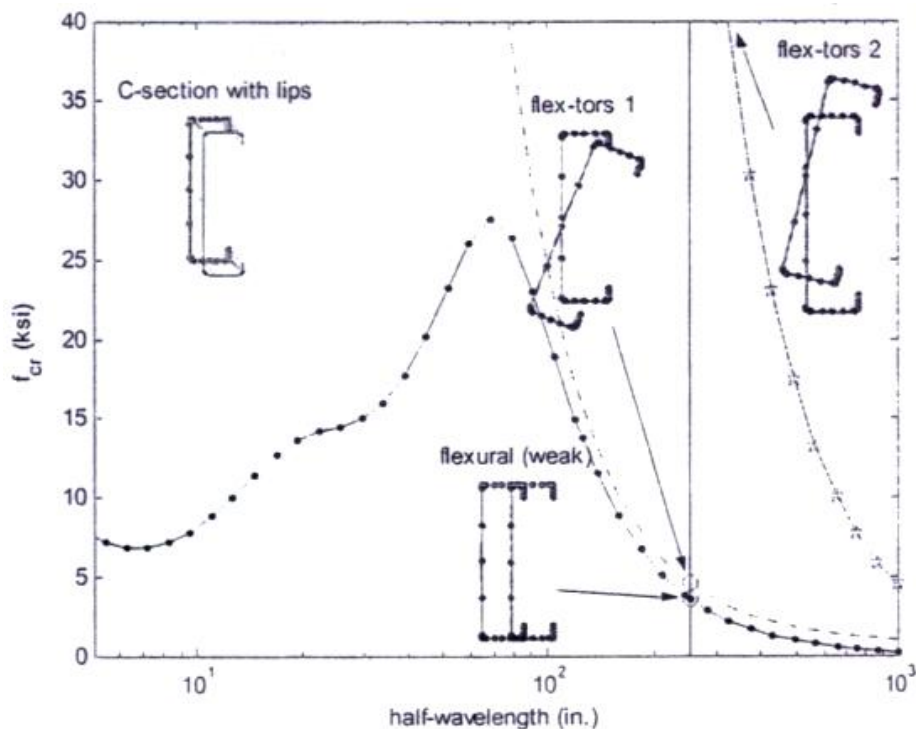
Back-to-back C-channel built-up compression members with a gap are popular in the construction industry particularly spanning over large area, and carrying high loads while maintaining low self-weight. However, current design standards do not provide comprehensive design guidelines for complex section such as back-to-back C-channel built-up section with a gap. There is little or no literature available for the design calculation of back-to-back C-channel built-up columns with a gap. Current design methods, i.e. the Effective Width Method (EWM) and the Direct Strength Method (DSM) are unable to accommodate such complex section. Thus, enhancement to these design methods is necessary to improve the design of back-to-back C-channel built-up columns. Therefore, the Thickness Reduction Method (TRem) is proposed in this research to improve the current design methods for the back-to-back C-channel built-up column.

8.2 Design Approach

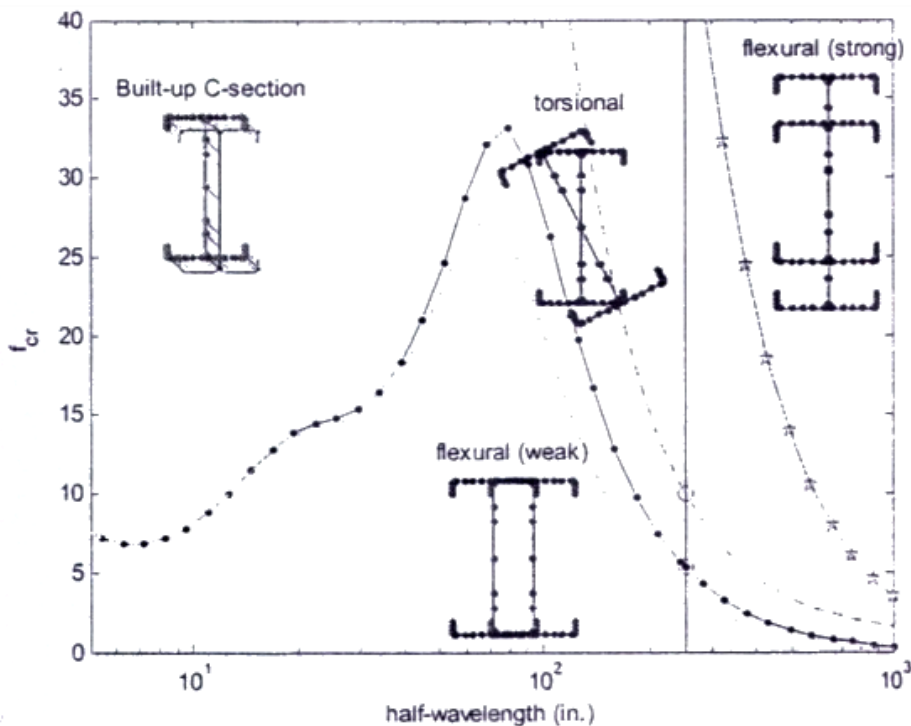
In the DSM, the elastic buckling loads (P_{cr1} , P_{crd} , and P_{cre}) are required to calculate the ultimate design strength of a column. The elastic buckling loads are either determined through manual calculations (DSM I) or using finite strip method software (DSM II) such as, the Cornell University Finite Strip Method (CUFSM). Schafer (AISI 2006, 54-55) proposed two different approaches for modelling built-up columns formed from two C-channels connected back-to-back in the CUFSM. They are:

- (i) modelled as a rigidly connected back-to-back C-channel, or
- (ii) modelled as two individual lipped C-channels.

According to Schafer (AISI 2006, 54-55), modelling the back-to-back C-channels as a rigidly connected section provides the upper bound model, whereas the latter provides the lower bound model as shown in Figure 8.1. Thus, there is a need to enhance the modelling of back-to-back C-channel built-up columns in the CUFSM.



(a) CUFSM Results from C-channel (Lower Bound)



(b) CUFSM Results from Built-up Back-to-back C-channel (Upper Bound)

Figure 8.1: CUFSM Result for Back-to-back C-channel Built-up Column (AISI 2006, 54)

A recent research by Zhang and Young (2012, 1-11) proposed to model back-to-back C-channel built-up section as an I-shape with a reduced web thickness rather than use the Schafer approaches. Several reduced web thicknesses were chosen to model the I-shape in the CUFSM. The reduced web thicknesses are verified by trial and error approach using test results to determine the thickness that provides the best arbitrary estimate of the column strength.

From the understanding of Schafer's and Zhang and Young's approaches, a modified method known as TReM based on the EWM and the DSM is proposed.

8.3 Thickness Reduction Method (TReM)

The TReM proposes changes to the web thickness and lead to enhanced CUFSM analysis model to design back-to-back C-channel built-up columns with a gap. Figure 8.2 shows the notations used for back-to-back C-channel built-up columns with a gap.

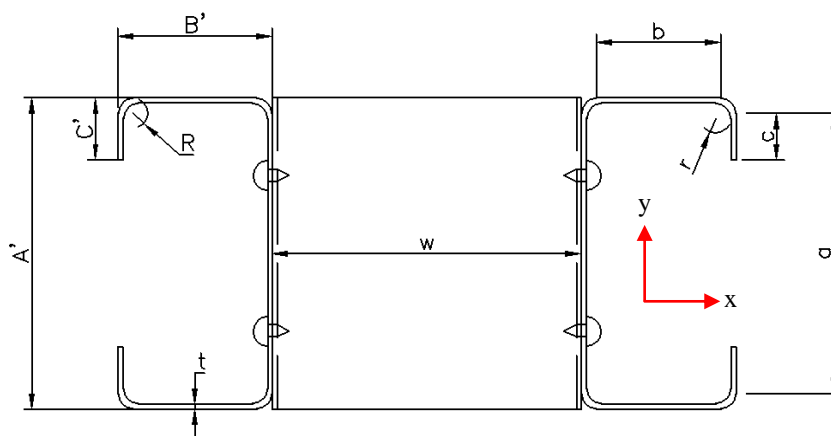


Figure 8.2: Notations for Back-to-back C-channel Built-up Section with a Gap

The applicability of the TReM is evaluated by comparing calculated results of back-to-back C-channel built-up columns with and without a gap with test results from this research. A sample spreadsheet for this method is in Appendix H.

Back-to-back C-channel built-up column with a gap has higher moment of inertia due to the gap between the two individual C-channels. The following equation proposed by Johnston (1971, 1465-1479) is used to calculate the moment of inertia of back-to-back C-channel built-up column with a gap, I_{yGBU} for this research.

$$I_{yGBU} = \frac{A_c (w + 2x_c + t)^2}{2} + 2I_{yc} \quad \text{Eq. 8-1}$$

where

A_c = cross sectional area of C-channel

w = distance of the gap

x_c = distance of the centroid to the web centreline of individual C-channel

t = material thickness

I_{yc} = moment of inertia of individual C-channel

For TReM, the back-to-back C-channel built-up column with a gap is modelled as an “I” in the CUFSM analysis as shown in Figure 8.3. The pre-programmed template in CUFSM is not available for the modelling of “I” shape. Therefore, coordinates and elements of the cross section need to be individually plotted. The thickness of the cross section is the material thickness of the test specimens e.g. 1.2mm. However, the webs of built-up sections are only screwed together at certain fastener spacing. This may not have resulted in the same effectiveness of two individual C-Channels of the back-to-back C-channel built-up section as assumed. Thus, the web is overestimated with twice the thickness of a single C-channel i.e. 2.4mm. Therefore, the yet to be determined thickness of web is the reduced thickness, t_{rw} .

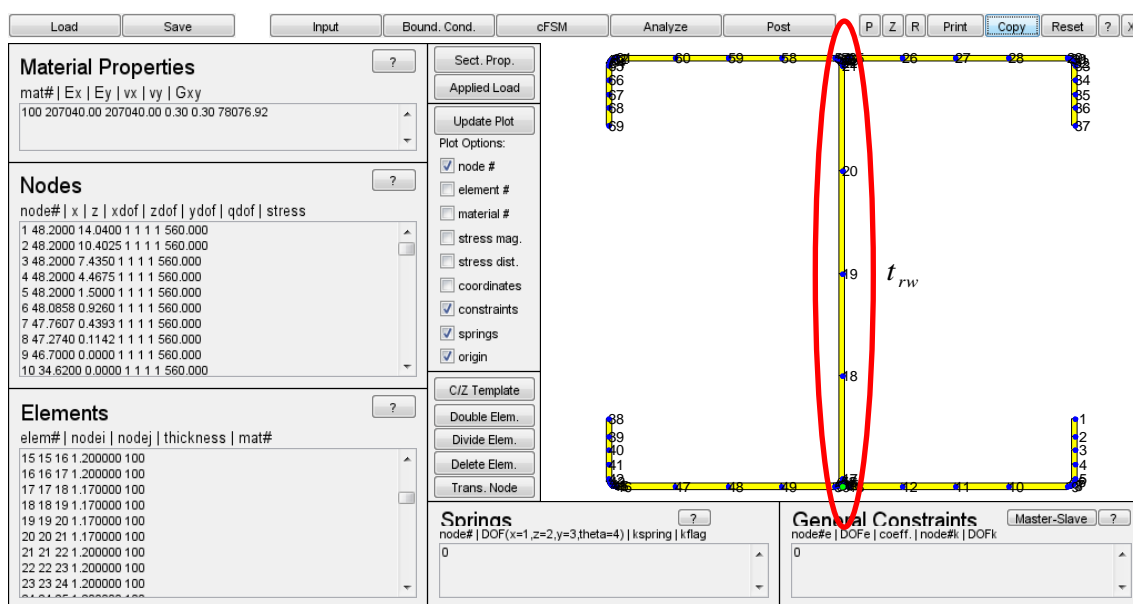


Figure 8.3: CUFSM Model for the Analysis of GBU Columns

In accordance with clause B2.1 of the AISI Specifications 2001 edition, the effectiveness of a web element is $b_{web} = \rho a$. The determination of the effective width of the web, ρa is similar to part of the EWM.

where

$$\rho = \frac{1 - 0.22}{\lambda_w}$$

where

$$\lambda_w = \sqrt{\frac{F_{ne}}{F_{cr}}}$$

When $\lambda_w \leq 0.673$, $\rho = 1.0$, then, $b_{web} = a$.

To obtain F_{ne} , λ_c is calculated as follows:

$$\lambda_c = \sqrt{\frac{F_y}{F_e}}$$

when

$$\lambda_c \leq 1.5, \quad F_{ne} = (0.658^{\lambda_c^2}) F_y$$

$$\lambda_c > 1.5, \quad F_{ne} = \left(\frac{0.877}{\lambda_c^2} \right) F_y$$

F_e is calculated as follows:

$$F_e = \min(F_{e1}, F_{e2})$$

where

Flexural buckling

$$F_{e1} = \frac{\pi^2 E}{(KL/r)^2}$$

where

$$\left(\frac{KL}{r} \right) = \left(\frac{KL}{r} \right)_m = \sqrt{\left(\frac{KL}{r} \right)_o^2 + \left(\frac{s}{r_{yc}} \right)^2}$$

Torsional buckling

$$F_{e2} = \sigma_t = \frac{1}{Ar_o^2} \left[GJ + \frac{\pi^2 EC_w}{(K_t L_t)^2} \right]$$

The slenderness factor, λ_w , can be rewritten as:

$$\lambda_w = \frac{1.052}{\sqrt{k}} \left(\frac{w}{t} \right) \sqrt{\frac{F_{ne}}{E}}$$

From the above equation, the slenderness factor, λ_w is influenced by the ratio of actual width to thickness, (w/t) .

The web to thickness ratio of the built-up column is $a/2t$. By considering the effectiveness of the web element in accordance with clause B2.1, the effective web to thickness ratio is $\rho a/t_{rw}$, where t_{rw} is the effective thickness of the web. Thus, it can be expressed as:

$$\frac{a}{2t} = \frac{\rho a}{t_{rw}}$$

From the above expression, the effective web thickness known as the reduced web thickness, t_{rw} is determined by:

$$t_{rw} = \frac{\rho a}{a} \times 2t \quad \text{Eq. 8-2}$$

where

ρ = a reduction factor

a = the clear width of web

t = the material's thickness of a built-up section

From the above equations, the reduction factor ρ varies depending on the dimensions, A , fasteners spacing, s , and end conditions, K of the specimens. Thus, the reduced web thickness, t_{rw} , accommodates for these governing factors.

8.3.1 Design Procedures

Figure 8.4 shows the summary of the processes in the determination of the design strength of a back-to-back C-channel built-up column with a gap according to the TReM.

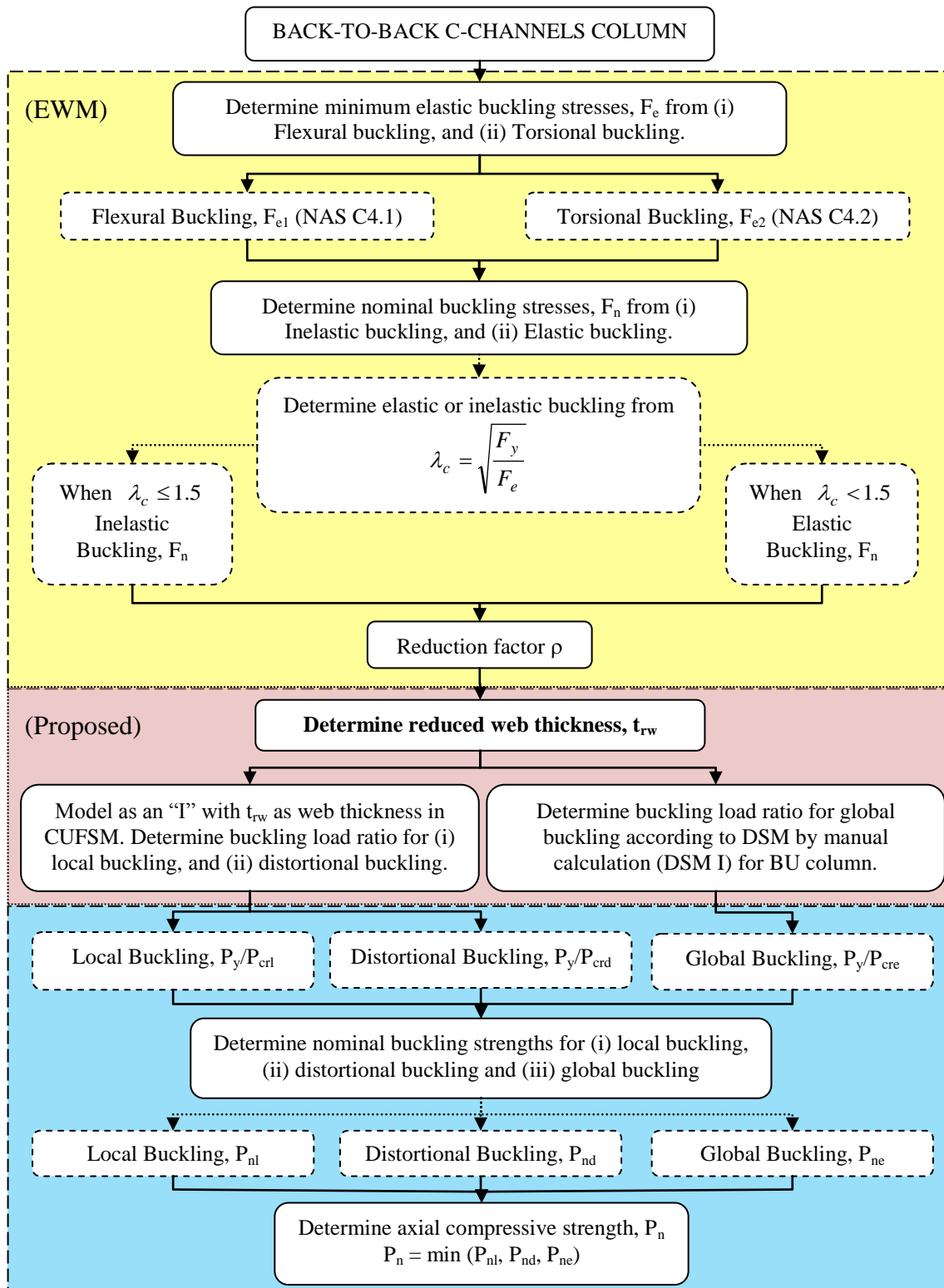


Figure 8.4: Design Procedure using TReM

The yellow box shows the design calculations which involve the determination of the effective web width in accordance with clause B2.1 of the AISI Specifications. This is also part of the design procedure for the EWM. The effective web width is then used to determine the reduced web thickness, t_{rw} . This thickness is required as input for the web thickness of the I-shape model in CUFSM. The buckling load ratios determined from analysing the CUFSM model are then used to determine nominal buckling strength and finally the axial compressive strength.

8.4 Evaluation of the Thickness Reduction Method (TRem)

8.4.1 Plain Back-to-back C-channel Built-up Columns

As detailed in section 8.2, Schafer's approach of modelling the plain back-to-back C-channels as a rigidly connected section provides the upper bound model, whereas modelling as C-channel provides the lower bound model. The upper bound model provides a buoyant estimation of the column strength and thus is not included for comparison in this research. Instead, the lower bound model is used as a comparison for the evaluation of the TRem on plain back-to-back C-channels column.

Table 8.1 and Table 8.2 show the comparison of compression test, finite element, and the DSMII results for the BU75 and BU90 plain back-to-back C-channel built-up columns.

Table 8.1: Comparison of Test and FE Results with TReM for BU75

Specimen	P_{test} (kN)	P_{FE} (kN)	P_{DSMII} (kN)	P_{trw} (kN)	$\frac{P_{test}}{P_{trw}}$	$\frac{P_{FE}}{P_{trw}}$	$\frac{P_{test}}{P_{DSMII}}$	$\frac{P_{FE}}{P_{DSMII}}$	$\frac{P_{DSMII}}{P_{trw}}$
BU75S50L300-1	120.66	120.13	114.39	128.75	0.94	0.93	1.05	1.05	0.89
BU75S50L300-2	118.87	120.78	114.39	128.74	0.92	0.94	1.04	1.03	0.89
BU75S50L300-3	118.65	122.04	112.77	127.97	0.93	0.95	1.05	1.08	0.88
Mean					0.93	0.94	1.05	1.05	0.89
BU75S100L300-1	Discard								
BU75S100L300-2	117.48	127	112.96	127.99	0.92	0.99	1.04	1.12	0.88
BU75S100L300-3	122.74	127.03	113.26	128.22	0.96	0.99	1.08	1.12	0.88
BU75S100L300-4	115.37	126.58	113.46	127.24	0.91	0.99	1.02	1.12	0.89
Mean					0.93	0.99	1.05	1.12	0.89
BU75S200L300-1	122.51	121.56	109.38	123.89	0.99	0.98	1.12	1.11	0.88
BU75S200L300-2	119.12	123.23	109.36	123.92	0.96	0.99	1.09	1.13	0.88
BU75S200L300-3	113.14	123.17	108.99	125.3	0.90	0.98	1.04	1.13	0.87
Mean					0.95	0.99	1.08	1.12	0.88

(contd.)

Specimen	P_{test} (kN)	P_{FE} (kN)	P_{DSMII} (kN)	P_{trw} (kN)	$\frac{P_{test}}{P_{trw}}$	$\frac{P_{FE}}{P_{trw}}$	$\frac{P_{test}}{P_{DSMII}}$	$\frac{P_{FE}}{P_{DSMII}}$	$\frac{P_{DSMII}}{P_{trw}}$
BU75S100L500-1	82.96	80.66	82.17	98.86	0.84	0.82	1.01	0.98	0.83
BU75S100L500-2	Discard								
BU75S100L500-3	74.07	71.70	79.27	93.84	0.79	0.76	0.93	0.90	0.84
Mean					0.81	0.79	0.97	0.94	0.84
BU75S200L500-1	86.21	78.93	78.11	91.86	0.94	0.86	1.10	1.01	0.85
BU75S200L500-2	88.93	72.01	76.36	88.69	1.00	0.81	1.16	0.94	0.86
BU75S200L500-3	93.61	79.62	76.26	88.56	1.06	0.90	1.23	1.04	0.86
Mean					1.00	0.86	1.17	1.00	0.86
BU75S400L500-1	74.77	65.01	64.60	69.25	1.08	0.94	1.16	1.01	0.93
BU75S400L500-2	80.56	64.72	64.31	68.81	1.17	0.94	1.25	1.01	0.93
BU75S400L500-3	87.64	62.94	64.80	69.55	1.26	0.90	1.35	0.97	0.93
Mean					1.17	0.93	1.25	0.99	0.93

(contd.)

Specimen	P_{test} (kN)	P_{FE} (kN)	P_{DSMII} (kN)	P_{trw} (kN)	$\frac{P_{test}}{P_{trw}}$	$\frac{P_{FE}}{P_{trw}}$	$\frac{P_{test}}{P_{DSMII}}$	$\frac{P_{FE}}{P_{DSMII}}$	$\frac{P_{DSMII}}{P_{trw}}$
BU75S225L1000-1	47.04	48.49	37.41	37.41	1.26	1.30	1.26	1.30	1.00
BU75S225L1000-2	46.28	38.05	35.94	35.94	1.29	1.06	1.29	1.06	1.00
BU75S225L1000-3	Discard								
Mean					1.27	1.18	1.27	1.18	1.00
BU75S450L1000-1	50.43	39.99	30.73	30.73	1.64	1.30	1.64	1.30	1.00
BU75S450L1000-2	45.02	39.58	30.09	30.09	1.50	1.32	1.50	1.32	1.00
BU75S450L1000-3	41.77	37.65	27.81	27.81	1.50	1.35	1.50	1.35	1.00
Mean					1.55	1.32	1.55	1.32	1.00
BU75S900L1000-1	39.90	36.30	18.74	18.74	2.13	1.94	2.13	1.94	1.00
BU75S900L1000-2	33.70	35.97	17.04	17.04	1.98	2.11	1.98	2.11	1.00
BU75S900L1000-3	31.48	36.46	17.63	17.63	1.79	1.79	1.79	1.79	1.00
Mean					1.97	2.04	1.97	2.04	1.00

(contd.)

Specimen	P_{test} (kN)	P_{FE} (kN)	P_{DSMII} (kN)	P_{trw} (kN)	$\frac{P_{test}}{P_{trw}}$	$\frac{P_{FE}}{P_{trw}}$	$\frac{P_{test}}{P_{DSMII}}$	$\frac{P_{FE}}{P_{DSMII}}$	$\frac{P_{DSMII}}{P_{trw}}$
BU75S475L2000-1	Discard								
BU75S475L2000-2	15.33	11.95	10.27	10.27	1.49	1.16	1.49	1.16	1.00
BU75S475L2000-3	12.87	13.00	10.22	10.22	1.26	1.27	1.26	1.27	1.00
Mean					1.38	1.22	1.38	1.22	1.00
BU75S950L2000-1	Discard								
BU75S950L2000-2	13.22	10.72	8.43	8.43	1.57	1.27	1.57	1.27	1.00
BU75S950L2000-3	12.99	9.13	8.36	8.36	1.55	1.09	1.55	1.09	1.00
Mean					1.56	1.18	1.56	1.18	1.00
BU75S1900L2000-1	Discard								
BU75S1900L2000-2	12.12	10.96	4.90	4.90	2.47	2.24	2.47	2.24	1.00
BU75S1900L2000-3	13.11	11.71	4.93	4.93	2.66	2.38	2.66	2.38	1.00
Mean					2.57	2.31	2.57	2.31	1.00
Overall Mean					1.31	1.21	1.38	1.27	0.94
Population Standard Deviation					0.47	0.44	0.43	0.40	0.06

As seen in Table 8.1 for BU75 test specimens, the TReM results are about 10% higher than the DSM II. The comparison shows that the TReM is unconservative while the DSM II is conservative in predicting the ultimate strength of stub columns from the BU75 test series. However, the calculation assumed fixed end condition whereas the columns were tested on fixed end condition. Thus, the finite element results serve as a better estimation of the column strength in these cases. When compared to the finite element results, the results calculated using the TReM are closer to the finite element results compared to the DSM II. The TReM is slightly unconservative; while the DSM II is overly conservative.

For longer BU75L500 columns, the TReM results are about 15% higher than the DSM II for columns with three and one intermediate fastener; whereas, for columns with no intermediate fastener, the TReM results are 7% higher than the DSM II. The TReM is generally conservative and closer to the experimental results compared to the DSM II. However, when considering the finite element results, the TReM is unconservative while the DSM II is conservative.

Results obtained from TReM and DSM II are the same for BU75L1000 and BU75L2000 columns. Both the TReM and DSM II are conservative. The calculated results are more conservative for specimens with larger fastener spacing. For specimens at $s/L > 0.50$ with no intermediate fasteners, both TReM and DSM II are overly conservative because specimens at $s/L > 0.50$ are beyond the clause C4.5 spacing requirements. The modified slenderness ratio is overly conservative in this case, thus the strength estimation of both the TReM and the DSM II are conservative.

Table 8.2: Comparison of Test and FE Results with TReM for BU90

Specimen	P_{test} (kN)	P_{FE} (kN)	P_{DSMII} (kN)	P_{trw} (kN)	$\frac{P_{test}}{P_{trw}}$	$\frac{P_{FE}}{P_{trw}}$	$\frac{P_{test}}{P_{DSMII}}$	$\frac{P_{FE}}{P_{DSMII}}$	$\frac{P_{DSMII}}{P_{trw}}$
BU90S50L300-1	172.49	185	166.83	163.14	1.06	1.13	1.03	1.11	1.02
BU90S50L300-2	171.61	186.58	166.47	162.97	1.05	1.14	1.03	1.12	1.02
BU90S50L300-3	167.56	187	165.61	160.44	1.04	1.17	1.01	1.13	1.03
Mean					1.05	1.15	1.03	1.12	1.03
BU90S100L300-1	Discard								
BU90S100L300-2	Discard								
BU90S100L300-3	171.18	188.44	166.91	164.22	1.04	1.15	1.03	1.13	1.02
BU90S100L300-4	173.87	185.52	166.80	164.26	1.06	1.13	1.04	1.11	1.02
Mean					1.05	1.14	1.03	1.12	1.02
BU90S200L300-1	170.25	187.72	165.77	162.76	1.05	1.15	1.03	1.13	1.02
BU90S200L300-2	177.50	188.12	165.92	162.94	1.09	1.15	1.07	1.14	1.02
BU90S200L300-3	Discard								
BU90S200L300-4	171.88	187.81	166.05	162.79	1.06	1.15	1.04	1.13	1.02
Mean					1.06	1.15	1.04	1.13	1.02

(contd.)

Specimen	P_{test} (kN)	P_{FE} (kN)	P_{DSMII} (kN)	P_{trw} (kN)	$\frac{P_{test}}{P_{trw}}$	$\frac{P_{FE}}{P_{trw}}$	$\frac{P_{test}}{P_{DSMII}}$	$\frac{P_{FE}}{P_{DSMII}}$	$\frac{P_{DSMII}}{P_{trw}}$
BU90S100L500-1	165.01	162.81	148.77	148.44	1.11	1.10	1.11	1.09	1.00
BU90S100L500-2	163.22	161.92	147.73	148.47	1.10	1.09	1.10	1.10	1.00
BU90S100L500-3	Discard								
Mean					1.11	1.09	1.11	1.10	1.00
BU90S200L500-1	170.48	158.13	149.37	148.24	1.15	1.07	1.15	1.06	1
BU90S200L500-2	173.17	159.29	148.19	147.51	1.17	1.08	1.17	1.08	1
BU90S200L500-3	151.53	151.53	148.06	148.33	1.02	1.02	1.03	1.03	0.99
Mean					1.12	1.06	1.11	1.05	1.00
BU90S400L500-1	170.01	162.16	148.59	148.58	1.14	1.09	1.15	1.1	1
BU90S400L500-2	151.41	168.28	148.41	148.64	1.02	1.13	1.02	1.14	1
BU90S400L500-3	Discard								
Mean					1.08	1.11	1.08	1.11	1.00

(contd.)

Specimen	P_{test} (kN)	P_{FE} (kN)	P_{DSMII} (kN)	P_{trw} (kN)	$\frac{P_{test}}{P_{trw}}$	$\frac{P_{FE}}{P_{trw}}$	$\frac{P_{test}}{P_{DSMII}}$	$\frac{P_{FE}}{P_{DSMII}}$	$\frac{P_{DSMII}}{P_{trw}}$
BU90S225L1000-1	167.81	153.71	121.61	133.07	1.26	1.16	1.38	1.26	0.91
BU90S225L1000-2	151.76	153.23	124.13	135.66	1.12	1.13	1.22	1.23	0.92
BU90S225L1000-3	Discard								
Mean					1.19	1.14	1.30	1.25	0.91
BU90S450L1000-1	Discard								
BU90S450L1000-2	175.18	155.82	124.53	136.03	1.29	1.15	1.41	1.25	0.92
BU90S450L1000-3	161.12	166.05	121.64	132.57	1.22	1.25	1.32	1.37	0.92
BU90S450L1000-4	Discard								
Mean					1.25	1.20	1.37	1.31	0.92
BU90S900L1000-1	164.86	154.68	119.39	130.27	1.27	1.19	1.38	1.30	0.92
BU90S900L1000-2	150.94	166.23	117.03	128.07	1.18	1.30	1.29	1.42	0.91
BU90S900L1000-3	Discard								
Mean					1.22	1.24	1.34	1.36	0.92
Overall Mean					1.12	1.14	1.14	1.16	0.98
Population Standard Deviation					0.08	0.06	0.13	0.10	0.04

As seen in Table 8.2, the TReM results compared to the DSM II results (i) are lower by 3% for the stub column length, and (ii) are similar for the 500mm column length, but (iii) greater by 8% for the 1000mm column length. Generally, when compared to test results and finite element results, both the TReM and the DSM II conservatively predicted the ultimate strength of columns from the BU90 test series. The TReM results show improved estimation of the ultimate strength of columns from the BU90 test series compared to the DSM II results for the BU90L1000 specimens.

Figure 8.5 shows the comparison of the TReM with compression test results for plain back-to-back C-channel built-up columns.

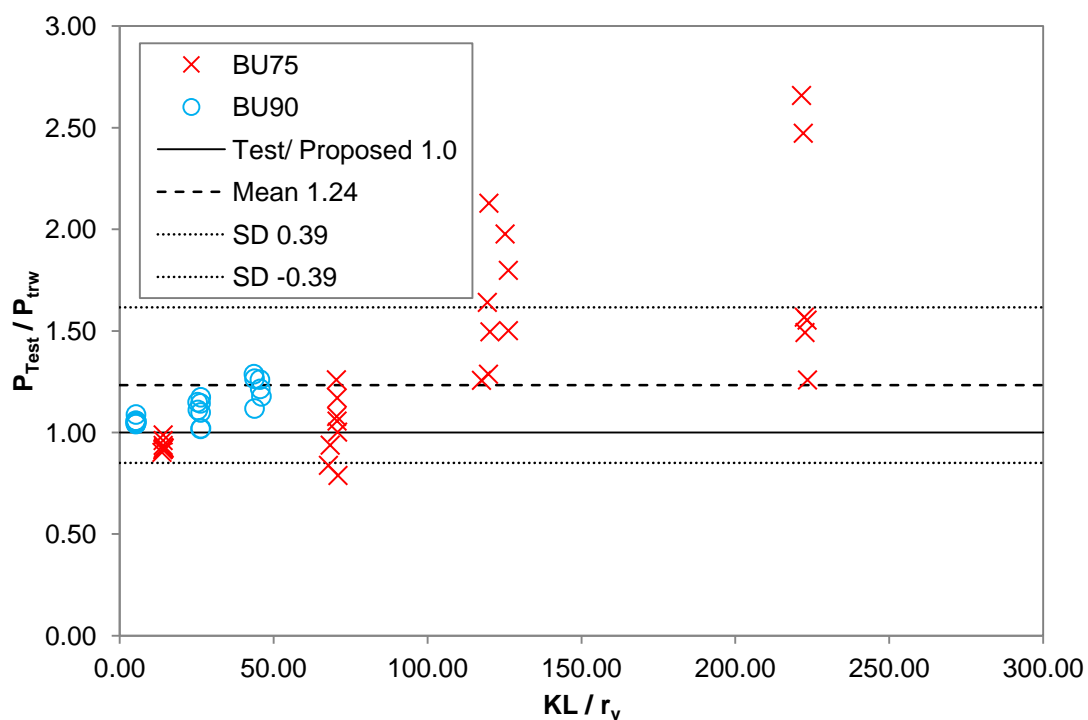


Figure 8.5: Comparison of Proposed Method with Test Results for BU

Figure 8.5 shows that the TReM is conservative for most columns from the GBU90 test series. However, the TReM is slightly unconservative for shorter GBU75 columns i.e. GBU75L300, GBU75L500, but overly conservative for longer GBU75 columns i.e. GBU75L1000, GBU75L2000. Overall, the TReM results when compared to the test results are conservative with a mean of 1.24 and a standard deviation of 0.39.

Figure 8.6 shows the comparison of the TReM with finite element results for plain back-to-back C-channel built-up columns.

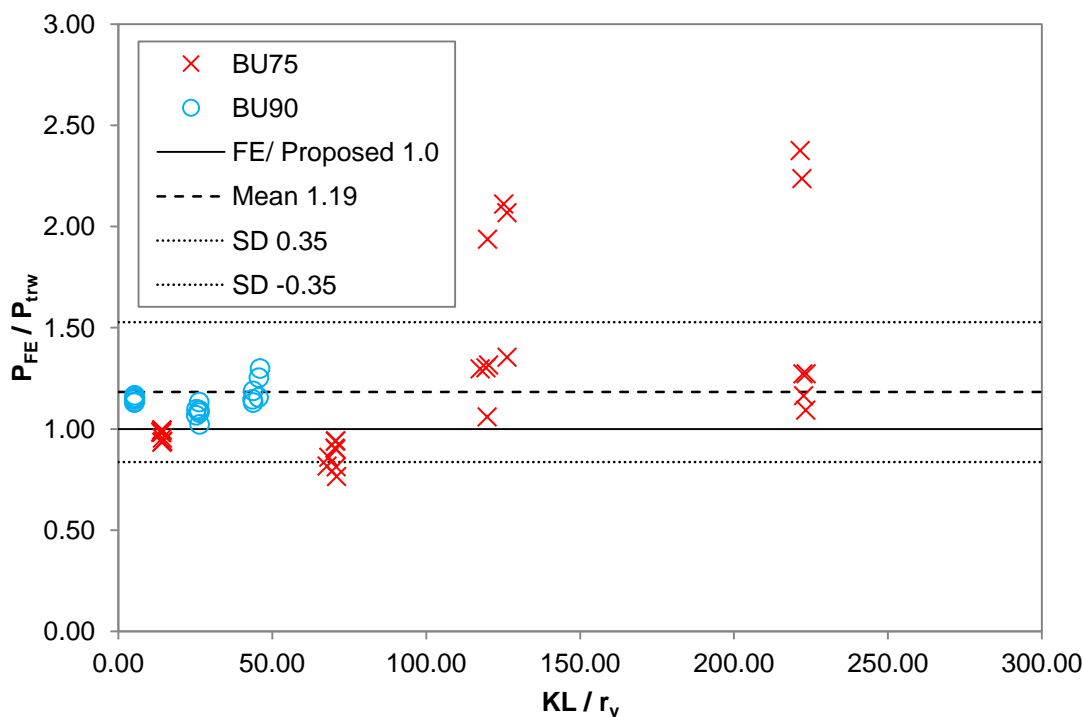


Figure 8.6: Comparison of Proposed Method with FE Results for BU

Similar to the previous graph, Figure 8.6 shows that the TReM is conservative when compared to the finite element results of all columns from the BU90 test series and shorter columns from the BU75 test series i.e. BU75L300, BU75L500. Moreover, the TReM is overly conservative for the BU75L1000 and BU75L2000 columns. Generally, the results are conservative when compared to the finite element results with a mean of 1.19 and a standard deviation of 0.35.

In general, the TReM predicts the strength of the plain back-to-back C-channel built-up columns well. The TReM serve to be an improved method to estimate the capacity of plain back-to-back C-channel built-up columns.

8.4.2 Back-to-back C-channel Built-up Columns with a Gap

Evaluation of the TReM on the back-to-back C-channel built-up columns with a gap was conducted using results from the GBU75 test series and the GBU90 test series. Table 8.3 and Table 8.4 show the comparison of compression test, finite element, and the DSMII results for GBU75 and GBU90 back-to-back C-channel built-up columns with a gap.

Table 8.3: Comparison of Test and FE Results with TReM for GBU75

Specimen	P_{test} (kN)	P_{FE} (kN)	P_{trw} (kN)	$\frac{P_{test}}{P_{trw}}$	$\frac{P_{FE}}{P_{trw}}$	Specimen	P_{test} (kN)	P_{FE} (kN)	P_{trw} (kN)	$\frac{P_{test}}{P_{trw}}$	$\frac{P_{FE}}{P_{trw}}$
GBU75S50L300-1	Discard					GBU75S200L300-1	105.19	120.06	124.03	0.85	0.97
GBU75S50L300-2	112.09	125.46	129.30	0.87	0.97	GBU75S200L300-2	107.06	121.49	124.22	0.86	0.98
GBU75S50L300-3	110.57	126.60	129.59	0.85	0.98	GBU75S200L300-3	Discard				
GBU75S50L300-4	128.94	122.44	129.47	1.00	0.95	GBU75S200L300-4	112.09	119.93	124.06	0.90	0.97
Mean				0.91	0.97	Mean				0.87	0.97
GBU75S100L500-1	101.68	108.71	99.16	1.03	1.10	GBU75S400L500-1	106.12	97.45	99.06	1.07	0.98
GBU75S100L500-2	98.05	101.18	99.20	0.99	1.02	GBU75S400L500-2	100.04	107.23	97.77	1.02	1.10
GBU75S100L500-3	105.78	117.50	98.69	1.07	1.19	GBU75S400L500-3	113.61	111.97	99.22	1.15	1.13
GBU75S100L500-4	-					GBU75S400L500-4	Discard				
Mean				1.03	1.10	Mean				1.08	1.07
GBU75S225L1000-1	86.62	105.20	46.40	1.87	2.27	GBU75S900L1000-1	73.36	80.57	34.75	2.11	2.32
GBU75S225L1000-2	85.63	99.86	48.10	1.78	2.08	GBU75S900L1000-2	64.12	77.60	34.98	1.83	2.22
GBU75S225L1000-3	72.19	99.73	43.48	1.66	2.29	GBU75S900L1000-3	69.74	77.09	29.70	2.35	2.60
Mean				1.77	2.21	Mean				2.10	2.38
GBU75S475L2000-1	29.25	28.15	21.93	1.33	1.28	GBU75S1900L2000-1	27.97	19.38	8.40	3.33	2.31
GBU75S475L2000-2	29.14	27.06	21.73	1.34	1.25	GBU75S1900L2000-2	27.73	20.43	8.39	3.31	2.44
GBU75S475L2000-3	29.37	27.20	21.83	1.35	1.25	GBU75S1900L2000-3	24.81	20.24	8.44	2.94	2.40
Mean				1.34	1.26	Mean				3.19	2.38

*(GBU75) (Test) Overall mean = 1.54, Population Standard Deviation = 0.75 **(FE) Overall mean = 1.54, Population Standard Deviation = 0.62

As seen in Table 8.3, the TReM results are unconservative in predicting the ultimate strength of stub columns from the GBU75 test series. This is because the calculation assumed fixed end condition whereas the columns were tested on fixed end condition. Thus, the finite element results serve as a better estimation of the column strength in these cases. When compared to the finite element results, the results calculated using the TReM are closer to the finite element results than the test results. The TReM is slightly unconservative when compared to the finite element results.

The TReM results are conservative for all other longer columns and are the most conservative for columns with 1000mm length. Moreover, similar to the plain back-to-back C-channel built-up columns, for the GBU75L500 and GBU75L1000 columns at $s/L > 0.50$, the TReM is overly conservative because the fastener spacing is beyond the clause C4.5 spacing requirements.

Table 8.4: Comparison of Test and FE Results with TRem for GBU90

Specimen	P_{test} (kN)	P_{FE} (kN)	P_{trw} (kN)	$\frac{P_{test}}{P_{trw}}$	$\frac{P_{FE}}{P_{trw}}$	Specimen	P_{test} (kN)	P_{FE} (kN)	P_{trw} (kN)	$\frac{P_{test}}{P_{trw}}$	$\frac{P_{FE}}{P_{trw}}$
GBU90S50L300-1	Discard					GBU90S200L300-1	Discard				
GBU90S50L300-2	Discard					GBU90S200L300-2	145.56	189.43	141.57	1.03	1.34
GBU90S50L300-3	147.66	190.23	142.26	1.04	1.34	GBU90S200L300-3	161.47	188.61	141.41	1.14	1.33
GBU90S50L300-4	164.40	189.63	141.46	1.16	1.34	GBU90S200L300-4	149.42	189.36	141.48	1.06	1.34
Mean				1.10	1.34	Mean				1.08	1.34
GBU90S100L500-1	161.82	180.76	149.49	0.90	1.21	GBU90S400L500-1	150.82	178.53	147.72	1.02	1.21
GBU90S100L500-2	159.01	180.74	149.48	0.88	1.21	GBU90S400L500-2	149.65	178.75	149.52	1.00	1.20
GBU90S100L500-3	160.65	182.14	149.48	0.88	1.22	GBU90S400L500-3	171.65	178.77	149.44	1.15	1.20
GBU90S100L500-4	-					GBU90S400L500-4	174.93	178.53	149.41	1.17	1.19
Mean				1.07	1.21	Mean				1.09	1.20
GBU90S225L1000-1	143.33	172.07	134.59	1.06	1.28	GBU90S900L1000-1	152.58	175.00	134.65	1.13	1.30
GBU90S225L1000-2	Discard					GBU90S900L1000-2	Discard				
GBU90S225L1000-3	146.14	182.00	131.38	1.11	1.39	GBU90S900L1000-3	141.70	182.65	131.34	1.08	1.39
Mean				1.09	1.33	Mean				1.11	1.35

*(GBU90) (Test) Overall mean = 1.09, Population Standard Deviation = 0.05 **(FE) Overall mean = 1.28, Population Standard Deviation = 0.07

For the GBU90, the TReM is conservative for all columns. The TReM is more conservative in predicting the finite element results than the test results of columns from the GBU90 test series. The TReM is more conservative in predicting the GBU90 compared to the GBU75 because the torsional buckling strength for back-to-back C-channel built-up column with a gap is calculated using section properties of a plain back-to-back C-channel built-up column. The back-to-back C-channel built-up column with a gap is conservatively assumed to have warping constant and radius of gyration of plain back-to-back C-channel built-up because the cross section of the built-up column with a gap is not constant along its length.

Figure 8.7 shows the comparison of the TReM with compression test results for back-to-back C-channel built-up columns with a gap.

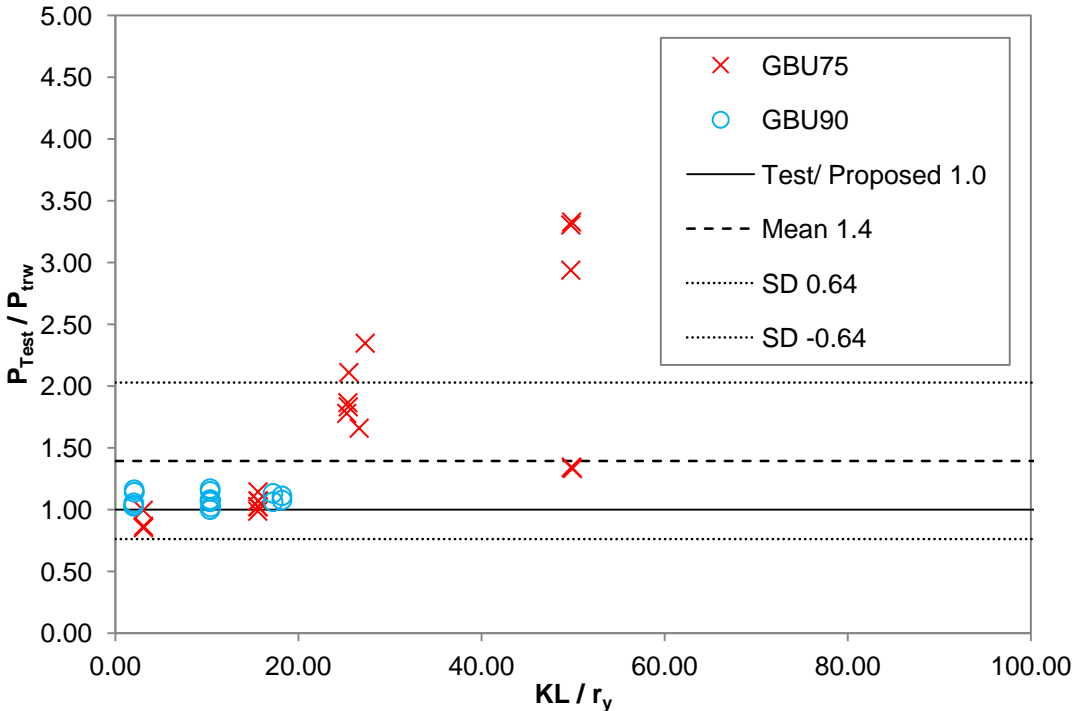


Figure 8.7: Comparison of Proposed Method with Test Results for GBU

Figure 8.7 shows that the TReM is close to 1.0 for shorter columns of the GBU75L300, GBU75L500, GBU90L300, GBU90L500, and GBU90L1000 test series. However, for the GBU75 test series, the TReM is overly conservative for longer columns i.e. the GBU75L1000, GBU75L2000. Overall, the TReM results when compared to the test results are conservative with a mean of 1.40 and a standard deviation of 0.64.

Figure 8.8 shows the comparison of the TReM with finite element results for back-to-back C-channel built-up columns with a gap.

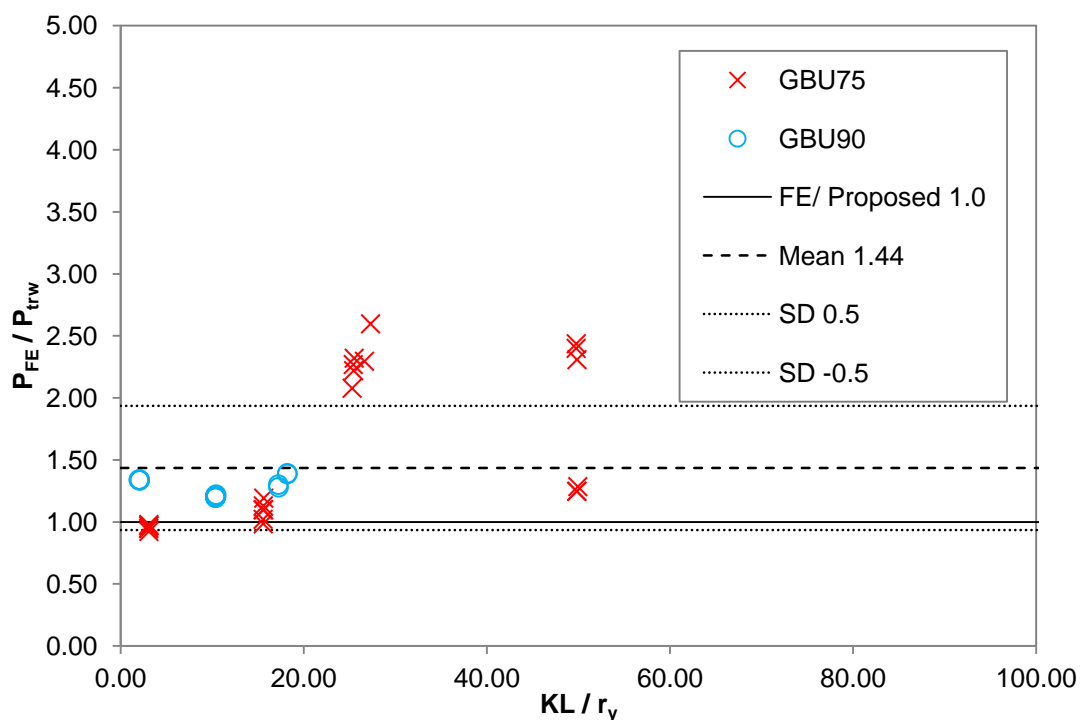


Figure 8.8: Comparison of Proposed Method with FE Results for GBU

Figure 8.8 shows that the TReM is conservative when compared to the finite element results of all columns from the GBU90 test series and most of the shorter columns from the GBU75 test series i.e. the GBU75L300, GBU75L500. Moreover, the TReM is overly conservative for the BU75L1000 and BU75L2000 columns. Generally, the results are conservative when compared to the finite element results with a mean of 1.44 and a standard deviation of 0.50.

The TReM is most conservative for longer columns with large fastener spacing beyond the clause C4.5 spacing requirements because the accuracy of the TReM is affected by the use of modified slenderness ratio. It is expected that the TReM results of back-to-back C-channel built-up columns with a gap can be enhanced with improved torsional buckling strength calculation. However, improvement to the buckling strength equation and modified slenderness ratio is not included in this research.

8.5 Conclusions

There are currently no design provisions for the back-to-back C-channel built-up columns with a gap. Therefore, an enhanced design method known as TReM is proposed. The TReM avoids tedious effective width calculation from EWM, and avoids transient assumptions in CUFSM for DSM, but at the same time incorporates the advantages of both EWM and DSM. The applicability of the TReM is evaluated on both built-up back-to-back C-channel columns with and without a gap. In general, TReM predicts the strength of the back-to-back C-channel built-up columns with and without a gap well. The TReM serves as an improved method to estimate the capacity of these built-up columns.

9 Conclusions

9.1 Introduction

This chapter concludes the investigation of the behaviour of axially loaded back-to-back C-channel built-up columns with findings and recommendations from the experimental works, finite element analysis and design evaluation. The specimens were designed with different dimensions, intermediate fasteners, and end support conditions which covered cases within and beyond the requirements of the provision for built-up columns documented in clause C4.5 of the AISI Specification (2001). A total of 24 C-channel columns, 66 plain back-to-back C-channel built-up columns, and 48 back-to-back C-channel built-up columns with a gap were tested in the compression test. Finite element analysis was conducted using LUSAS version 14.4 to model the test specimens. A total of 115 experimental results were compared with the finite element analysis results of 22 C-channel columns, 53 plain back-to-back C-channel built-up columns, and 40 back-to-back C-channel built-up columns with a gap.

The current design guidelines on C-channel columns and plain back-to-back C-channel built-up columns using Effective Width Method (EWM) and Direct Strength Method (DSM) were evaluated using the test results. Due to lack of guidelines, an enhanced design method known as Thickness Reduction Method (TReM) was proposed for back-to-back C-channel built-up columns with a gap. TReM was evaluated using test and finite element results in this research.

The following objectives of the research were achieved.

- (a) The calculation of the design strength of cold formed steel built-up columns was successfully completed using EWM of North American Specification (NAS) (1946) and DSM of North American Specification (NAS) (2001) for Cold-Formed Steel (CFS) structures.
- (b) The buckling behaviour of the stub, short, intermediate and slender columns were studied through test results and experimental observations during compression tests.

- (c) Finite element models for C-channel, back-to-back built-up column with and without a gap were created using LUSAS version 14.4 and evaluated using test results.
- (d) The provision C4.5 of the AISI Specifications 2001 edition for built-up columns were evaluated with specimens designed to include fastener spacing within and beyond the requirements of clause C4.5.

9.2 Conclusions

The EWM and DSM are conservative in predicting the capacity of cold-formed steel plain back-to-back C-channel built-up columns, especially when the fastener spacing is beyond the spacing requirements from clause C4.5 of the AISI Specifications 2001 Edition.

For the design of back-to-back C-channel built-up columns with a gap, the TReM was proposed to enhance the current design method. The TReM is able to predict the capacity of the back-to-back C-channel built-up column with and without a gap well based on the cross sections (C75 and C90) considered in this research. The TReM results for the plain back-to-back C-channel built-up column show good correlation with the experimental and finite element results. The strength of back-to-back C-channel built-up column with a gap is higher than plain back-to-back C-channel built up column for specimens with smaller cross sections e.g. BU75. However, for the specimens with larger cross sections e.g. the BU90, the capacity for all the tested back-to-back C-channel built-up columns with a gap decreased slightly due to the shift of the failure axis.

Generally, the plain back-to-back C-channel built-up columns failed with local buckling for stub columns, distortional buckling for short and intermediate columns and global buckling for slender columns. Specifically to stub built-up columns, the result shows that plate element slenderness plays an important role. Buckling failure is dominant for columns with larger web-flange ratio (A'/B') while strength failure is dominant for columns with smaller web-flange ratio (A'/B'). Different from plain back-to-back C-channel built-up columns, the failure modes of back-to-back

C-channel built-up columns with a gap are categorised into two types, i.e. S-shaped buckling and O-shaped buckling as observed by Johnston (1971).

Finite element models created from LUSAS version 14.4 predict the strength and behaviour of C-channel, back-to-back C-channel built-up columns with and without a gap well. The two key criteria in modelling built-up columns are the screw connection and the surface contact. The surface-to-surface contact was modelled using the slideline function with master and slave feature in LUSAS. As for screws, a simplified model with 2mm thin strips was used to model the screw connections between the two web surfaces.

The modified slenderness ratio from clause C4.5 of the AISI Specifications 2001 edition is conservative for built-up columns. The modified slenderness ratio is more conservative for longer columns than the shorter back-to-back C-channel built-up columns. Back-to-back C-channel built-up columns with and without a gap with fastener spacing at $s/L < 0.25$ and $0.25 < s/L < 0.50$ achieved higher ultimate strength than those with fastener spacing at $s/L > 0.50$. For columns with fastener spacing beyond the clause requirement, i.e. specimens with $s/L > 0.50$, the provision C4.5 for built-up columns is significantly conservative. The restraint at the mid-length of the back-to-back C-channel built-up columns is critical regardless of the number of fasteners along the length of the built-up column.

9.3 Recommendations & Future Works

This research has met all of its objectives, and from the findings presented, it is recommended that:

- (a) short C-channels can be introduced as intermediate fasteners for plain built-up columns consisted of slender cross section forming built-up columns with a gap to increase the strength and stiffness of the built-up column.
- (b) restraints such as fasteners can be provided at ends and mid-length of built-up columns to prevent the separation of individual C-channels and improve the strength and rigidity of the built-up columns.
- (c) the modified slenderness ratio of clause C4.5 from AISI Specifications 2001 Edition should be included in the design of built-up columns since it is

recommended in (b) that fasteners should be provided at both ends and at mid-length of the column.

This research also provides a solid framework allowing future researchers and practitioners to further investigate the behaviour of built-up columns. The following recommendations can be considered for future research.

- (a) Study on the effect of varying plate slenderness ratios e.g. web-flange ratio (A'/B') and flange-thickness ratio (B'/t) on the behaviour of back-to-back C-channel built-up columns with and without a gap with more finite element modelling.
- (b) Evaluation of TReM with different cross section parameters.
- (c) Determination of torsional properties to determine torsional buckling strength for back-to-back C-channel built-up columns with a gap.
- (d) Further in-depth study on the behaviour of slender built-up columns.

References

(Chicago Referencing)

- AISI. 1997. *Cold-formed steel back-to-back header assembly tests*. Publication RG-9719. North American Steel Framing Alliance.
<http://www.toolbase.org/PDF/CaseStudies/BacktoBackHeaderAssembly.pdf>
- AISI. 2002a. *AISI manual cold-formed steel design*. American Iron and Steel Institute.
- AISI. 2002b. *Commentary on Appendix 1 design of cold-formed steel structural members with the Direct Strength Method*. American Iron and Steel Institute.
- AISI. 2002c. *North American Specification for the design of cold-formed steel structural members (2001 edition)*. American Iron and Steel Institute.
- AISI. 2005. *Supplement 2004 to the North American Specification for the design of cold-formed steel structural members 2001 edition*. American Iron and Steel Institute.
- AISI. 2006. *Direct Strength Method (DSM) Design Guide*. CF06-1. American Iron and Steel Institute.
- AISI. 2007. *North American Specification for the design of cold-formed steel structural members (2007 edition)*. American Iron and Steel Institute.
- Allen, D. 2006. *History of cold-formed steel*. Structure Magazine (Issue November). 28-32.
<http://www.structuremag.org/Archives/2006-11/C-BB-History-AllenLowndes-Nov06.pdf>
- Aslani, F. and S. C. Goel. 1991. An analytical criterion for buckling strength of built-up compression members. *Engineering Journal*. 28(4): 159-168. AISC.
<http://www.aisc.org> (accessed May 03, 2010)
- ASTM International. 2008. *Standard test methods for time of setting of hydraulic cement by Vicat needle*. ASTM C191-08. ASTM.
www.astm.org/Standards/C191.htm (accessed January 10, 2011)
- ASTM International. 2008. *Standard test methods for compressive strength of hydraulic cement mortars (using 2in. or [50mm] cube specimens)*. ASTM C109/

- C109M-01. ASTM. www.astm.org/Standards/C191.htm (accessed January 10, 2011)
- Barrios, D. B., E. Angelo, and E. Goncalves. 2005. Finite element shot peening simulation for residual stress analysis and comparison with experimental results. MECOM 2005 – 8th Congress on computational mechanics. November, 2005. Buenos Aires, Argentina. *Computational Mechanics* 24(3): 413 – 422.
- Becque, J. and K. J. R. Rasmussen. 2009. Numerical investigation of the interaction of local and overall buckling of stainless steel I-columns. *Journal of Structural Engineering*. 135(11): 1349 – 1356. ASCE. <http://www.asce.org> (accessed July 08, 2010)
- Bleich F. 1952. Buckling strength of metal structures. New York: McGraw-Hill. 167 – 192. Quoted in Aslani and Goel 1991, 159-168.
- Brueggen, B., and C. Ramseyer. 2005. Capacity of built-up cold-formed steel axial compression members. *Proceedings of the annual stability conference*. Rolla, Missouri. Structural stability research council (2005). Quoted in Whittle and Ramseyer 2009, 190-201.
- Butterworth, J. 1999. Finite element analysis of structural steelwork beam to column bolted connections. Constructional Research Unit, School of Science and Technology, University of Teesside, UK. CS502 (1) <http://www.lusas.com/> (accessed February 09, 2011)
- Chin, H. K. H. 2008. Finite element investigation on the strength of semi rigid steel connection. Bachelor thesis. Universiti Teknologi Malaysia, Skudai, Johor Darul Takzim, Malaysia. <http://www.efka.utm.my/thesis/> (accessed January 20, 2011)
- Crisfield, M. A. 1991. *Non-linear finite element analysis of solids and structures: volume 1 – essentials*. England. John Wiley and Sons Ltd.
- Dos Santos, E. S., E. M. Batista, and D. Camotim. 2012. Experimental investigation concerning lipped channel columns undergoing local–distortional–global buckling mode interaction. *Thin-Walled Structures* 54: 19-34. Science Direct. <http://www.sciencedirect.com> (accessed December 06, 2012).

- Dubina D., R. Zaharia, and V. Ungureanu. 2002. Behaviour of Built-up Columns made of C sections Connected with Bolted C Stitches. International Colloquium on Stability and Ductility of Steel Structures (SDSS 2002) 179 – 186. Akadémiai Kiadó, Budapest.
- FEA Co., Ltd. (2011) Lusas element reference manual & user's manual (version 14.4), United Kingdom.
- Gao, L., H. Sun, F. Jin, and H. Fan. 2009. Load-carrying capacity of high strength steel box-sections I: stub columns. *Journal of Constructional Steel Research*. 65(4): 918 – 924. Science Direct. <http://www.sciencedirect.com> (accessed June 18, 2009).
- Georgieva, I., L. Schueremans, and L. Pyl. 2012. Composed columns from cold-formed steel Z-profiles: experiments and code-based predictions of the overall compression capacity. *Engineering Structures*. 37: 125-134. Science Direct. <http://www.sciencedirect.com> (accessed December 05, 2012).
- Hancock, G. J., T. M. Murray, and D. S. Ellifritt. 2001. *Cold-formed steel structures to the AISI specification*. New York. CRC Press.
- Hussin, M. A. 2001. Prestasi Sambungan pada Paksi Major Menggunakan Keratan Keluli Tempatan. Bachelor thesis. Universiti Teknologi Malaysia, Skudai, Johor Darul Takzim, Malaysia. Quoted in Chin 2008.
- Johnston, B. G. 1971. Spaced steel columns. *Journal of the Structural Division*, 97(5): 1465 – 1479. ASCE. <http://www.asce.org> (purchased May 10, 2012)
- Kwon, Y. B., B. S. Kim, G. J. Hancock. 2009. Compression tests of high strength cold-formed steel channels with buckling interaction. *Journal of Constructional Steel Research*. 65(2): 278-289. Science Direct. <http://www.sciencedirect.com> (accessed May 26, 2009).
- Lue, D. M., T. Yen, and J. L. Liu. 2006. Experimental investigation on built-up columns. *Journal of Constructional Steel Research*. 62(12): 1325–1332. Science Direct. <http://www.sciencedirect.com> (accessed November 10, 2009).
- Liu, J. L., D. M. Lue, and C. H. Lin. 2009. Investigation on slenderness ratio of built-up compression members. *Journal of Constructional Steel Research*. 65(1):

- 237-248. Science Direct. <http://www.sciencedirect.com> (accessed September 25, 2007).
- Macdonald, M., M. A. Heiyantuduwa, and J. Rhodes. 2008. Recent Developments in the Design of Cold-Formed Steel Members and Structures. *Thin-Walled Structures*. 46(7–9): 1047-1053. Science Direct. <http://www.sciencedirect.com> (accessed May 05, 2009).
- Megnounif, A., M. Djafour, A. Belarbi, and D. Kerdal. 2008. Strength buckling predictions of cold-formed steel built-up columns. *Structural engineering and mechanics*. 28(4): 443-460.
- Mei, C.C., A. L. Y. Ng, H. H. Lau, and S. L. Toh. 2009. Applications of Built-up Sections in Lightweight Steel Trusses, *Sixth International Conference on Advances in Steel Structures*. December 16, 2009. 857-864. Hong Kong, China: The Hong Kong Institute of Steel Construction.
- Reyes, W. and A. Guzmán. 2011. Evaluation of the slenderness ratio in built-up cold-formed box sections. *Journal of Constructional Steel Research*. 67(6): 929-935. Science Direct. <http://www.sciencedirect.com> (accessed December 05, 2011).
- Rhodes, J. and J. M. Harvey. 1977. Interaction behaviour of plain channel columns under concentric or eccentric loading. *Proceedings of the Second International Colloquium on the Stability of Steel Structures*. Liege. 439–444. Quoted in Young 2006, 119-132.
- Rondal, J. and M. Niazi. 1990. Stability of built-up beams and columns with thin-walled members. *Journal of Constructional Steel Research*. 16(4): 329 - 335. Science Direct. <http://www.sciencedirect.com> (accessed May 05, 2009).
- Salem, A. H., M. A. El Aghoury, S. K. Hassan, and A. A. Amin. 2004. Post-buckling strength of battened columns built from cold formed lipped channels. *Emirates Journal for Engineering Research*. 9(2): 117 - 125. United Arab Emirates University. www.engg.uaeu.ac.ae/ejer/ (accessed 10 April, 2008)
- Schafer, B. W. 2002. Local, distortional, and euler buckling of thin-walled columns. *Journal of Structural Engineering*. 128(3): 289 – 299. ASCE. <http://www.asce.org> (accessed May 02, 2009)

- Schafer, B. W. 2008. Review: the direct strength method of cold-formed steel member design. *Journal of Constructional Steel Research*. 64(7-8): 766 – 778. Science Direct. <http://www.sciencedirect.com> (accessed May 06, 2009).
- Schafer, B. W. and S. Ádány. 2005. Understanding and classifying local, distortional and global buckling in open thin-walled members. *Proceedings of Annual Conference Structural Stability Research Council*, Montreal, Canada. 27-46.
- Schafer, B. W. and S. Ádány. 2006. Buckling analysis of cold-formed steel members using CUFSM: Conventional and constrained finite strip methods. *18th International Specialty Conference on Cold-Formed Steel Structures: Recent Research and Developments in Cold-Formed Steel Design and Construction*. October 26-27, 2006. Orlando, Florida. 39-54.
- Standards Australia. 2005. *Cold-formed steel design*. AS 4600-2005. Standards Australia Online. <http://www.saiglobal.com> (accessed March 25, 2009).
- Standards Australia. 2007. *Methods of tensile testing of metals*. AS1391-2007. Standards Australia Online. <http://www.saiglobal.com> (accessed March 25, 2009).
- Stone, T. A. and R. A. LaBoube. 2005. Behaviour of cold-formed steel built-up I-sections. *Thin-Walled Structures*. 43(12) 1805 – 1817. Science Direct. <http://www.sciencedirect.com> (accessed May 06, 2009).
- Tahir, M. M., S. b. Mohamed, M. A. Hussin, and A. A. Saim. 2004. Performance of Extended End Plate Connection Connected to Column Flange. Bachelor thesis. Universiti Teknologi Malaysia, Skudai, Johor Darul Takzim, Malaysia. Quoted in Chin 2008.
- Tan, E. H. 2006. Behavior and strength study on steel semi rigid connection using LUSAS. Bachelor thesis. Universiti Teknologi Malaysia, Skudai, Johor Darul Takzim, Malaysia. Quoted in Chin 2008.
- Tang, X. M. and H. W. Ma. 2005. A study on bolted connection of built-up I-shaped member consisting of double thin-walled cold-formed lipped channels. *4th International conference on advances in steel structures*. 1: 523 – 528. Science Direct. <http://www.sciencedirect.com> (accessed May 06, 2009).

- Temple, M.C. and G.M. Elmahdy. 1996. Slenderness ratio of main member between interconnectors of built-up compression members. *Canadian Journal of Civil Engineering* 23(1996): 1295 – 1304. <http://www.nrcresearchpress.com> (accessed March 05, 2011).
- Von Karman, T., E. E. Sechler, and L. H. Donnell. 1932. The strength of thin plates in compression. *Transactions. ASME.* 54(MP 54-5). Quoted in Hancock, Murray, and Ellifritt 2001, 375.
- Whittle, J., & C. Ramseyer. 2009. Buckling capacities of axially loaded, cold-formed, built-up C-channels. *Thin-walled structures* 47(2): 190-201. Science Direct. <http://www.sciencedirect.com> (accessed May 06, 2009).
- Winter, G. 1947. Strength of thin steel compression flanges. *Transactions. ASCE.* Paper No. 2305. 112() 527-576. Quoted in Hancock, Murray, and Ellifritt 2001, 375.
- Yan, J. and B. Young. 2002. Column tests of cold-formed steel channels with complex stiffeners. *Journal of Structural Engineering* 128(6): 737-745. ASCE. <http://www.asce.org> (accessed May 02, 2009).
- Yiu, F. and T. Peköz. 2000. Design of cold-formed steel plain channels. *Fifteenth International Specialty Conference on Cold-Formed Steel Structures*, St. Louis, Missouri. October 19-20, 2000. 13-22.
- Young, B. 2005. Experimental investigation of cold-formed steel lipped angle concentrically loaded compression members. *Journal of Structural Engineering.* 131(9): 1390-1396. ASCE. <http://www.asce.org> (accessed May 02, 2009)
- Young, B. 2006. Local buckling and shift of effective centroid of slender sections. *Advanced Facade Engineering and Technology Symposium*, April 21, 2006. Hong Kong, China. 119-132.
- Young, B. and J. Chen. 2008. Design of cold-formed steel built-up closed sections with intermediate stiffeners. *Journal of Structural Engineering.* 134(5): 727 – 737. ASCE. <http://www.asce.org> (accessed Jun 05, 2013)
- Young, B. and K. J. R. Rasmussen. 1998a. Design of lipped channel columns. *Journal of Structural Engineering.* 124(2): 140 – 148. ASCE. <http://www.asce.org> (accessed Dec 22, 2009)

- Young, B. and K.J.R. Rasmussen. 1998b. Tests of Cold-Formed Channel Columns. Proceedings of the 14th International Specialty Conference on Cold-Formed Steel Structures, St. Louis, University of Missouri-Rolla, Mo, USA, 239-264.
- Young, B. and K. J. R. Rasmussen. 1998c. Tests of fixed-ended plain channel columns. *Journal of Structural Engineering*. 124(2): 131 – 139. ASCE. <http://www.asce.org> (accessed May 02, 2009)
- Young, B and J. T. Yan. 2000. Finite element analysis of cold-formed channel columns. *15th International Specialty Conference on Cold-formed Steel Structures*, October 19-20, 2000. St. Louis, Missouri U.S.A. pp 281 – 305.
- Young, B. and J. T. Yan. 2002. Channel columns undergoing local, distortional and overall buckling. *Journal of structural engineering*. 128(6): 728-736. ASCE. <http://www.asce.org> (accessed June 08, 2009)
- Young, B. and J. T. Yan. 2004. Design of cold-formed steel channel columns with complex edge stiffeners by Direct Strength Method. *Journal of structural engineering*. 130(11): 1756–1763. ASCE. <http://www.asce.org> (accessed June 08, 2009)
- Yu, W. W., and R. A. LaBoube. 2010. *Cold formed steel design*. 4th ed. [image] New Jersey: John Wiley & Sons.
- Zaharia, R. and D. Dubina. 2005. Numerical study of stability of cold-formed built-up columns. *Bulletin of the Polytechnic Institute of Jassy, Constructions, Architecture Section*. LI(LV)(1-2): 61-68. <http://www.ce.tuiasi.ro/~bipcons/Archive/23.pdf> (accessed May 07, 2012)
- Zhang, J. H. and B. Young. 2012. Compression tests of cold-formed steel I-shaped open sections with edge and web stiffeners. *Thin-Walled Structures*. 52: 1-11. Science Direct. <http://www.sciencedirect.com> (accessed December 05, 2012)

“Every reasonable effort has been made to acknowledge the owners of copyright material. I would be pleased to hear from any copyright owner who has been omitted or incorrectly acknowledged.”

Volume II

Table of Contents

TABLE OF CONTENTS	I
LIST OF FIGURES	III
A. TENSILE COUPON TEST RESULTS	1
B. IMPERFECTION RESULTS FOR C-CHANNEL	4
B.1 Stub Column	4
B.2 Short Column	6
B.3 Intermediate Column	7
B.4 Slender Column	11
C. IMPERFECTION RESULTS FOR PLAIN BUILT-UP BACK-TO-BACK C-CHANNELS	12
C.1 Stub Column	12
C.2 Short Column	18
C.3 Intermediate Column	27
C.4 Slender Column	30
D. IMPERFECTION RESULTS GAPPED BUILT-UP BACK-TO-BACK C-CHANNELS	36
D.1 Stub Column	36
D.2 Short Column (L=500mm)	40
D.3 Short Column (L=1000mm)	44
D.4 Short Column (L=2000mm)	48
E. RESULTS FOR C-CHANNEL	52
E.1 Stub Column	52
E.2 Short Column	59
E.3 Intermediate Column	62
E.4 Slender Column	70
F. RESULTS FOR PLAIN BUILT-UP BACK-TO-BACK C-CHANNELS	73
F.1 Stub Column	73
F.2 Short Column	91

F.3	Intermediate Column	112
F.4	Slender Column	120
G.	RESULTS FOR GAPPED BUILT-UP BACK-TO-BACK C-CHANNELS	126
G.1	Stub Column	126
G.2	Short Column (L=500mm)	137
G.3	Short Column (L=1000mm)	154
G.4	Short Column (L=2000mm)	160
H.	DESIGN SPREADSHEETS	166
H.1	Design Methods	166
	H.1.1 Effective Width Method (EWM)	166
	H.1.2 Direct Strength Method by Manual Calculation (DSM I)	172
	H.1.3 Direct Strength Method by CUFSM (DSM II)	177
	H.1.4 Beam-column Design	179
H.2	C-channel Column Spreadsheets	187
	H.2.1 Effective Width Method (EWM)	187
	H.2.2 Direct Strength Method (DSM I & DSM II)	192
H.3	Plain Built-up Back-to-back Channels Column Spreadsheets	198
	H.3.1 Effective Width Method (EWM)	198
	H.3.2 Direct Strength Method (DSM I & DSM II)	201
H.4	Gapped Built-up Back-to-back Channels Column Spreadsheet	204
	H.4.1 Thickness Reduction Method (TReM)	204

List of Figures

Figure A.1	Tensile Coupon Test Results of C75-2	1
Figure A.2	Tensile Coupon Test Results of C75-3	1
Figure A.3	Tensile Coupon Test Results of C90-1	2
Figure A.4	Tensile Coupon Test Results of C90-2	2
Figure A.5	Tensile Coupon Test Results of C90-3	3
Figure B.1	Imperfection Results for C75L300-1	4
Figure B.2	Imperfection Results for C90L300-2	5
Figure B.3	Imperfection Results for C90L1000-1	6
Figure B.4	Imperfection Results for C75L500-2	7
Figure B.5	Imperfection Results for C90L500-1	8
Figure B.6	Imperfection Results for C75L1000-1	9
Figure B.7	Imperfection Results for C90L1000-1	10
Figure B.8	Imperfection Results for C75L2000-1	11
Figure C.1	Imperfection Results for BU75S50L300-1	12
Figure C.2	Imperfection Results for BU75S100L300-2	13
Figure C.3	Imperfection Results for BU75S200L300-1	14
Figure C.4	Imperfection Results for BU90S50L300-1	15
Figure C.5	Imperfection Results for BU90S100L300-3	16
Figure C.6	Imperfection Results for BU90S200L300-1	17
Figure C.7	Imperfection Results for BU75S100L500-1	18
Figure C.8	Imperfection Results for BU75S200L500-1	19
Figure C.9	Imperfection Results for BU75S400L500-1	20
Figure C.10	Imperfection Results for BU90S100L500-1	21
Figure C.11	Imperfection Results for BU90S200L500-1	22
Figure C.12	Imperfection Results for BU90S400L500-1	23
Figure C.13	Imperfection Results for BU90S225L1000-1	24
Figure C.14	Imperfection Results for BU90S450L1000-2	25
Figure C.15	Imperfection Results for BU90S900L1000-1	26
Figure C.16	Imperfection Results for BU75S225L1000-1	27
Figure C.17	Imperfection Results for BU75S450L1000-1	28
Figure C.18	Imperfection Results for BU75S900L1000-1	29
Figure C.19	Imperfection Results for BU75S475L2000-2 (Left)	30
Figure C.20	Imperfection Results for BU75S475L2000-2 (Right)	31
Figure C.21	Imperfection Results for BU75S950L2000-2 (Left)	32

Figure C.22	Imperfection Results for BU75S950L2000-2 (Right)	33
Figure C.23	Imperfection Results for BU75S1900L2000-2 (Left)	34
Figure C.24	Imperfection Results for BU75S1900L2000-2 (Right)	35
Figure D.1	Imperfection Results for GBU75S50L300-2	36
Figure D.2	Imperfection Results for GBU75S200L300-1	37
Figure D.3	Imperfection Results for GBU90S50L300-3	38
Figure D.4	Imperfection Results for GBU90S200L300-2	39
Figure D.5	Imperfection Results for GBU75S100L500-1	40
Figure D.6	Imperfection Results for GBU75S400L500-1	41
Figure D.7	Imperfection Results for GBU90S100L500-1	42
Figure D.8	Imperfection Results for GBU90S400L500-1	43
Figure D.9	Imperfection Results for GBU75S225L1000-1	44
Figure D.10	Imperfection Results for GBU75S900L1000-1	45
Figure D.11	Imperfection Results for GBU90S225L1000-1	46
Figure D.12	Imperfection Results for GBU90S900L1000-1	47
Figure D.13	Imperfection Results for GBU75S475L2000-1 (Left)	48
Figure D.14	Imperfection Results for GBU75S475L2000-1 (Right)	49
Figure D.15	Imperfection Results for GBU75S1900L2000-1 (Left)	50
Figure D.16	Imperfection Results for GBU75S1900L2000-1 (Right)	51
Figure E.1	Axial Load versus Shortening Curve for C75L300-1	52
Figure E.2	Axial Load versus Deformation Curve for C75L300-1	52
Figure E.3	Axial Load versus Shortening Curve for C75L300-2	53
Figure E.4	Axial Load versus Deformation Curve for C75L300-2	53
Figure E.5	Axial Load versus Shortening Curve for C75L300-3	54
Figure E.6	Axial Load versus Deformation Curve for C75L300-3	54
Figure E.7	Axial Load versus Shortening Curve for C75L300-4	55
Figure E.8	Axial Load versus Deformation Curve for C75L300-4	55
Figure E.9	Axial Load versus Shortening Curve for C90L300-2	56
Figure E.10	Axial Load versus Deformation Curve for C90L300-2	56
Figure E.11	Axial Load versus Shortening Curve for C90L300-3	57
Figure E.12	Axial Load versus Deformation Curve for C90L300-3	57
Figure E.13	Axial Load versus Shortening Curve for C90L300-4	58
Figure E.14	Axial Load versus Deformation Curve for C90L300-4	58
Figure E.15	Axial Load versus Shortening Curve for C90L500-1	59
Figure E.16	Axial Load versus Deformation Curve for C90L500-1	59
Figure E.17	Axial Load versus Shortening Curve for C90L500-2	60

Figure E.18	Axial Load versus Deformation Curve for C90L500-2	60
Figure E.19	Axial Load versus Shortening Curve for C90L500-3	61
Figure E.20	Axial Load versus Deformation Curve for C90L500-3	61
Figure E.21	Axial Load versus Shortening Curve for C75L500-2	62
Figure E.22	Axial Load versus Deformation Curve for C75L500-2	62
Figure E.23	Axial Load versus Shortening Curve for C75L500-3	63
Figure E.24	Axial Load versus Deformation Curve for C75L500-3	63
Figure E.25	Axial Load versus Shortening Curve for C75L500-4	64
Figure E.26	Axial Load versus Deformation Curve for C75L500-4	64
Figure E.27	Axial Load versus Shortening Curve for C75L1000-1	65
Figure E.28	Axial Load versus Deformation Curve for C75L1000-1	65
Figure E.29	Axial Load versus Shortening Curve for C75L1000-2	66
Figure E.30	Axial Load versus Deformation Curve for C75L1000-2	66
Figure E.31	Axial Load versus Shortening Curve for C90L1000-1	67
Figure E.32	Axial Load versus Deformation Curve for C90L1000-1	67
Figure E.33	Axial Load versus Shortening Curve for C90L1000-2	68
Figure E.34	Axial Load versus Deformation Curve for C90L1000-2	68
Figure E.35	Axial Load versus Shortening Curve for C90L1000-3	69
Figure E.36	Axial Load versus Deformation Curve for C90L1000-3	69
Figure E.37	Axial Load versus Shortening Curve for C75L2000-1	70
Figure E.38	Axial Load versus Deformation Curve for C75L2000-1	70
Figure E.39	Axial Load versus Shortening Curve for C75L2000-2	71
Figure E.40	Axial Load versus Deformation Curve for C75L2000-2	71
Figure E.41	Axial Load versus Shortening Curve for C75L2000-3	72
Figure E.42	Axial Load versus Deformation Curve for C75L2000-3	72
Figure F.1	Axial Load versus Shortening Curve for BU75S50L300-1	73
Figure F.2	Axial Load versus Deformation Curve for BU75S50L300-1	73
Figure F.3	Axial Load versus Shortening Curve for BU75S50L300-2	74
Figure F.4	Axial Load versus Deformation Curve for BU75S50L300-2	74
Figure F.5	Axial Load versus Shortening Curve for BU75S50L300-3	75
Figure F.6	Axial Load versus Deformation Curve for BU75S50L300-3	75
Figure F.7	Axial Load versus Shortening Curve for BU75S100L300-2	76
Figure F.8	Axial Load versus Deformation Curve for BU75S100L300-2	76
Figure F.9	Axial Load versus Shortening Curve for BU75S100L300-3	77
Figure F.10	Axial Load versus Deformation Curve for BU75S100L300-3	77
Figure F.11	Axial Load versus Shortening Curve for BU75S100L300-4	78

Figure F.12	Axial Load versus Deformation Curve for BU75S100L300-4	78
Figure F.13	Axial Load versus Shortening Curve for BU75S200L300-1	79
Figure F.14	Axial Load versus Deformation Curve for BU75S200L300-1	79
Figure F.15	Axial Load versus Shortening Curve for BU75S200L300-2	80
Figure F.16	Axial Load versus Deformation Curve for BU75S200L300-2	80
Figure F.17	Axial Load versus Shortening Curve for BU75S200L300-3	81
Figure F.18	Axial Load versus Deformation Curve for BU75S200L300-3	81
Figure F.19	Axial Load versus Shortening Curve for BU75S200L300-4	82
Figure F.20	Axial Load versus Deformation Curve for BU75S200L300-4	82
Figure F.21	Axial Load versus Shortening Curve for BU90S50L300-1	83
Figure F.22	Axial Load versus Deformation Curve for BU90S50L300-1	83
Figure F.23	Axial Load versus Shortening Curve for BU90S50L300-2	84
Figure F.24	Axial Load versus Deformation Curve for BU90S50L300-2	84
Figure F.25	Axial Load versus Shortening Curve for BU90S50L300-3	85
Figure F.26	Axial Load versus Deformation Curve for BU90S50L300-3	85
Figure F.27	Axial Load versus Shortening Curve for BU90S100L300-3	86
Figure F.28	Axial Load versus Deformation Curve for BU90S100L300-3	86
Figure F.29	Axial Load versus Shortening Curve for BU90S100L300-4	87
Figure F.30	Axial Load versus Deformation Curve for BU90S100L300-4	87
Figure F.31	Axial Load versus Shortening Curve for BU90S200L300-1	88
Figure F.32	Axial Load versus Deformation Curve for BU90S200L300-1	88
Figure F.33	Axial Load versus Shortening Curve for BU90S200L300-2	89
Figure F.34	Axial Load versus Deformation Curve for BU90S200L300-2	89
Figure F.35	Axial Load versus Shortening Curve for BU90S200L300-4	90
Figure F.36	Axial Load versus Deformation Curve for BU90S200L300-4	90
Figure F.37	Axial Load versus Shortening Curve for BU75S100L500-1	91
Figure F.38	Axial Load versus Deformation Curve for BU75S100L500-1	91
Figure F.39	Axial Load versus Shortening Curve for BU75S100L500-3	92
Figure F.40	Axial Load versus Deformation Curve for BU75S100L500-3	92
Figure F.41	Axial Load versus Shortening Curve for BU75S200L500-1	93
Figure F.42	Axial Load versus Deformation Curve for BU75S200L500-1	93
Figure F.43	Axial Load versus Shortening Curve for BU75S200L500-2	94
Figure F.44	Axial Load versus Deformation Curve for BU75S200L500-2	94
Figure F.45	Axial Load versus Shortening Curve for BU75S200L500-3	95
Figure F.46	Axial Load versus Deformation Curve for BU75S200L500-3	95
Figure F.47	Axial Load versus Shortening Curve for BU75S400L500-1	96

Figure F.48	Axial Load versus Deformation Curve for BU75S400L500-1	96
Figure F.49	Axial Load versus Shortening Curve for BU75S400L500-2	97
Figure F.50	Axial Load versus Deformation Curve for BU75S400L500-2	97
Figure F.51	Axial Load versus Shortening Curve for BU75S400L500-3	98
Figure F.52	Axial Load versus Deformation Curve for BU75S400L500-3	98
Figure F.53	Axial Load versus Shortening Curve for BU90S100L500-1	99
Figure F.54	Axial Load versus Deformation Curve for BU90S100L500-1	99
Figure F.55	Axial Load versus Shortening Curve for BU90S100L500-2	100
Figure F.56	Axial Load versus Deformation Curve for BU90S100L500-2	100
Figure F.57	Axial Load versus Shortening Curve for BU90S200L500-1	101
Figure F.58	Axial Load versus Deformation Curve for BU90S200L500-1	101
Figure F.59	Axial Load versus Shortening Curve for BU90S200L500-2	102
Figure F.60	Axial Load versus Deformation Curve for BU90S200L500-2	102
Figure F.61	Axial Load versus Shortening Curve for BU90S200L500-3	103
Figure F.62	Axial Load versus Deformation Curve for BU90S200L500-3	103
Figure F.63	Axial Load versus Shortening Curve for BU90S400L500-1	104
Figure F.64	Axial Load versus Deformation Curve for BU90S400L500-1	104
Figure F.65	Axial Load versus Shortening Curve for BU90S400L500-2	105
Figure F.66	Axial Load versus Deformation Curve for BU90S400L500-2	105
Figure F.67	Axial Load versus Shortening Curve for BU90S225L1000-1	106
Figure F.68	Axial Load versus Deformation Curve for BU90S225L1000-1	106
Figure F.69	Axial Load versus Shortening Curve for BU90S225L1000-2	107
Figure F.70	Axial Load versus Deformation Curve for BU90S225L1000-2	107
Figure F.71	Axial Load versus Shortening Curve for BU90S450L1000-2	108
Figure F.72	Axial Load versus Deformation Curve for BU90S450L1000-2	108
Figure F.73	Axial Load versus Shortening Curve for BU90S450L1000-3	109
Figure F.74	Axial Load versus Deformation Curve for BU90S450L1000-3	109
Figure F.75	Axial Load versus Shortening Curve for BU90S900L1000-1	110
Figure F.76	Axial Load versus Deformation Curve for BU90S900L1000-1	110
Figure F.77	Axial Load versus Shortening Curve for BU90S900L1000-2	111
Figure F.78	Axial Load versus Deformation Curve for BU90S900L1000-2	111
Figure F.79	Axial Load versus Shortening Curve for BU75S225L1000-1	112
Figure F.80	Axial Load versus Deformation Curve for BU75S225L1000-1	112
Figure F.81	Axial Load versus Shortening Curve for BU75S225L1000-2	113
Figure F.82	Axial Load versus Deformation Curve for BU75S225L1000-2	113
Figure F.83	Axial Load versus Shortening Curve for BU75S450L1000-1	114

Figure F.84	Axial Load versus Deformation Curve for BU75S450L1000-1	114
Figure F.85	Axial Load versus Shortening Curve for BU75S450L1000-2	115
Figure F.86	Axial Load versus Deformation Curve for BU75S450L1000-2	115
Figure F.87	Axial Load versus Shortening Curve for BU75S450L1000-3	116
Figure F.88	Axial Load versus Deformation Curve for BU75S450L1000-3	116
Figure F.89	Axial Load versus Shortening Curve for BU75S900L1000-1	117
Figure F.90	Axial Load versus Deformation Curve for BU75S900L1000-1	117
Figure F.91	Axial Load versus Shortening Curve for BU75S900L1000-2	118
Figure F.92	Axial Load versus Deformation Curve for BU75S900L1000-2	118
Figure F.93	Axial Load versus Shortening Curve for BU75S900L1000-3	119
Figure F.94	Axial Load versus Deformation Curve for BU75S900L1000-3	119
Figure F.95	Axial Load versus Shortening Curve for BU75S475L2000-2	120
Figure F.96	Axial Load versus Deformation Curve for BU75S475L2000-2	120
Figure F.97	Axial Load versus Shortening Curve for BU75S475L2000-3	121
Figure F.98	Axial Load versus Deformation Curve for BU75S475L2000-3	121
Figure F.99	Axial Load versus Shortening Curve for BU75S950L2000-2	122
Figure F.100	Axial Load versus Deformation Curve for BU75S950L2000-2	122
Figure F.101	Axial Load versus Shortening Curve for BU75S950L2000-3	123
Figure F.102	Axial Load versus Deformation Curve for BU75S950L2000-3	123
Figure F.103	Axial Load versus Shortening Curve for BU75S1900L2000-2	124
Figure F.104	Axial Load versus Deformation Curve for BU75S1900L2000-2	124
Figure F.105	Axial Load versus Shortening Curve for BU75S1900L2000-3	125
Figure F.106	Axial Load versus Deformation Curve for BU75S1900L2000-3	125
Figure G.1	Axial Load versus Shortening Curve for GBU75S50L300-2	126
Figure G.2	Axial Load versus Deformation Curve for GBU75S50L300-2	126
Figure G.3	Axial Load versus Shortening Curve for GBU75S50L300-3	127
Figure G.4	Axial Load versus Deformation Curve for GBU75S50L300-3	127
Figure G.5	Axial Load versus Shortening Curve for GBU75S50L300-4	128
Figure G.6	Axial Load versus Deformation Curve for GBU75S50L300-4	128
Figure G.7	Axial Load versus Shortening Curve for GBU75S200L300-1	129
Figure G.8	Axial Load versus Deformation Curve for GBU75S200L300-1	129
Figure G.9	Axial Load versus Shortening Curve for GBU75S200L300-2	130
Figure G.10	Axial Load versus Deformation Curve for GBU75S200L300-2	130
Figure G.11	Axial Load versus Shortening Curve for GBU75S200L300-4	131
Figure G.12	Axial Load versus Deformation Curve for GBU75S200L300-4	131
Figure G.13	Axial Load versus Shortening Curve for GBU90S50L300-3	132

Figure G.14	Axial Load versus Deformation Curve for GBU90S50L300-3	132
Figure G.15	Axial Load versus Shortening Curve for GBU90S50L300-4	133
Figure G.16	Axial Load versus Deformation Curve for GBU90S50L300-4	133
Figure G.17	Axial Load versus Shortening Curve for GBU90S200L300-2	134
Figure G.18	Axial Load versus Deformation Curve for GBU90S200L300-2	134
Figure G.19	Axial Load versus Shortening Curve for GBU90S200L300-3	135
Figure G.20	Axial Load versus Deformation Curve for GBU90S200L300-3	135
Figure G.21	Axial Load versus Shortening Curve for GBU90S200L300-4	136
Figure G.22	Axial Load versus Deformation Curve for GBU90S200L300-4	136
Figure G.23	Axial Load versus Shortening Curve for GBU75S100L500-1	137
Figure G.24	Axial Load versus Deformation Curve for GBU75S100L500-1	137
Figure G.25	Axial Load versus Shortening Curve for GBU75S100L500-2	138
Figure G.26	Axial Load versus Deformation Curve for GBU75S100L500-2	138
Figure G.27	Axial Load versus Shortening Curve for GBU75S100L500-3	139
Figure G.28	Axial Load versus Deformation Curve for GBU75S100L500-3	139
Figure G.29	Axial Load versus Shortening Curve for GBU75S400L500-1	140
Figure G.30	Axial Load versus Deformation Curve for GBU75S400L500-1	140
Figure G.31	Axial Load versus Shortening Curve for GBU75S400L500-2	141
Figure G.32	Axial Load versus Deformation Curve for GBU75S400L500-2	141
Figure G.33	Axial Load versus Shortening Curve for GBU75S400L500-3	142
Figure G.34	Axial Load versus Deformation Curve for GBU75S400L500-3	142
Figure G.35	Axial Load versus Shortening Curve for GBU90S100L500-1	143
Figure G.36	Axial Load versus Deformation Curve for GBU90S100L500-1	143
Figure G.37	Axial Load versus Shortening Curve for GBU90S100L500-2	144
Figure G.38	Axial Load versus Deformation Curve for GBU90S100L500-2	144
Figure G.39	Axial Load versus Shortening Curve for GBU90S100L500-3	145
Figure G.40	Axial Load versus Deformation Curve for GBU90S100L500-3	145
Figure G.41	Axial Load versus Shortening Curve for GBU90S400L500-1	146
Figure G.42	Axial Load versus Deformation Curve for GBU90S400L500-1	146
Figure G.43	Axial Load versus Shortening Curve for GBU90S400L500-2	147
Figure G.44	Axial Load versus Deformation Curve for GBU90S400L500-2	147
Figure G.45	Axial Load versus Shortening Curve for GBU90S400L500-3	148
Figure G.46	Axial Load versus Deformation Curve for GBU90S400L500-3	148
Figure G.47	Axial Load versus Shortening Curve for GBU90S400L500-4	149
Figure G.48	Axial Load versus Deformation Curve for GBU90S400L500-4	149
Figure G.49	Axial Load versus Shortening Curve for GBU90S225L1000-1	150

Figure G.50	Axial Load versus Deformation Curve for GBU90S225L1000-1	150
Figure G.51	Axial Load versus Shortening Curve for GBU90S225L1000-3	151
Figure G.52	Axial Load versus Deformation Curve for GBU90S225L1000-3	151
Figure G.53	Axial Load versus Shortening Curve for GBU90S900L1000-1	152
Figure G.54	Axial Load versus Deformation Curve for GBU90S900L1000-1	152
Figure G.55	Axial Load versus Shortening Curve for GBU90S900L1000-3	153
Figure G.56	Axial Load versus Deformation Curve for GBU90S900L1000-3	153
Figure G.57	Axial Load versus Shortening Curve for GBU75S225L1000-1	154
Figure G.58	Axial Load versus Deformation Curve for GBU75S225L1000-1	154
Figure G.59	Axial Load versus Shortening Curve for GBU75S225L1000-2	155
Figure G.60	Axial Load versus Deformation Curve for GBU75S225L1000-2	155
Figure G.61	Axial Load versus Shortening Curve for GBU75S225L1000-3	156
Figure G.62	Axial Load versus Deformation Curve for GBU75S225L1000-3	156
Figure G.63	Axial Load versus Shortening Curve for GBU75S900L1000-1	157
Figure G.64	Axial Load versus Deformation Curve for GBU75S900L1000-1	157
Figure G.65	Axial Load versus Shortening Curve for GBU75S900L1000-2	158
Figure G.66	Axial Load versus Deformation Curve for GBU75S900L1000-2	158
Figure G.67	Axial Load versus Shortening Curve for GBU75S900L1000-3	159
Figure G.68	Axial Load versus Deformation Curve for GBU75S900L1000-3	159
Figure G.69	Axial Load versus Shortening Curve for GBU75S475L2000-1	160
Figure G.70	Axial Load versus Deformation Curve for GBU75S475L2000-1	160
Figure G.71	Axial Load versus Shortening Curve for GBU75S475L2000-2	161
Figure G.72	Axial Load versus Deformation Curve for GBU75S475L2000-2	161
Figure G.73	Axial Load versus Shortening Curve for GBU75S475L2000-3	162
Figure G.74	Axial Load versus Deformation Curve for GBU75S475L2000-3	162
Figure G.75	Axial Load versus Shortening Curve for GBU75S1900L2000-1	163
Figure G.76	Axial Load versus Deformation Curve for GBU75S1900L2000-1	163
Figure G.77	Axial Load versus Shortening Curve for GBU75S1900L2000-2	164
Figure G.78	Axial Load versus Deformation Curve for GBU75S1900L2000-2	164
Figure G.79	Axial Load versus Shortening Curve for GBU75S1900L2000-3	165
Figure G.80	Axial Load versus Deformation Curve for GBU75S1900L2000-3	165
Figure H.1:	Notations for C-channel Section	166
Figure H.2:	Effective Width of C-channel Section	169
Figure H.3:	Illustration for Plain Back-to-back C-channels Built-up Section Centre-to-centre Dimensions	172
Figure H.4:	Interpretation of CUFSM Results (Schafer 2006)	178

A. Tensile Coupon Test Results

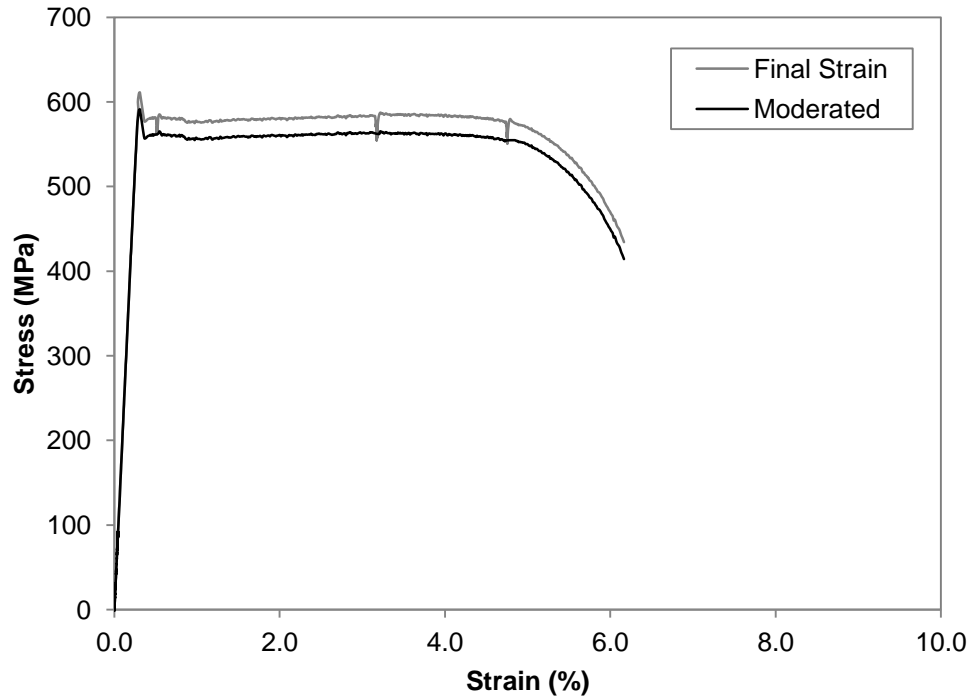


Figure A.1 Tensile Coupon Test Results of C75-2

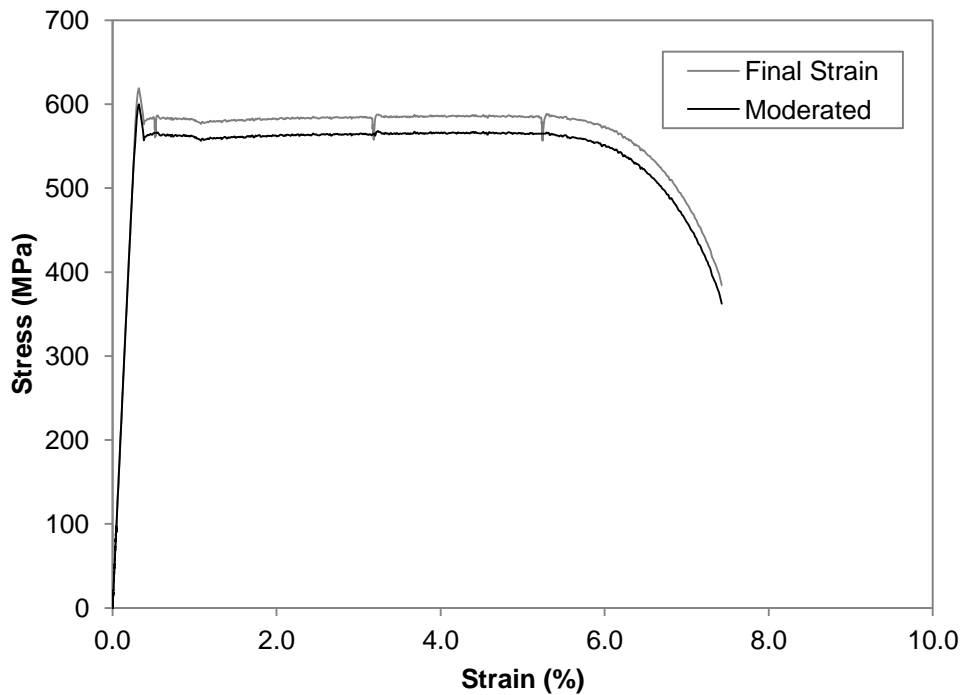


Figure A.2 Tensile Coupon Test Results of C75-3

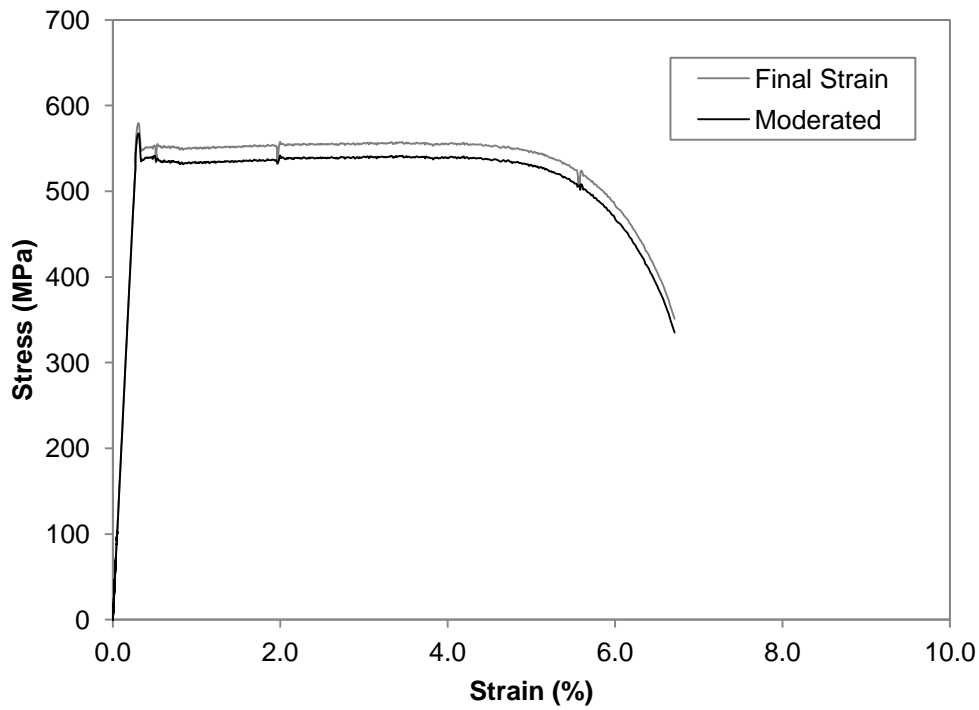


Figure A.3 Tensile Coupon Test Results of C90-1

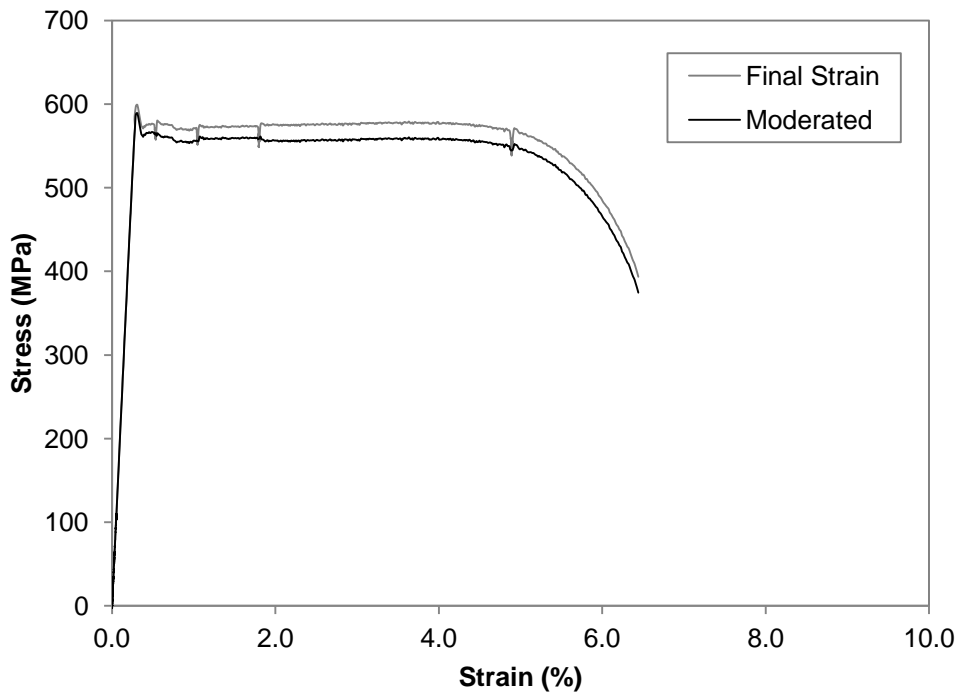


Figure A.4 Tensile Coupon Test Results of C90-2

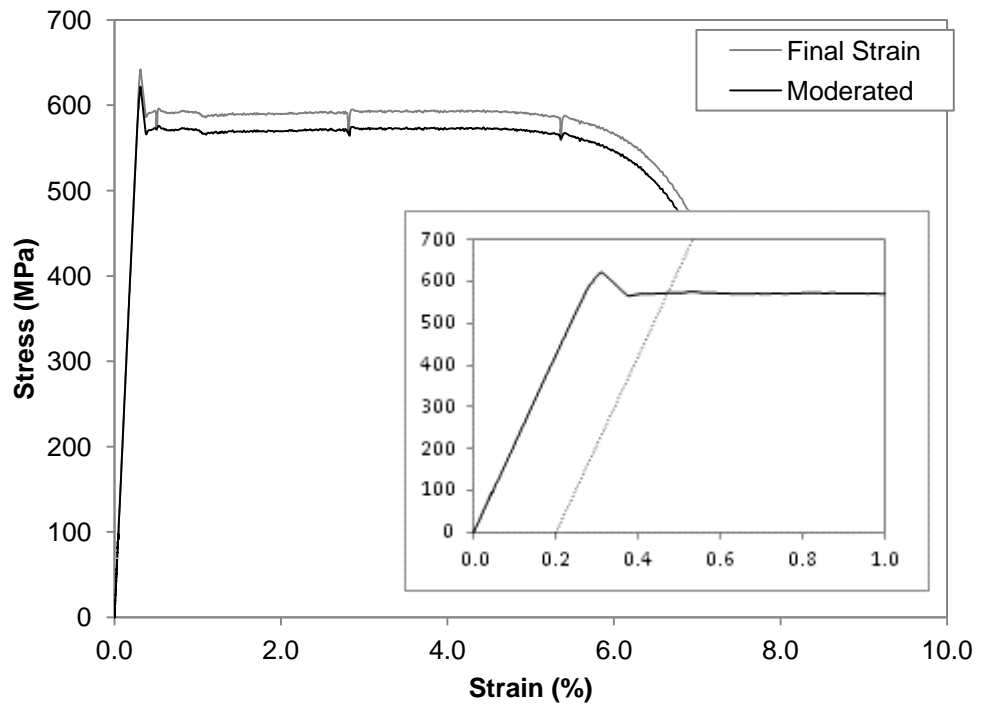


Figure A.5 Tensile Coupon Test Results of C90-3

B. Imperfection Results for C-channel

B.1 Stub Column

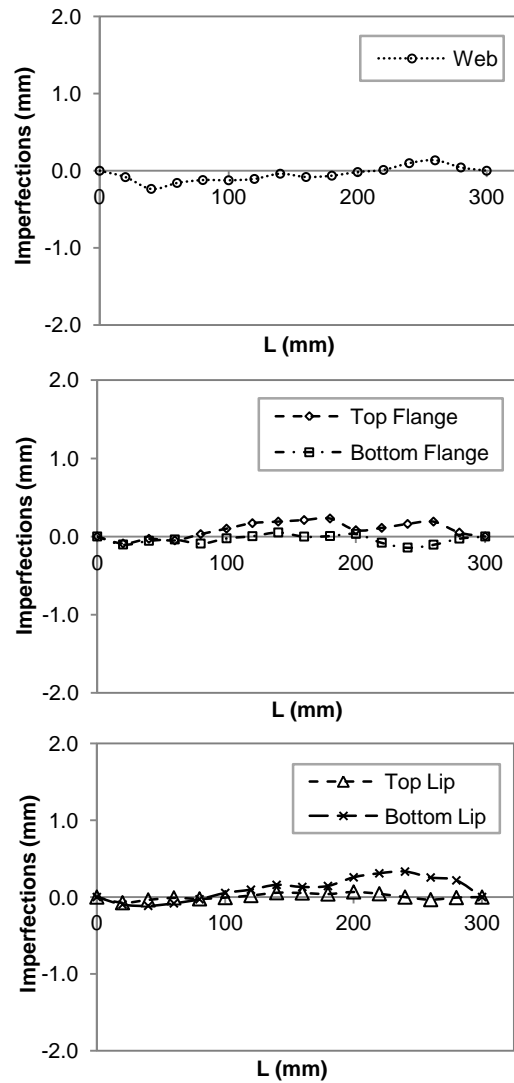


Figure B.1 Imperfection Results for C75L300-1

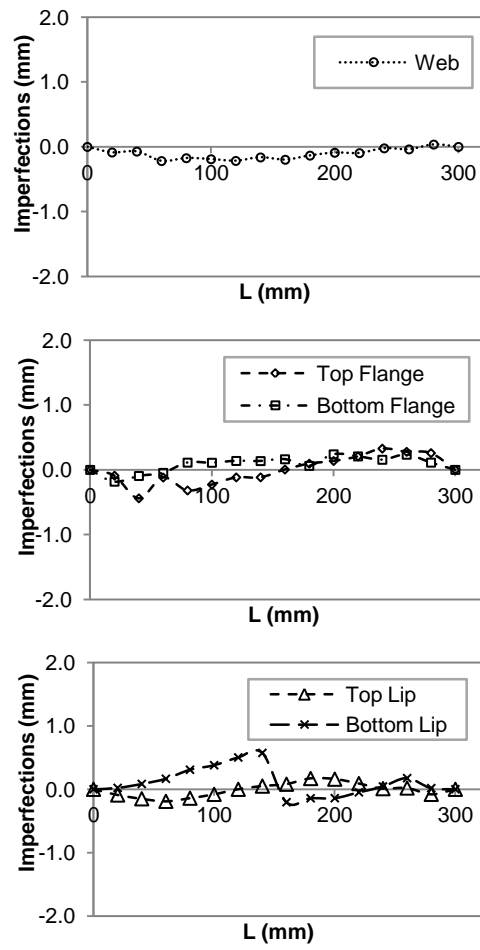


Figure B.2 Imperfection Results for C90L300-2

B.2 Short Column

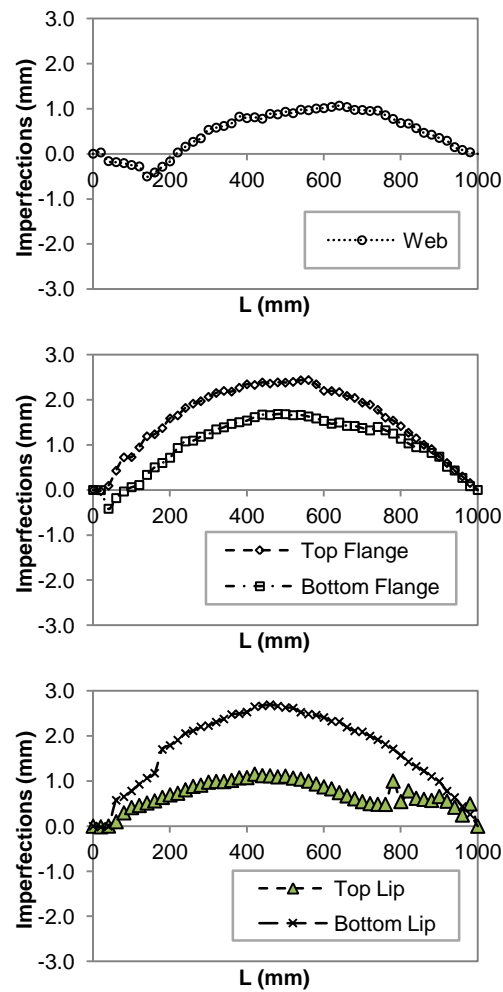


Figure B.3 Imperfection Results for C90L1000-1

B.3 Intermediate Column

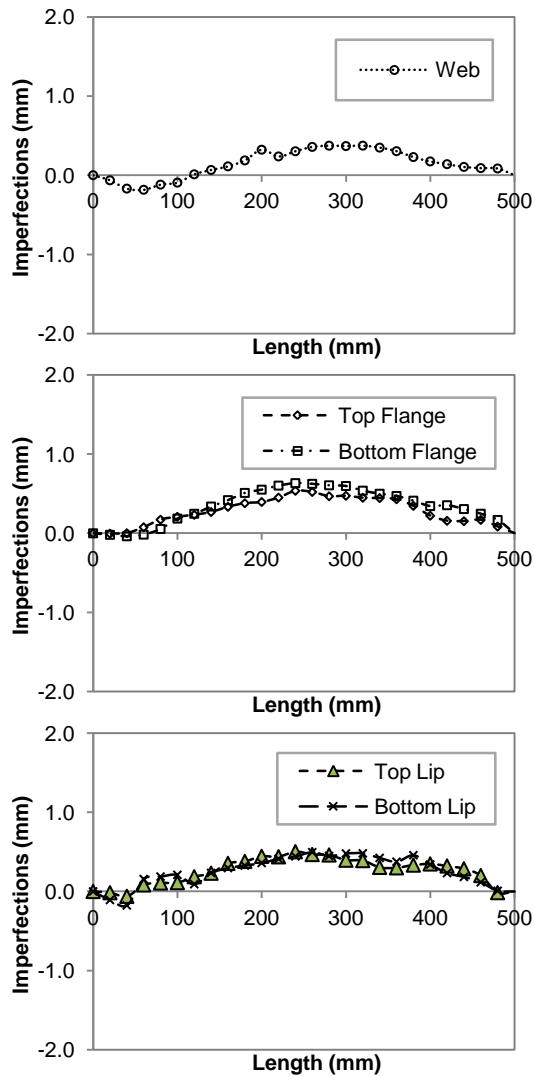


Figure B.4 Imperfection Results for C75L500-2

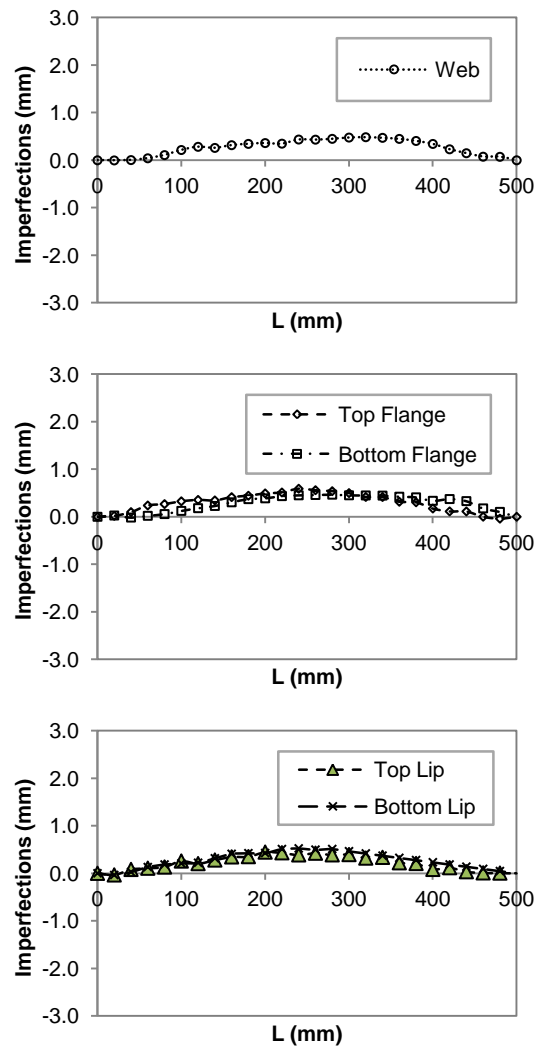


Figure B.5 Imperfection Results for C90L500-1

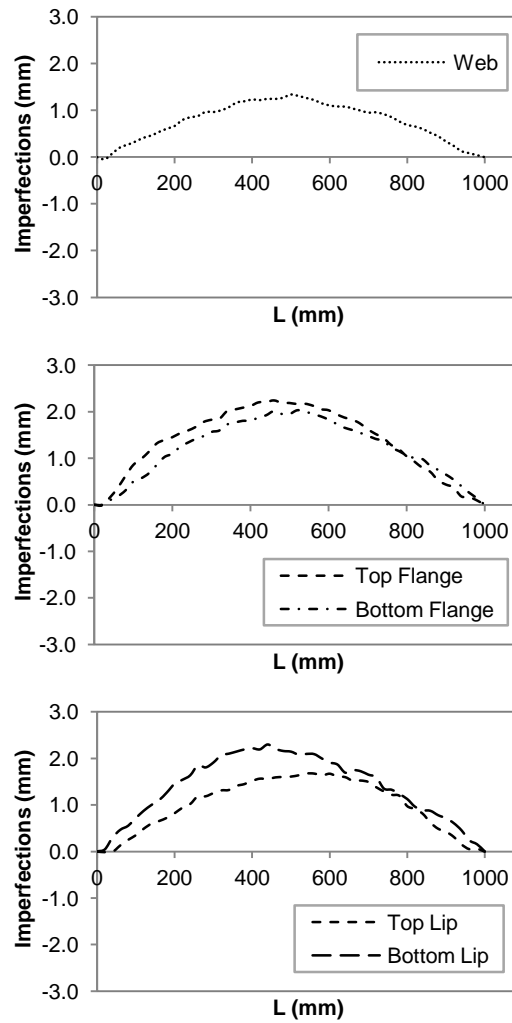


Figure B.6 Imperfection Results for C75L1000-1

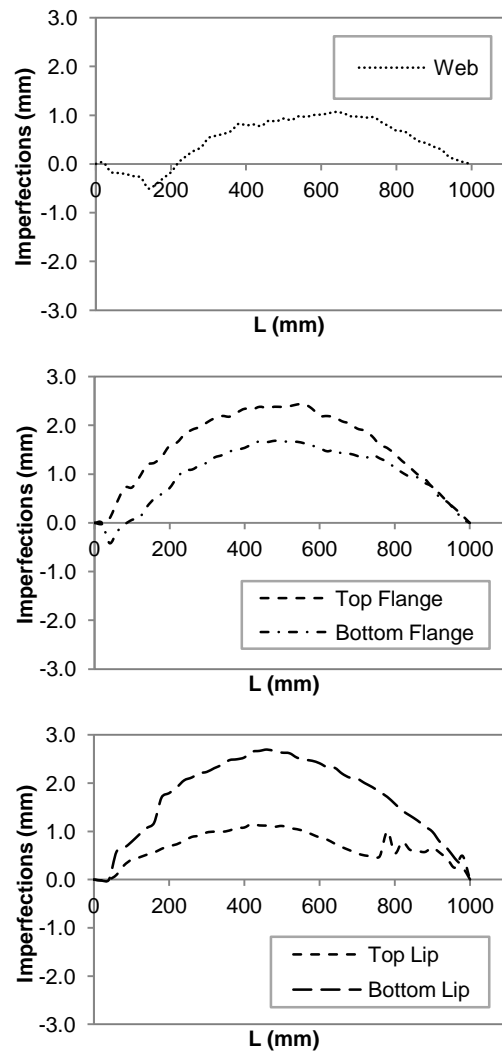


Figure B.7 Imperfection Results for C90L1000-1

B.4 Slender Column

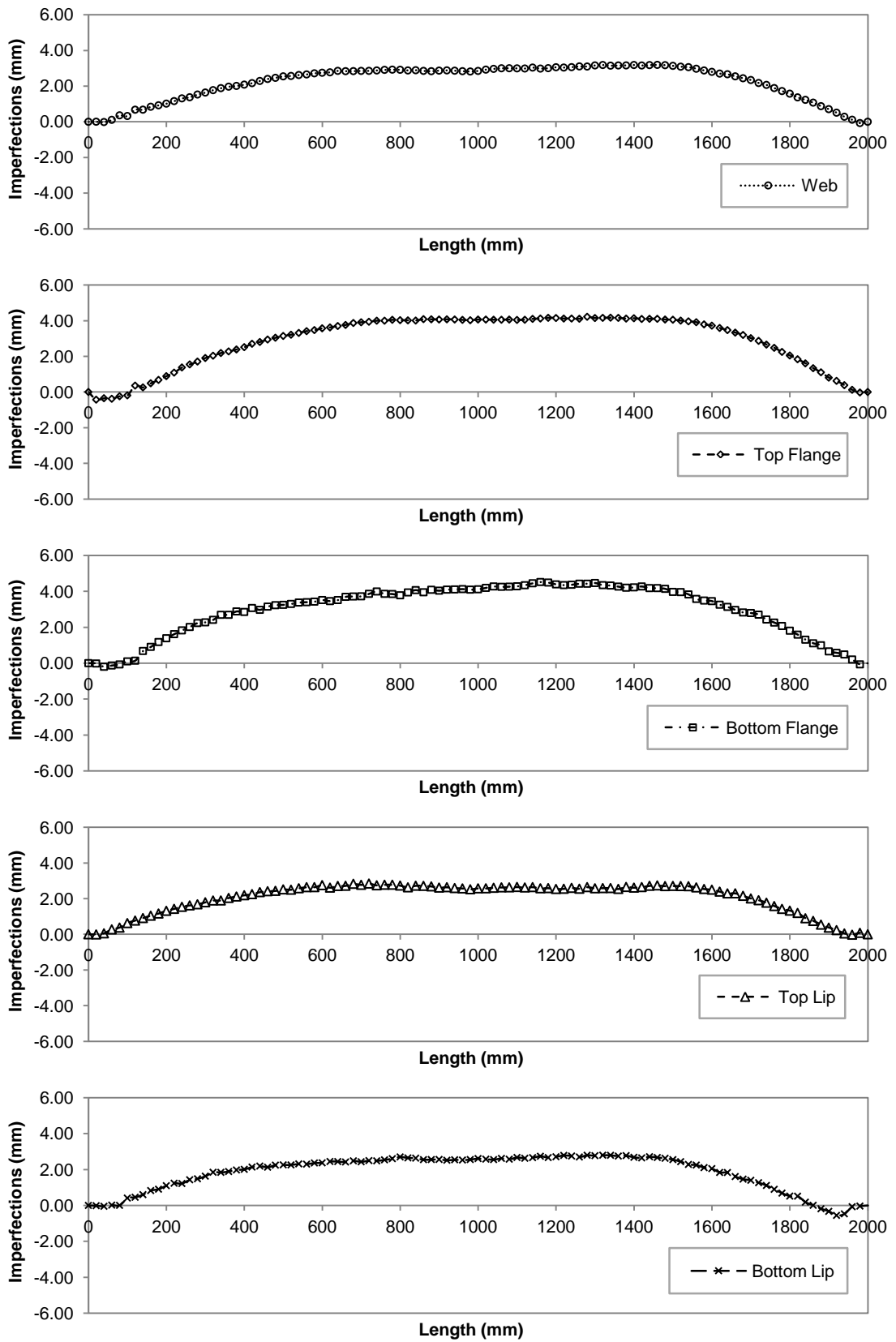


Figure B.8 Imperfection Results for C75L2000-1

C. Imperfection Results for Plain Built-up Back-to-back C-channels

C.1 Stub Column

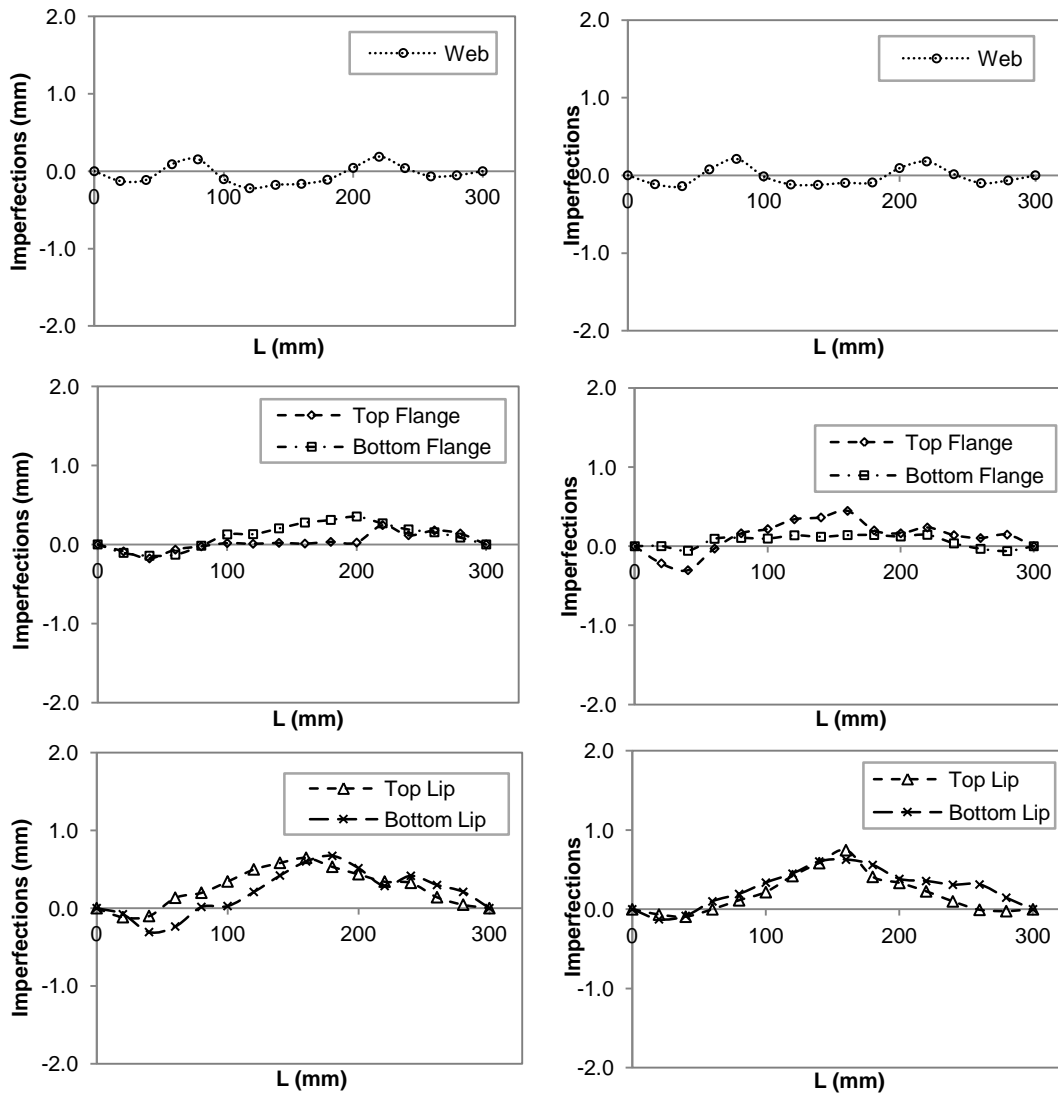


Figure C.1 Imperfection Results for BU75S50L300-1

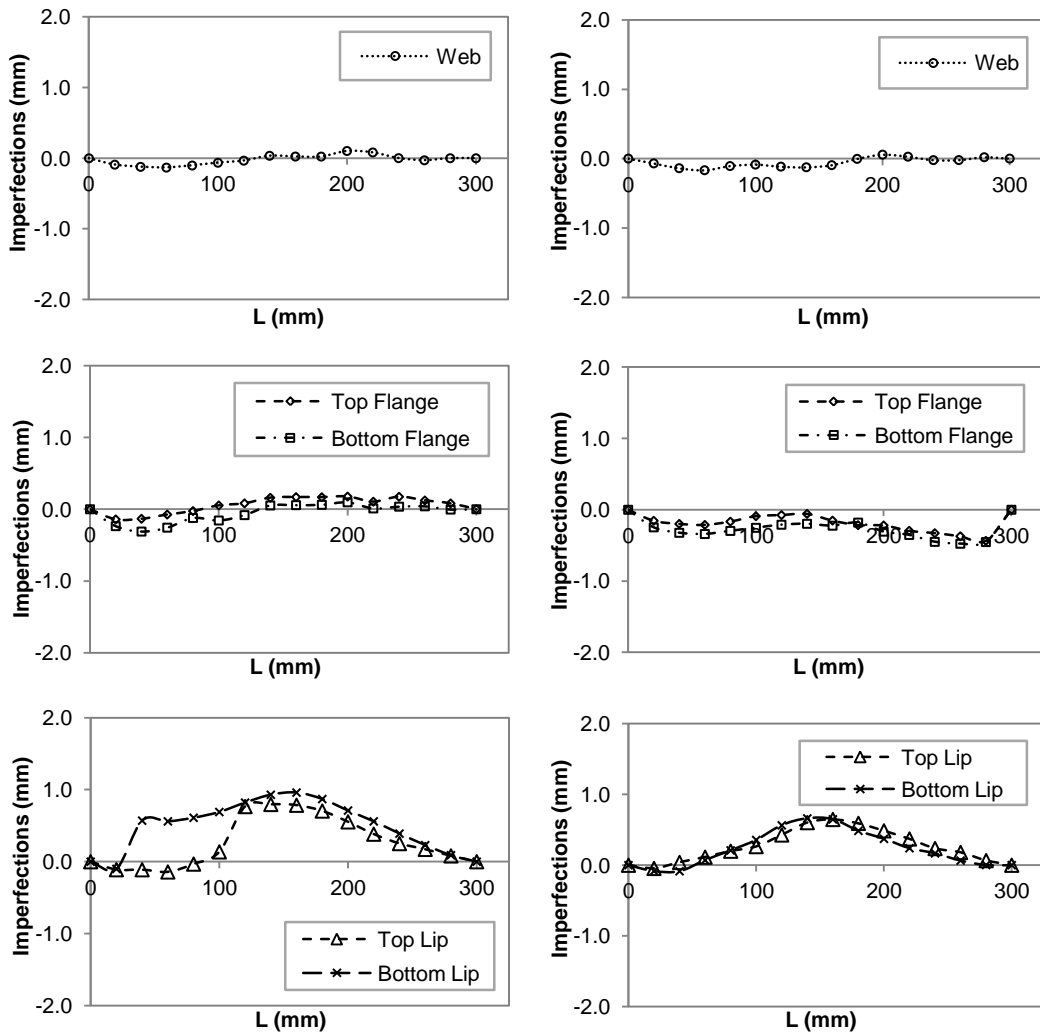


Figure C.2 Imperfection Results for BU75S100L300-2

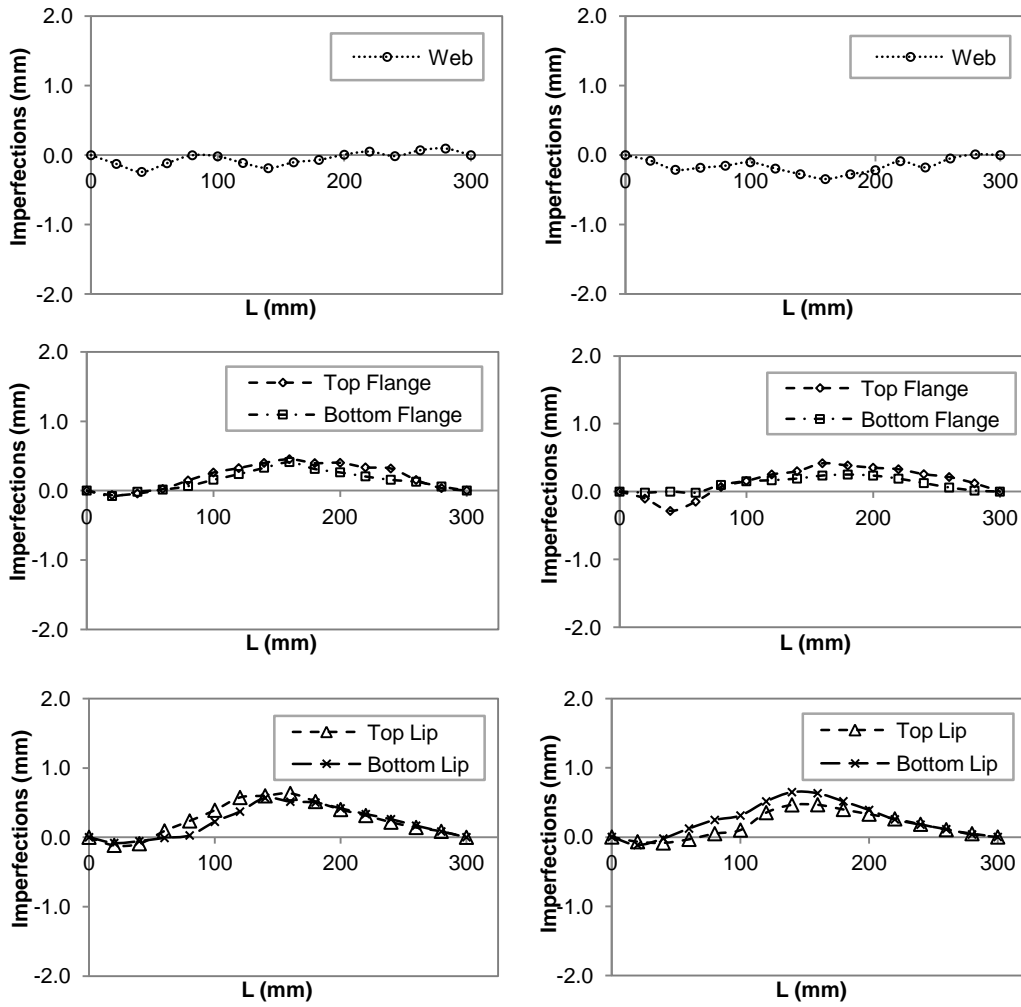


Figure C.3 Imperfection Results for BU75S200L300-1

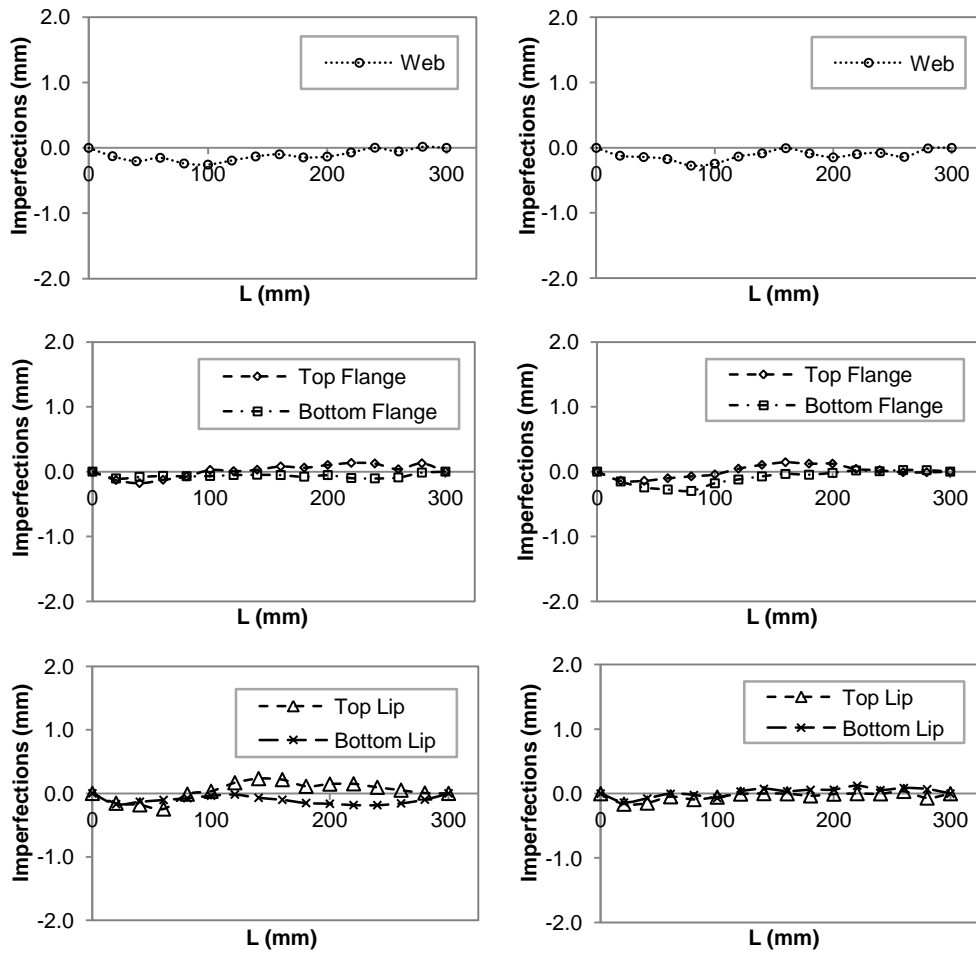


Figure C.4 Imperfection Results for BU90S50L300-1

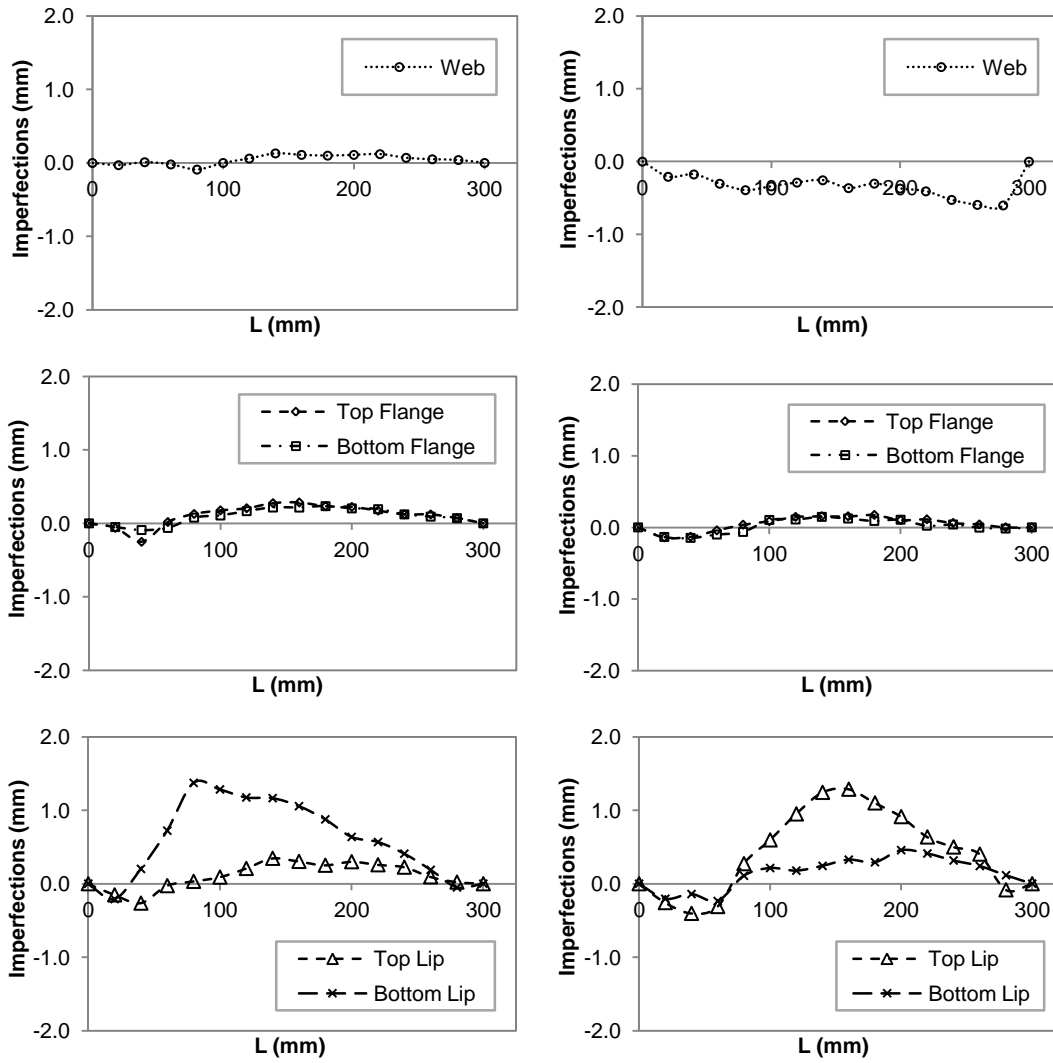


Figure C.5 Imperfection Results for BU90S100L300-3

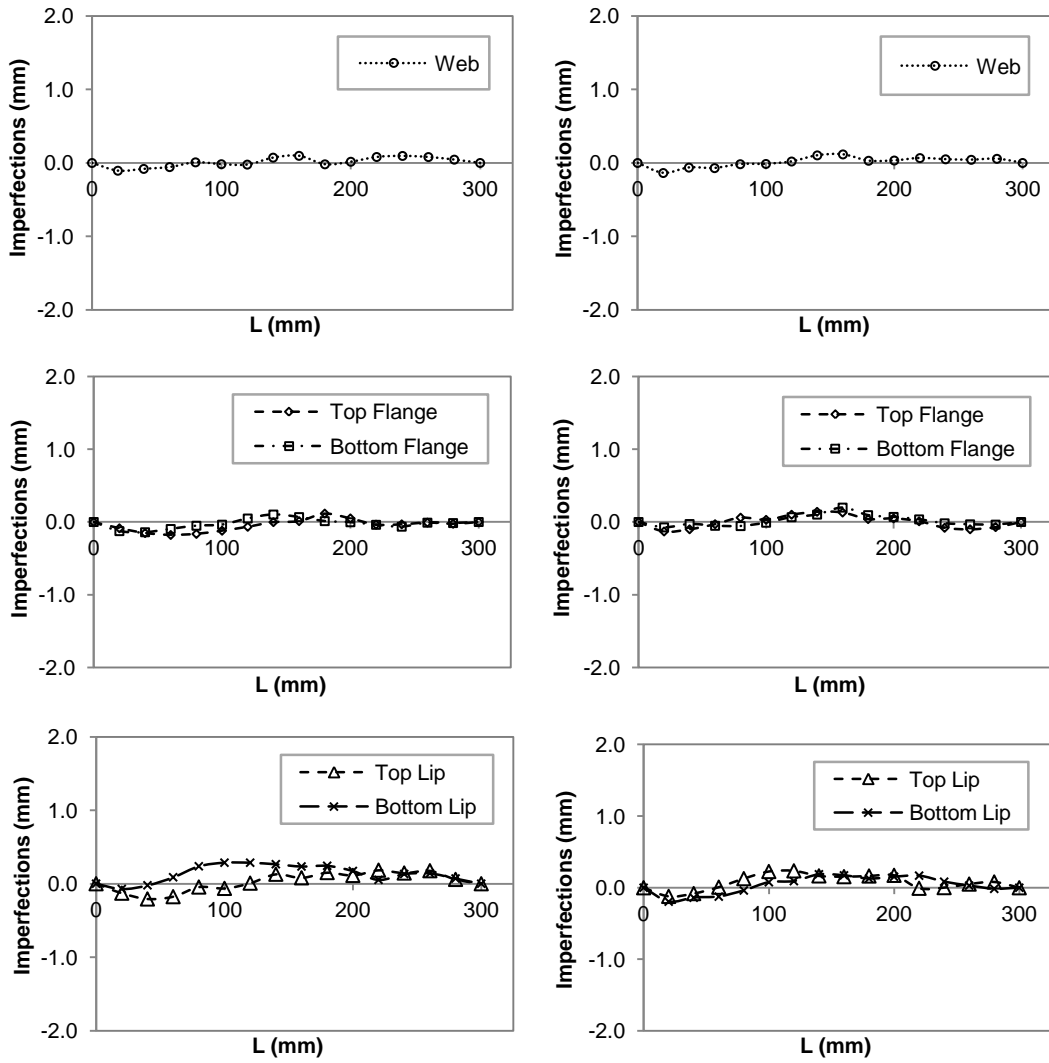


Figure C.6 Imperfection Results for BU90S200L300-1

C.2 Short Column

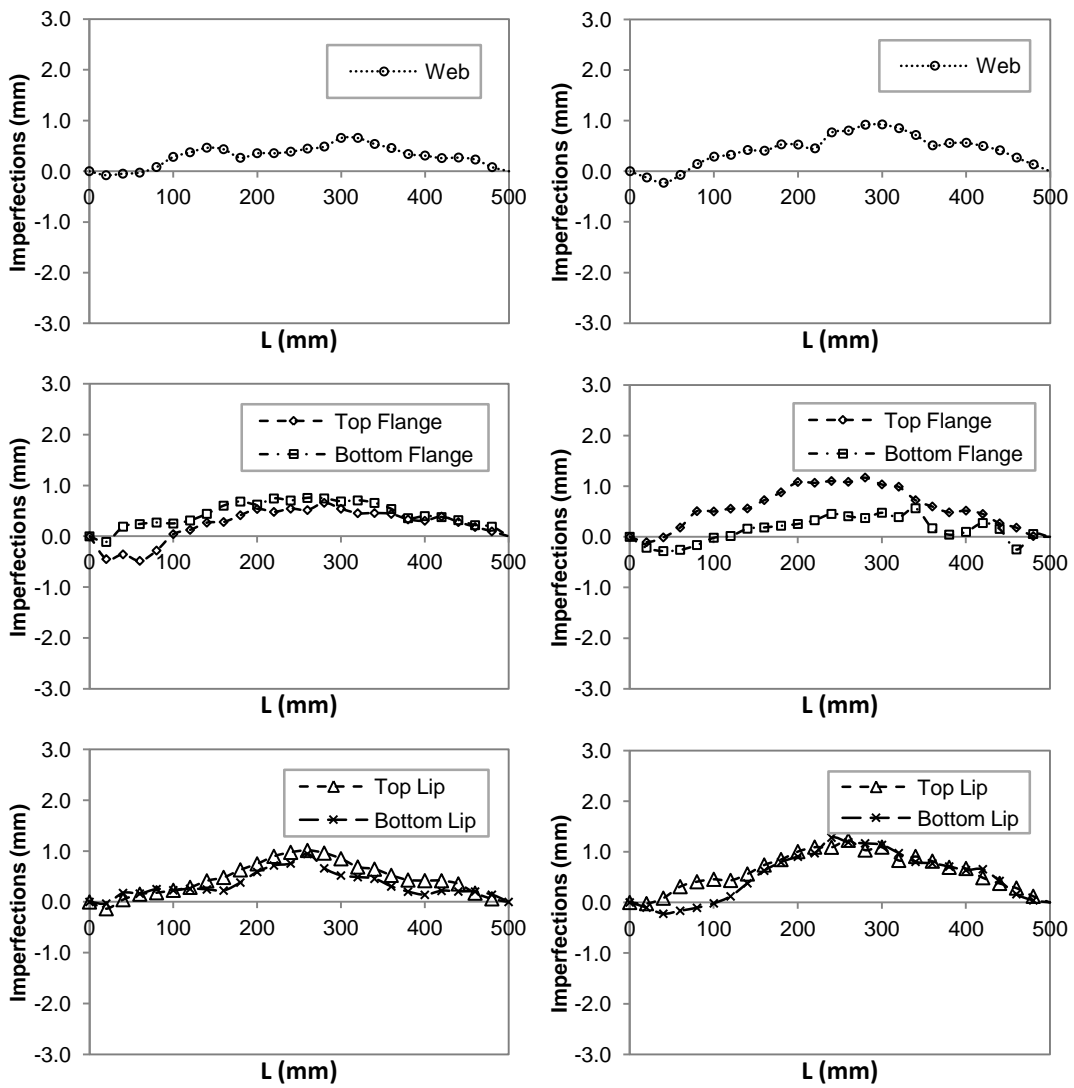


Figure C.7 Imperfection Results for BU75S100L500-1

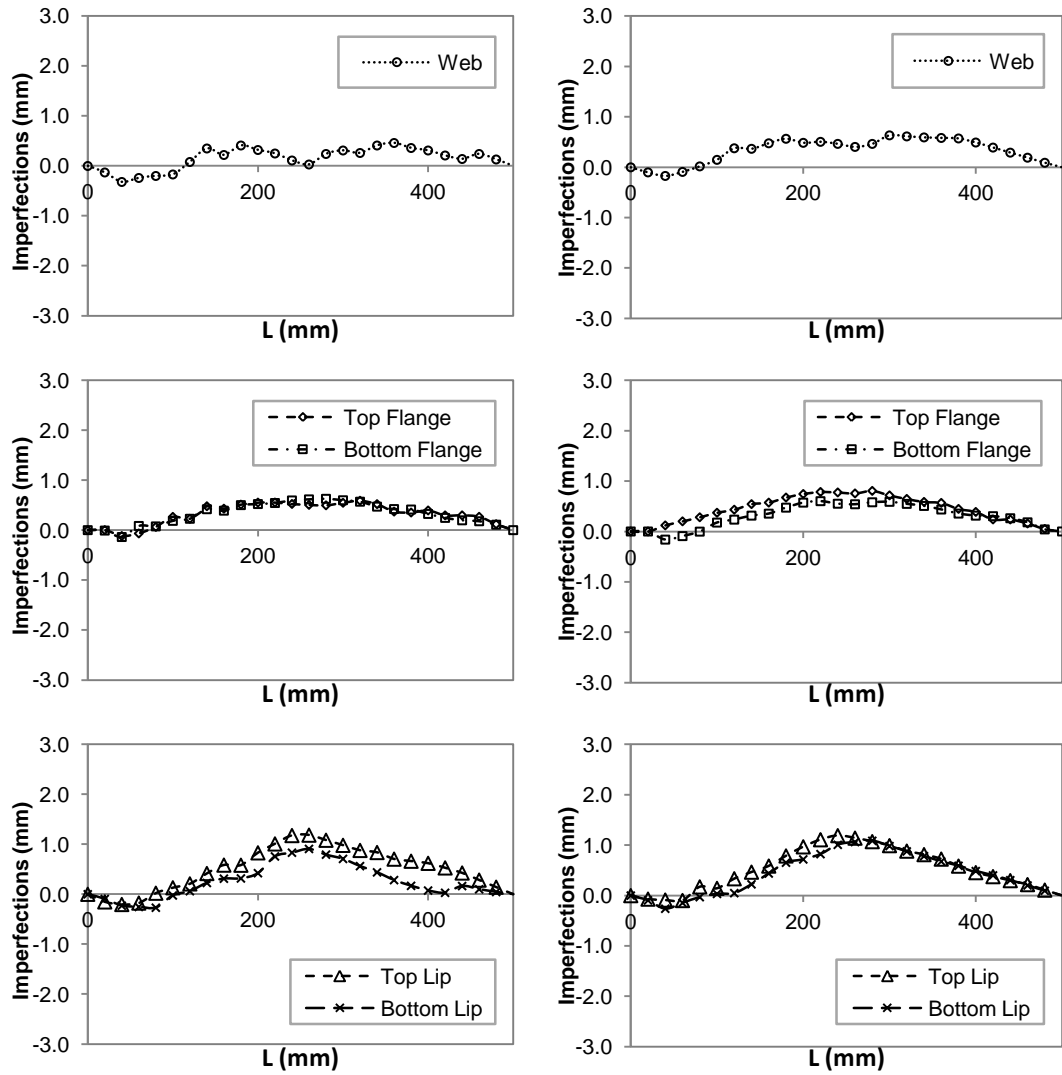


Figure C.8 Imperfection Results for BU75S200L500-1

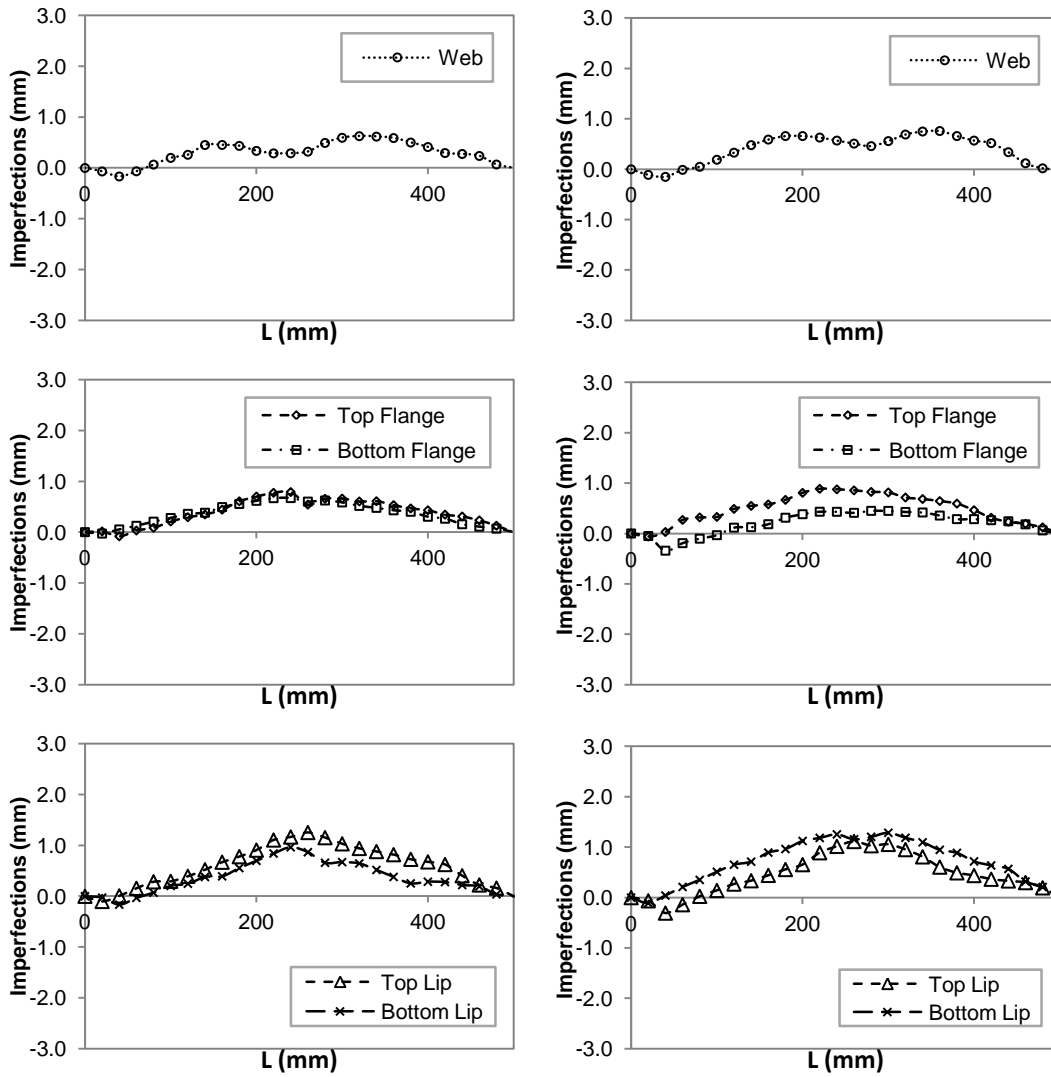


Figure C.9 Imperfection Results for BU75S400L500-1

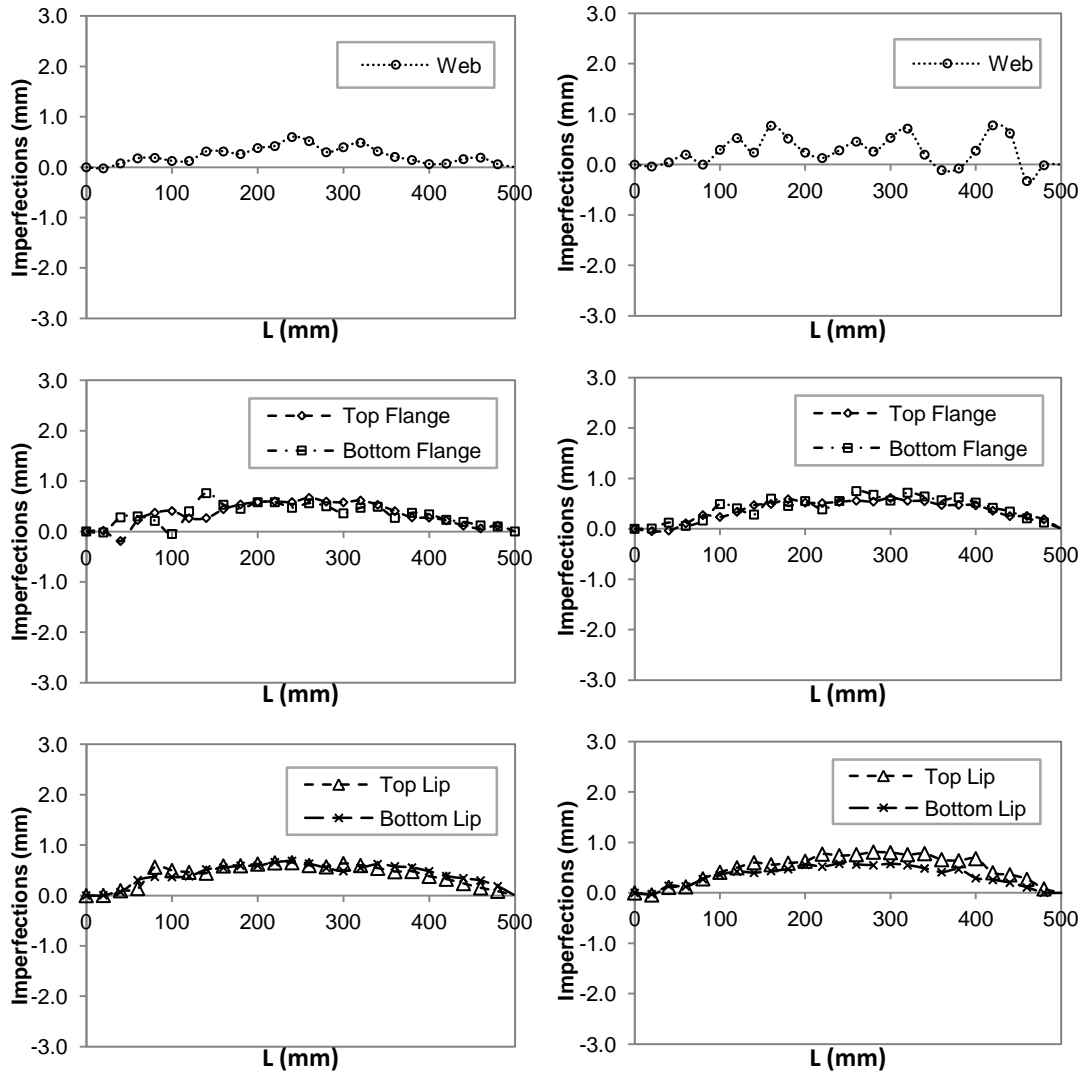


Figure C.10 Imperfection Results for BU90S100L500-1

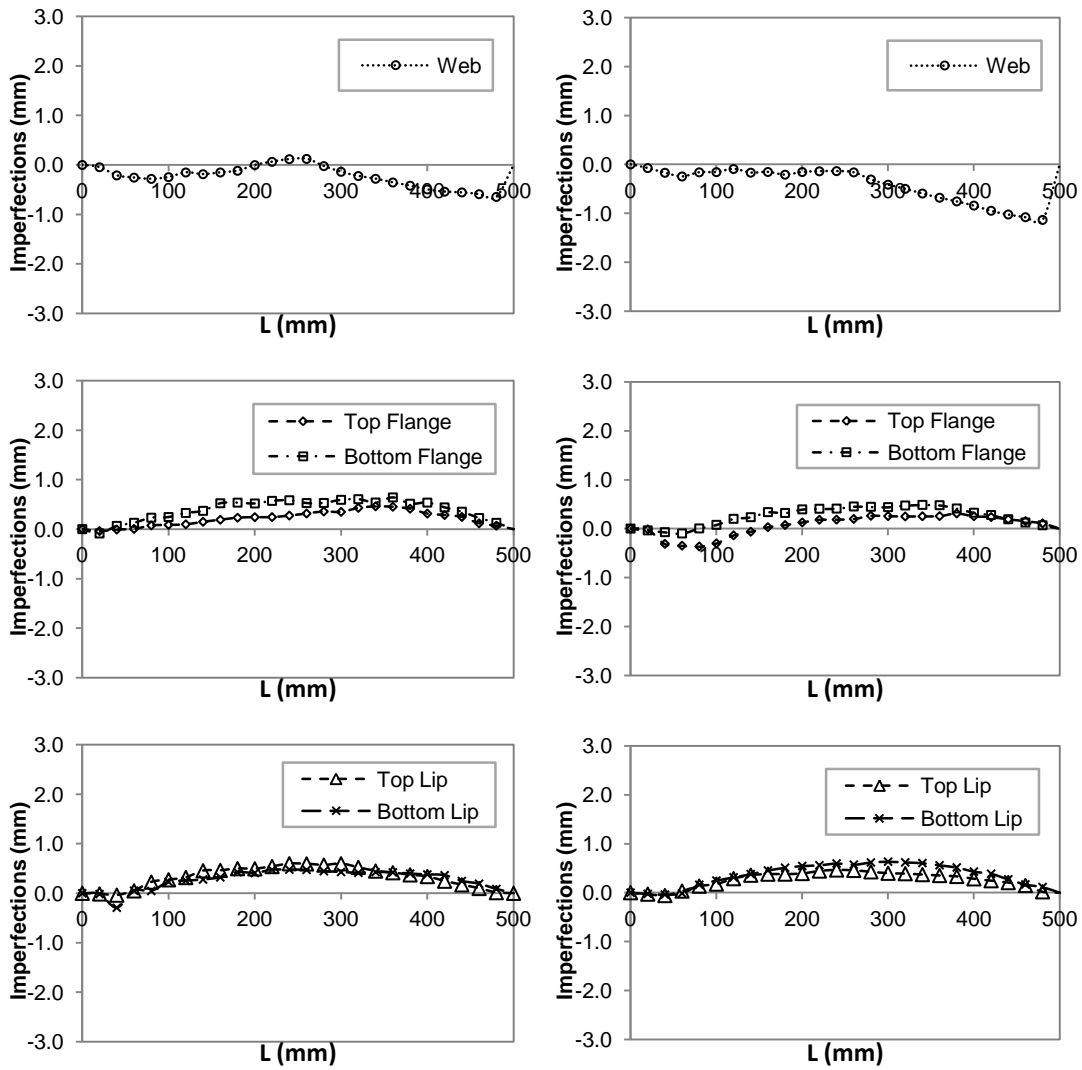


Figure C.11 Imperfection Results for BU90S200L500-1

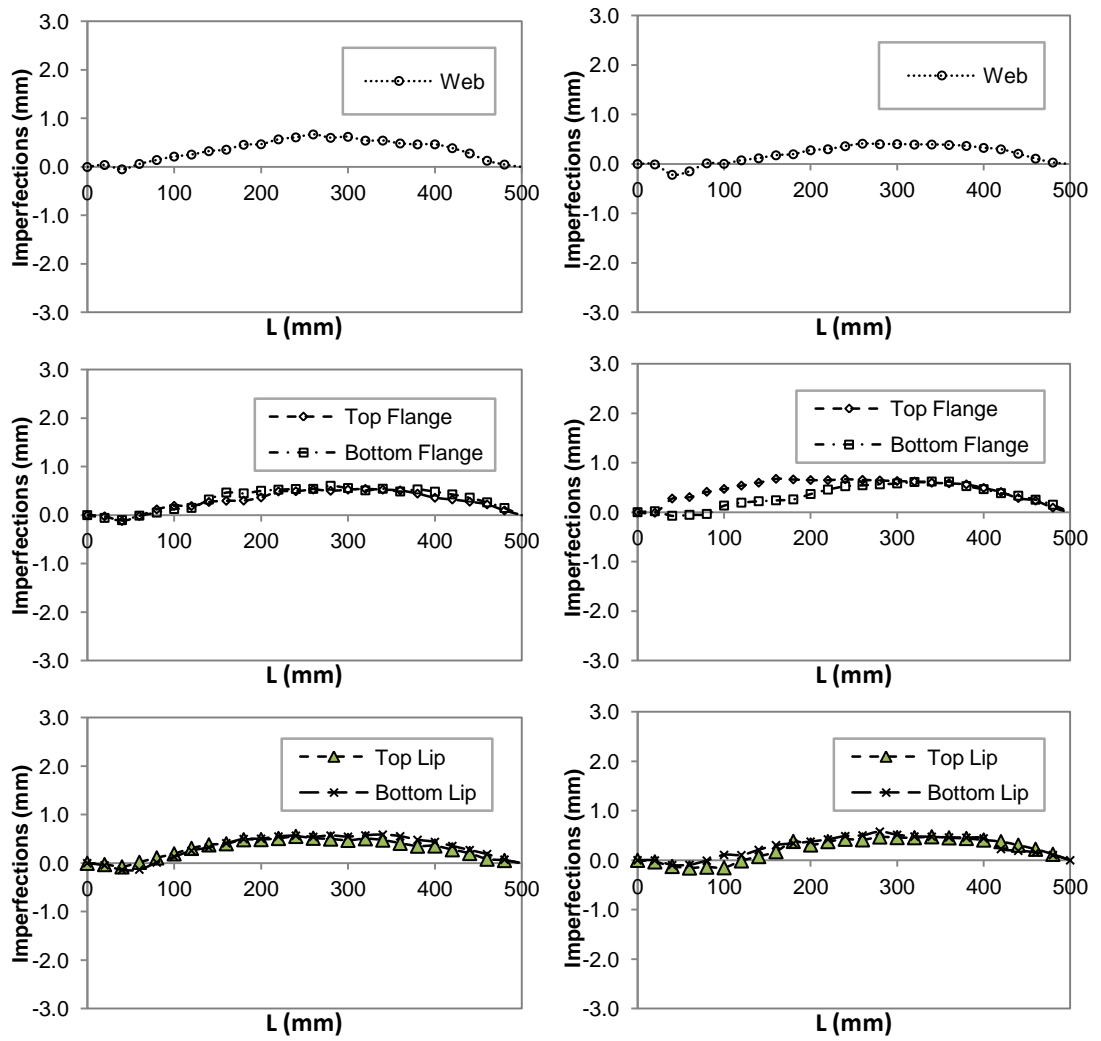


Figure C.12 Imperfection Results for BU90S400L500-1

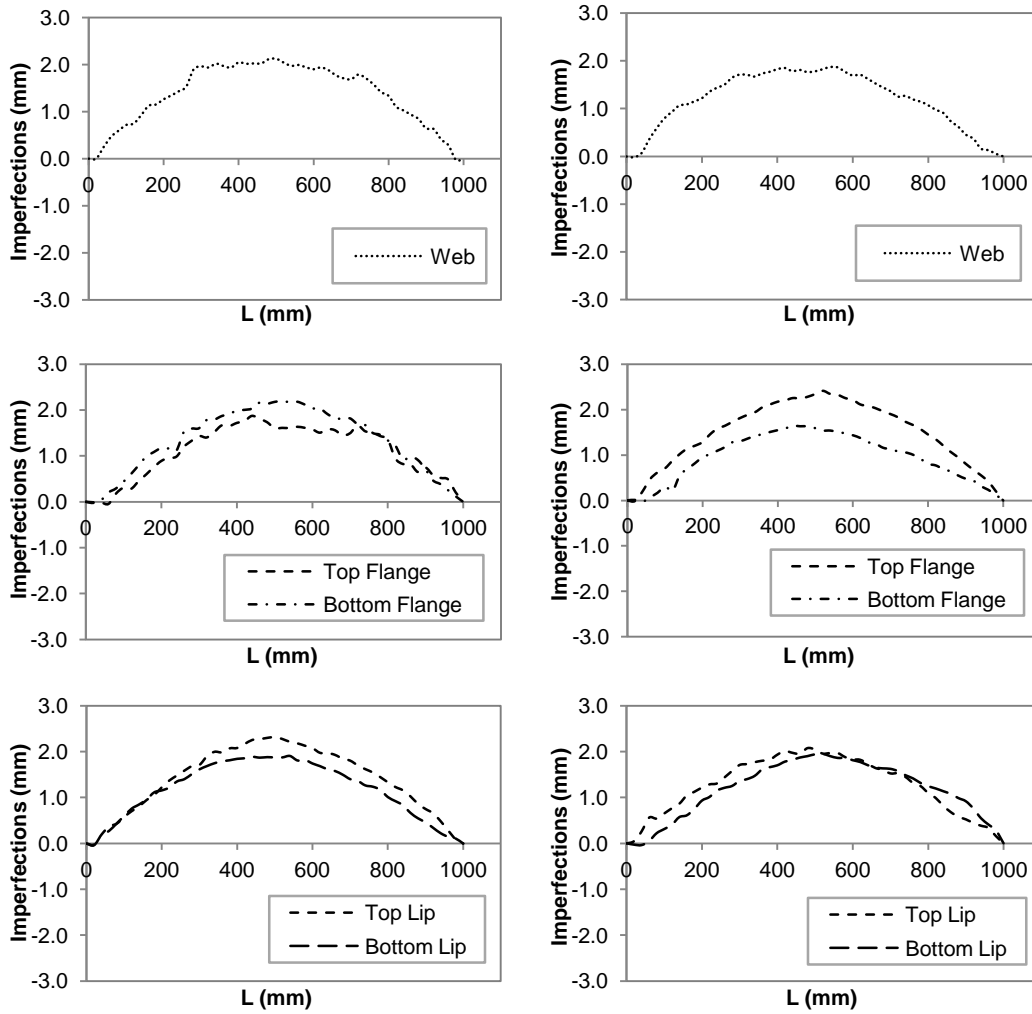


Figure C.13 Imperfection Results for BU90S225L1000-1

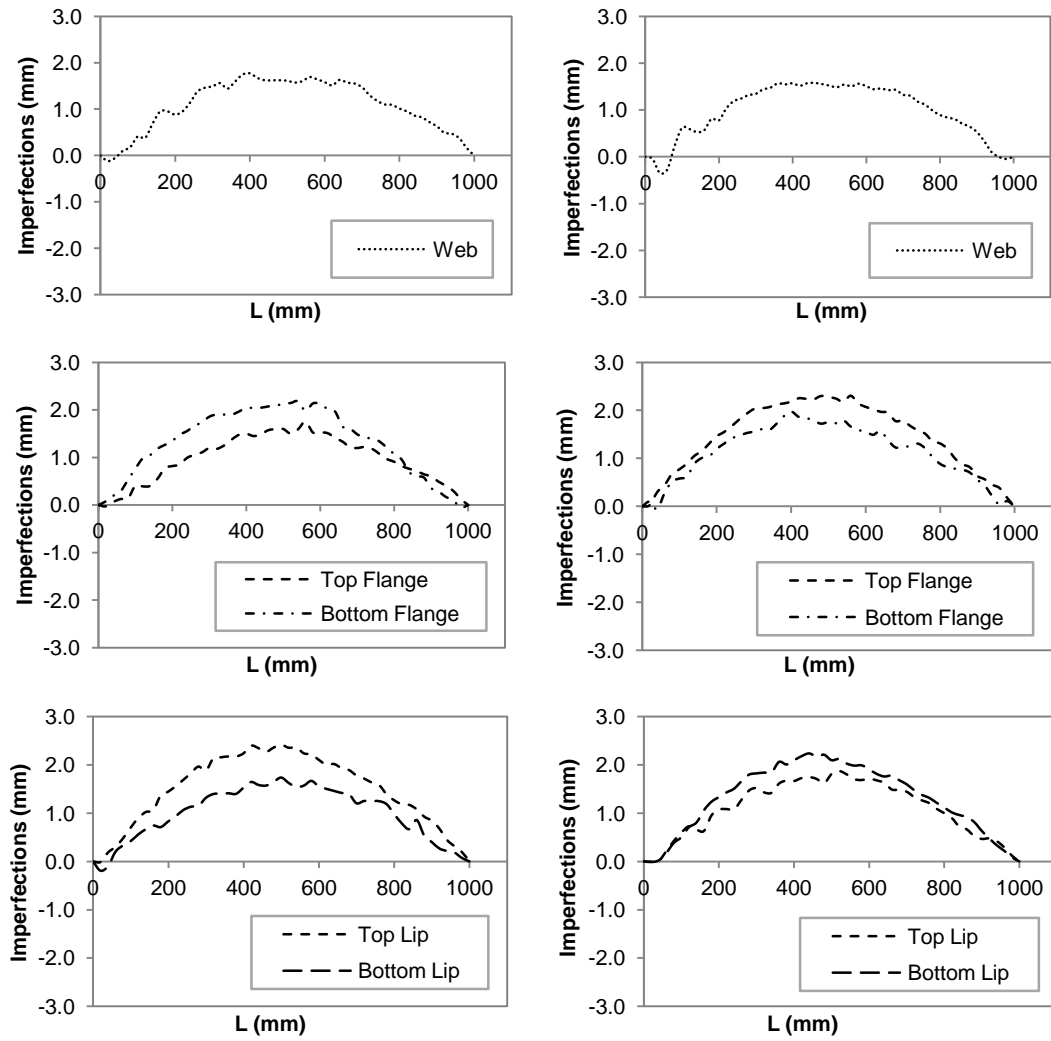


Figure C.14 Imperfection Results for BU90S450L1000-2

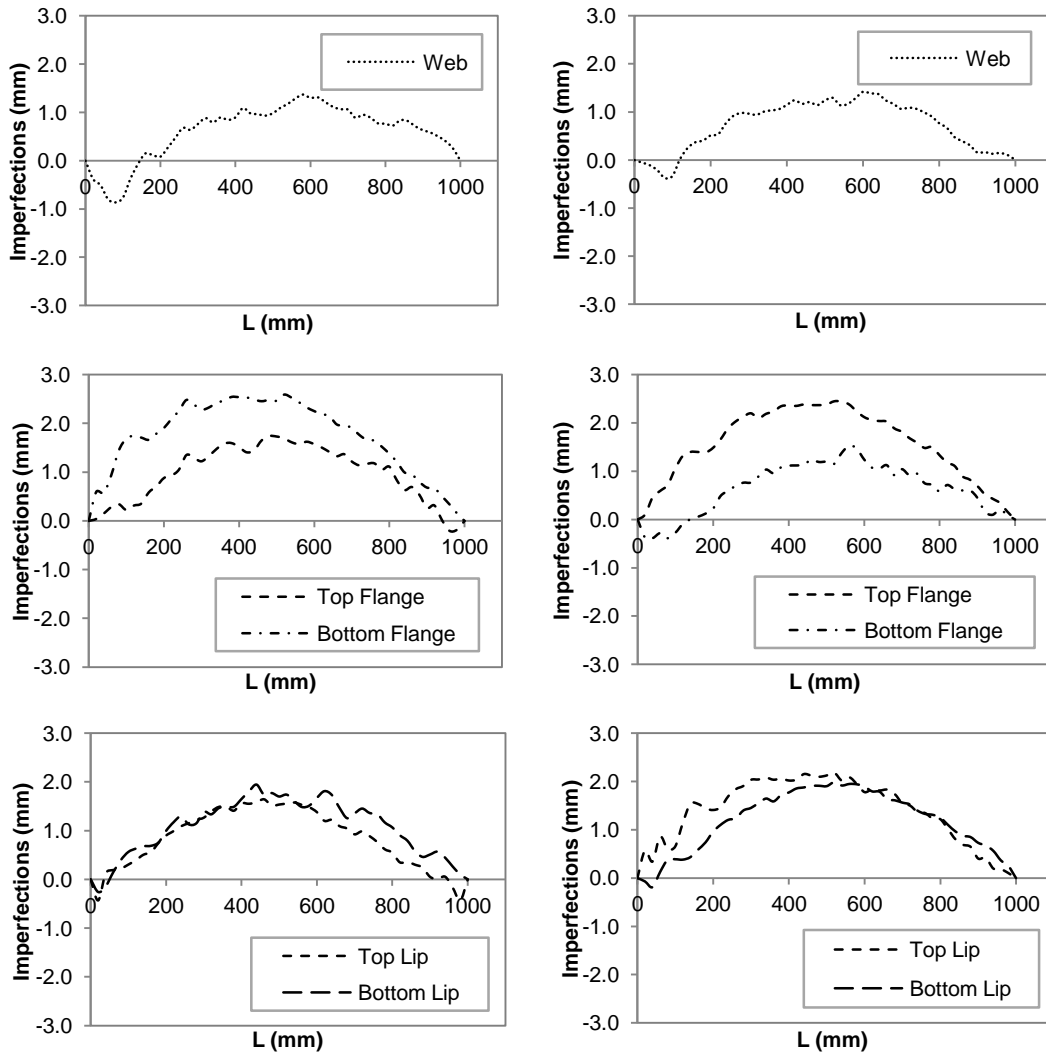


Figure C.15 Imperfection Results for BU90S900L1000-1

C.3 Intermediate Column

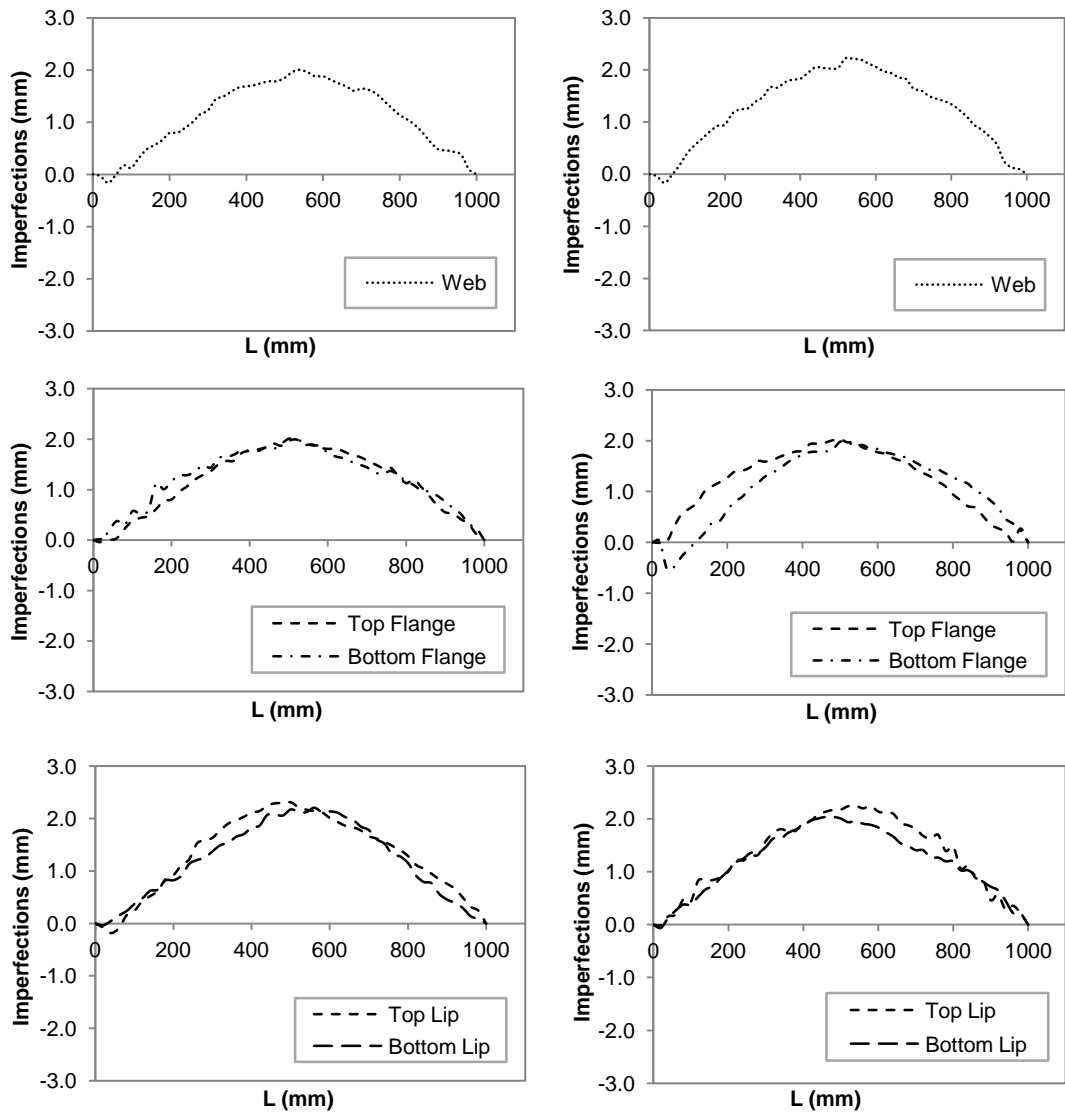


Figure C.16 Imperfection Results for BU75S225L1000-1

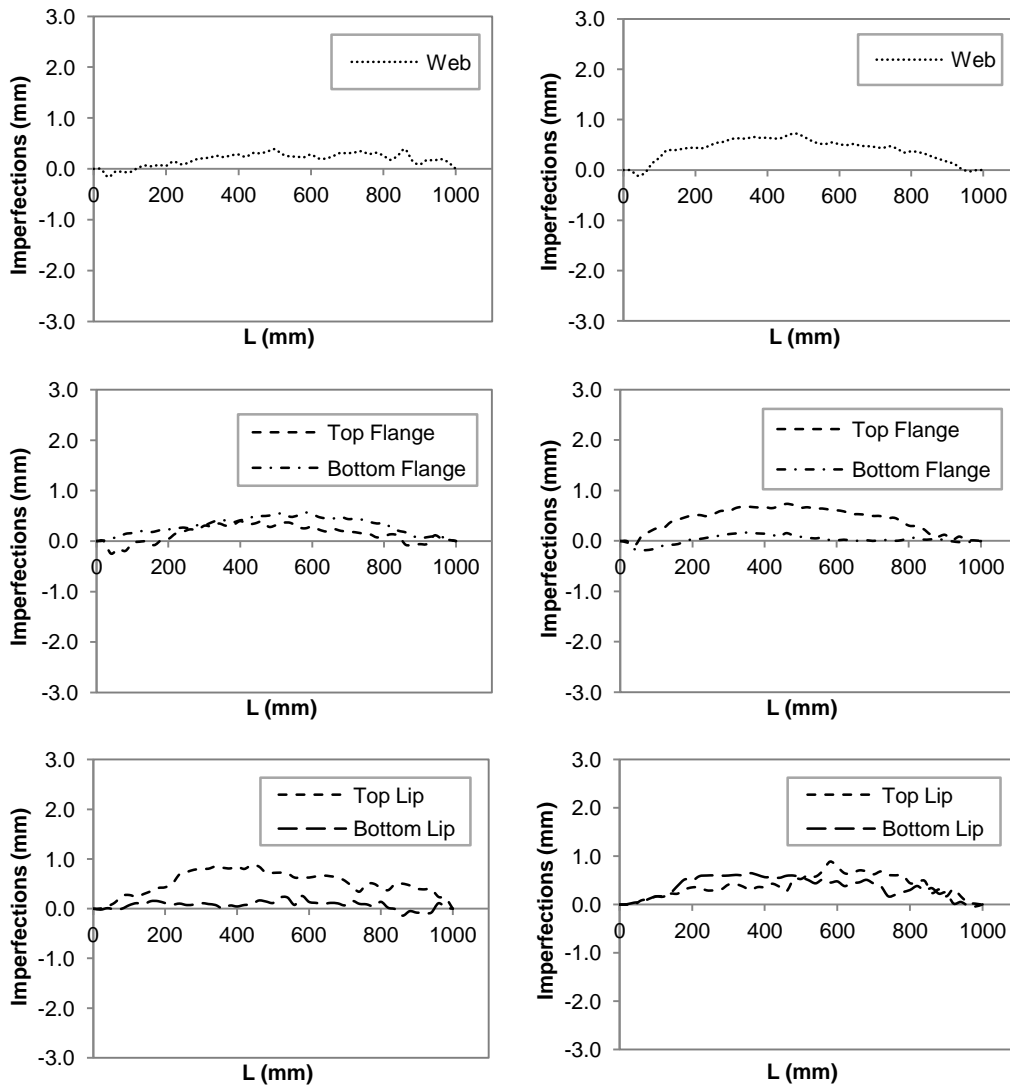


Figure C.17 Imperfection Results for BU75S450L1000-1

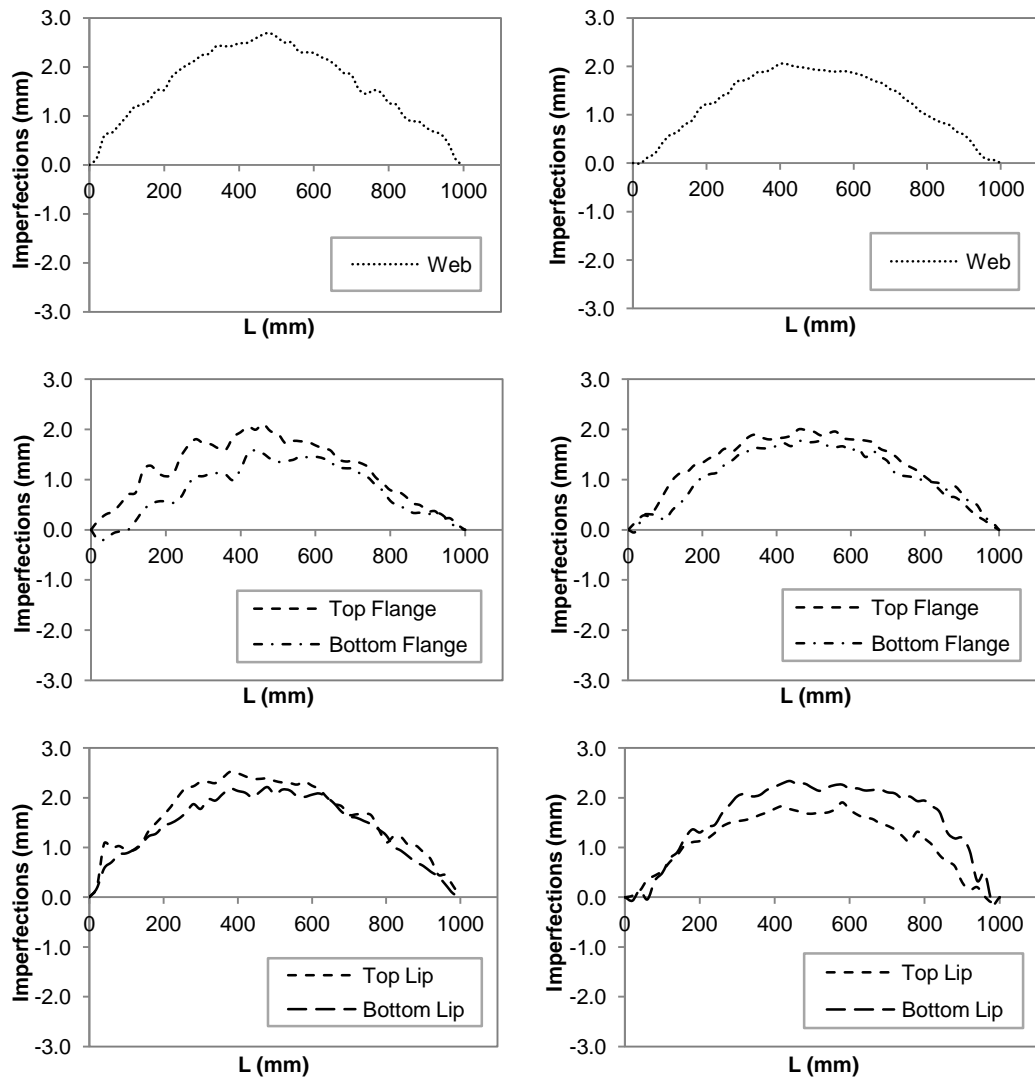


Figure C.18 Imperfection Results for BU75S900L1000-1

C.4 Slender Column

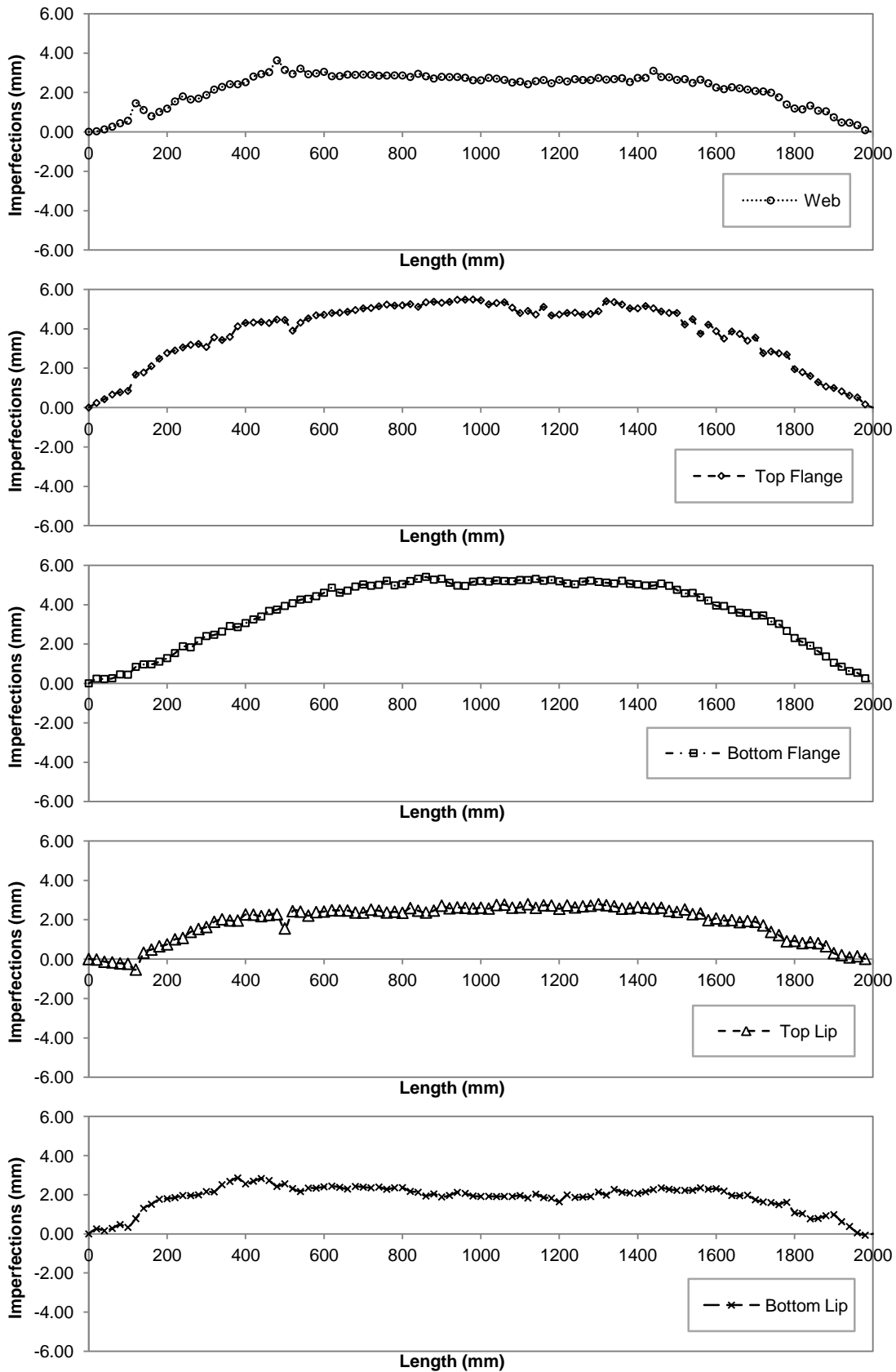


Figure C.19 Imperfection Results for BU75S475L2000-2 (Left)

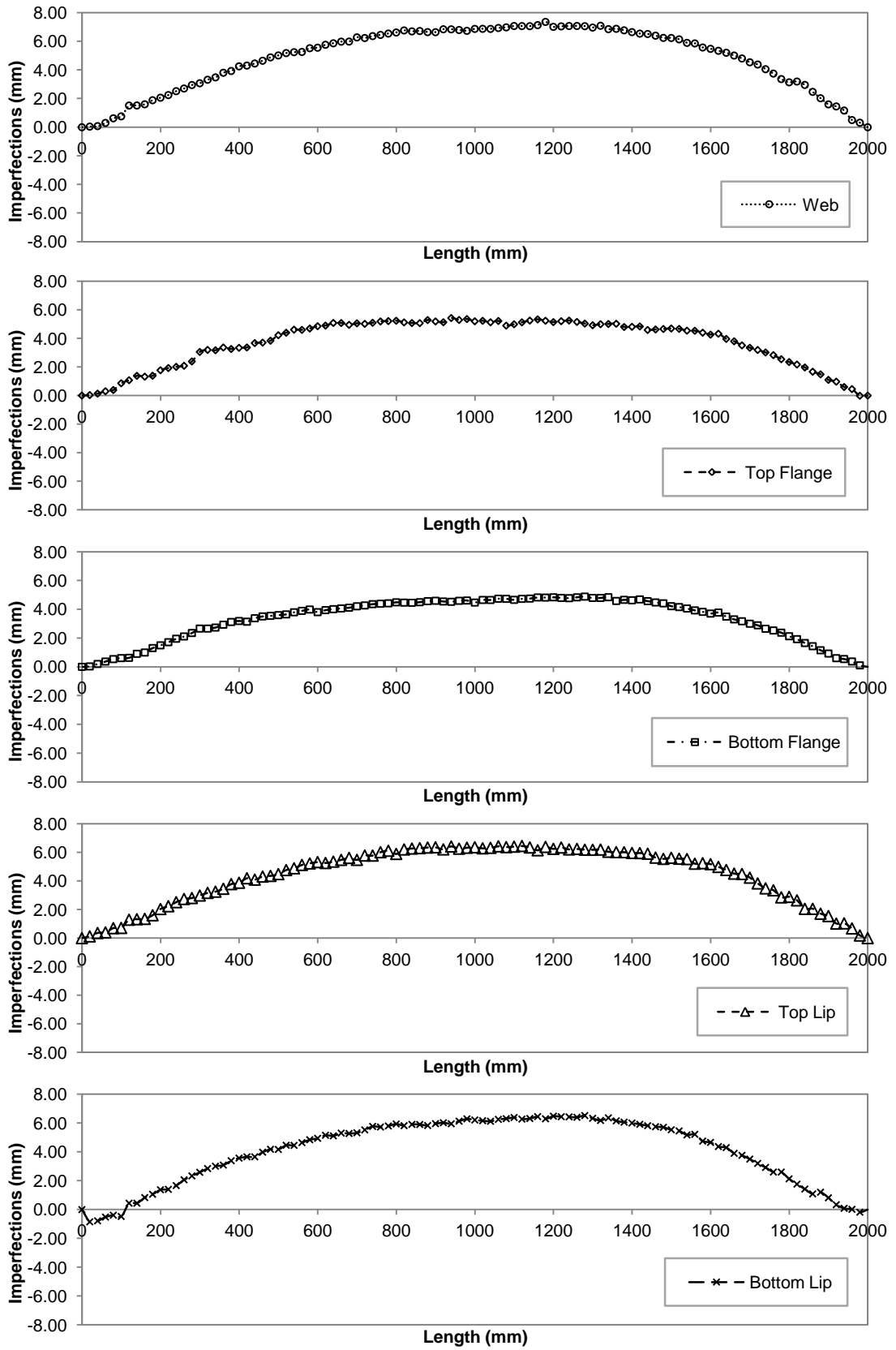


Figure C.20 Imperfection Results for BU75S475L2000-2 (Right)

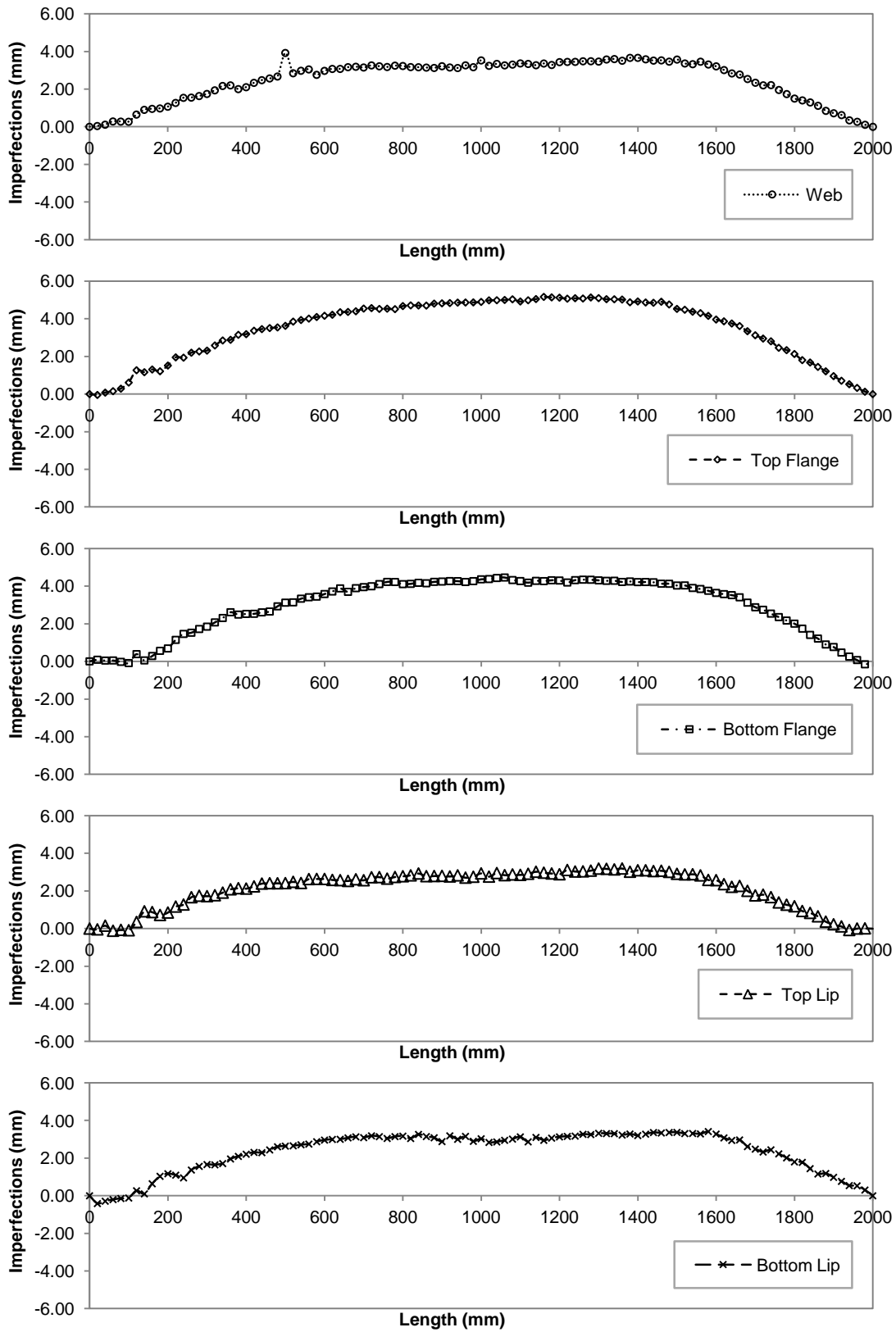


Figure C.21 Imperfection Results for BU75S950L2000-2 (Left)

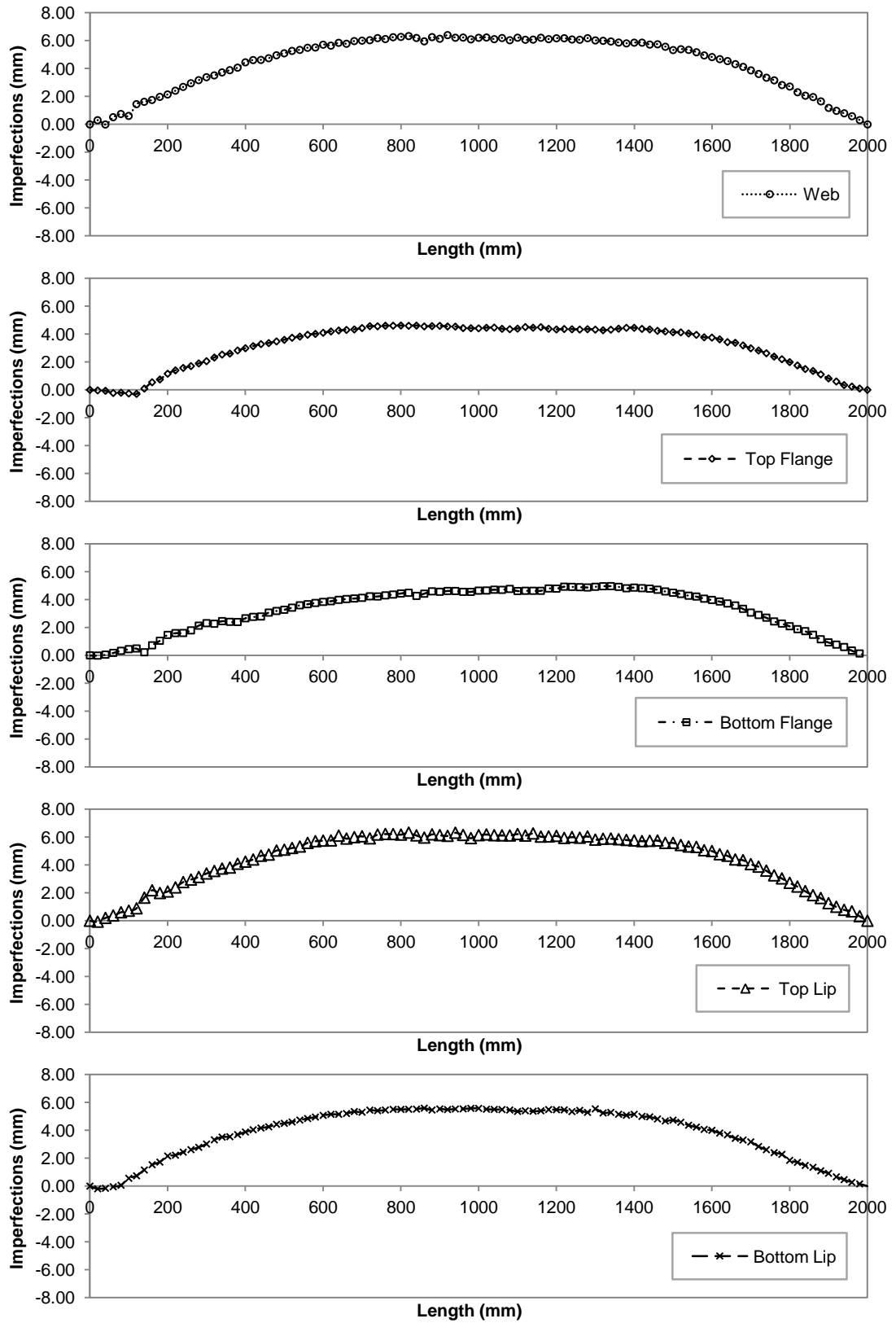


Figure C.22 Imperfection Results for BU75S950L2000-2 (Right)

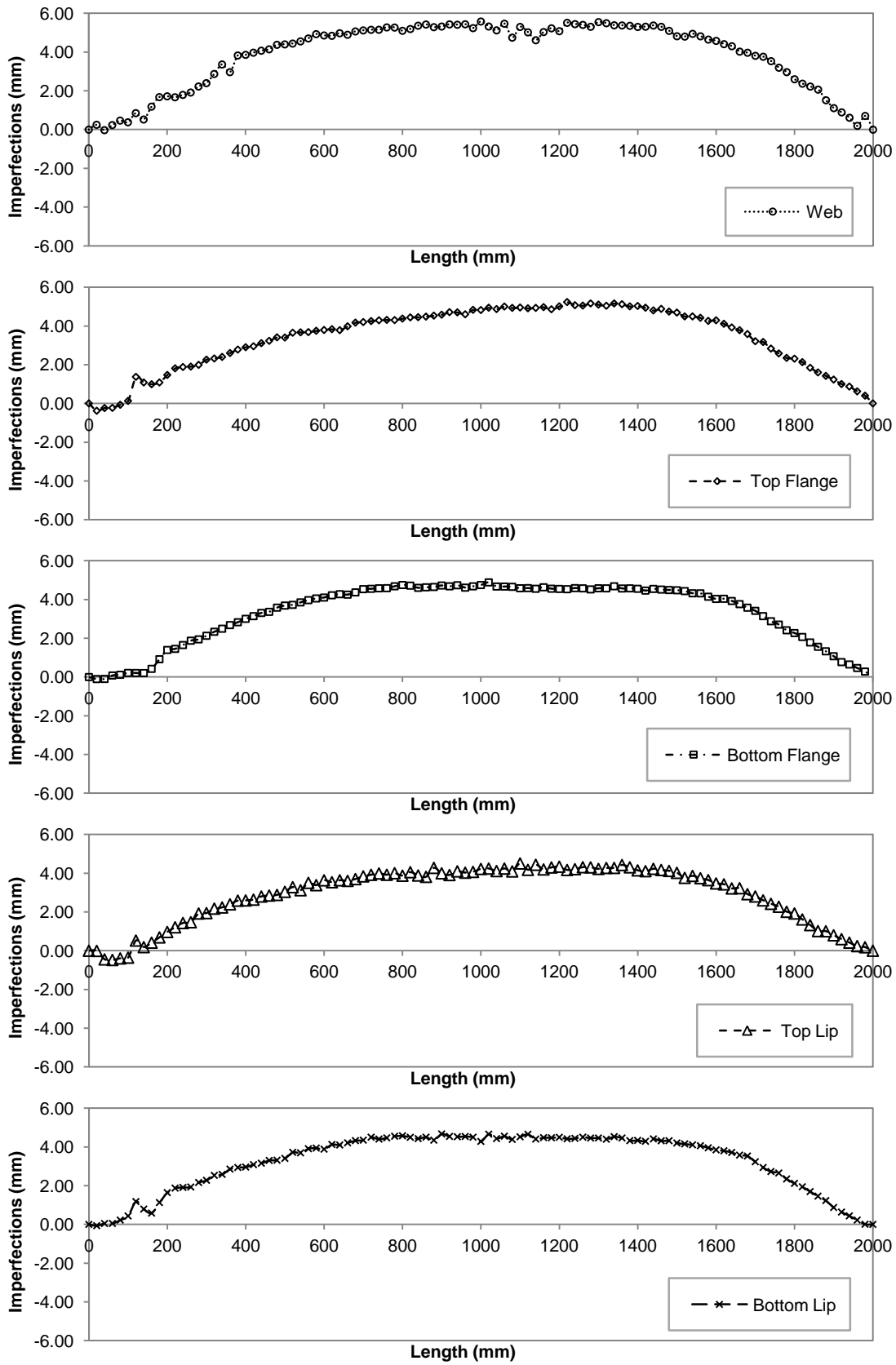


Figure C.23 Imperfection Results for BU75S1900L2000-2 (Left)

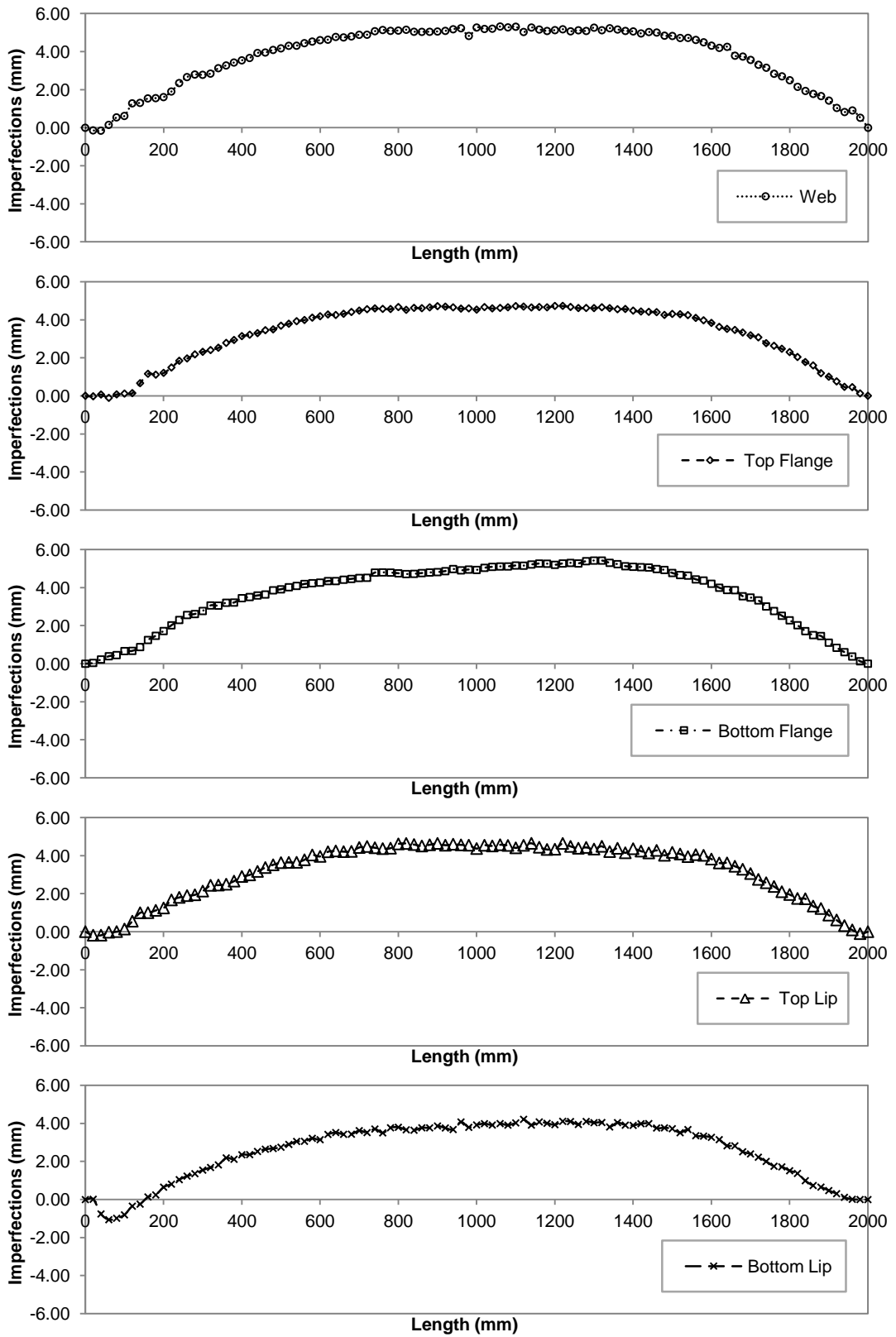


Figure C.24 Imperfection Results for BU75S1900L2000-2 (Right)

D. Imperfection Results Gapped Built-up Back-to-back C-channels

D.1 Stub Column

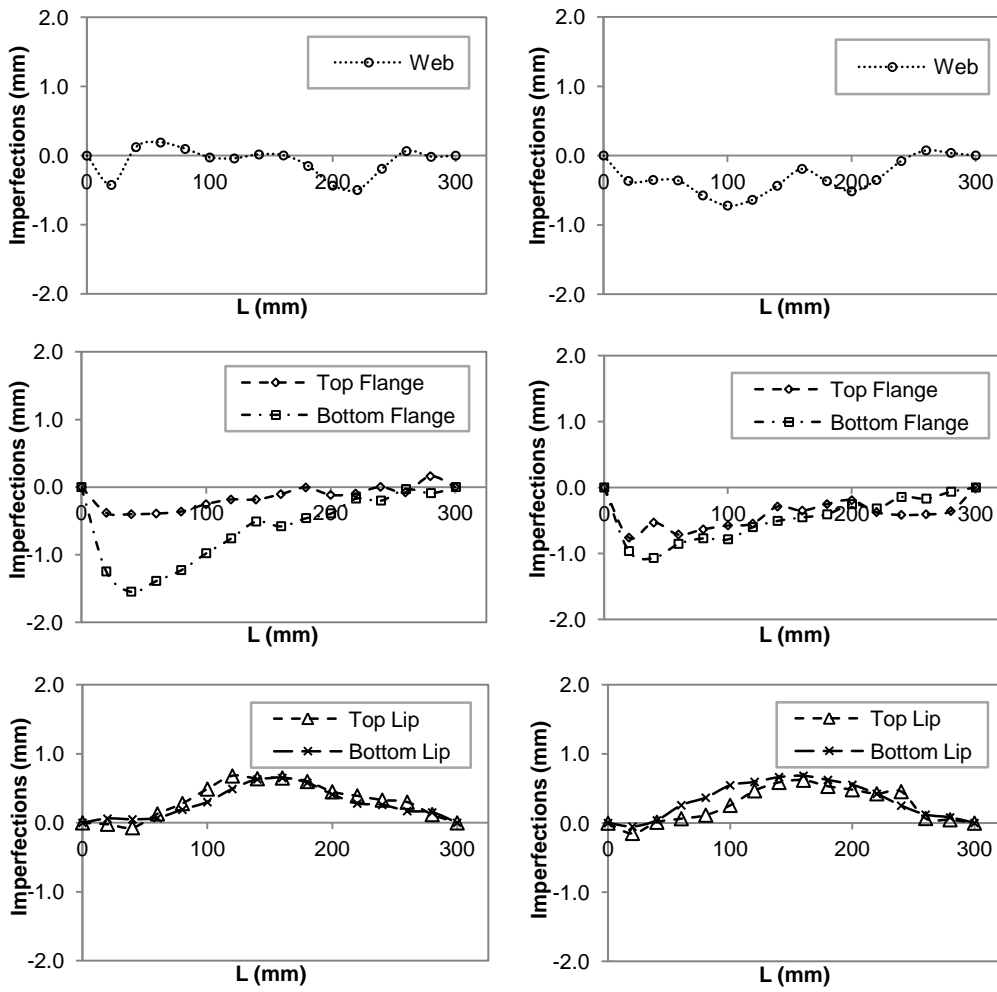


Figure D.1 Imperfection Results for GBU75S50L300-2

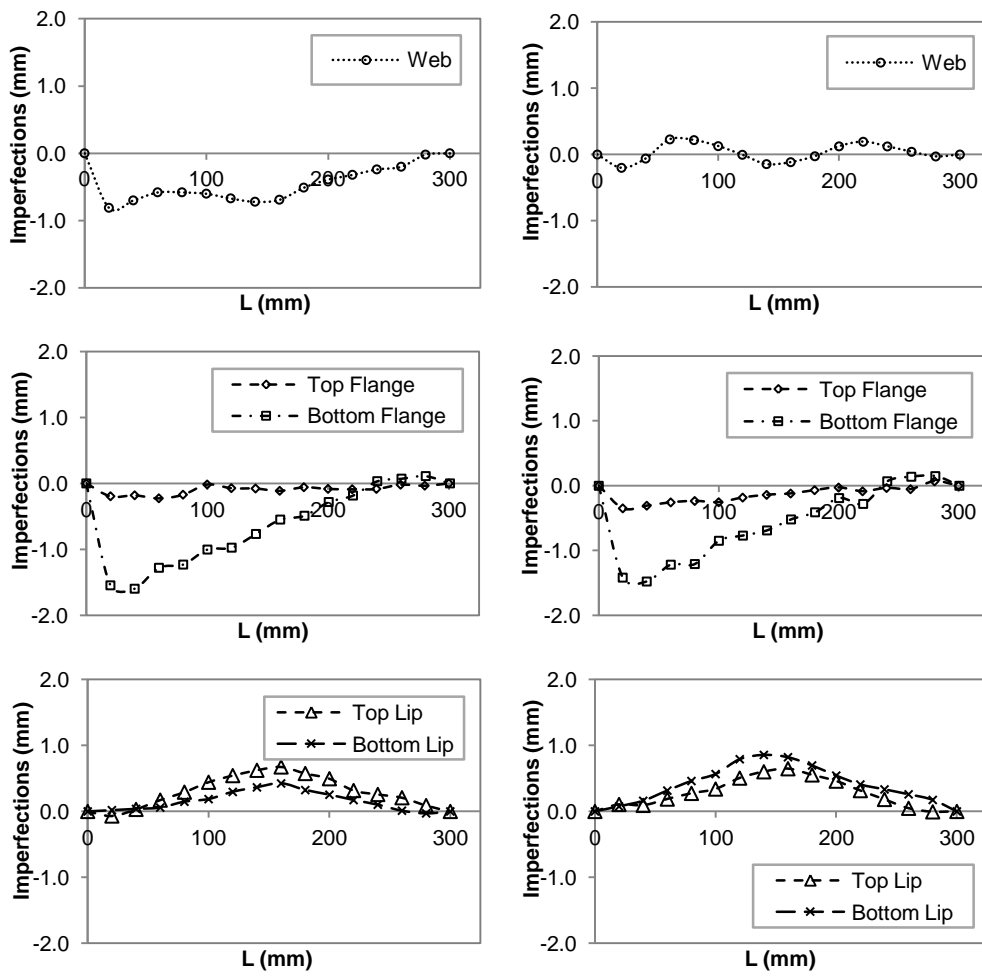


Figure D.2 Imperfection Results for GBU75S200L300-1

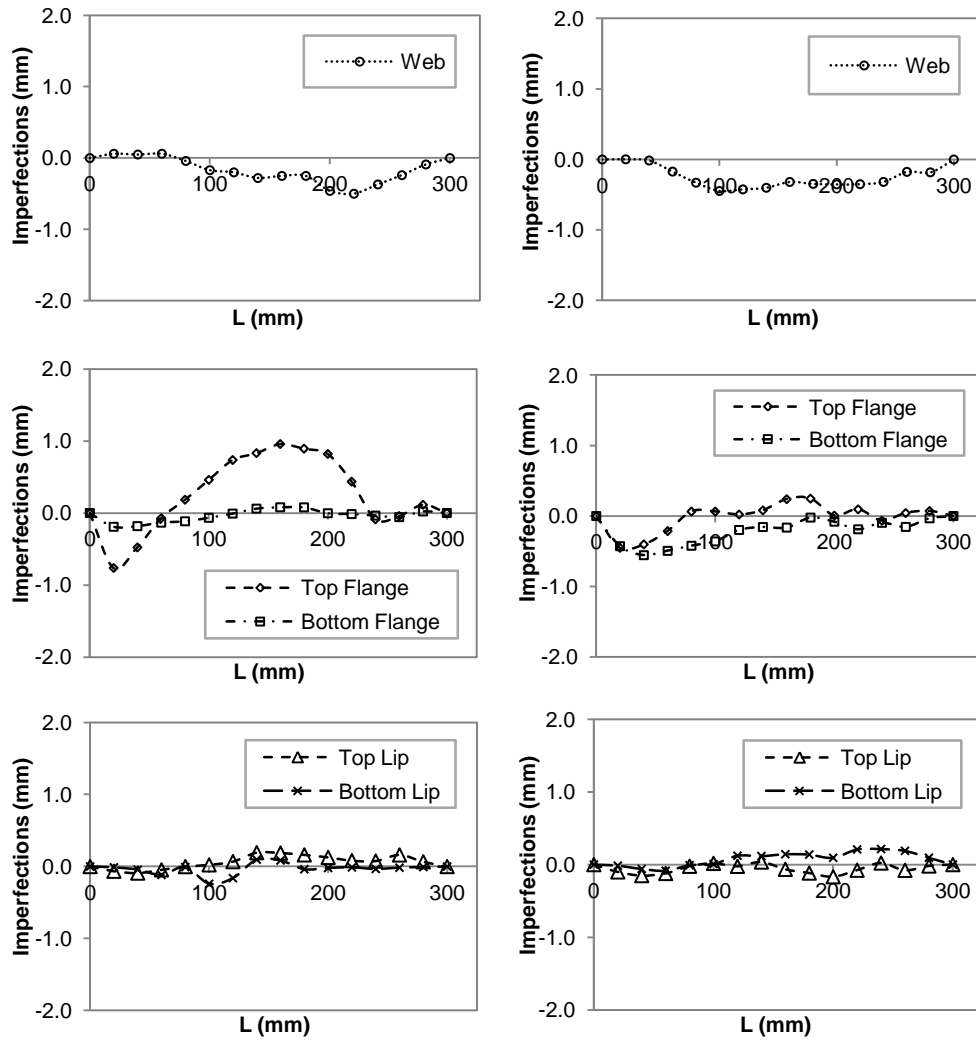


Figure D.3 Imperfection Results for GBU90S50L300-3

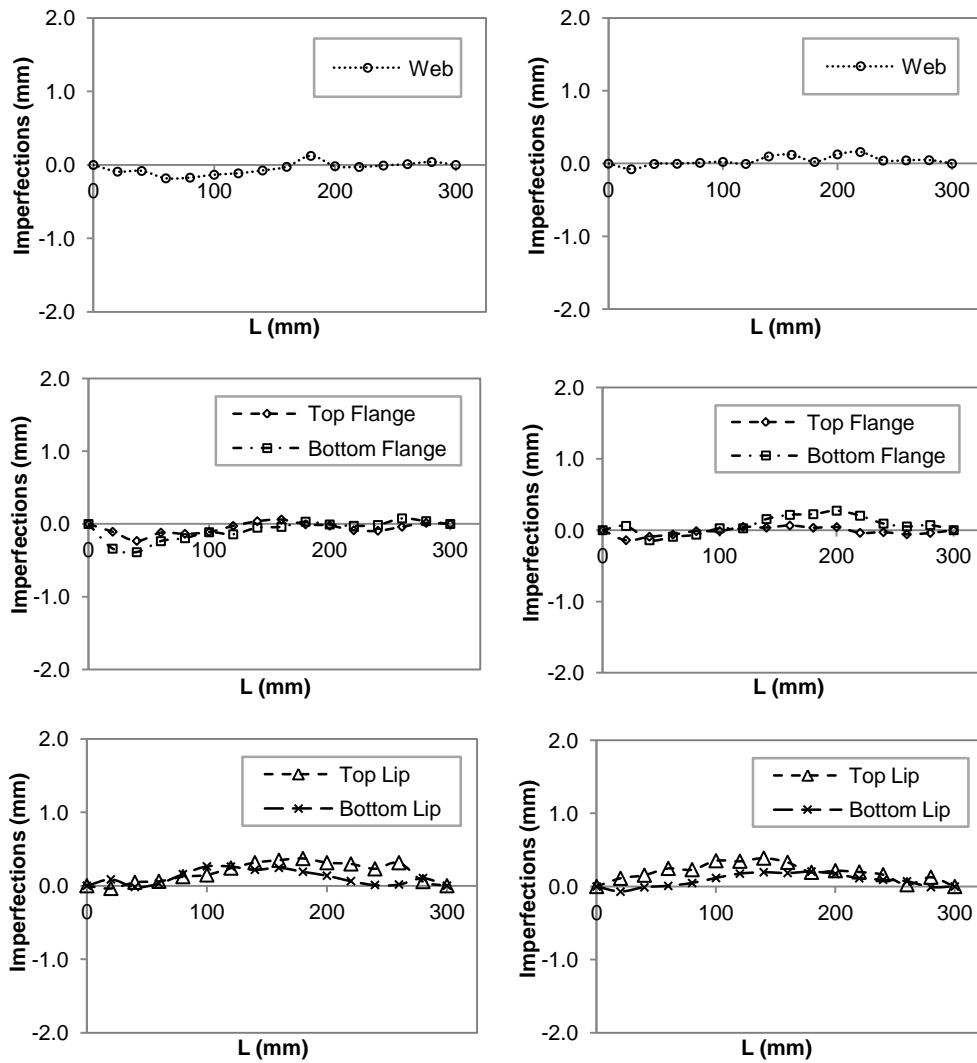


Figure D.4 Imperfection Results for GBU90S200L300-2

D.2 Short Column (L=500mm)

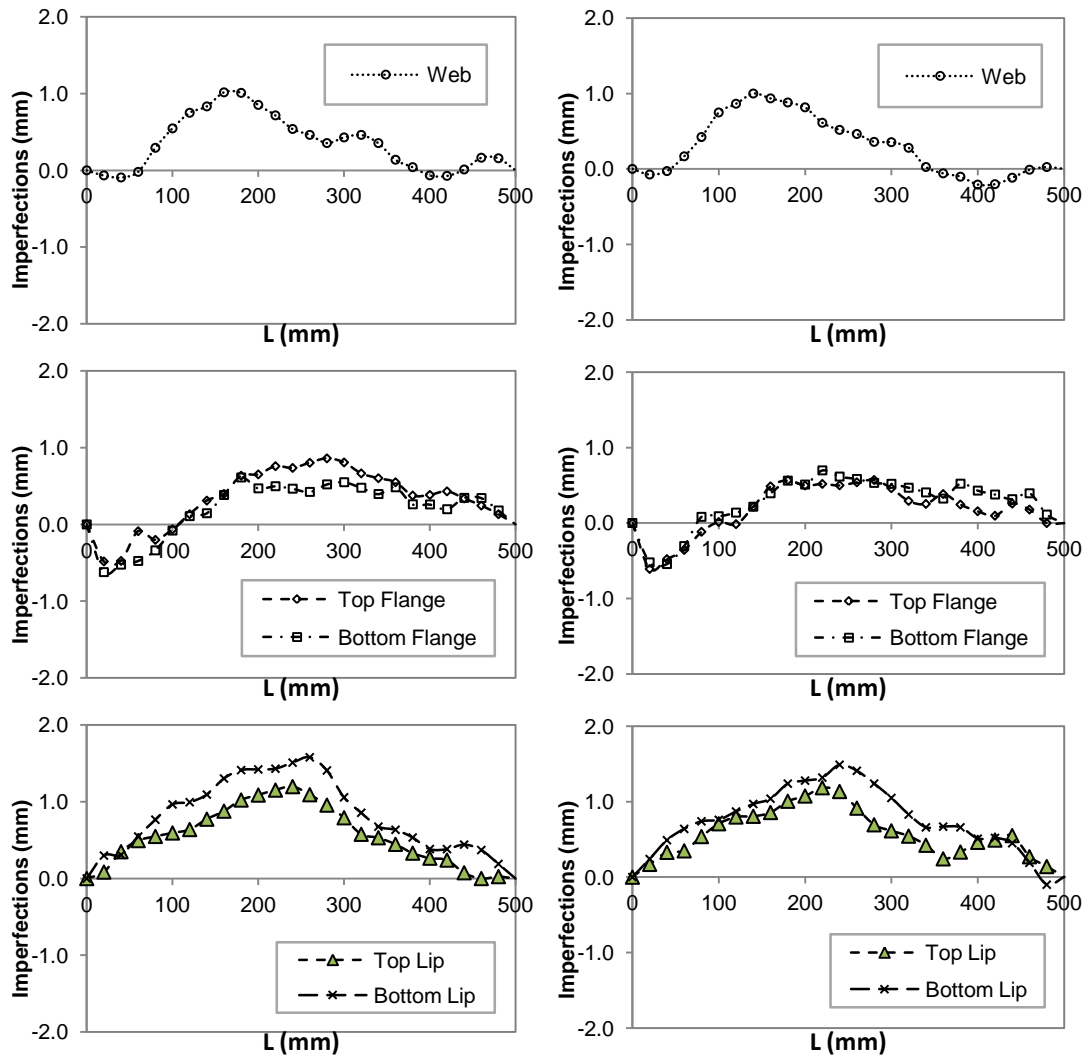


Figure D.5 Imperfection Results for GBU75S100L500-1

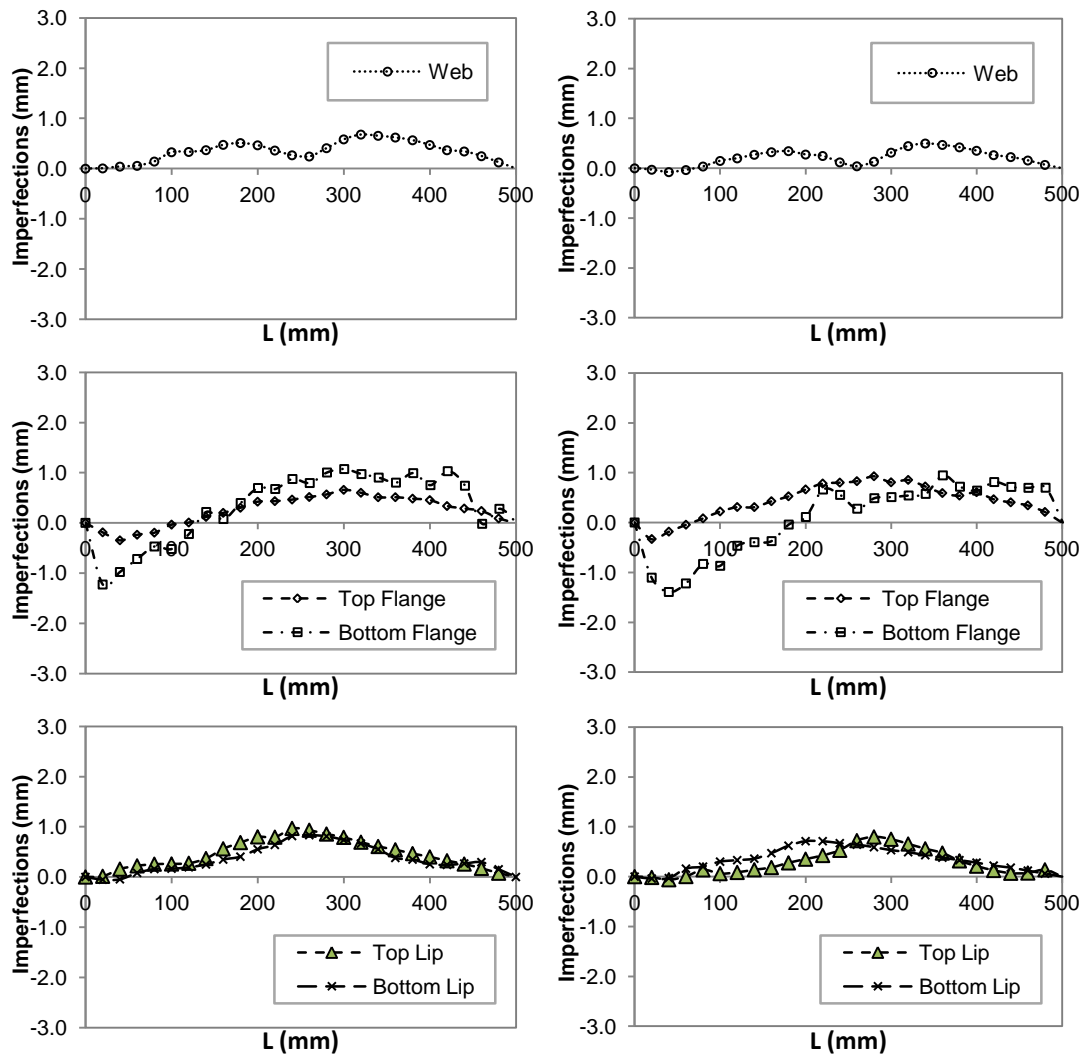


Figure D.6 Imperfection Results for GBU75S400L500-1

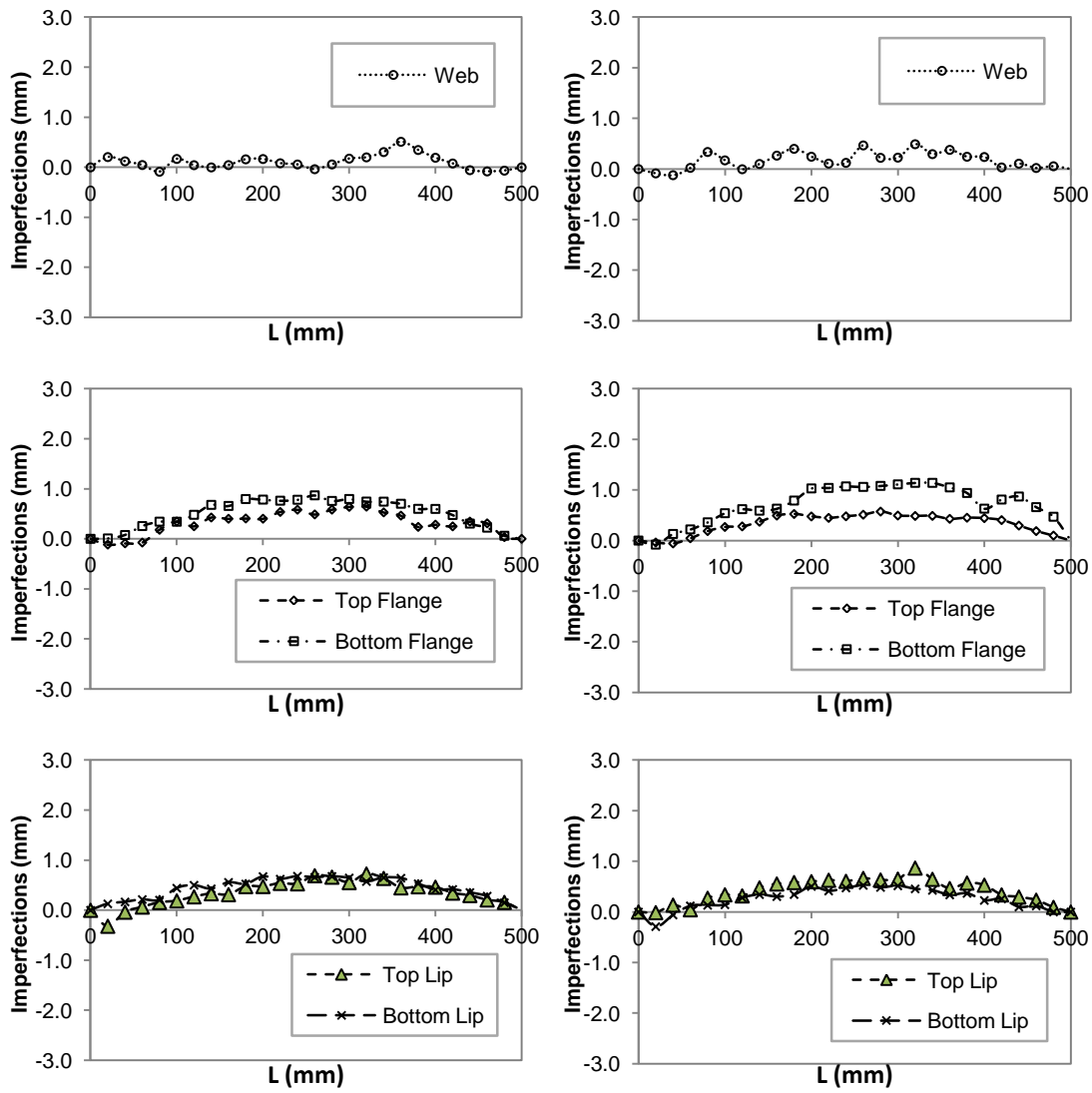


Figure D.7 Imperfection Results for GBU90S100L500-1

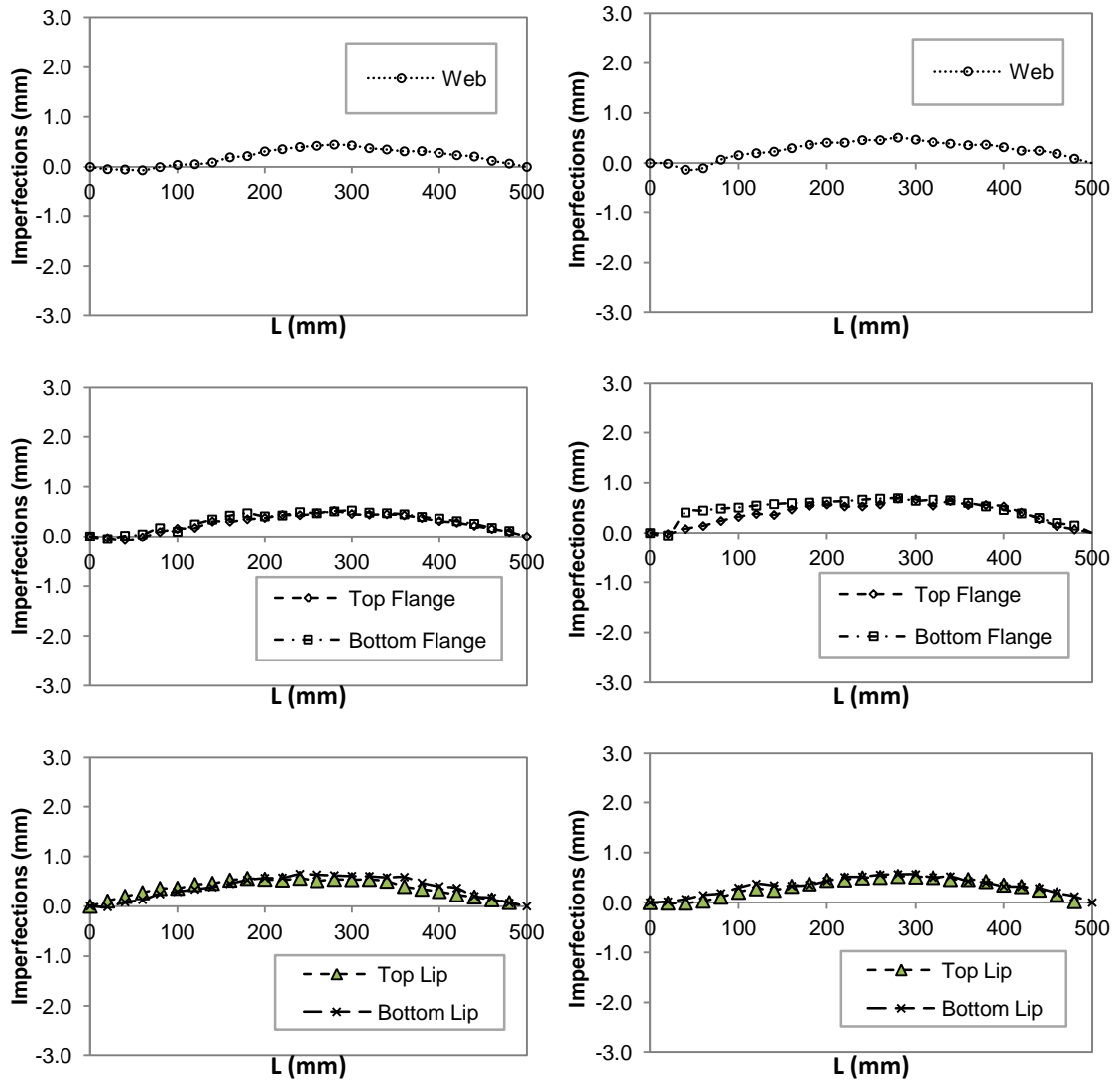


Figure D.8 Imperfection Results for GBU90S400L500-1

D.3 Short Column (L=1000mm)

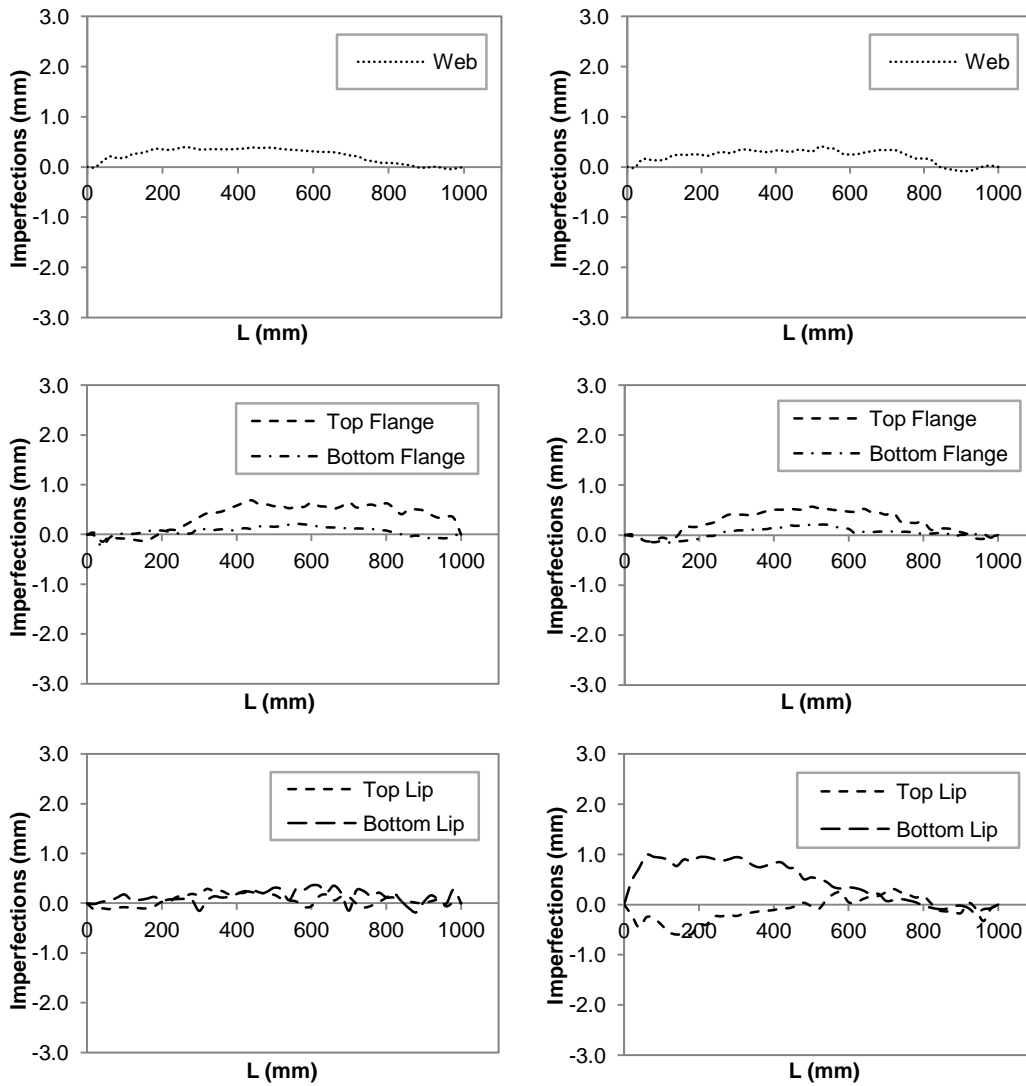


Figure D.9 Imperfection Results for GBU75S225L1000-1

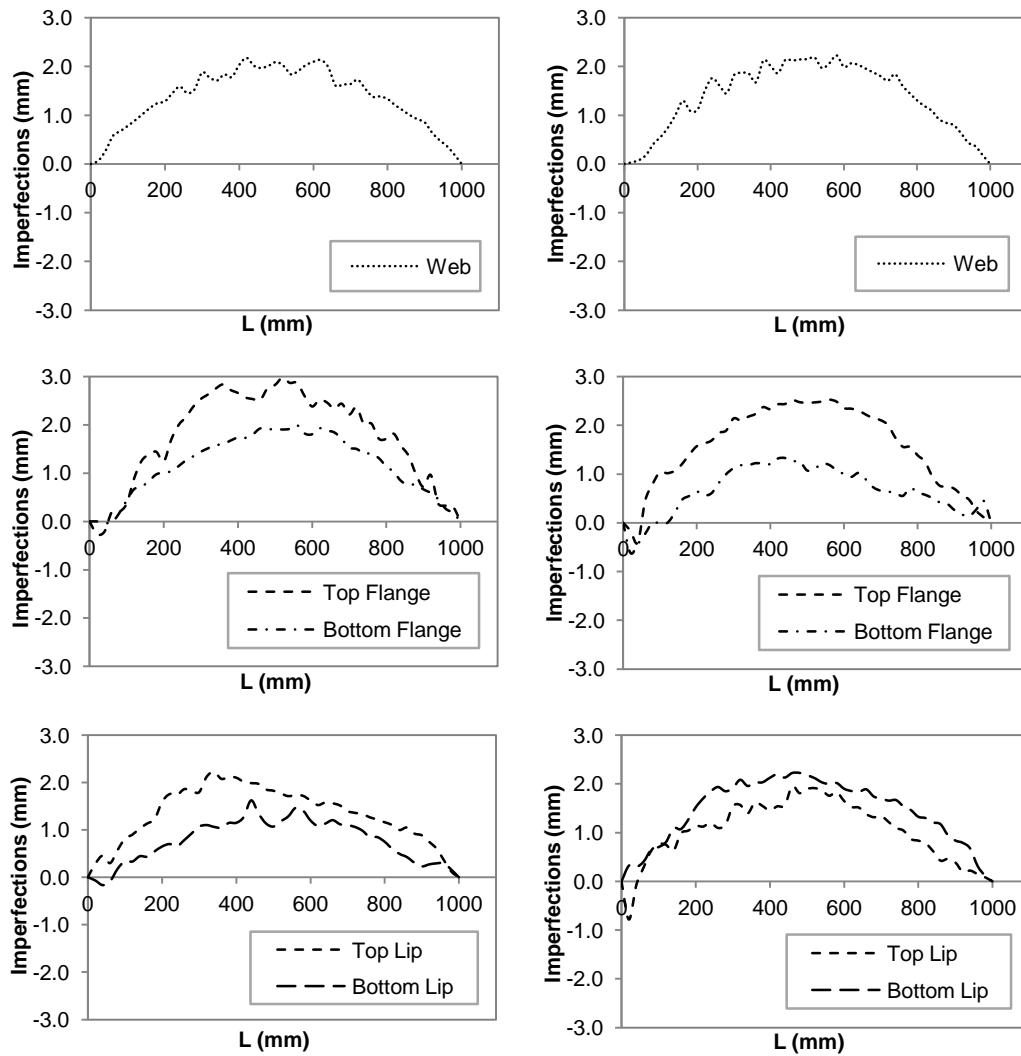


Figure D.10 Imperfection Results for GBU75S900L1000-1

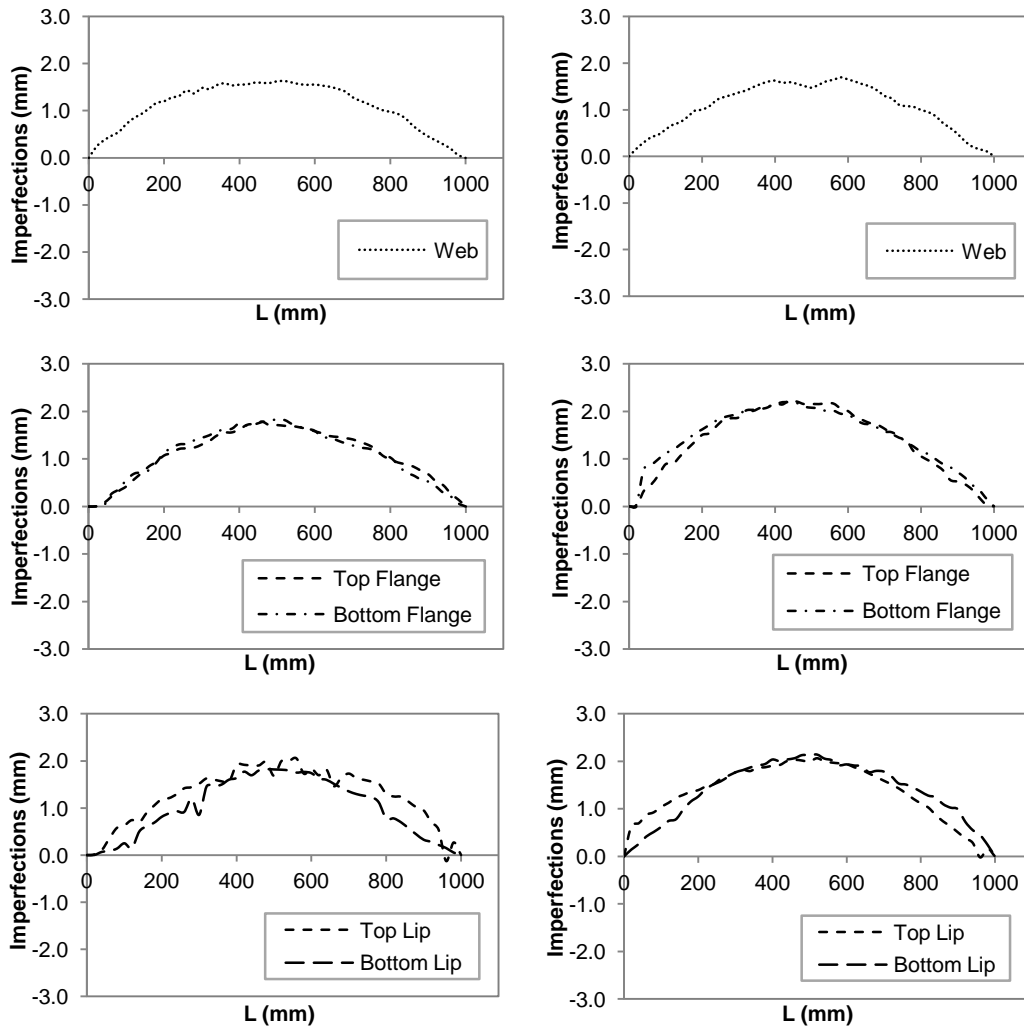


Figure D.11 Imperfection Results for GBU90S225L1000-1

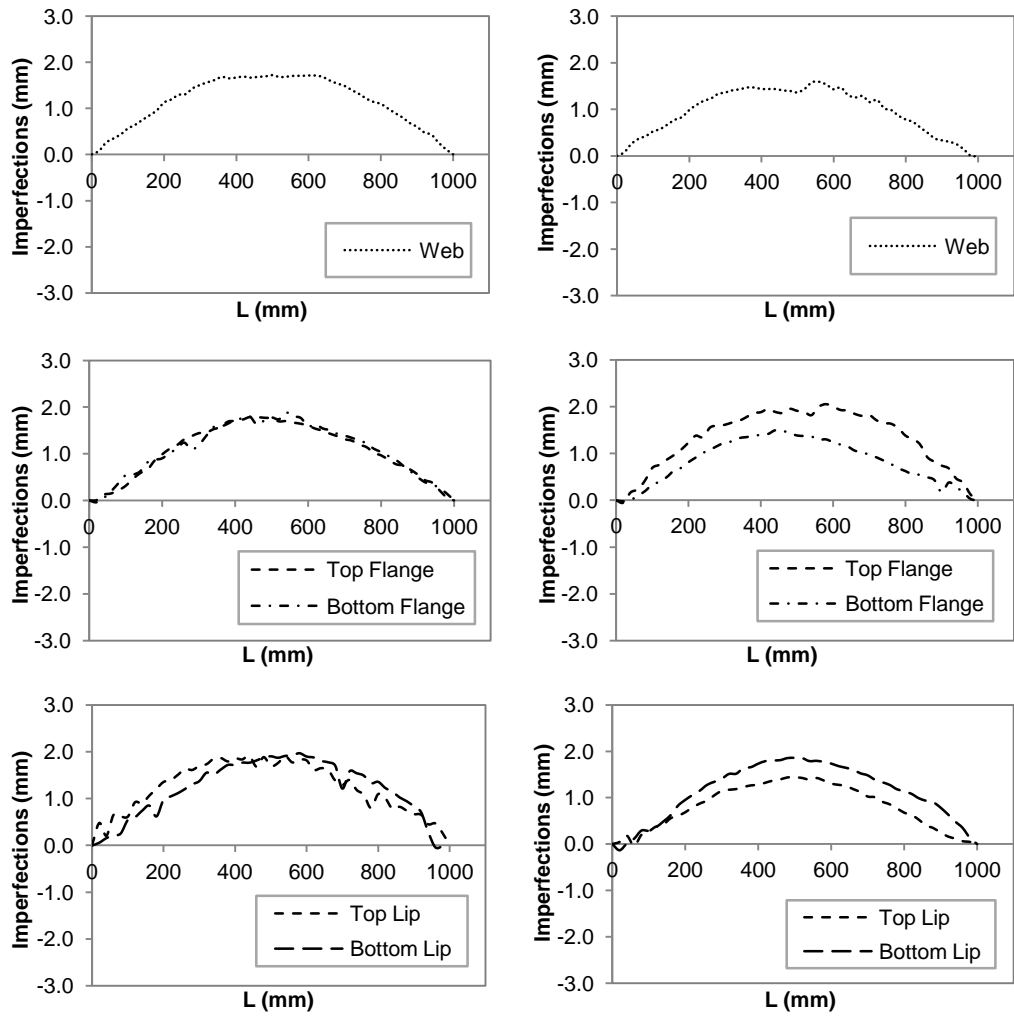


Figure D.12 Imperfection Results for GBU90S900L1000-1

D.4 Short Column (L=2000mm)

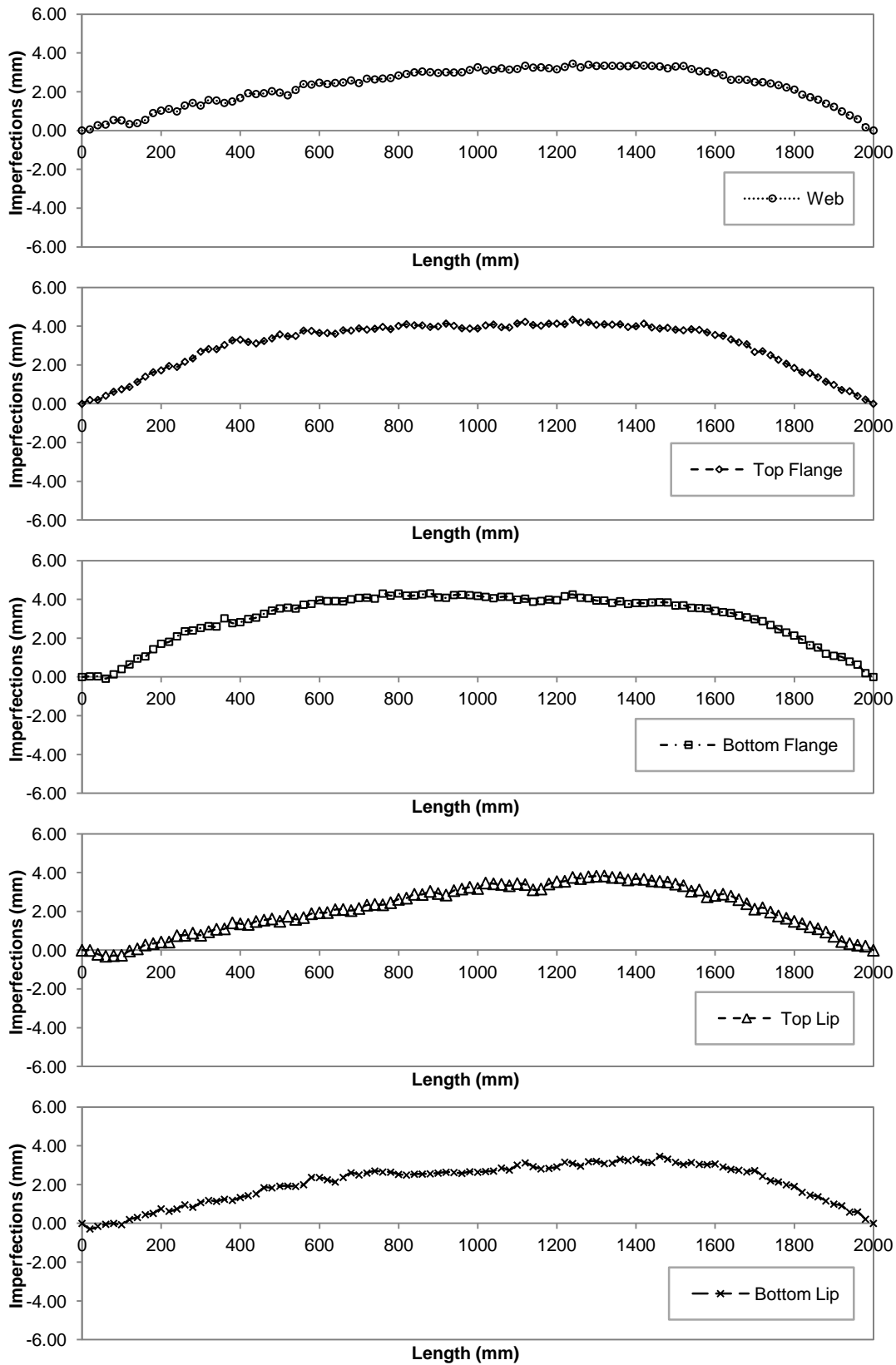


Figure D.13 Imperfection Results for GBU75S475L2000-1 (Left)

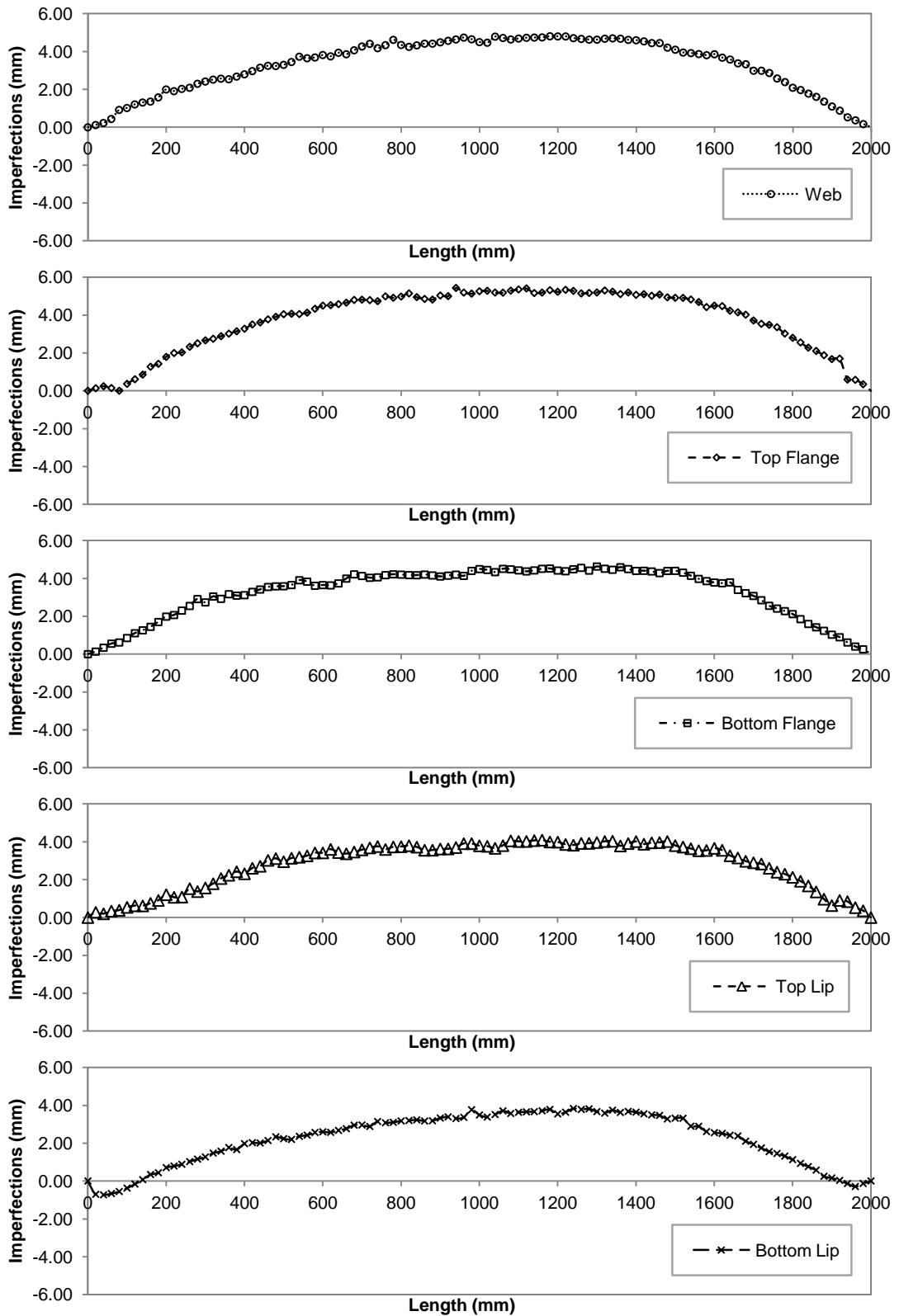


Figure D.14 Imperfection Results for GBU75S475L2000-1 (Right)

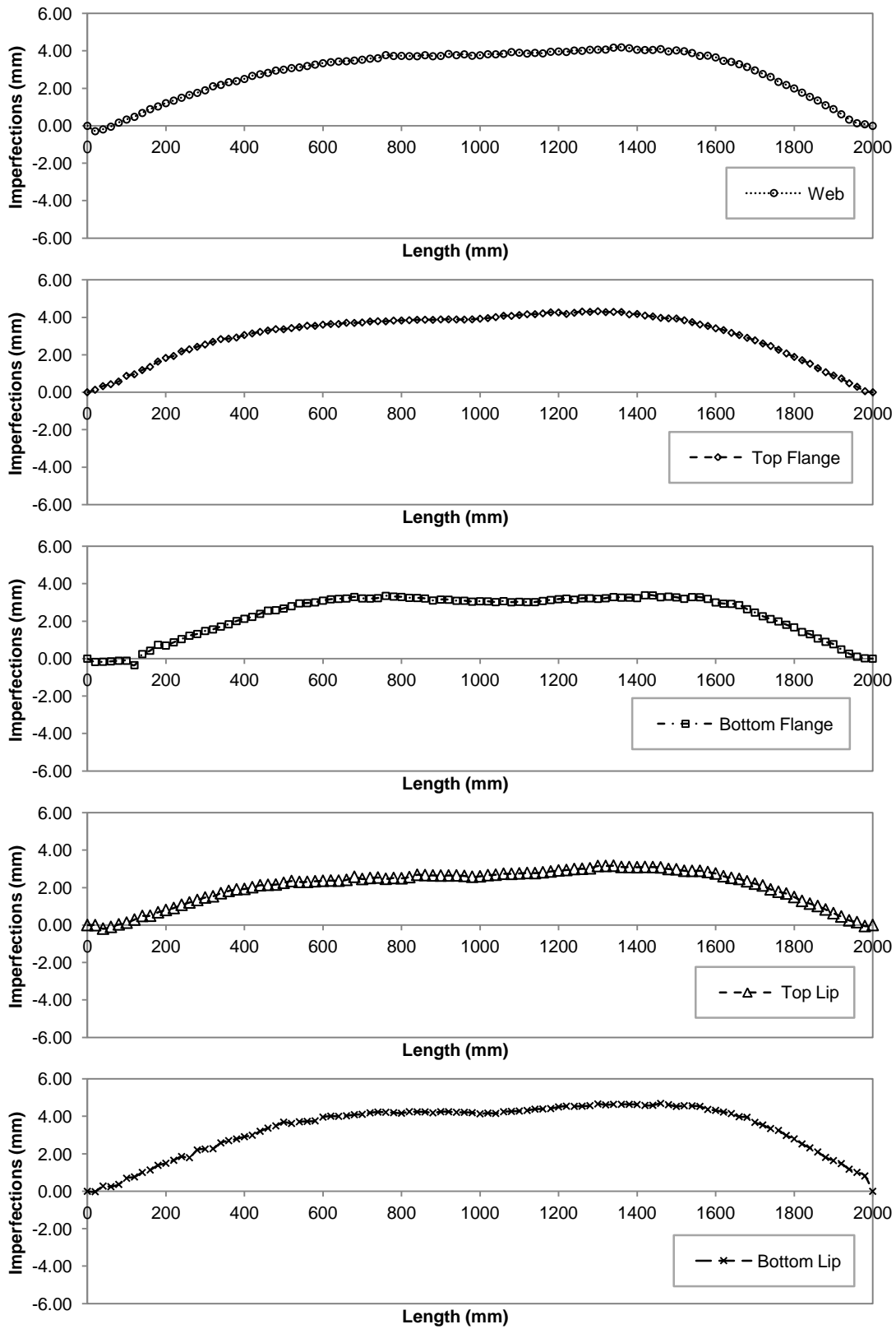


Figure D.15 Imperfection Results for GBU75S1900L2000-1 (Left)

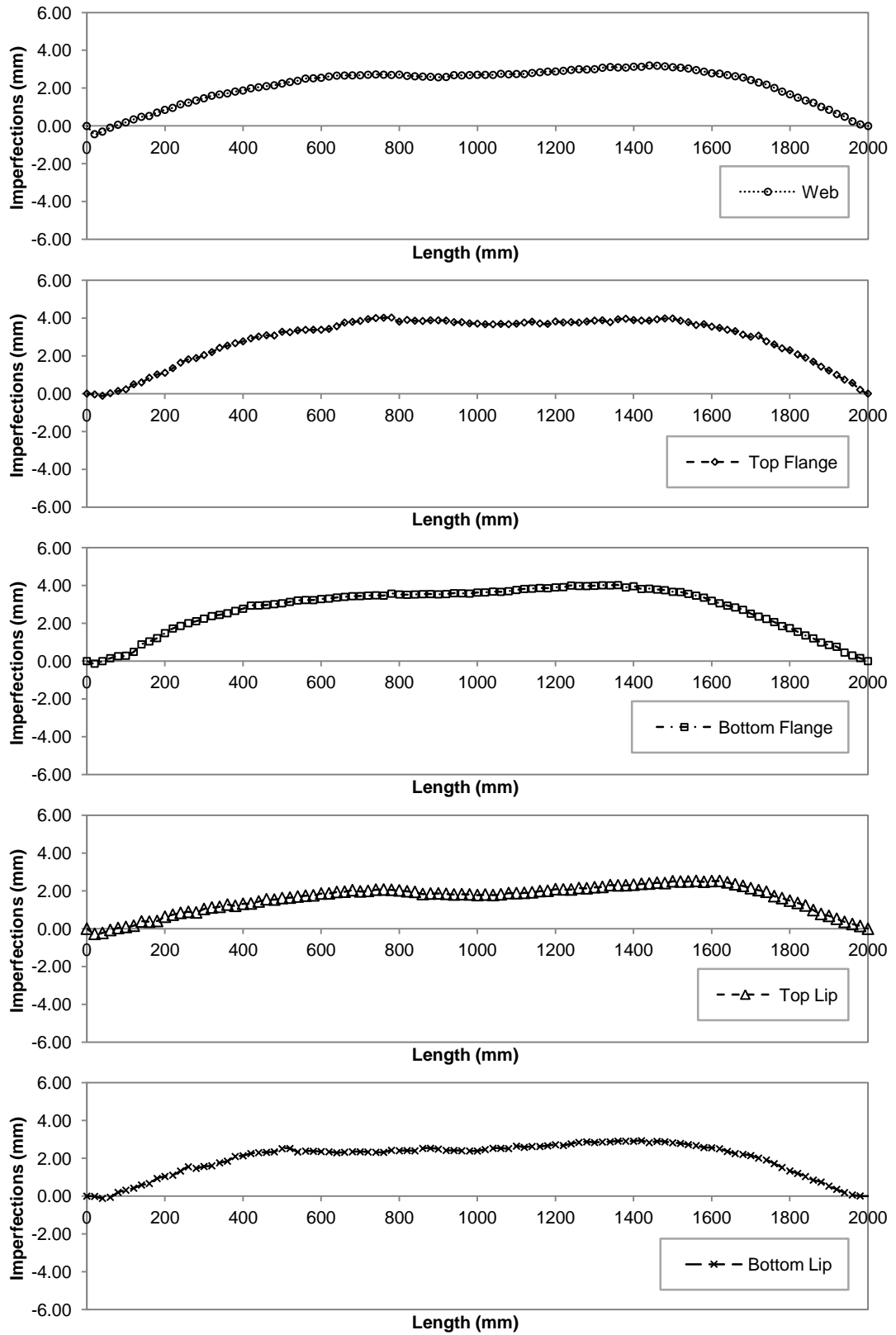


Figure D.16 Imperfection Results for GBU75S1900L2000-1 (Right)

E. Results for C-channel

E.1 Stub Column

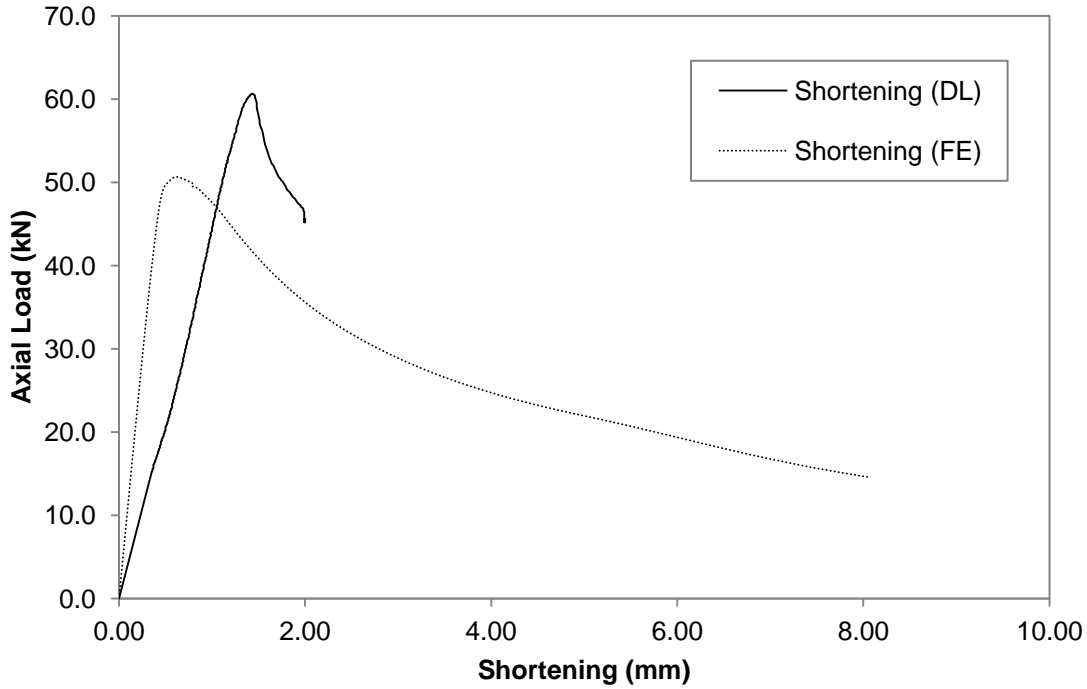


Figure E.1 Axial Load versus Shortening Curve for C75L300-1

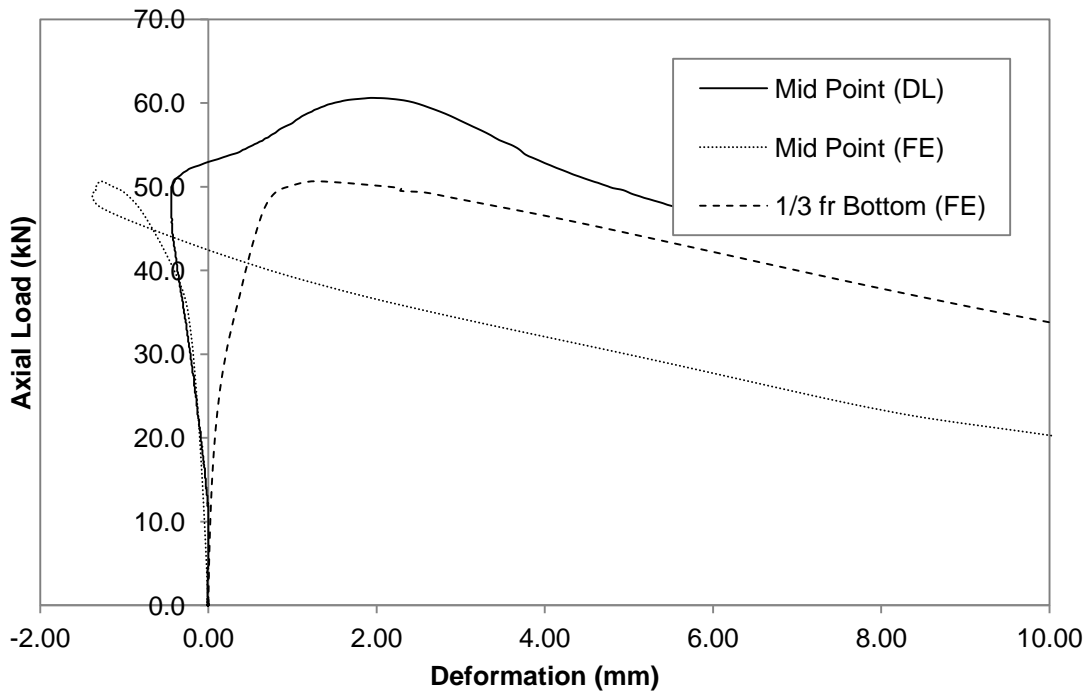


Figure E.2 Axial Load versus Deformation Curve for C75L300-1

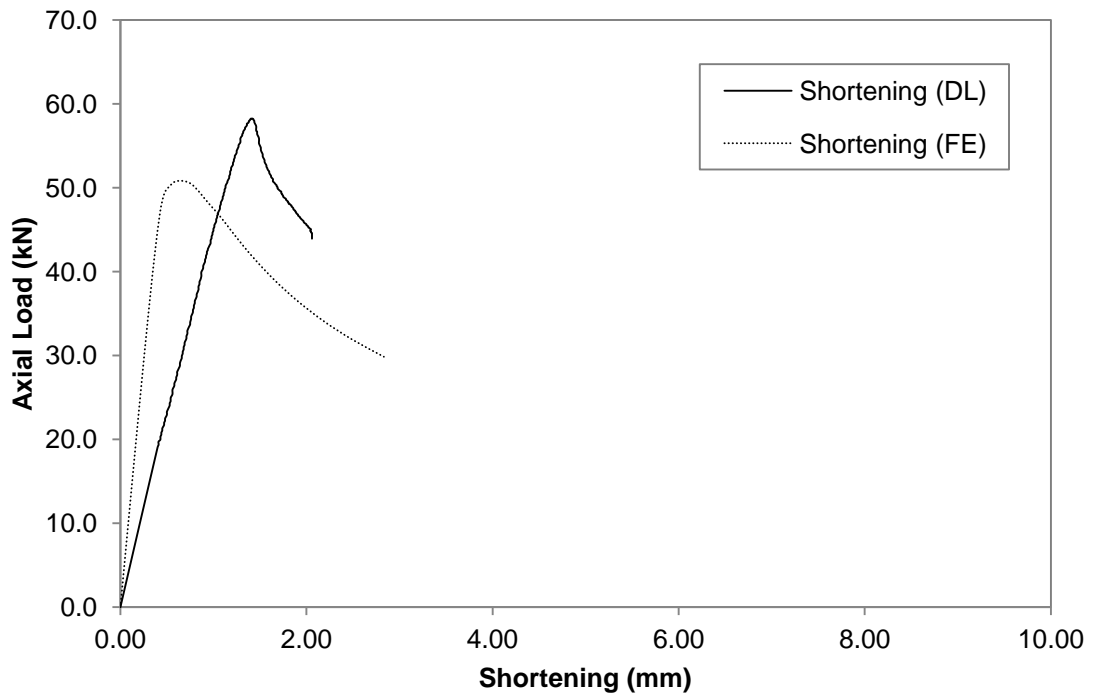


Figure E.3 Axial Load versus Shortening Curve for C75L300-2

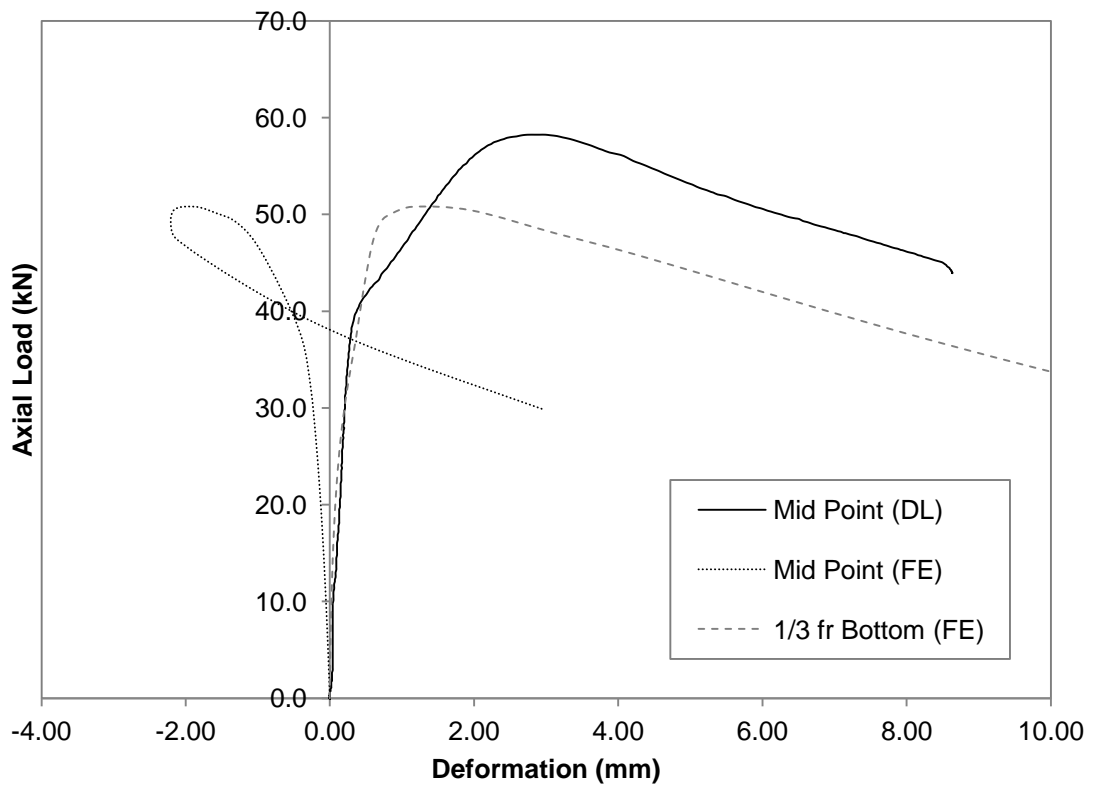


Figure E.4 Axial Load versus Deformation Curve for C75L300-2

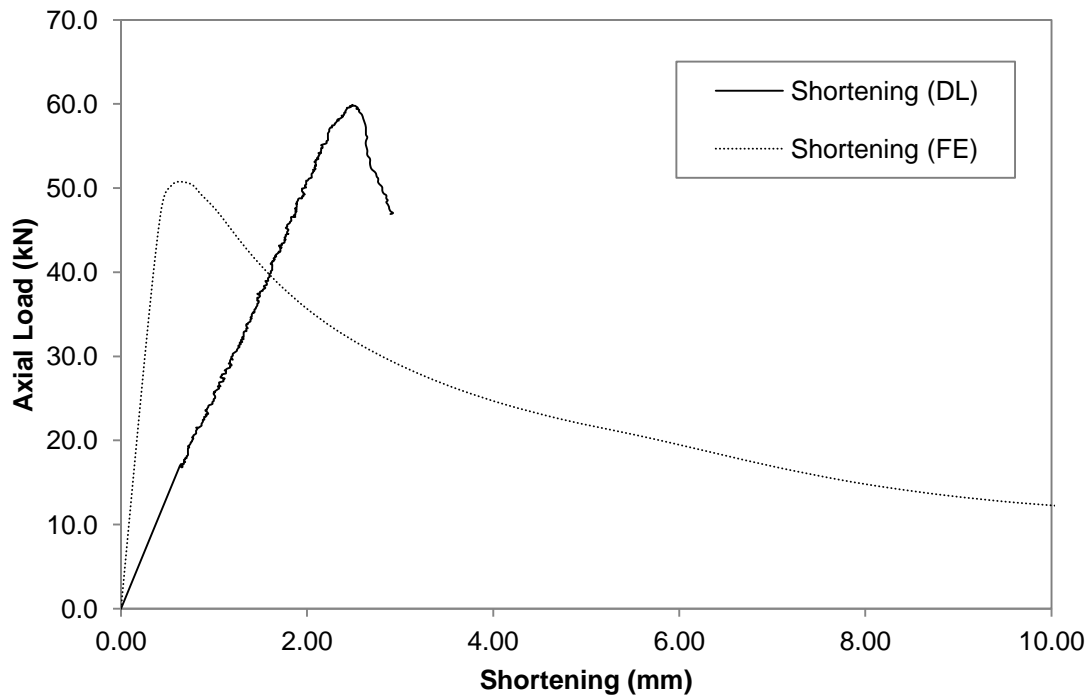


Figure E.5 Axial Load versus Shortening Curve for C75L300-3

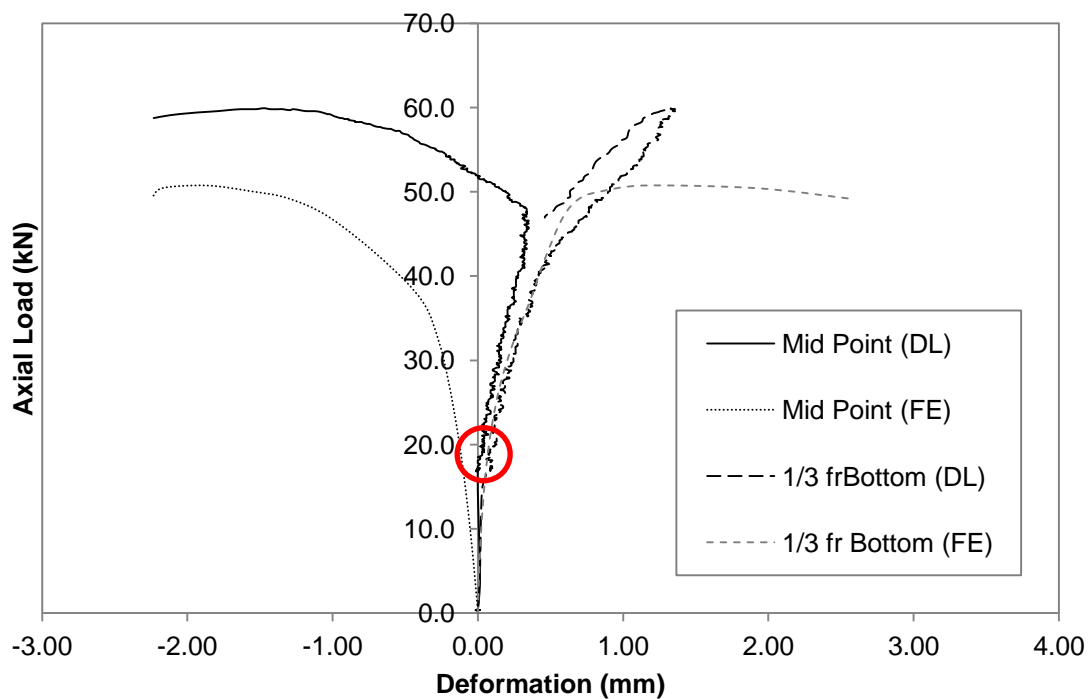


Figure E.6 Axial Load versus Deformation Curve for C75L300-3

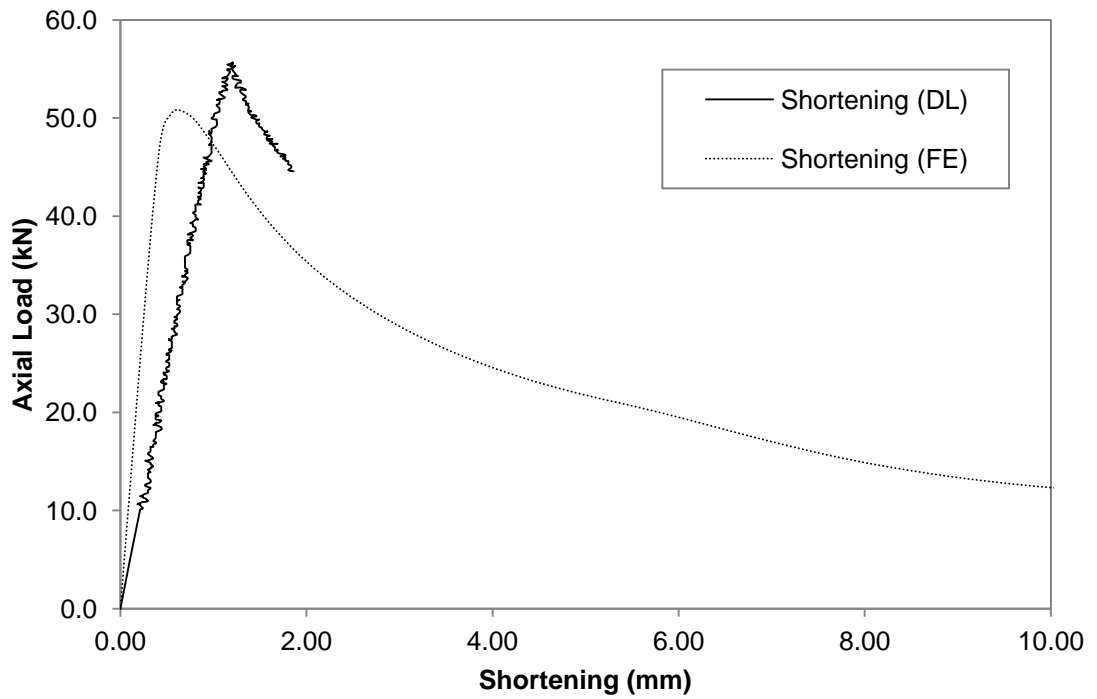


Figure E.7 Axial Load versus Shortening Curve for C75L300-4

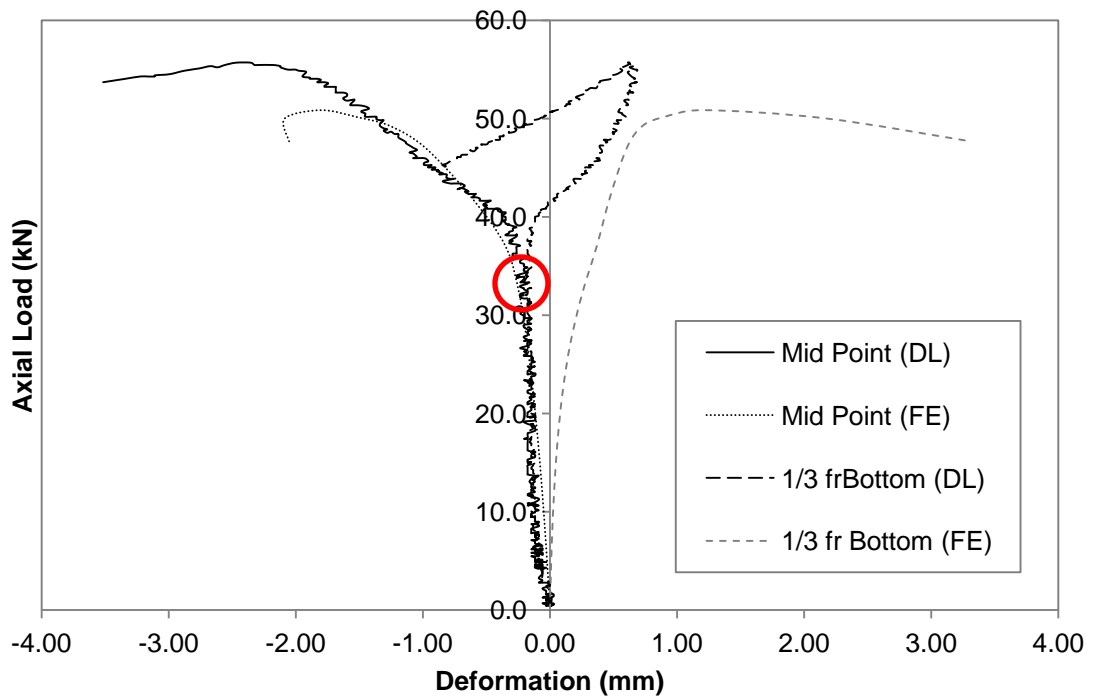


Figure E.8 Axial Load versus Deformation Curve for C75L300-4

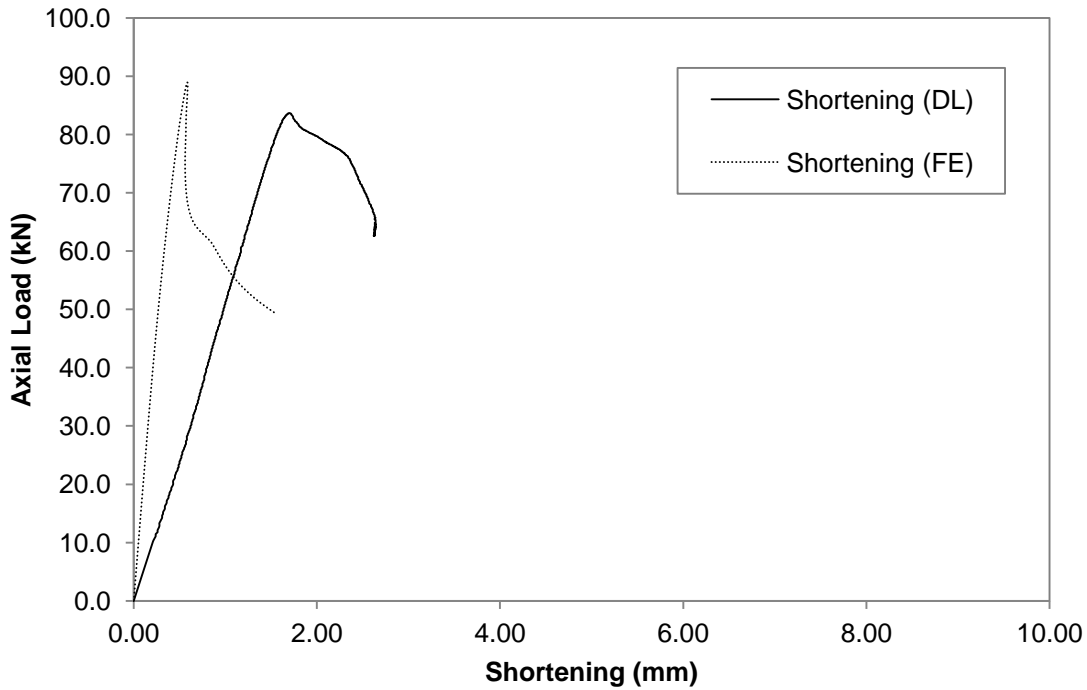


Figure E.9 Axial Load versus Shortening Curve for C90L300-2

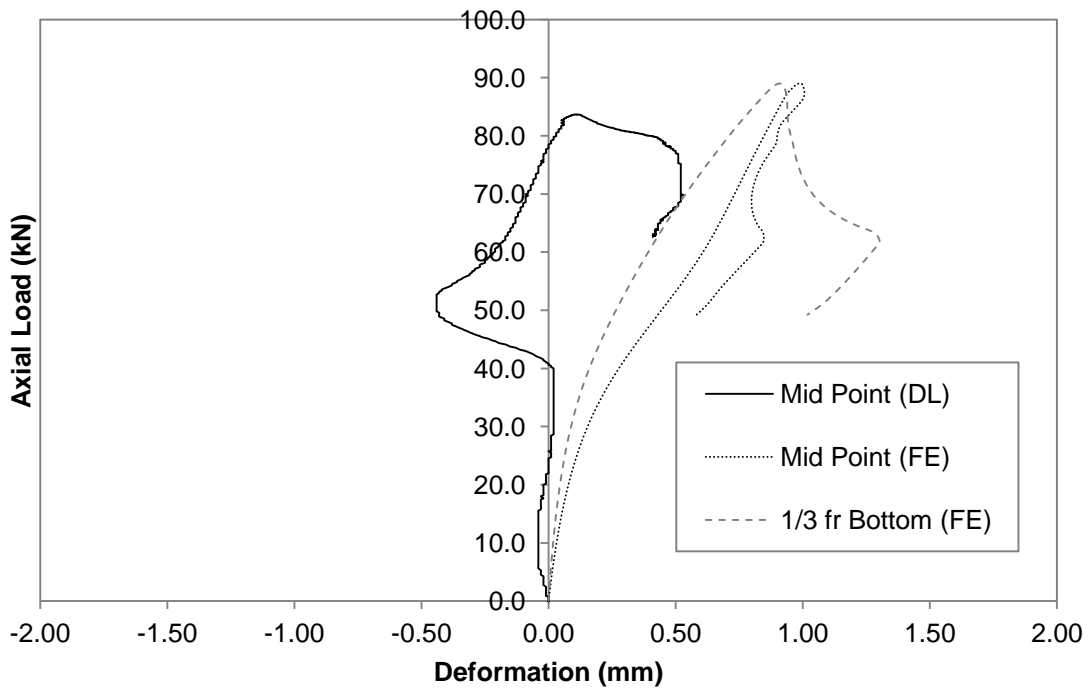


Figure E.10 Axial Load versus Deformation Curve for C90L300-2

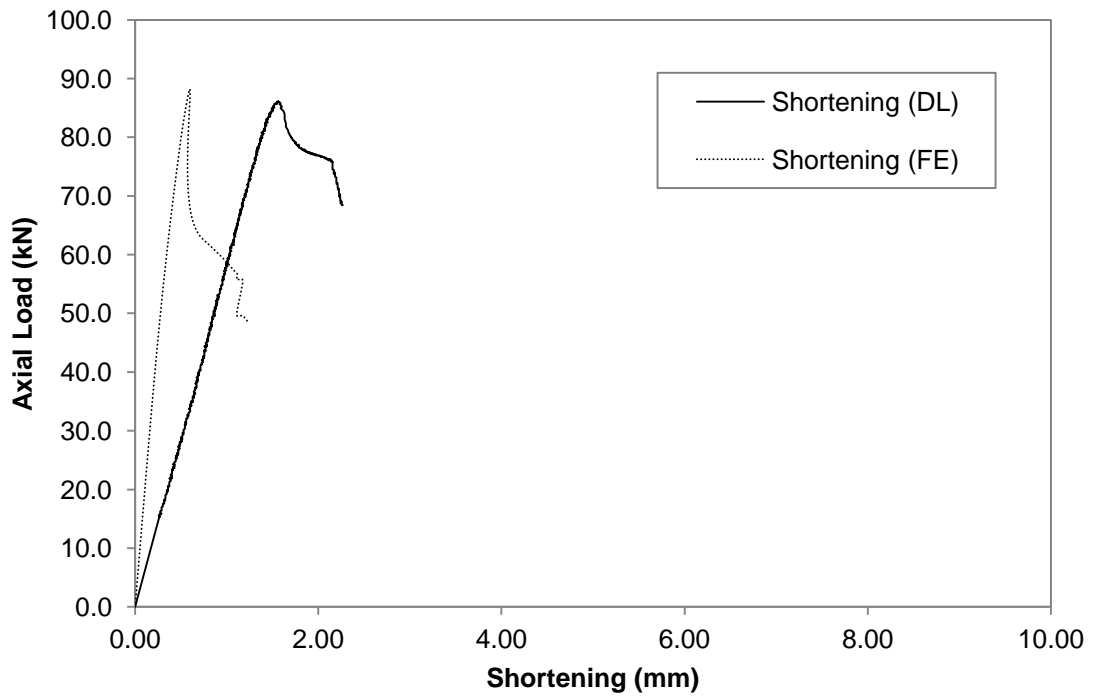


Figure E.11 Axial Load versus Shortening Curve for C90L300-3

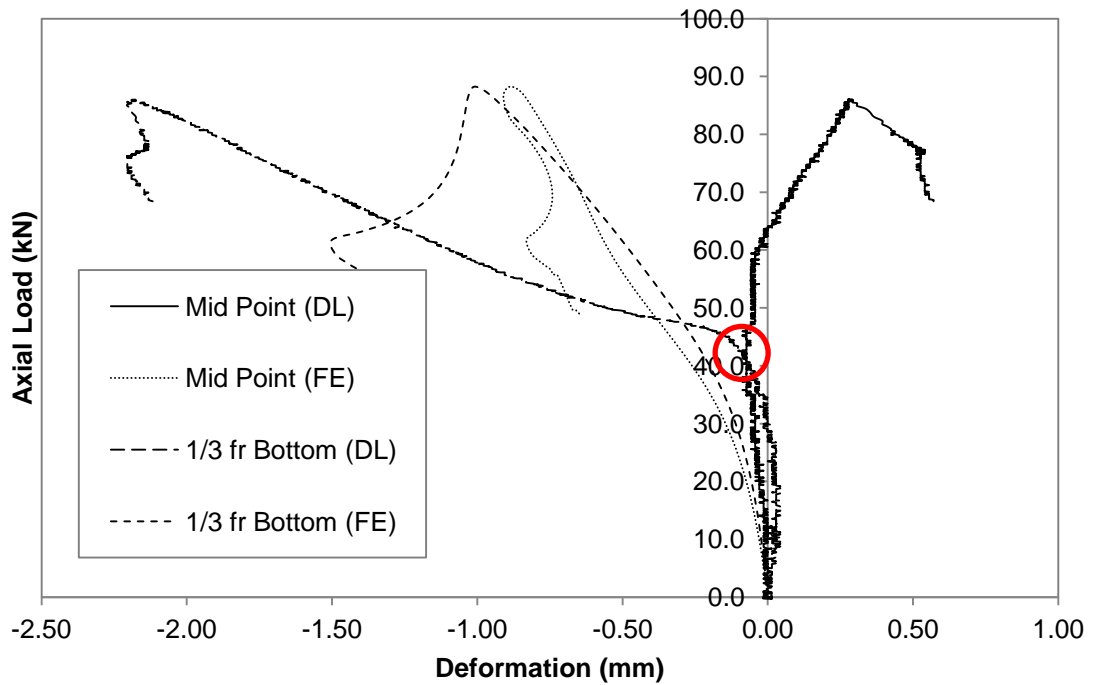


Figure E.12 Axial Load versus Deformation Curve for C90L300-3

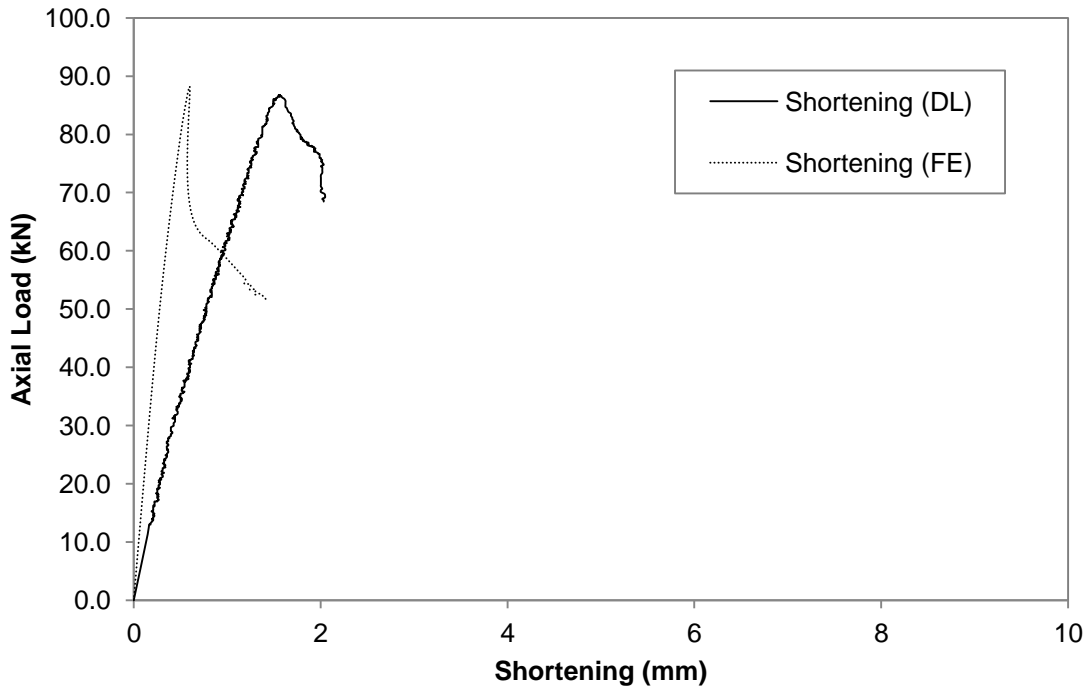


Figure E.13 Axial Load versus Shortening Curve for C90L300-4

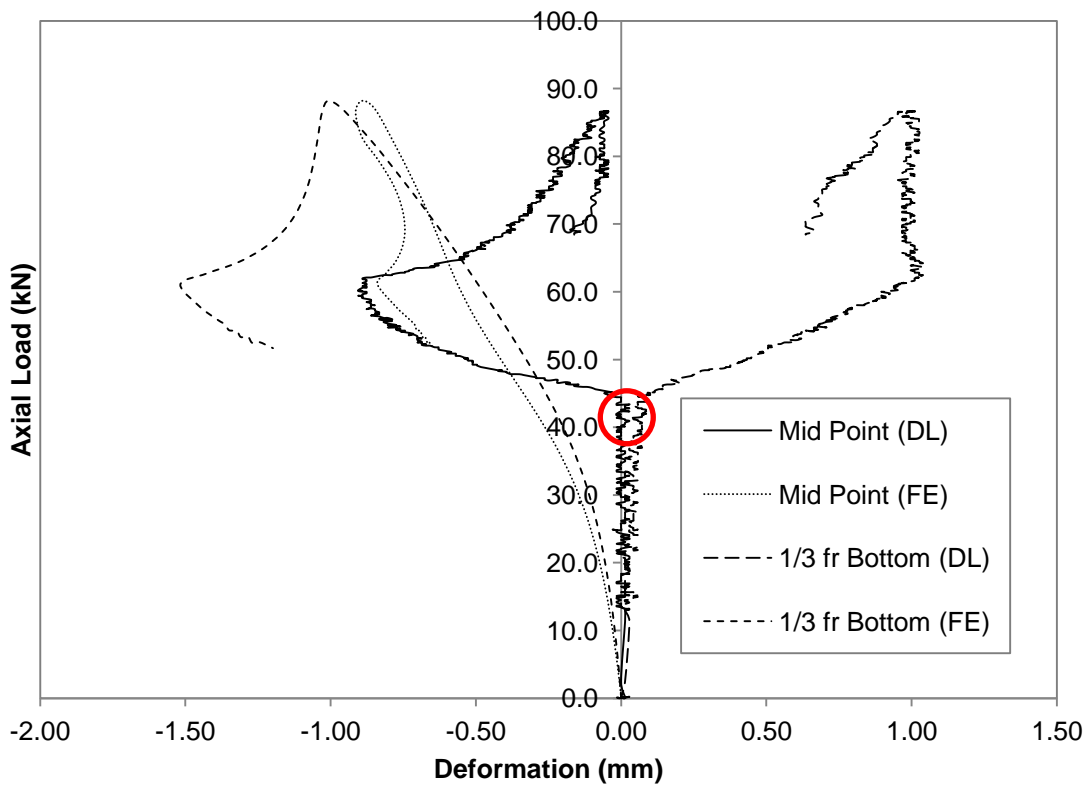


Figure E.14 Axial Load versus Deformation Curve for C90L300-4

E.2 Short Column

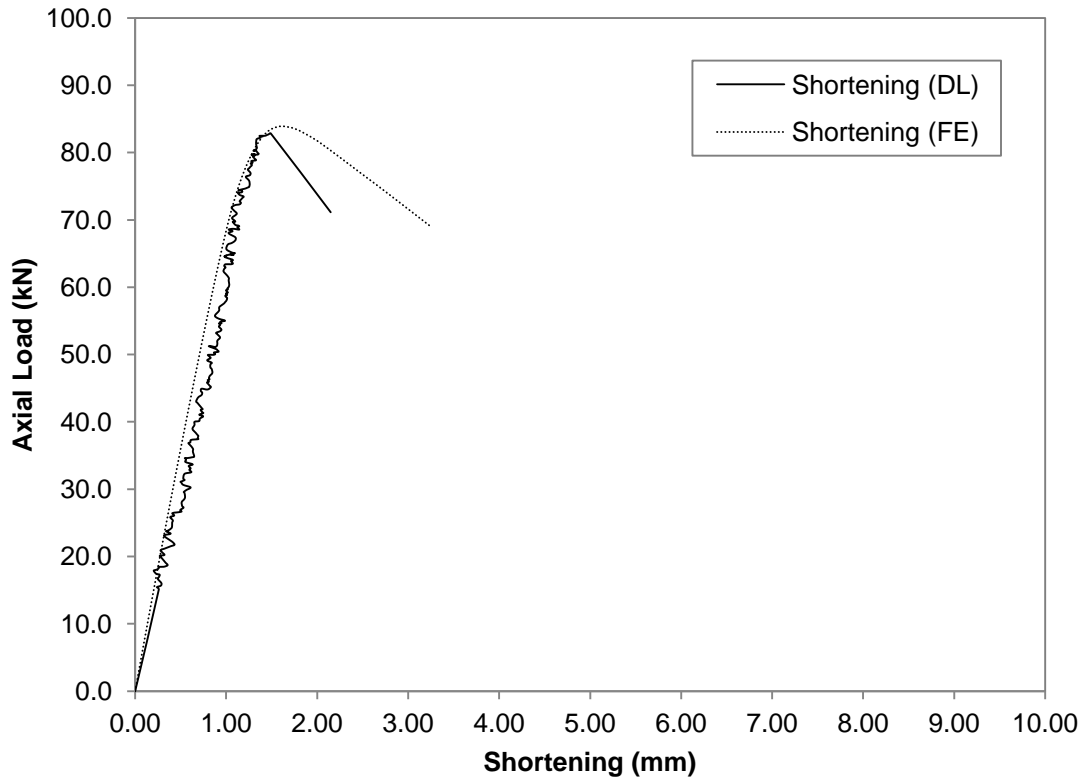


Figure E.15 Axial Load versus Shortening Curve for C90L500-1

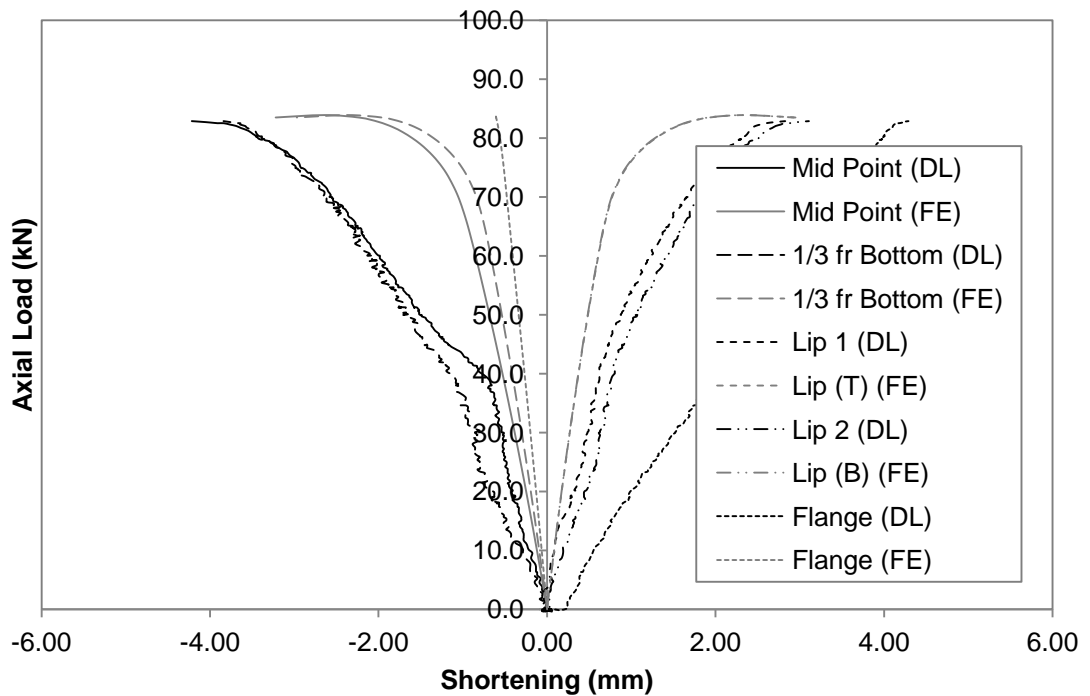


Figure E.16 Axial Load versus Deformation Curve for C90L500-1

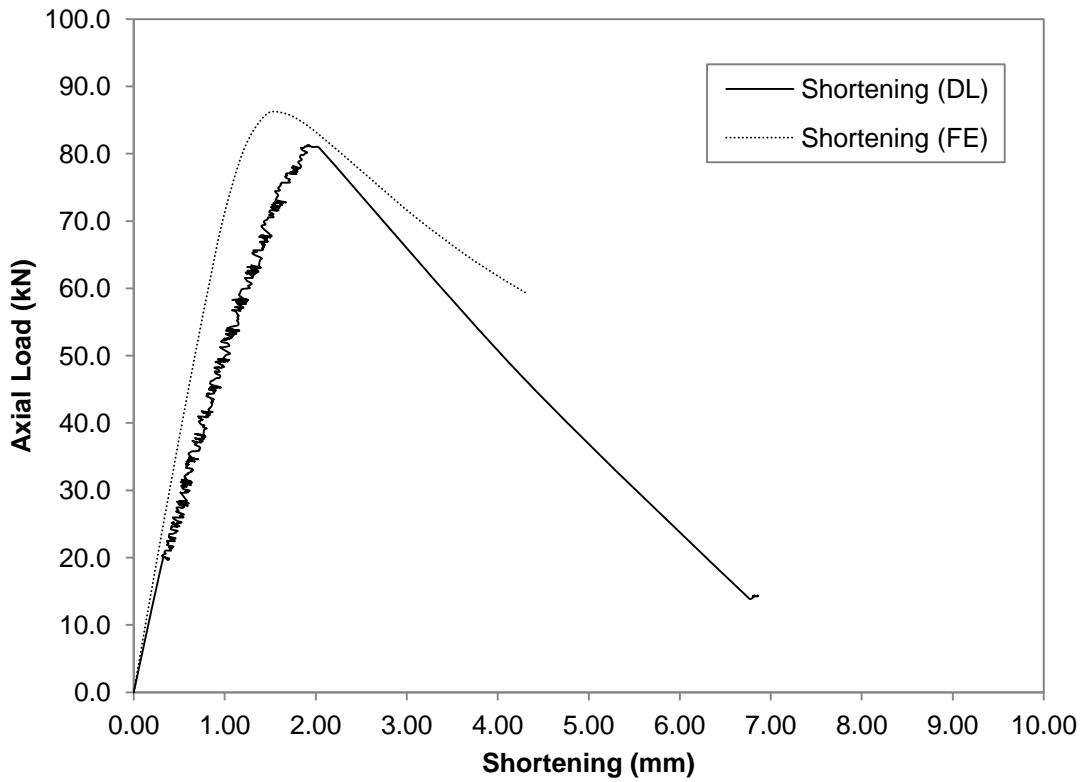


Figure E.17 Axial Load versus Shortening Curve for C90L500-2

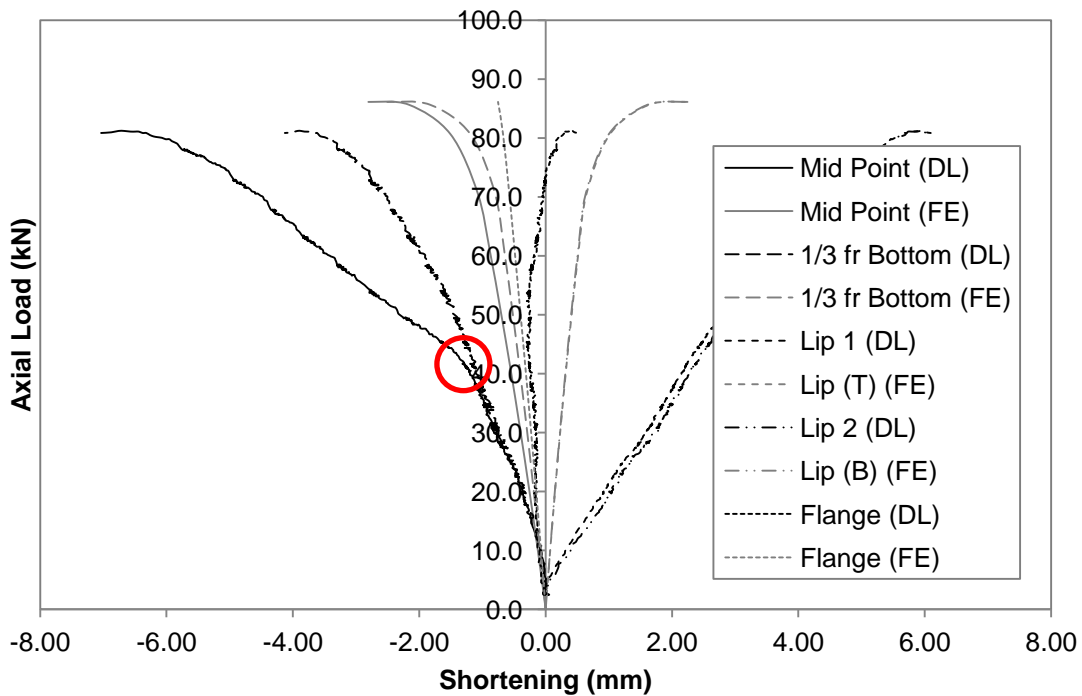


Figure E.18 Axial Load versus Deformation Curve for C90L500-2

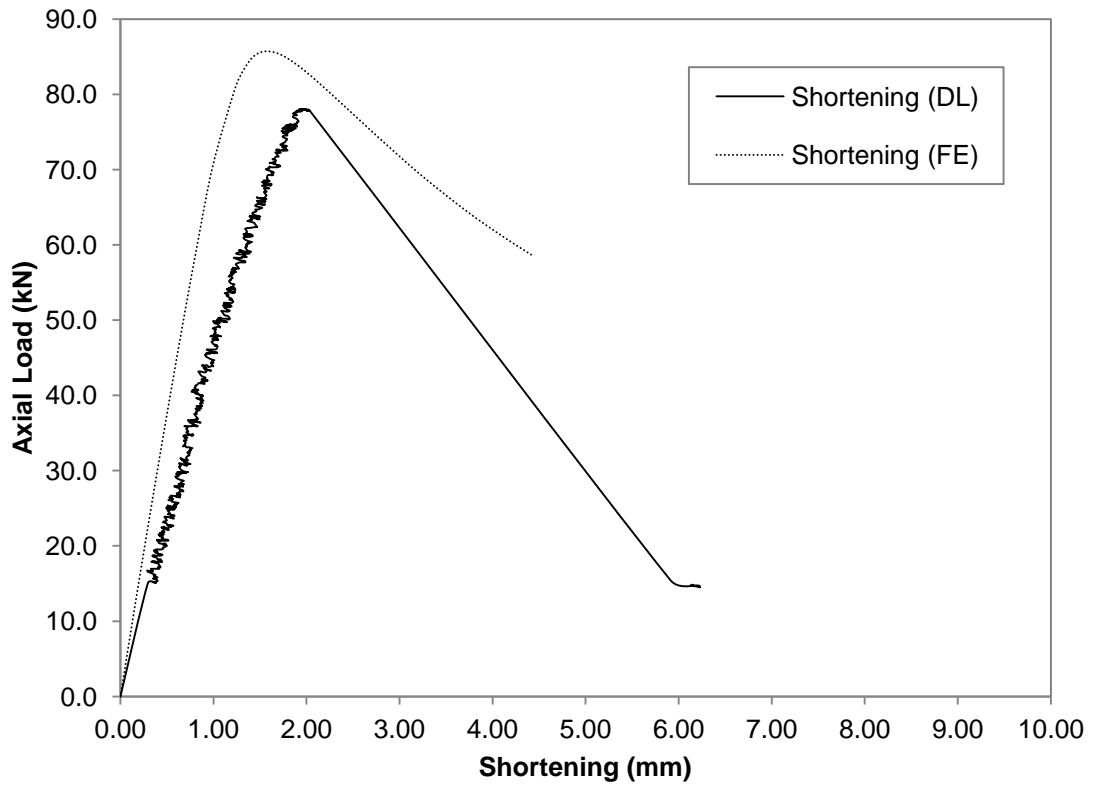


Figure E.19 Axial Load versus Shortening Curve for C90L500-3

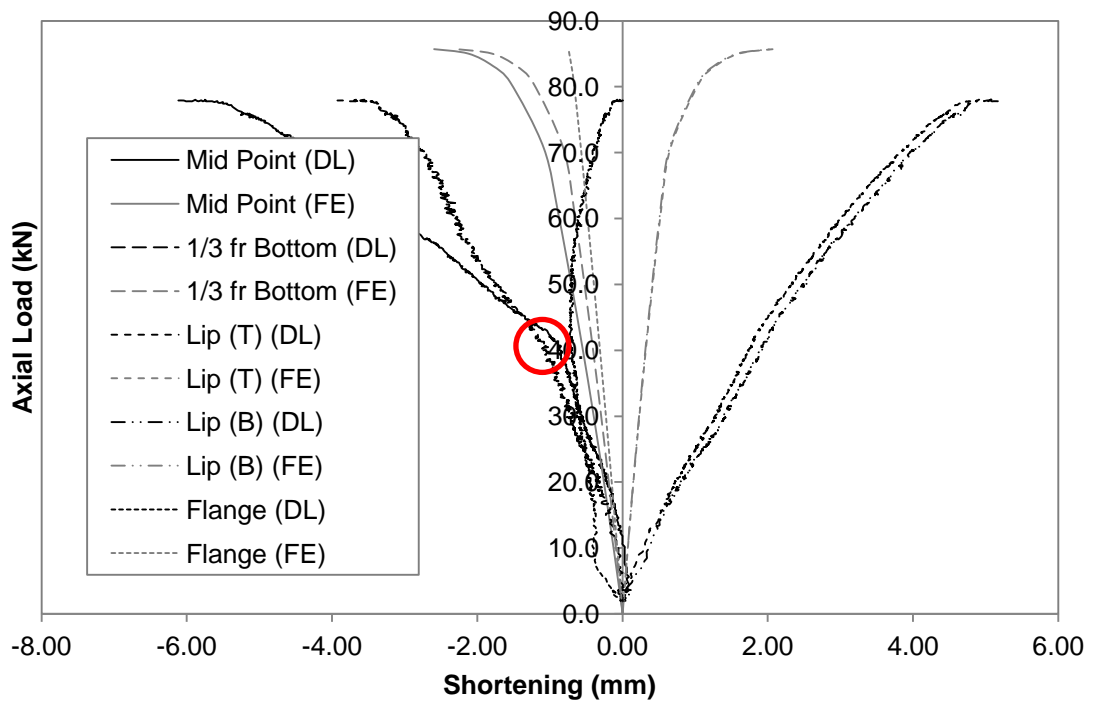


Figure E.20 Axial Load versus Deformation Curve for C90L500-3

E.3 Intermediate Column

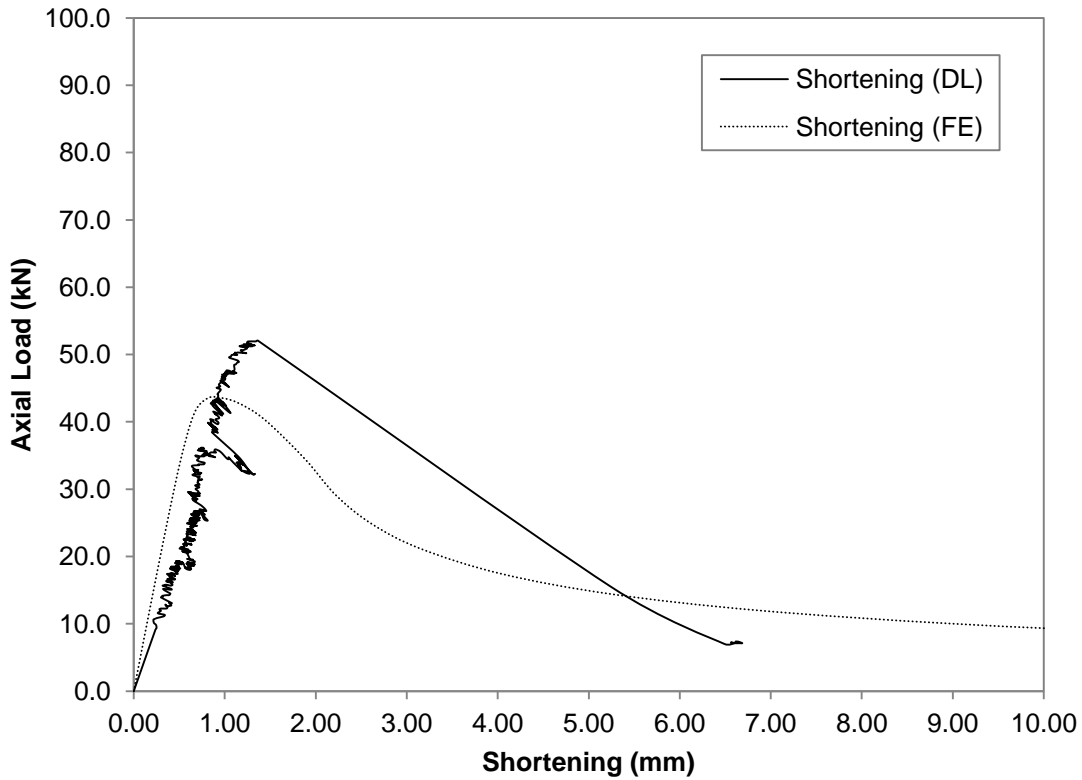


Figure E.21 Axial Load versus Shortening Curve for C75L500-2

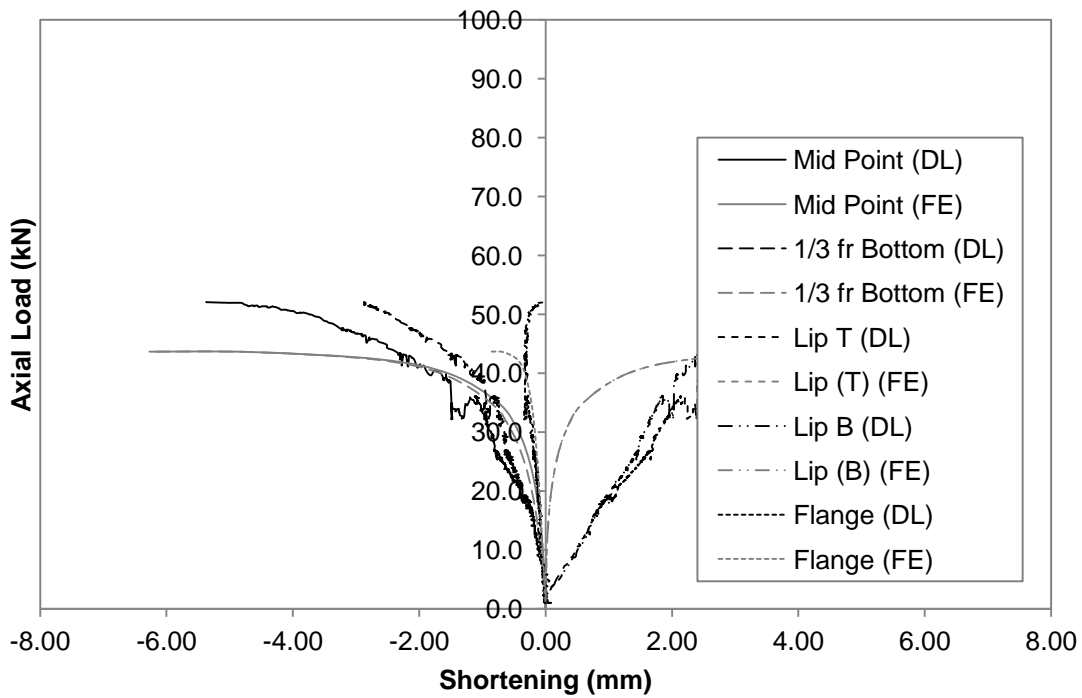


Figure E.22 Axial Load versus Deformation Curve for C75L500-2

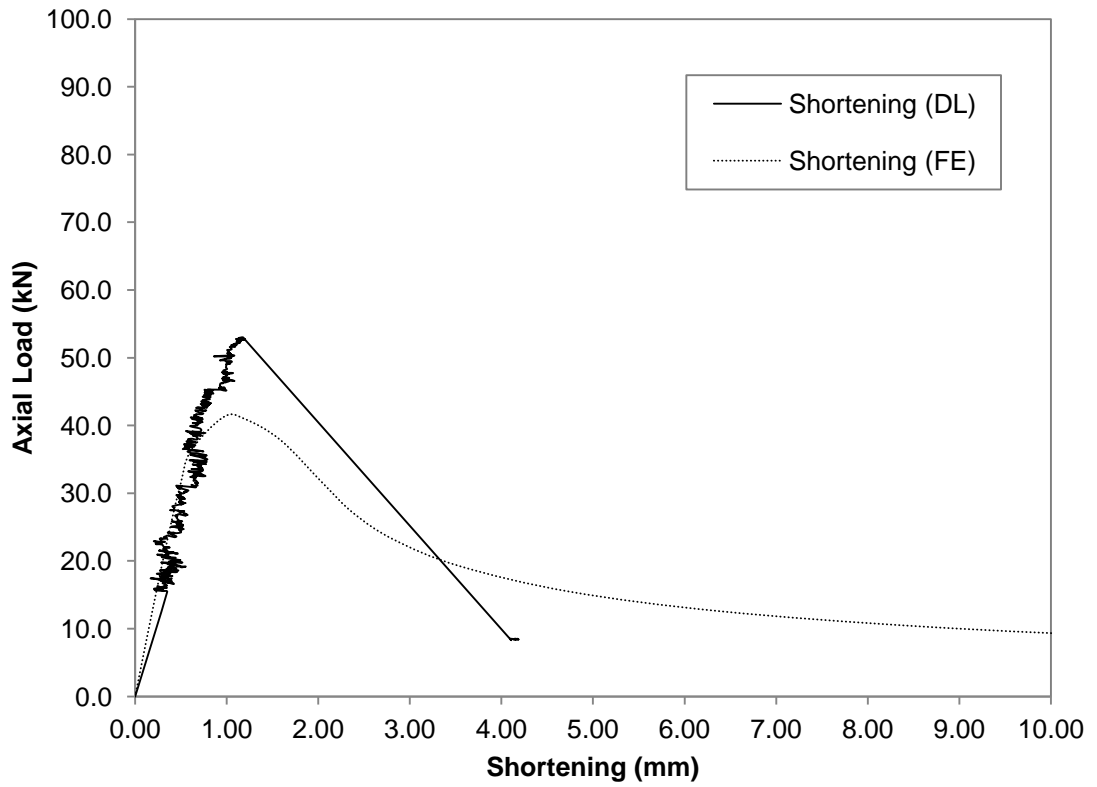


Figure E.23 Axial Load versus Shortening Curve for C75L500-3

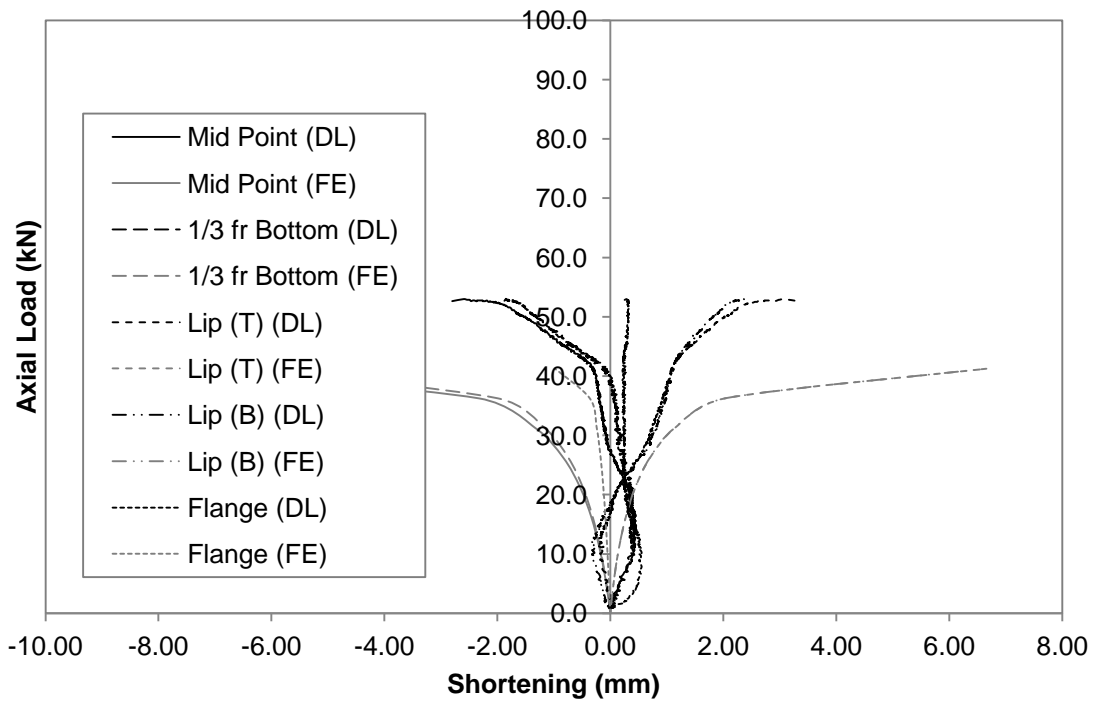


Figure E.24 Axial Load versus Deformation Curve for C75L500-3

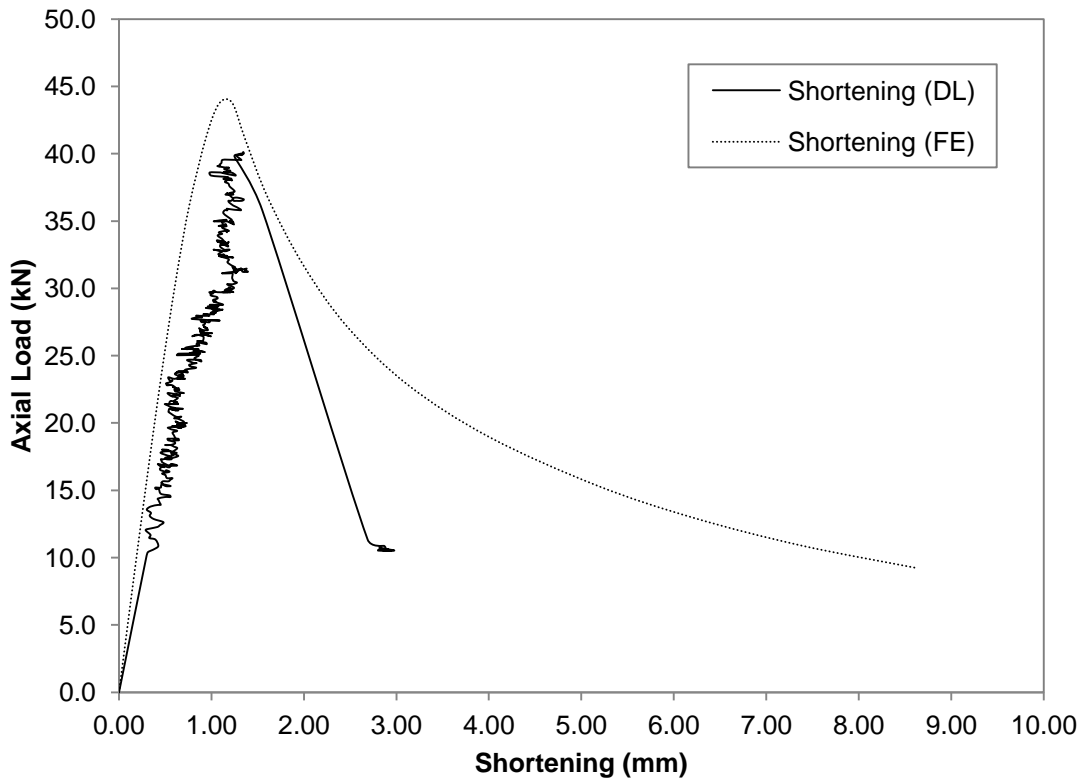


Figure E.25 Axial Load versus Shortening Curve for C75L500-4

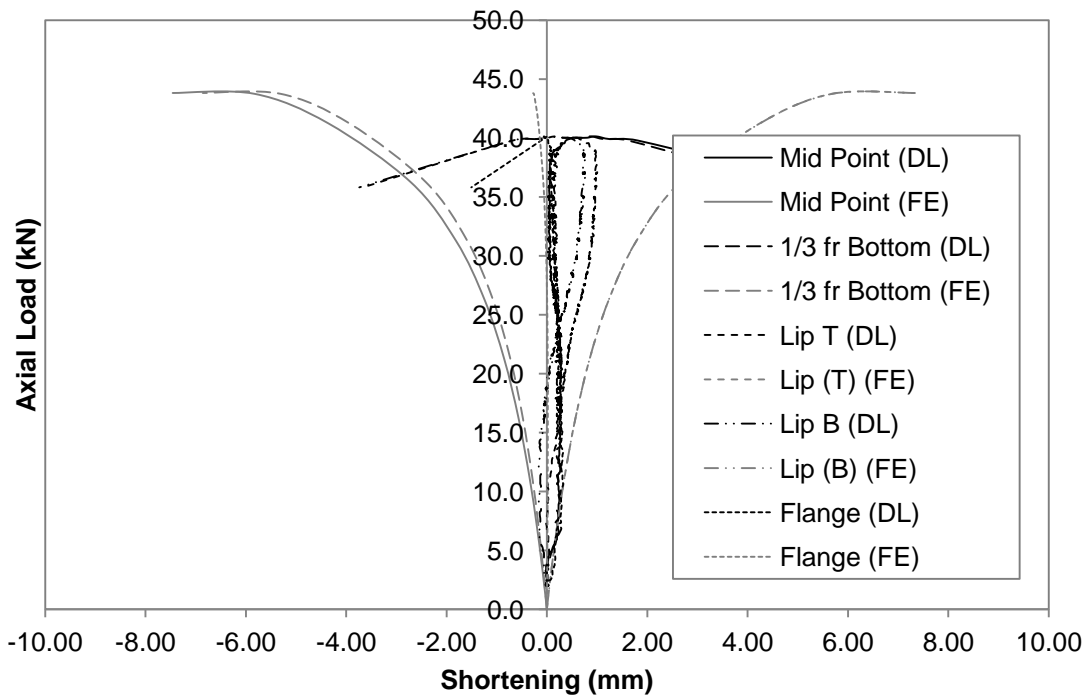


Figure E.26 Axial Load versus Deformation Curve for C75L500-4

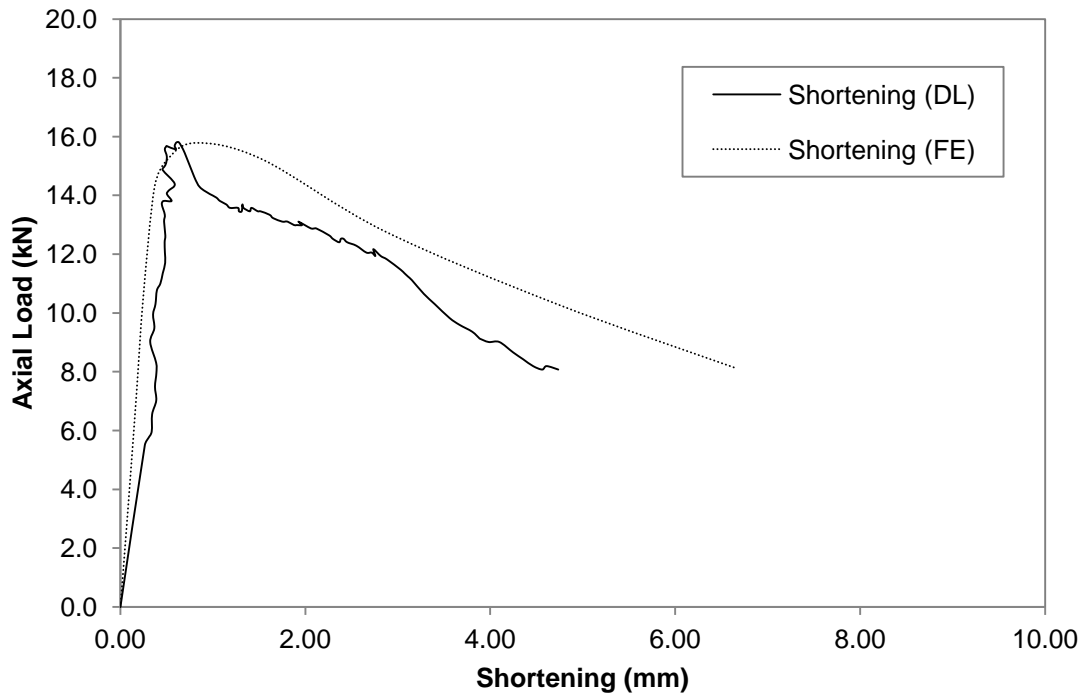


Figure E.27 Axial Load versus Shortening Curve for C75L1000-1

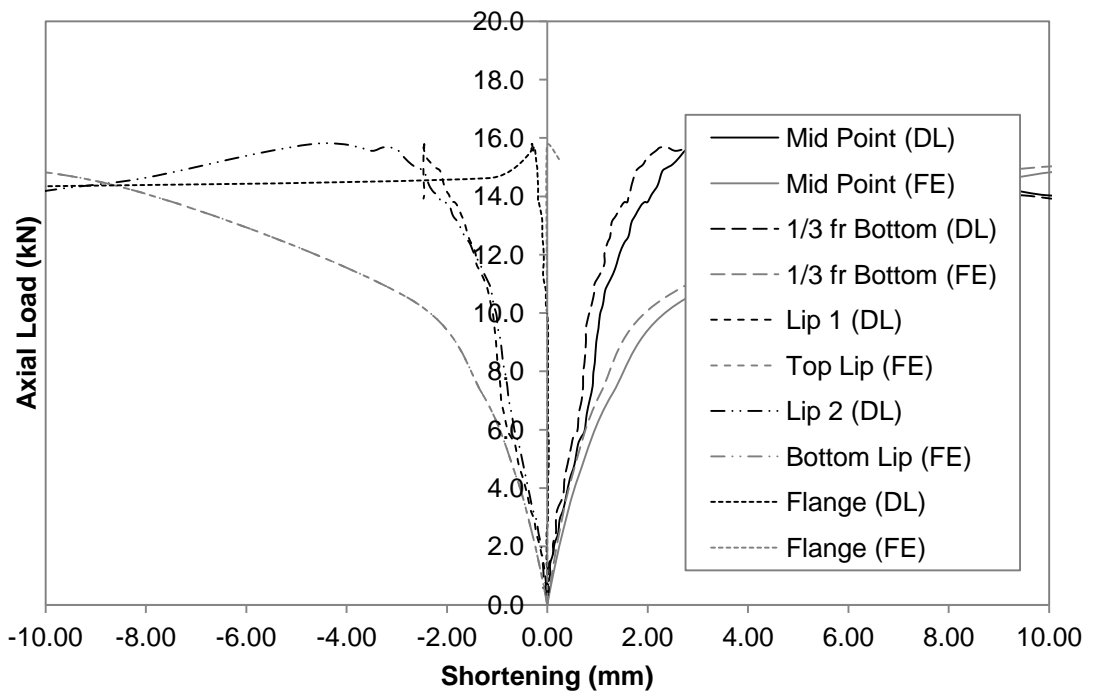


Figure E.28 Axial Load versus Deformation Curve for C75L1000-1

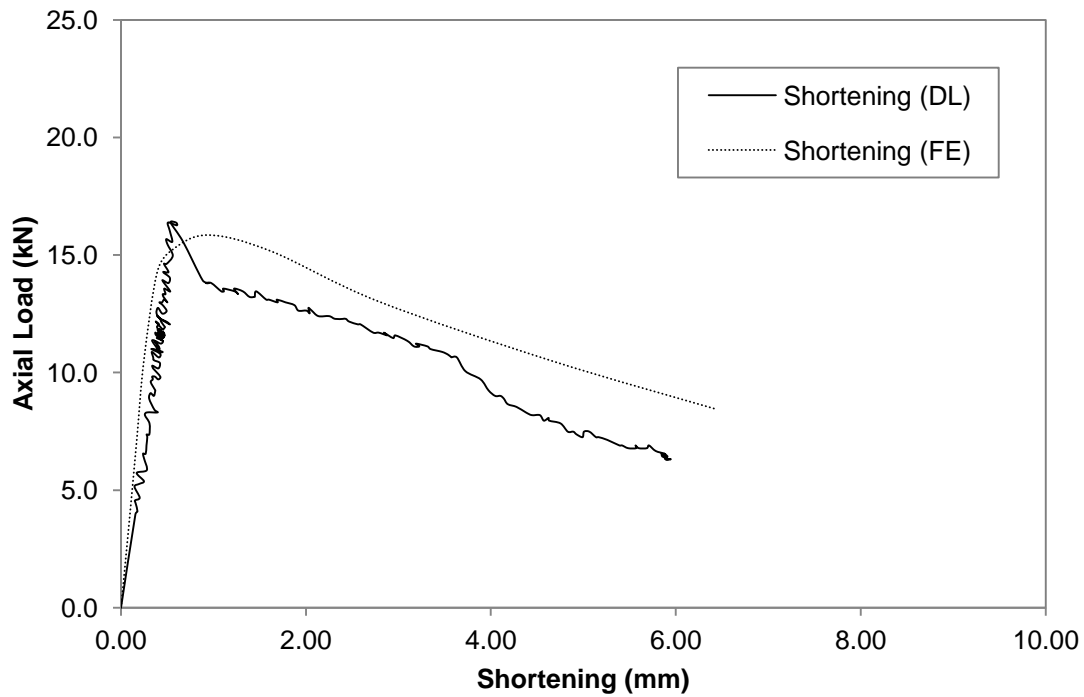


Figure E.29 Axial Load versus Shortening Curve for C75L1000-2

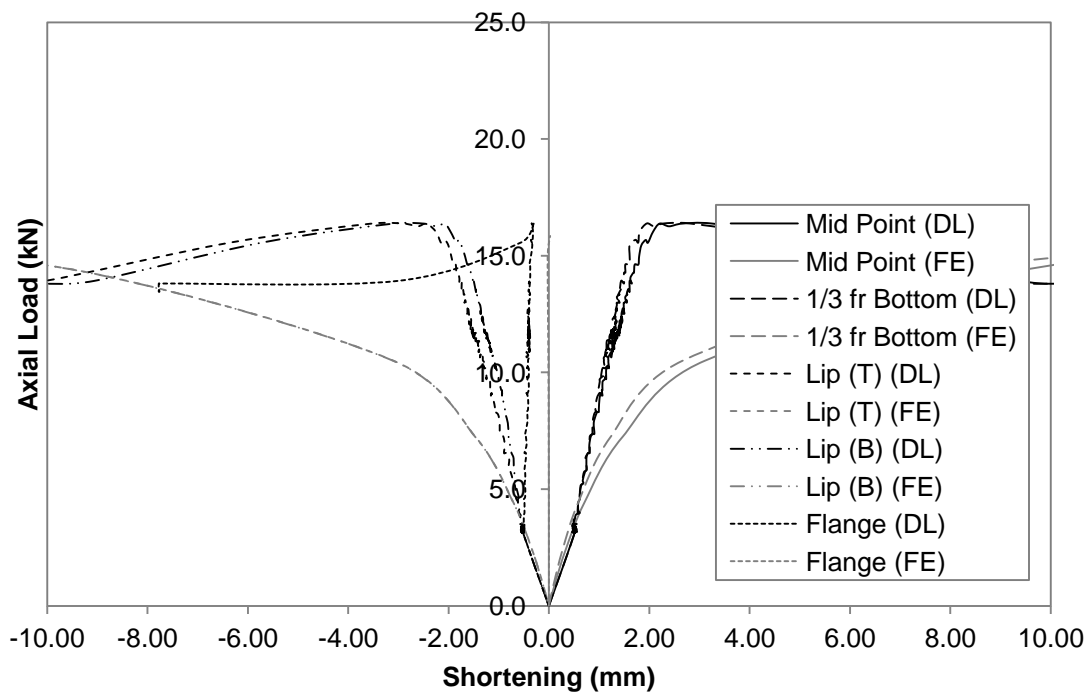


Figure E.30 Axial Load versus Deformation Curve for C75L1000-2

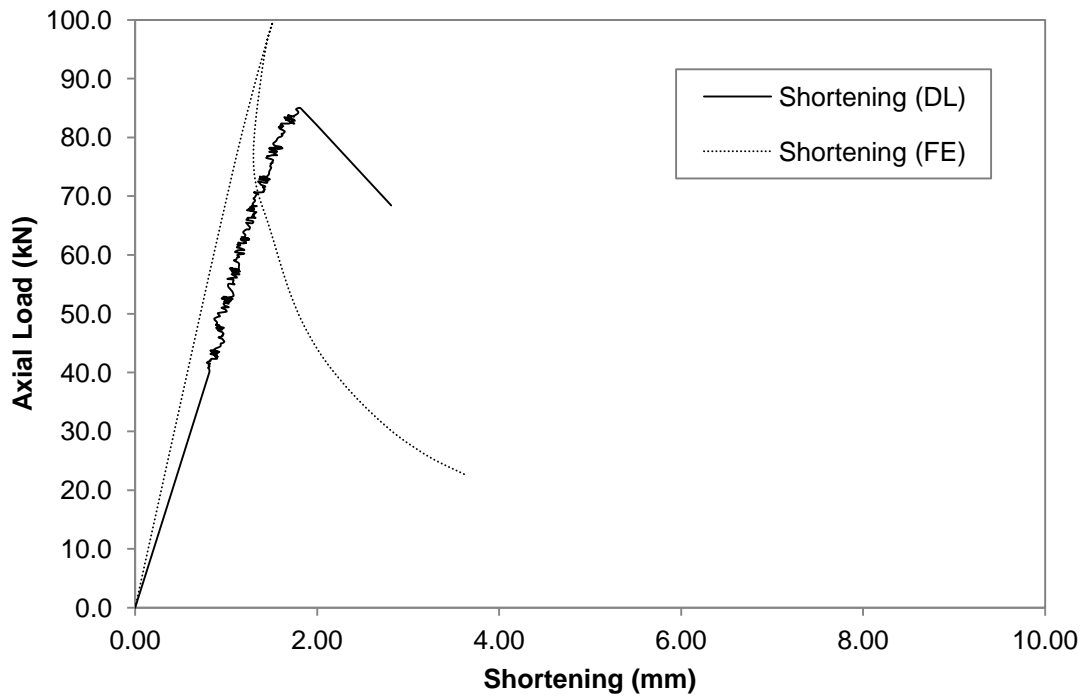


Figure E.31 Axial Load versus Shortening Curve for C90L1000-1

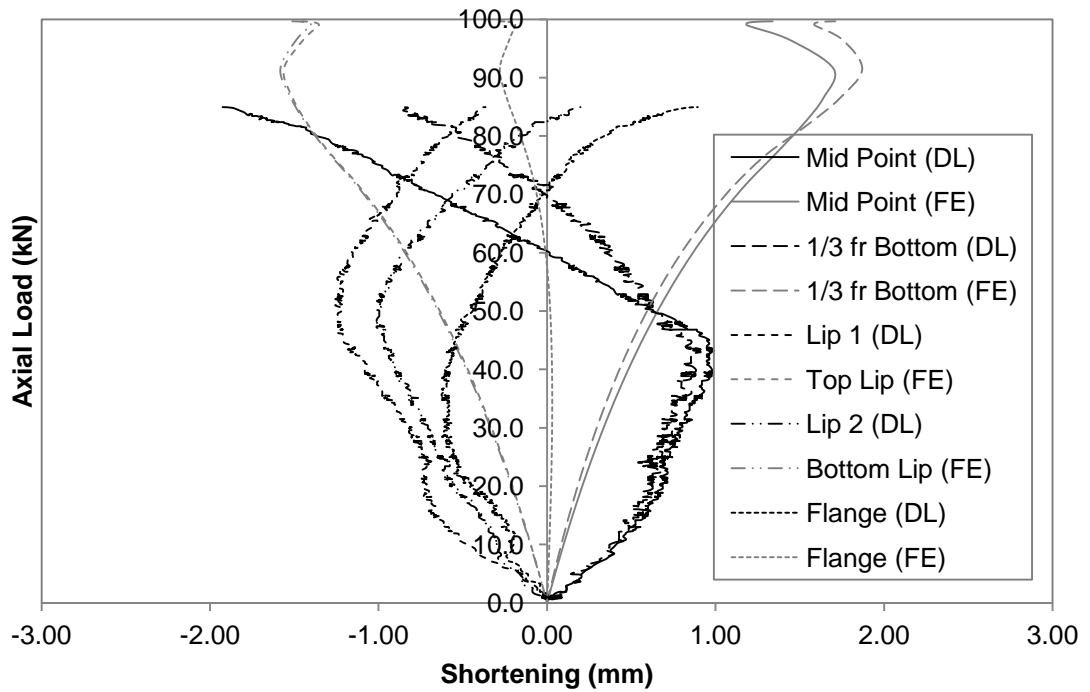


Figure E.32 Axial Load versus Deformation Curve for C90L1000-1

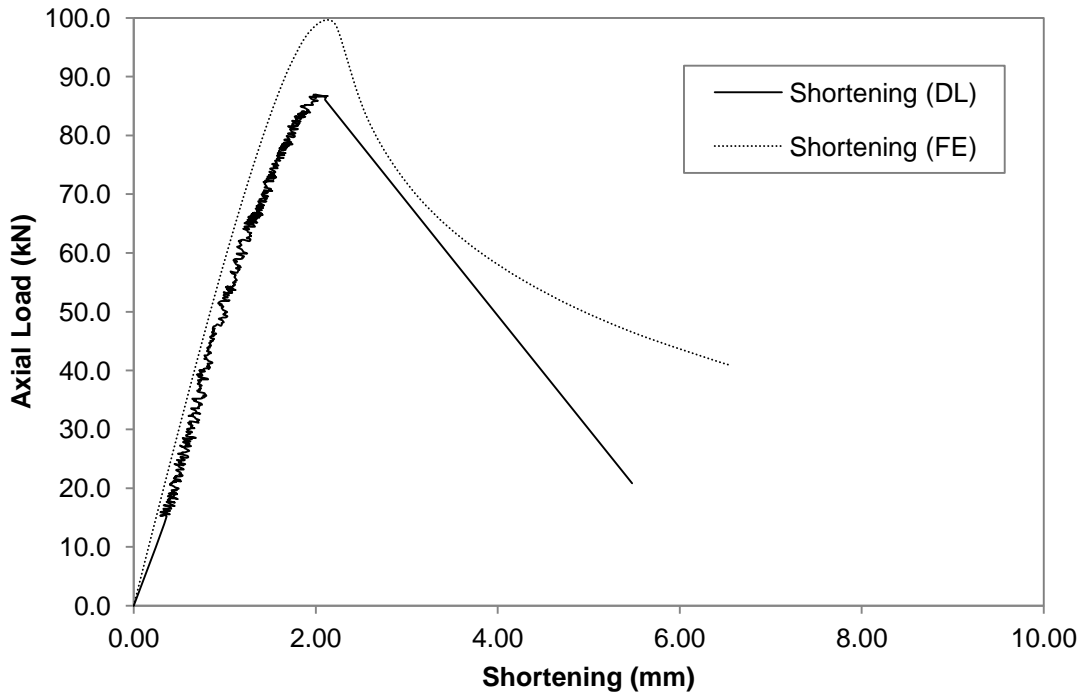


Figure E.33 Axial Load versus Shortening Curve for C90L1000-2

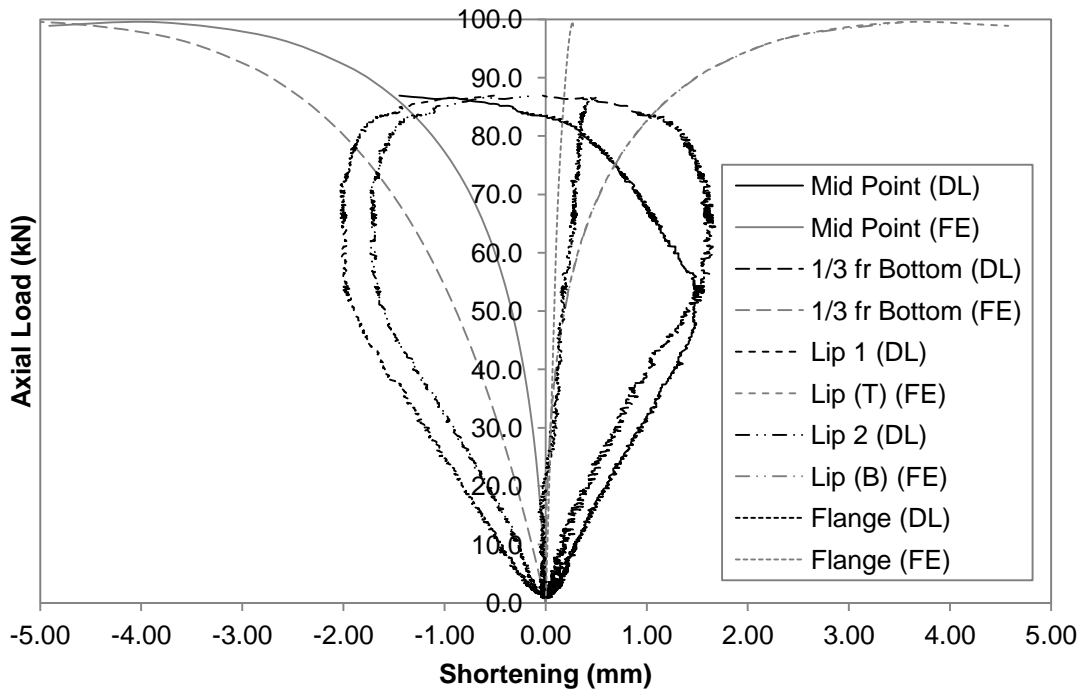


Figure E.34 Axial Load versus Deformation Curve for C90L1000-2

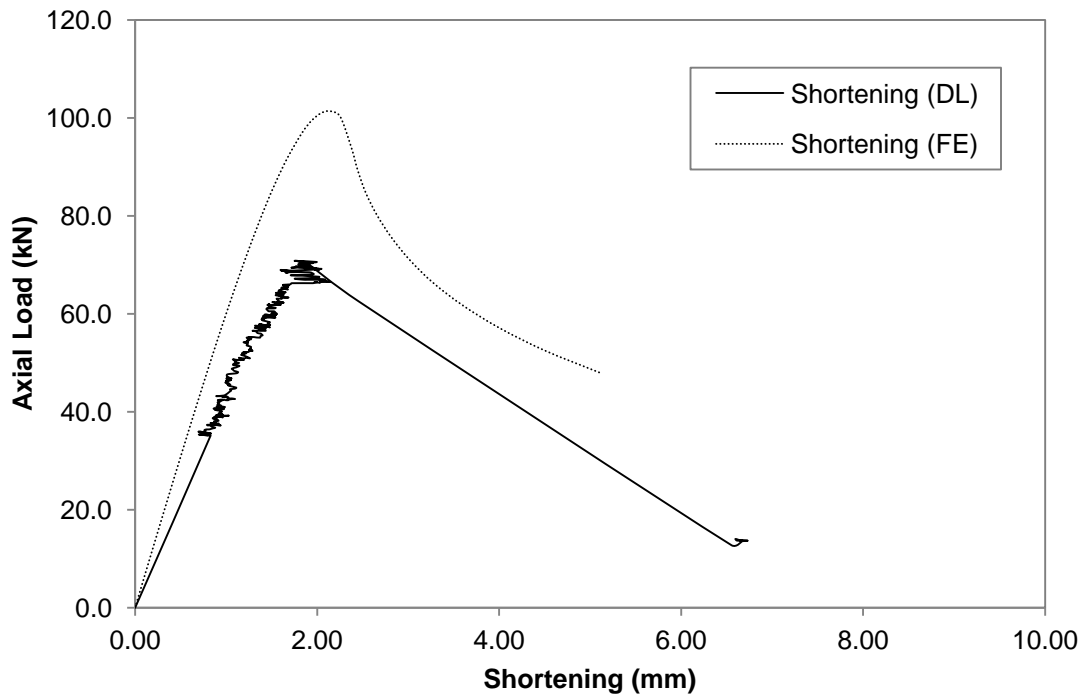


Figure E.35 Axial Load versus Shortening Curve for C90L1000-3

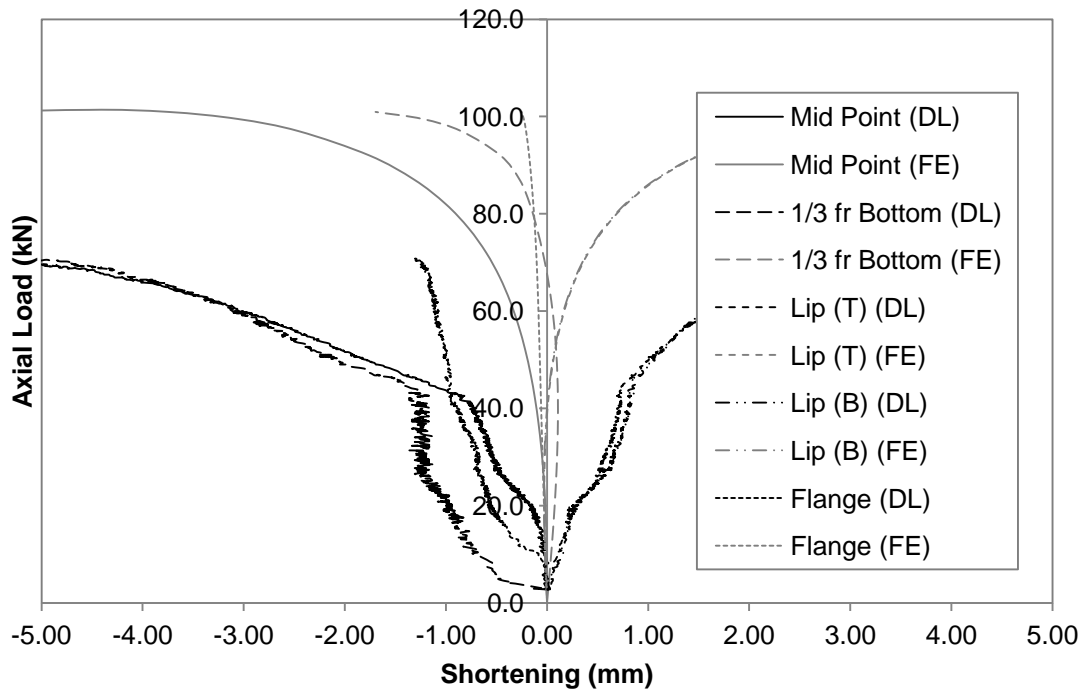


Figure E.36 Axial Load versus Deformation Curve for C90L1000-3

E.4 Slender Column

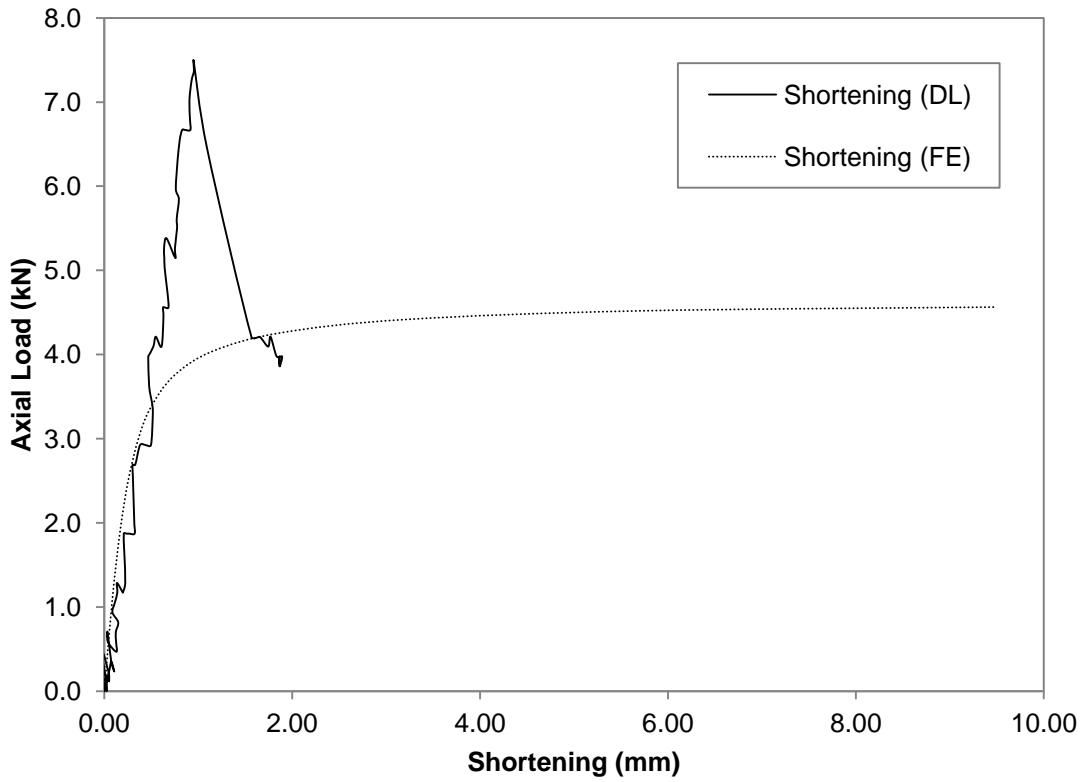


Figure E.37 Axial Load versus Shortening Curve for C75L2000-1

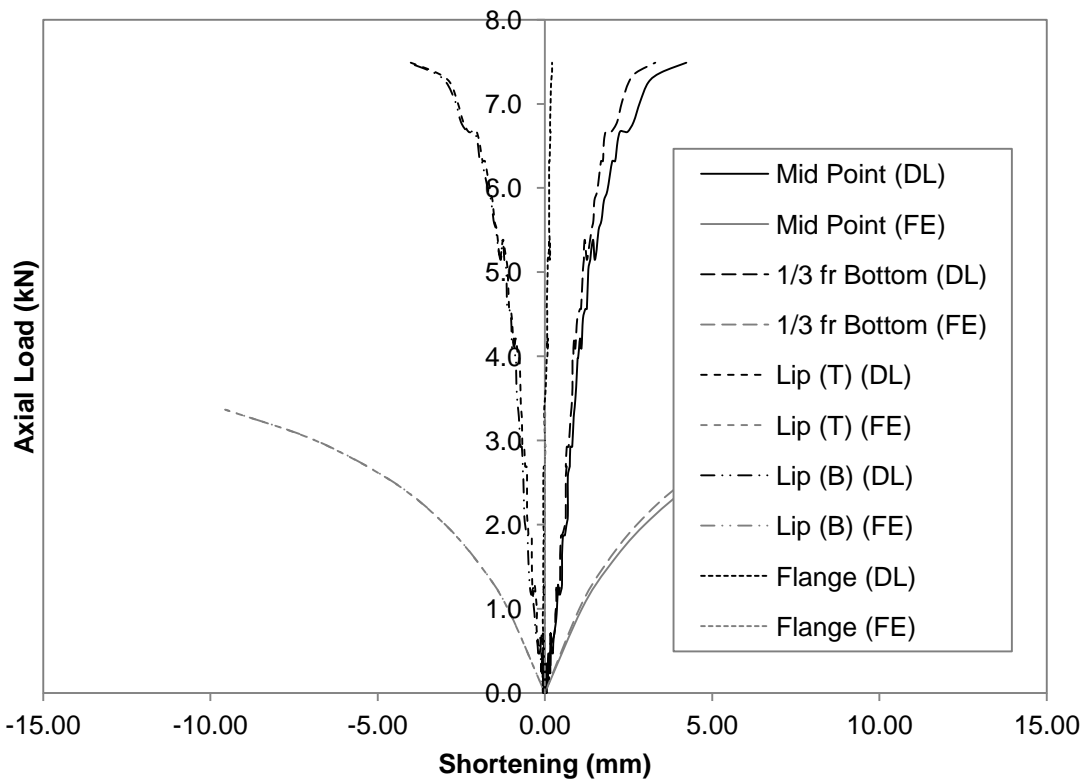


Figure E.38 Axial Load versus Deformation Curve for C75L2000-1

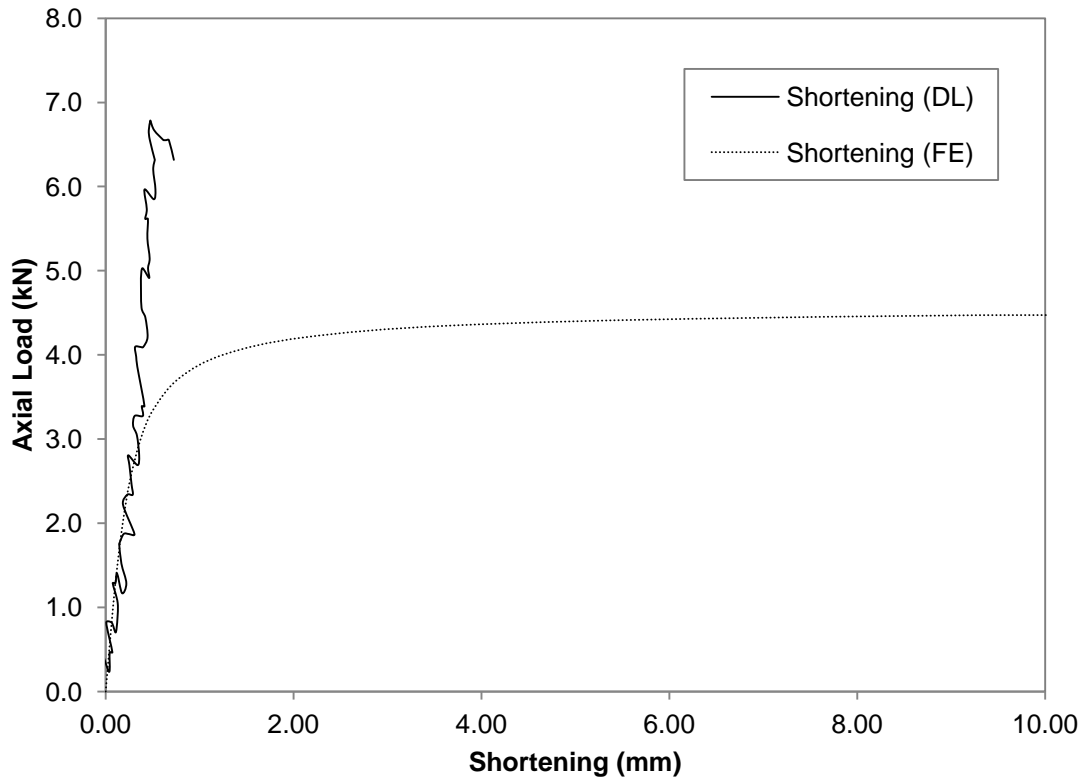


Figure E.39 Axial Load versus Shortening Curve for C75L2000-2

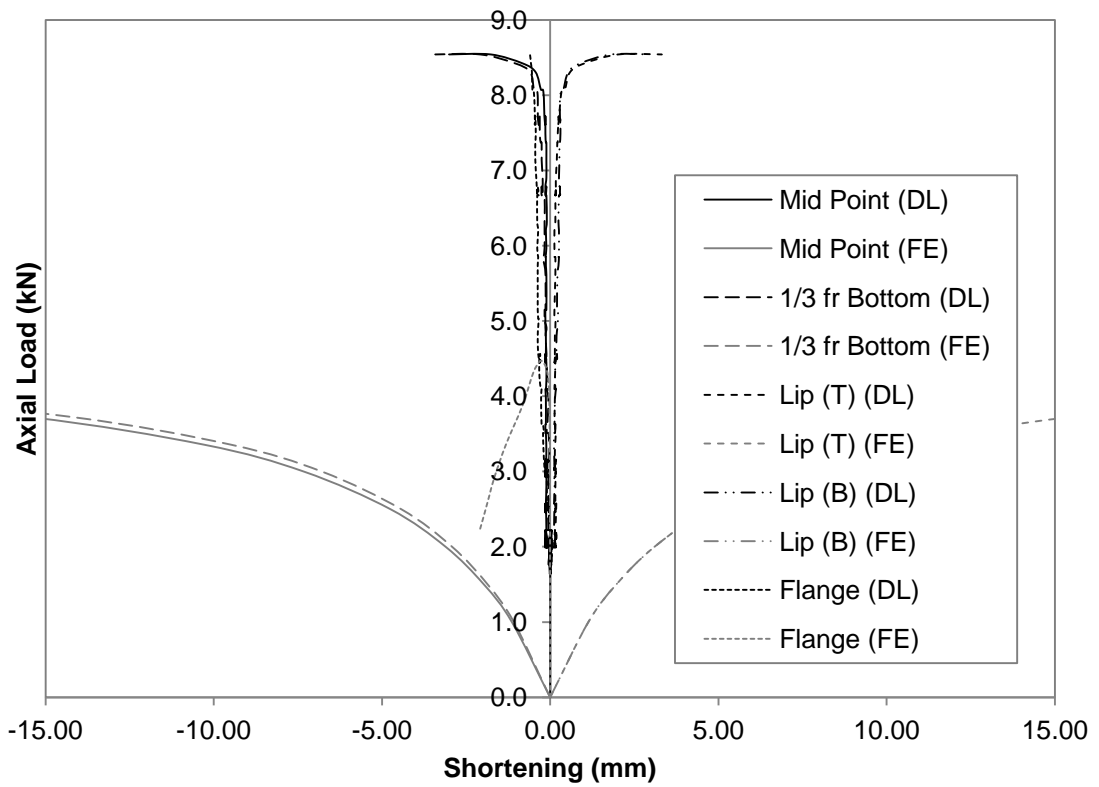


Figure E.40 Axial Load versus Deformation Curve for C75L2000-2

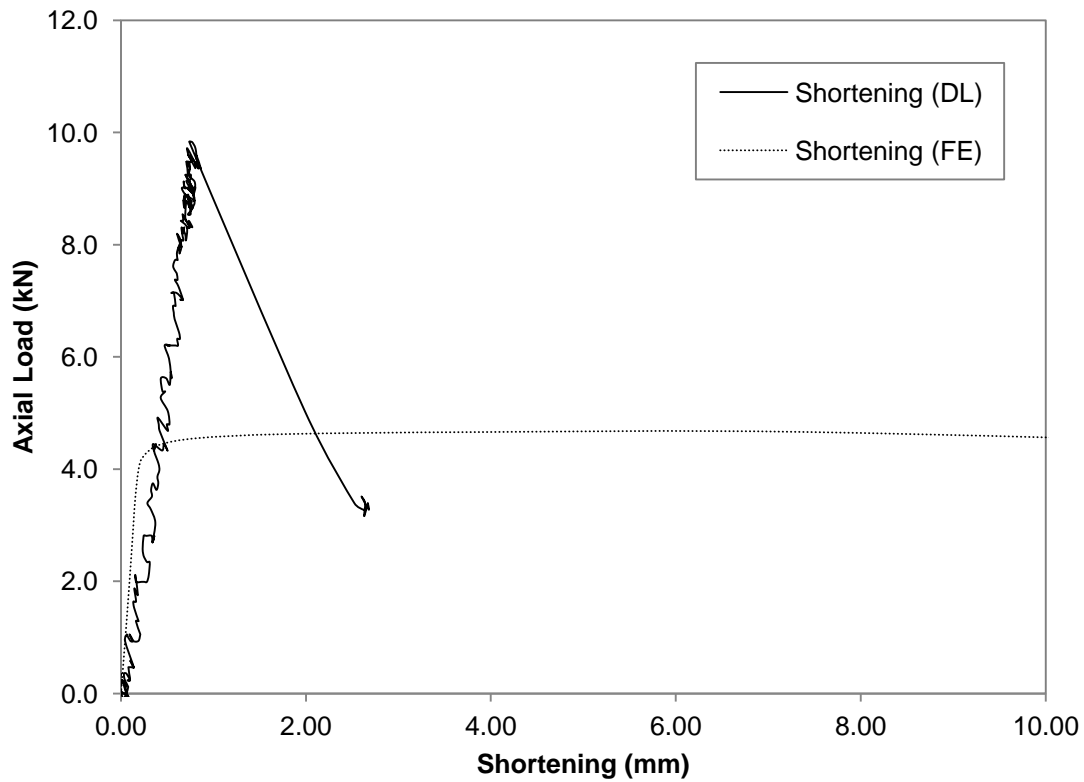


Figure E.41 Axial Load versus Shortening Curve for C75L2000-3

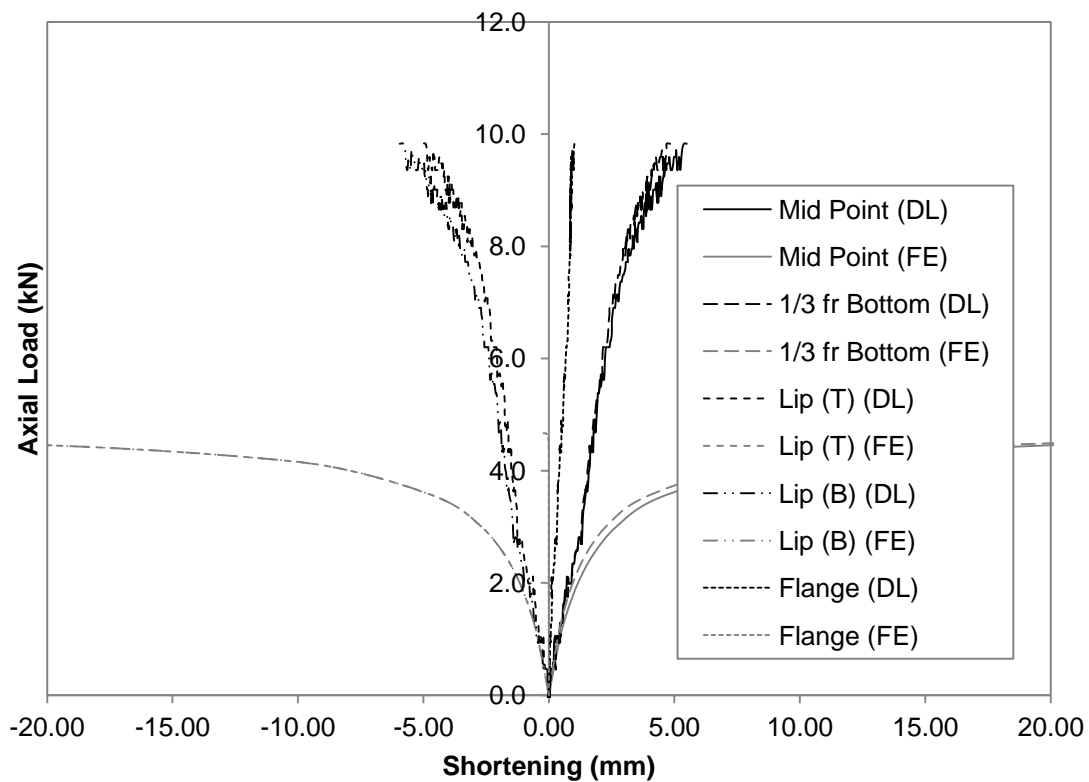


Figure E.42 Axial Load versus Deformation Curve for C75L2000-3

F. Results for Plain Built-up Back-to-back C-channels

F.1 Stub Column

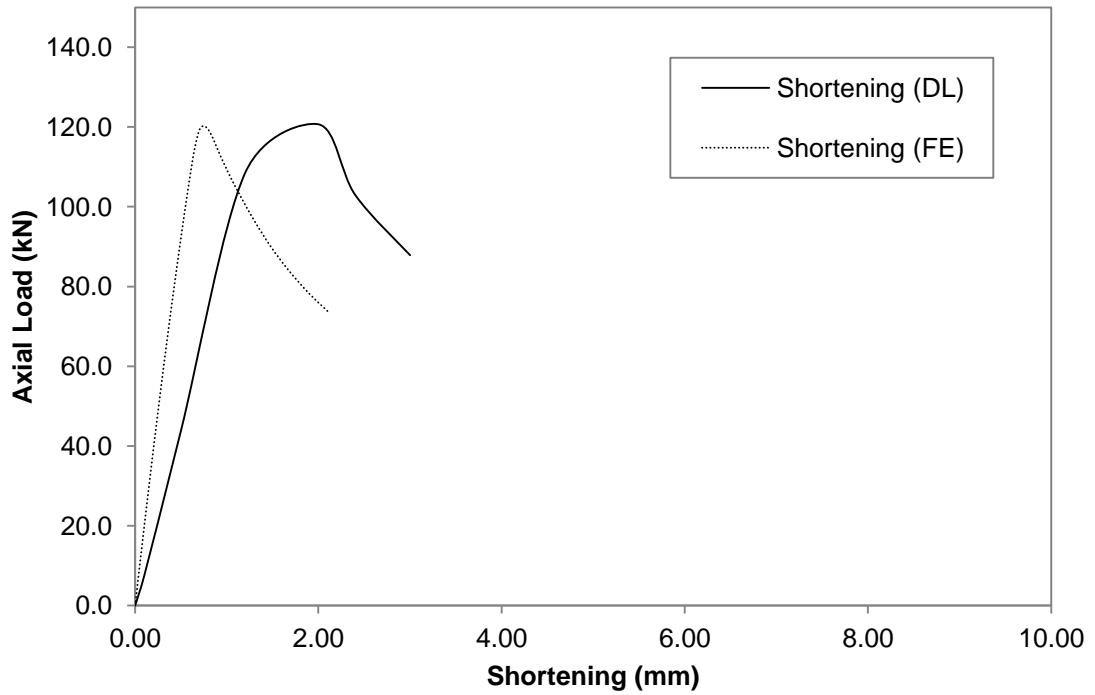


Figure F.1 Axial Load versus Shortening Curve for BU75S50L300-1

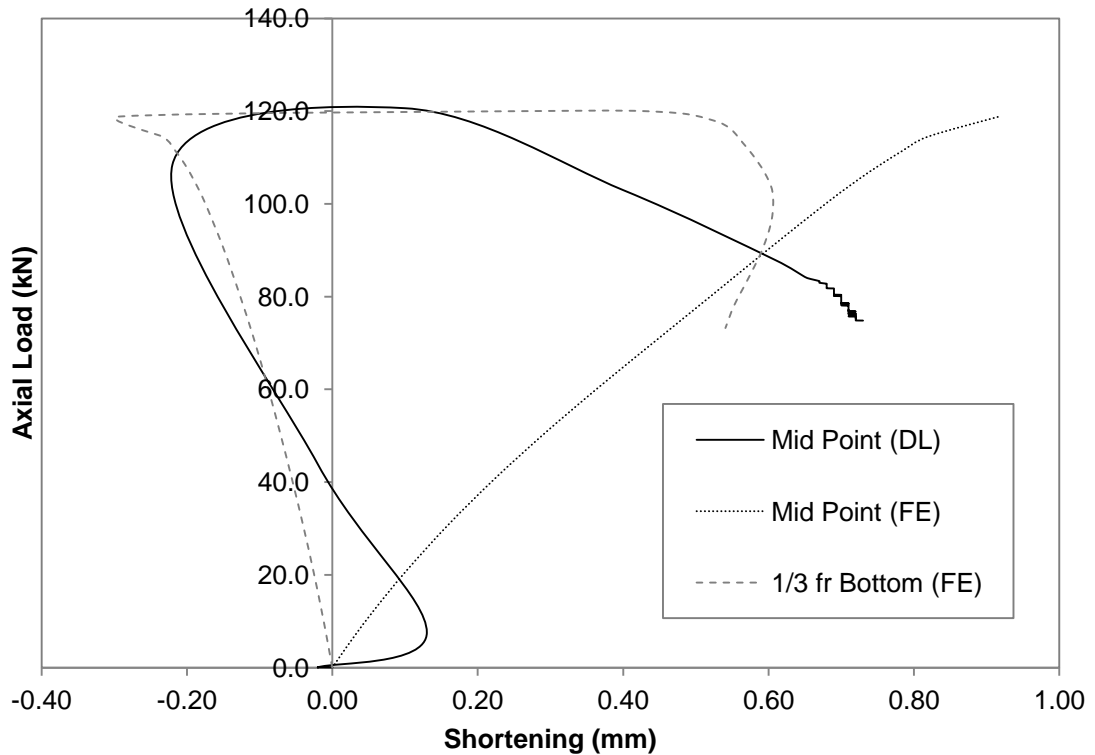


Figure F.2 Axial Load versus Deformation Curve for BU75S50L300-1

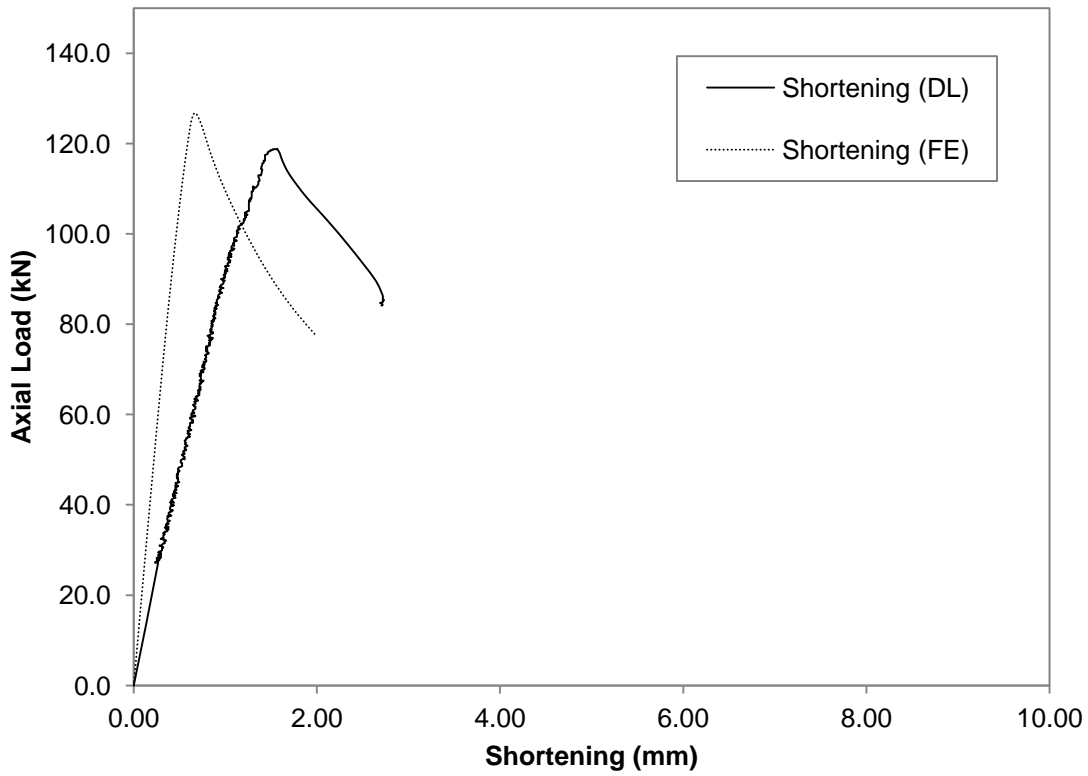


Figure F.3 Axial Load versus Shortening Curve for BU75S50L300-2

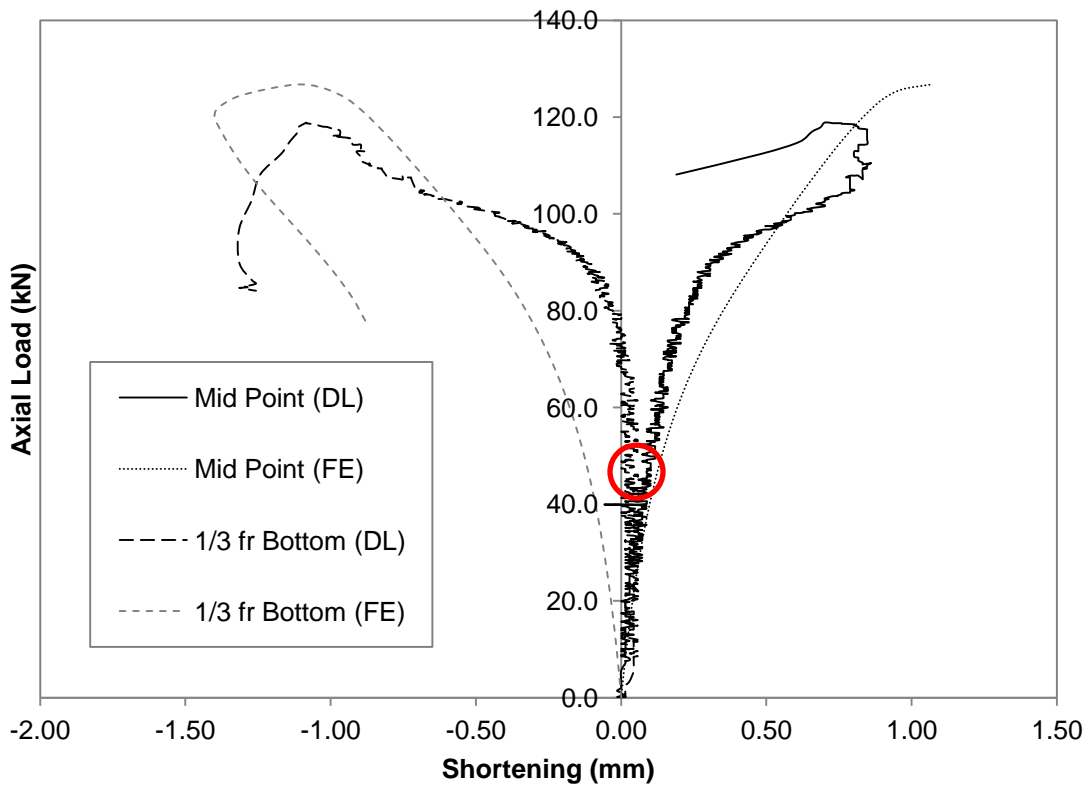


Figure F.4 Axial Load versus Deformation Curve for BU75S50L300-2

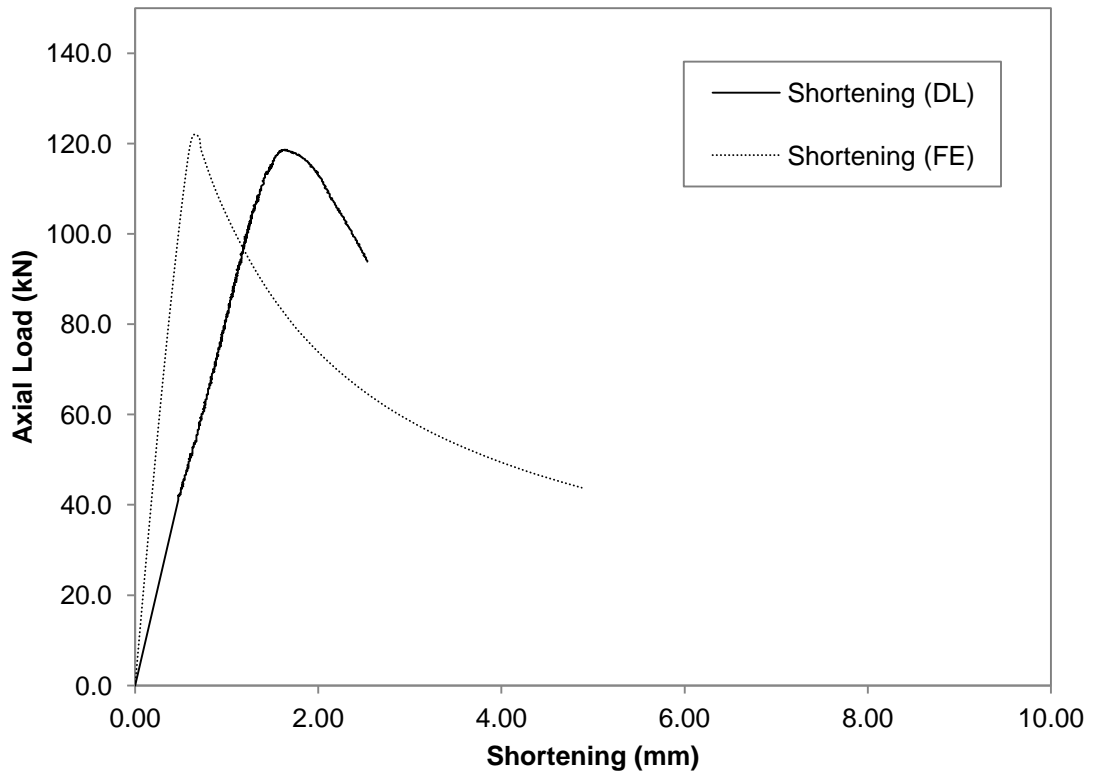


Figure F.5 Axial Load versus Shortening Curve for BU75S50L300-3

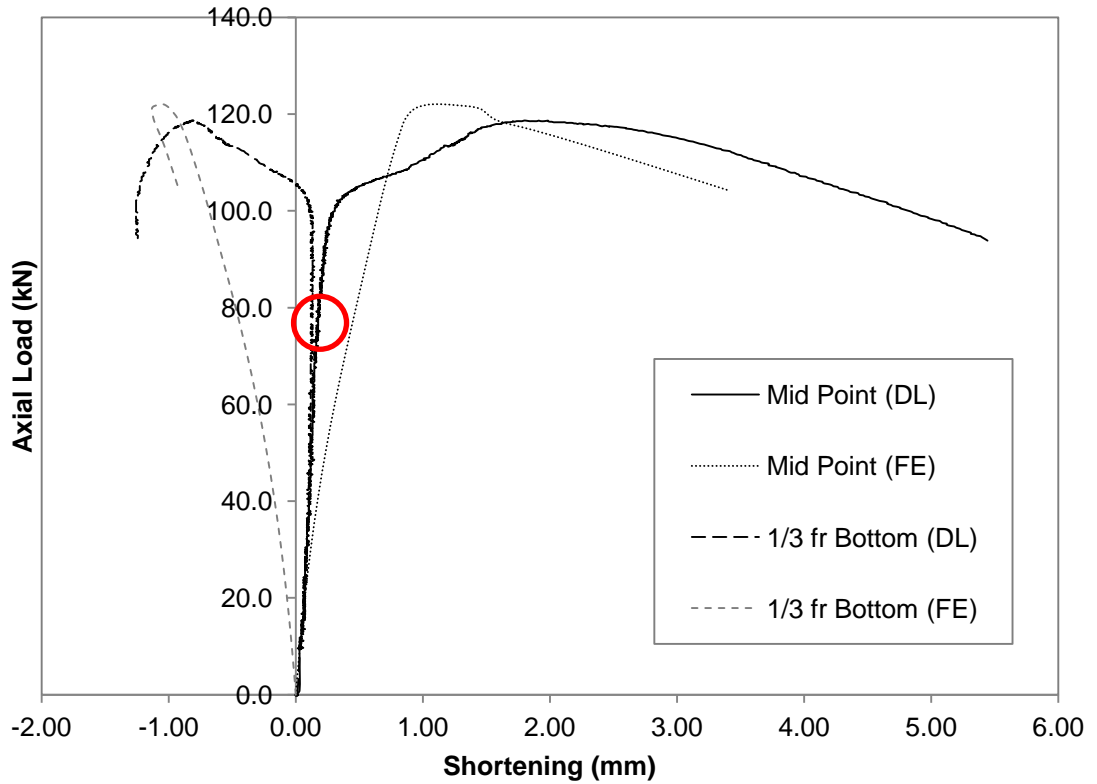


Figure F.6 Axial Load versus Deformation Curve for BU75S50L300-3

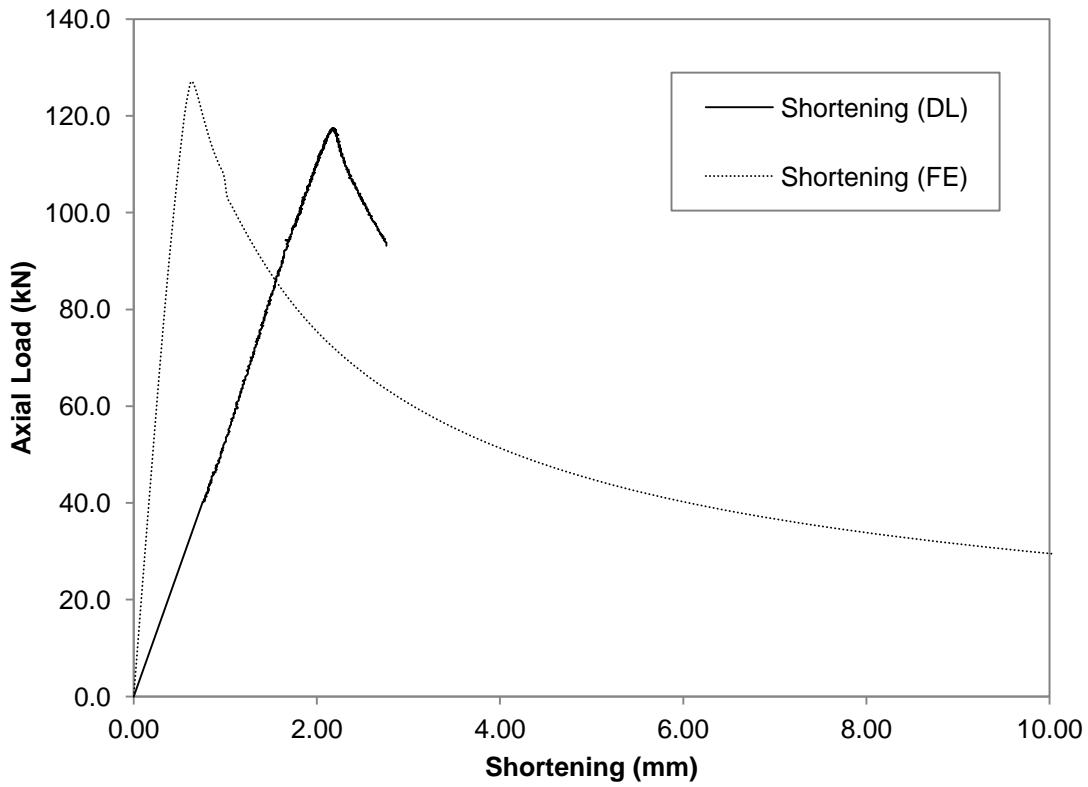


Figure F.7 Axial Load versus Shortening Curve for BU75S100L300-2

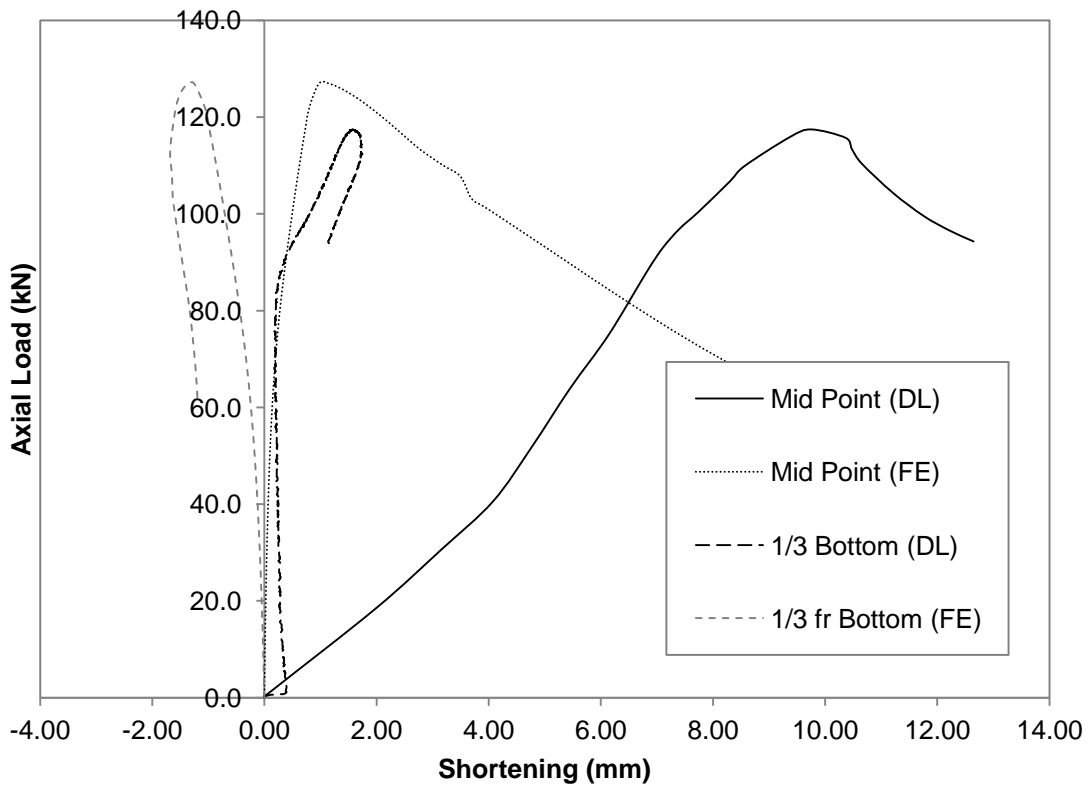


Figure F.8 Axial Load versus Deformation Curve for BU75S100L300-2

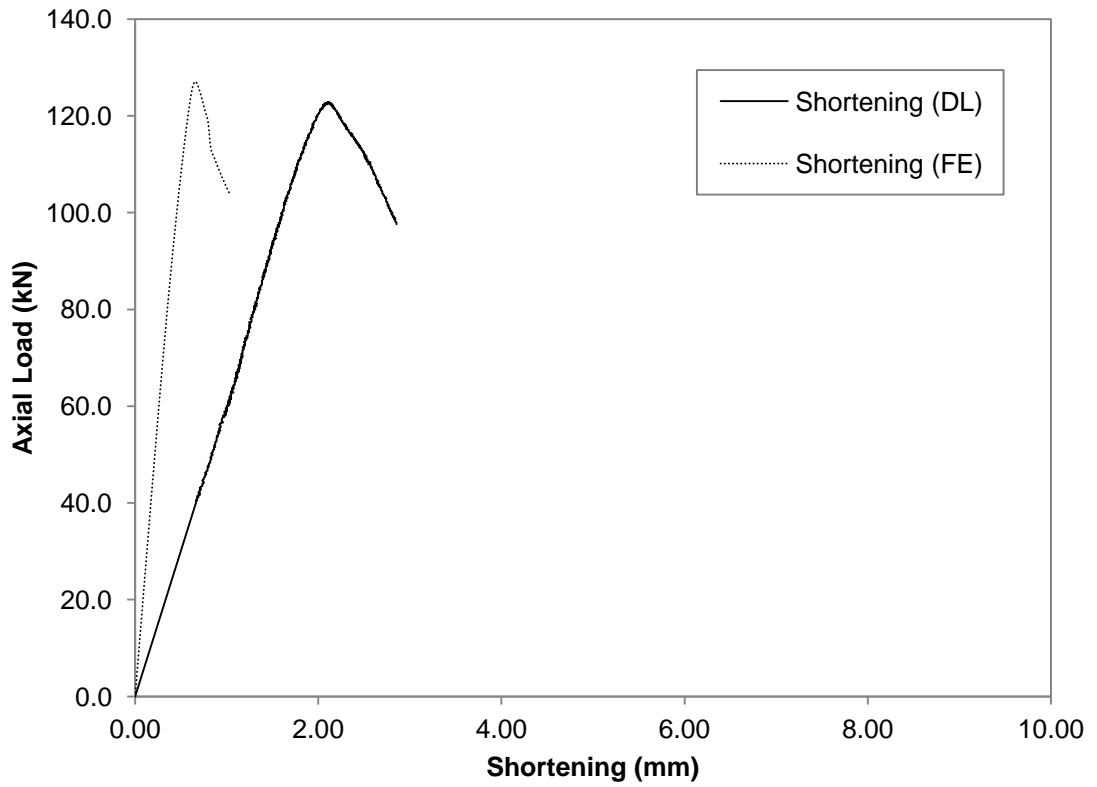


Figure F.9 Axial Load versus Shortening Curve for BU75S100L300-3

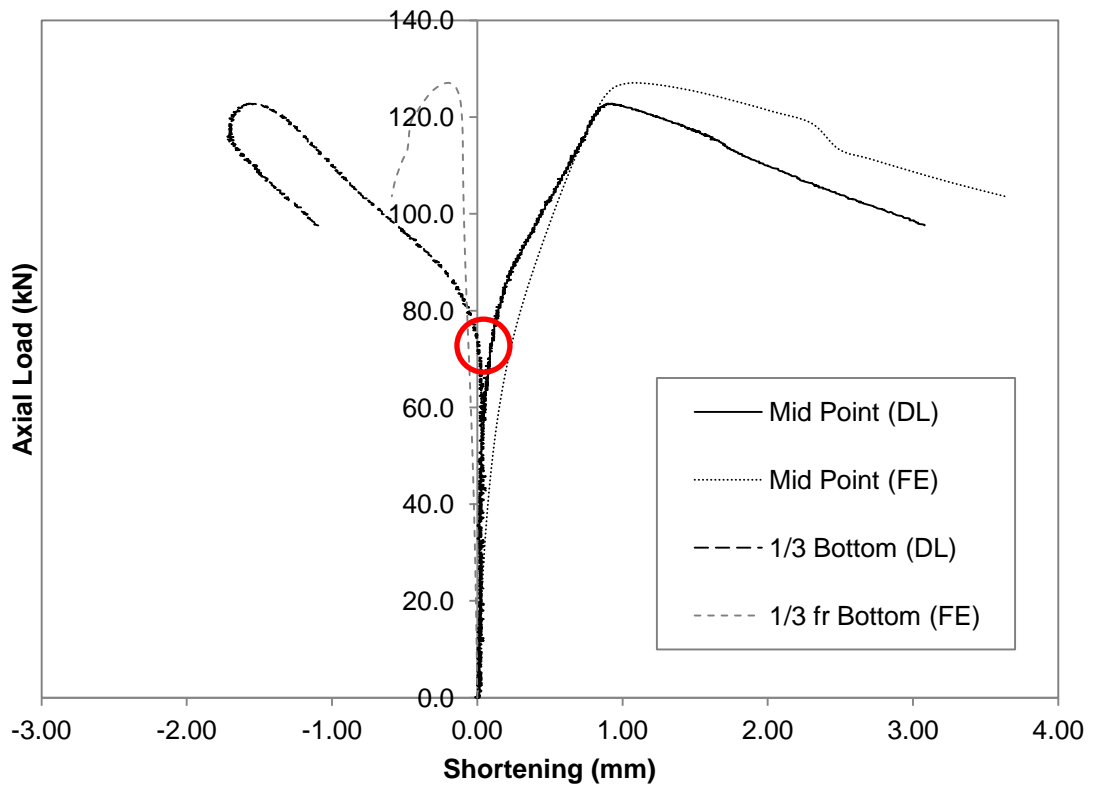


Figure F.10 Axial Load versus Deformation Curve for BU75S100L300-3

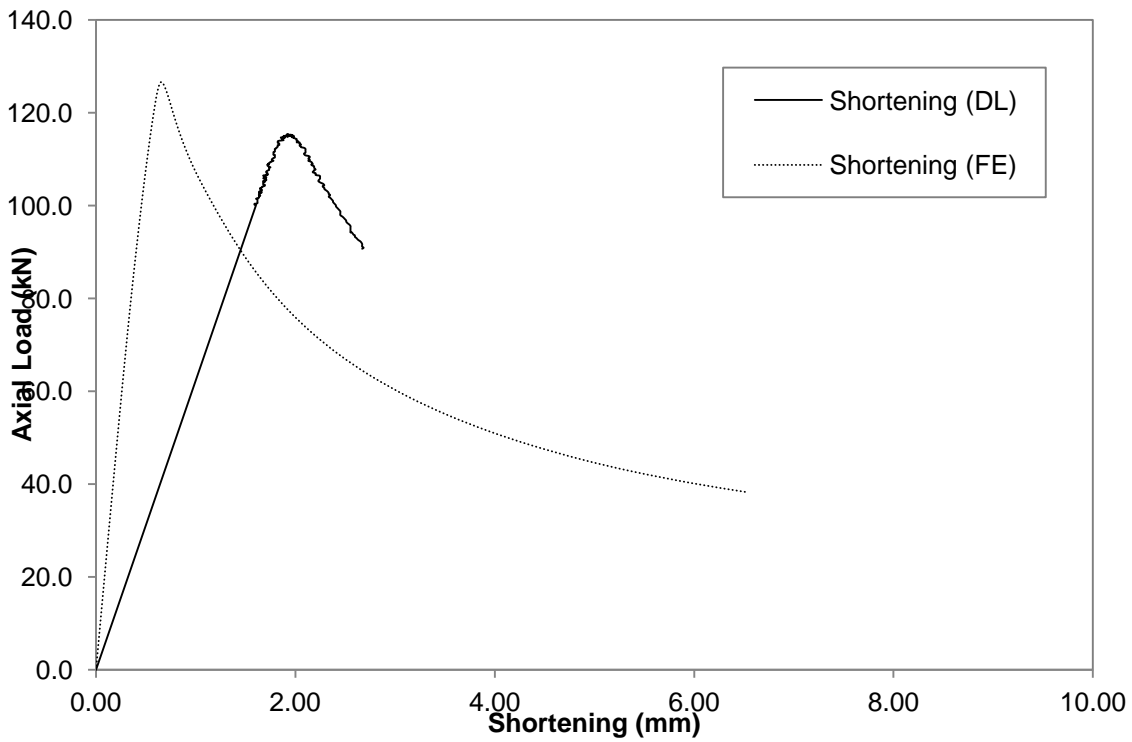


Figure F.11 Axial Load versus Shortening Curve for BU75S100L300-4

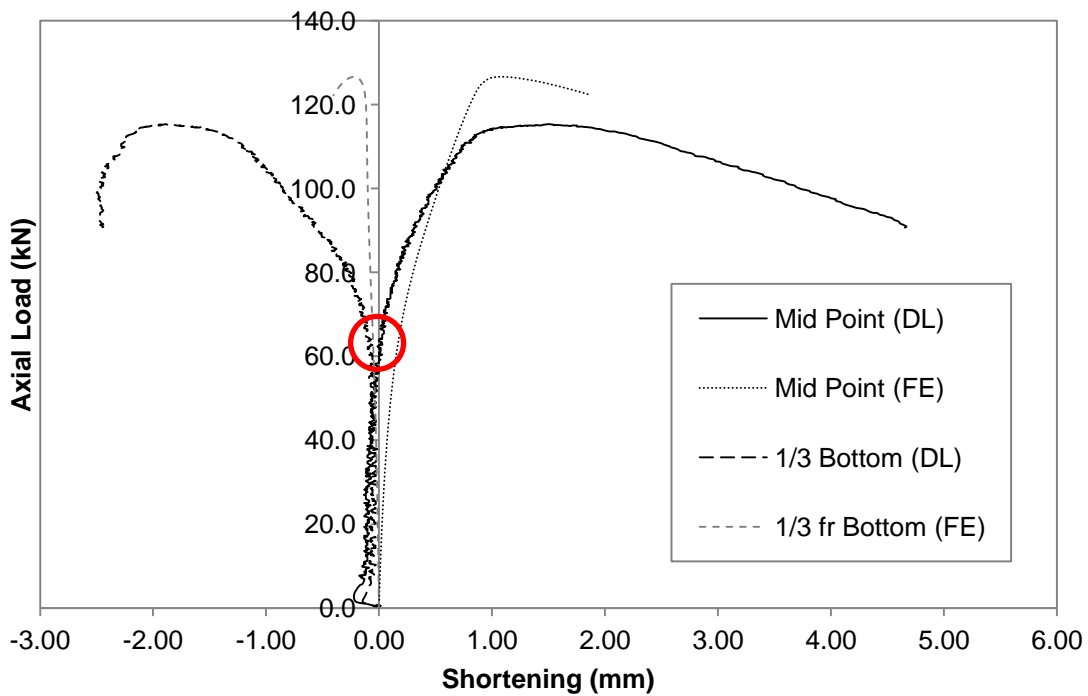


Figure F.12 Axial Load versus Deformation Curve for BU75S100L300-4

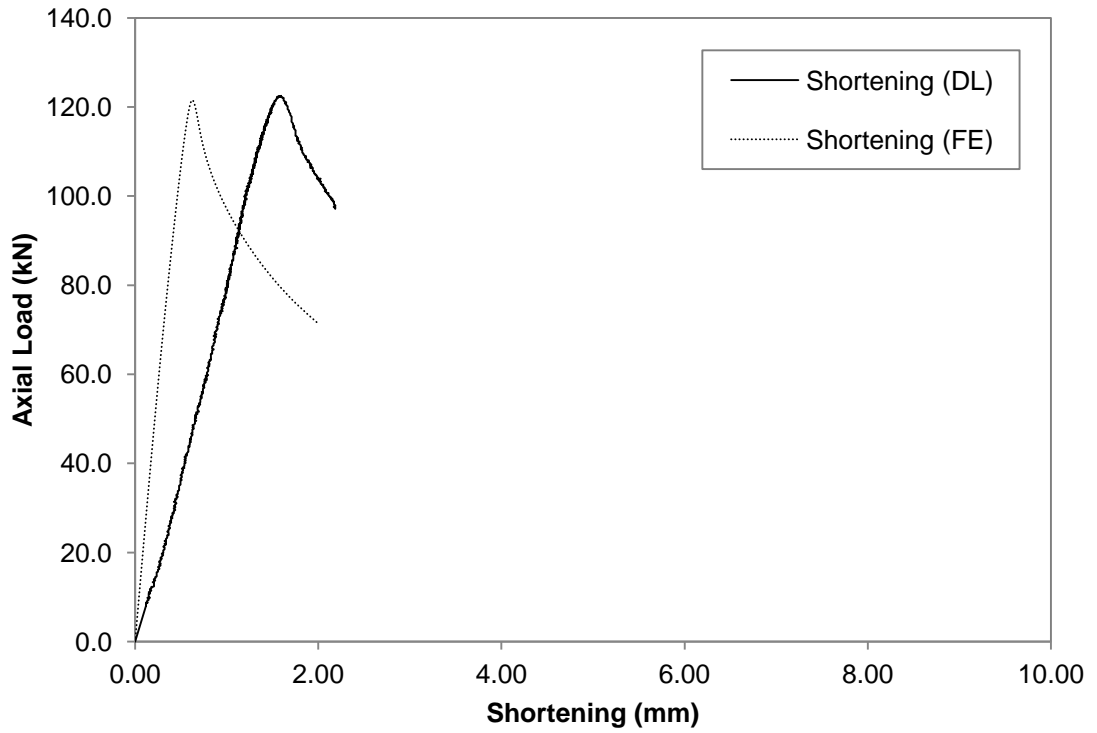


Figure F.13 Axial Load versus Shortening Curve for BU75S200L300-1

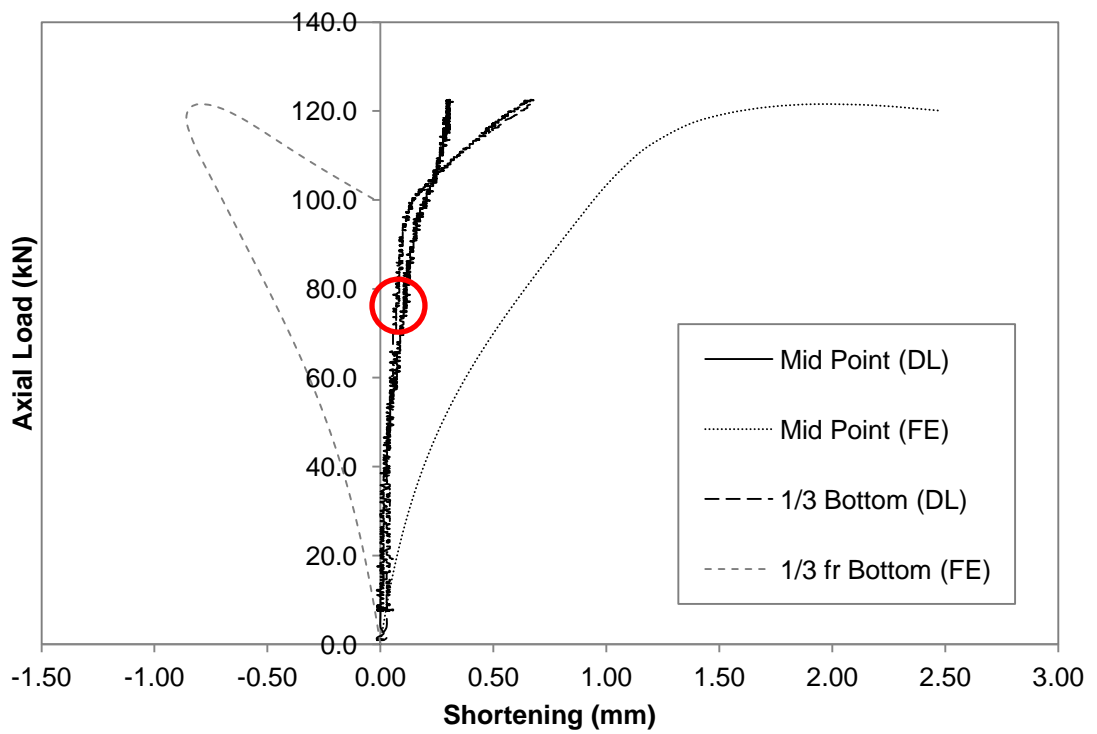


Figure F.14 Axial Load versus Deformation Curve for BU75S200L300-1

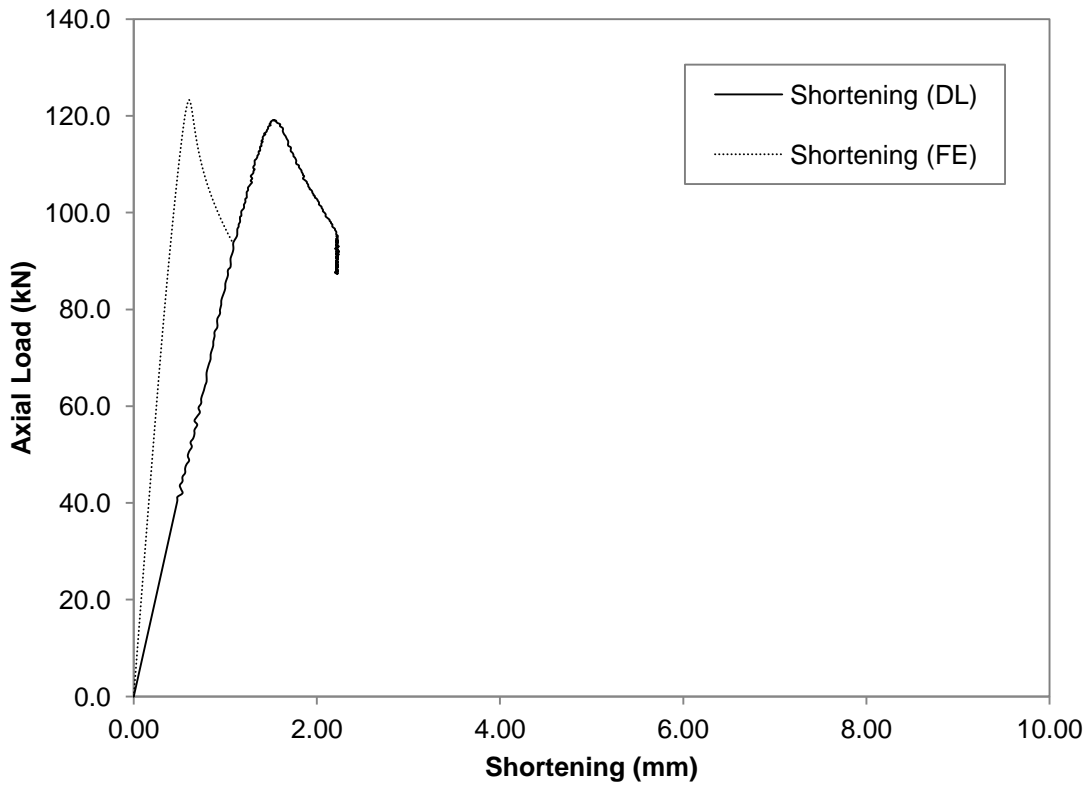


Figure F.15 Axial Load versus Shortening Curve for BU75S200L300-2

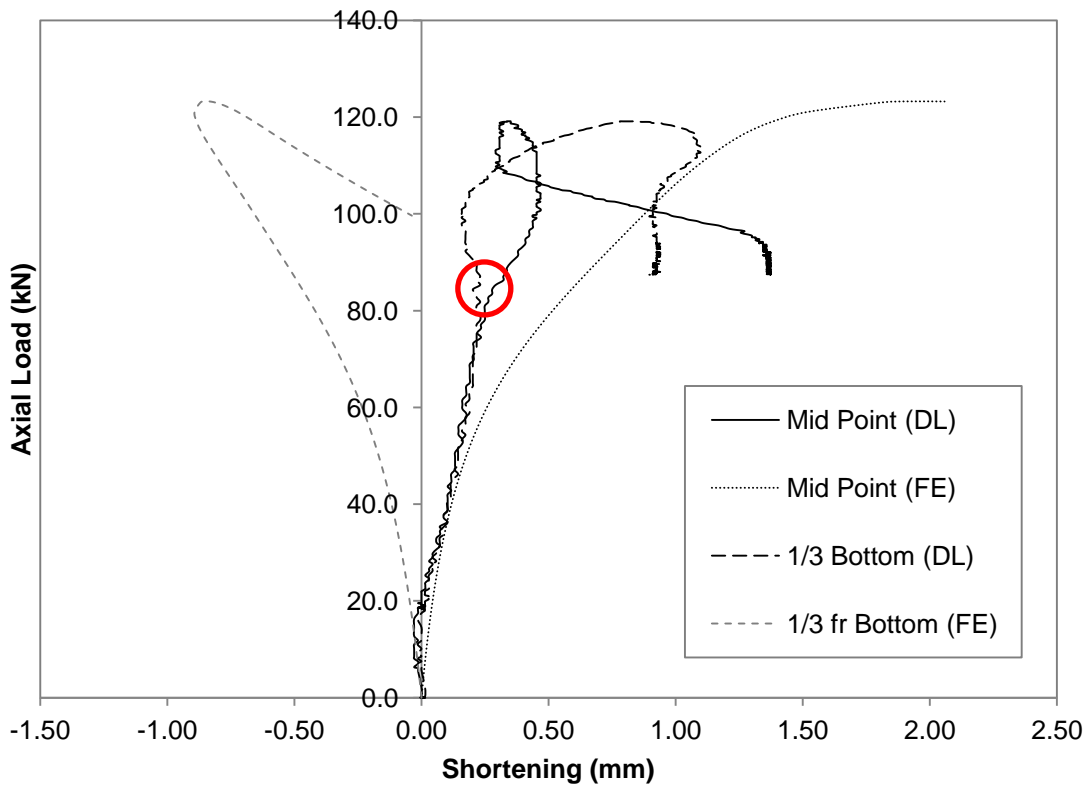


Figure F.16 Axial Load versus Deformation Curve for BU75S200L300-2

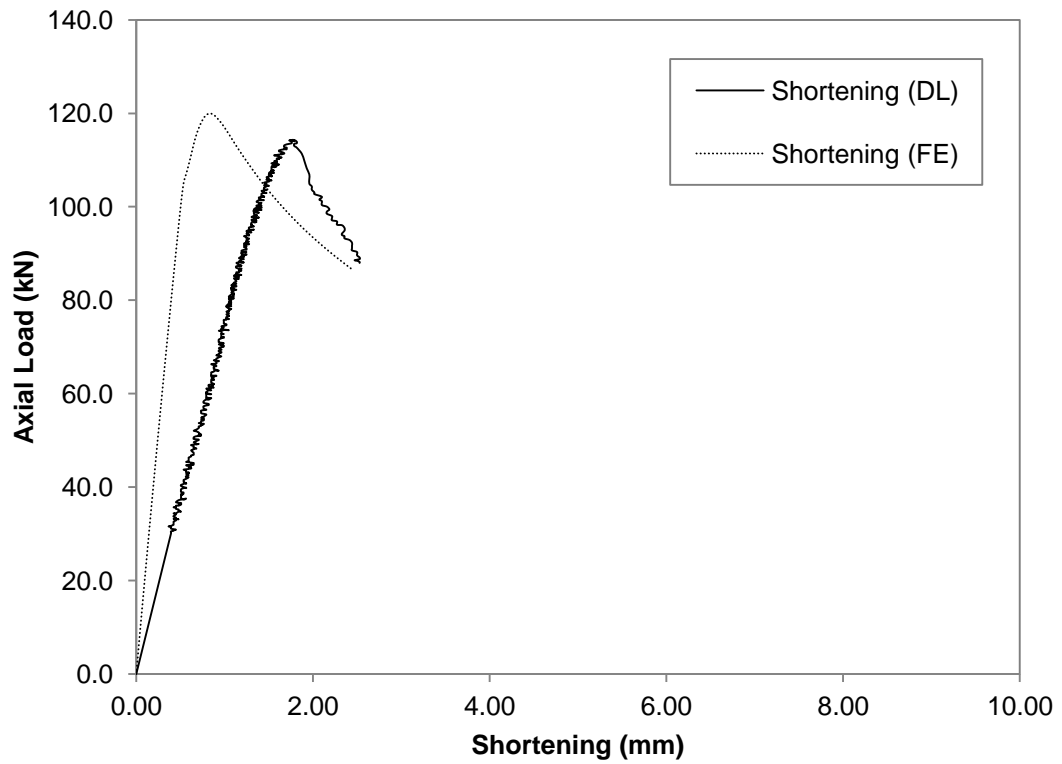


Figure F.17 Axial Load versus Shortening Curve for BU75S200L300-3

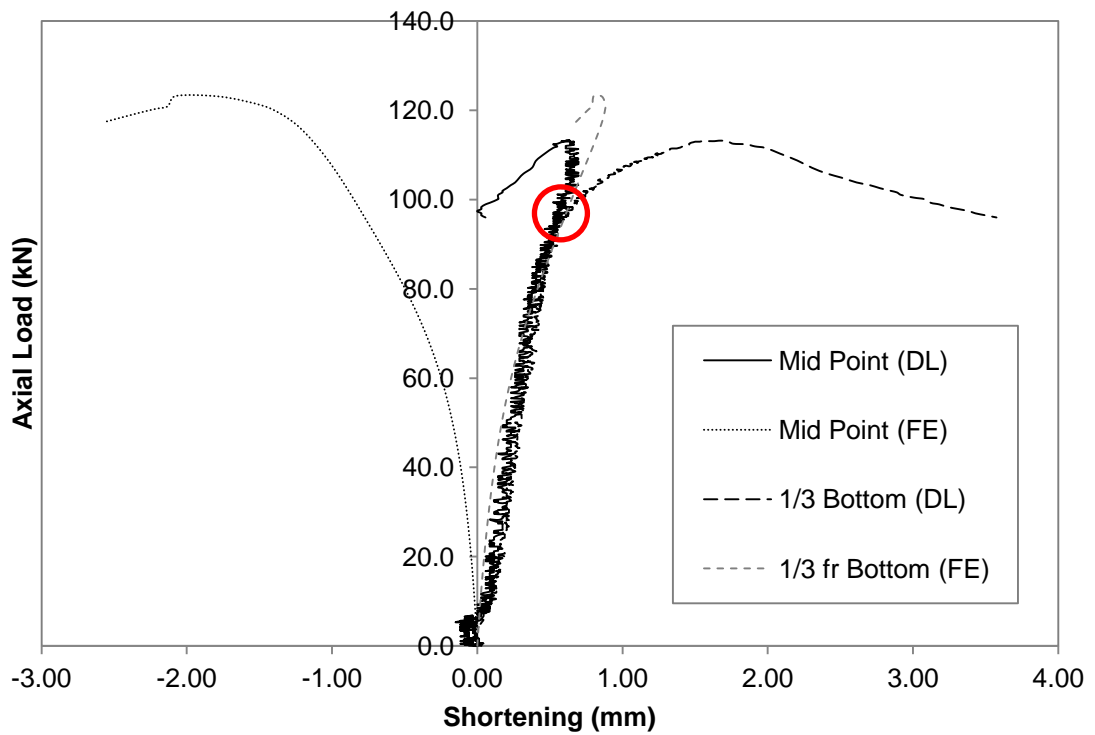


Figure F.18 Axial Load versus Deformation Curve for BU75S200L300-3

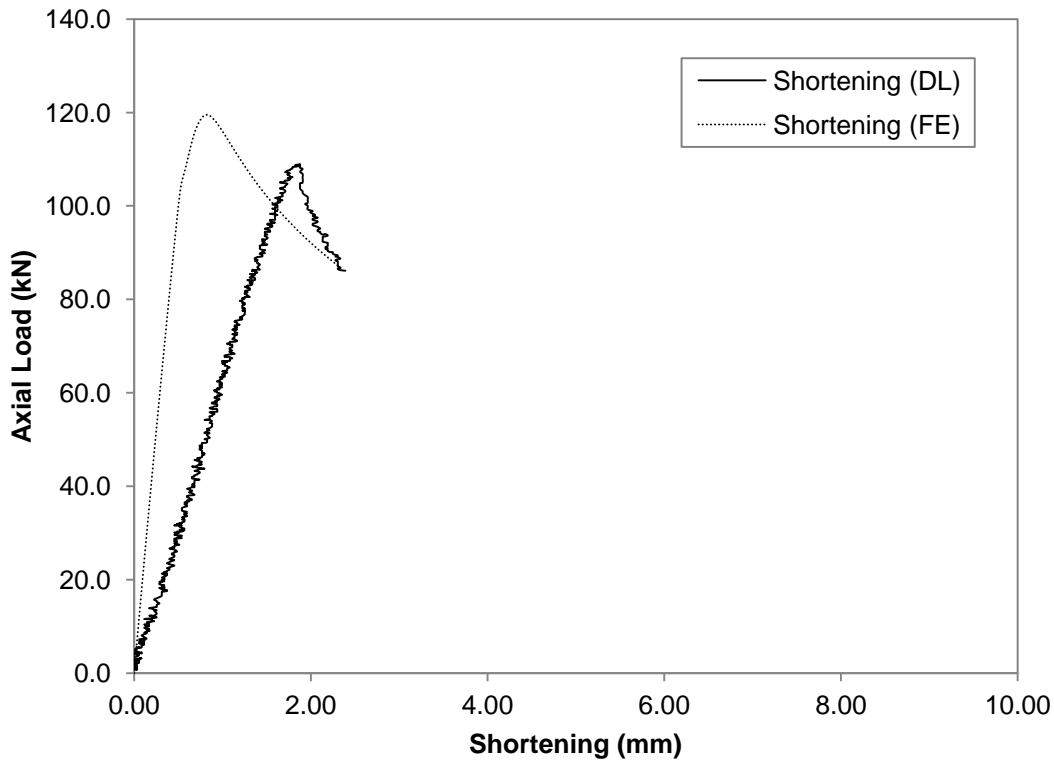


Figure F.19 Axial Load versus Shortening Curve for BU75S200L300-4

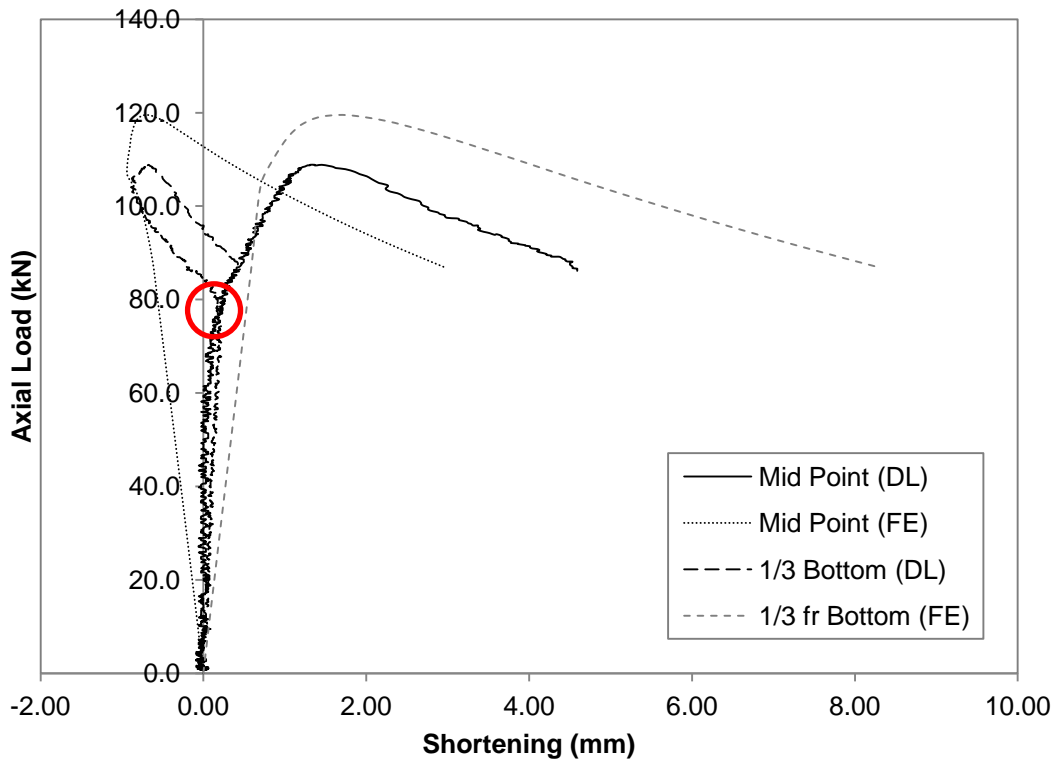


Figure F.20 Axial Load versus Deformation Curve for BU75S200L300-4

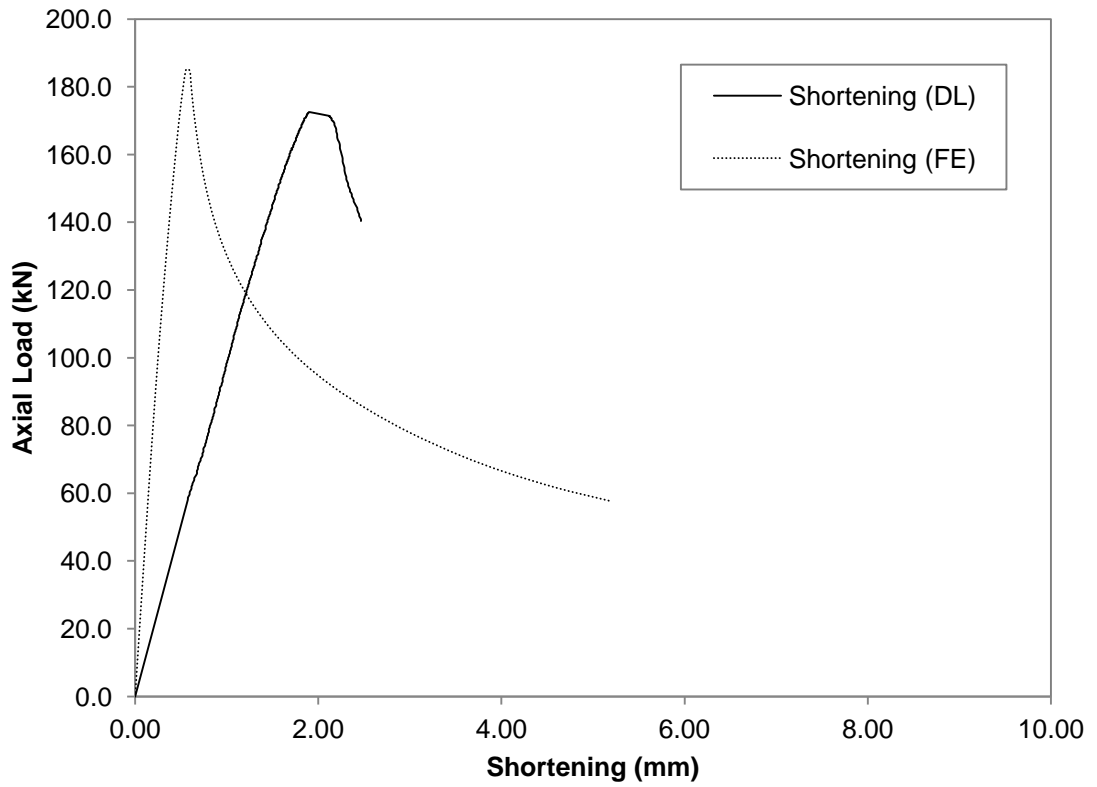


Figure F.21 Axial Load versus Shortening Curve for BU90S50L300-1

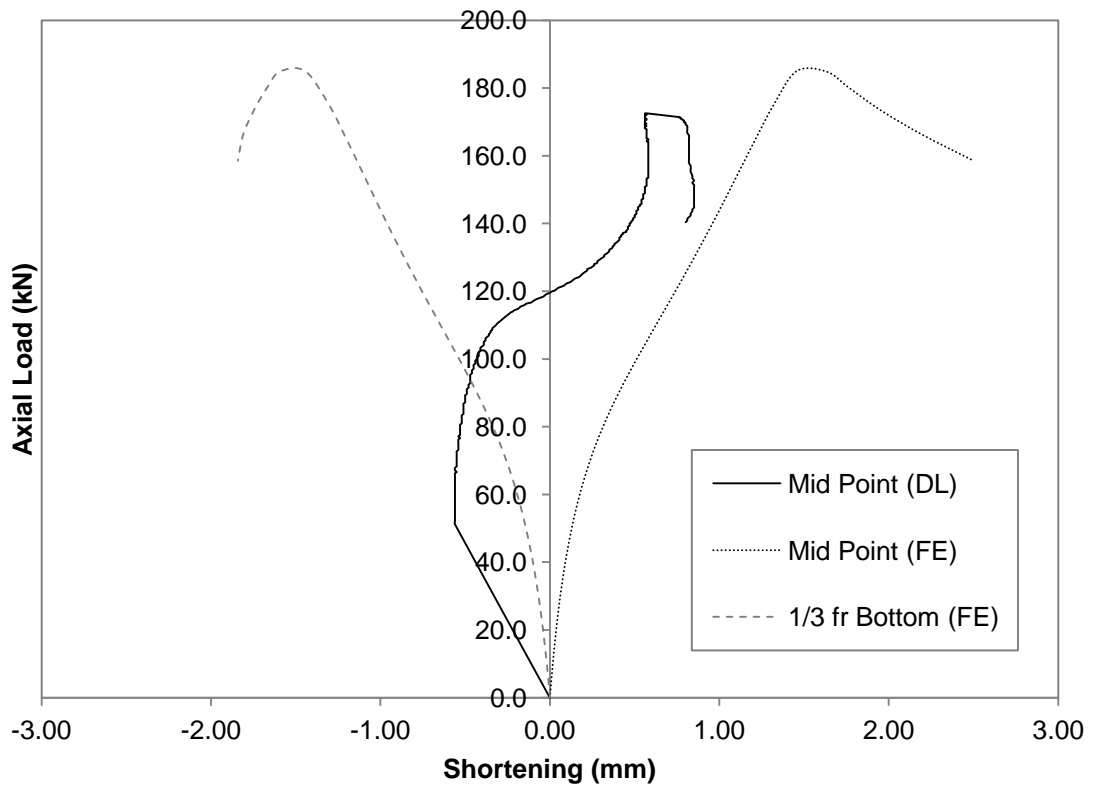


Figure F.22 Axial Load versus Deformation Curve for BU90S50L300-1

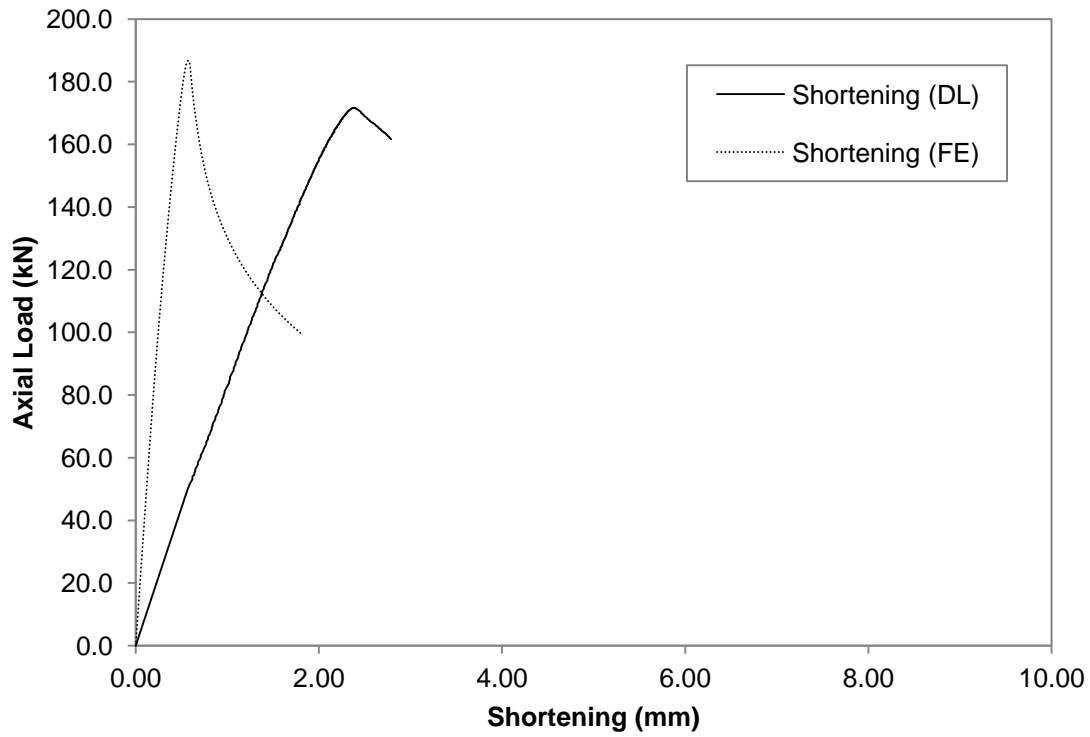


Figure F.23 Axial Load versus Shortening Curve for BU90S50L300-2

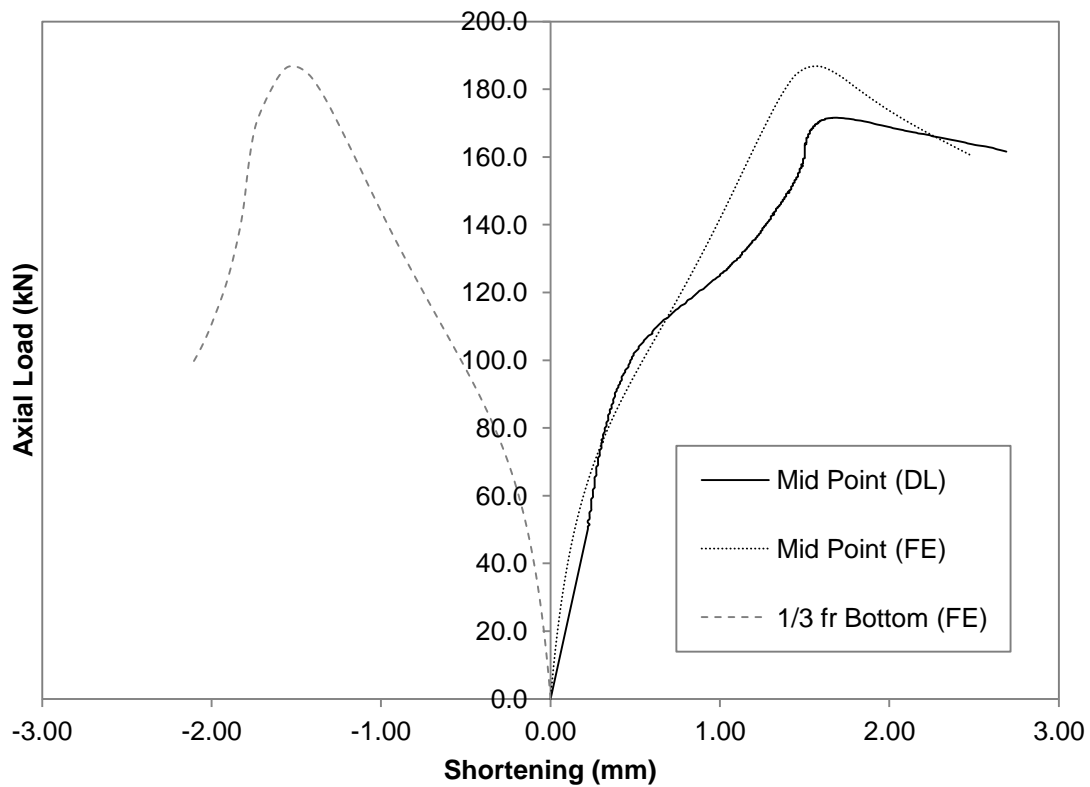


Figure F.24 Axial Load versus Deformation Curve for BU90S50L300-2

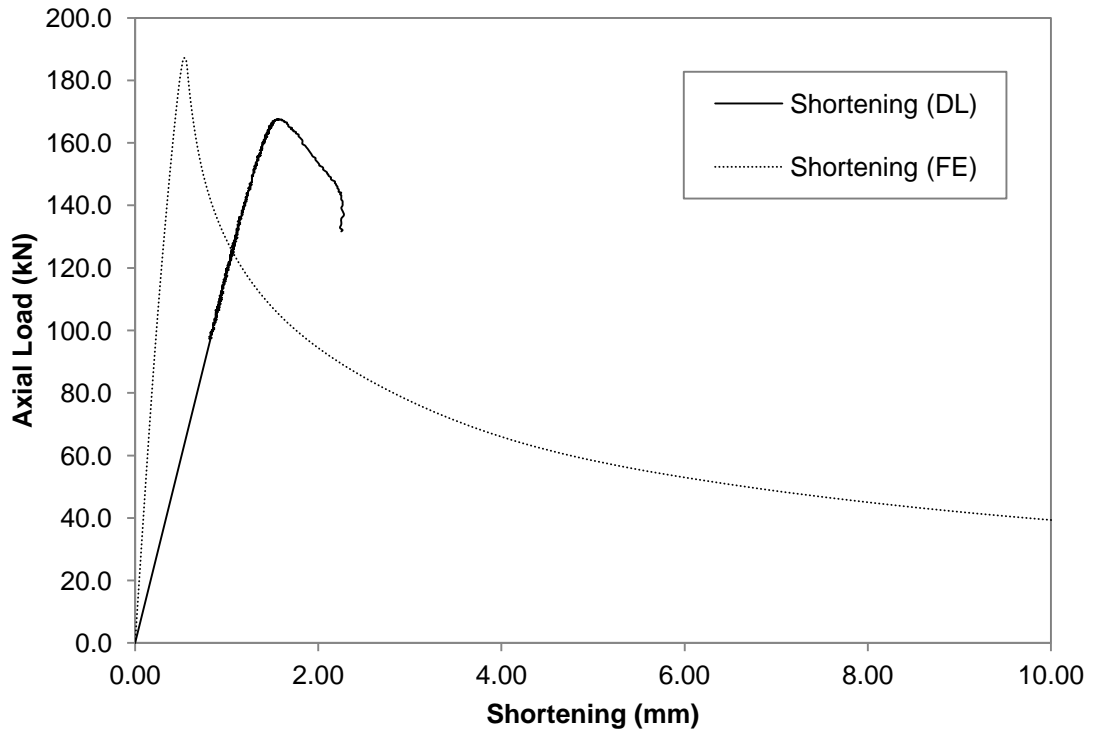


Figure F.25 Axial Load versus Shortening Curve for BU90S50L300-3

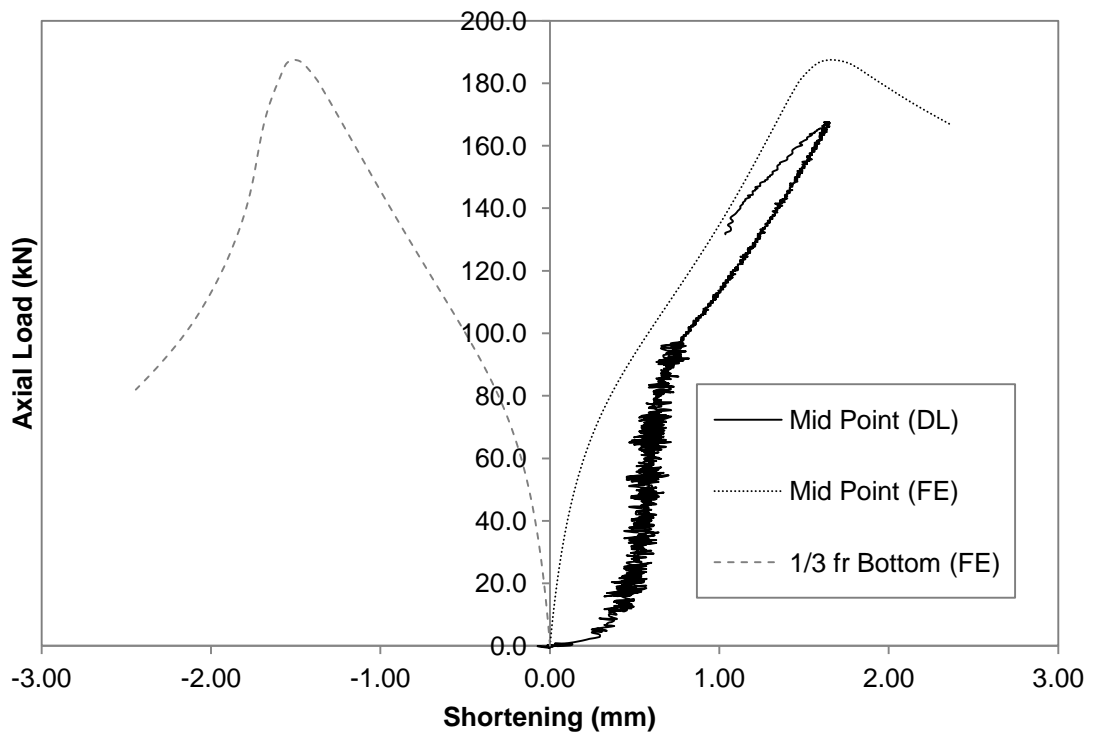


Figure F.26 Axial Load versus Deformation Curve for BU90S50L300-3

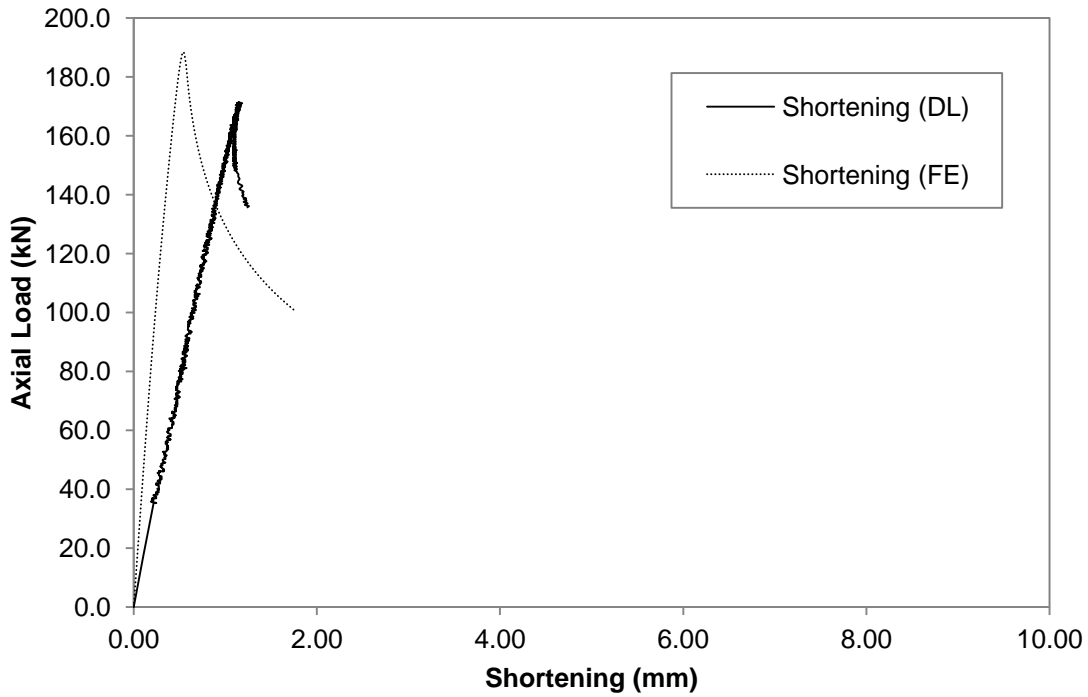


Figure F.27 Axial Load versus Shortening Curve for BU90S100L300-3

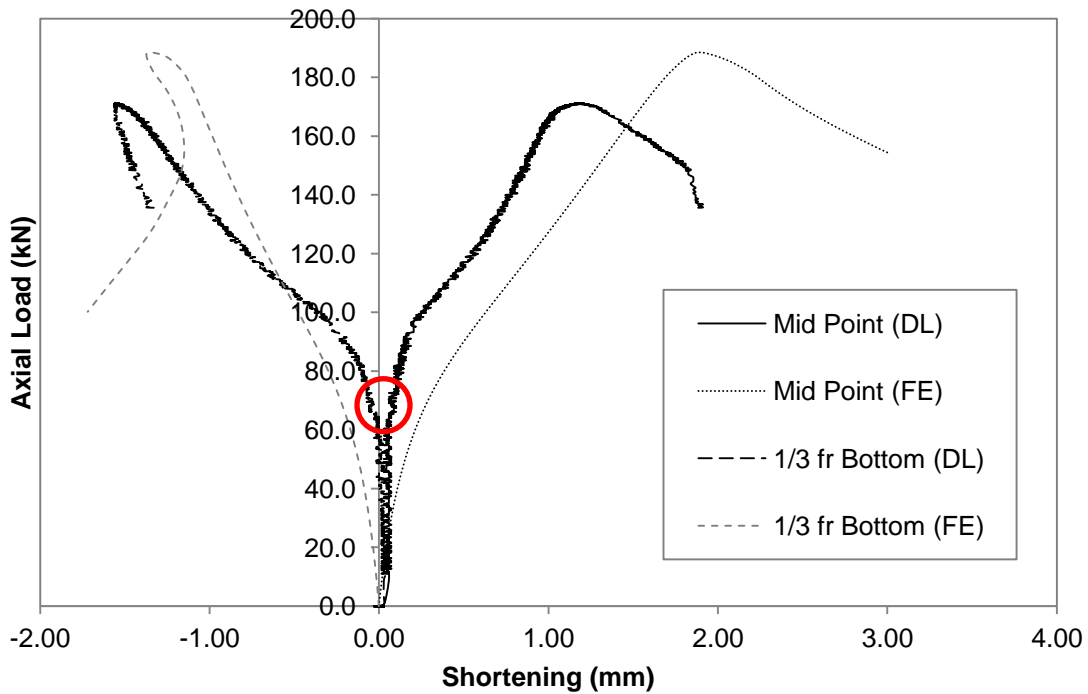


Figure F.28 Axial Load versus Deformation Curve for BU90S100L300-3

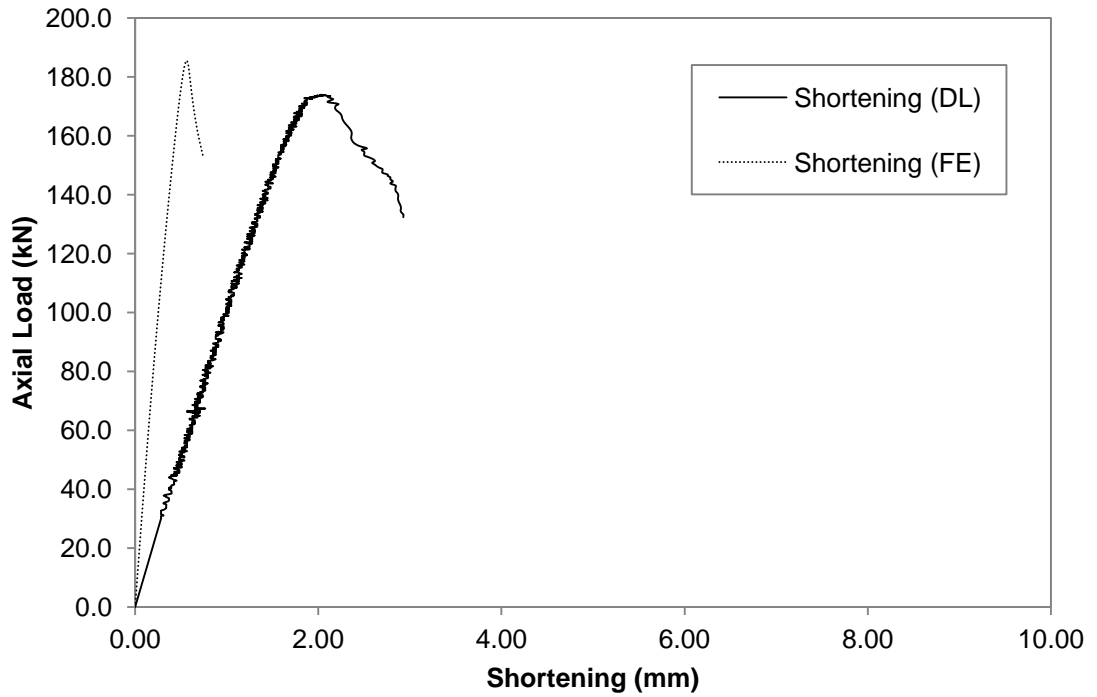


Figure F.29 Axial Load versus Shortening Curve for BU90S100L300-4

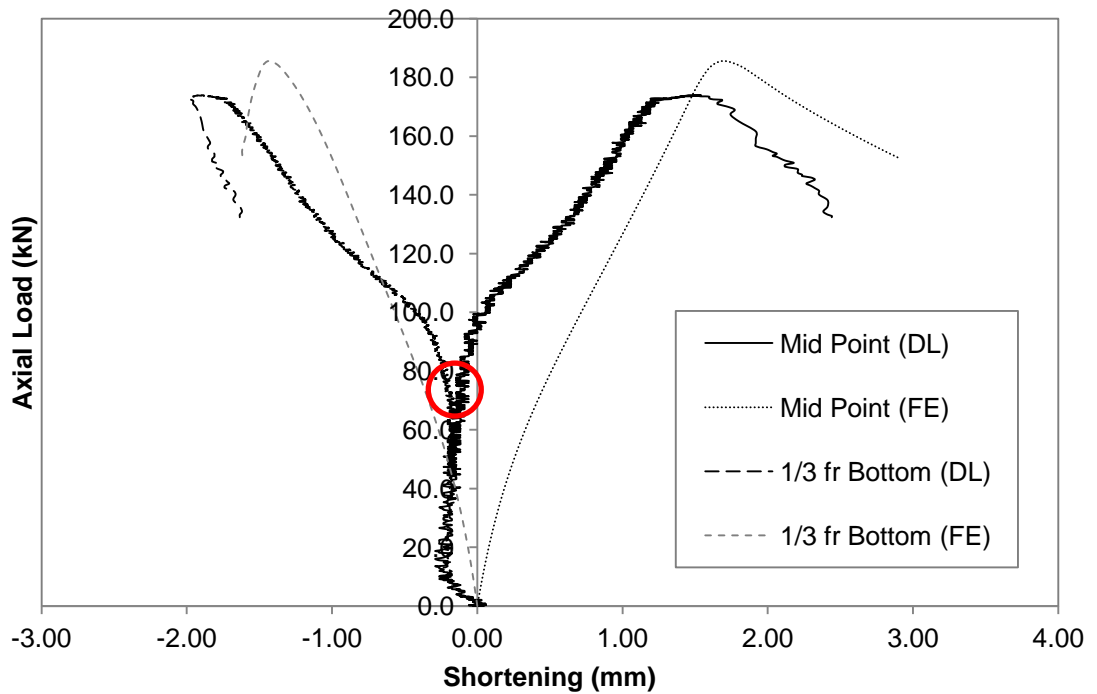


Figure F.30 Axial Load versus Deformation Curve for BU90S100L300-4

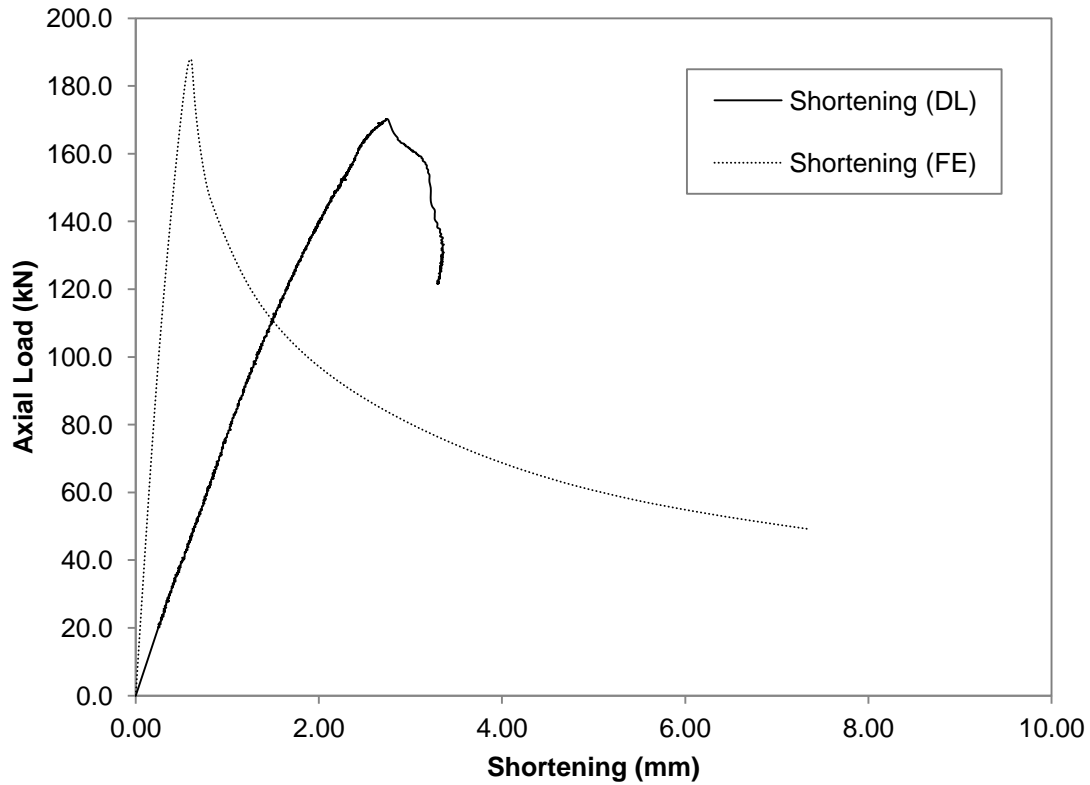


Figure F.31 Axial Load versus Shortening Curve for BU90S200L300-1

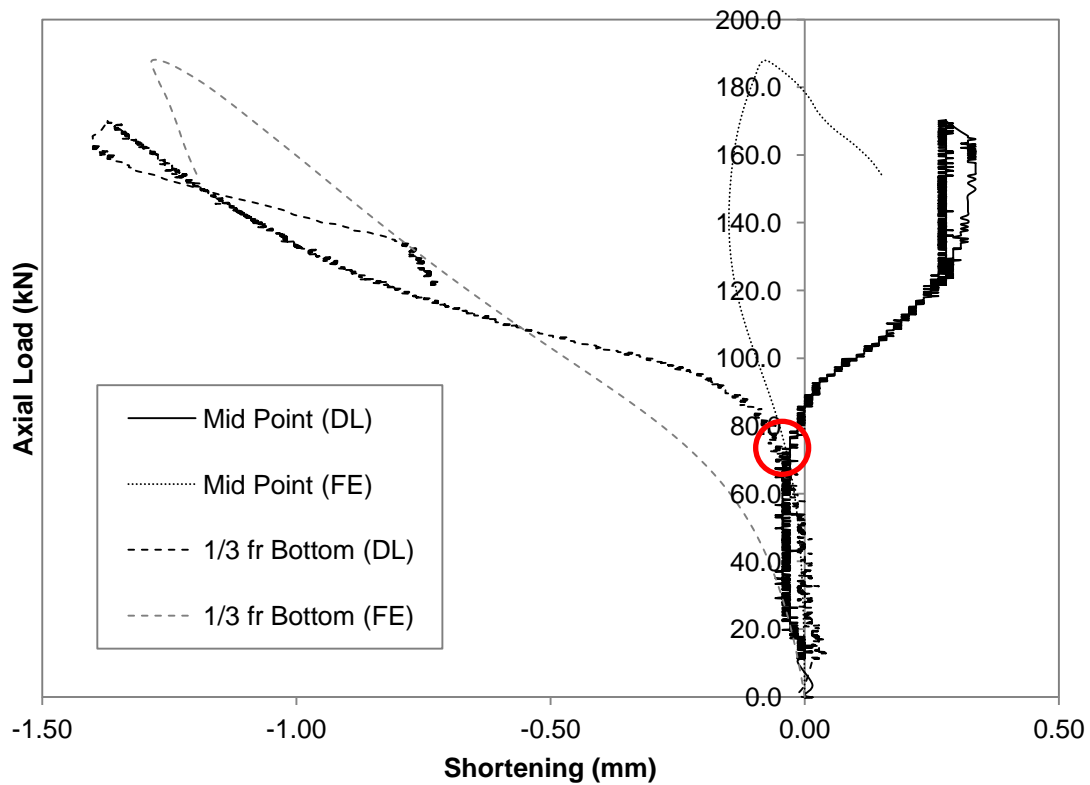


Figure F.32 Axial Load versus Deformation Curve for BU90S200L300-1

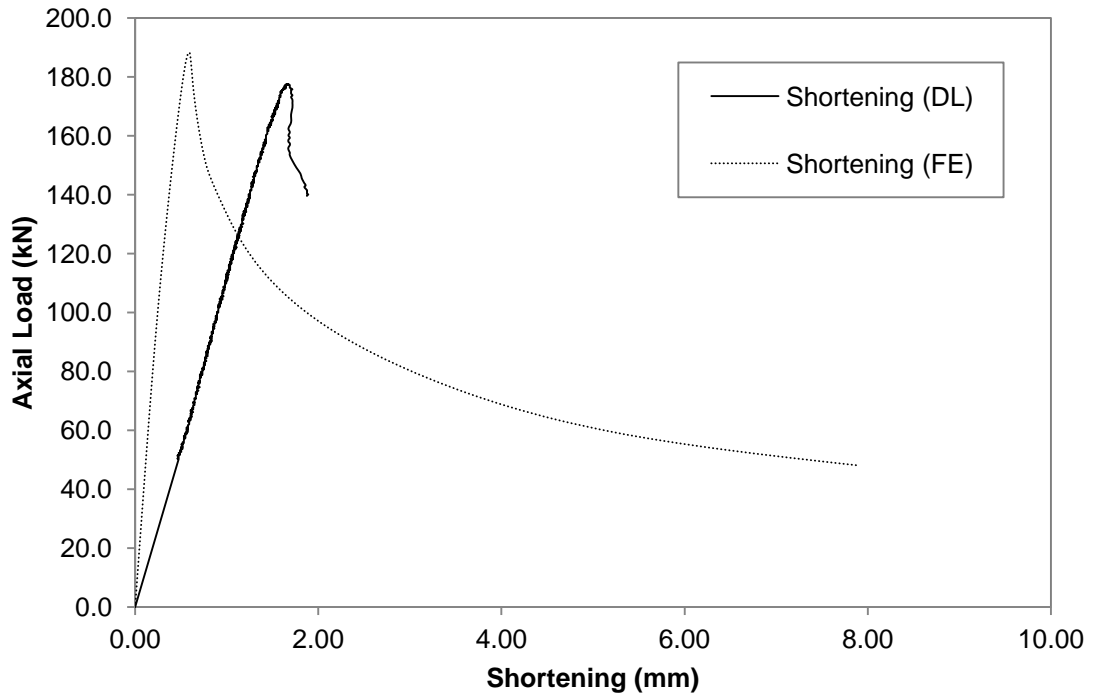


Figure F.33 Axial Load versus Shortening Curve for BU90S200L300-2

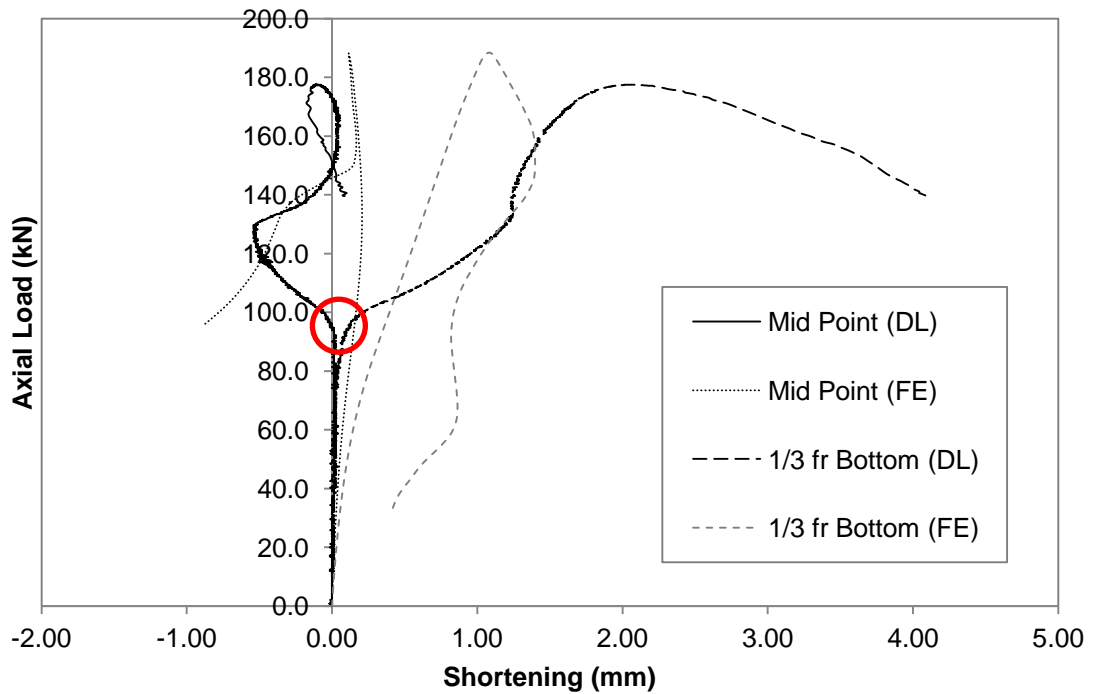


Figure F.34 Axial Load versus Deformation Curve for BU90S200L300-2

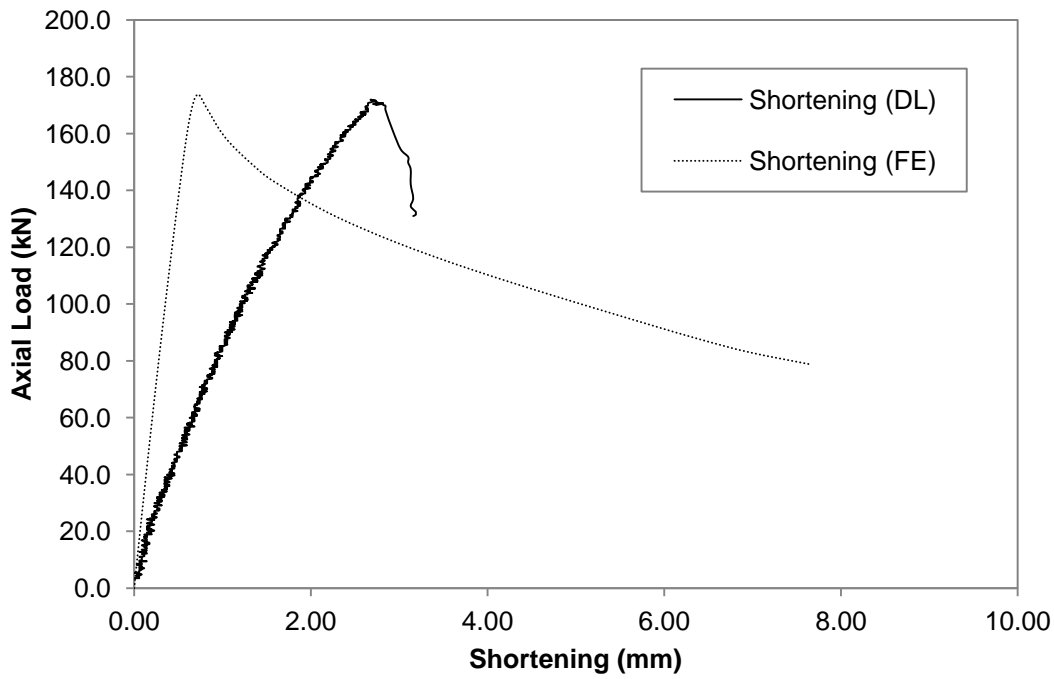


Figure F.35 Axial Load versus Shortening Curve for BU90S200L300-4

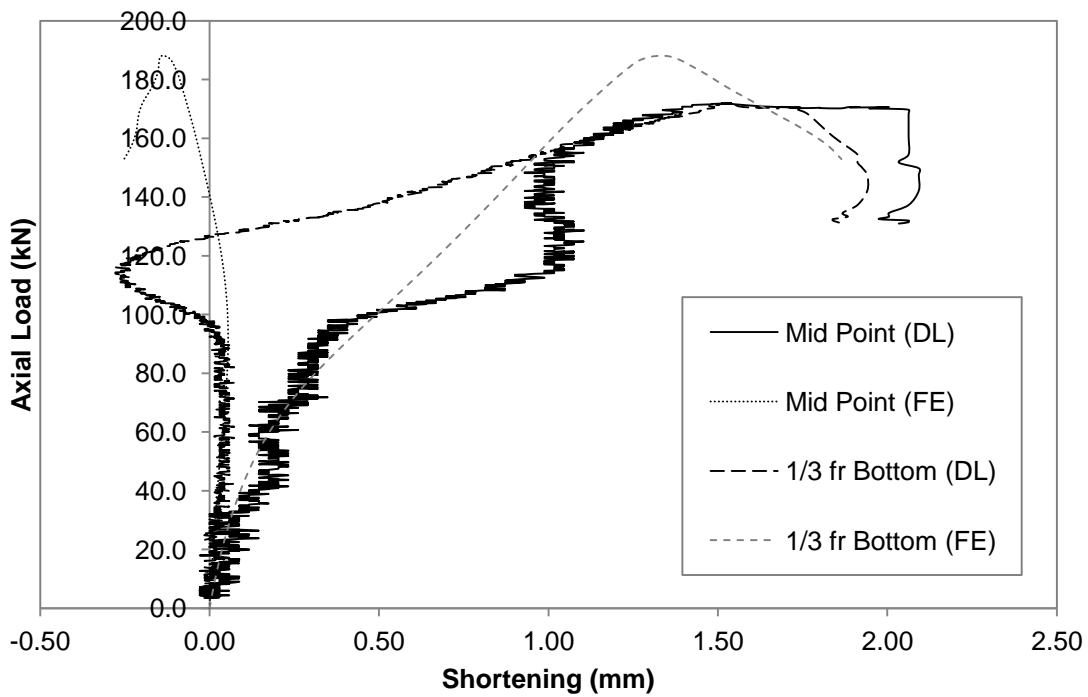


Figure F.36 Axial Load versus Deformation Curve for BU90S200L300-4

F.2 Short Column

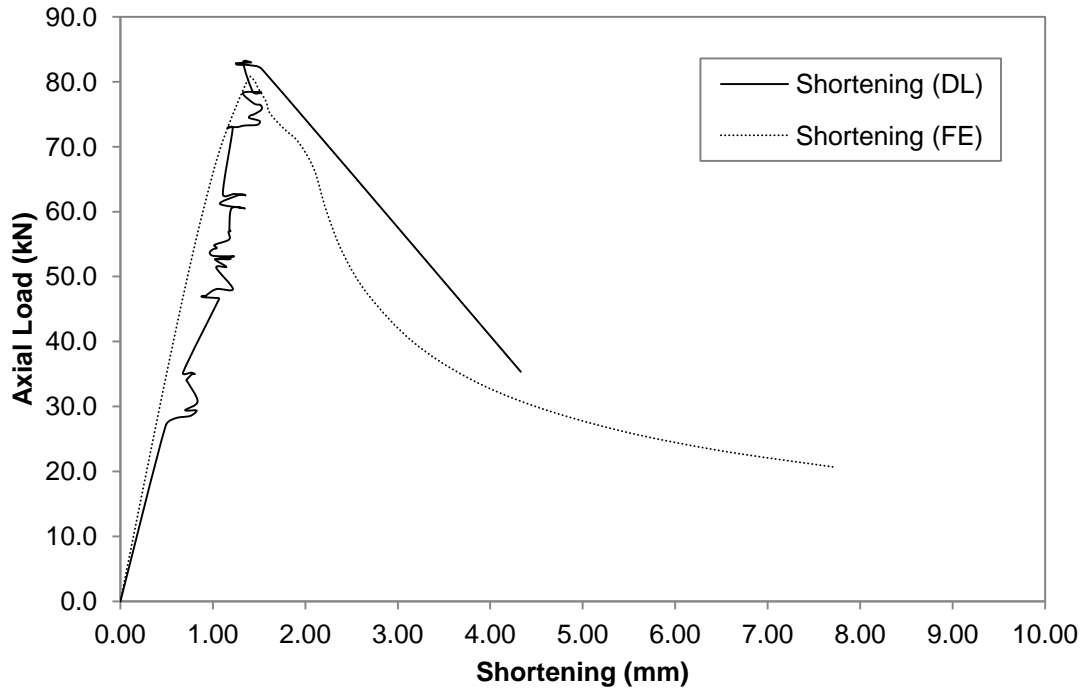


Figure F.37 Axial Load versus Shortening Curve for BU75S100L500-1

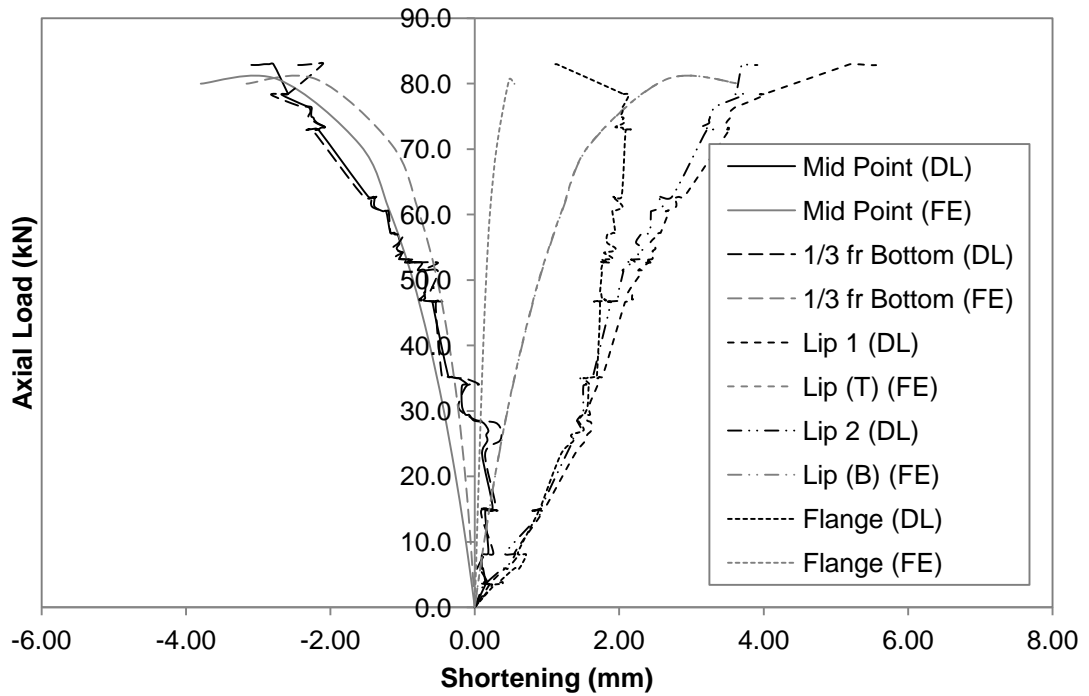


Figure F.38 Axial Load versus Deformation Curve for BU75S100L500-1

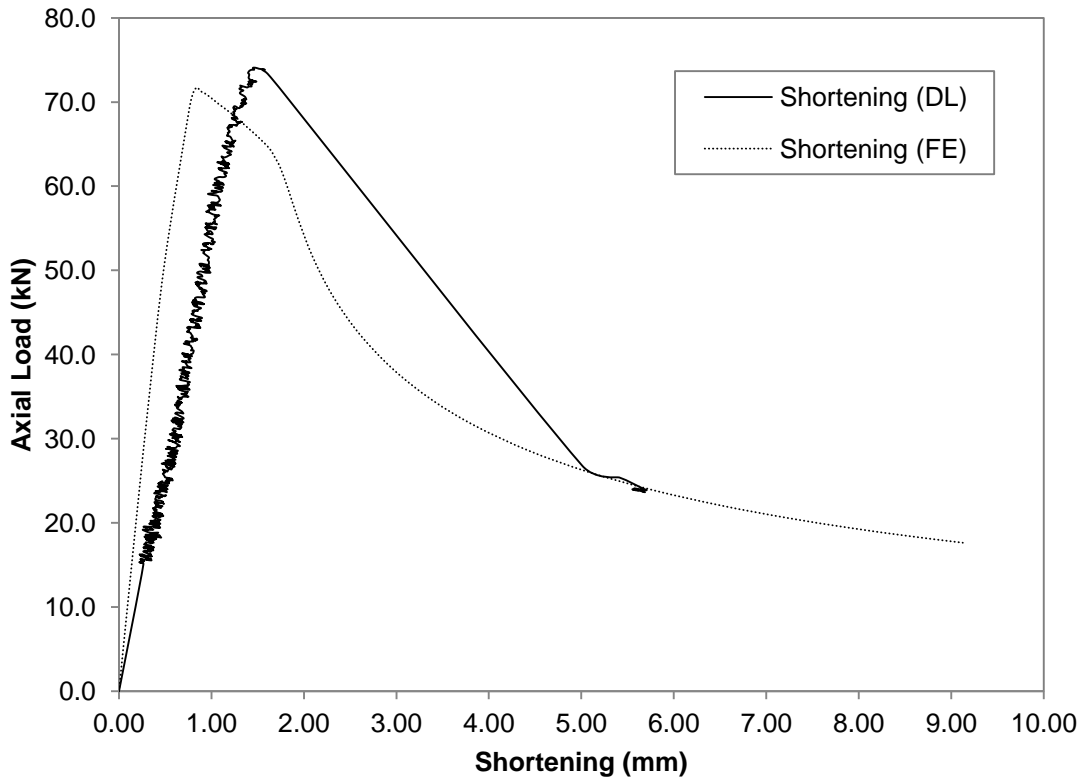


Figure F.39 Axial Load versus Shortening Curve for BU75S100L500-3

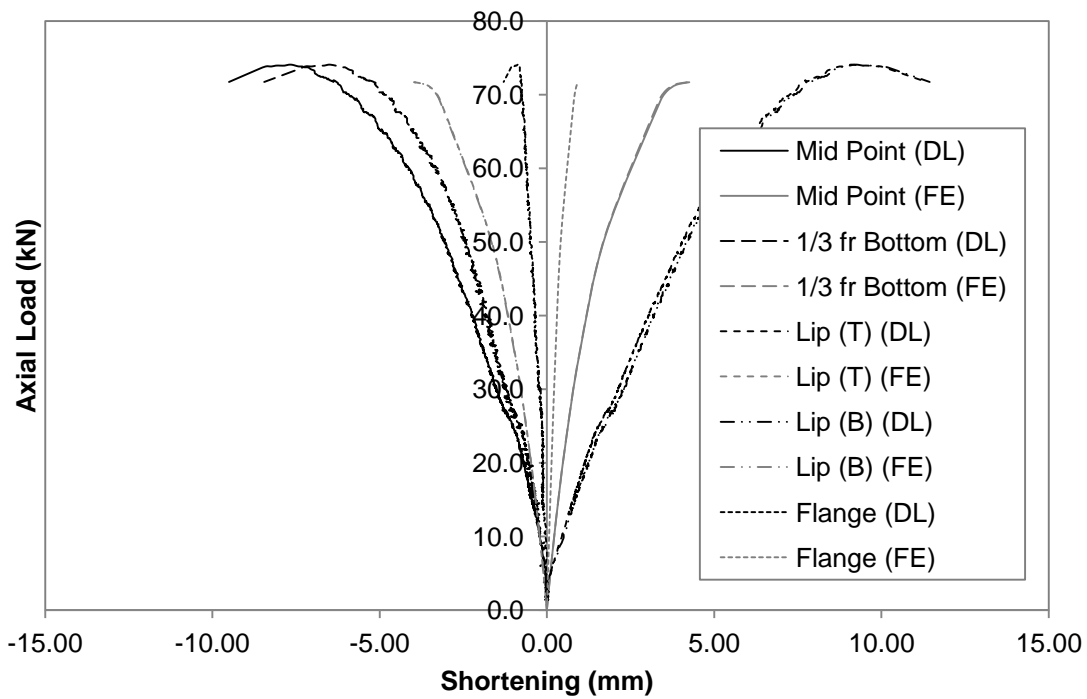


Figure F.40 Axial Load versus Deformation Curve for BU75S100L500-3

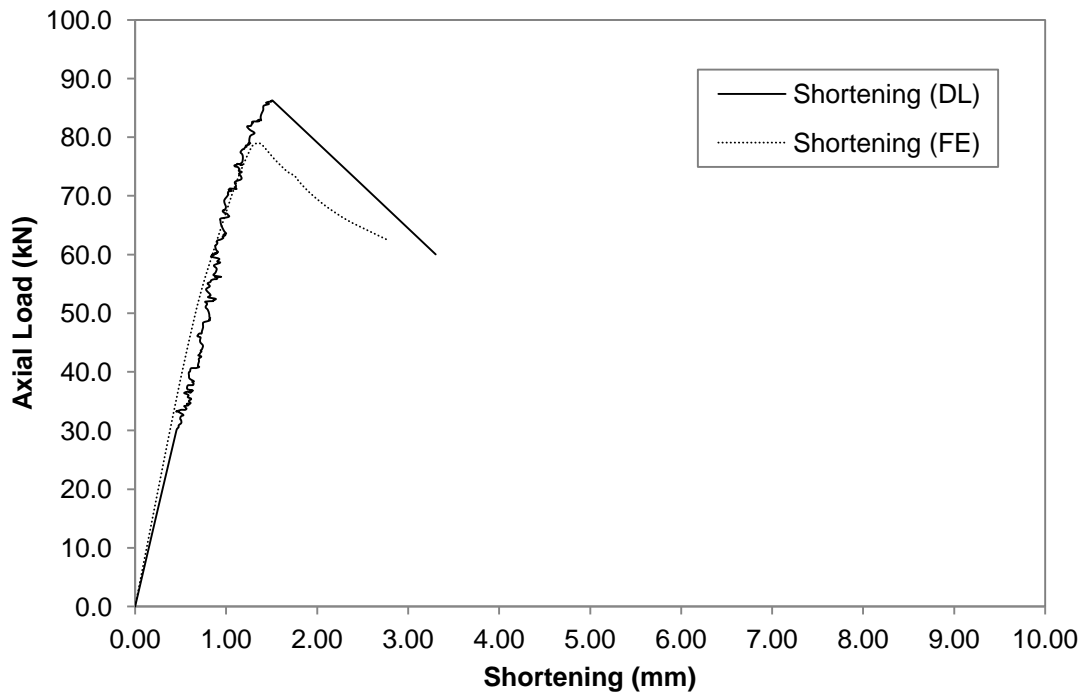


Figure F.41 Axial Load versus Shortening Curve for BU75S200L500-1

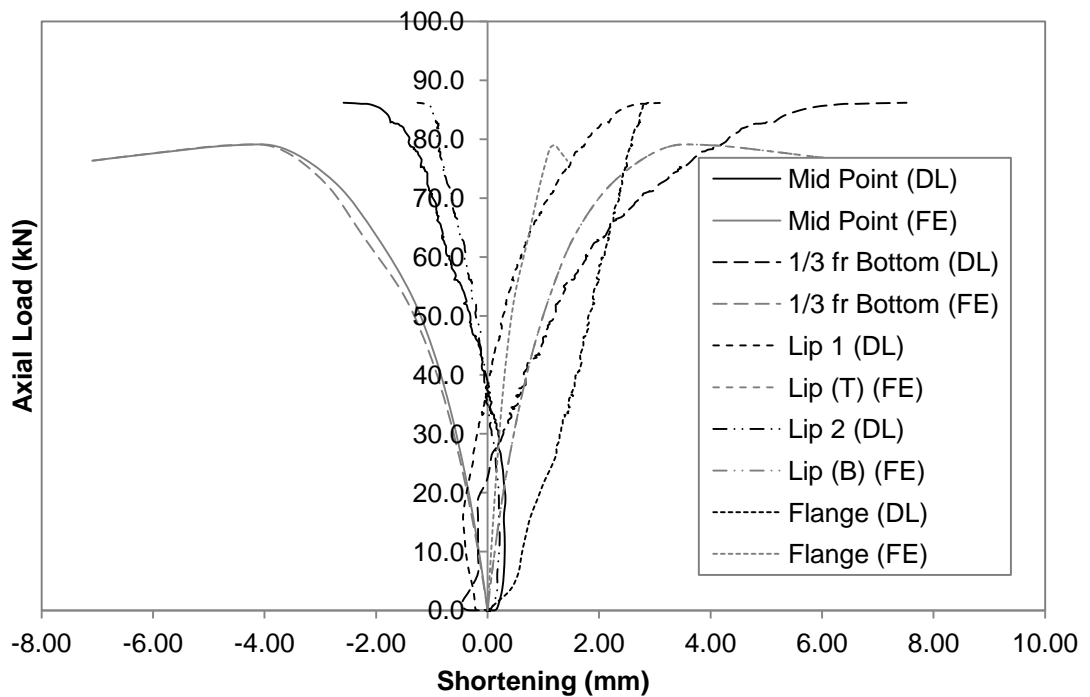


Figure F.42 Axial Load versus Deformation Curve for BU75S200L500-1

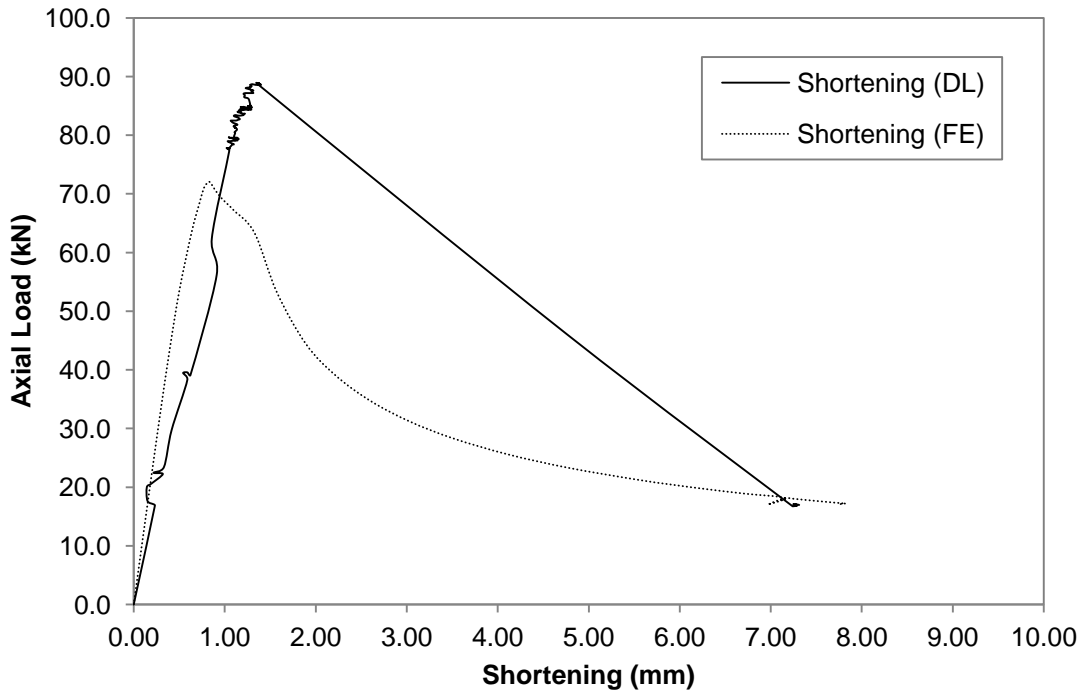


Figure F.43 Axial Load versus Shortening Curve for BU75S200L500-2

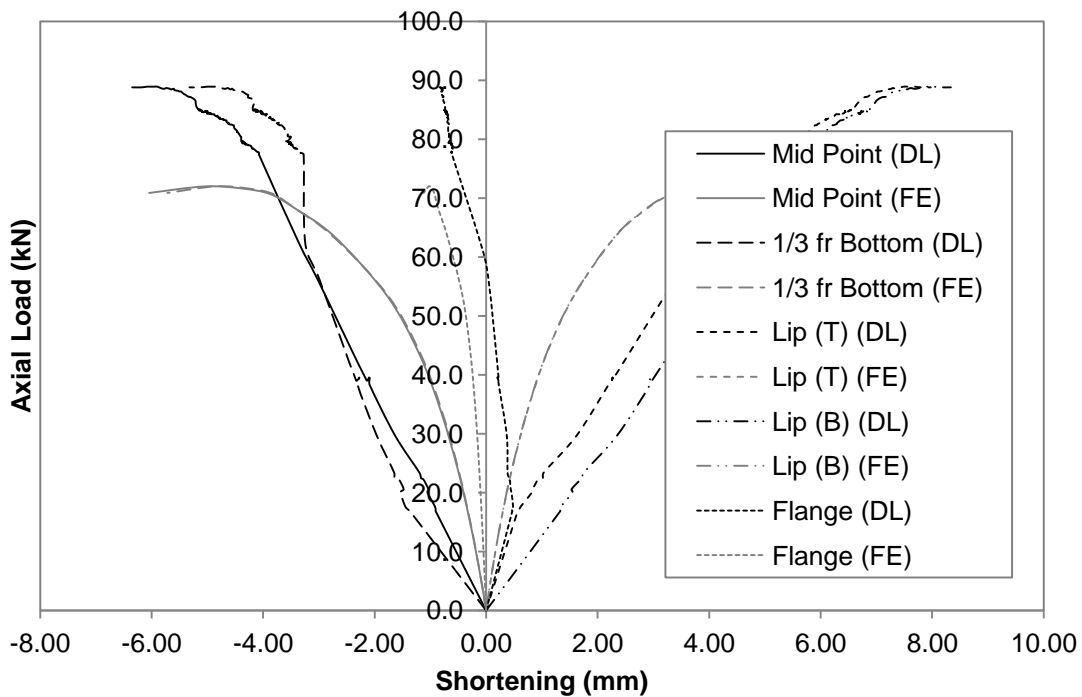


Figure F.44 Axial Load versus Deformation Curve for BU75S200L500-2

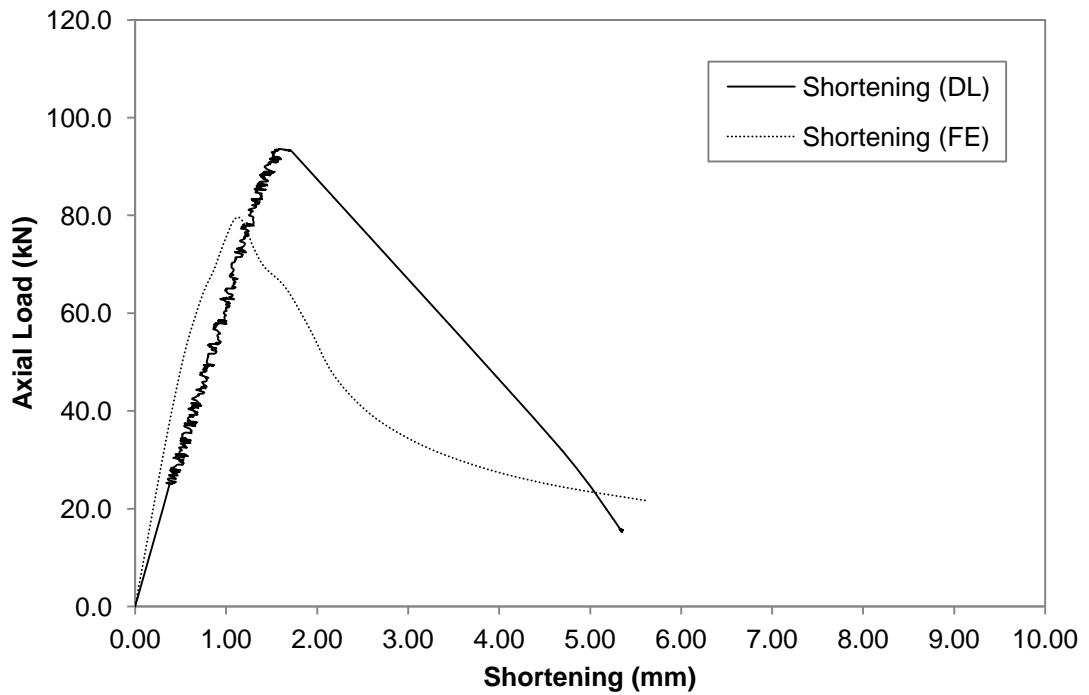


Figure F.45 Axial Load versus Shortening Curve for BU75S200L500-3

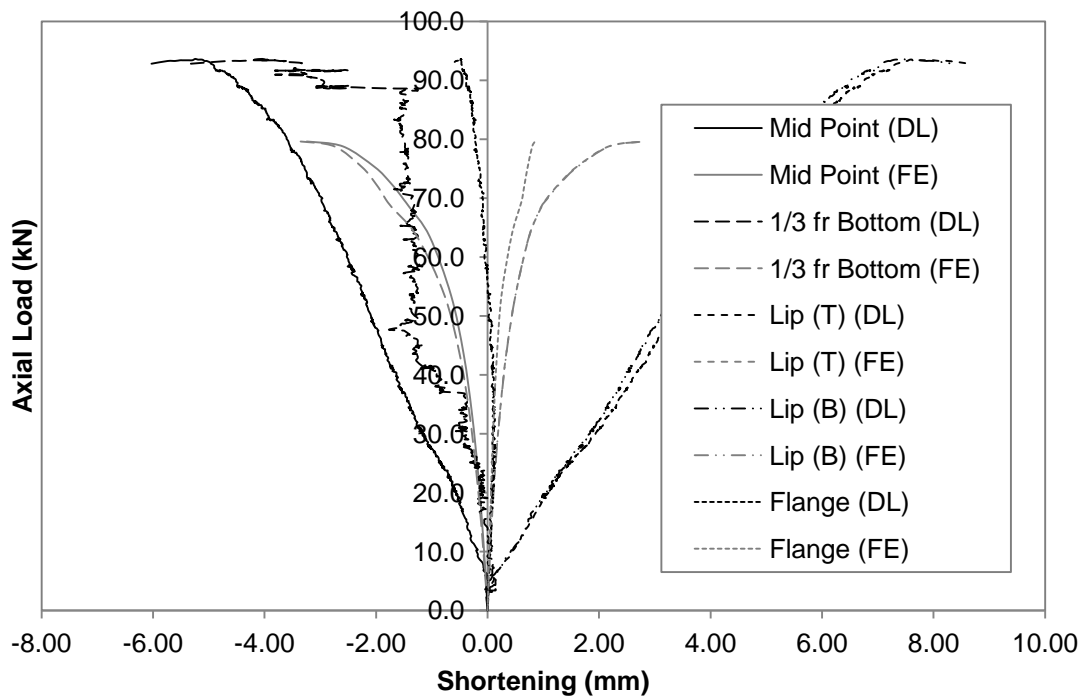


Figure F.46 Axial Load versus Deformation Curve for BU75S200L500-3

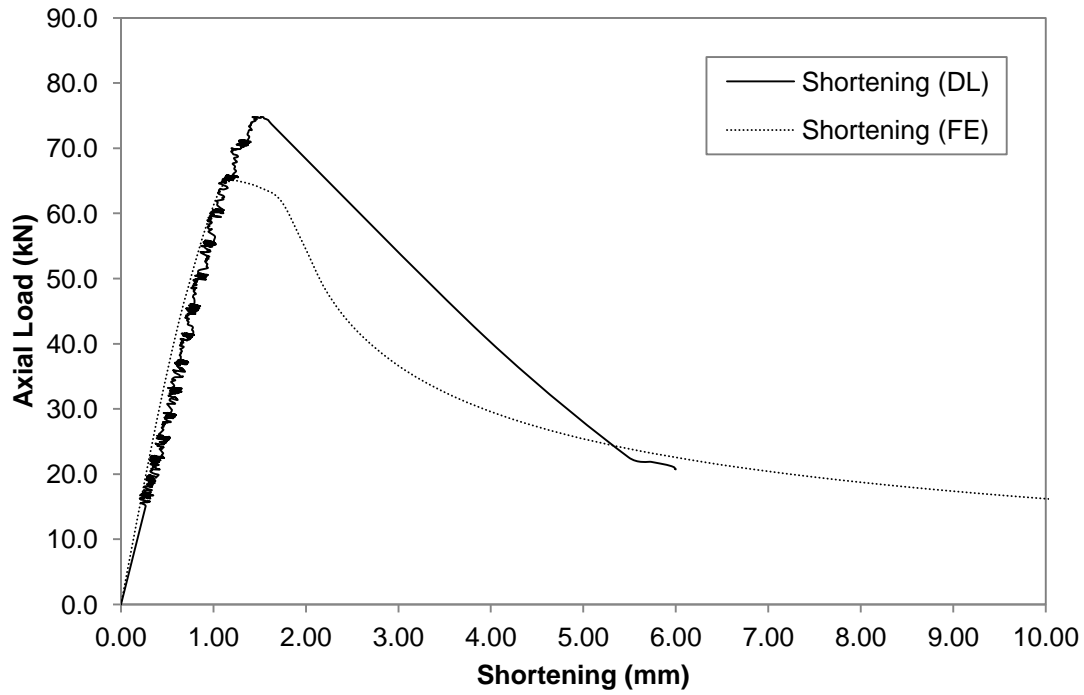


Figure F.47 Axial Load versus Shortening Curve for BU75S400L500-1

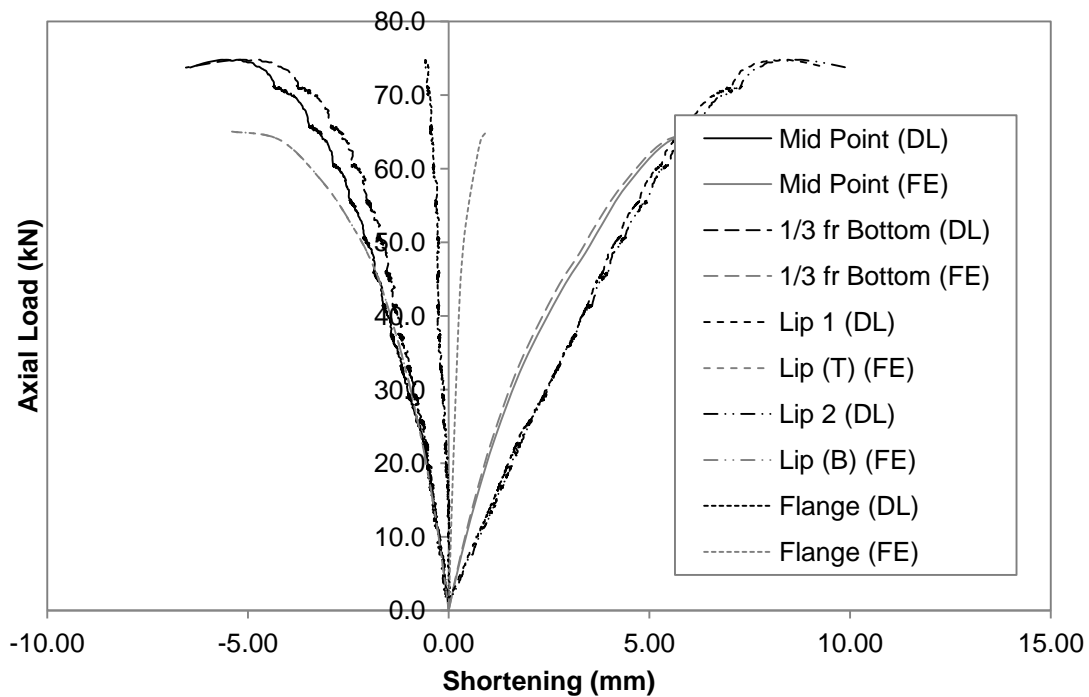


Figure F.48 Axial Load versus Deformation Curve for BU75S400L500-1

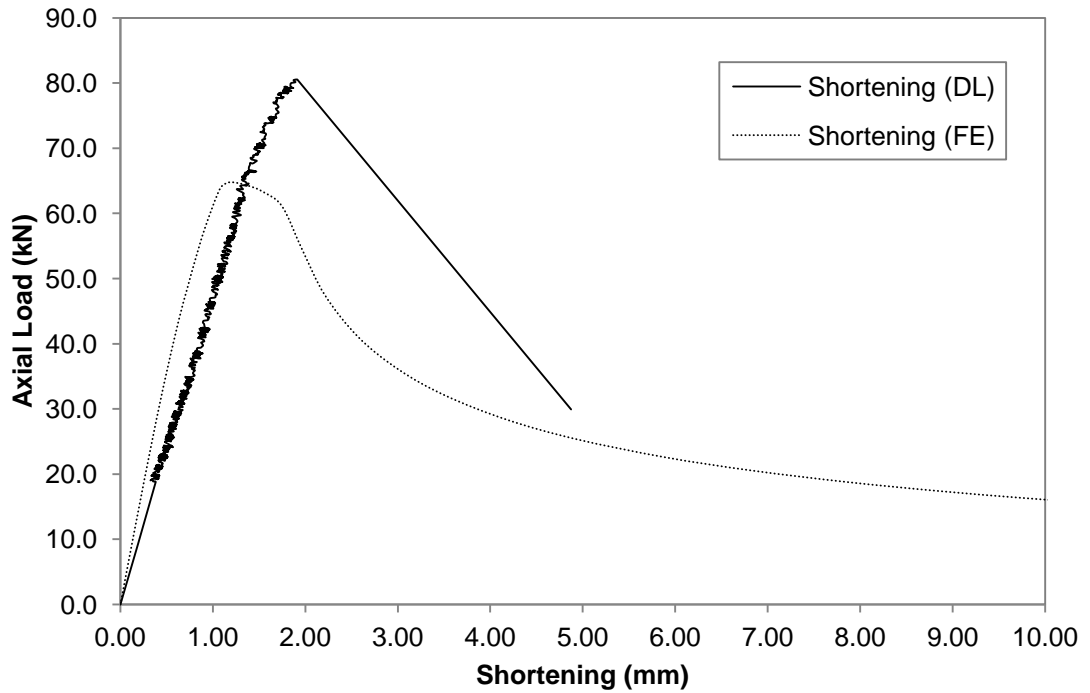


Figure F.49 Axial Load versus Shortening Curve for BU75S400L500-2

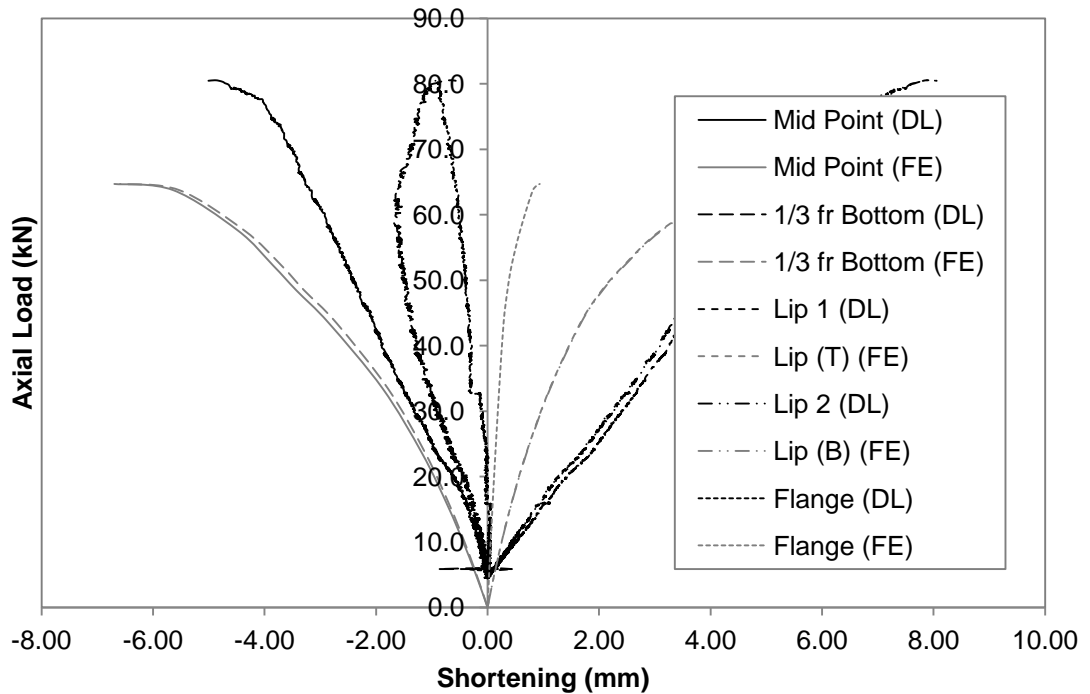


Figure F.50 Axial Load versus Deformation Curve for BU75S400L500-2

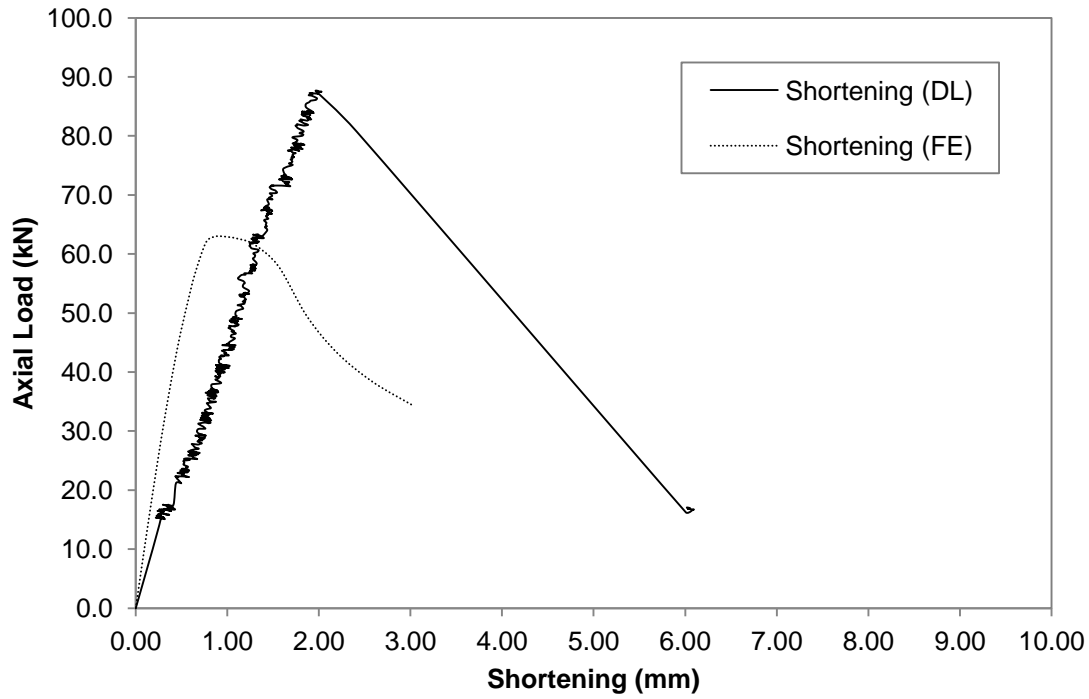


Figure F.51 Axial Load versus Shortening Curve for BU75S400L500-3

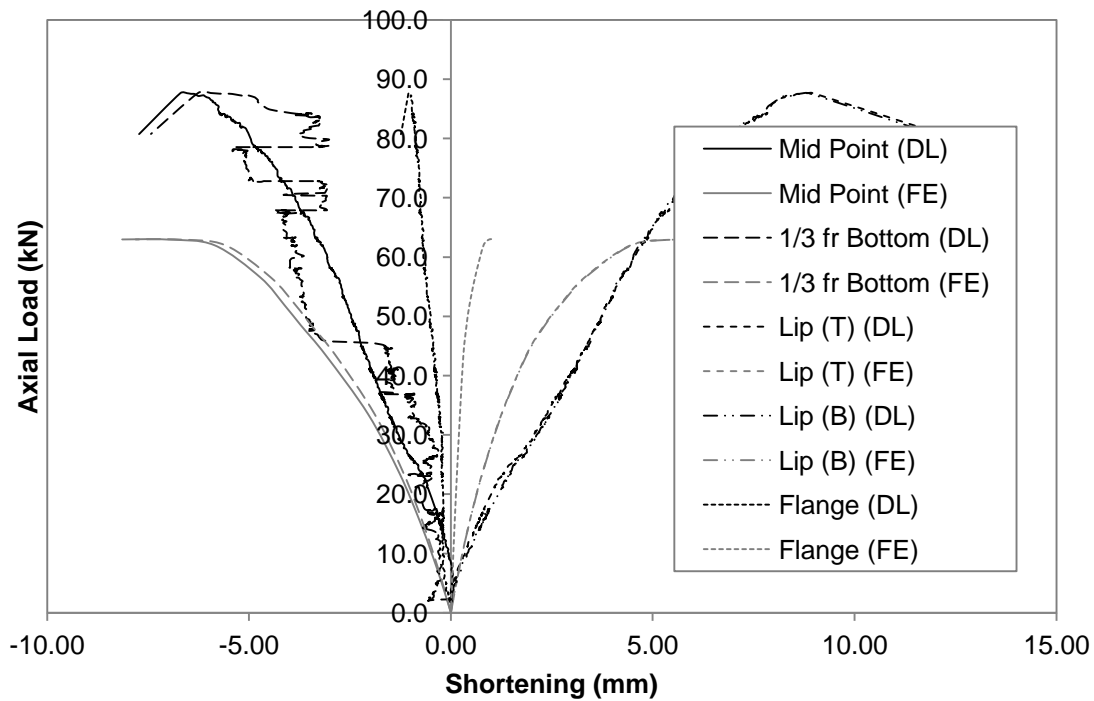


Figure F.52 Axial Load versus Deformation Curve for BU75S400L500-3

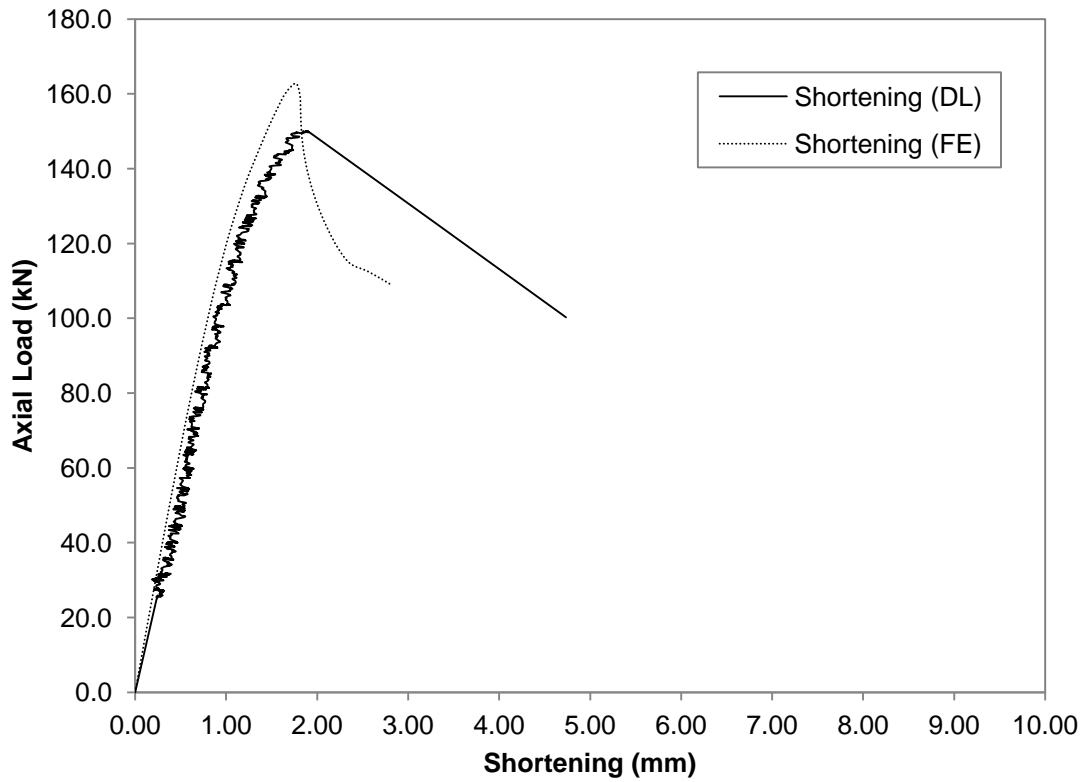


Figure F.53 Axial Load versus Shortening Curve for BU90S100L500-1

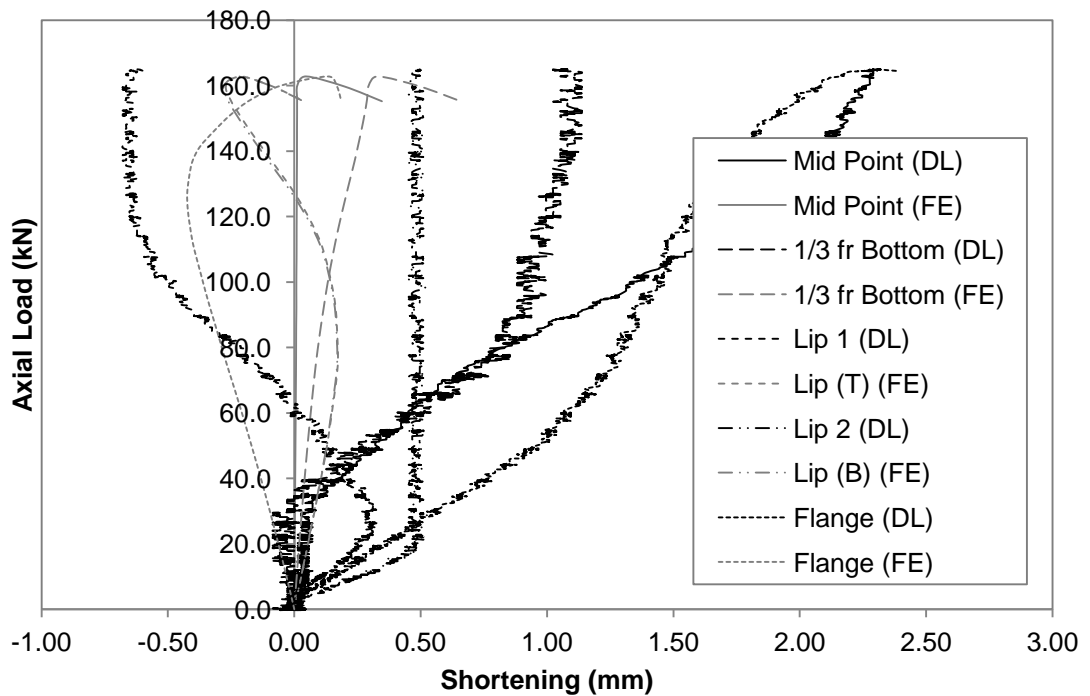


Figure F.54 Axial Load versus Deformation Curve for BU90S100L500-1

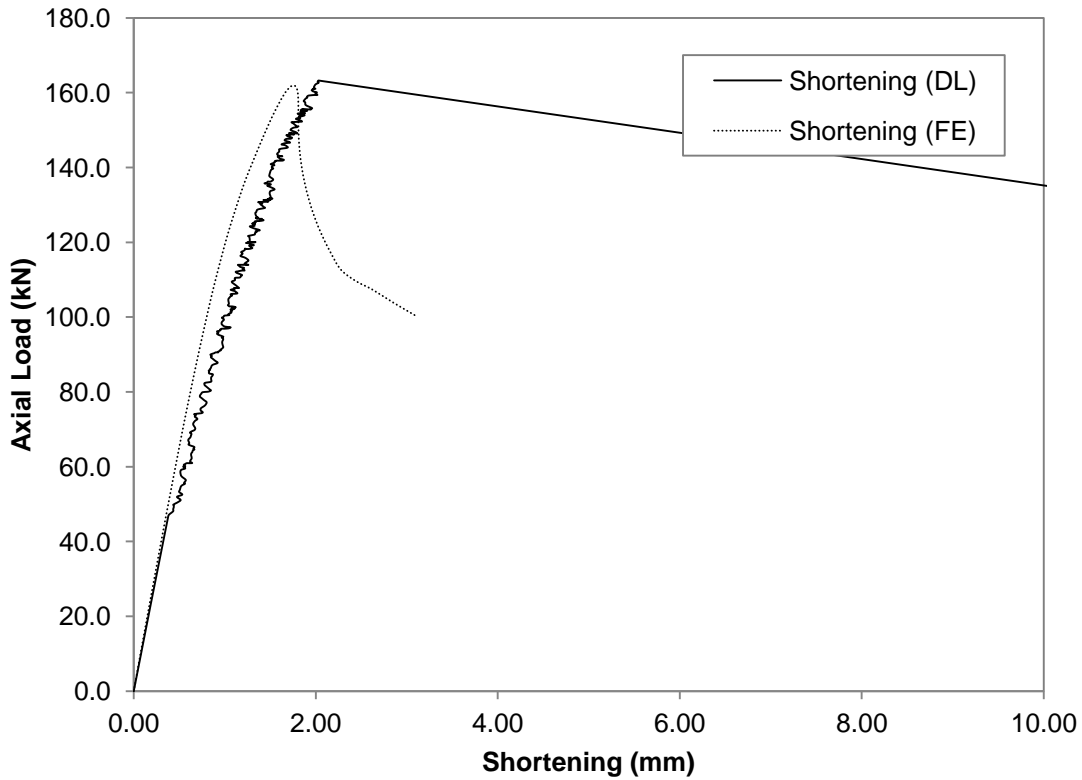


Figure F.55 Axial Load versus Shortening Curve for BU90S100L500-2

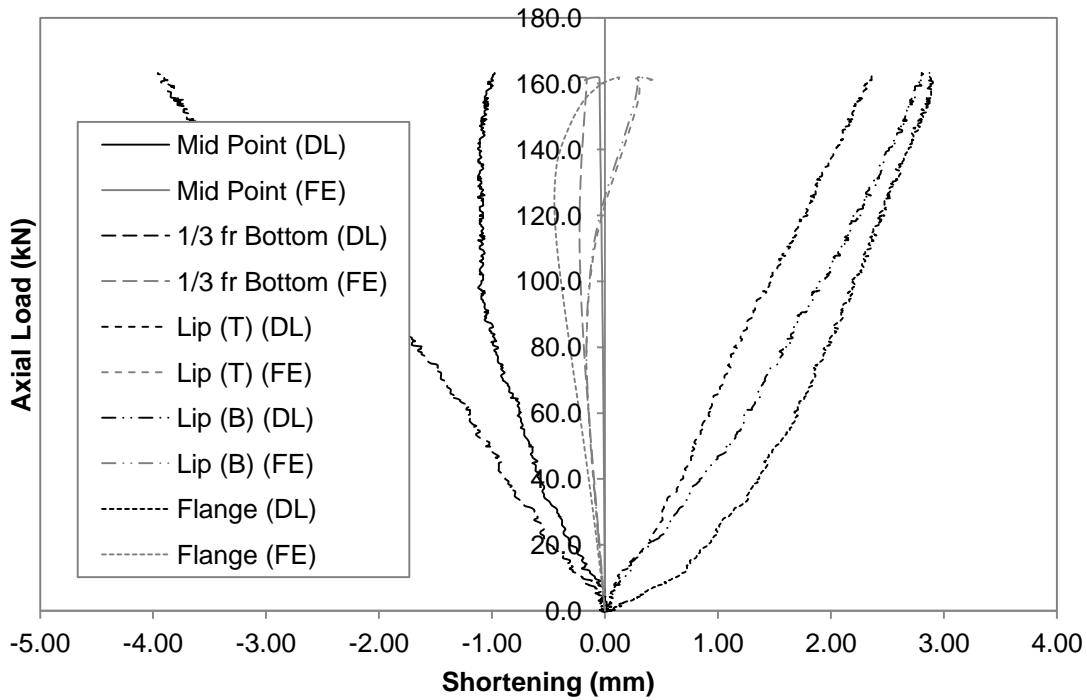


Figure F.56 Axial Load versus Deformation Curve for BU90S100L500-2

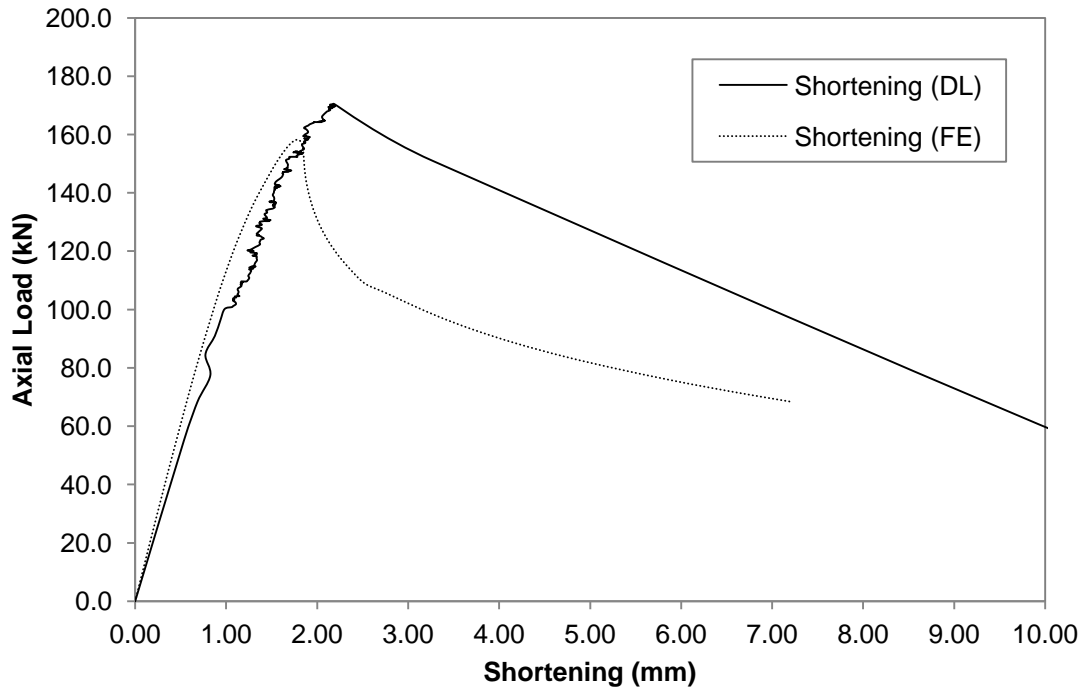


Figure F.57 Axial Load versus Shortening Curve for BU90S200L500-1

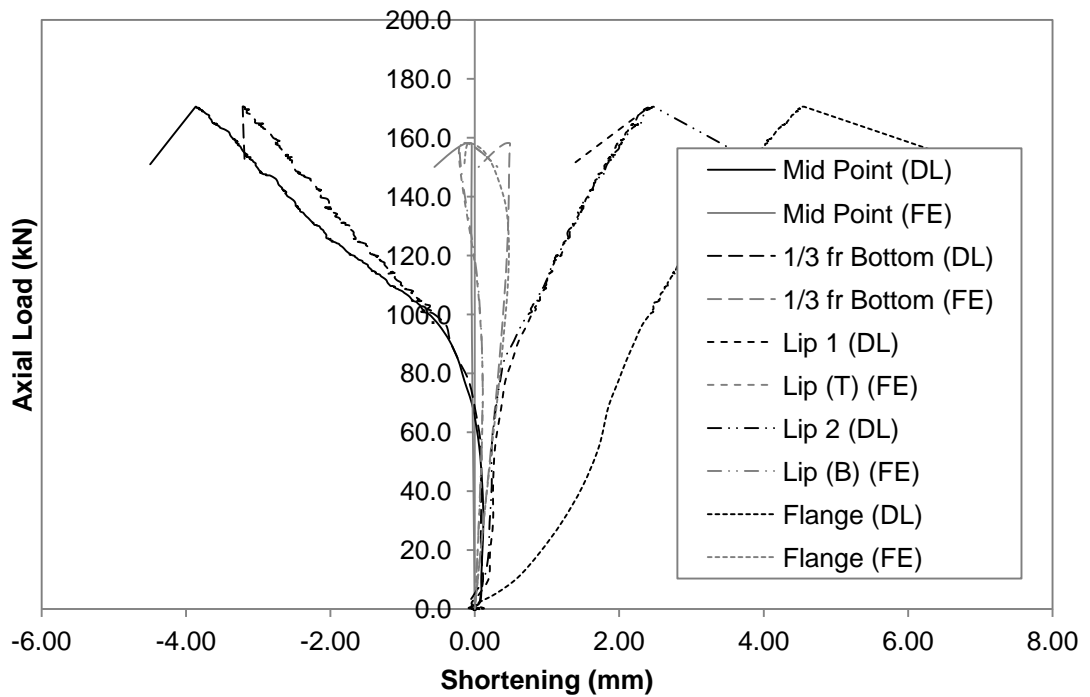


Figure F.58 Axial Load versus Deformation Curve for BU90S200L500-1

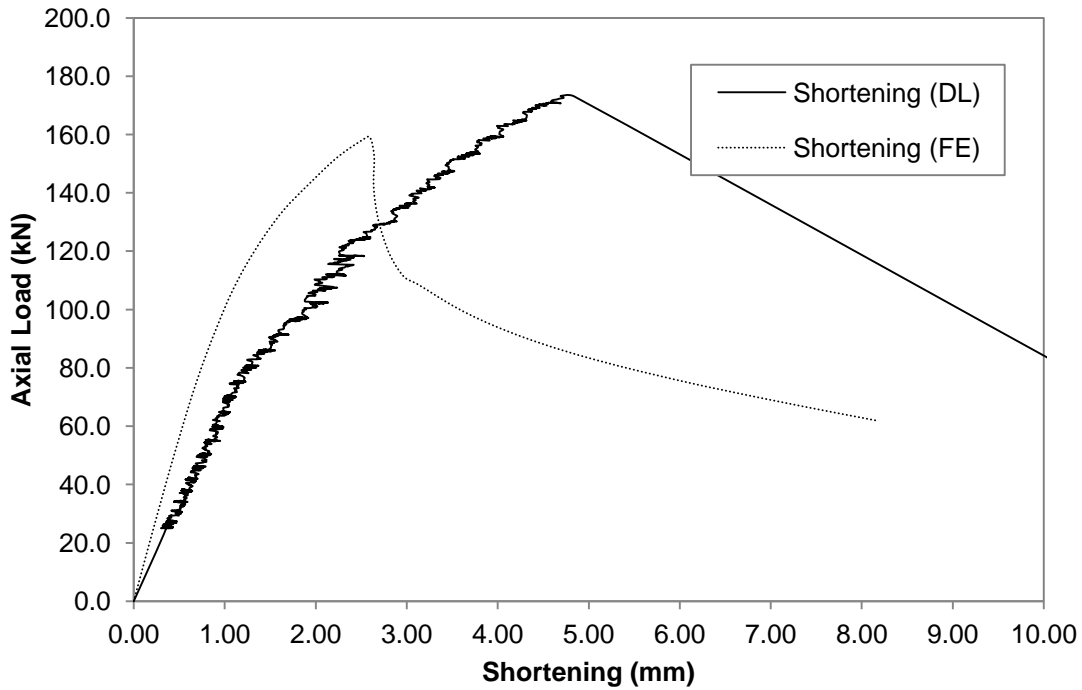


Figure F.59 Axial Load versus Shortening Curve for BU90S200L500-2

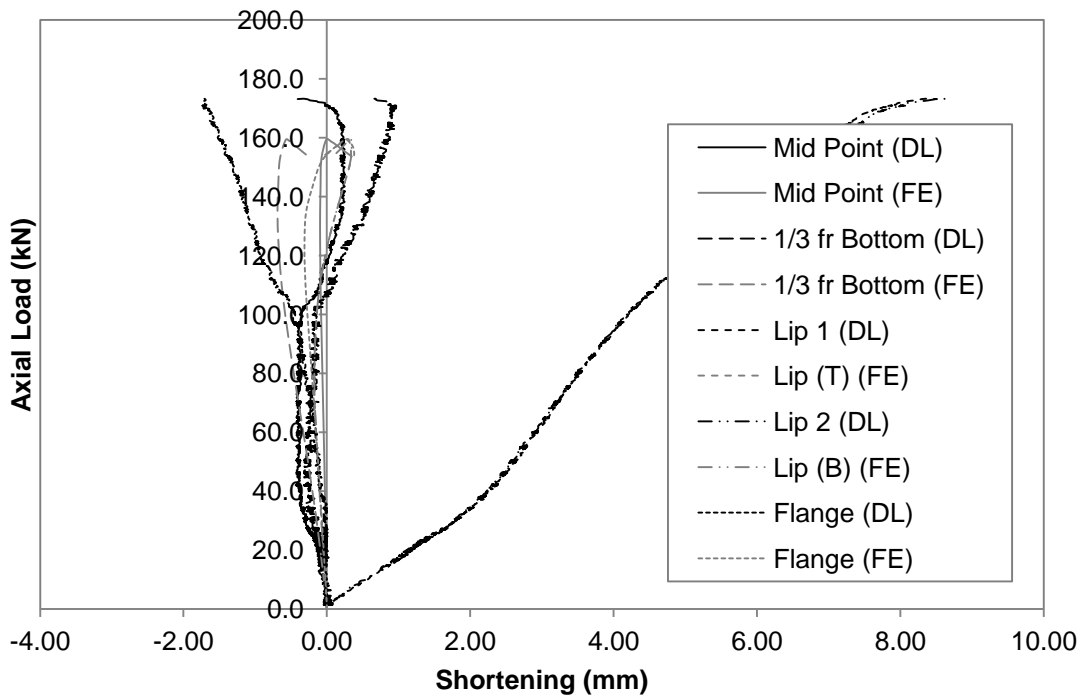


Figure F.60 Axial Load versus Deformation Curve for BU90S200L500-2

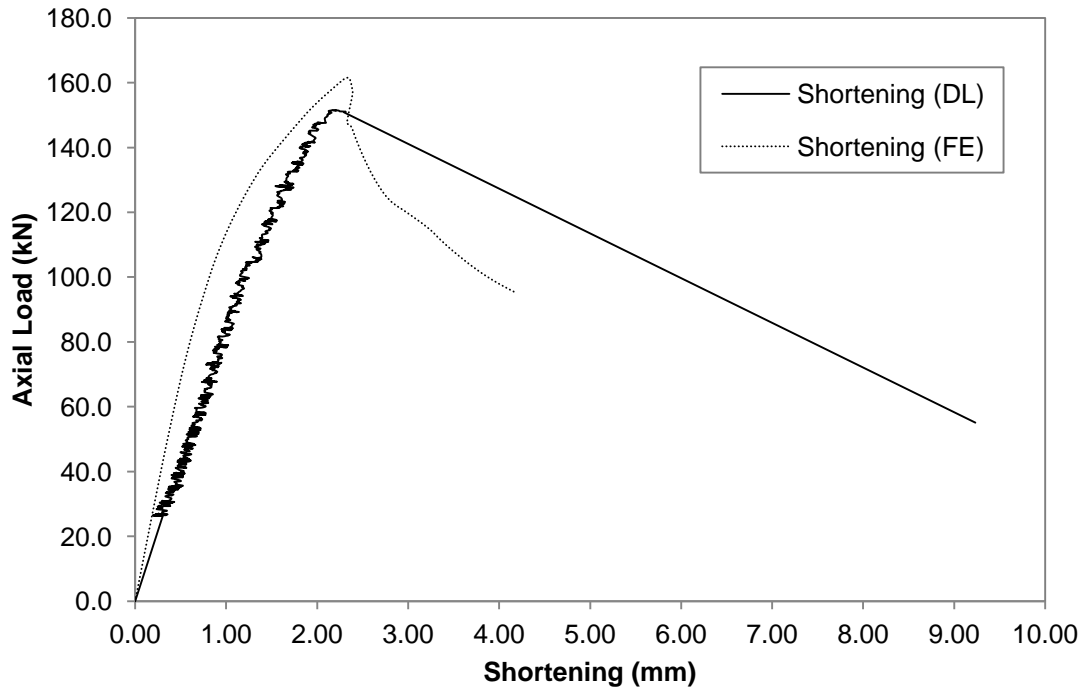


Figure F.61 Axial Load versus Shortening Curve for BU90S200L500-3

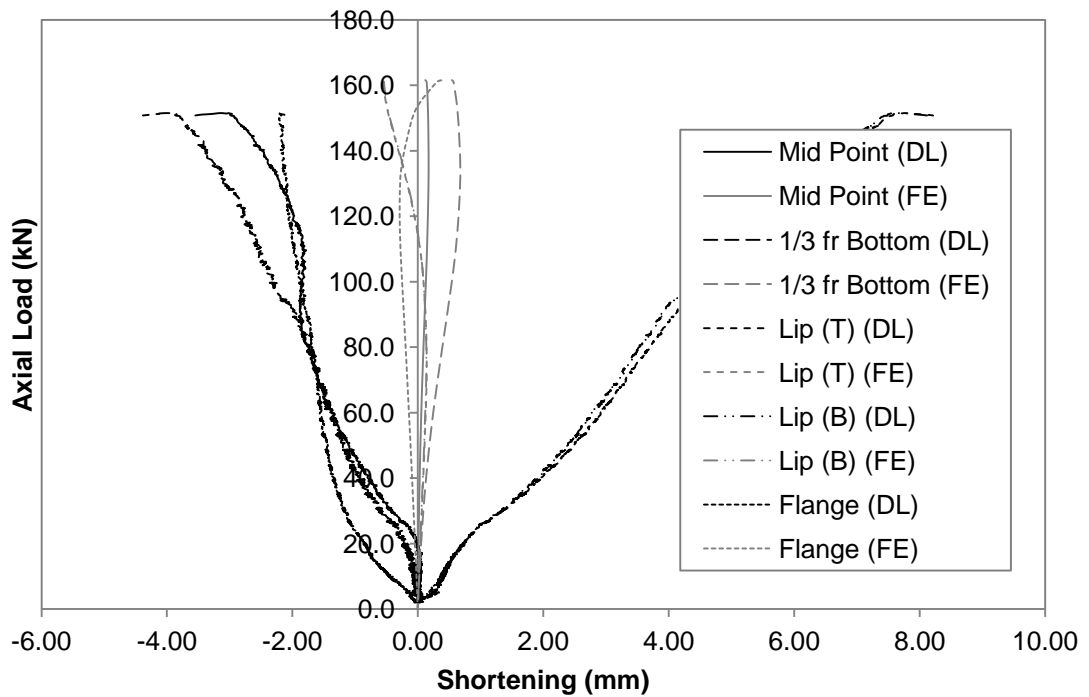


Figure F.62 Axial Load versus Deformation Curve for BU90S200L500-3

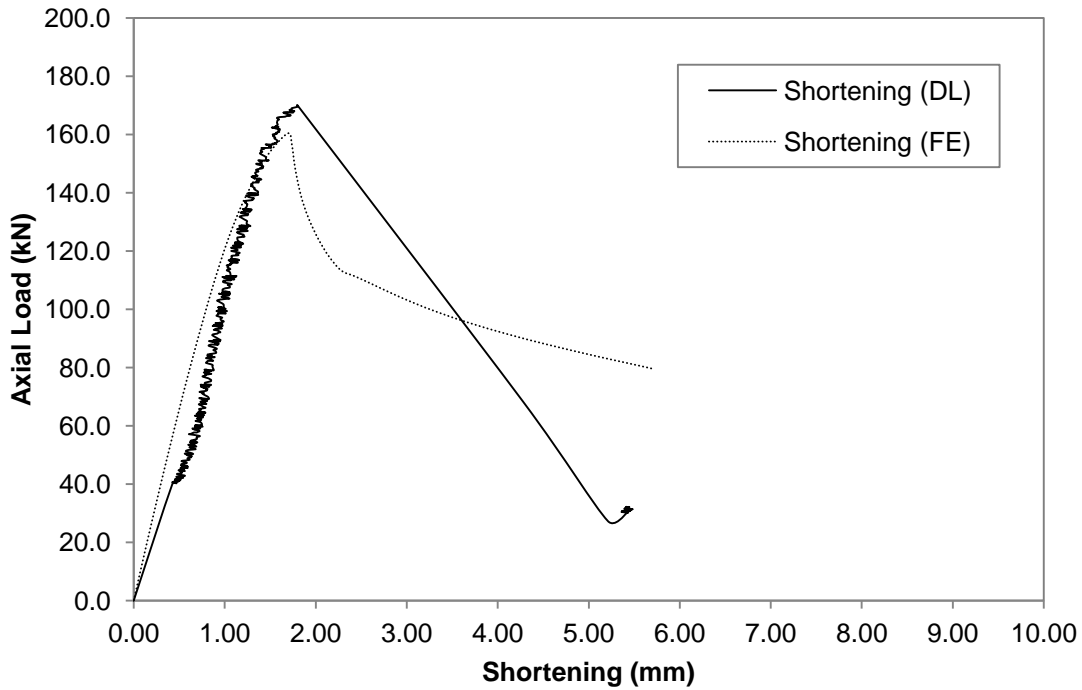


Figure F.63 Axial Load versus Shortening Curve for BU90S400L500-1

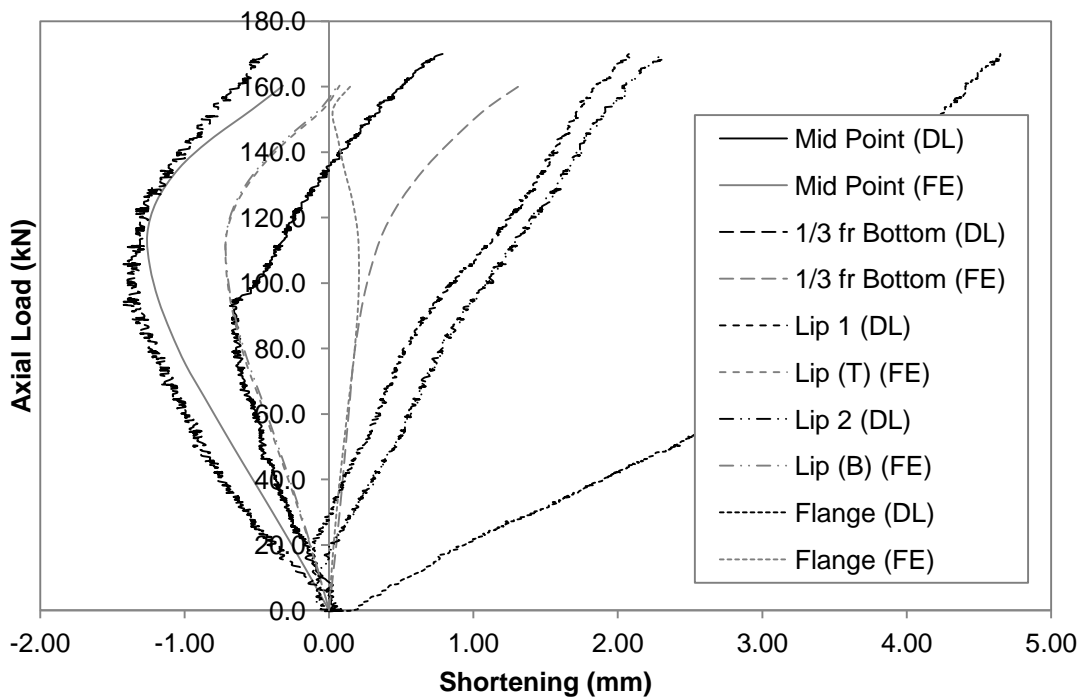


Figure F.64 Axial Load versus Deformation Curve for BU90S400L500-1

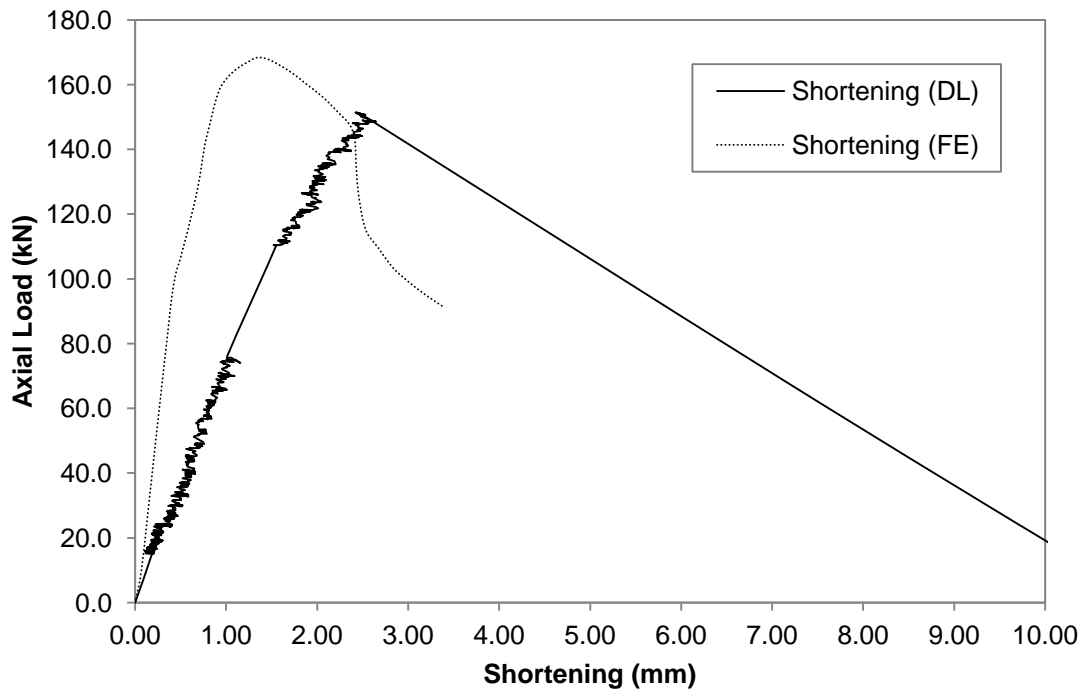


Figure F.65 Axial Load versus Shortening Curve for BU90S400L500-2

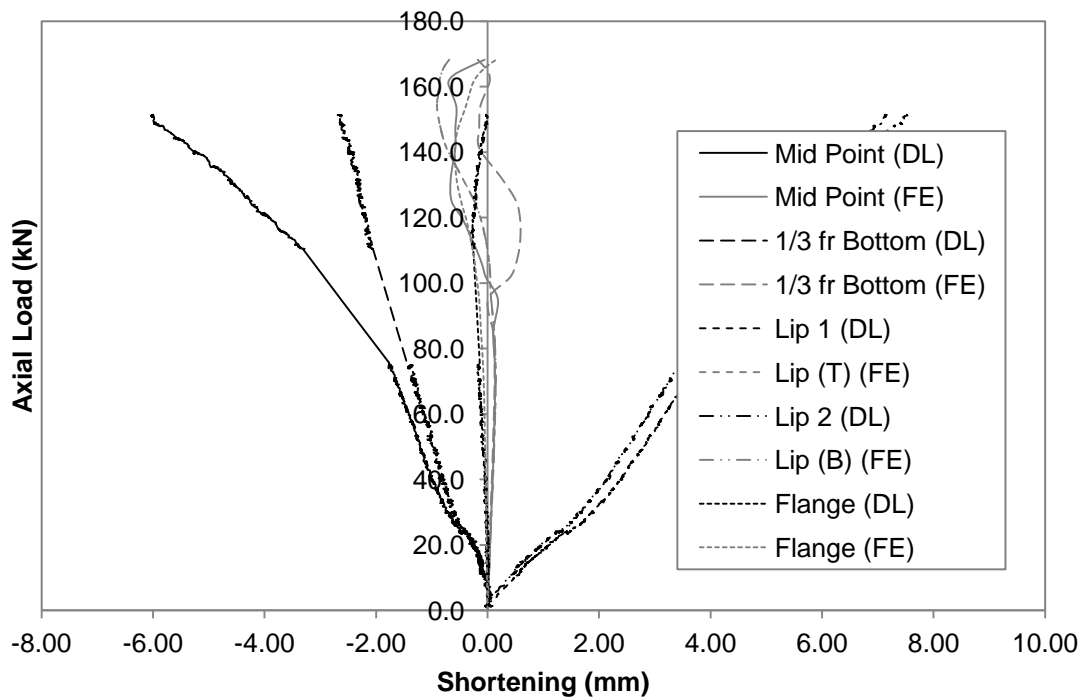


Figure F.66 Axial Load versus Deformation Curve for BU90S400L500-2

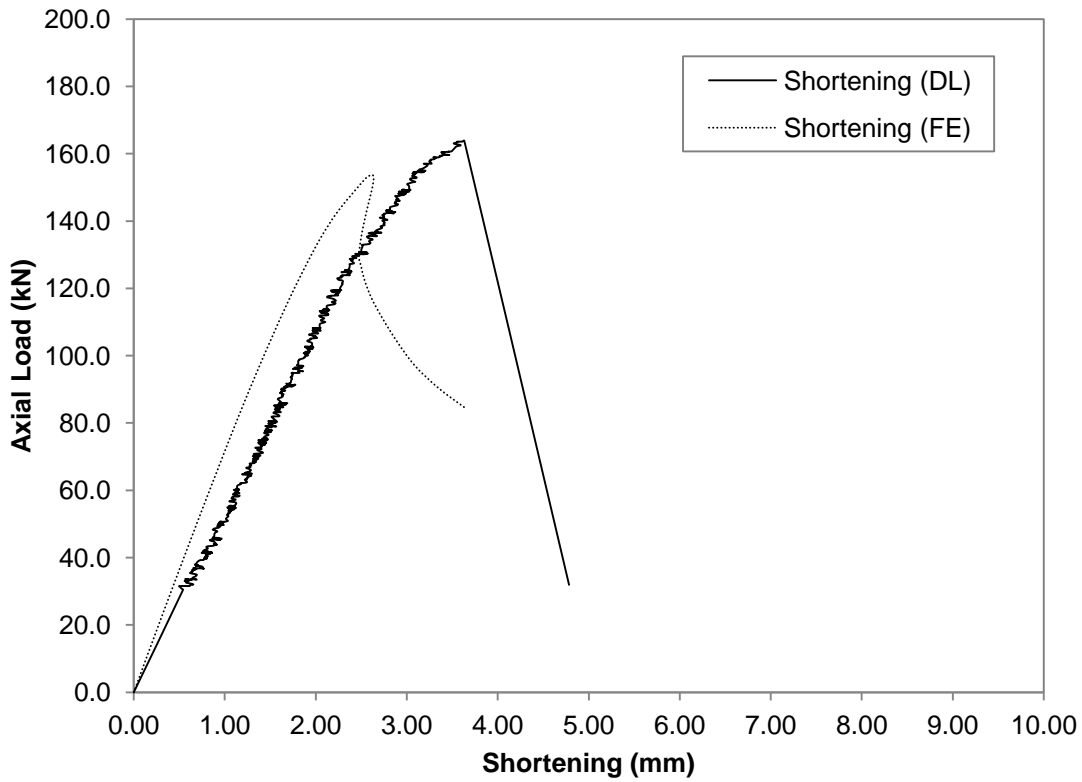


Figure F.67 Axial Load versus Shortening Curve for BU90S225L1000-1

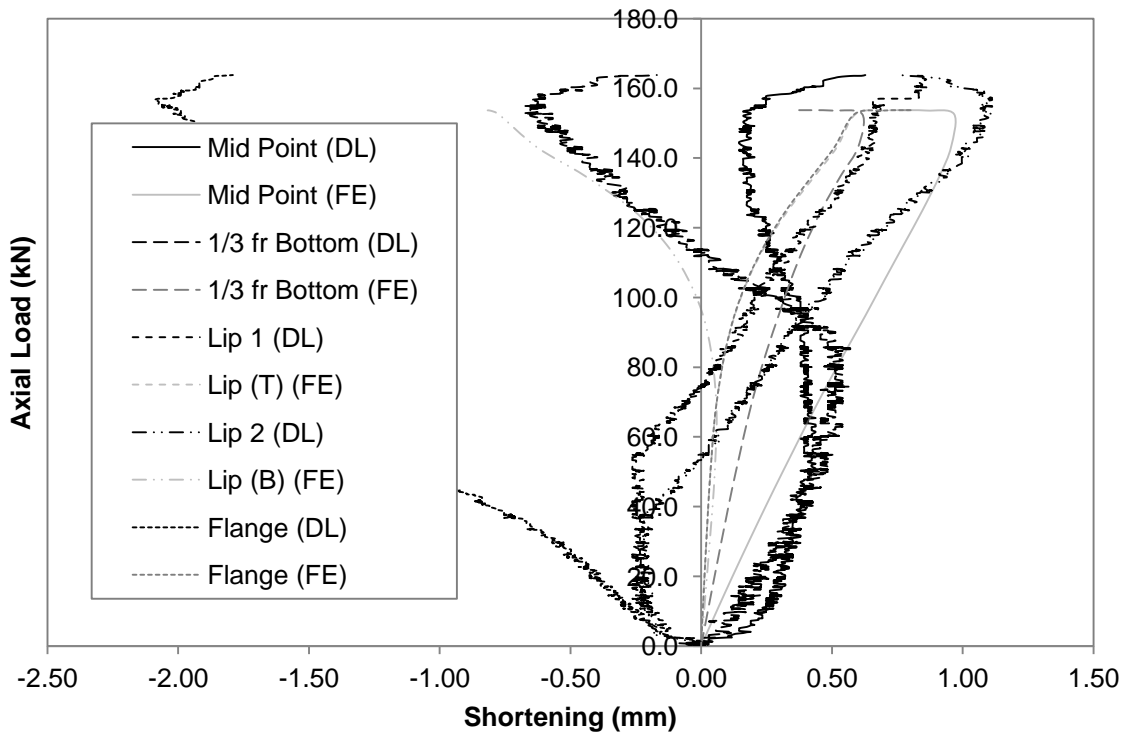


Figure F.68 Axial Load versus Deformation Curve for BU90S225L1000-1

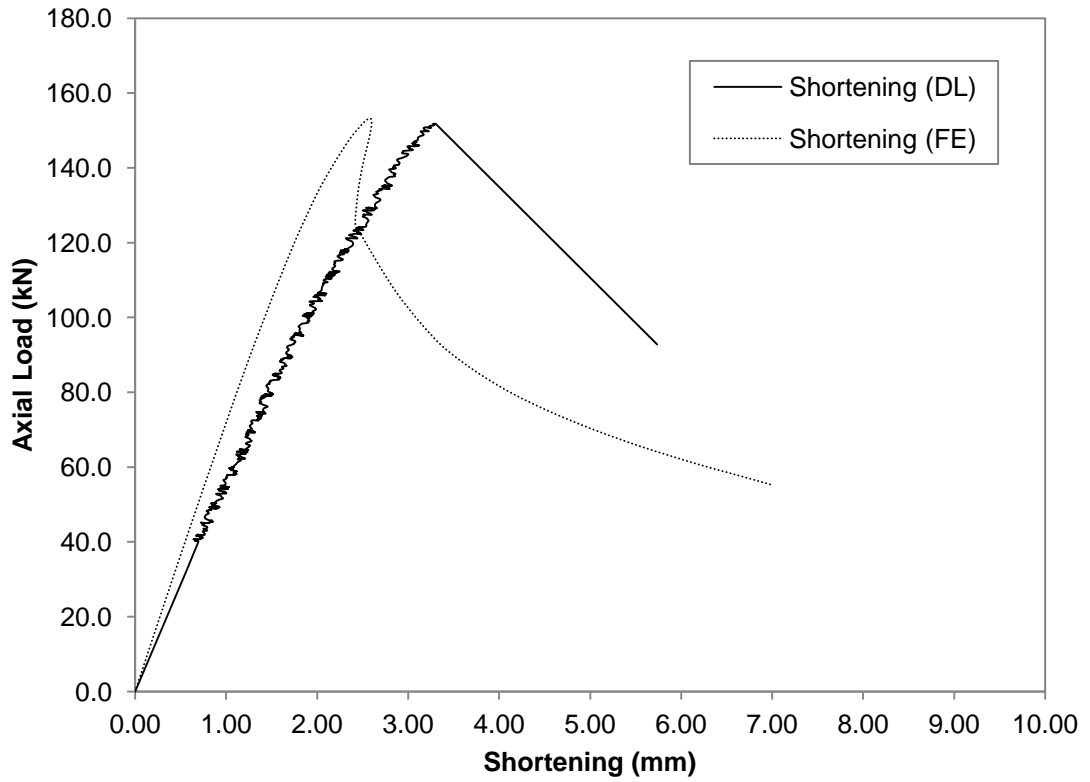


Figure F.69 Axial Load versus Shortening Curve for BU90S225L1000-2

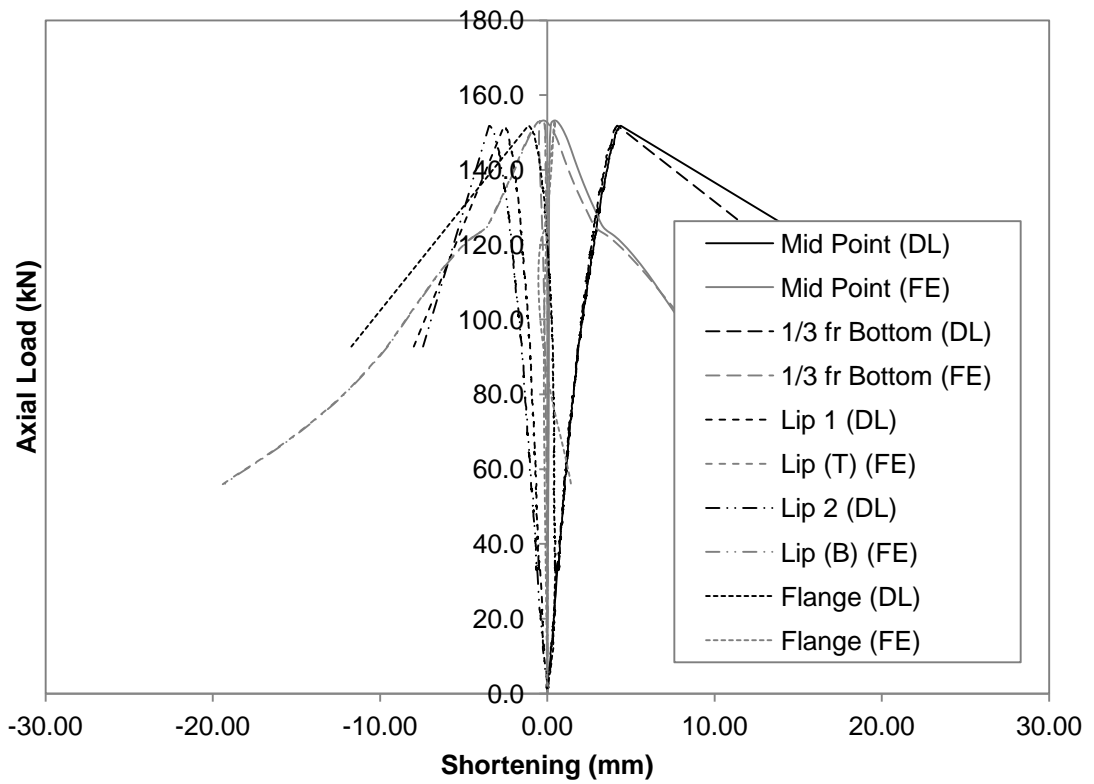


Figure F.70 Axial Load versus Deformation Curve for BU90S225L1000-2

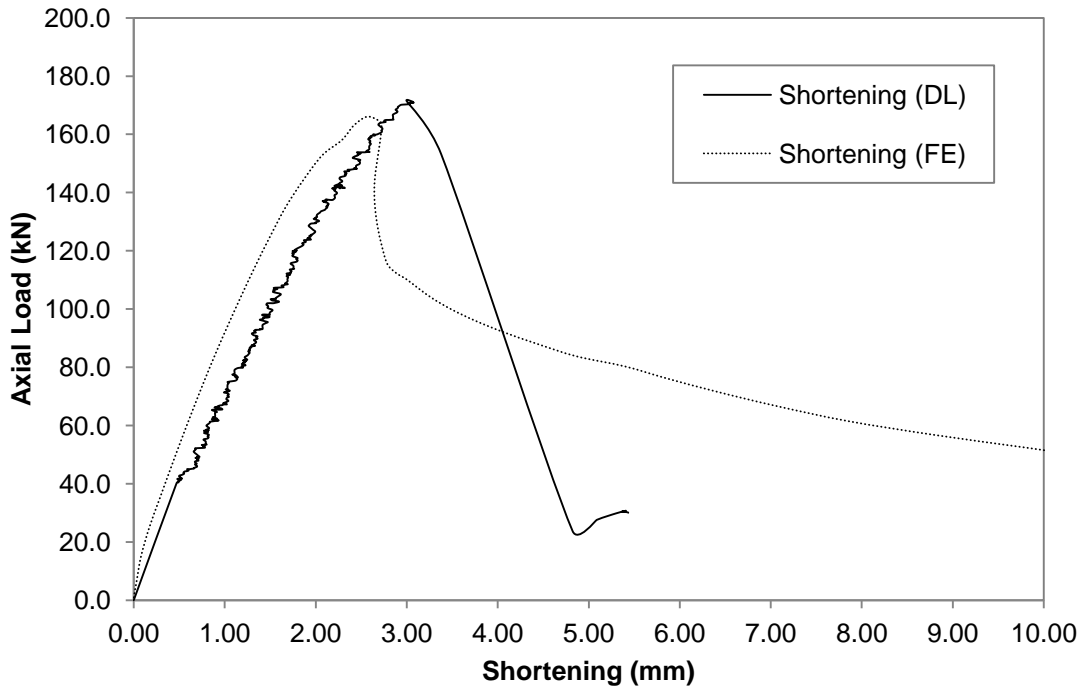


Figure F.71 Axial Load versus Shortening Curve for BU90S450L1000-2

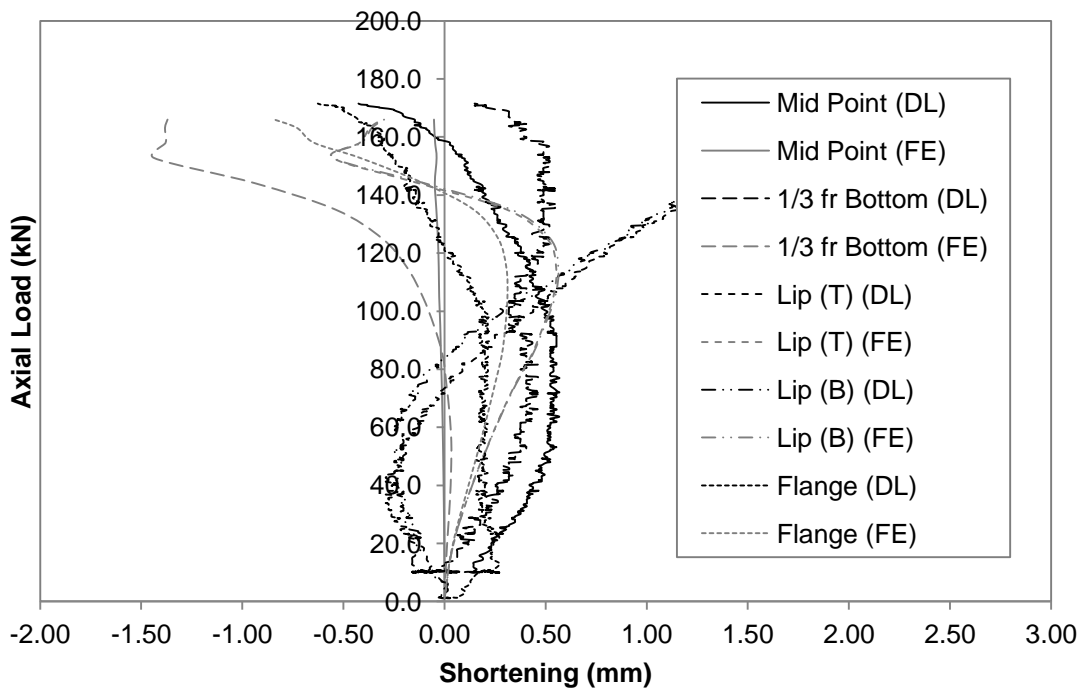


Figure F.72 Axial Load versus Deformation Curve for BU90S450L1000-2

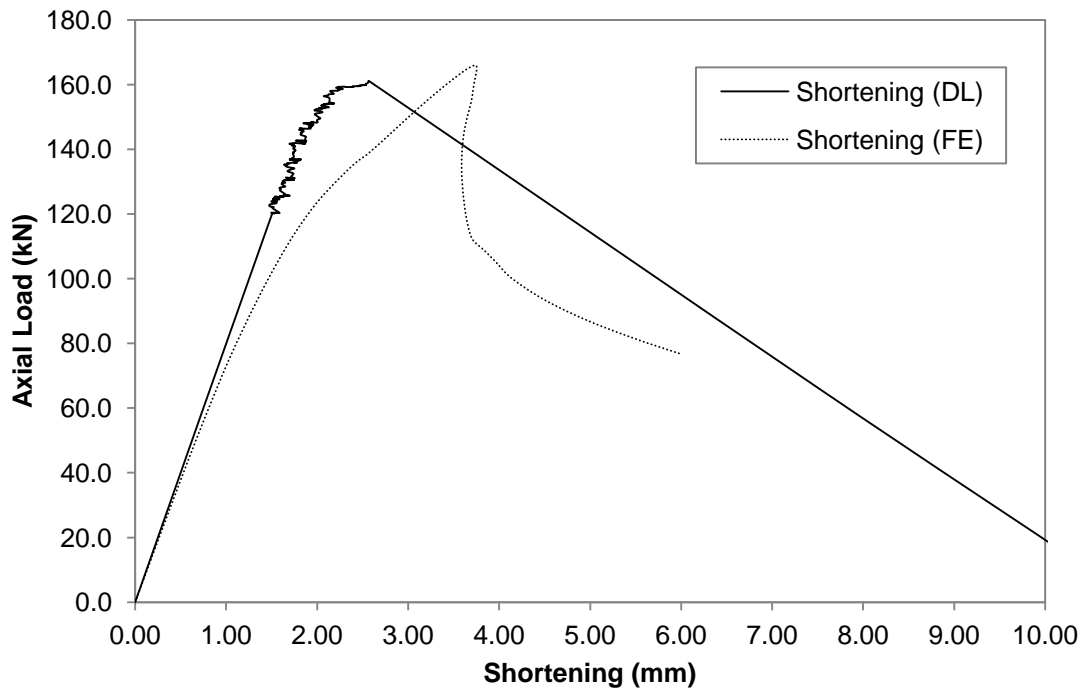


Figure F.73 Axial Load versus Shortening Curve for BU90S450L1000-3

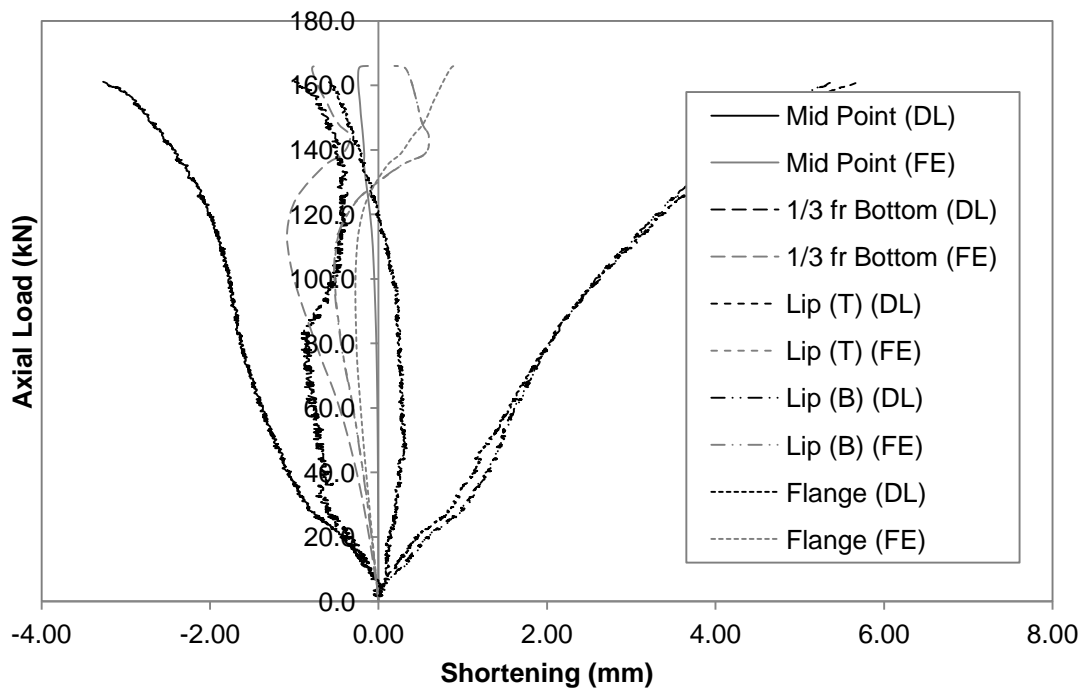


Figure F.74 Axial Load versus Deformation Curve for BU90S450L1000-3

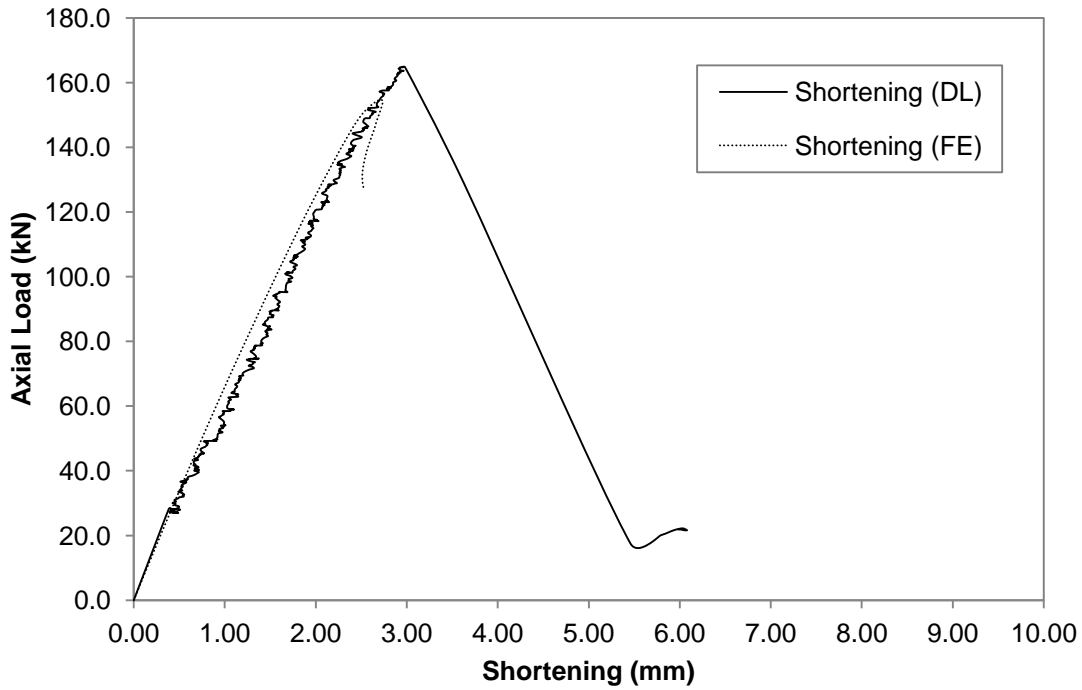


Figure F.75 Axial Load versus Shortening Curve for BU90S900L1000-1

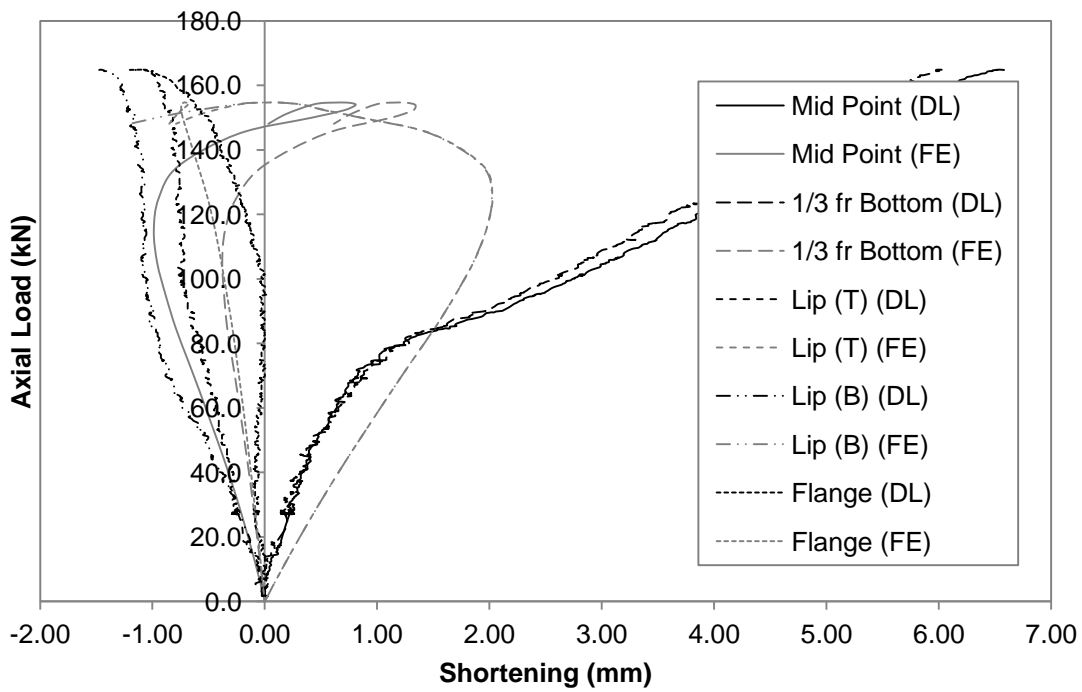


Figure F.76 Axial Load versus Deformation Curve for BU90S900L1000-1

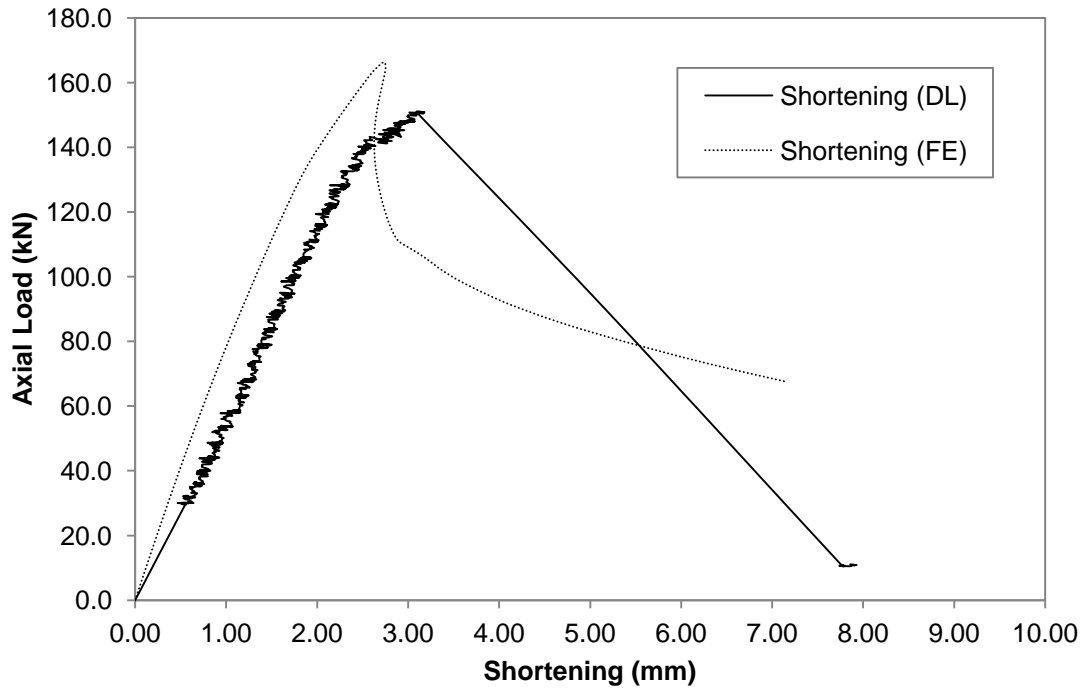


Figure F.77 Axial Load versus Shortening Curve for BU90S900L1000-2

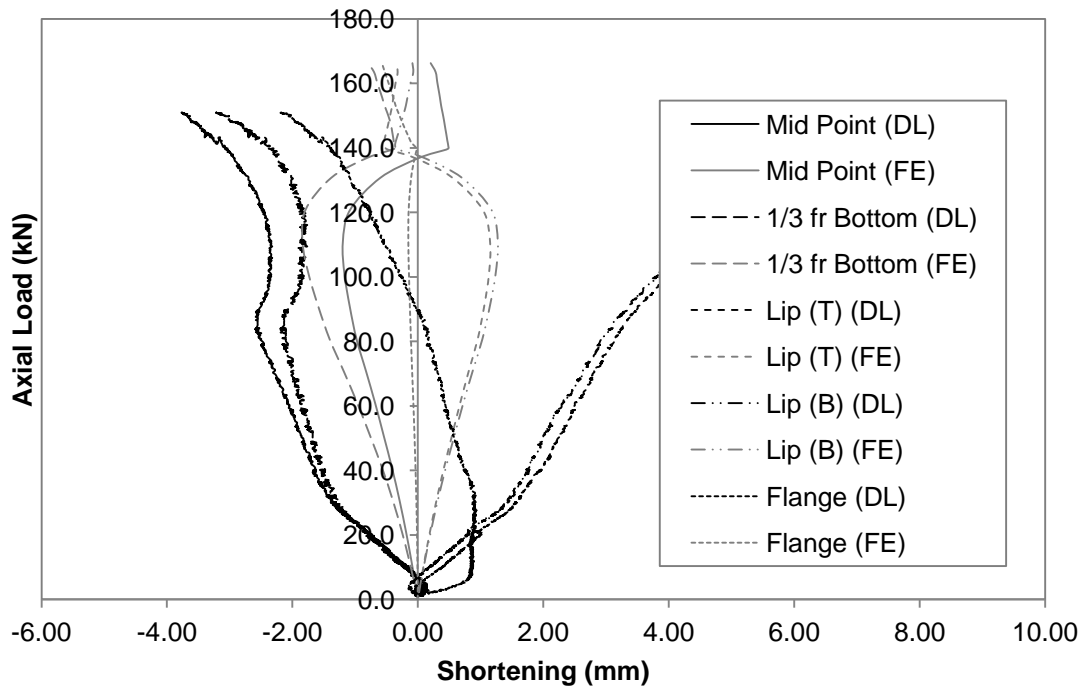


Figure F.78 Axial Load versus Deformation Curve for BU90S900L1000-2

F.3 Intermediate Column

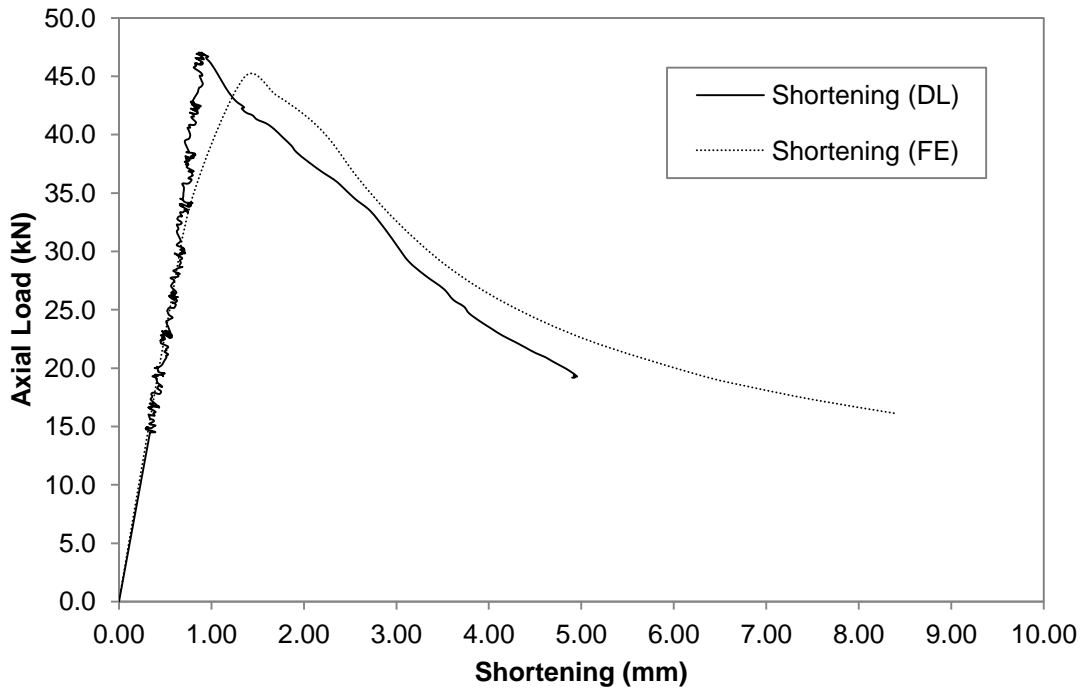


Figure F.79 Axial Load versus Shortening Curve for BU75S225L1000-1

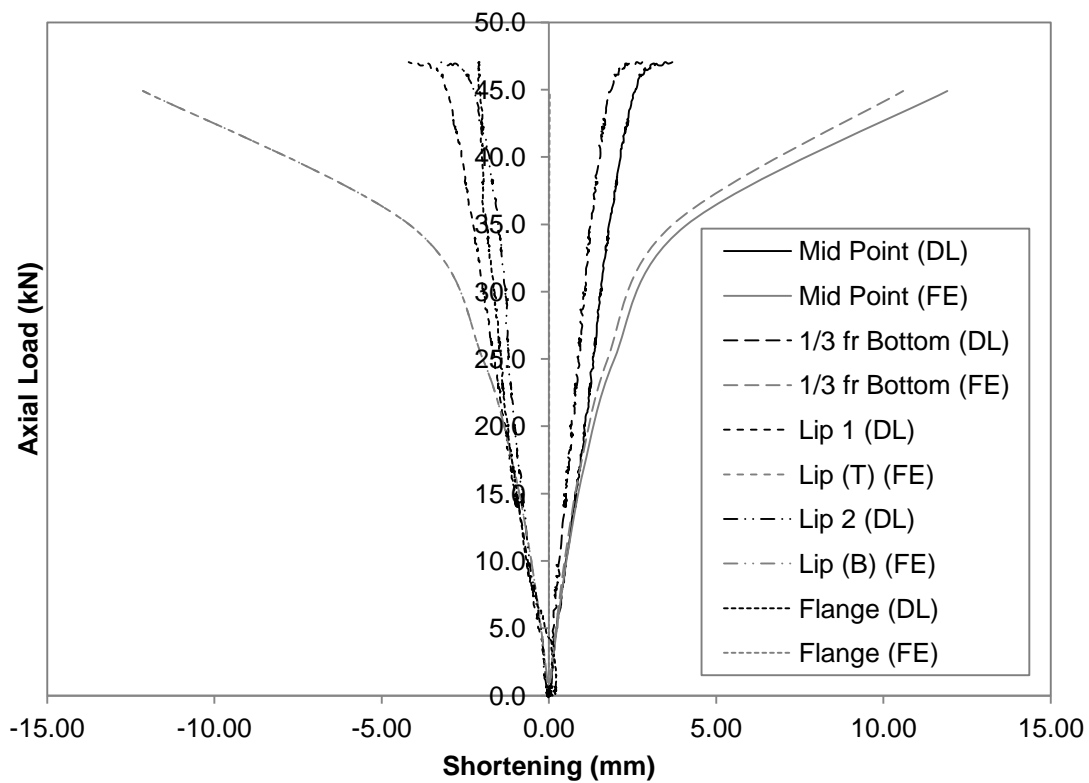


Figure F.80 Axial Load versus Deformation Curve for BU75S225L1000-1

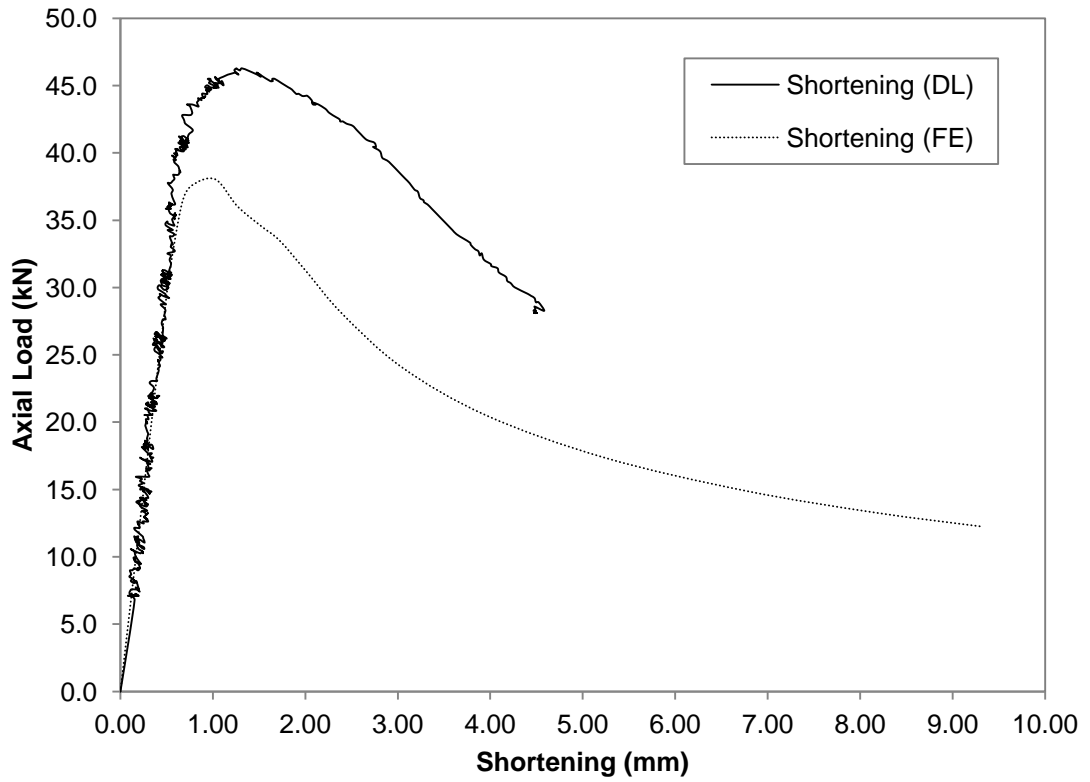


Figure F.81 Axial Load versus Shortening Curve for BU75S225L1000-2

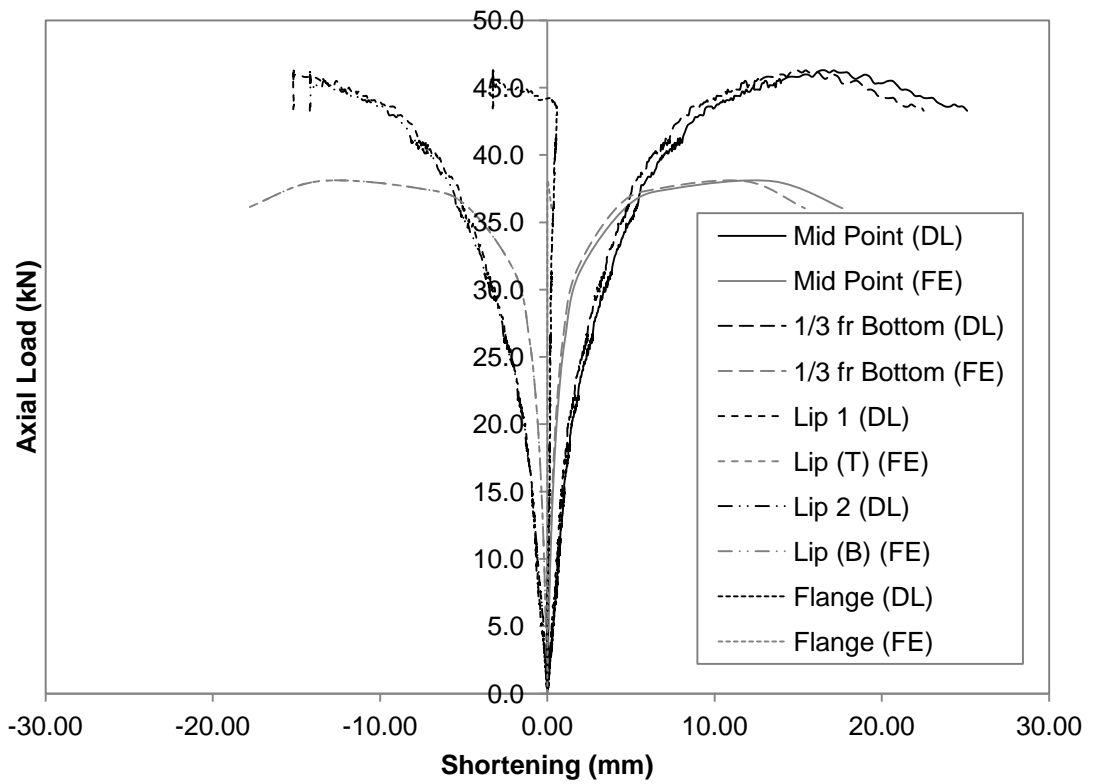


Figure F.82 Axial Load versus Deformation Curve for BU75S225L1000-2

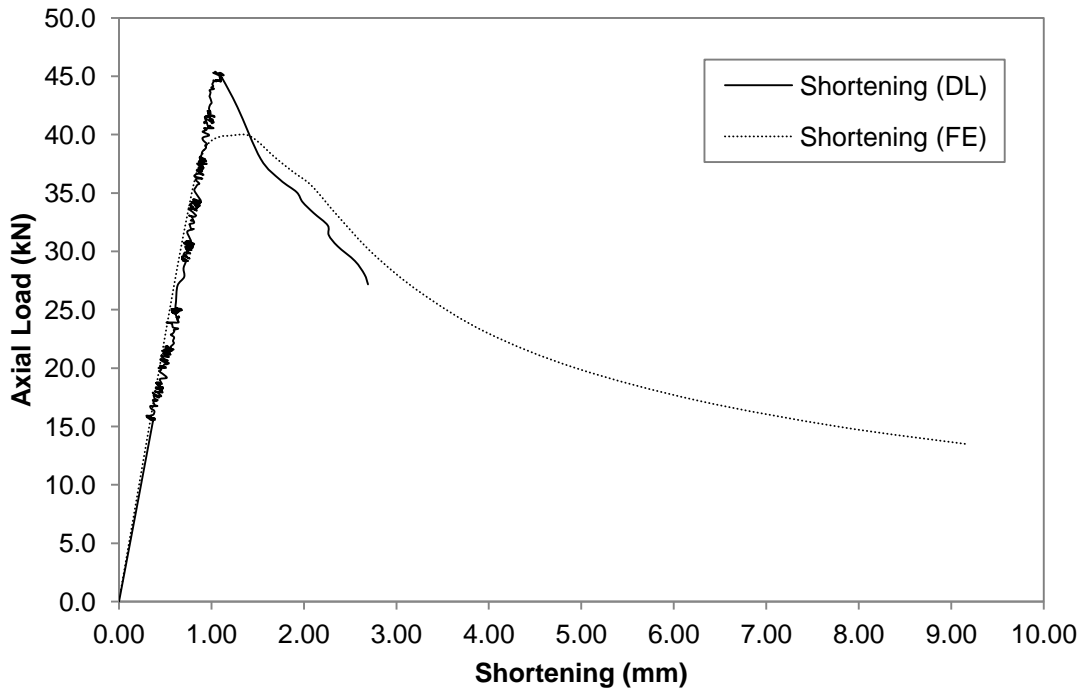


Figure F.83 Axial Load versus Shortening Curve for BU75S450L1000-1

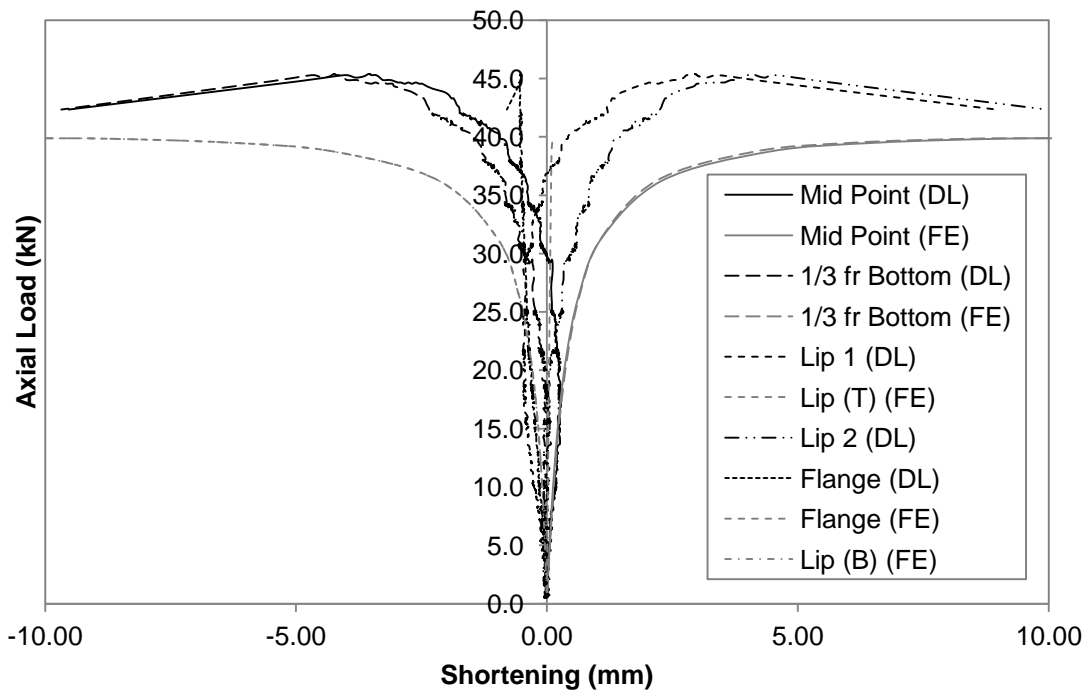


Figure F.84 Axial Load versus Deformation Curve for BU75S450L1000-1

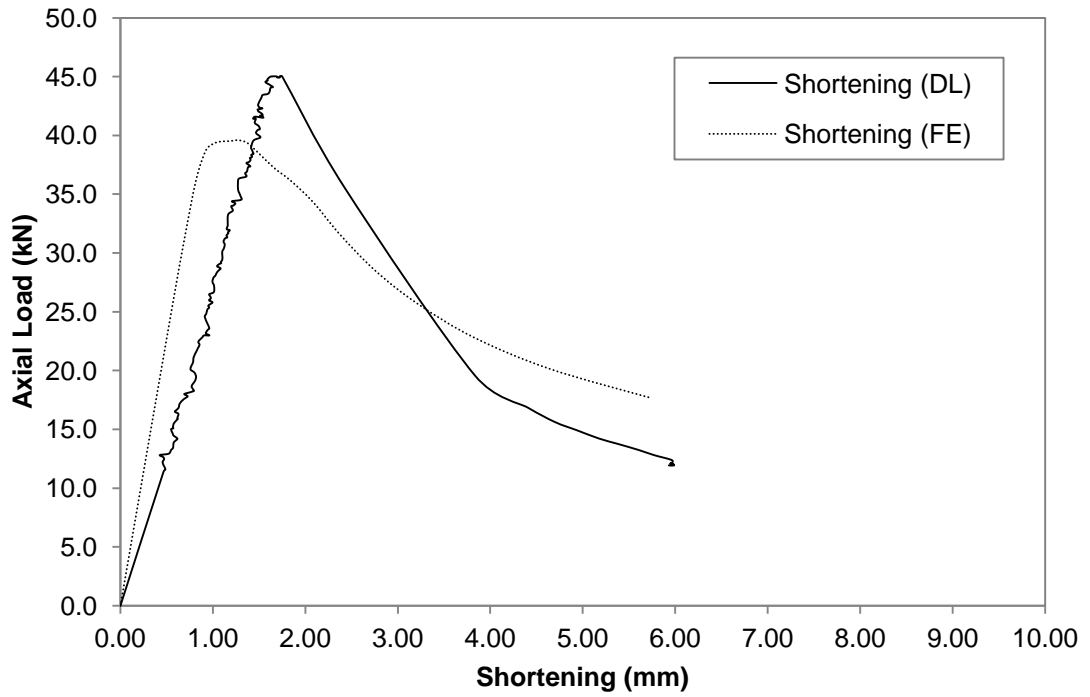


Figure F.85 Axial Load versus Shortening Curve for BU75S450L1000-2

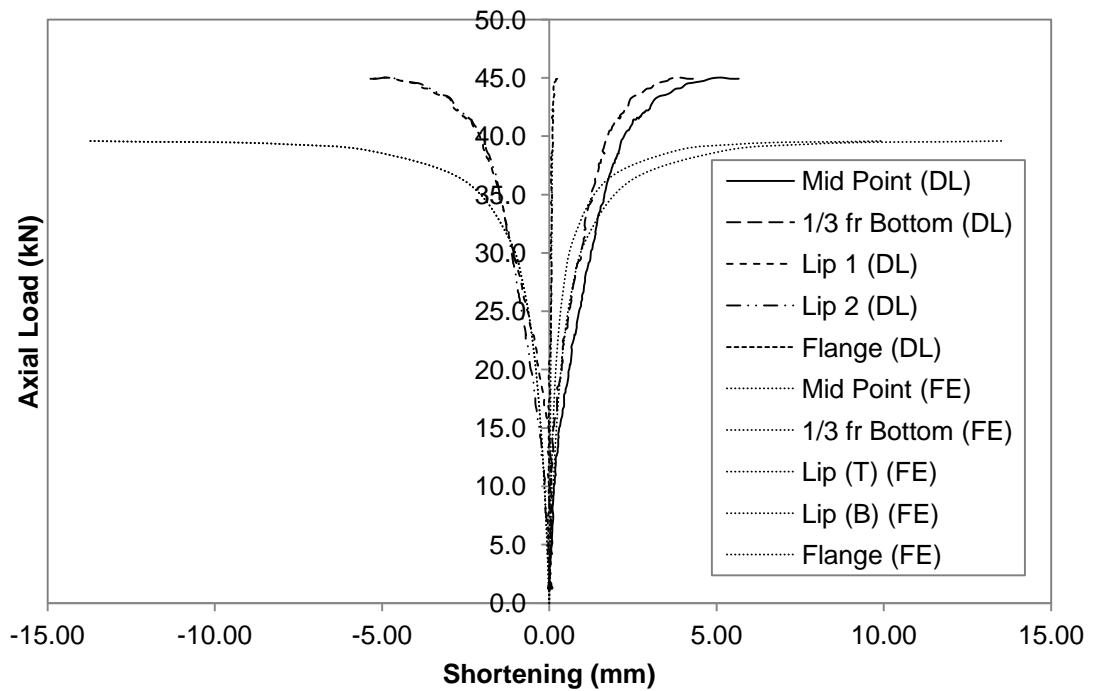


Figure F.86 Axial Load versus Deformation Curve for BU75S450L1000-2

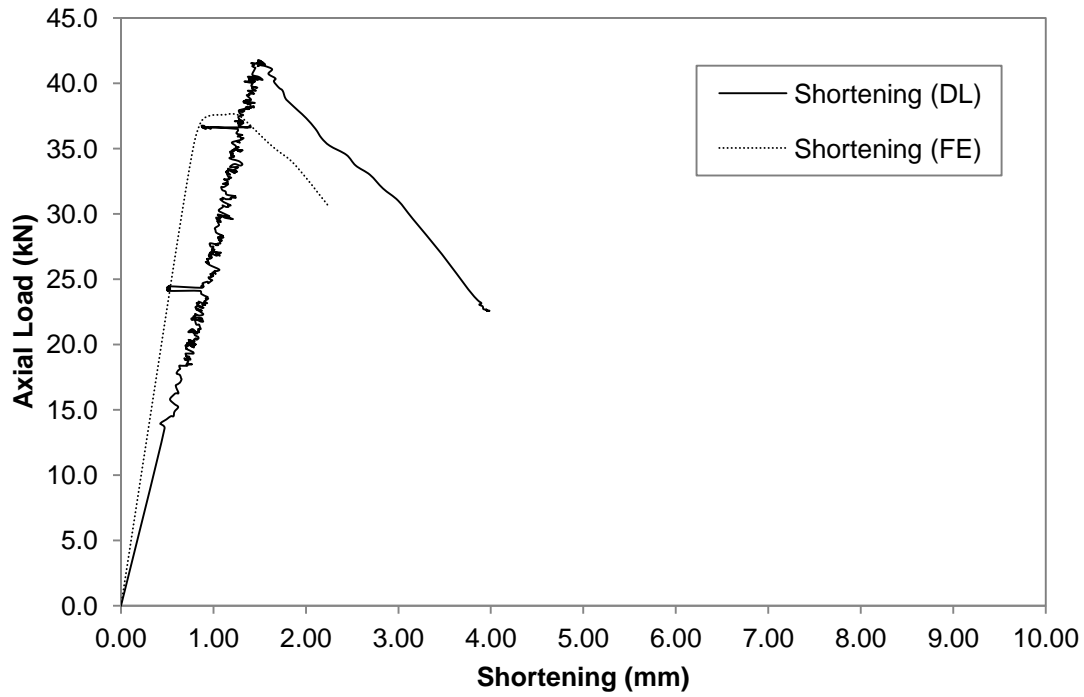


Figure F.87 Axial Load versus Shortening Curve for BU75S450L1000-3

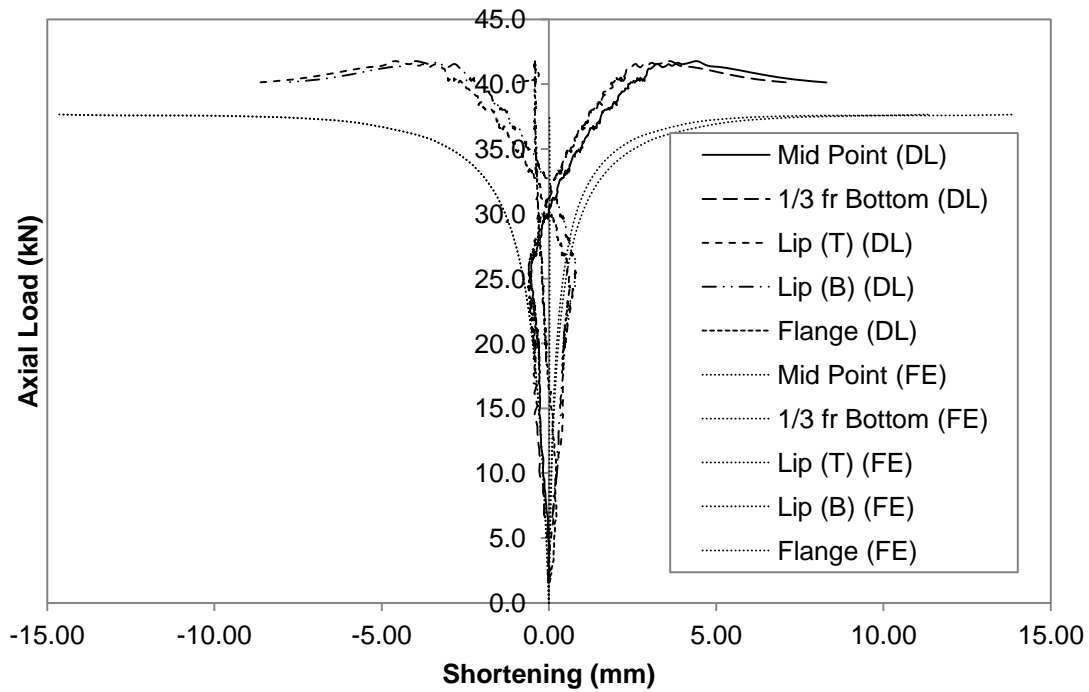


Figure F.88 Axial Load versus Deformation Curve for BU75S450L1000-3

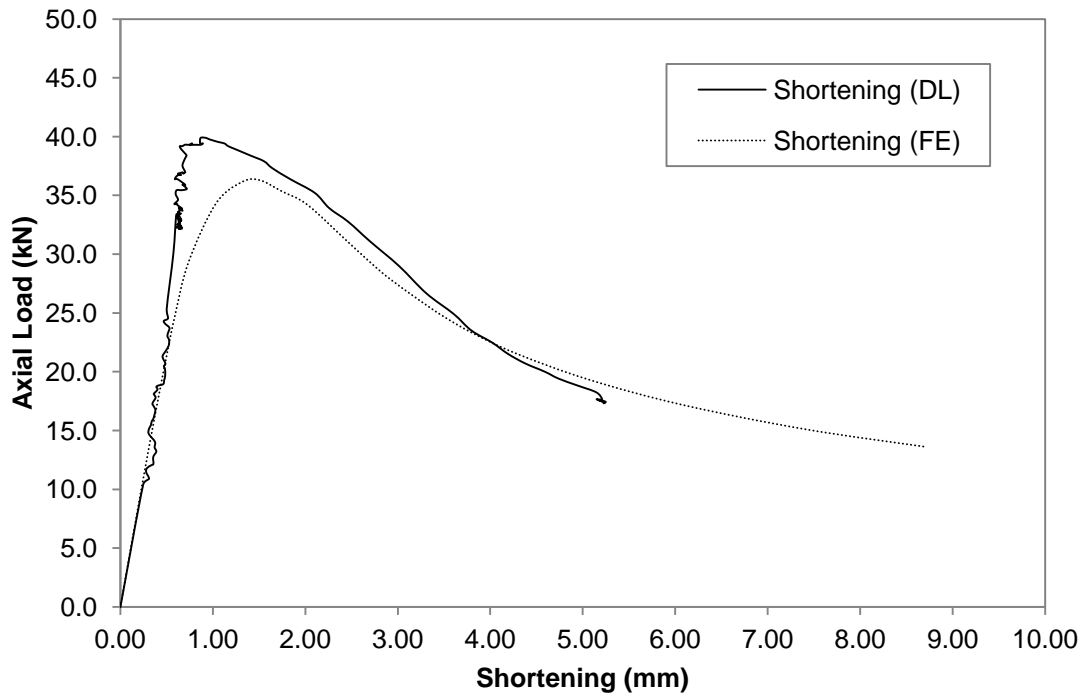


Figure F.89 Axial Load versus Shortening Curve for BU75S900L1000-1

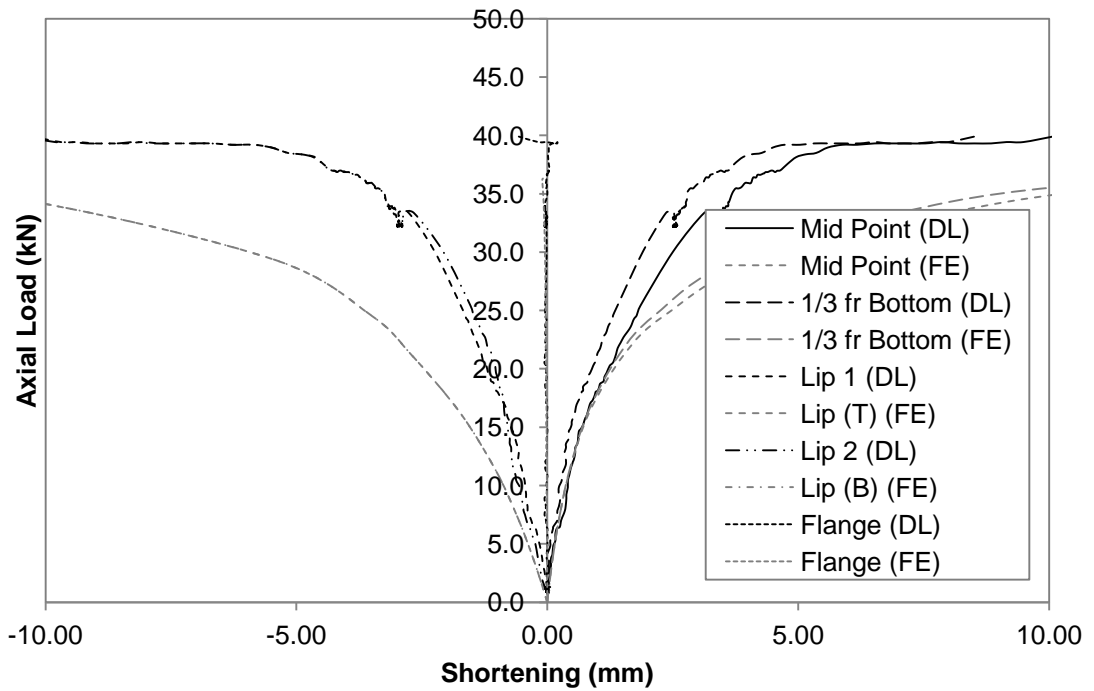


Figure F.90 Axial Load versus Deformation Curve for BU75S900L1000-1

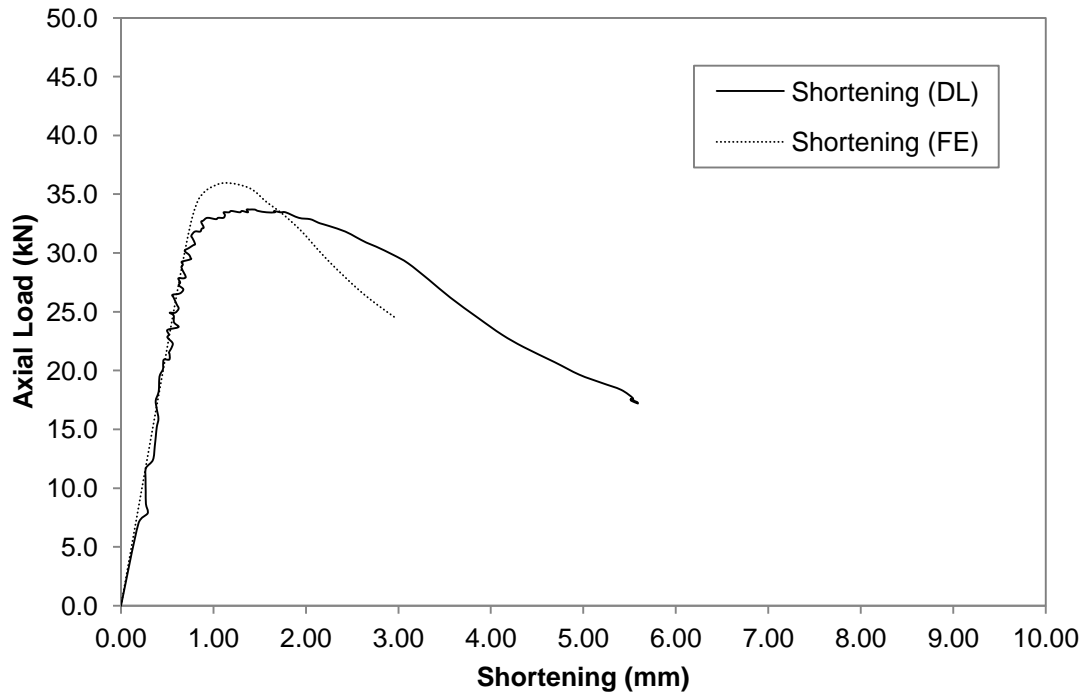


Figure F.91 Axial Load versus Shortening Curve for BU75S900L1000-2

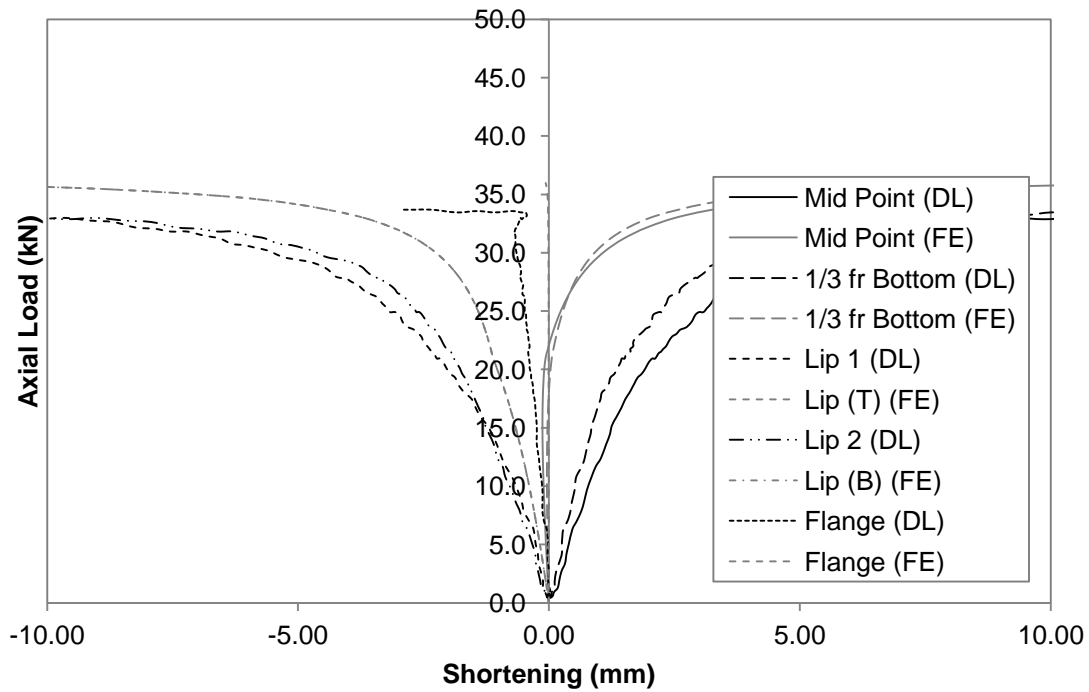


Figure F.92 Axial Load versus Deformation Curve for BU75S900L1000-2

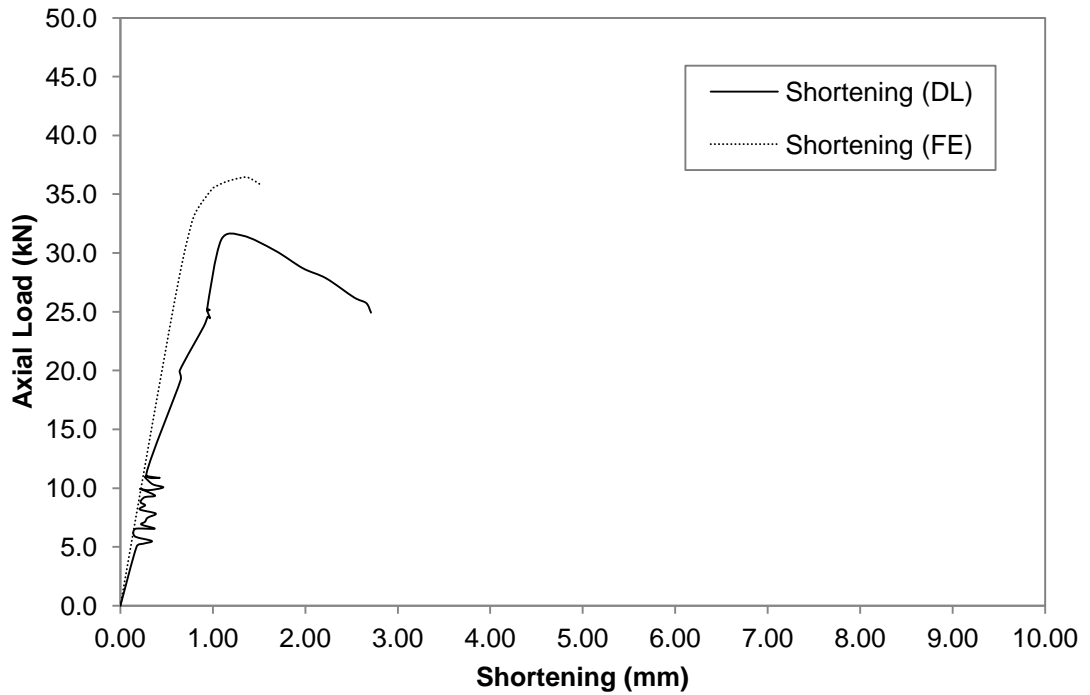


Figure F.93 Axial Load versus Shortening Curve for BU75S900L1000-3

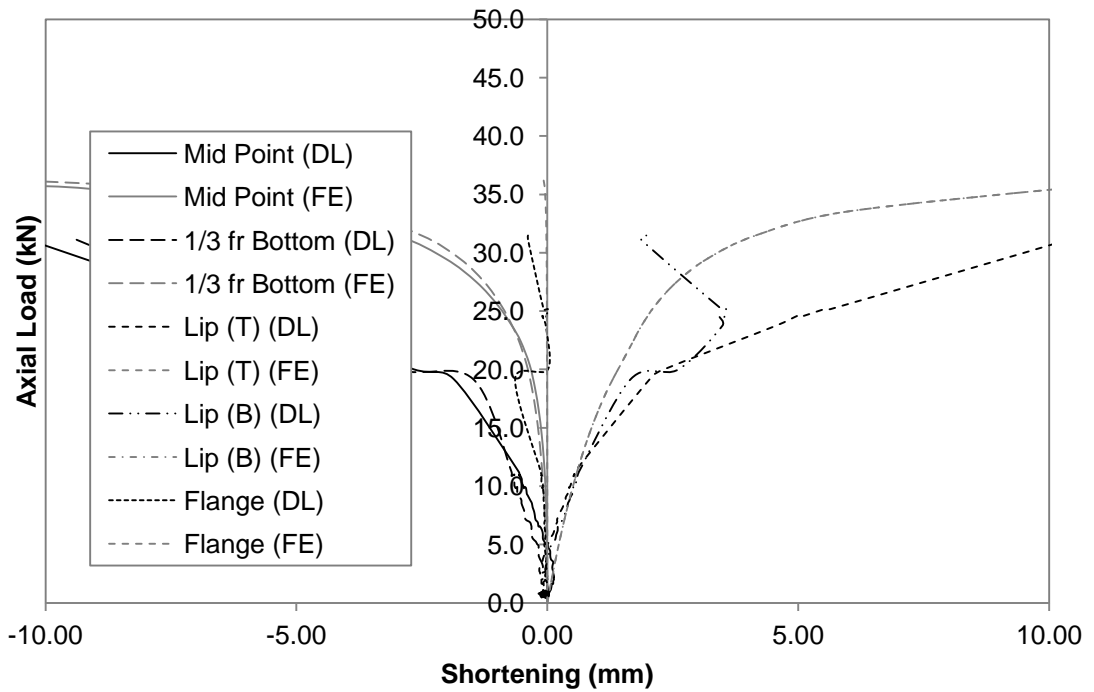


Figure F.94 Axial Load versus Deformation Curve for BU75S900L1000-3

F.4 Slender Column

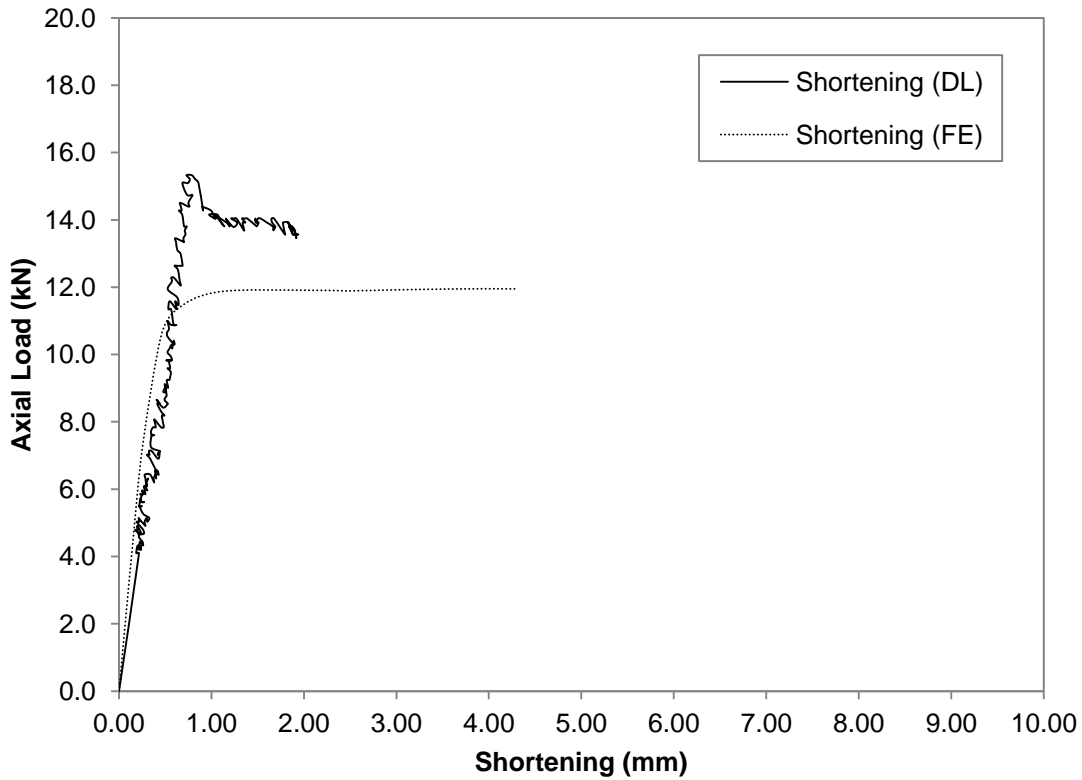


Figure F.95 Axial Load versus Shortening Curve for BU75S475L2000-2

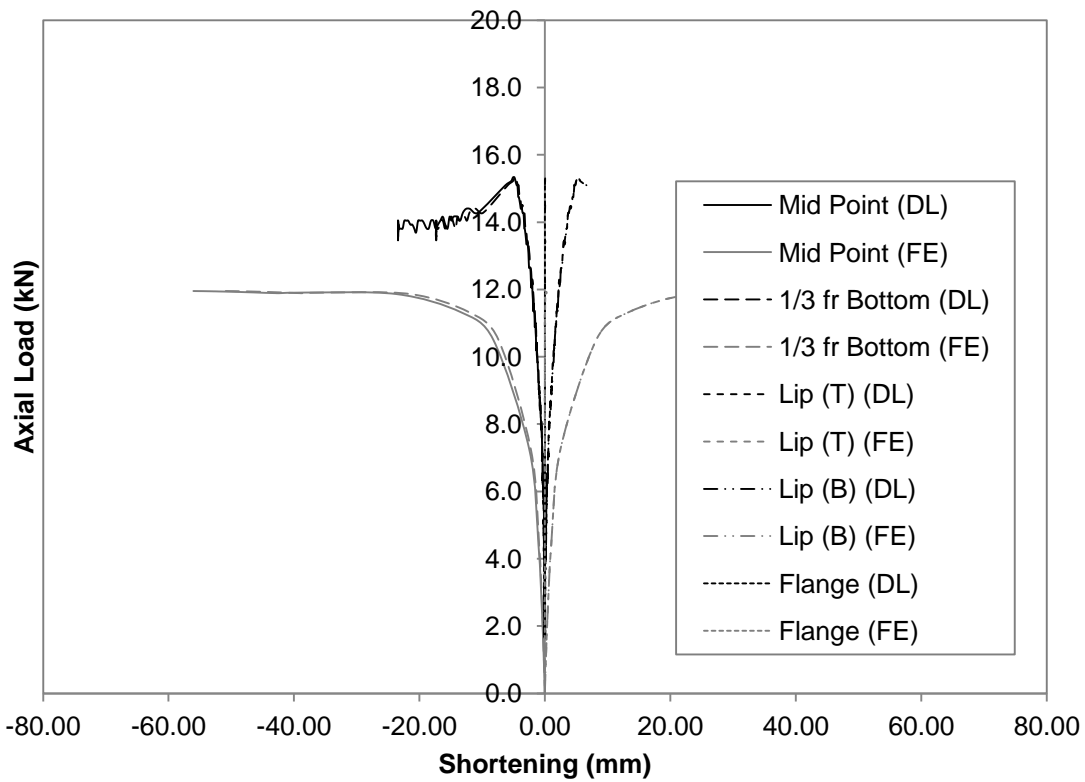


Figure F.96 Axial Load versus Deformation Curve for BU75S475L2000-2

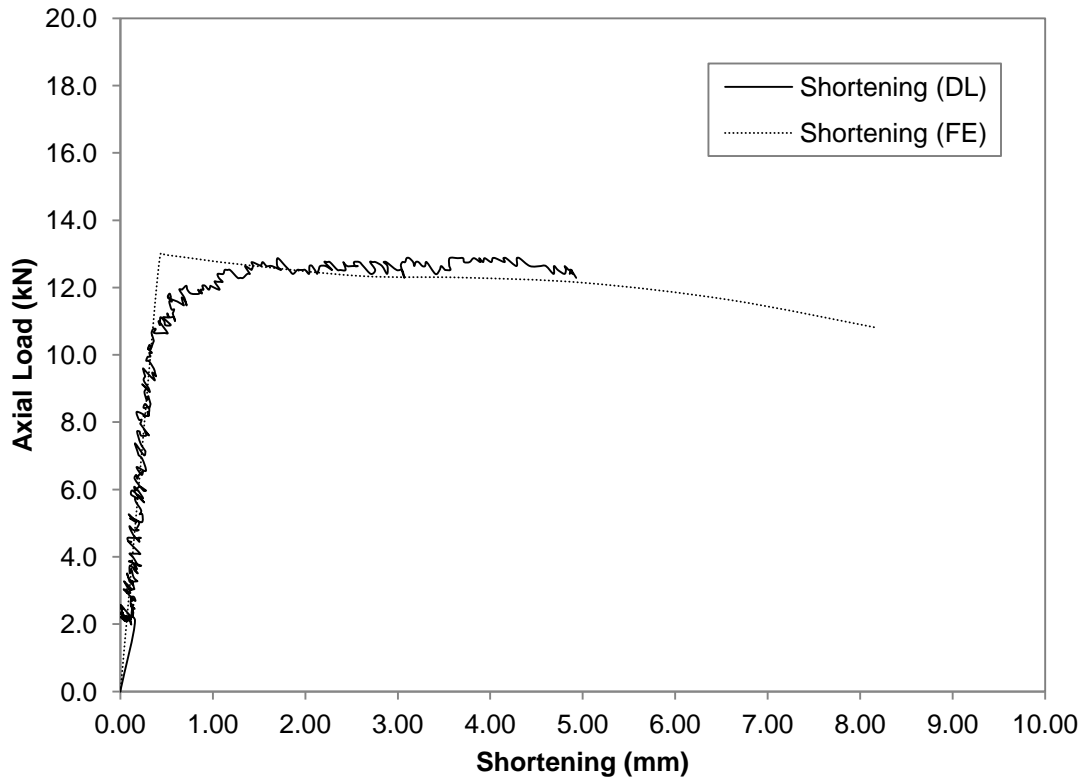


Figure F.97 Axial Load versus Shortening Curve for BU75S475L2000-3

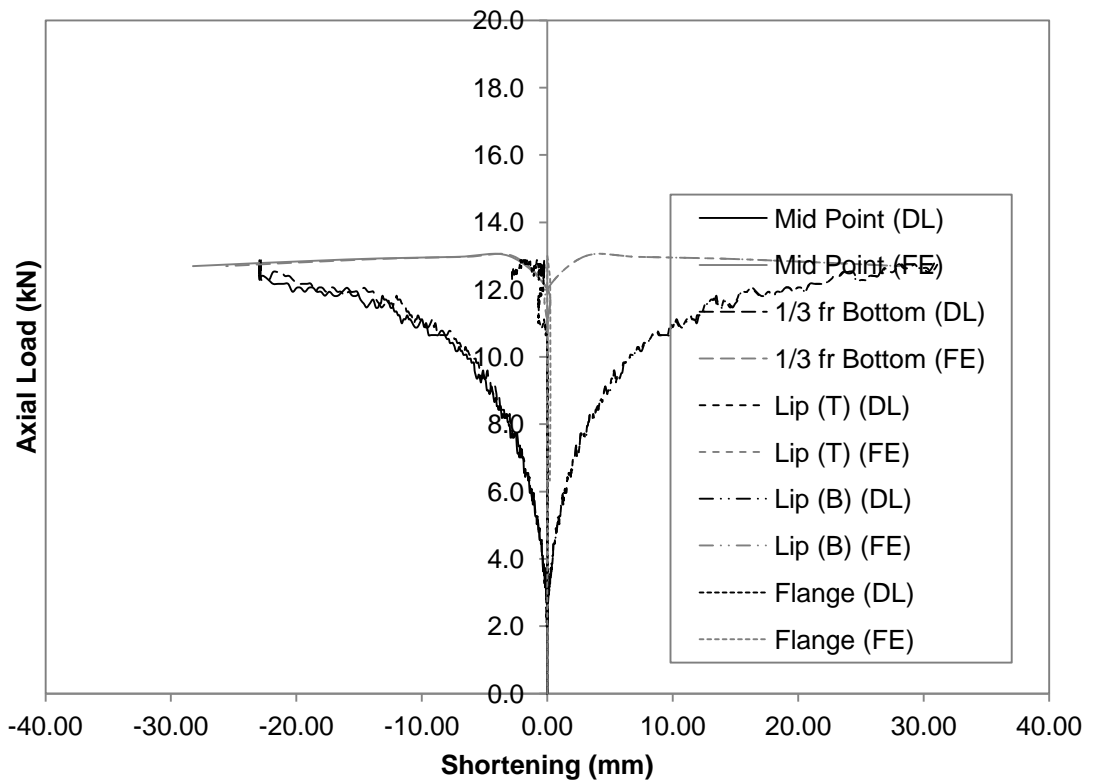


Figure F.98 Axial Load versus Deformation Curve for BU75S475L2000-3

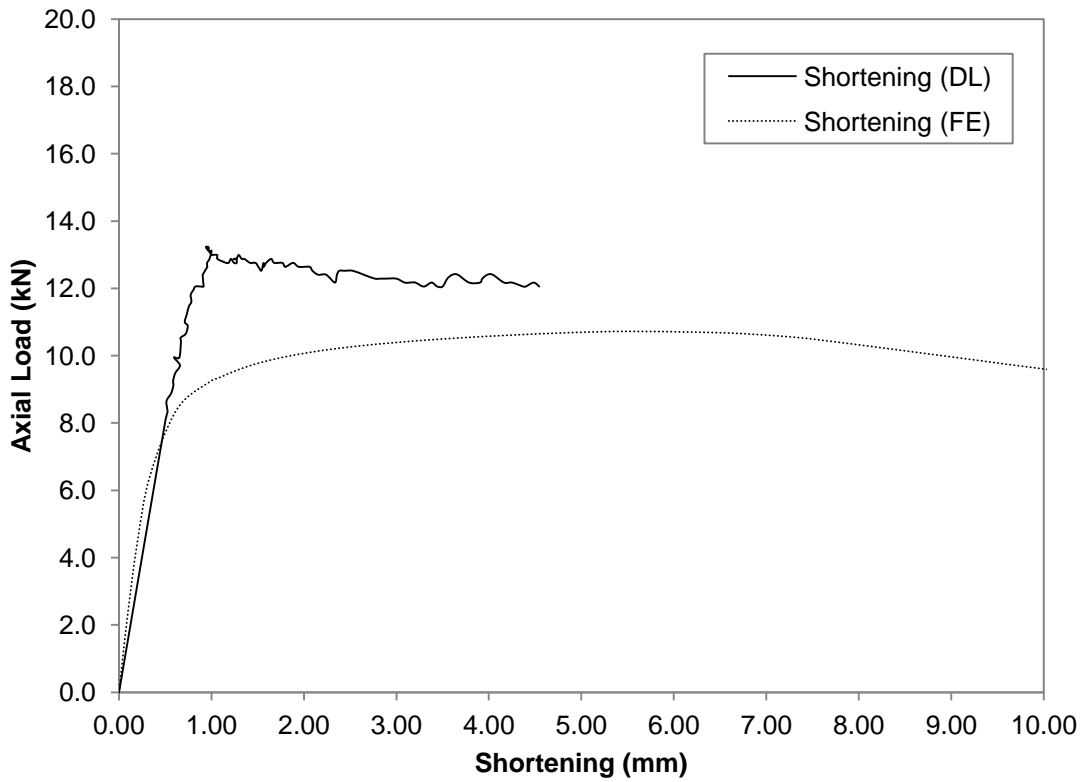


Figure F.99 Axial Load versus Shortening Curve for BU75S950L2000-2

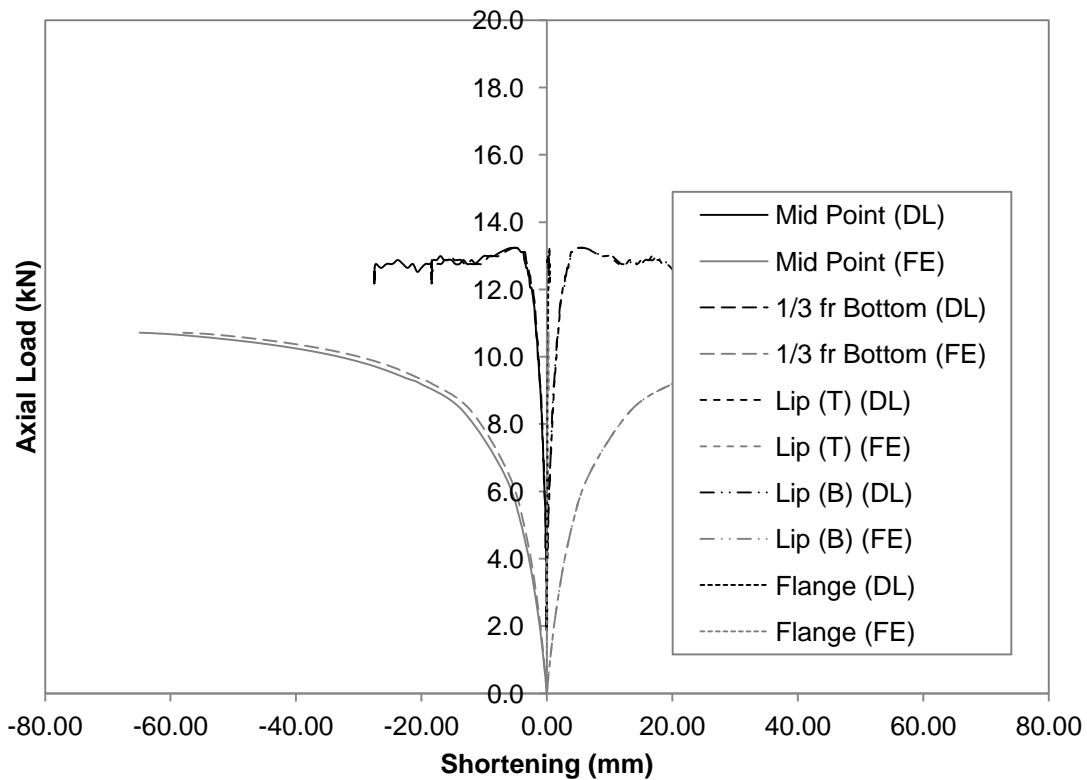


Figure F.100 Axial Load versus Deformation Curve for BU75S950L2000-2

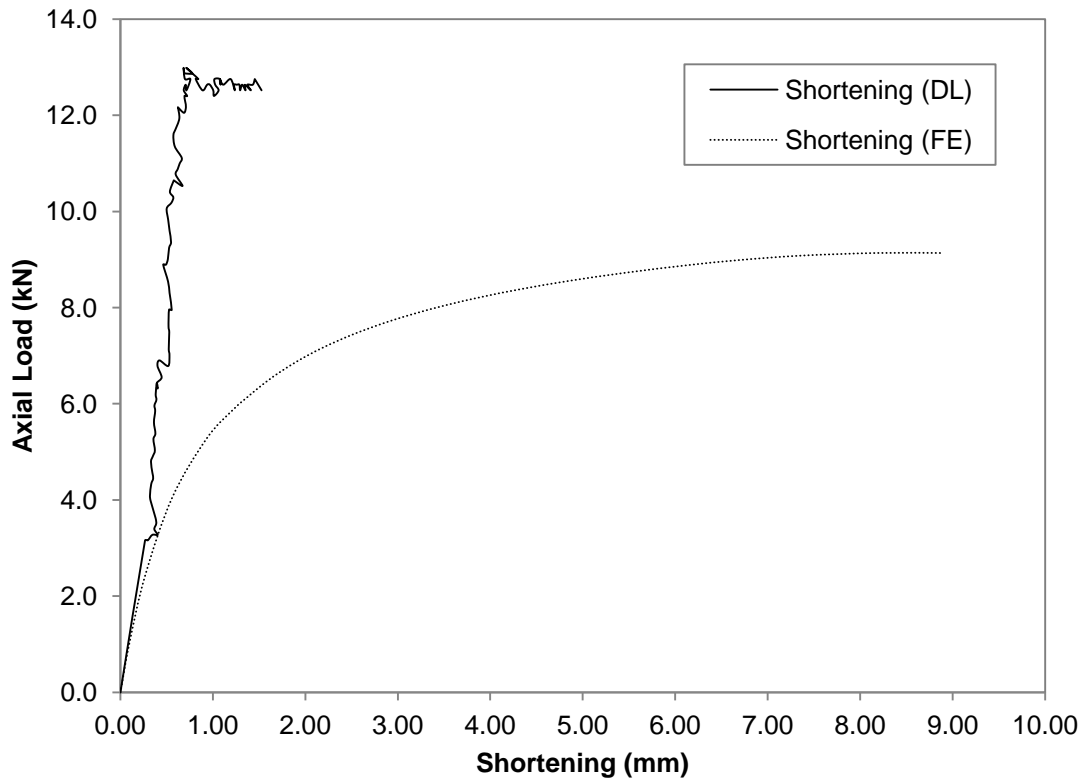


Figure F.101 Axial Load versus Shortening Curve for BU75S950L2000-3

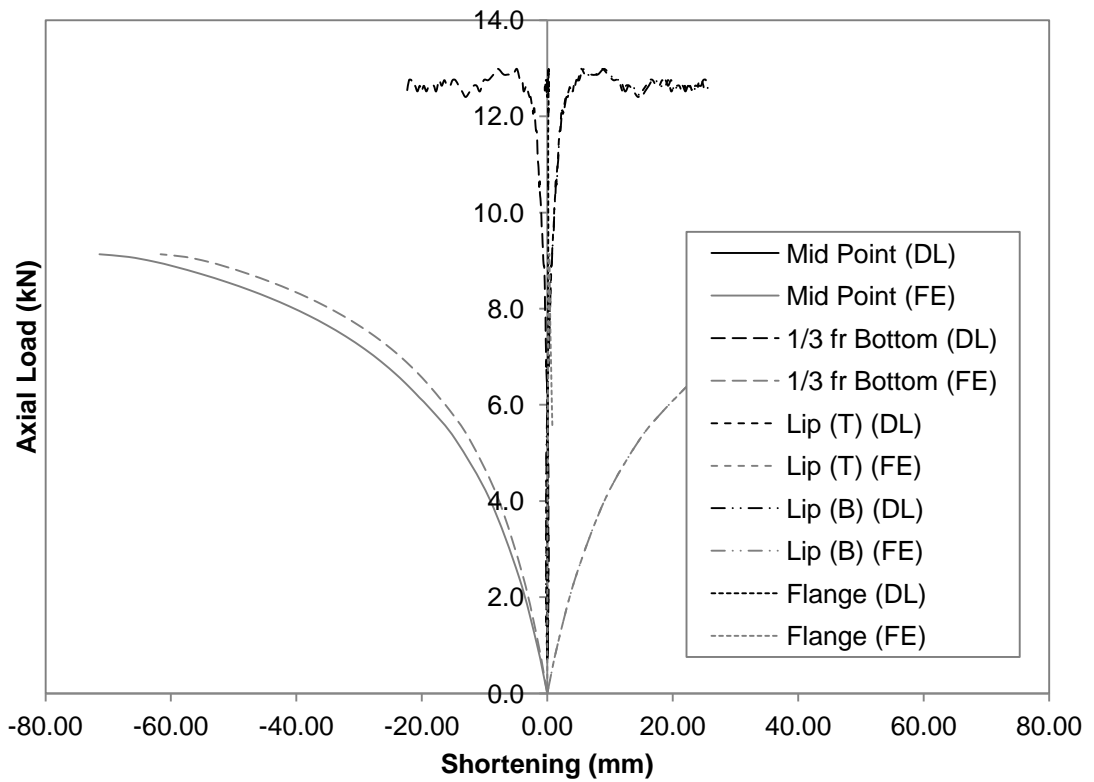


Figure F.102 Axial Load versus Deformation Curve for BU75S950L2000-3

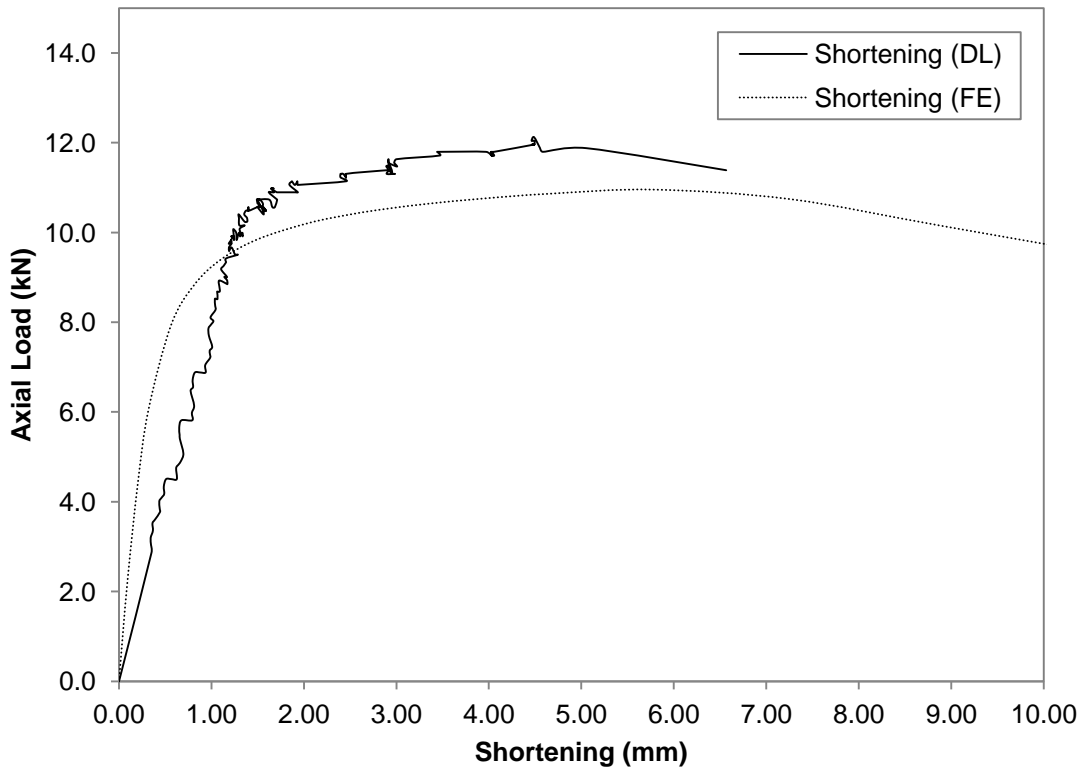


Figure F.103 Axial Load versus Shortening Curve for BU75S1900L2000-2

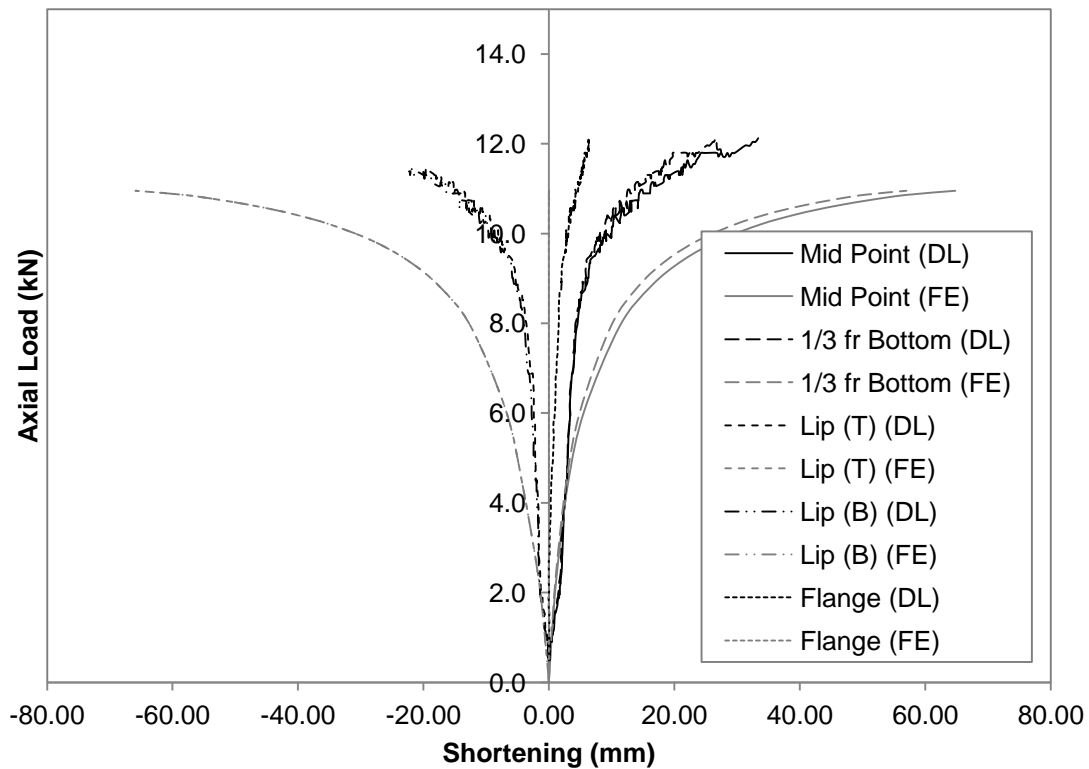


Figure F.104 Axial Load versus Deformation Curve for BU75S1900L2000-2

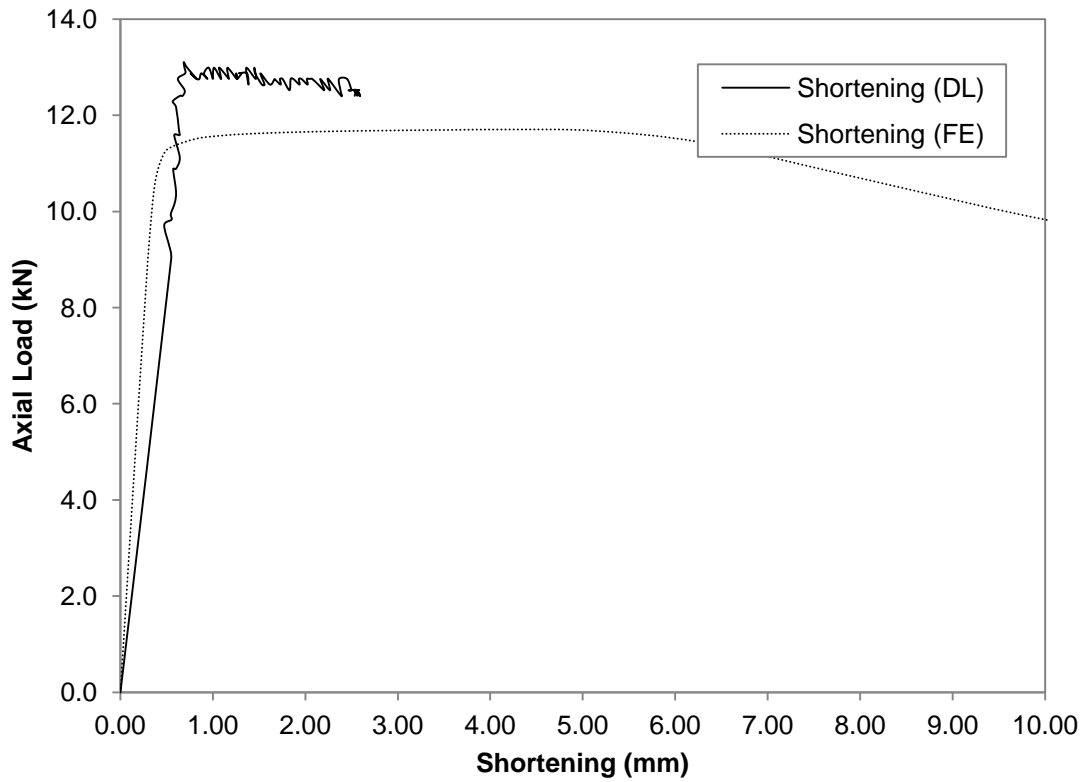


Figure F.105 Axial Load versus Shortening Curve for BU75S1900L2000-3

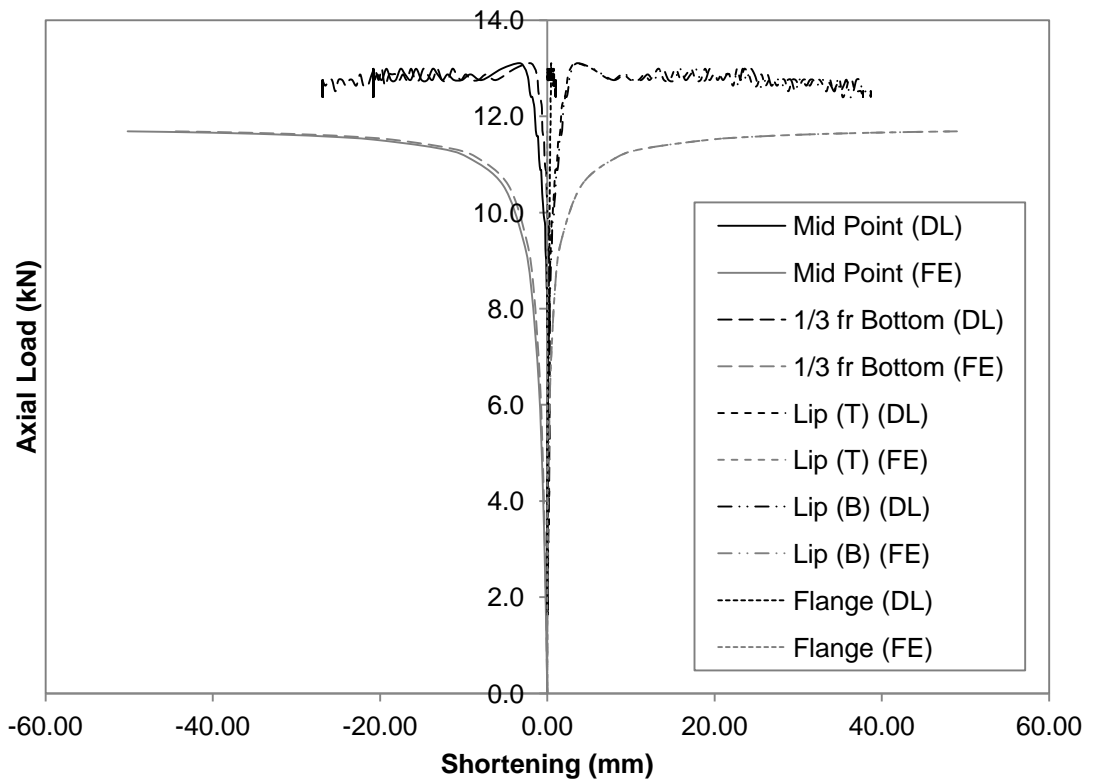


Figure F.106 Axial Load versus Deformation Curve for BU75S1900L2000-3

G. Results for Gapped Built-up Back-to-back C-channels

G.1 Stub Column

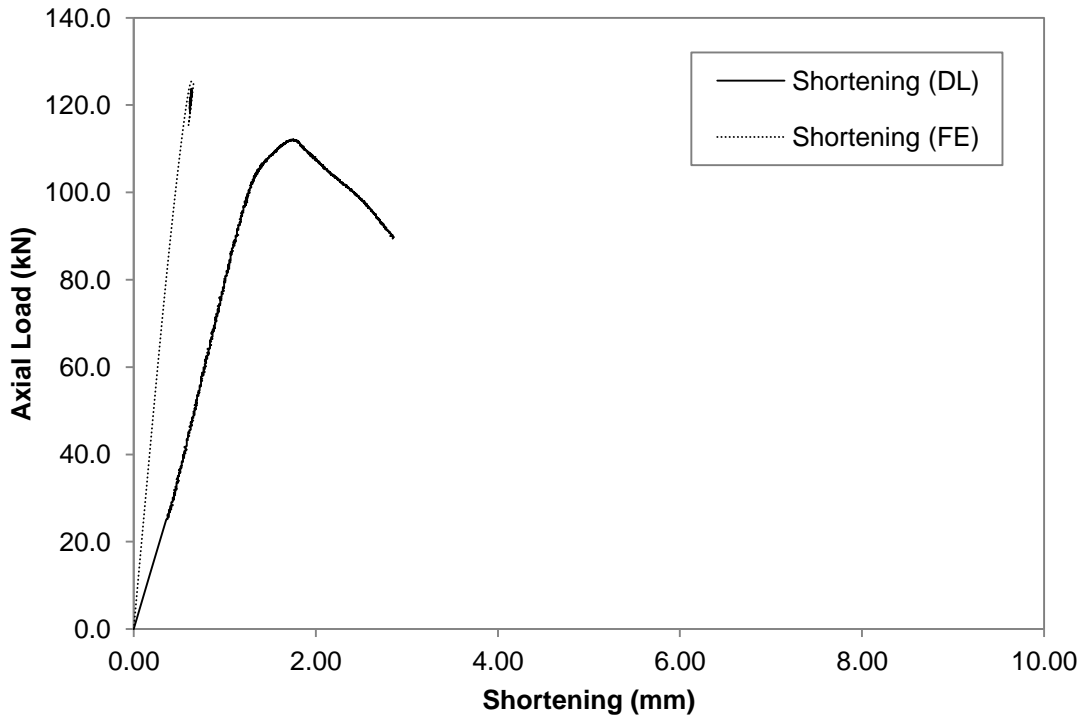


Figure G.1 Axial Load versus Shortening Curve for GBU75S50L300-2

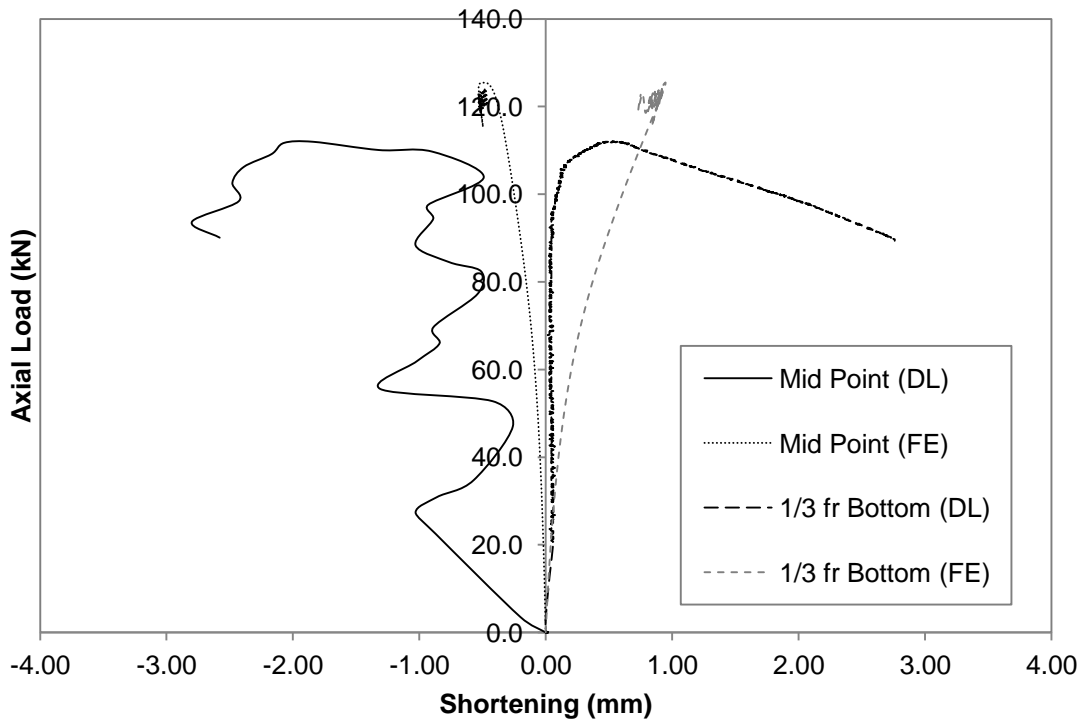


Figure G.2 Axial Load versus Deformation Curve for GBU75S50L300-2

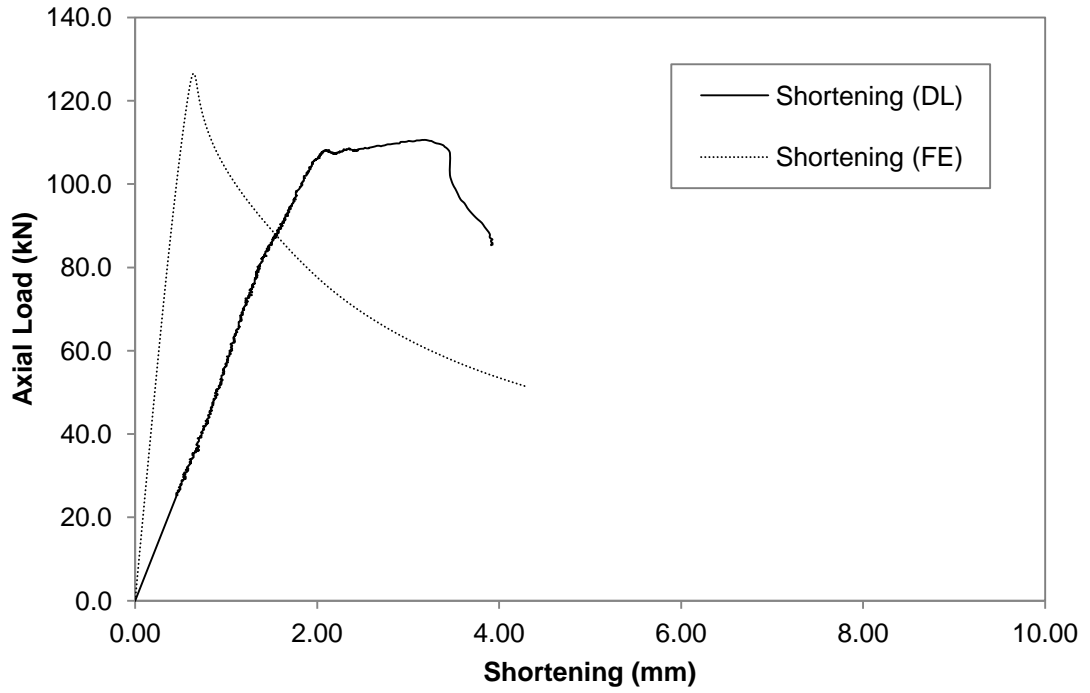


Figure G.3 Axial Load versus Shortening Curve for GBU75S50L300-3

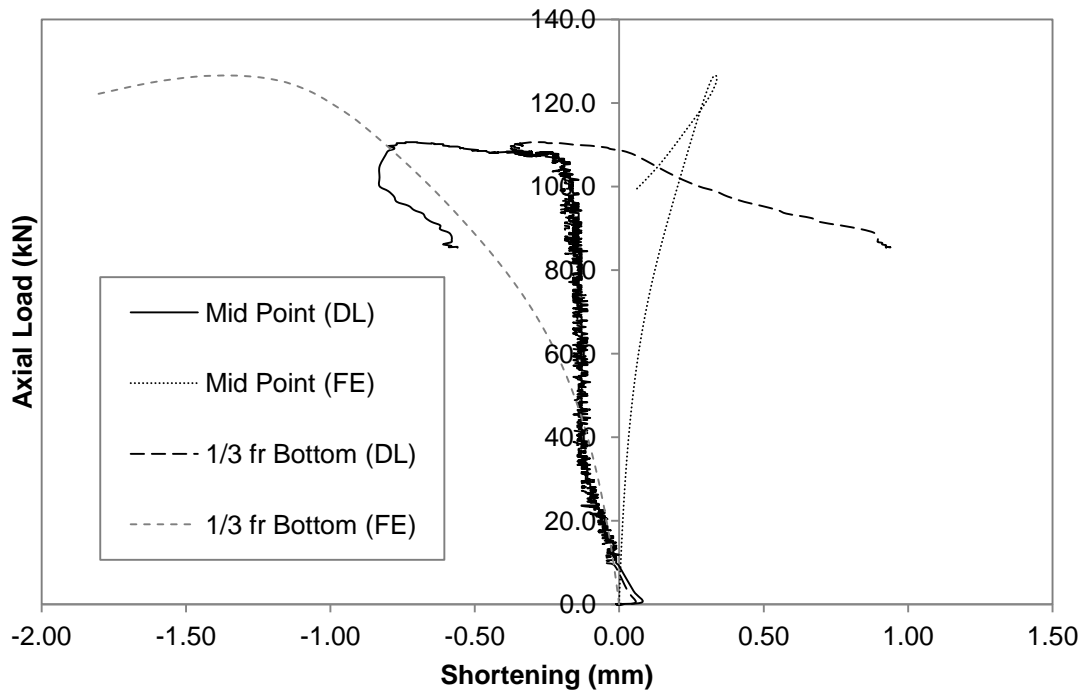


Figure G.4 Axial Load versus Deformation Curve for GBU75S50L300-3

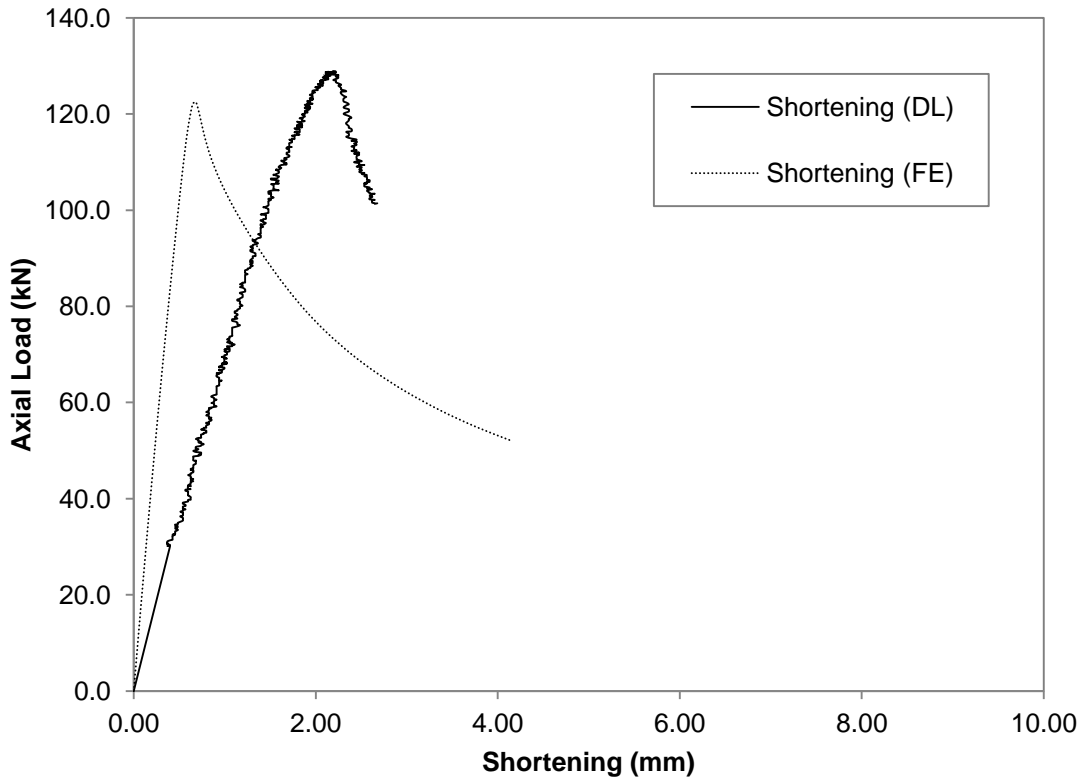


Figure G.5 Axial Load versus Shortening Curve for GBU75S50L300-4

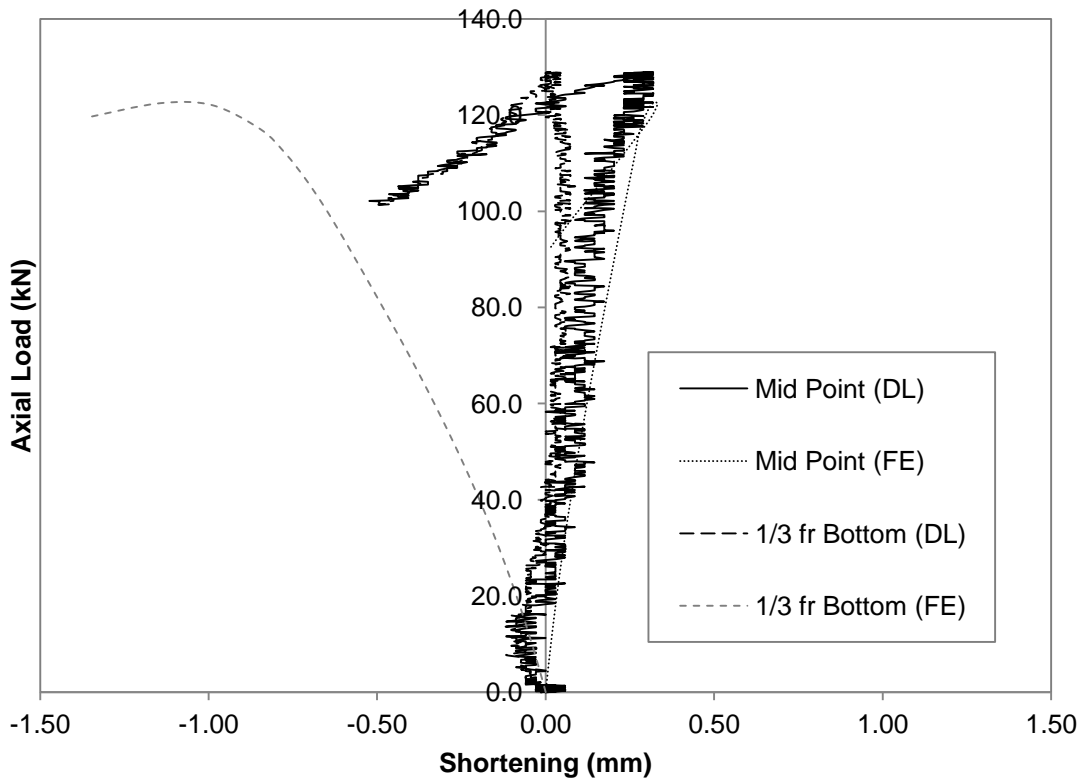


Figure G.6 Axial Load versus Deformation Curve for GBU75S50L300-4

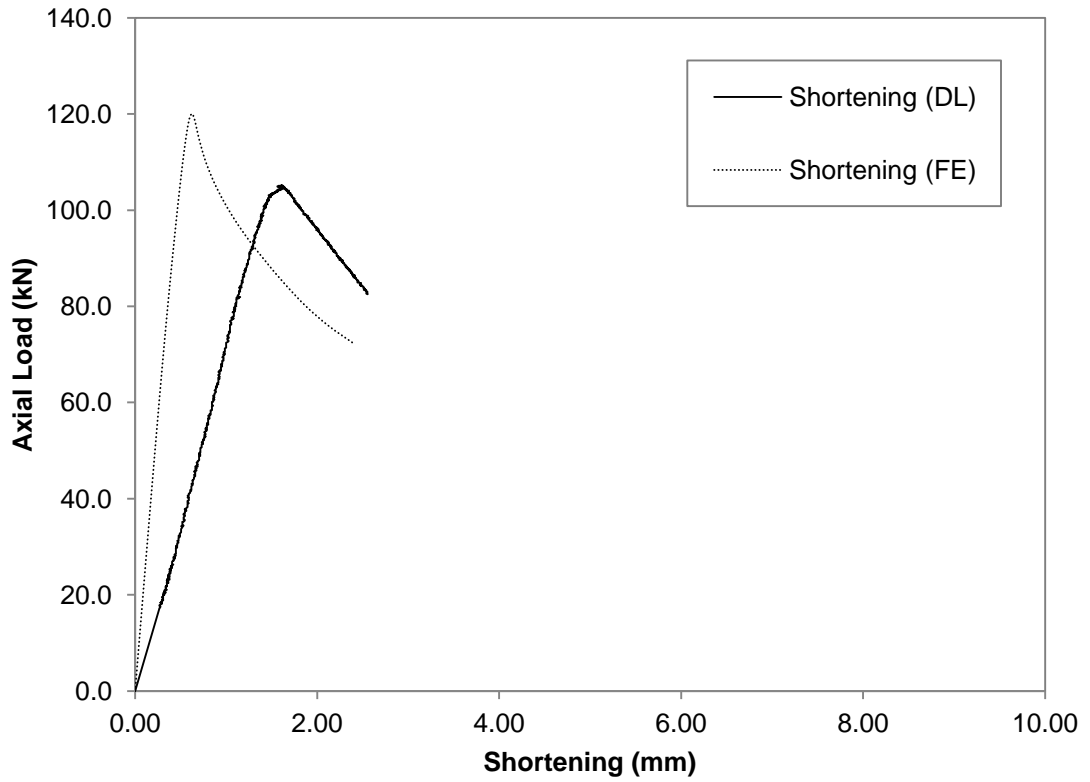


Figure G.7 Axial Load versus Shortening Curve for GBU75S200L300-1

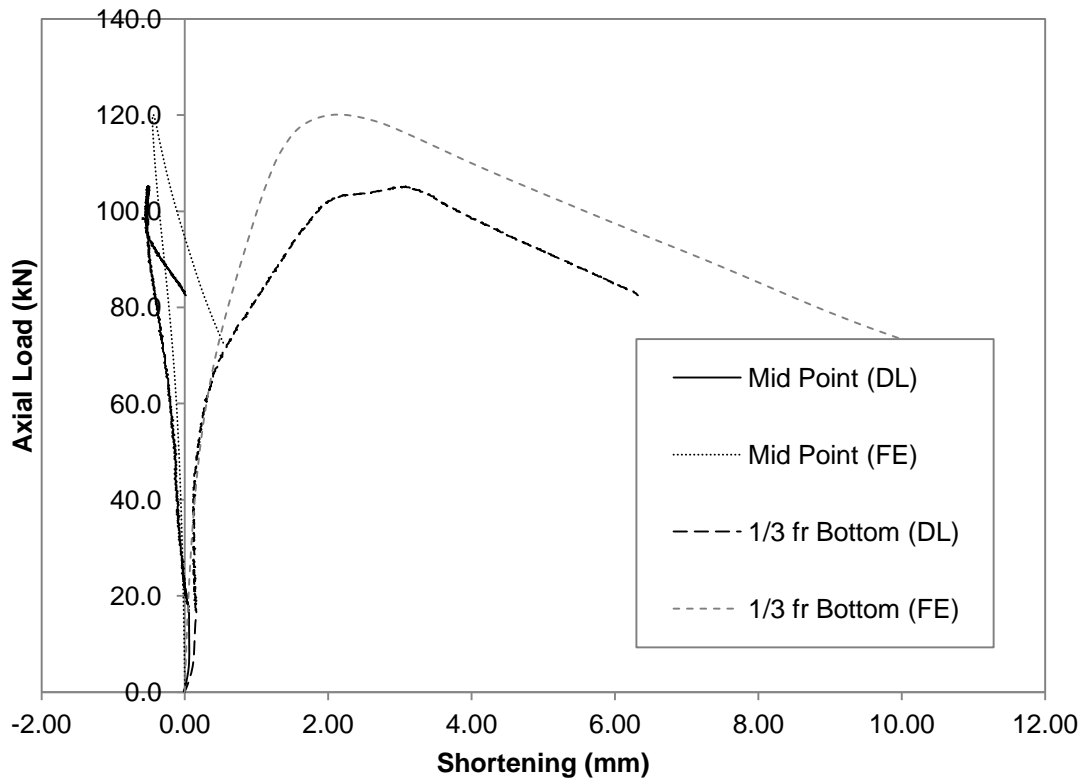


Figure G.8 Axial Load versus Deformation Curve for GBU75S200L300-1

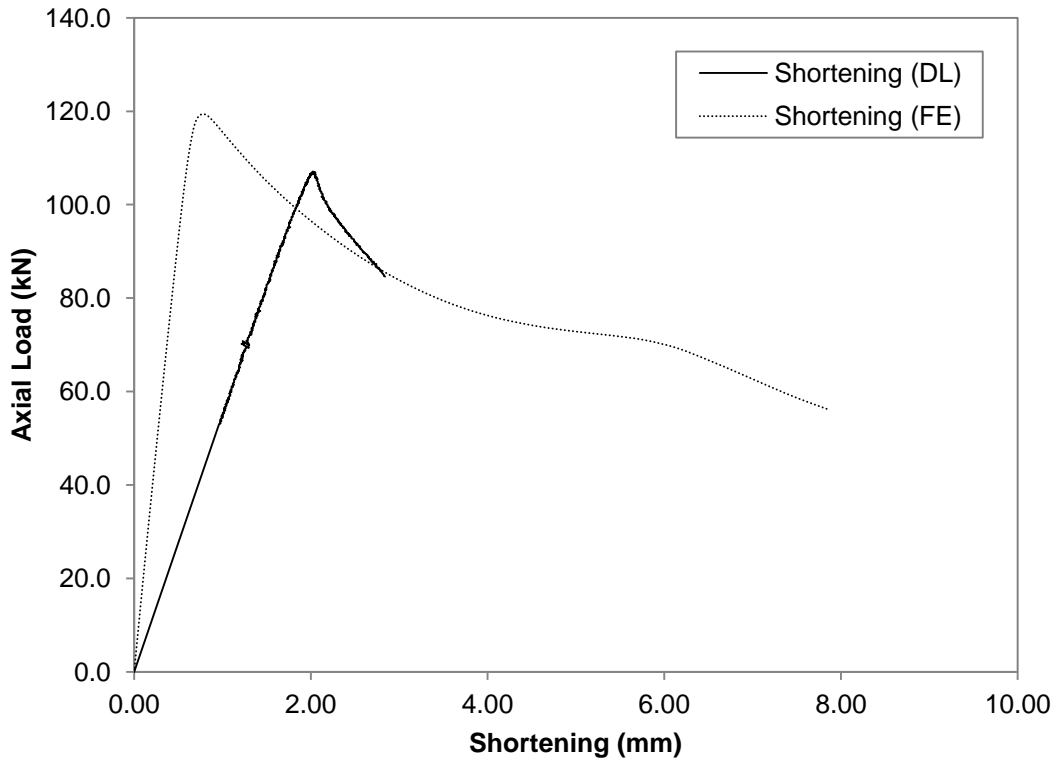


Figure G.9 Axial Load versus Shortening Curve for GBU75S200L300-2

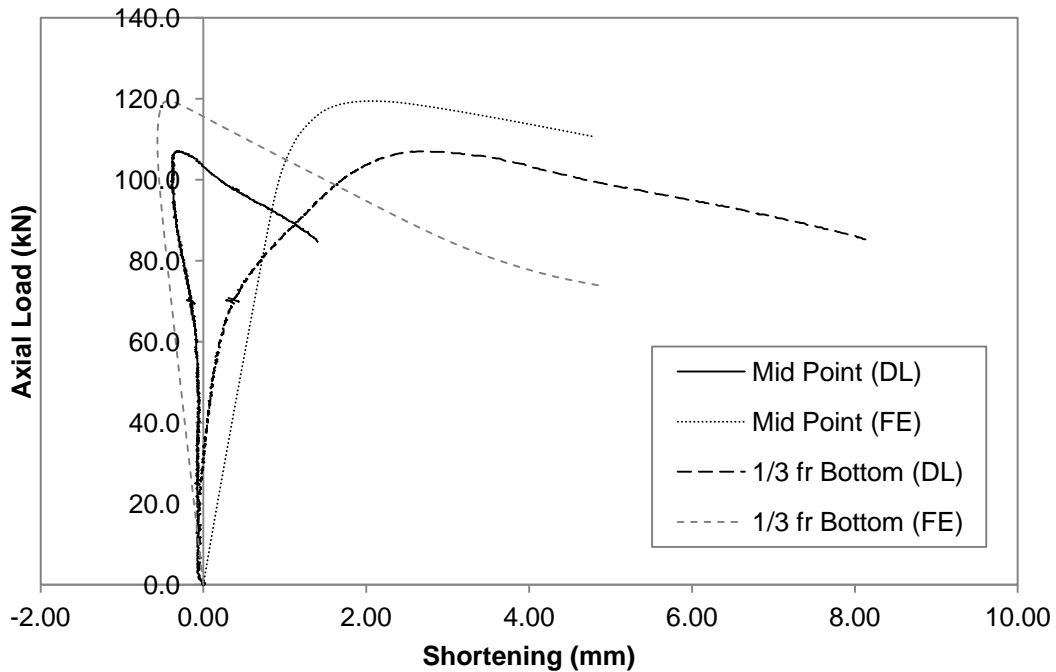


Figure G.10 Axial Load versus Deformation Curve for GBU75S200L300-2

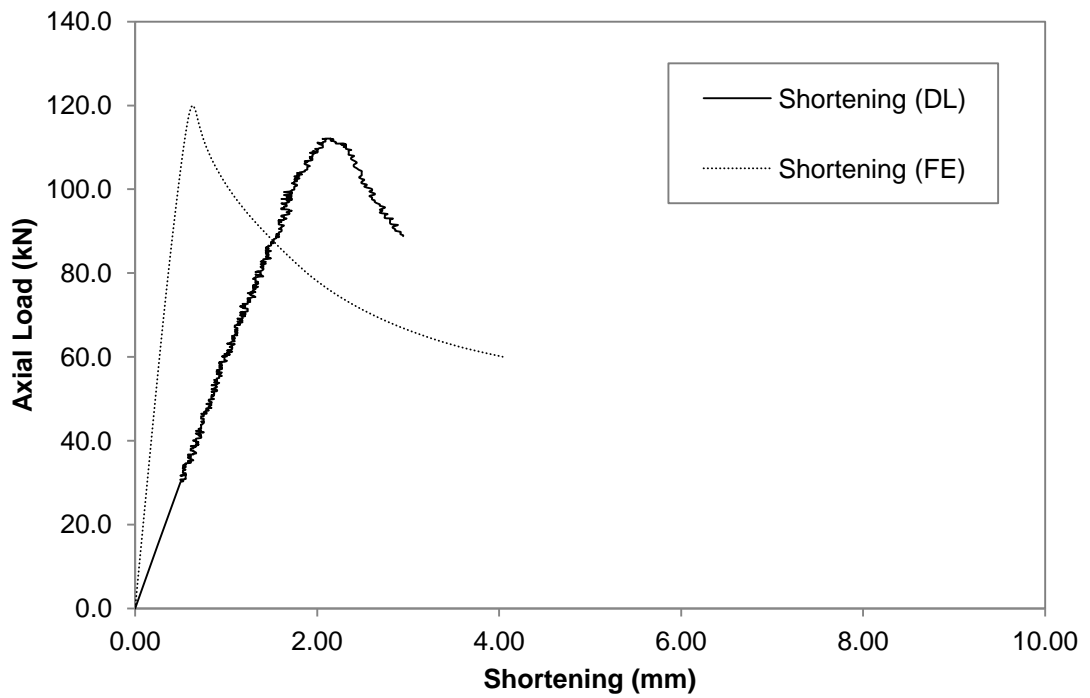


Figure G.11 Axial Load versus Shortening Curve for GBU75S200L300-4

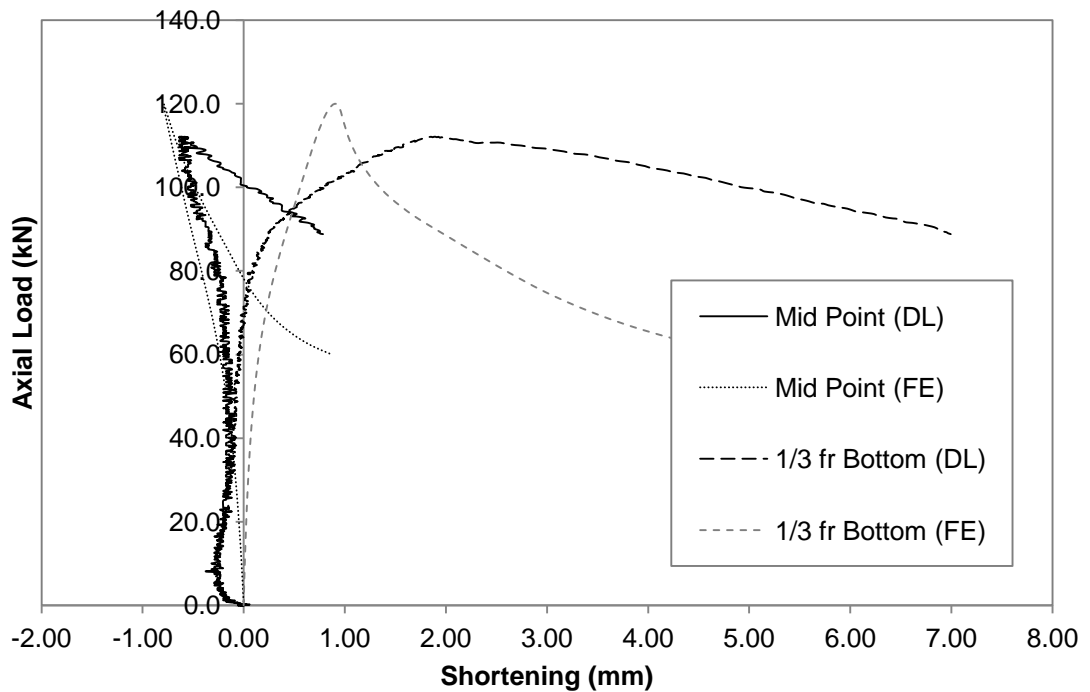


Figure G.12 Axial Load versus Deformation Curve for GBU75S200L300-4

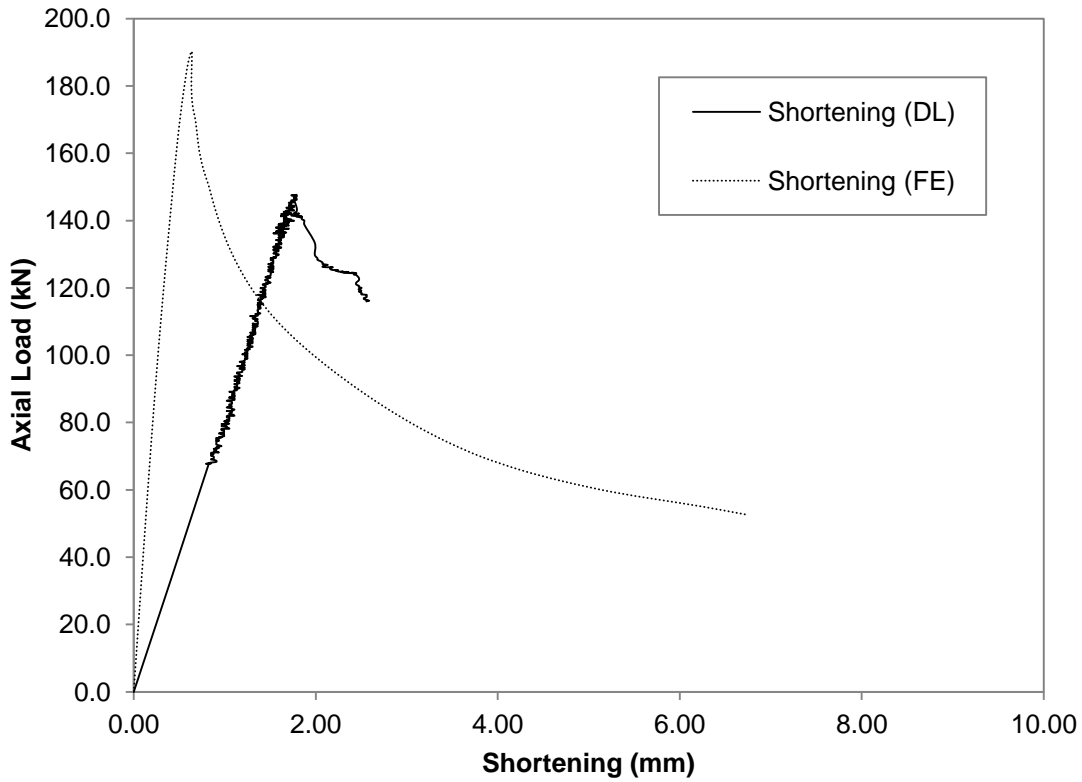


Figure G.13 Axial Load versus Shortening Curve for GBU90S50L300-3

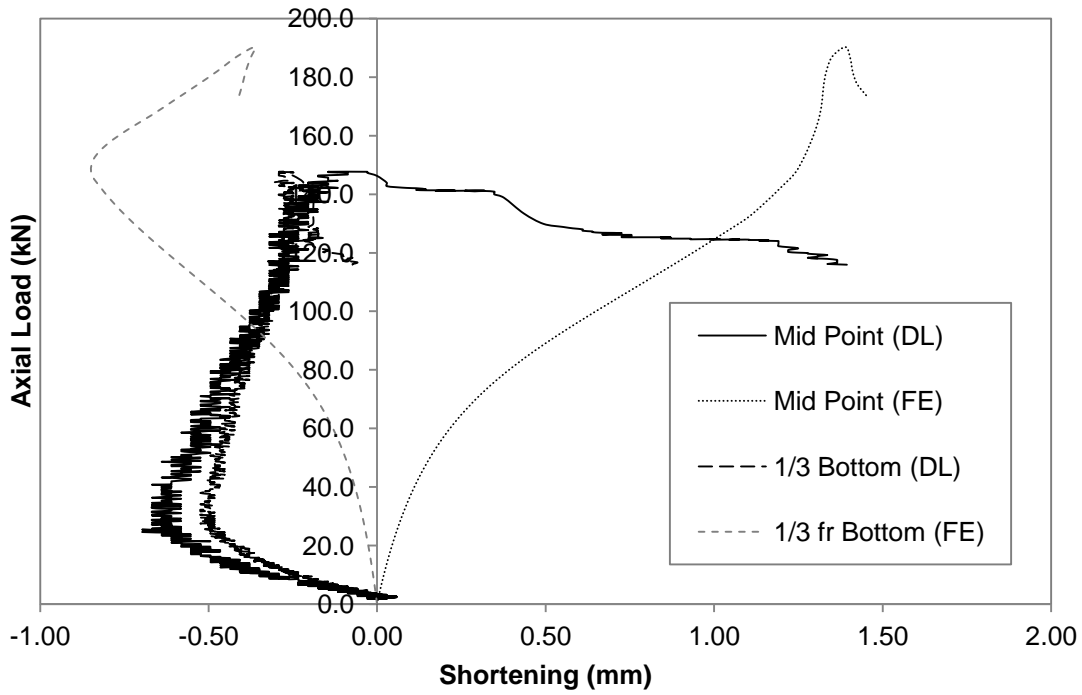


Figure G.14 Axial Load versus Deformation Curve for GBU90S50L300-3

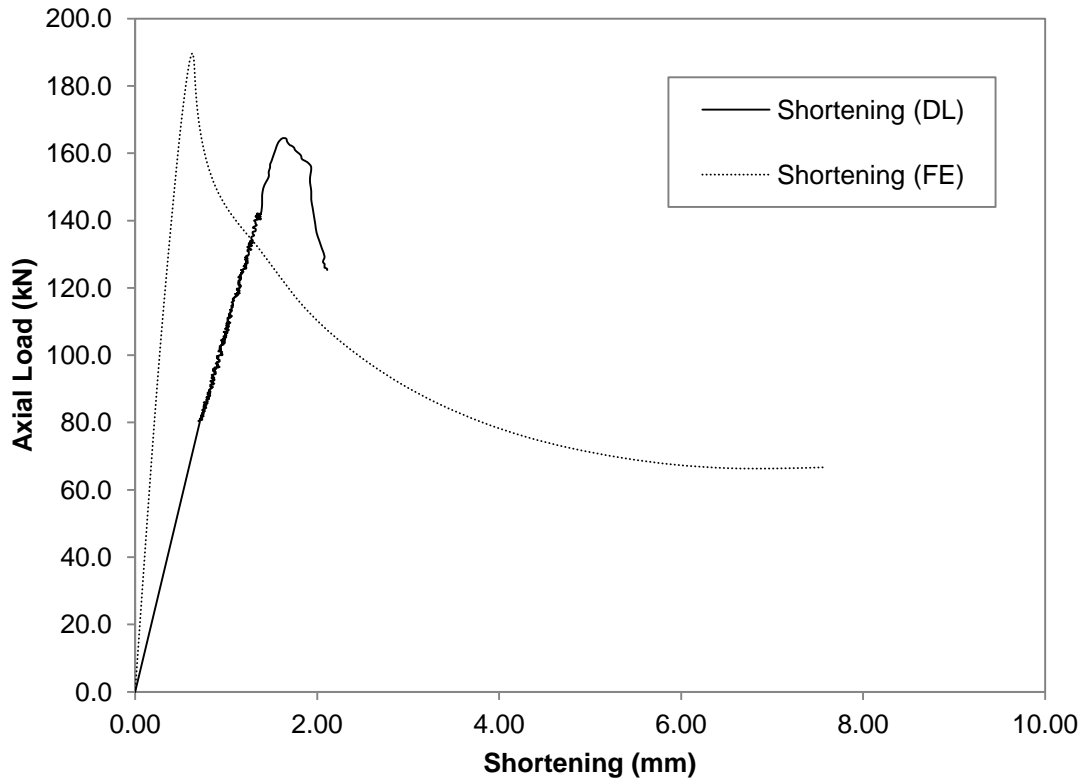


Figure G.15 Axial Load versus Shortening Curve for GBU90S50L300-4

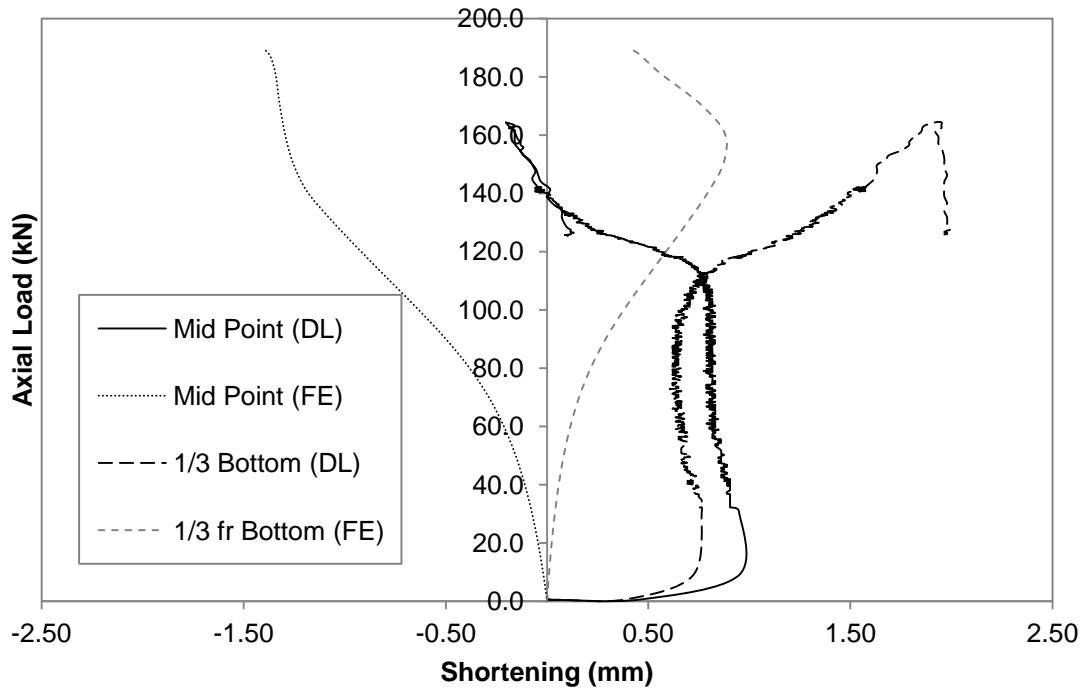


Figure G.16 Axial Load versus Deformation Curve for GBU90S50L300-4

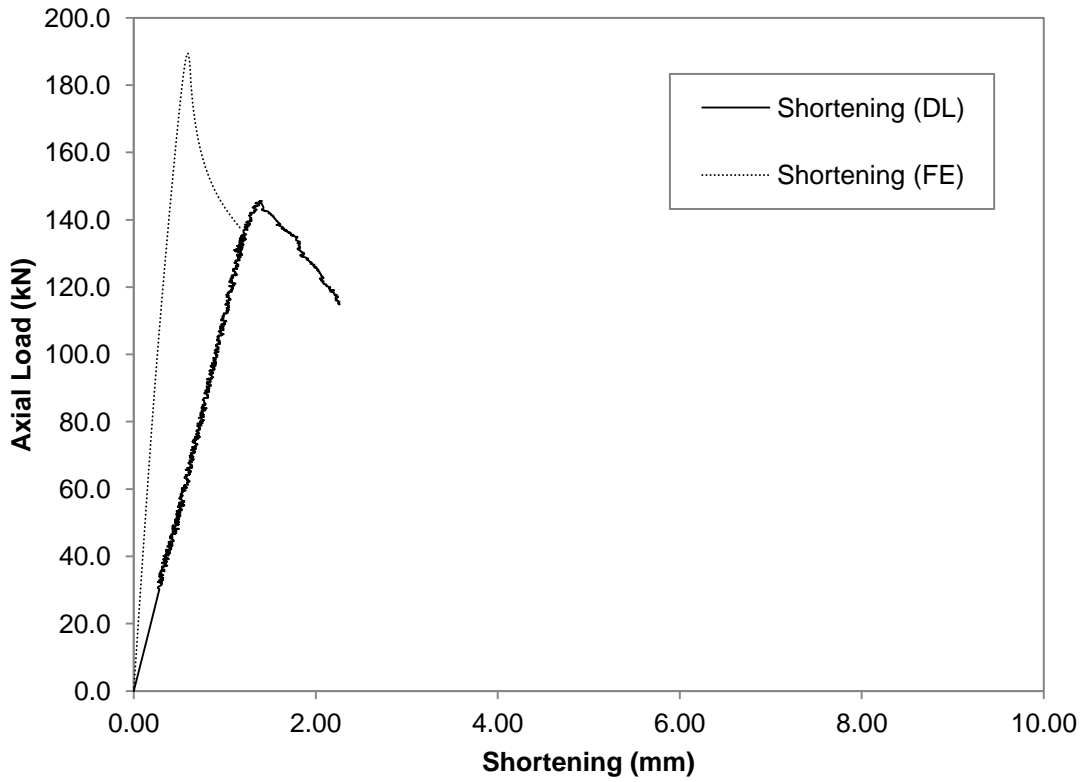


Figure G.17 Axial Load versus Shortening Curve for GBU90S200L300-2

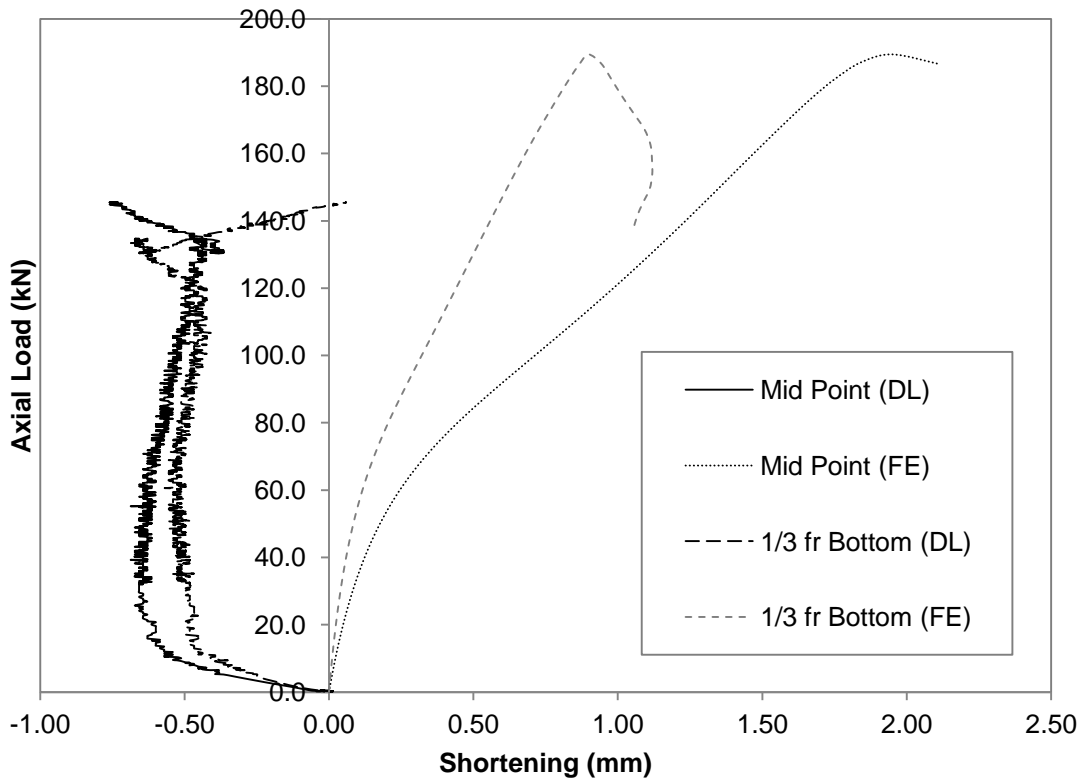


Figure G.18 Axial Load versus Deformation Curve for GBU90S200L300-2

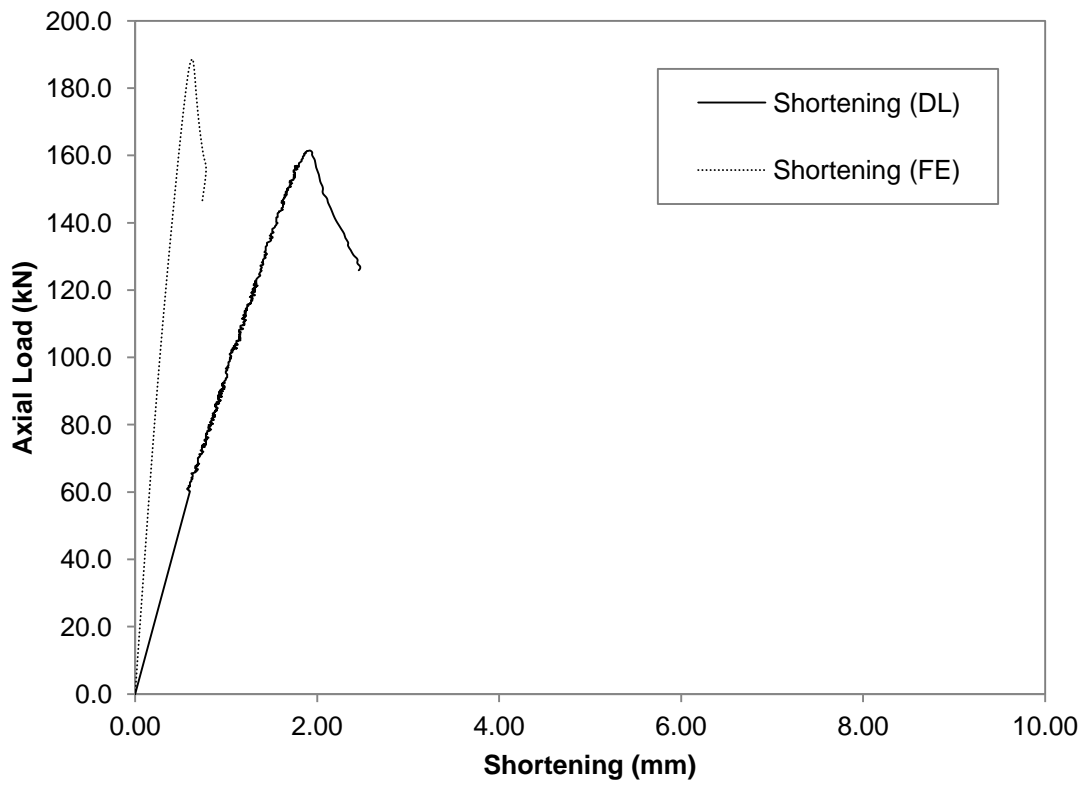


Figure G.19 Axial Load versus Shortening Curve for GBU90S200L300-3

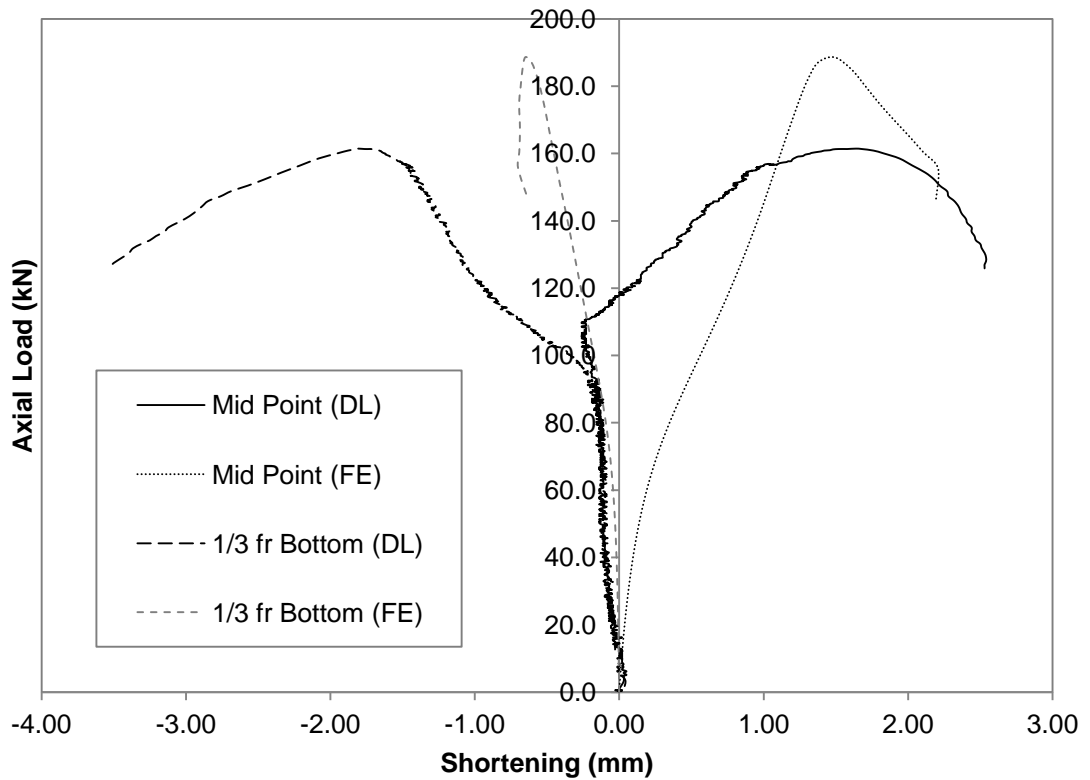


Figure G.20 Axial Load versus Deformation Curve for GBU90S200L300-3

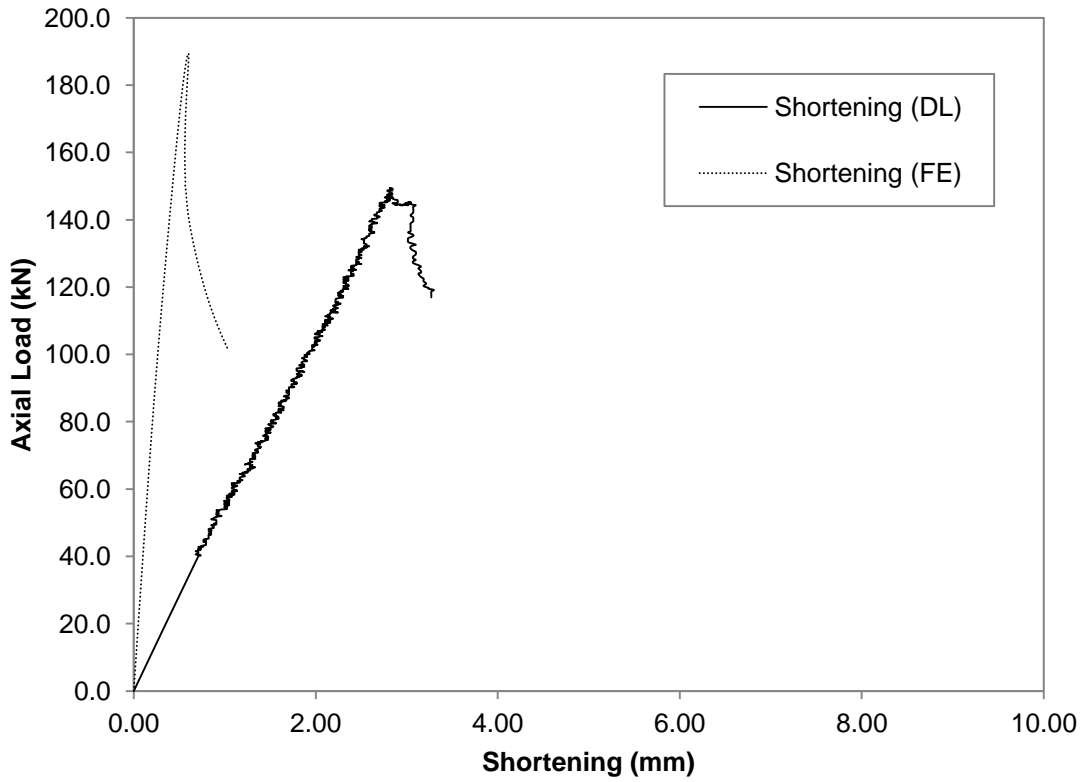


Figure G.21 Axial Load versus Shortening Curve for GBU90S200L300-4

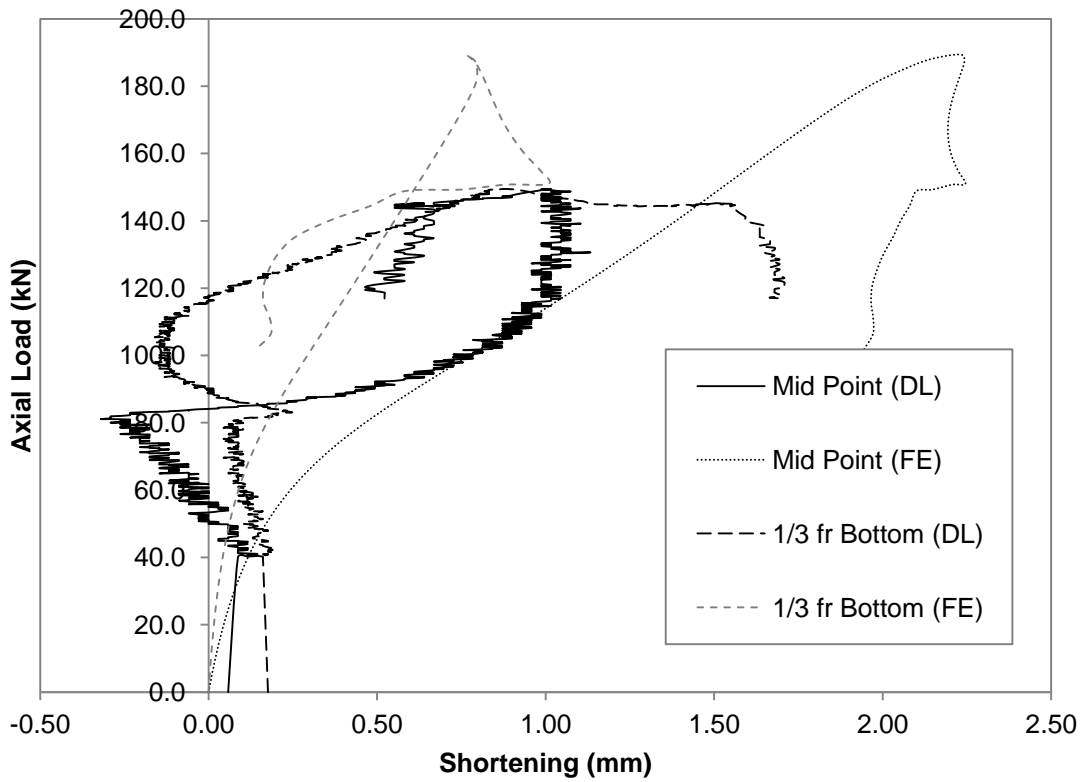


Figure G.22 Axial Load versus Deformation Curve for GBU90S200L300-4

G.2 Short Column (L=500mm)

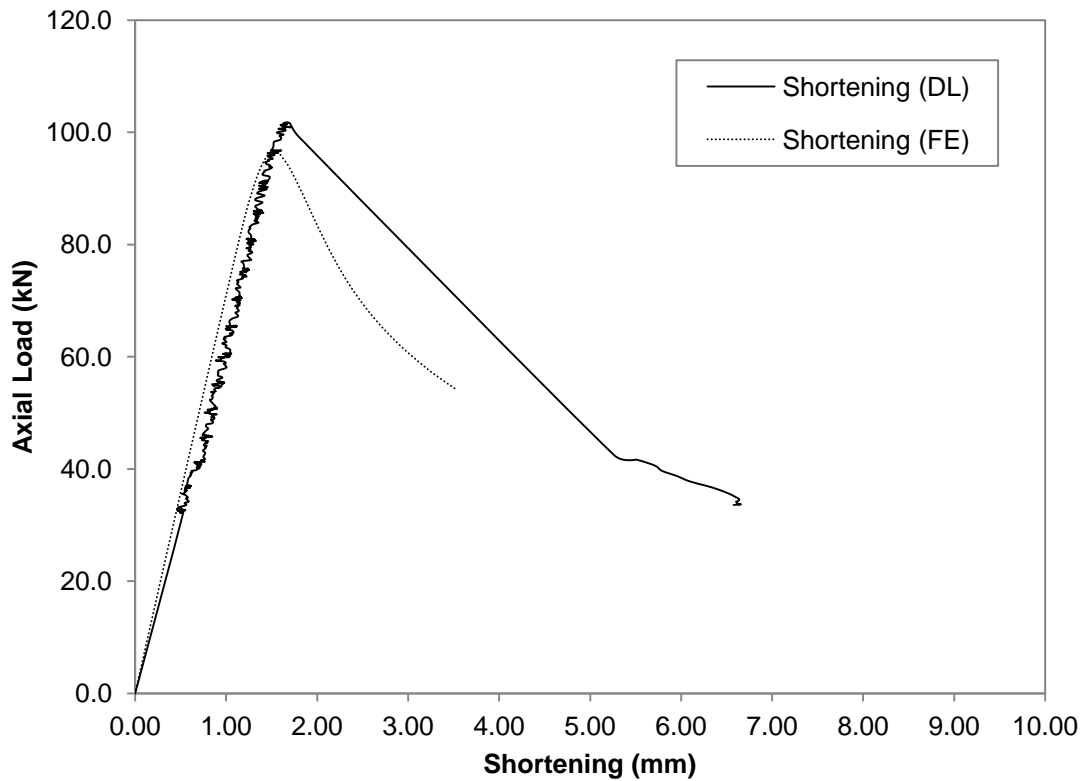


Figure G.23 Axial Load versus Shortening Curve for GBU75S100L500-1

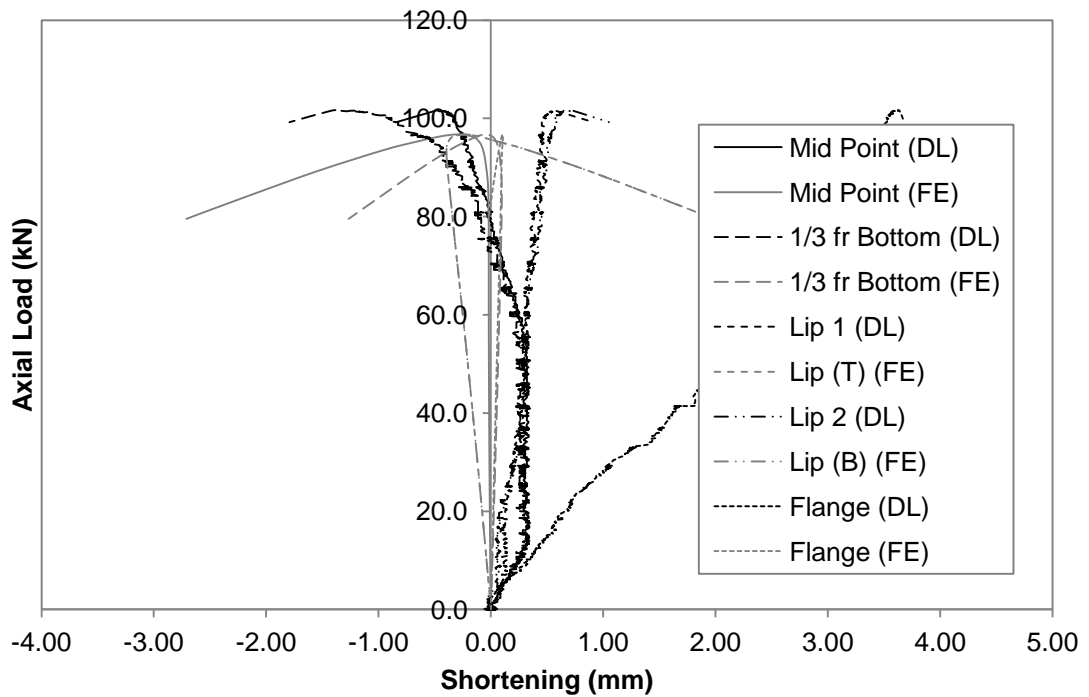


Figure G.24 Axial Load versus Deformation Curve for GBU75S100L500-1

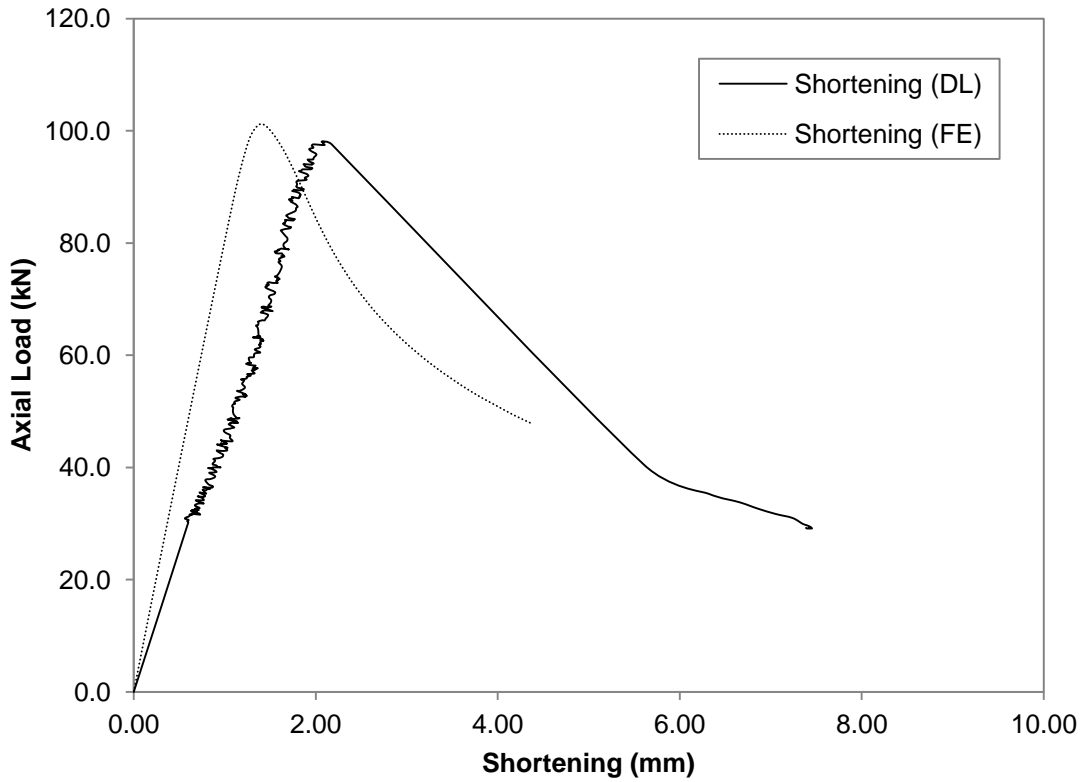


Figure G.25 Axial Load versus Shortening Curve for GBU75S100L500-2

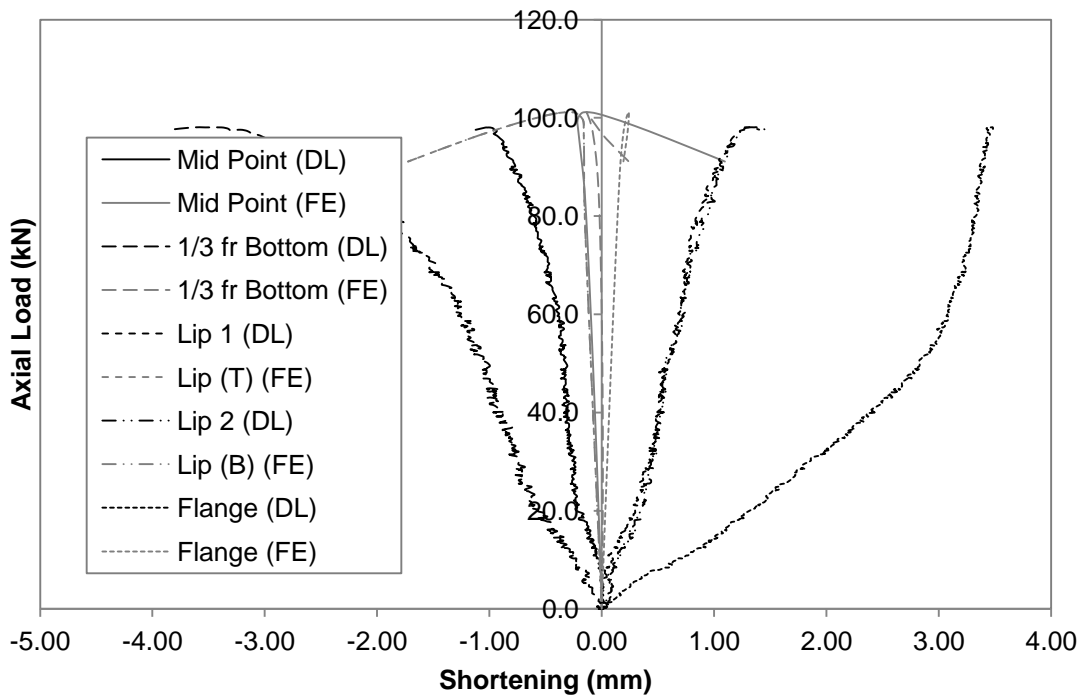


Figure G.26 Axial Load versus Deformation Curve for GBU75S100L500-2

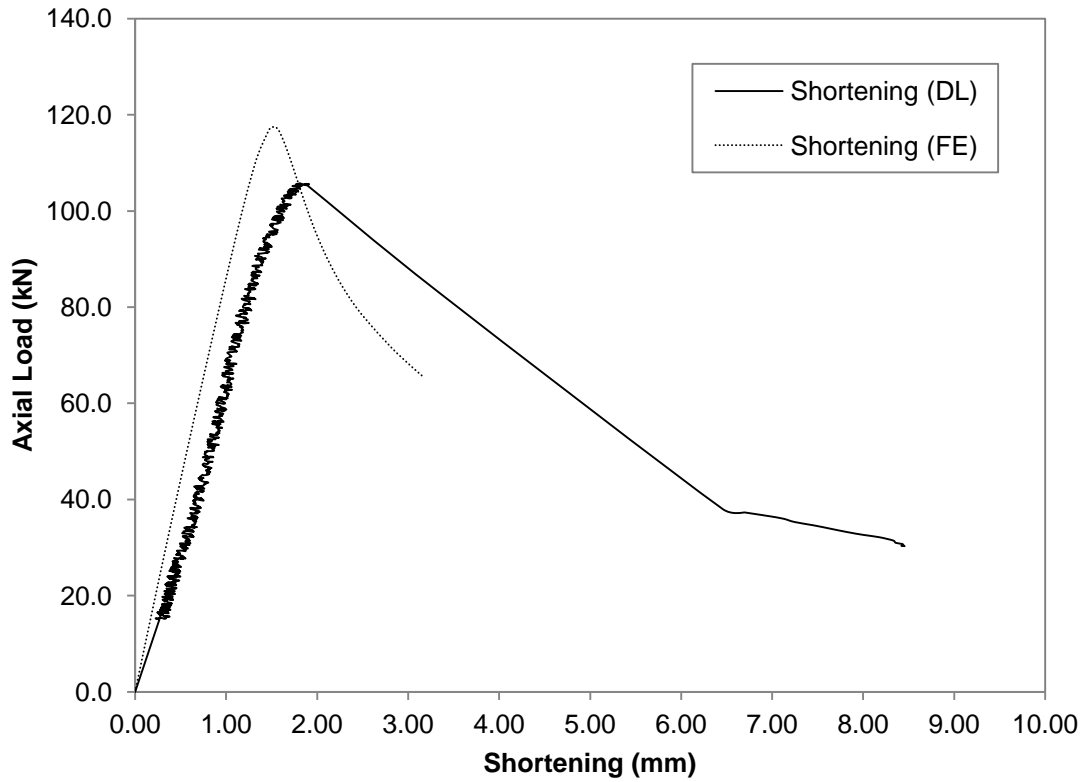


Figure G.27 Axial Load versus Shortening Curve for GBU75S100L500-3

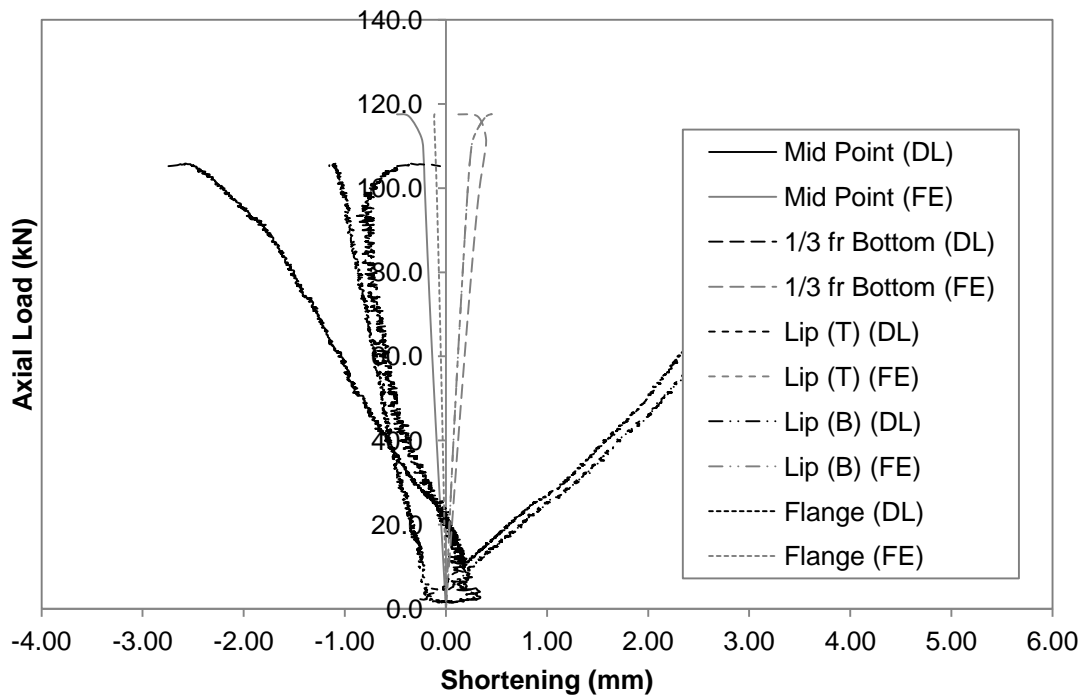


Figure G.28 Axial Load versus Deformation Curve for GBU75S100L500-3

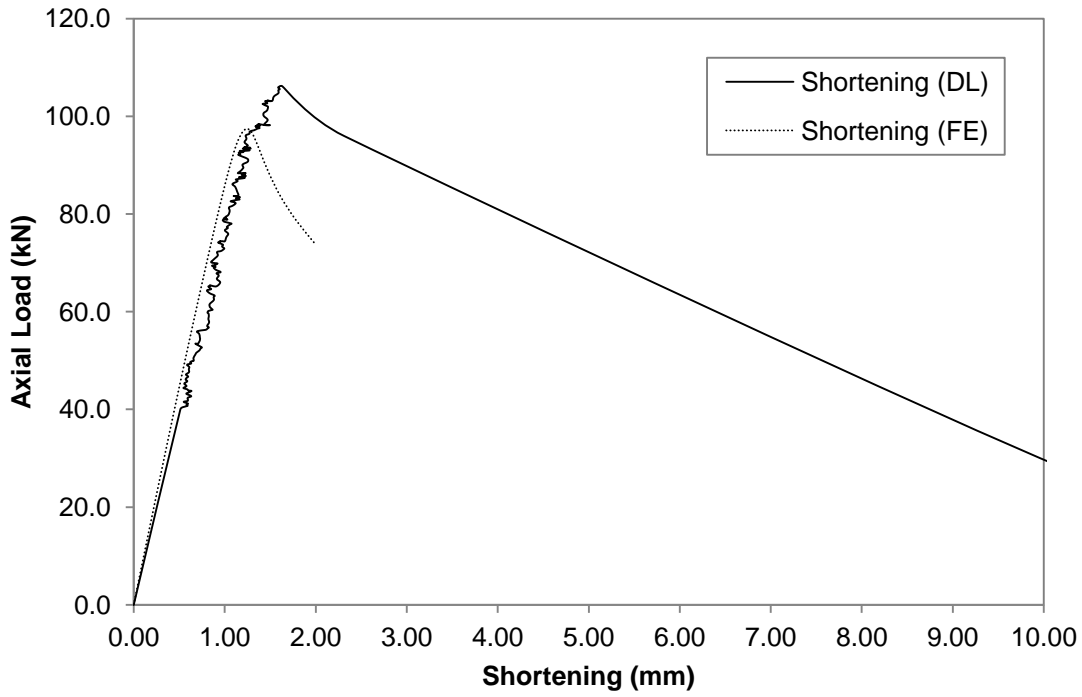


Figure G.29 Axial Load versus Shortening Curve for GBU75S400L500-1

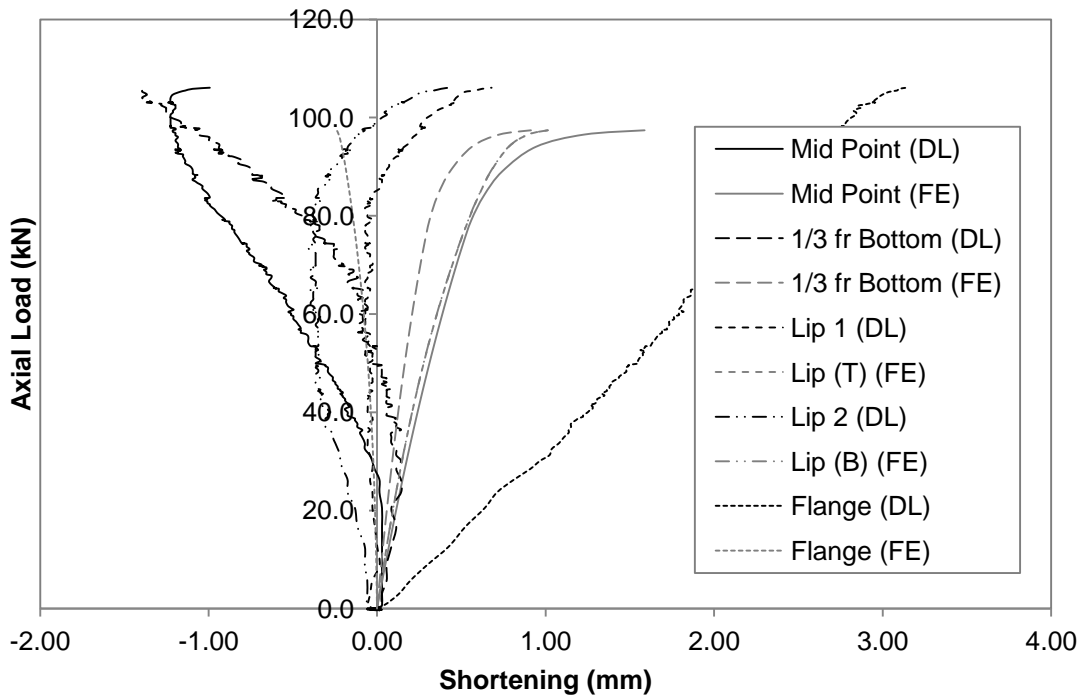


Figure G.30 Axial Load versus Deformation Curve for GBU75S400L500-1

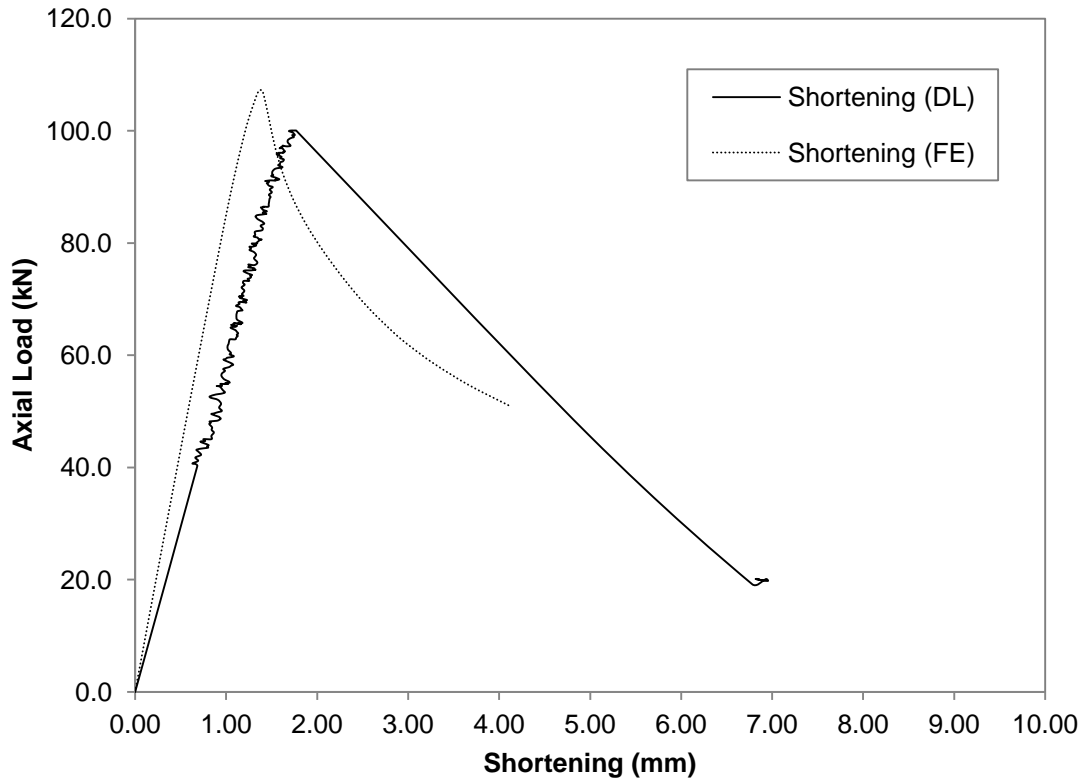


Figure G.31 Axial Load versus Shortening Curve for GBU75S400L500-2

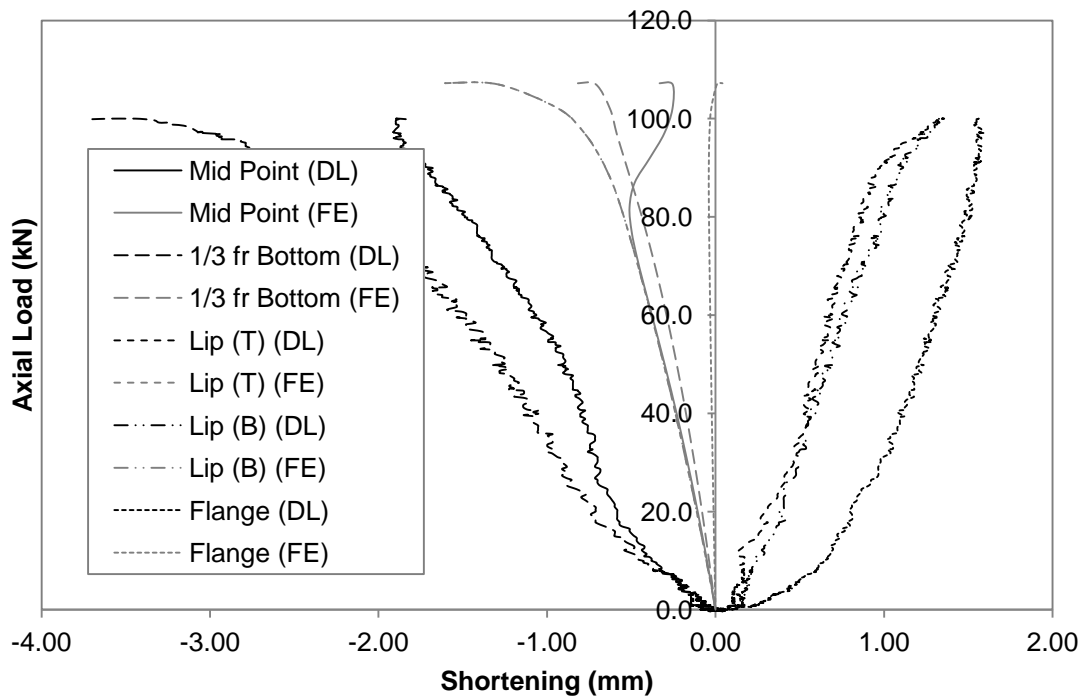


Figure G.32 Axial Load versus Deformation Curve for GBU75S400L500-2

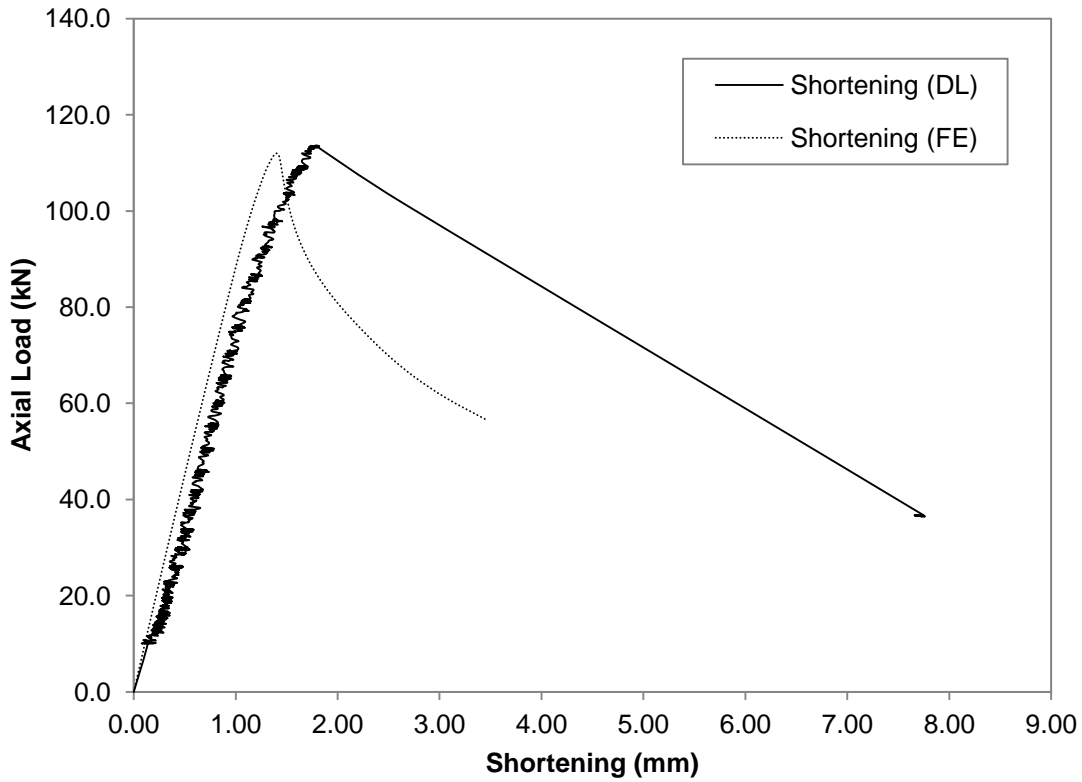


Figure G.33 Axial Load versus Shortening Curve for GBU75S400L500-3

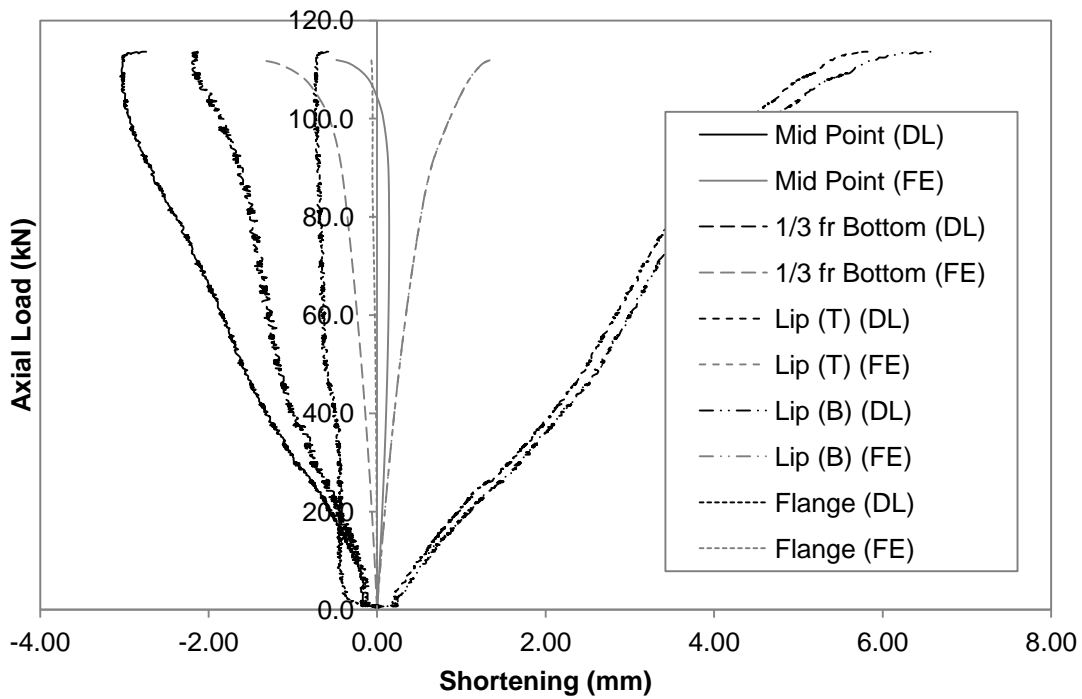


Figure G.34 Axial Load versus Deformation Curve for GBU75S400L500-3

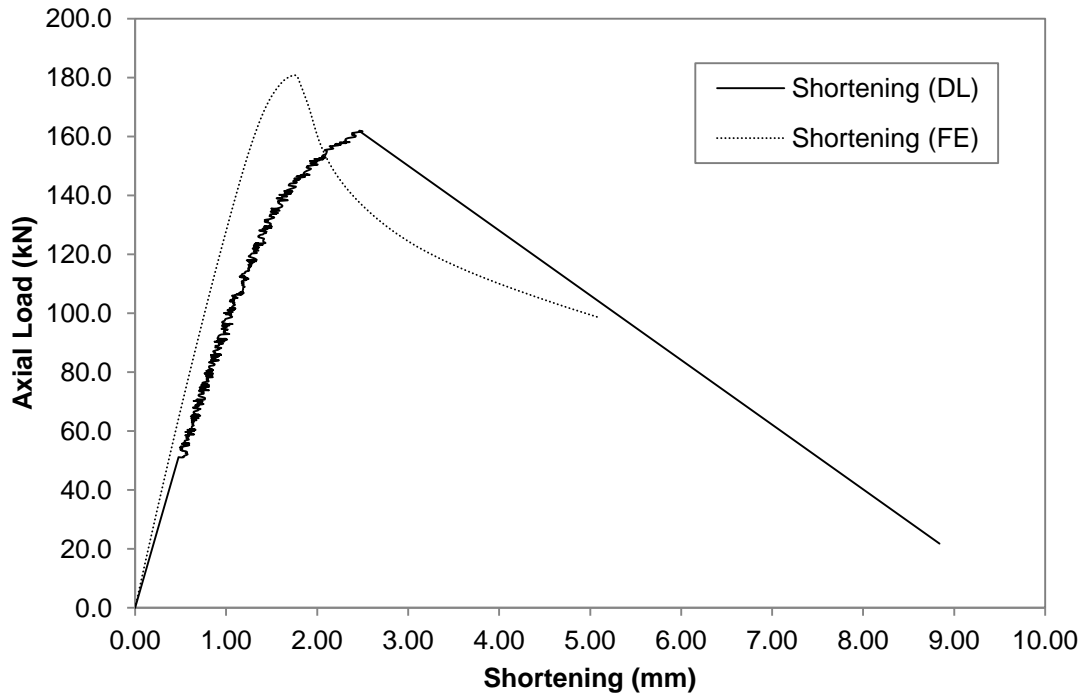


Figure G.35 Axial Load versus Shortening Curve for GBU90S100L500-1

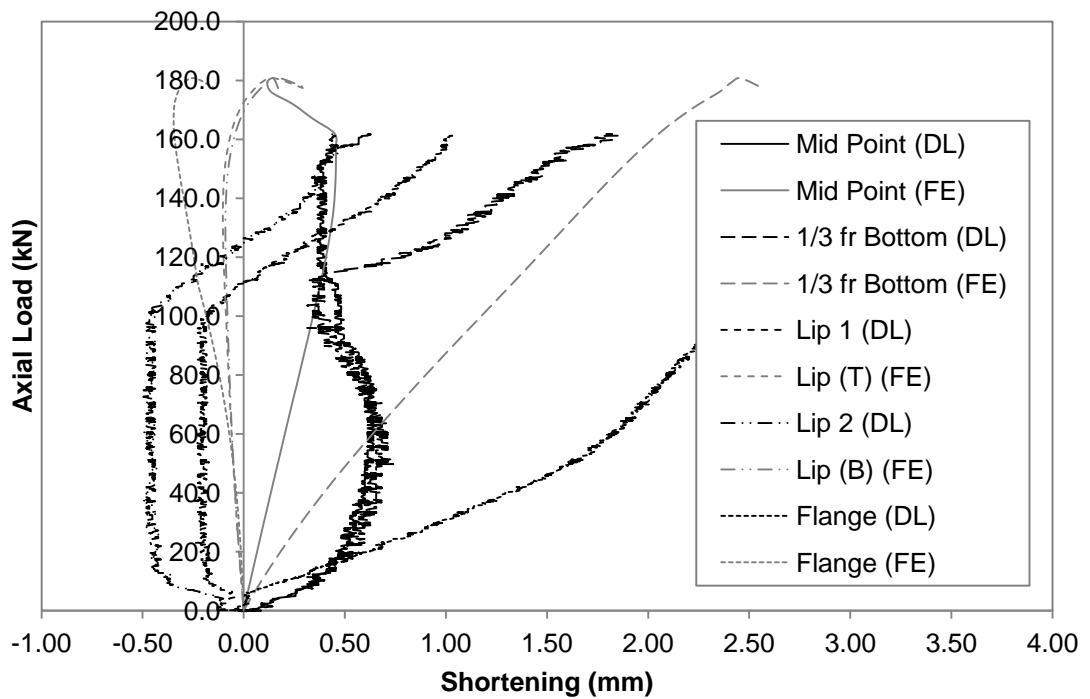


Figure G.36 Axial Load versus Deformation Curve for GBU90S100L500-1

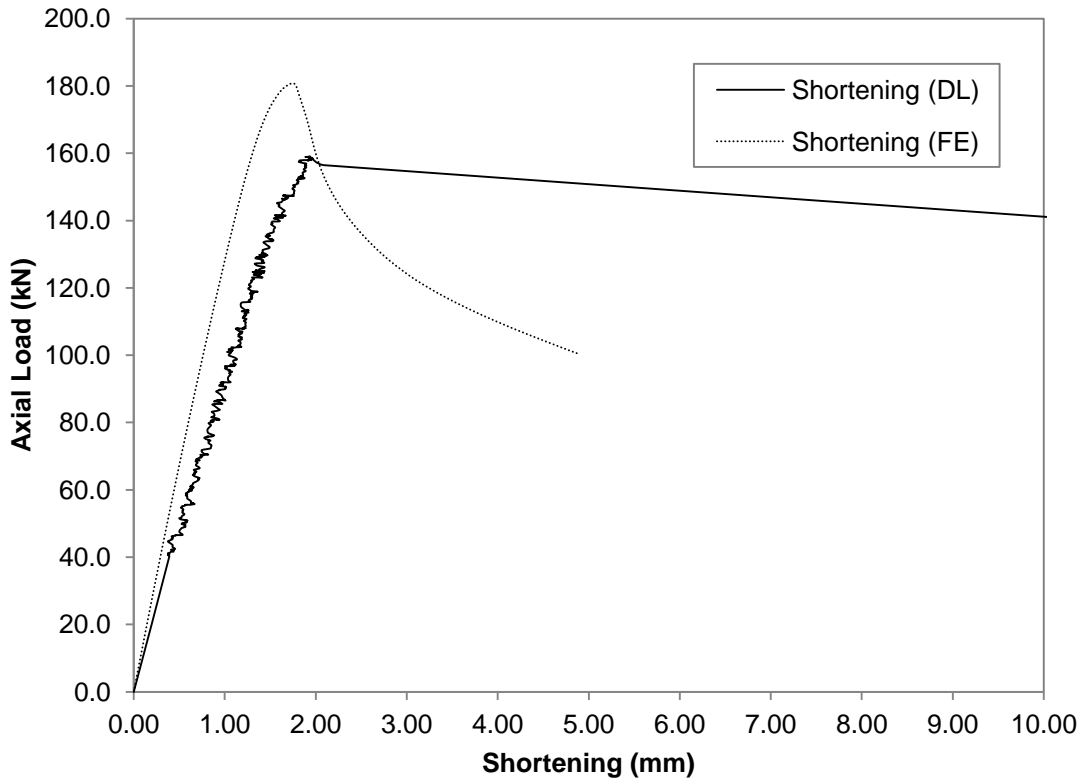


Figure G.37 Axial Load versus Shortening Curve for GBU90S100L500-2

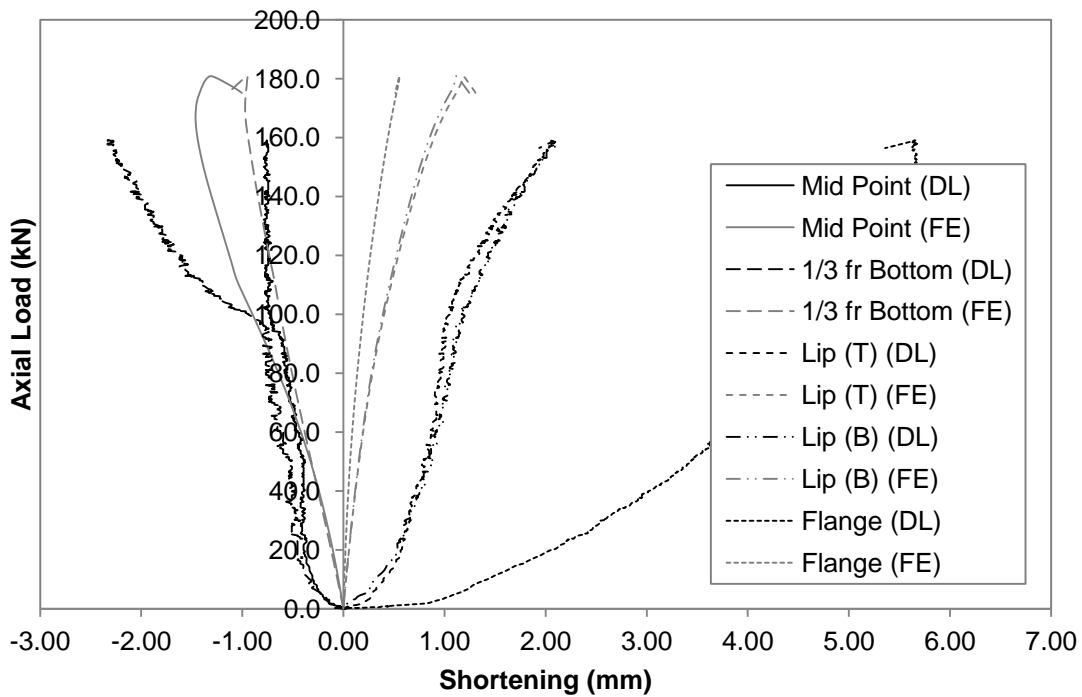


Figure G.38 Axial Load versus Deformation Curve for GBU90S100L500-2

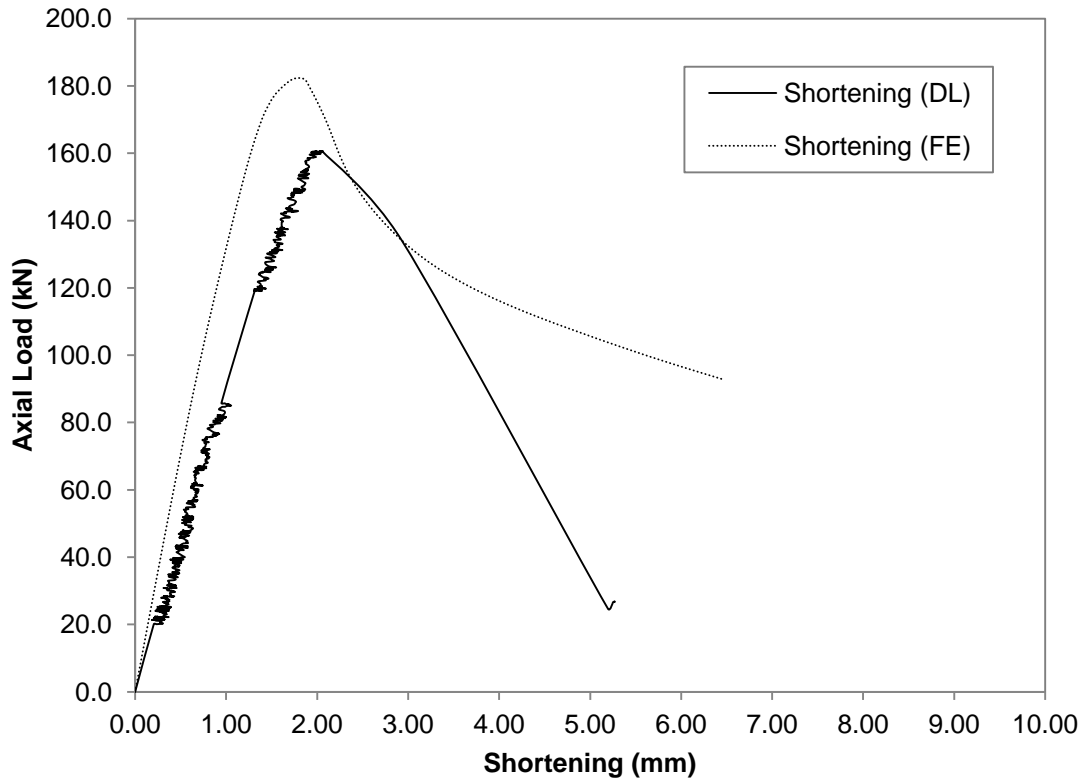


Figure G.39 Axial Load versus Shortening Curve for GBU90S100L500-3

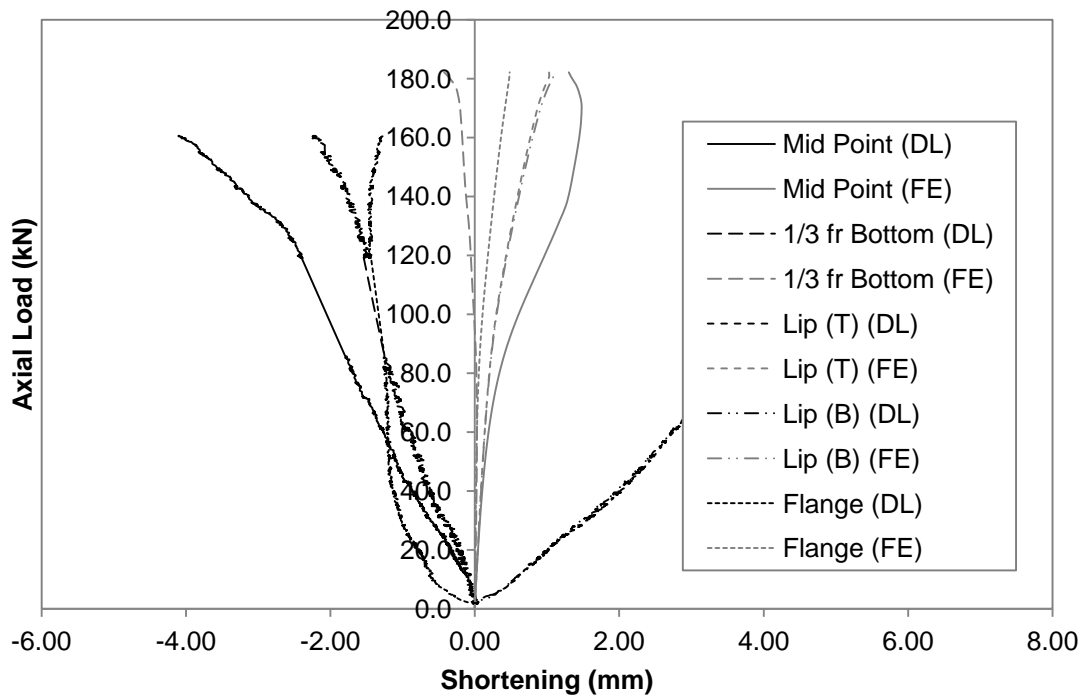


Figure G.40 Axial Load versus Deformation Curve for GBU90S100L500-3

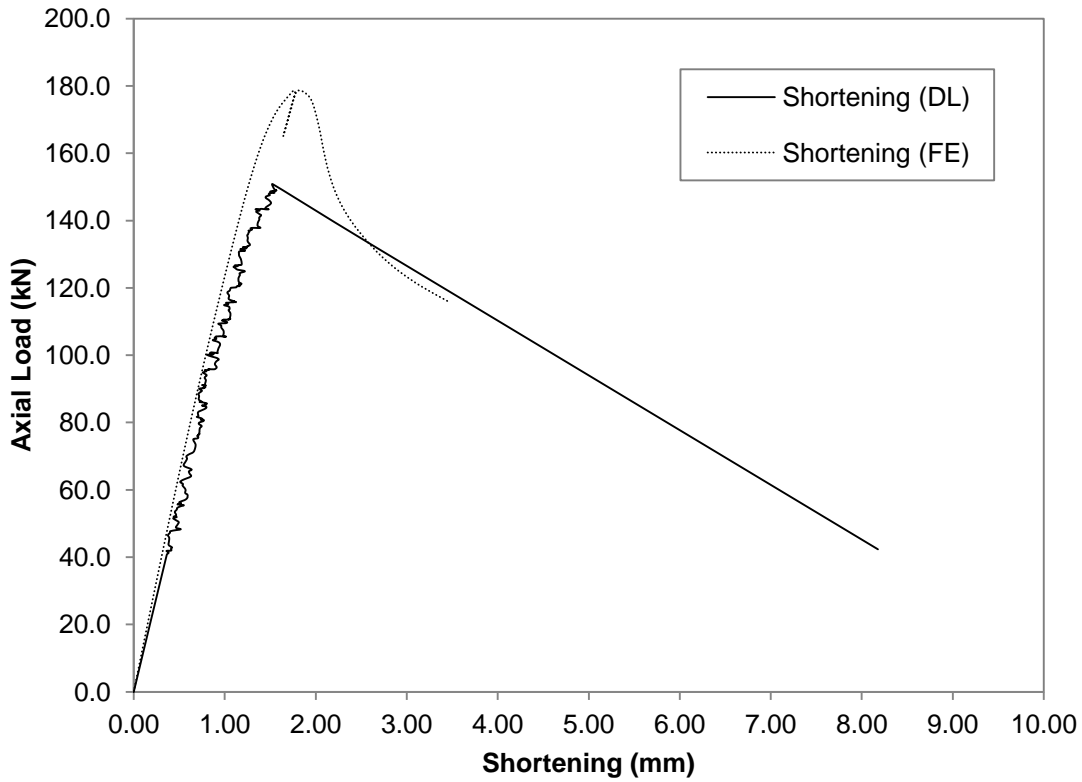


Figure G.41 Axial Load versus Shortening Curve for GBU90S400L500-1

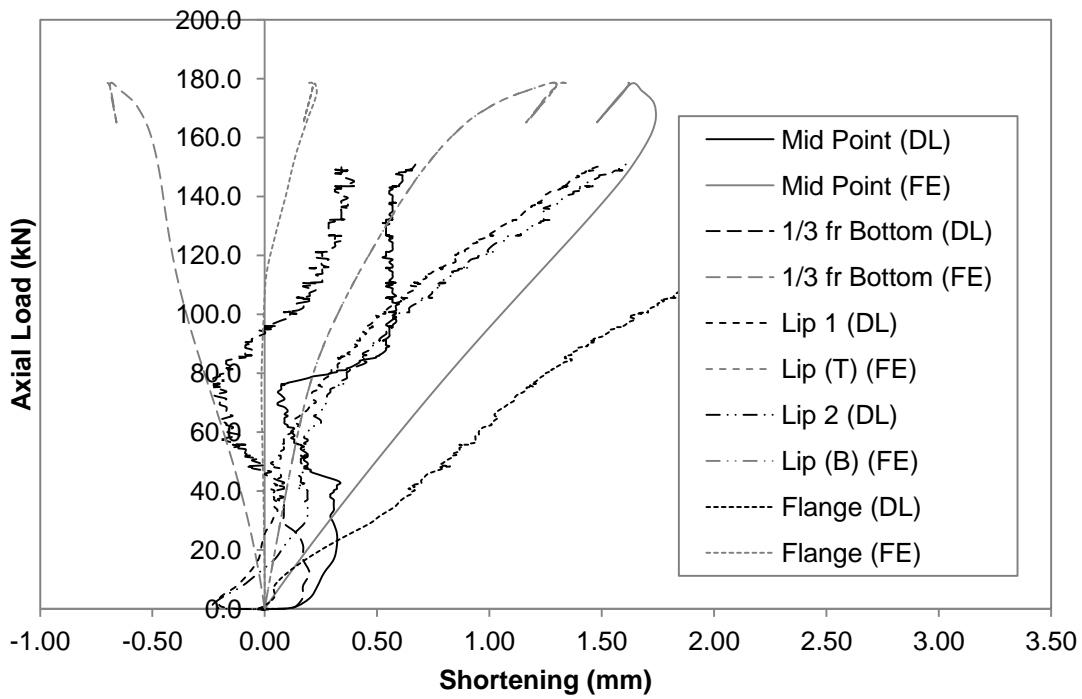


Figure G.42 Axial Load versus Deformation Curve for GBU90S400L500-1

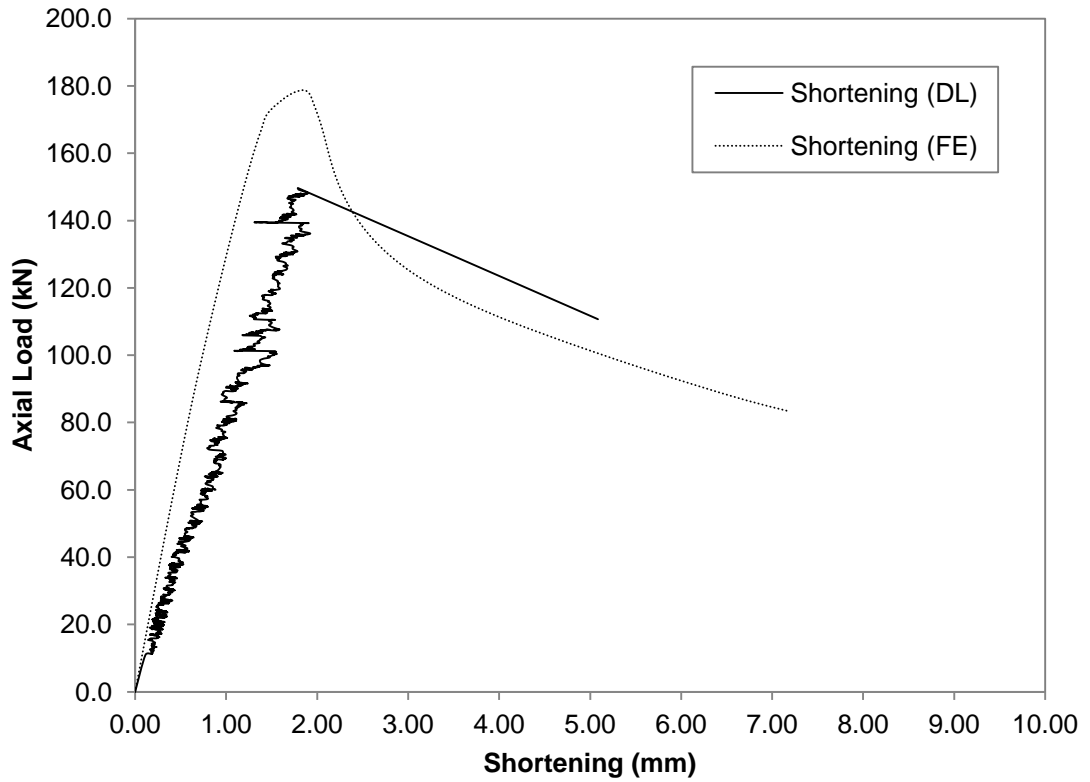


Figure G.43 Axial Load versus Shortening Curve for GBU90S400L500-2

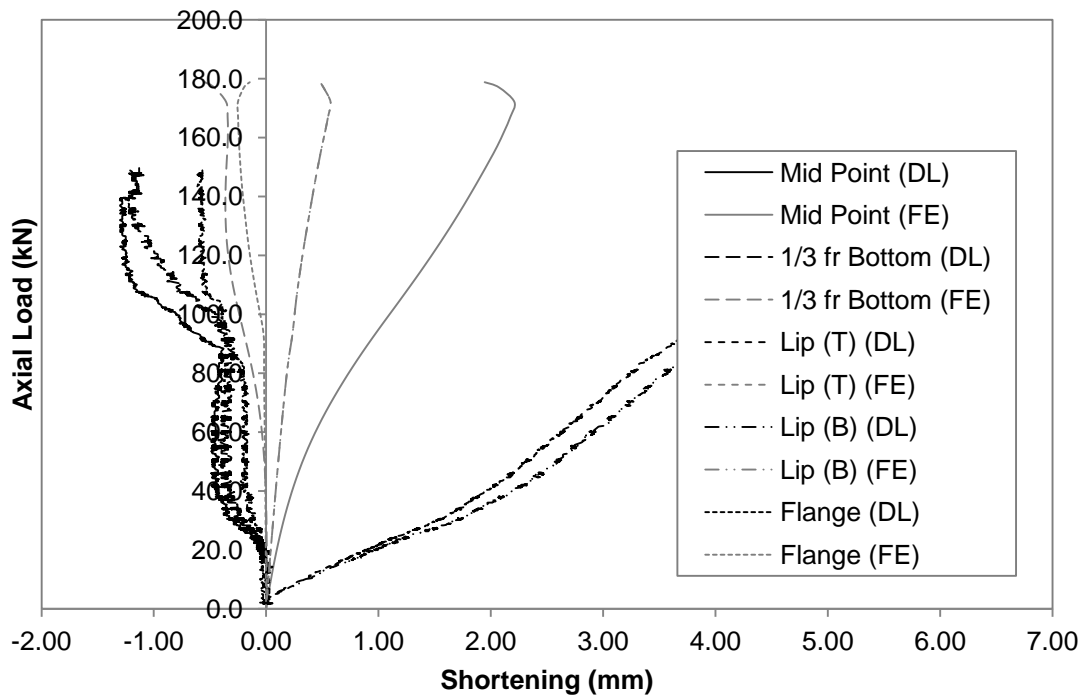


Figure G.44 Axial Load versus Deformation Curve for GBU90S400L500-2

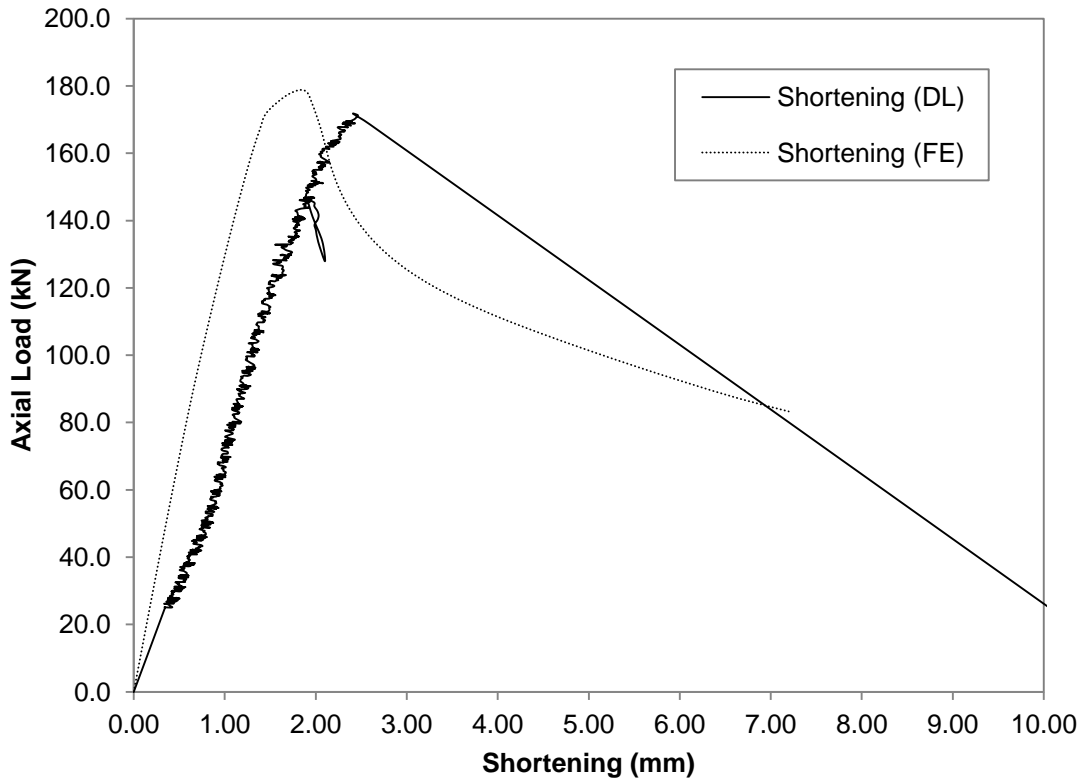


Figure G.45 Axial Load versus Shortening Curve for GBU90S400L500-3

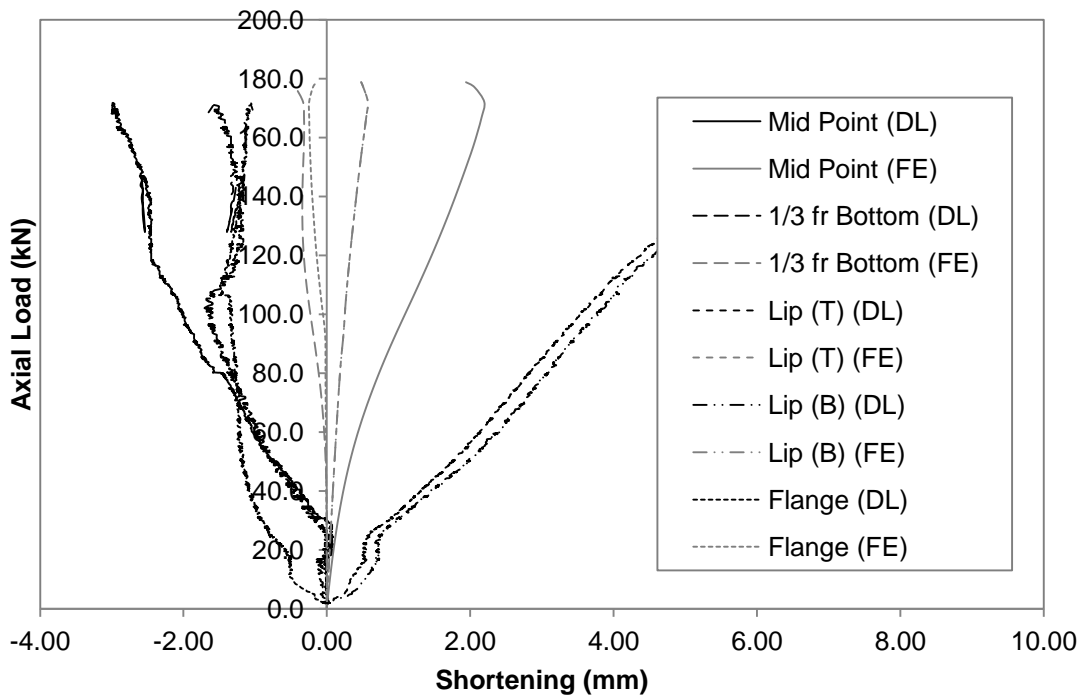


Figure G.46 Axial Load versus Deformation Curve for GBU90S400L500-3

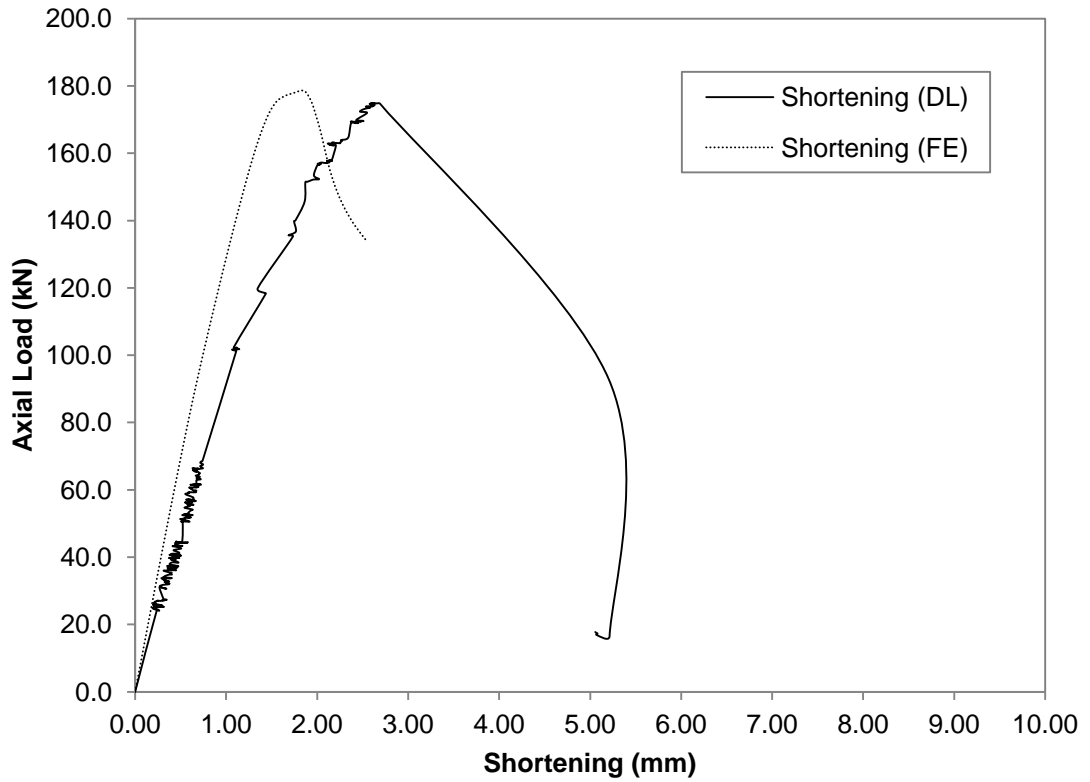


Figure G.47 Axial Load versus Shortening Curve for GBU90S400L500-4

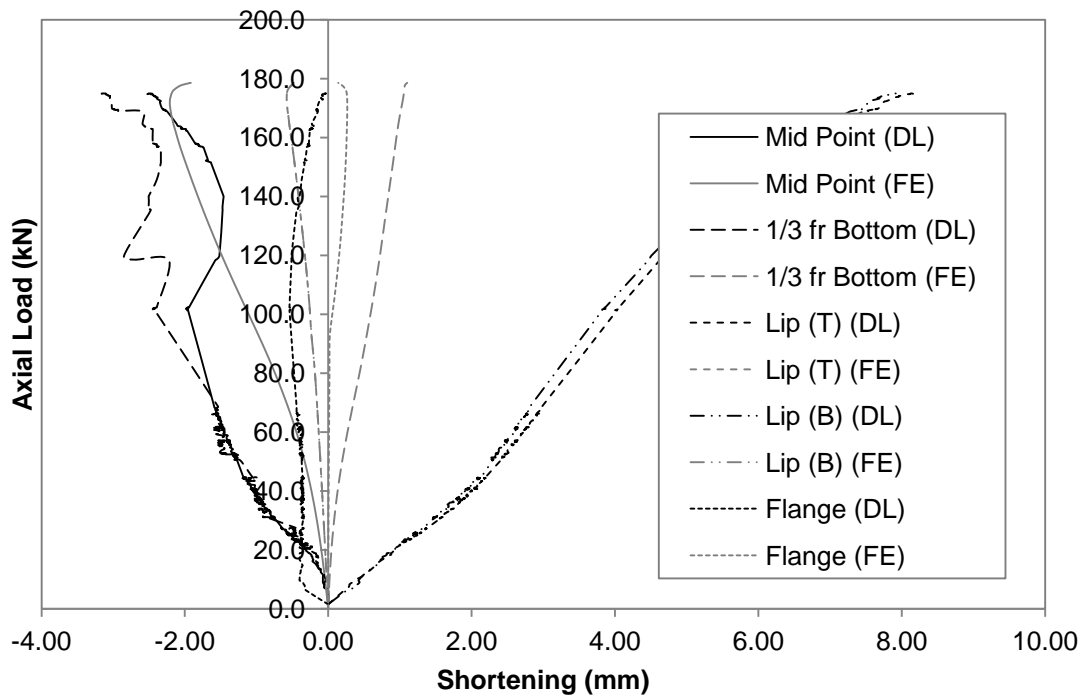


Figure G.48 Axial Load versus Deformation Curve for GBU90S400L500-4

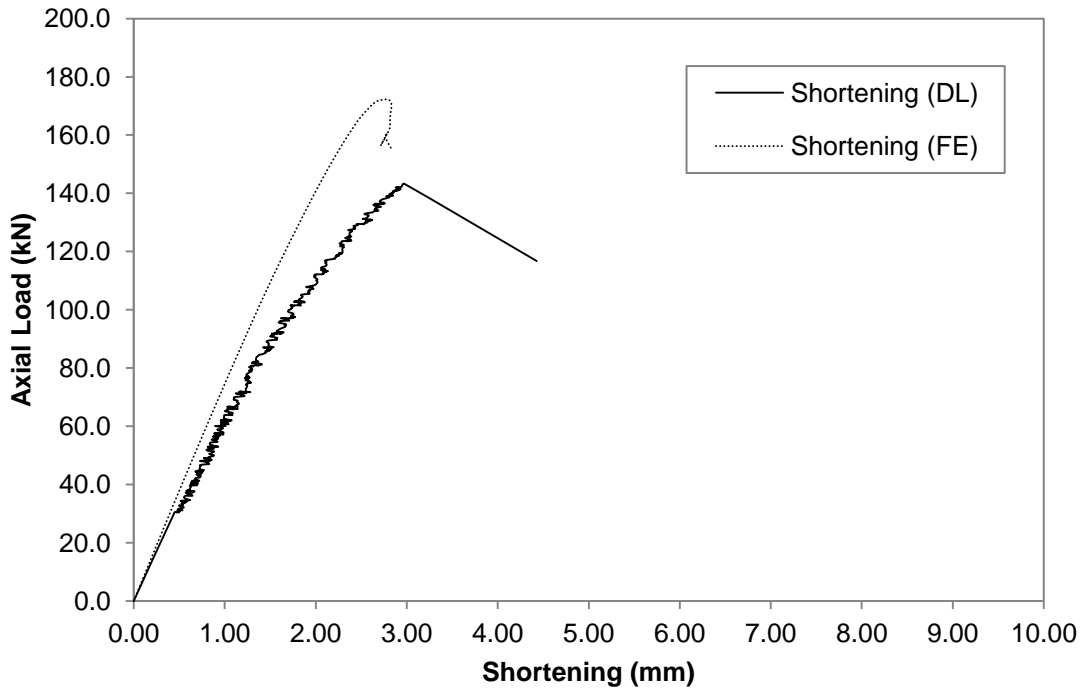


Figure G.49 Axial Load versus Shortening Curve for GBU90S225L1000-1

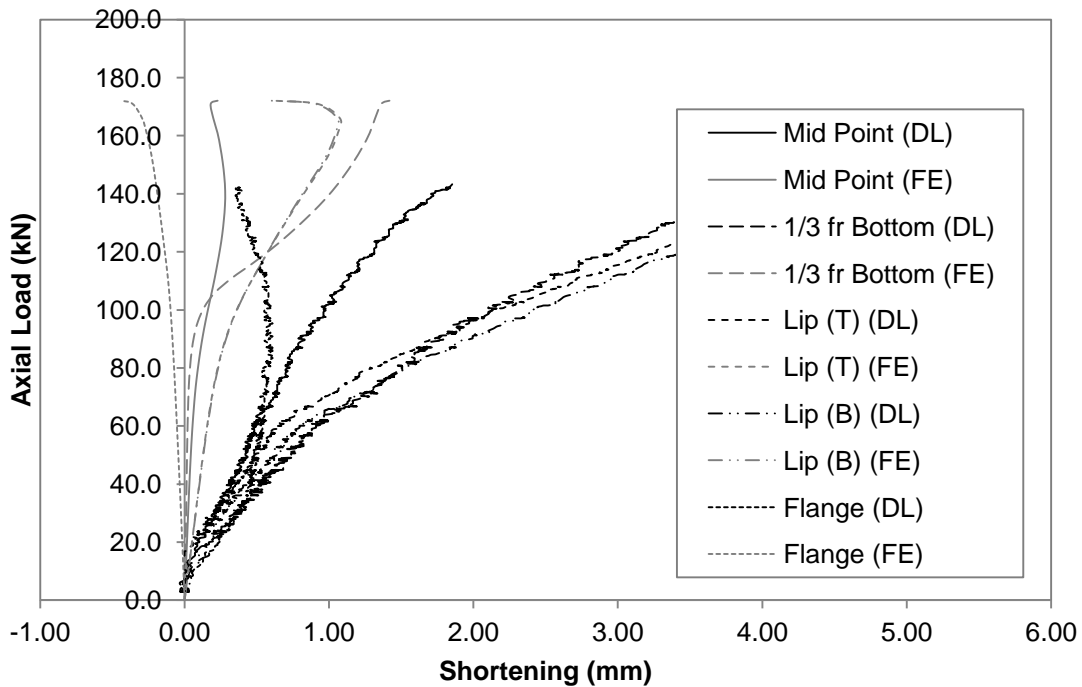


Figure G.50 Axial Load versus Deformation Curve for GBU90S225L1000-1

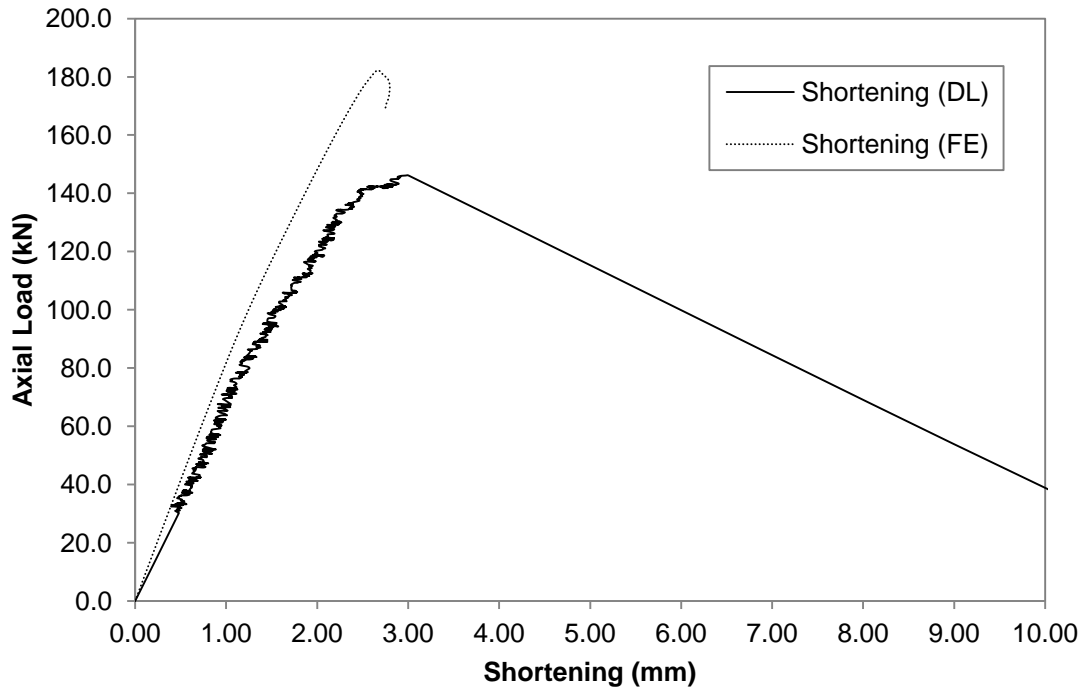


Figure G.51 Axial Load versus Shortening Curve for GBU90S225L1000-3

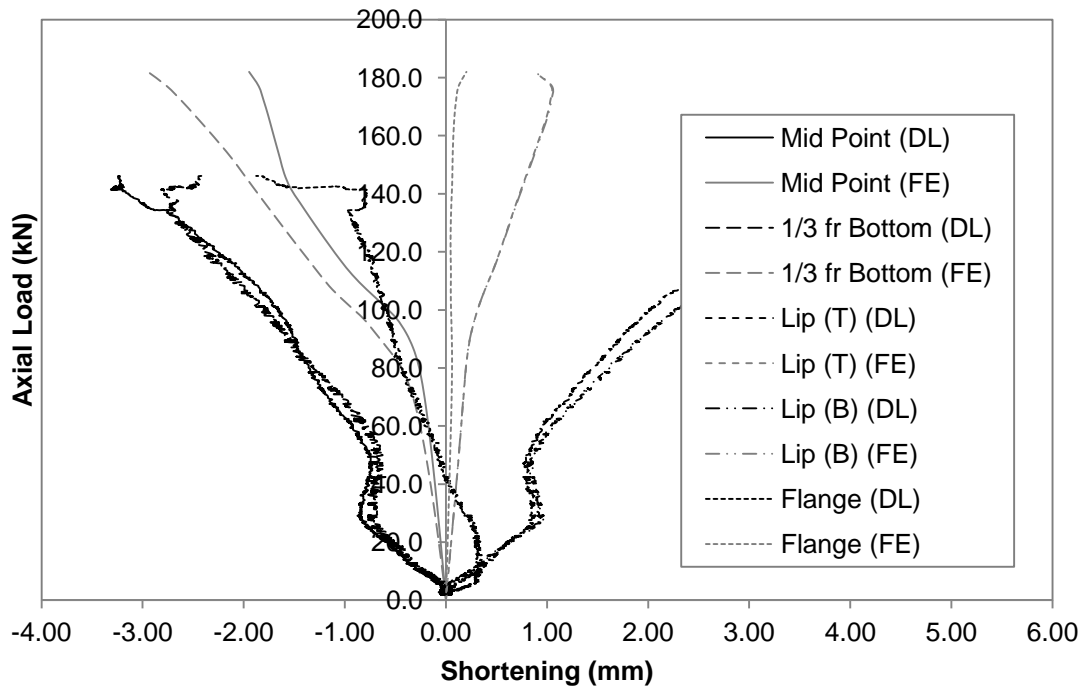


Figure G.52 Axial Load versus Deformation Curve for GBU90S225L1000-3

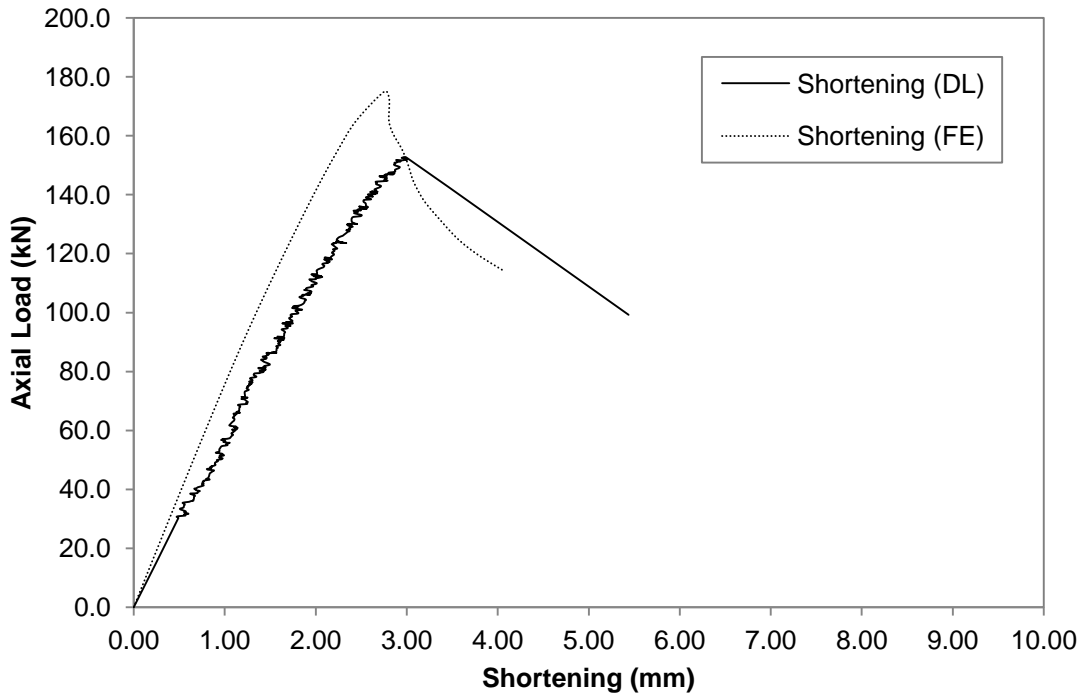


Figure G.53 Axial Load versus Shortening Curve for GBU90S900L1000-1

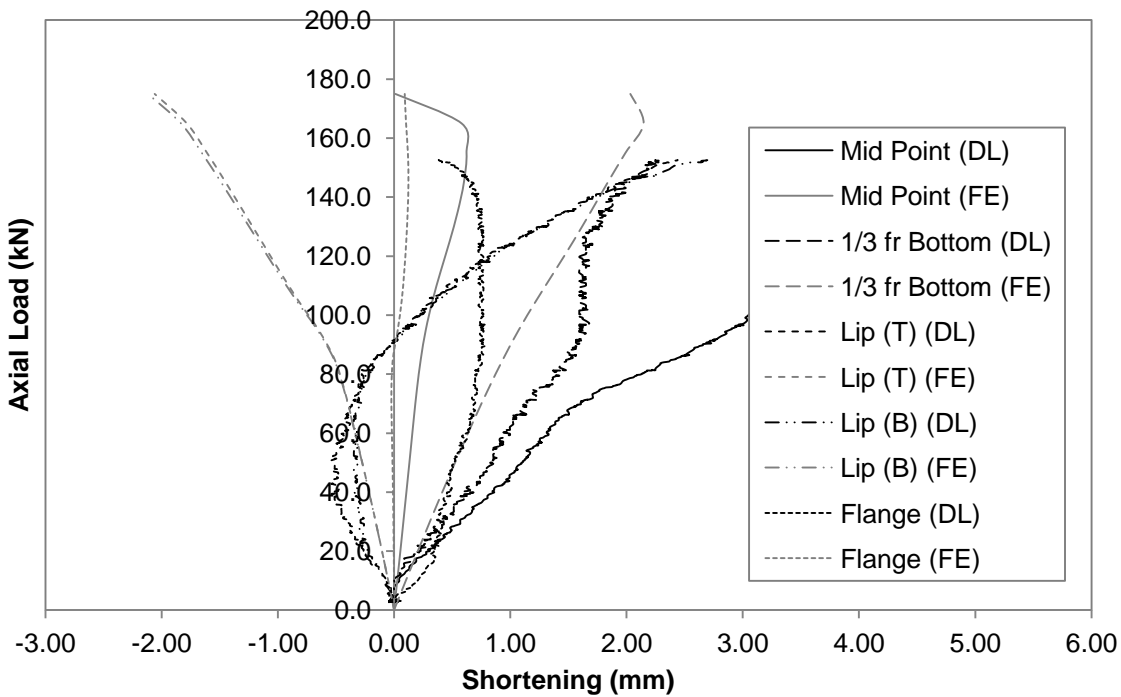


Figure G.54 Axial Load versus Deformation Curve for GBU90S900L1000-1

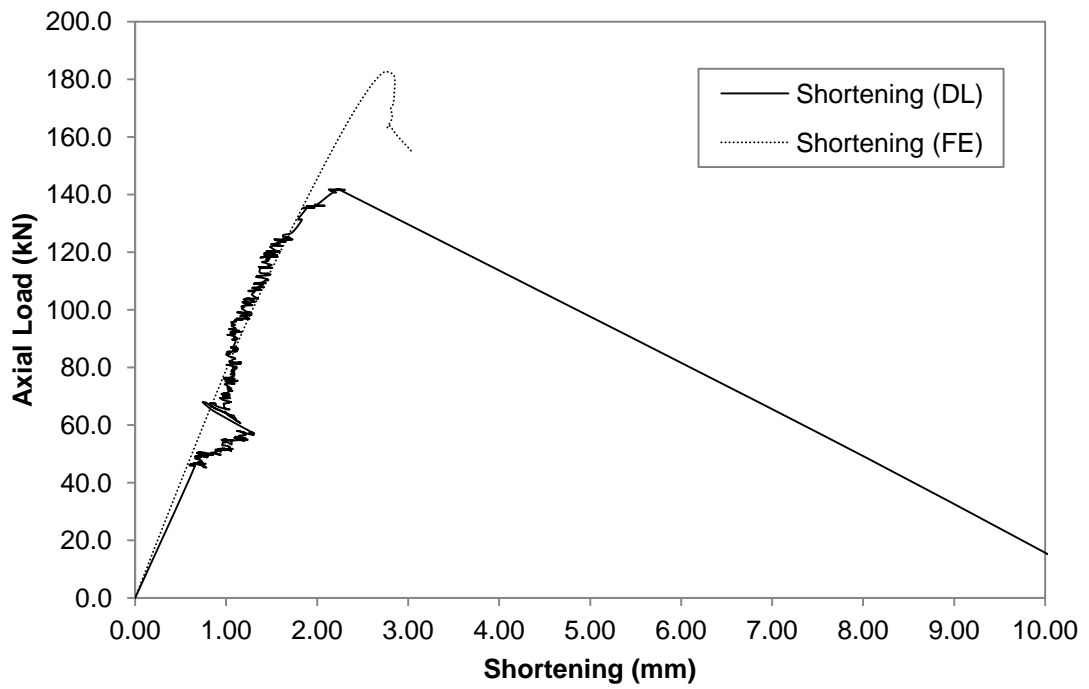


Figure G.55 Axial Load versus Shortening Curve for GBU90S900L1000-3

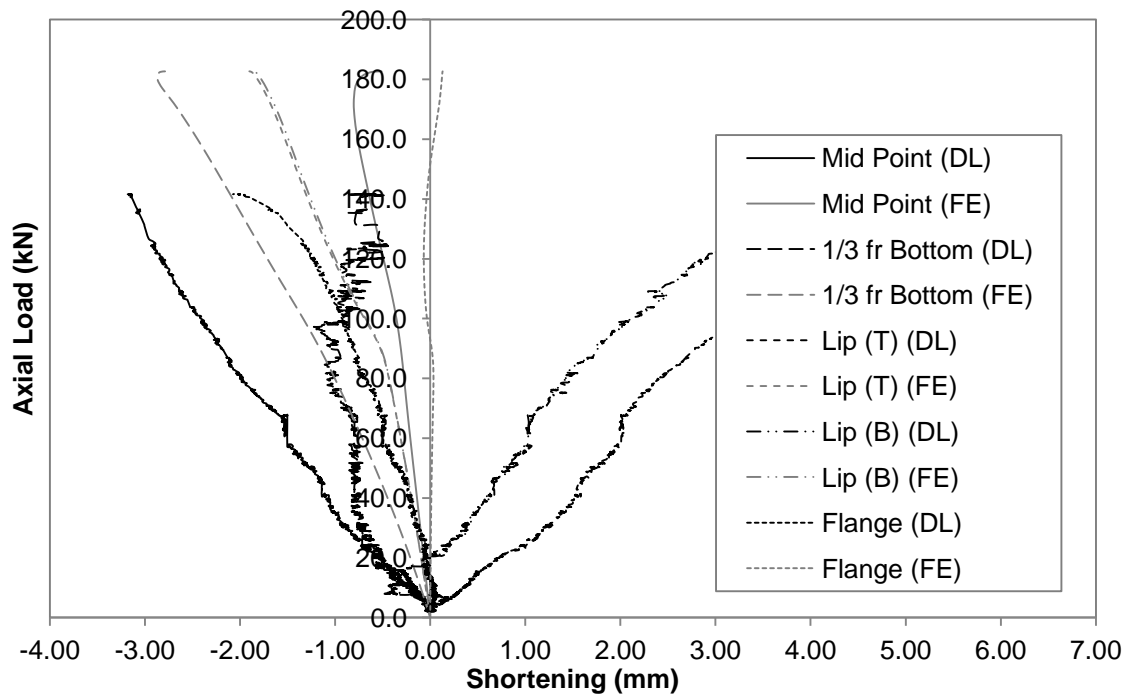


Figure G.56 Axial Load versus Deformation Curve for GBU90S900L1000-3

G.3 Short Column (L=1000mm)

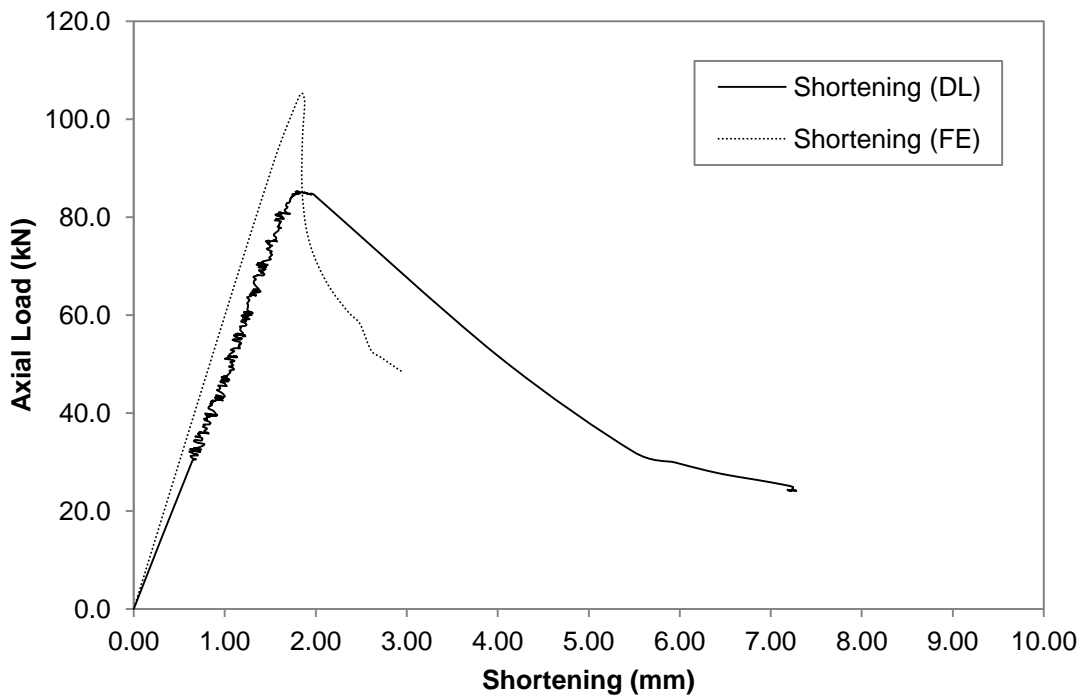


Figure G.57 Axial Load versus Shortening Curve for GBU75S225L1000-1

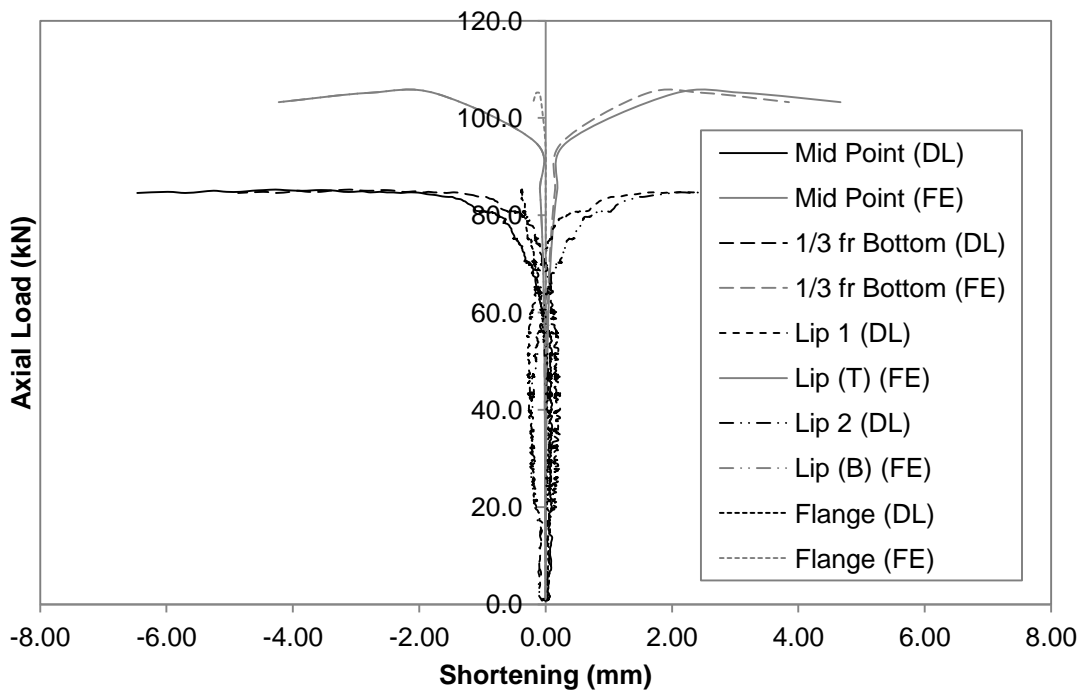


Figure G.58 Axial Load versus Deformation Curve for GBU75S225L1000-1

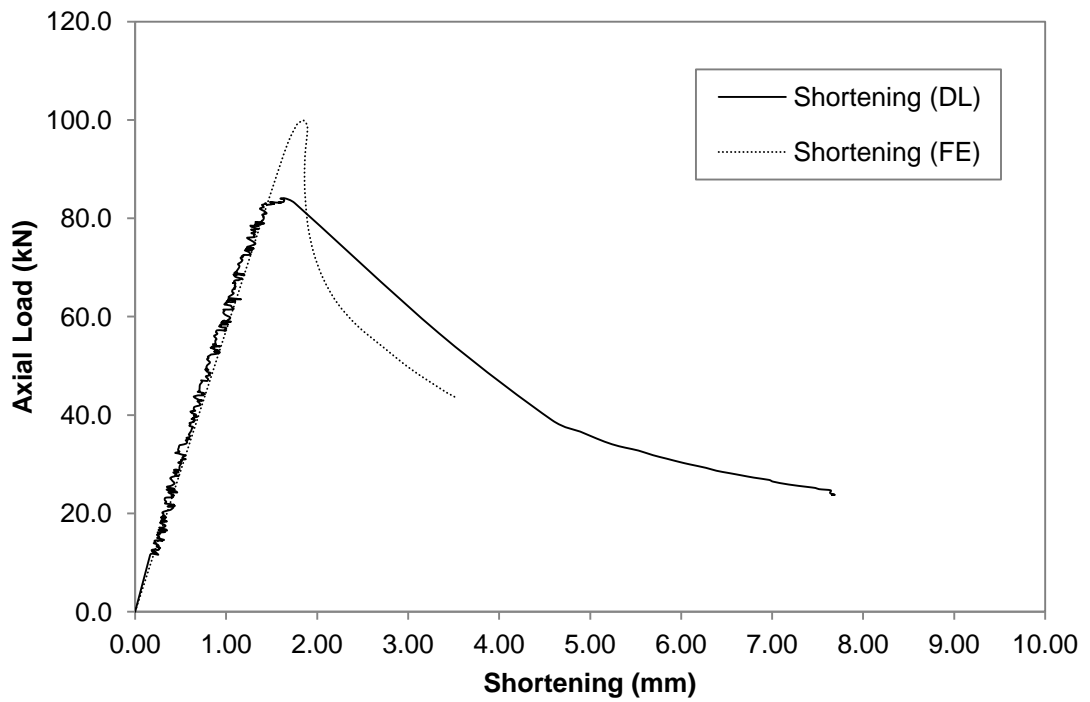


Figure G.59 Axial Load versus Shortening Curve for GBU75S225L1000-2

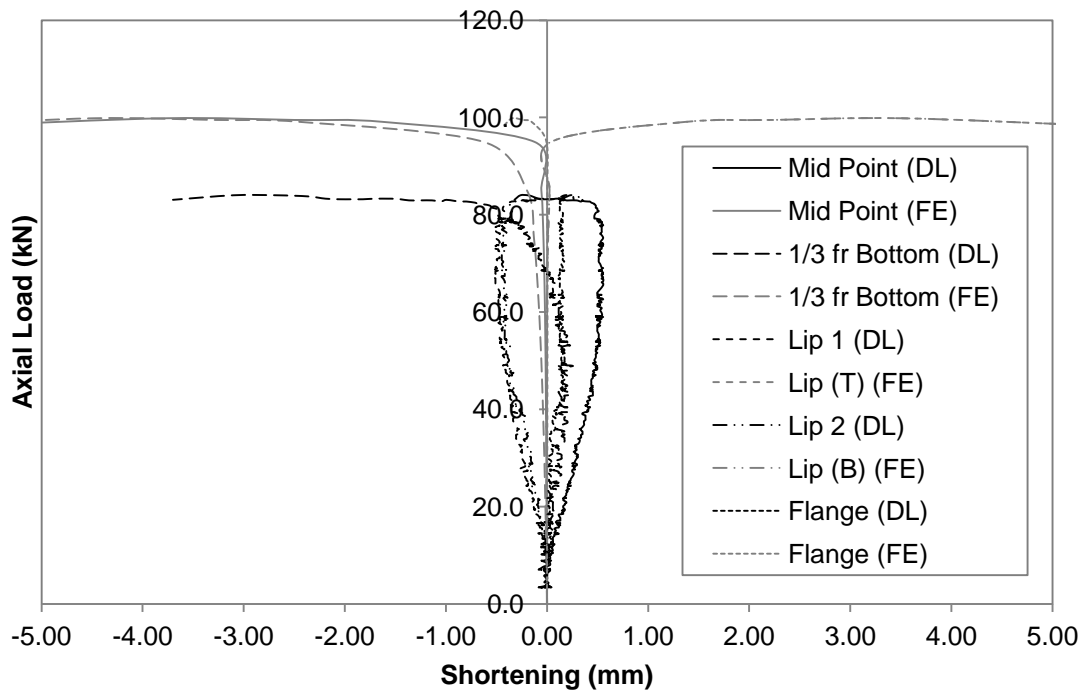


Figure G.60 Axial Load versus Deformation Curve for GBU75S225L1000-2

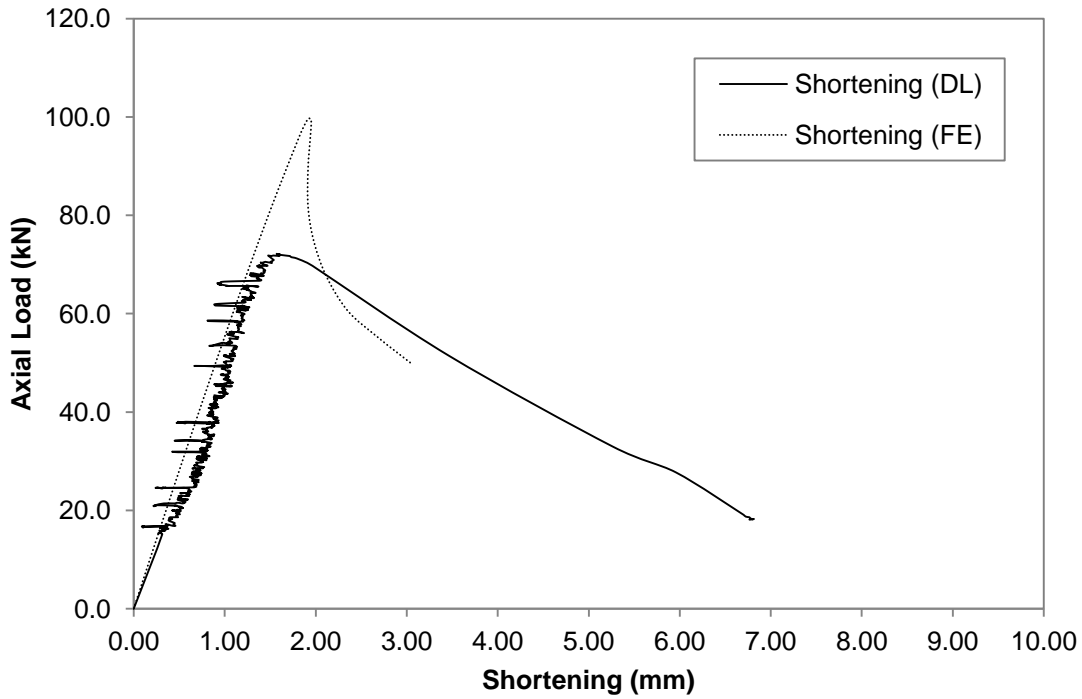


Figure G.61 Axial Load versus Shortening Curve for GBU75S225L1000-3

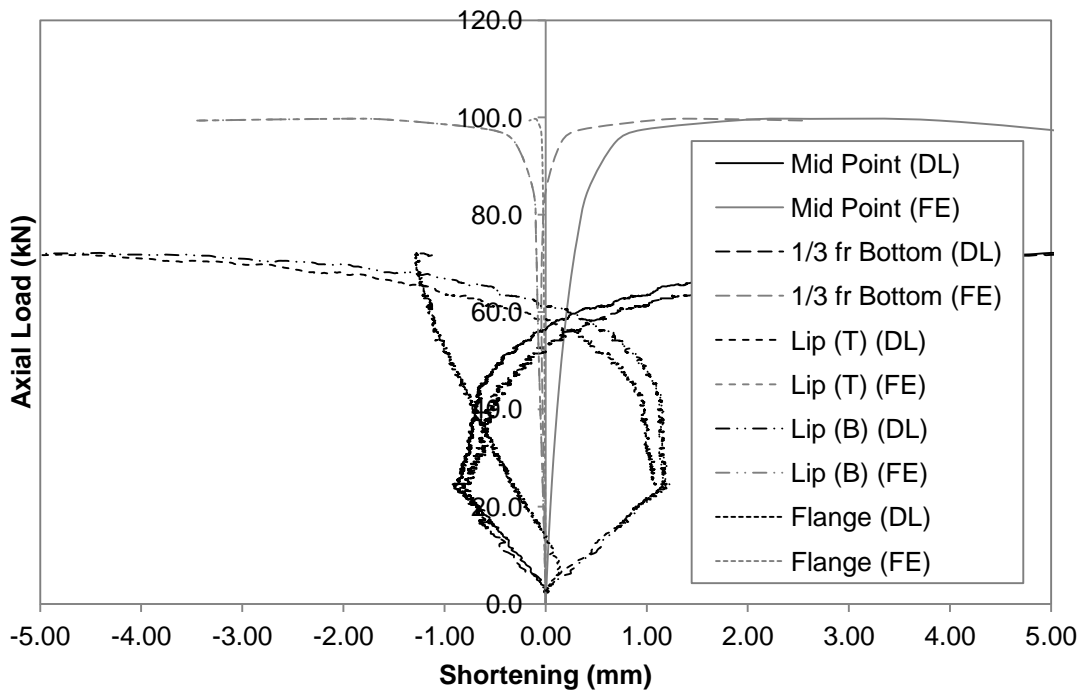


Figure G.62 Axial Load versus Deformation Curve for GBU75S225L1000-3

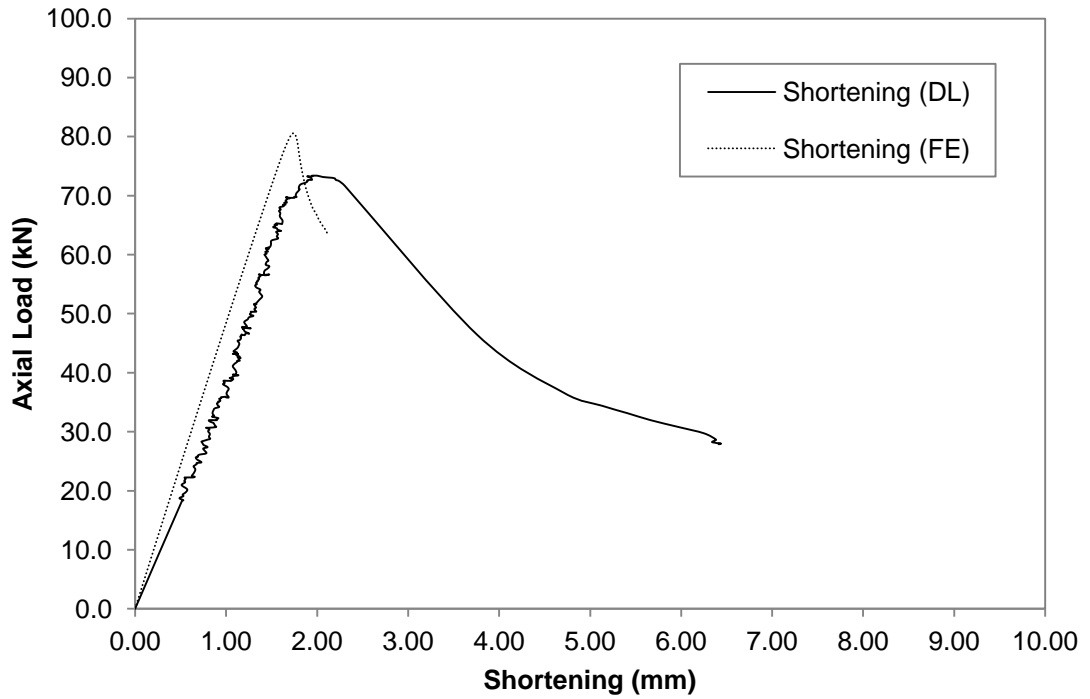


Figure G.63 Axial Load versus Shortening Curve for GBU75S900L1000-1

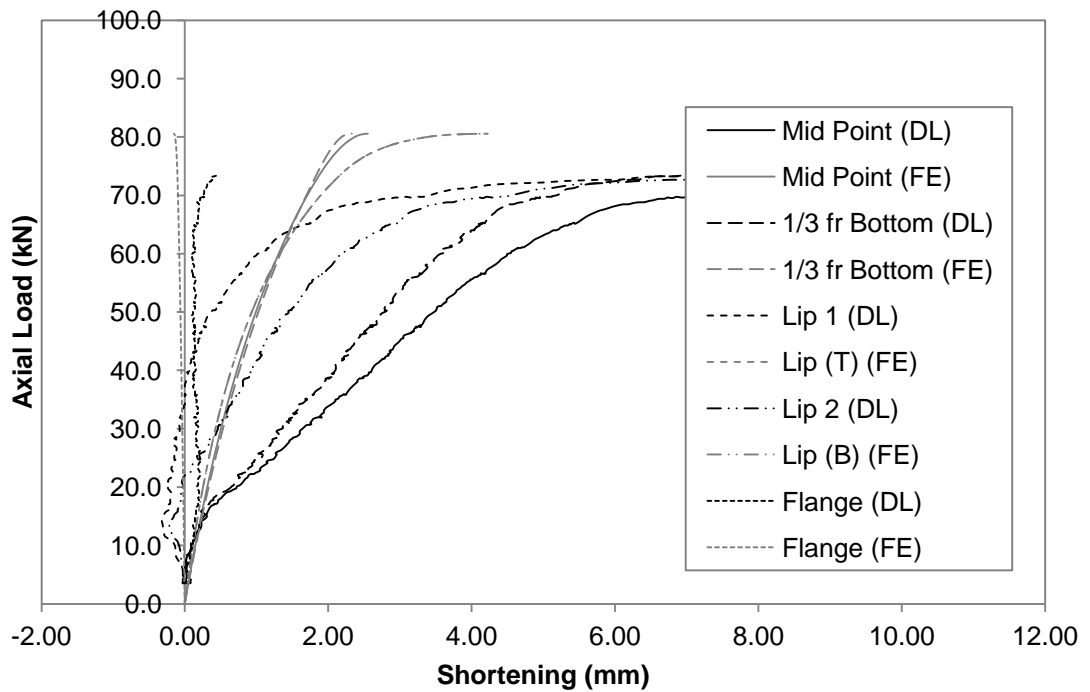


Figure G.64 Axial Load versus Deformation Curve for GBU75S900L1000-1

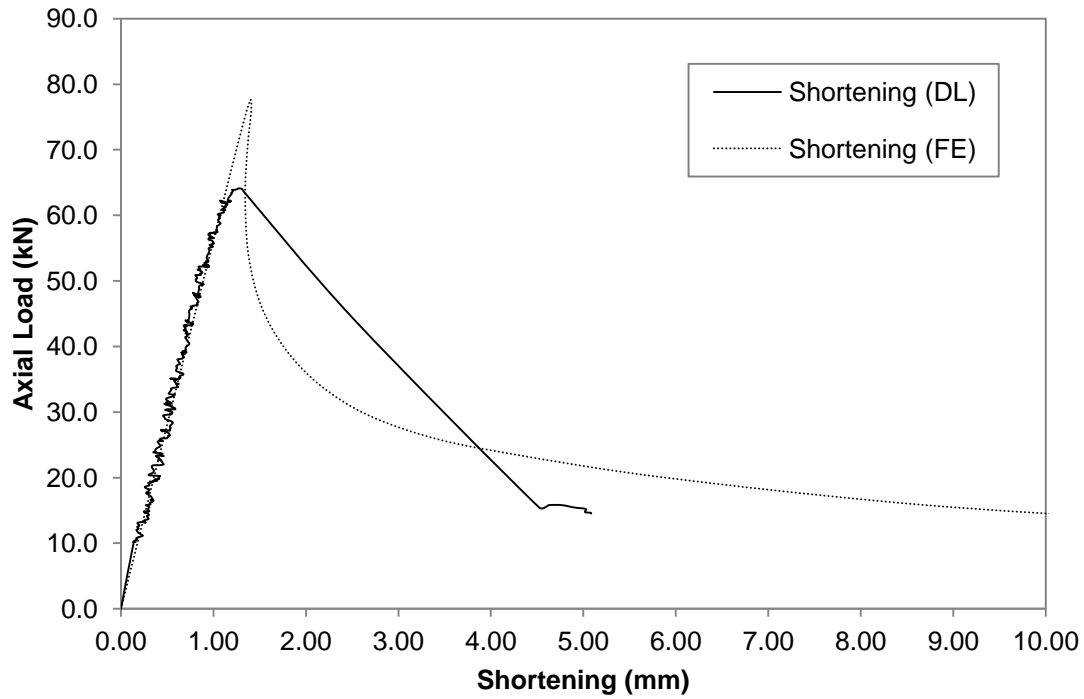


Figure G.65 Axial Load versus Shortening Curve for GBU75S900L1000-2

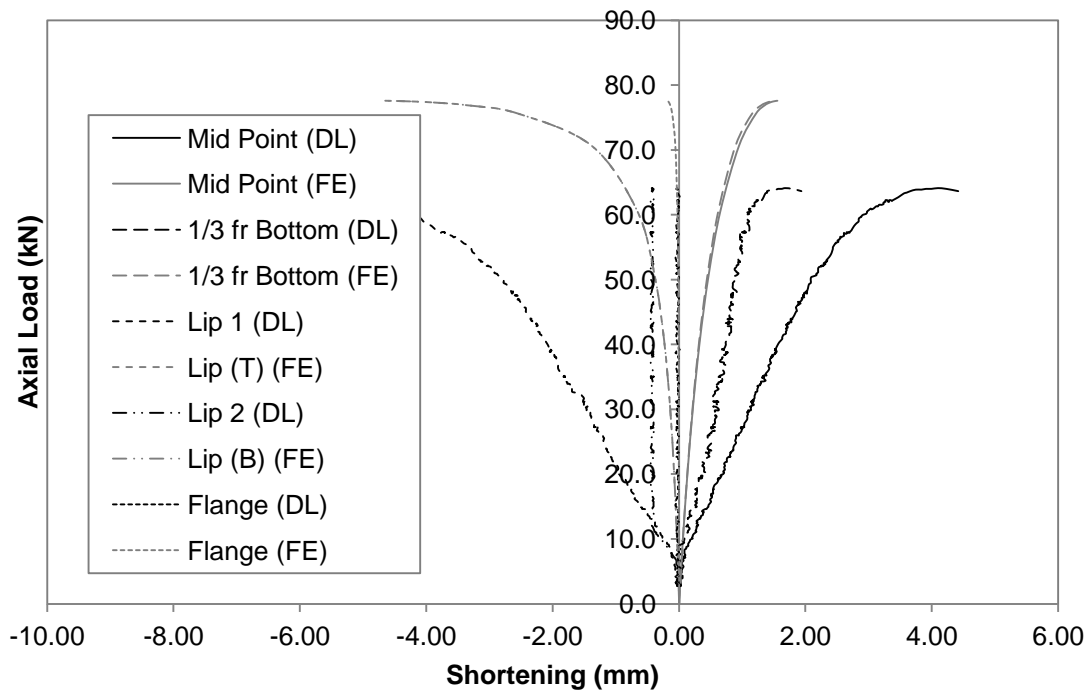


Figure G.66 Axial Load versus Deformation Curve for GBU75S900L1000-2

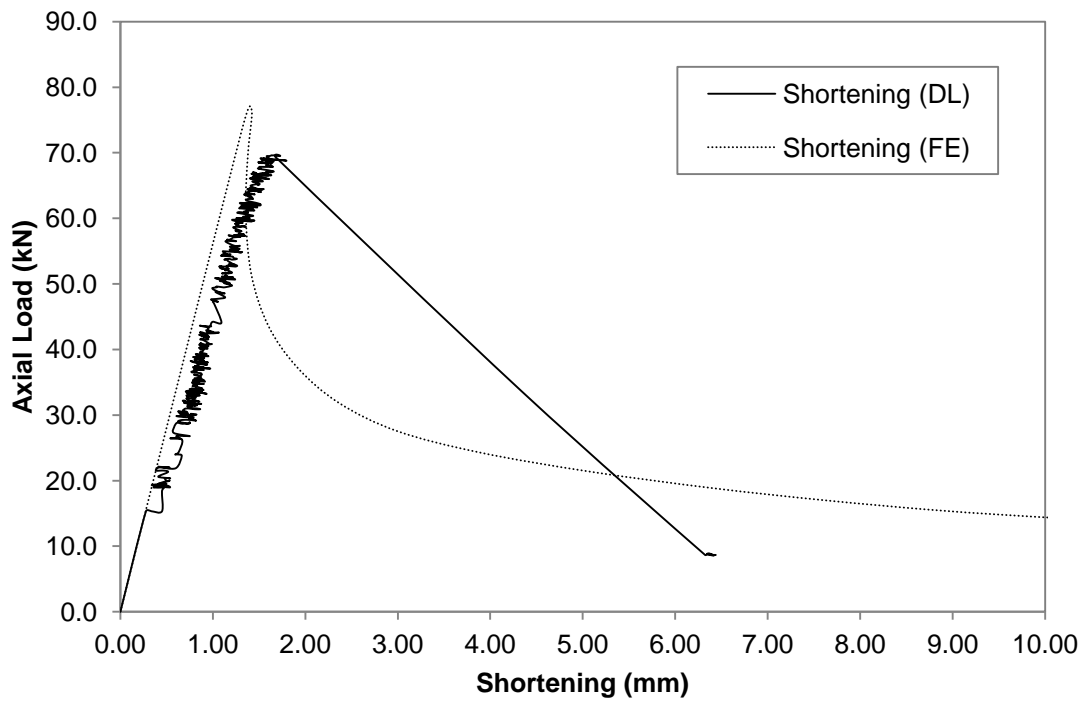


Figure G.67 Axial Load versus Shortening Curve for GBU75S900L1000-3

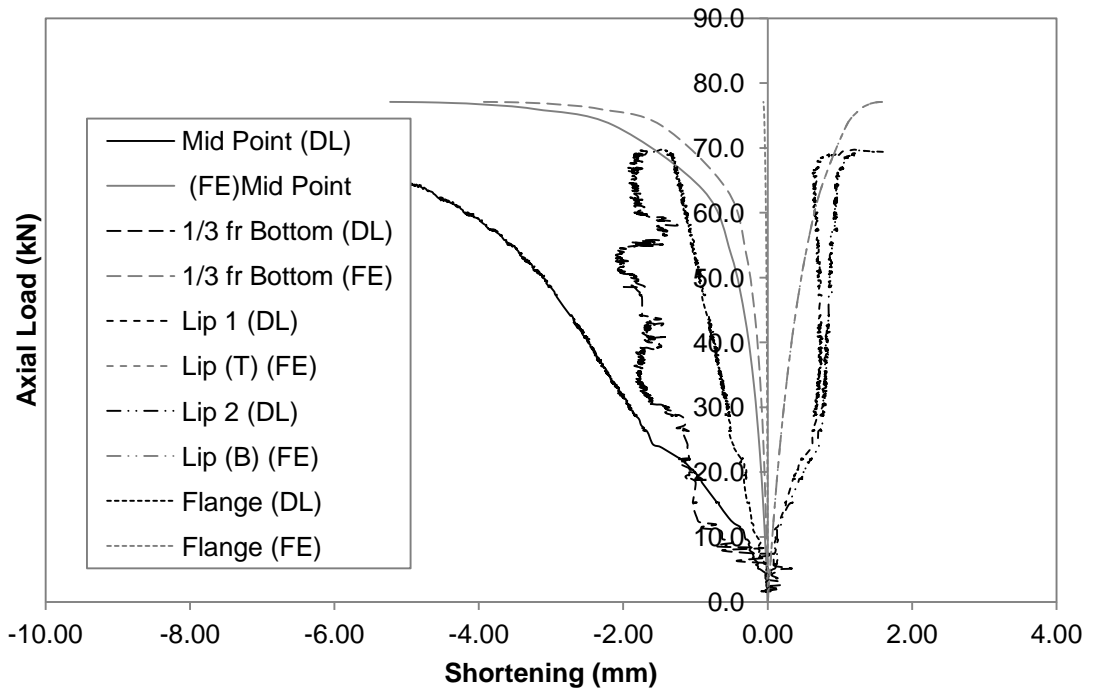


Figure G.68 Axial Load versus Deformation Curve for GBU75S900L1000-3

G.4 Short Column (L=2000mm)

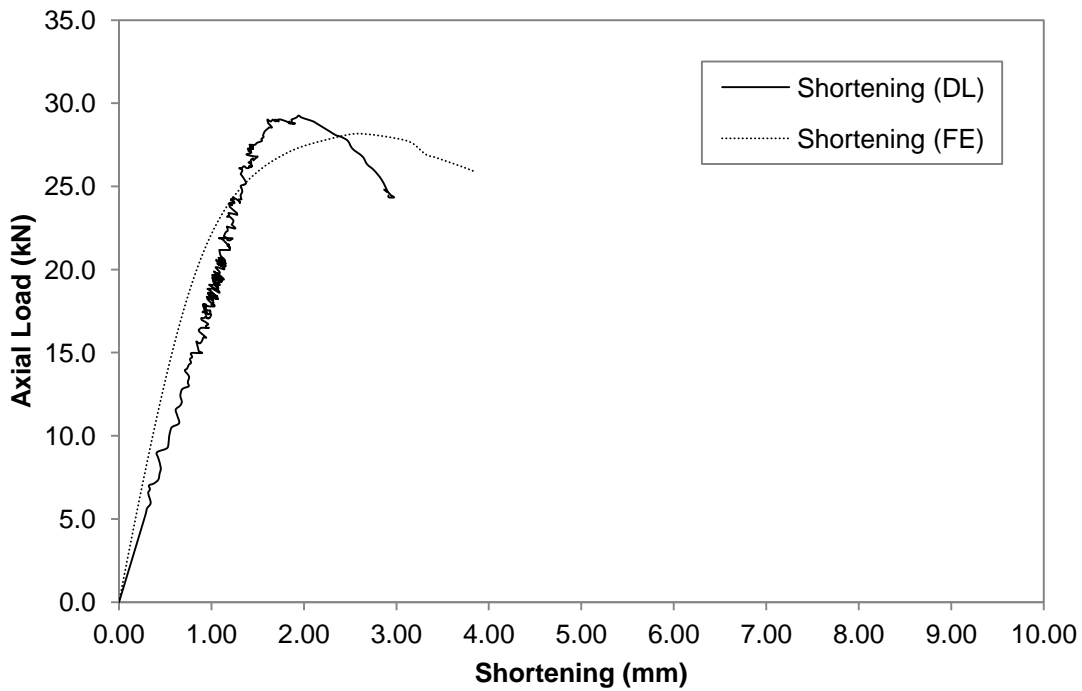


Figure G.69 Axial Load versus Shortening Curve for GBU75S475L2000-1

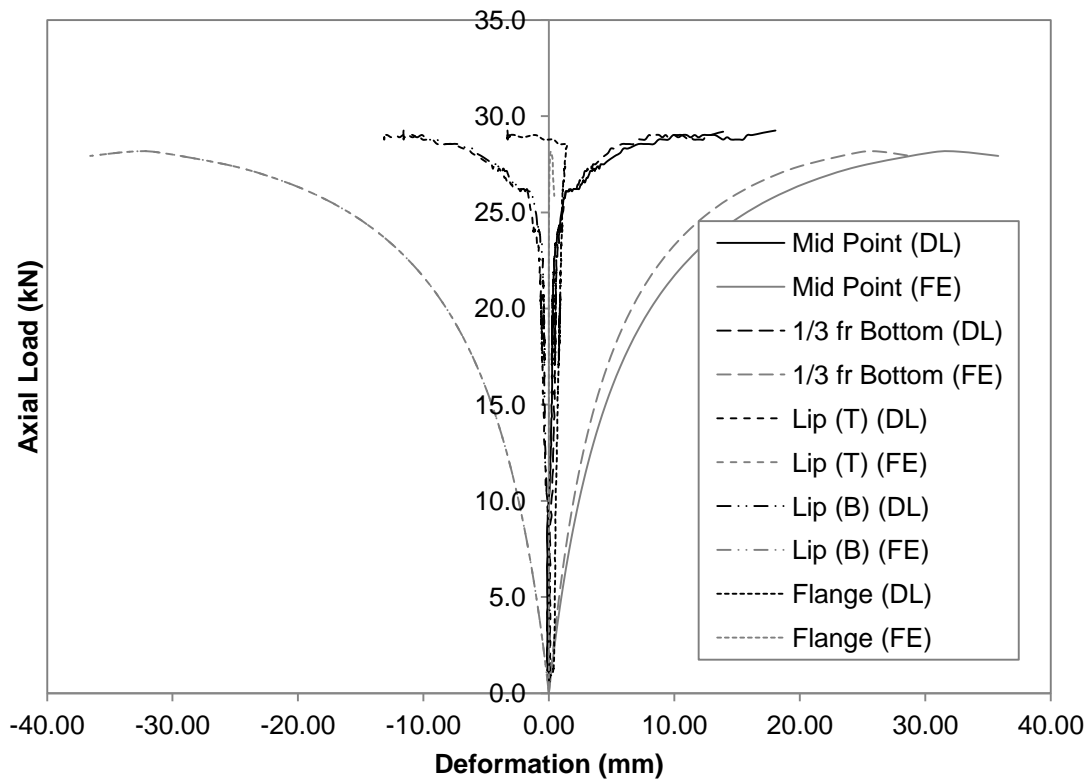


Figure G.70 Axial Load versus Deformation Curve for GBU75S475L2000-1

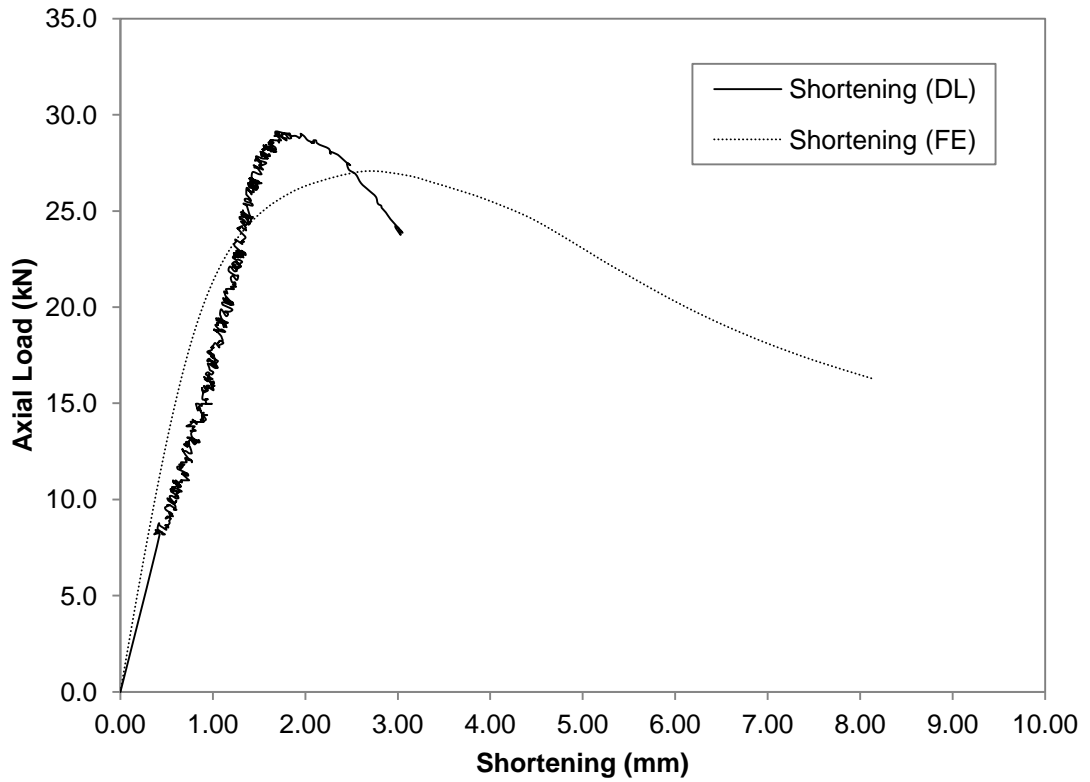


Figure G.71 Axial Load versus Shortening Curve for GBU75S475L2000-2

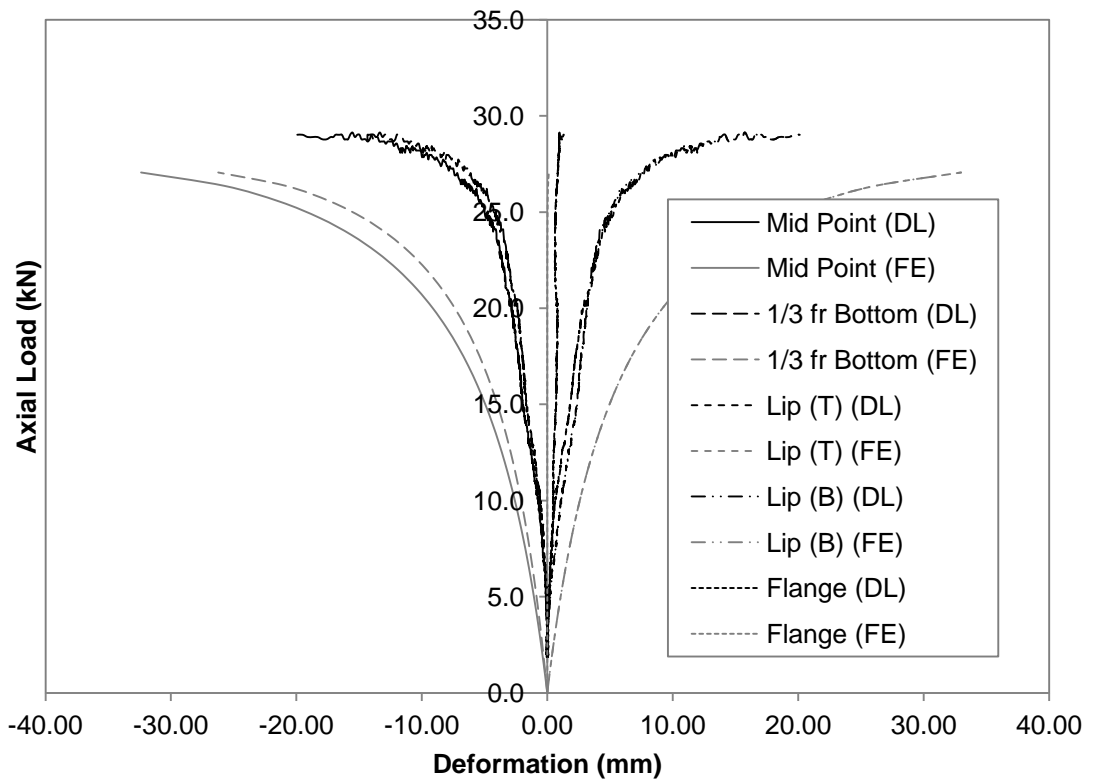


Figure G.72 Axial Load versus Deformation Curve for GBU75S475L2000-2

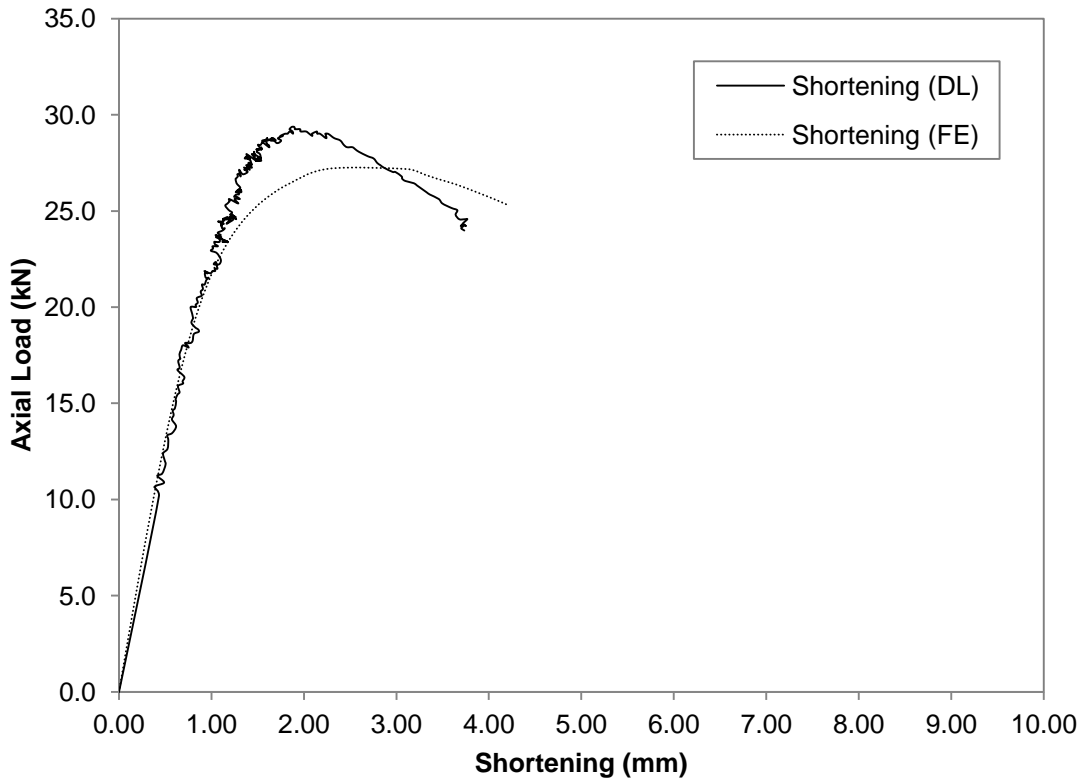


Figure G.73 Axial Load versus Shortening Curve for GBU75S475L2000-3

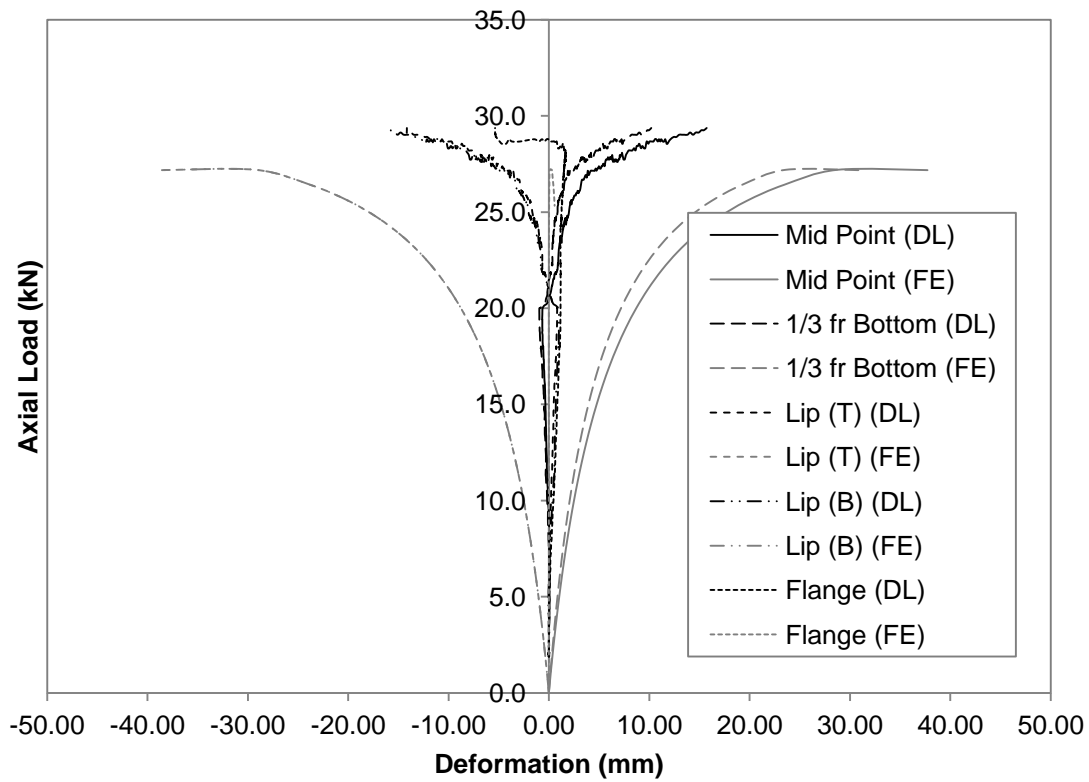


Figure G.74 Axial Load versus Deformation Curve for GBU75S475L2000-3

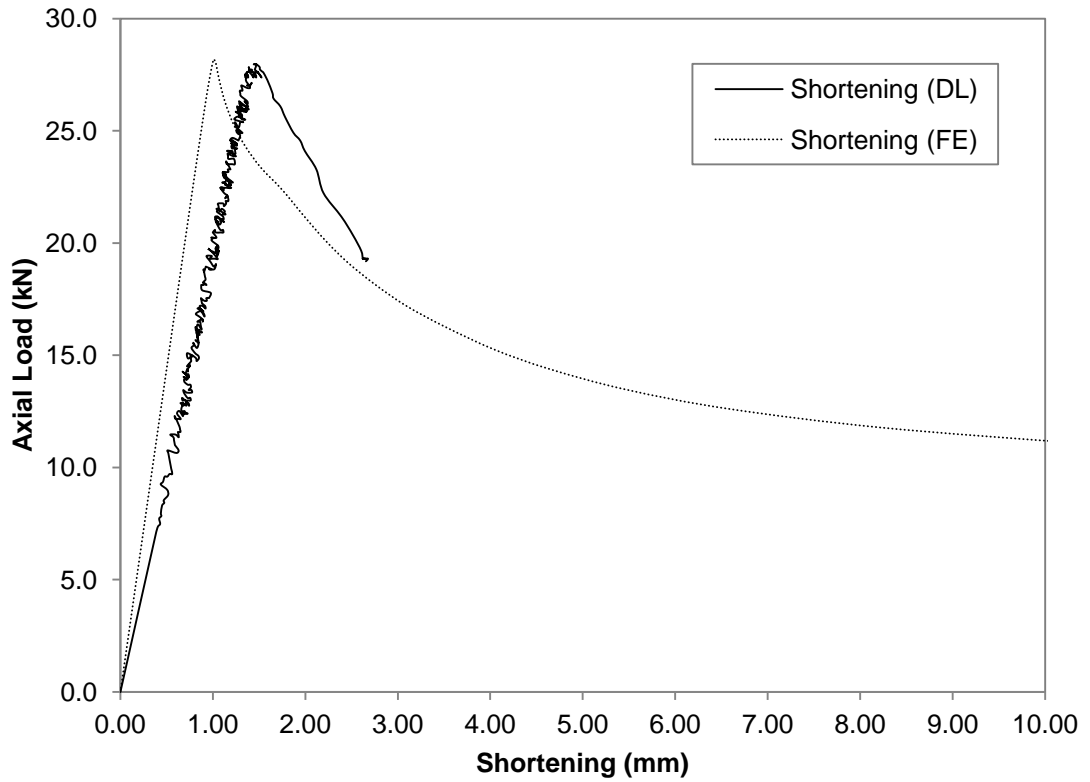


Figure G.75 Axial Load versus Shortening Curve for GBU75S1900L2000-1

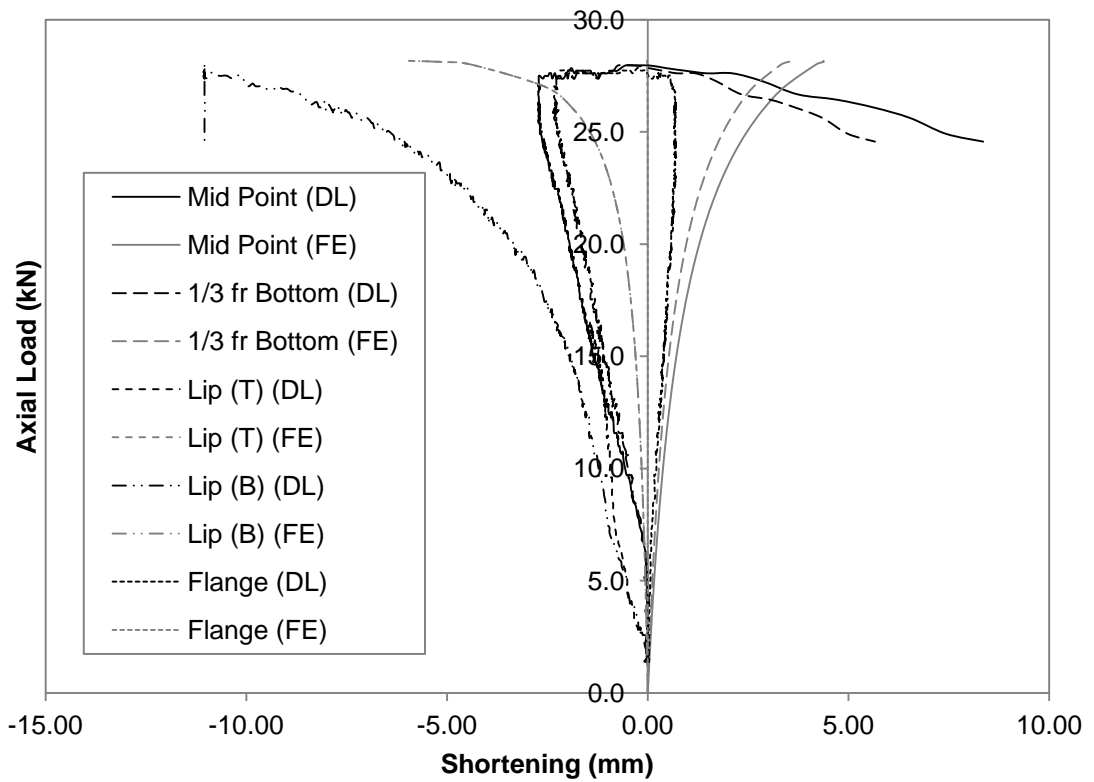


Figure G.76 Axial Load versus Deformation Curve for GBU75S1900L2000-1

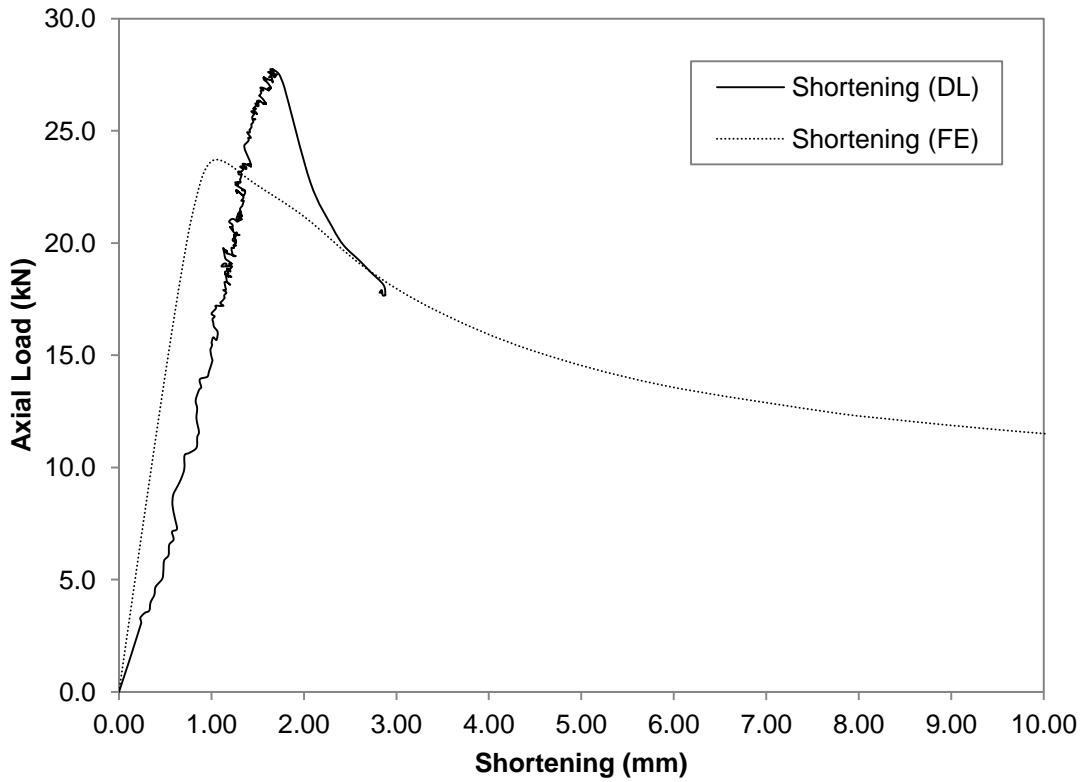


Figure G.77 Axial Load versus Shortening Curve for GBU75S1900L2000-2

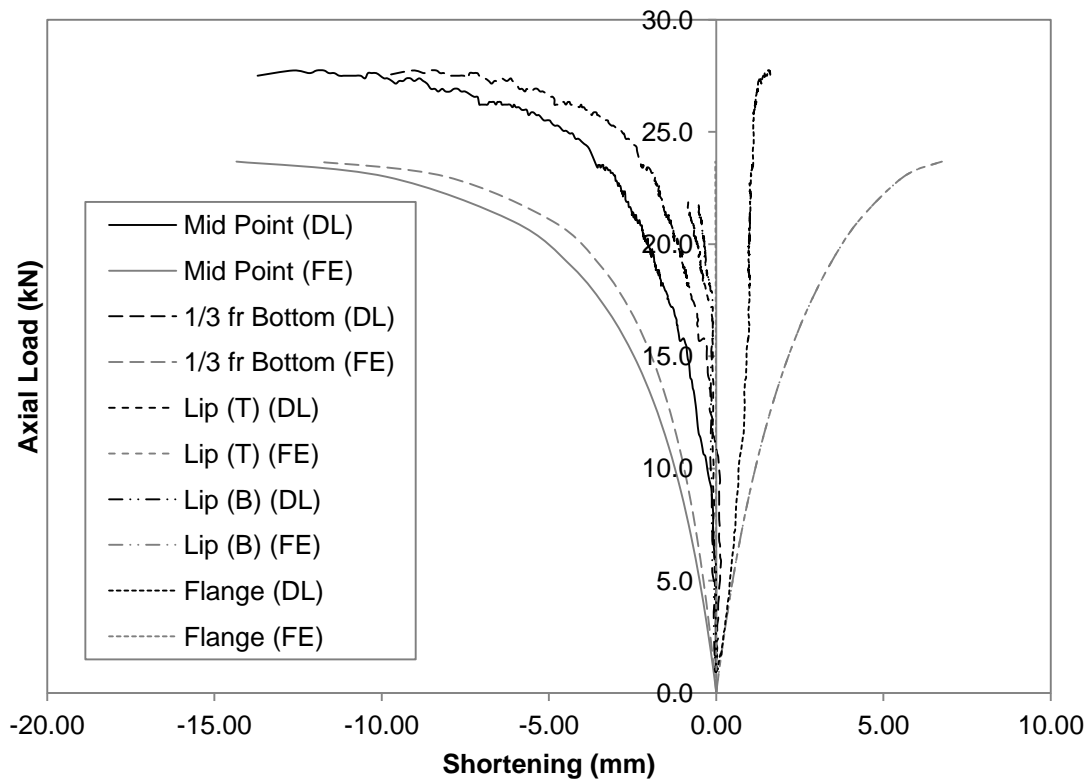


Figure G.78 Axial Load versus Deformation Curve for GBU75S1900L2000-2

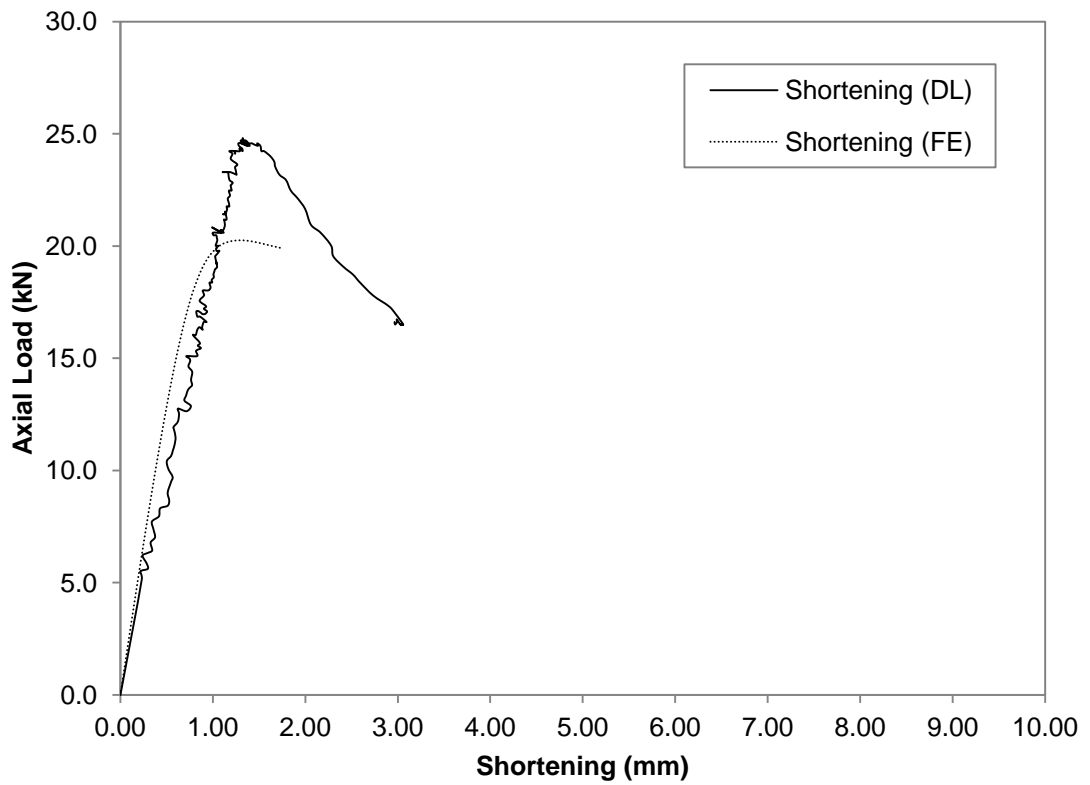


Figure G.79 Axial Load versus Shortening Curve for GBU75S1900L2000-3

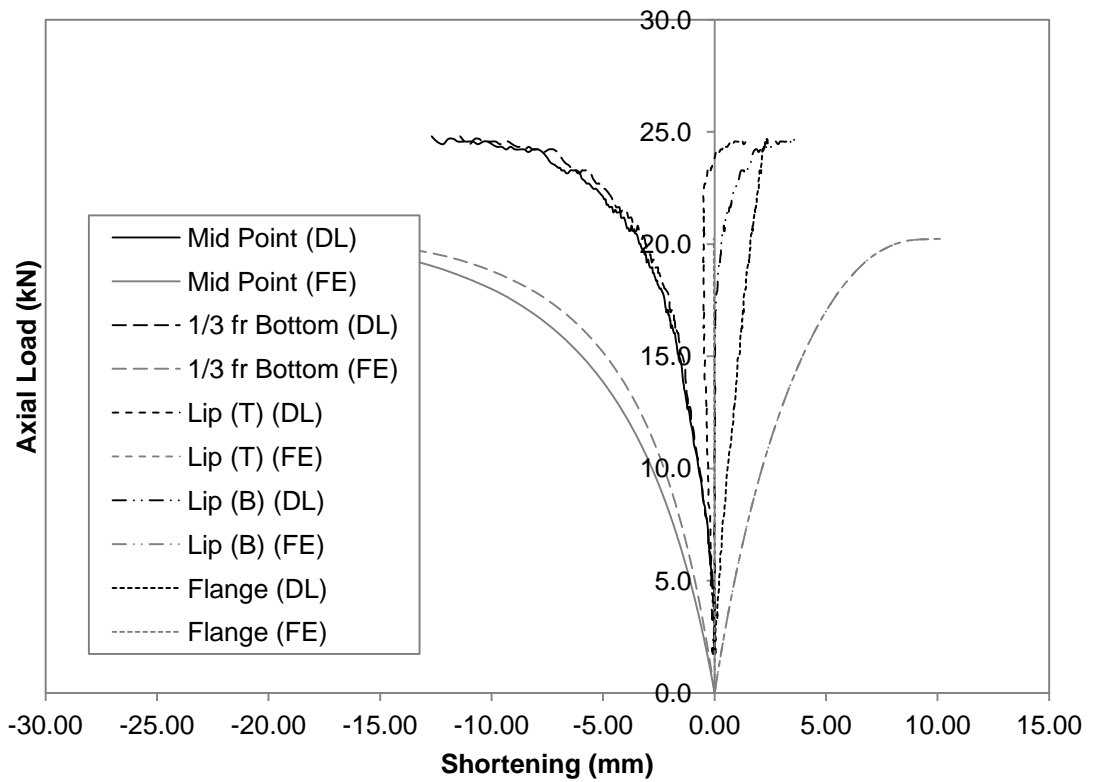


Figure G.80 Axial Load versus Deformation Curve for GBU75S1900L2000-3

H. Design Spreadsheets

H.1 Design Methods

H.1.1 Effective Width Method (EWM)

H.1.1.1 Section Properties

This thesis used section properties formulae for C-channel column based on the AISI specifications. The notations used are denoted in Figure H.1.

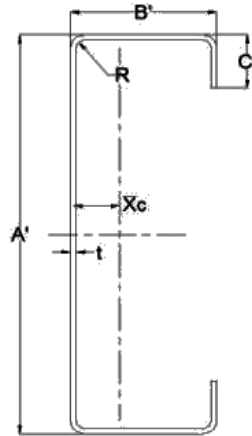


Figure H.1: Notations for C-channel Section

The following are formulae used to calculate the section properties of C-channel sections.

Radii at corner center to center

$$r = R + \frac{t}{2} \quad \text{Eq. H-1}$$

Clear width of web

$$a = A' - 2r + t \quad \text{Eq. H-2}$$

Clear width of flanges

$$b = B' - \left[t + \frac{t}{2} + \alpha \left(t + \frac{t}{2} \right) \right] \quad \text{Eq. H-3}$$

Clear width of lips

$$c = \alpha \left[C' - \left(t + \frac{t}{2} \right) \right] \quad \text{Eq. H-4}$$

Corner length centre to centre

$$u = \frac{\pi r}{2} \quad \text{Eq. H-5}$$

Cross sectional area

$$A_c = t \left[b + 2b + 2u + \alpha (c + 2u) \right] \quad \text{Eq. H-6}$$

Distance between centroid and web centreline

$$x_c = \frac{2t}{A} \left[b \left(\frac{b}{2} + r \right) + u (0.363r) + \alpha \left[c - 1.637r + c + 2r \right] \right] \quad \text{Eq. H-7}$$

Distance between centroid & outside of web

$$x_{ic} = x_c + \frac{t}{2} \quad \text{Eq. H-8}$$

Second Moment of Inertia for C-channel

$$I_{xc} = 2t \left\{ \begin{array}{l} 0.0417a^3 + b \left(\frac{b}{2} + r \right)^2 + u \left(\frac{b}{2} + 0.637r \right)^2 + 0.149r^3 + \\ \alpha \left[0.0833c^3 + \frac{c}{4} (c - c)^2 + u \left(\frac{a}{2} + 0.637r \right)^2 + 0.149r^3 \right] \end{array} \right\} \quad \text{Eq. H-9}$$

$$I_{yc} = 2t \left\{ \begin{array}{l} b \left(\frac{b}{2} + r \right)^2 + \frac{b^3}{12} + 0.356r^3 + \\ \alpha \left[c + 2r \right]^2 + u \left(c + 1.637r \right)^2 + 0.149r^3 \end{array} \right\} - Ax_c^2 \quad \text{Eq. H-10}$$

Radius of gyration

$$r_{xc} = \sqrt{\frac{I_{xc}}{A_c}} \quad \text{Eq. H-11}$$

$$r_{yc} = \sqrt{\frac{I_{yc}}{A_c}} \quad \text{Eq. H-12}$$

$$r_o = \sqrt{r_{xc}^2 + r_{yc}^2} \quad \text{Eq. H-13}$$

Torsional Constant

$$J = \frac{t^3}{3} \left[b + 2b + 2u + \alpha (c + 2u) \right] \quad \text{Eq. H-14}$$

Warping Constant

$$C_w = 2 \times \frac{\bar{a}^2 \bar{b}^2 t}{12} \left[\frac{2\bar{a}^3 \bar{b} + 3\bar{a}^2 \bar{b}^2 + \alpha \left(48\bar{c}^4 + 112\bar{b} \bar{c}^3 + 8\bar{a} \bar{c}^3 + 48\bar{a} \bar{b} \bar{c}^2 \right)}{6\bar{a}^2 \bar{b} + c + \alpha 2\bar{c} - \alpha 24\bar{a} \bar{c}^2} \right] \quad \text{Eq. H-15}$$

H.1.1.2 Nominal Axial Strength, P_{n-EWM}

In the Effective Width Method (EWM), the nominal axial compressive strength, P_n , of C-channel column is the product of effective area, A_e and elastic buckling stress, F_n . The nominal axial strength is calculated as follows:

$$P_n = A_e F_n \quad \text{Eq. H-16}$$

According to clause C4 of the AISI Specification (2001), nominal axial buckling stress is calculated as follows:

Inelastic buckling

$$\text{For } \lambda_c \leq 1.5 \quad F_n = 0.658^{\lambda_c^2} F_y \quad \text{Eq. H-17}$$

Elastic buckling

$$\text{For } \lambda_c > 1.5 \quad F_n = \left(\frac{0.877}{\lambda_c^2} \right) F_y \quad \text{Eq. H-18}$$

where,

$$\lambda_c = \sqrt{\frac{F_y}{F_e}} \quad \text{Eq. H-19}$$

F_y = Yield stress of the section

F_e = minimum of Elastic Flexural, Torsional and Torsional-Flexural Buckling Stresses

From clause C4.1 of AISI Specification (2001), nominal elastic buckling stresses for yielding, flexural, flexural-torsional and torsional buckling are determined as follows:

Flexural Buckling

$$F_e = \frac{\pi^2 E}{(KL/r)^2} \quad \text{Eq. H-20}$$

Torsional Buckling

Singly Symmetric Sections

$$F_e = \frac{1}{2\beta} \left[\sigma_{ex} + \sigma_t \pm \sqrt{(\sigma_{ex} + \sigma_t)^2 - 4\beta\sigma_{ex}\sigma_t} \right] \quad \text{Eq. H-21}$$

Doubly Symmetric Sections

$$F_e = \frac{\sigma_t \sigma_{ex}}{\sigma_t + \sigma_{ex}} \quad \text{Eq. H-22}$$

The fundamental of the Effective Width Method takes the effective area into account because cold working process induces differential stress distribution along the cross section. The general formula to calculate A_e is effective width of elements multiplied by thickness of each element as shown below.

$$A_e = b_t t \quad \text{Eq. H-23}$$

$$b_t = b_{web} + 2b_{flange} + 2b_{lip} + 4b_{corner} \quad \text{Eq. H-24}$$

Corner length between flange/web and flange/lip is considered fully effective as it is the most cold-worked area throughout the manufacturing process. Hence, there is no reduction for the corner length. The effective corner width, b_{corner} equals to the centre-to-centre corner length, u as shown by equation 7-5 in Section H.1.1.1. For web, flange and lip element, a reduction factor, ρ is introduced, so that the effective width of element, b_e is the product of the reduction factor, ρ and the clear width of element. The effective width of a C-channel section is illustrated in Figure H.2

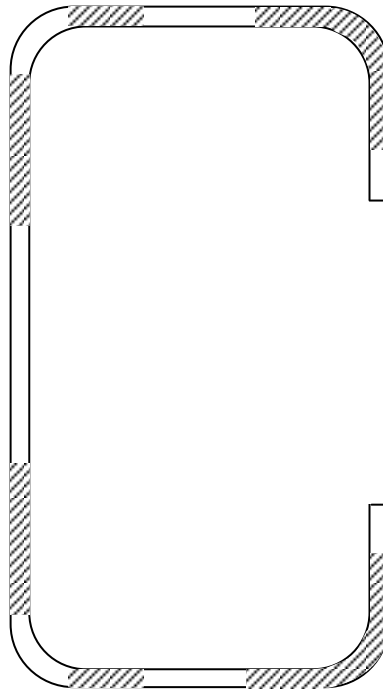


Figure H.2: Effective Width of C-channel Section

In terms of web element, the effective width of web, b_{web} is:

$$b_{web} = \rho a \quad \text{Eq. H-25}$$

where,

$$\text{For } \lambda \leq 0.673 \quad \rho = 1.0 \quad \text{Eq. H-26}$$

$$\text{For } \lambda > 0.673 \quad \rho = \frac{\left(1 - \frac{0.22}{\lambda}\right)}{\lambda} \quad \text{Eq. H-27}$$

where

$$\lambda = \sqrt{\frac{f}{F_{cr}}} \quad \text{Eq. H-28}$$

where

$$f = F_n \quad (\text{as determined by Eq. 7.17 or Eq. 7.18})$$

$$F_{cr} = \frac{k\pi^2 E}{12(1-\mu^2)} \left(\frac{t}{a}\right)^2 \quad (\text{Plate elastic buckling stress}) \quad \text{Eq. H-29}$$

For the critical elastic buckling stress, F_{cr} , the coefficient k and clear width varies for each element. The clear width of the elements is denoted as a for web, b for flange and c for lip. The coefficient k is taken as 4.0 for stiffened element i.e. web, whereas for unstiffened element i.e. lip, it is taken as 0.43. Determination of k is more complex for edge stiffened element i.e. flange. The plate buckling coefficient, k for flange is calculated as follows for C-channel columns with perpendicular flange/lip junction:

$$\text{For } C'/b \leq 0.25 \quad k = 3.57 \left(R_l\right)^n + 0.43 \leq 4 \quad \text{Eq. H-30}$$

$$\text{For } 0.25 < C'/b \leq 0.8 \quad k = \left(4.82 - \frac{5C'}{b}\right) \left(R_l\right)^n + 0.43 \leq 4 \quad \text{Eq. H-31}$$

The n and R_l value in the above equations is determined using the following equations:

$$n = \left[0.582 - \frac{b/t}{4S}\right] \geq \frac{1}{3} \quad \text{Eq. H-32}$$

where

$$S = 1.28 \sqrt{\frac{E}{f}} \quad \text{Eq. H-33}$$

where

$$S = \text{maximum } b_o/t \text{ ratio for a stiffened element to be fully effective}$$

f = Nominal buckling stress, F_n as determined by Eq. 7.17 or Eq. 7.18

$$R_I = \frac{I_x}{I_a} \leq 1 \quad \text{Eq. H-34}$$

where

$$I_a = 399t^4 \left[\frac{b}{S} - 0.328 \right]^3 \leq t^4 \left[115 \frac{b}{S} + 5 \right] \quad \text{Eq. H-35}$$

$$I_a = 0 \quad \text{for} \quad \frac{b}{t} \leq \frac{S}{3} \quad \text{Eq. H-36}$$

where

I_a = adequate moment of inertia of stiffener, so that each component element behaves as a stiffened element

b = clear width of flange

t = thickness of flange

S = as determined in Eq. 7-32

$$I_s = (c^3 t \sin^2 \theta) / 12 \quad \text{Eq. H-37}$$

where

I_s = Moment of inertia of full section of stiffener about its own centroidal axis parallel to element to be stiffened. For edge stiffeners, the round corner between stiffener and element to be stiffened shall not be considered as part of the stiffener

θ = angle between flange and lip

c = clear width of lip

For uniformly compressed unstiffened element i.e. lip, the reduced effective width of the stiffener is considered. Thus, the final effective width of the lip element, b_{lip} needs to be further reduced by reduction factor, R_I as determined previously. The final effective width of the lip element, b_{lip} is determined as:

$$\text{Final } b_{lip} = b_{lip} R_I \quad \text{Eq. H-38}$$

H.1.2 Direct Strength Method by Manual Calculation (DSM I)

H.1.2.1 Centre-to-centre Section Properties

Centre-to-centre dimensions are required for the calculation of the section properties for the Direct Strength Method by manual calculation. Notations used are as in Figure H.3. The equations used are listed on the following page.

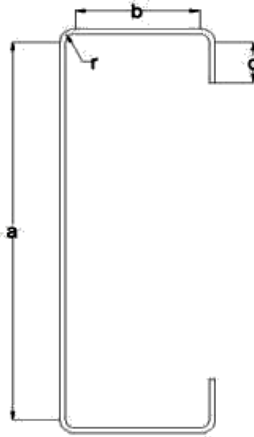


Figure H.3: Illustration for Plain Back-to-back C-channels Built-up Section Centre-to-centre Dimensions

Centre-to-centre width of web,

$$\bar{a} = A' - t \quad \text{Eq. H-39}$$

Centre-to-centre width of flanges,

$$\bar{b} = B' - \left[\frac{t}{2} + \frac{\alpha t}{2} \right] \quad \text{Eq. H-40}$$

Centre-to-centre width of lips,

$$\bar{c} = \alpha \left[t - \frac{t}{2} \right] \quad \text{Eq. H-41}$$

where, $\alpha = 1$ (For stiffened lipped section)

Cross-sectional area of flange

$$A_f = \bar{b} + \bar{c} \quad \text{Eq. H-42}$$

St. Venant torsion constant of the flange

$$J_f = \frac{1}{3\bar{b}t^3} + \frac{1}{3\bar{c}t^3} \quad \text{Eq. H-43}$$

Moment of inertia of flange

$$I_{xf} = \frac{t(t^2\bar{b}^2 + 4\bar{b}\bar{c}^3 - 4\bar{b}\bar{c}^3 \cos^2 \Phi) + t^2\bar{b}\bar{c} + \bar{c}^4 - \bar{c}^4 \cos^2 \Phi}{12(\bar{b} + \bar{c})} \quad \text{Eq. H-44}$$

$$I_{yf} = \frac{t(\bar{b}^4 + 4c\bar{b}^3 + 6\bar{c}^2\bar{b}^2 \cos^2 \Phi + 4\bar{c}^3\bar{b} \cos^2 \Phi + \bar{c}^4 \cos^2 \Phi)}{12(\bar{b} + \bar{c})} \quad \text{Eq. H-45}$$

Product of the moment of inertia of flange

$$I_{xyf} = \frac{t\bar{b}c^2 \sin \theta (\bar{b} + c \cos \theta)}{4(\bar{b} + c)}$$

Eq. H-46

Distance from flange/web junction to the centroid of the flange

$$x_0 = \frac{\bar{b}^2 - \bar{c}^2 \cos \phi}{2(\bar{b} + \bar{c})} \quad \text{Eq. H-47}$$

Distance from centroid of flange to shear centre of flange

$$h_x = \frac{-\left(\bar{b}^2 + 2\bar{c}\bar{b} + \bar{c}^2 \cos \phi\right)}{2(\bar{b} + \bar{c})} \quad \text{Eq. H-48}$$

$$h_y = y_0 = \frac{-\bar{c} \sin \phi}{2(\bar{b} + \bar{c})} \quad \text{Eq. H-49}$$

$$x_0 - h_x = \bar{b} \quad \text{Eq. H-50}$$

Warping constant of flange

$$C_{wf} = 0 \quad \text{Eq. H-51}$$

Warping Constant

$$C_w = 2 \times \frac{\bar{a}^2 \bar{b}^2 t}{12} \left[\frac{2\bar{a}^3 \bar{b} + 3\bar{a}^2 \bar{b}^2 + \alpha \left(\begin{array}{l} 48\bar{c}^4 + 112\bar{b}\bar{c}^3 + 8\bar{a}\bar{c}^3 + 48\bar{a}\bar{b}\bar{c}^2 \\ + 12\bar{a}^2 \bar{c}^2 + 12\bar{a}^2 \bar{b}\bar{c} + 6\bar{a}^3 \bar{c} \end{array} \right)}{6\bar{a}^2 \bar{b} + \bar{c} + \alpha 2\bar{c} - \alpha 24\bar{a}\bar{c}^2} \right] \quad \text{Eq. H-52}$$

Critical Length

Compression:

$$L_{cr} = \left\{ \frac{6\pi^4 \bar{a} (1 - \nu^2)}{t^3} \left[I_{xf} (x_0 - h_x) + C_{wf} - \frac{I_{xyf}^2}{I_{yf}} (x_0 - h_x) \right] \right\}^{1/4} \quad \text{Eq. H-53}$$

Bending:

$$L_{cr} = \left\{ \frac{4\pi^4 \bar{a} (1 - \nu^2)}{t^3} \left[I_{xf} (x_{0f} - h_{xf}) + C_{wf} - \frac{I_{xyf}^2}{I_{yf}} (x_{0f} - h_{xf}) + \frac{\pi^4 \bar{a}^4}{720} \right] \right\}^{1/4} \quad \text{Eq. H-54}$$

H.1.2.2 Nominal Axial Strength, P_{n-DSM1}

Nominal axial strength for column is the minimum nominal axial strength for local, distortional and global buckling. Thus, by hand calculation, P_n is:

$$P_n = \min (P_{nl}, P_{nd}, P_{ne}) \quad \text{Eq. H-55}$$

Global Buckling:

$$\lambda_c \leq 1.5 \quad P_{ne} = 0.658 \lambda_c^2 P_y \quad \text{Eq. H-56}$$

$$\lambda_c > 1.5 \quad P_{ne} = \left(\frac{0.877}{\lambda_c} \right)^2 P_y \quad \text{Eq. H-57}$$

Local Buckling:

$$\lambda_\ell \leq 0.776 \quad P_{nl} = P_{ne} \quad \text{Eq. H-58}$$

$$\lambda_\ell > 0.776 \quad P_{nl} = \left[1 - 0.15 \left(\frac{P_{crl}}{P_{ne}} \right)^{0.4} \right] \left(\frac{P_{crl}}{P_{ne}} \right)^{0.4} P_{ne} \quad \text{Eq. H-59}$$

Distortional:

$$\lambda_d \leq 0.561 \quad P_{nd} = P_y \quad \text{Eq. H-60}$$

$$\lambda_d > 0.561 \quad P_{nd} = \left[1 - 0.25 \left(\frac{P_{crd}}{P_y} \right)^{0.6} \right] \left(\frac{P_{crd}}{P_y} \right)^{0.6} P_y \quad \text{Eq. H-61}$$

The critical local buckling stress, f_{crl} is the minimum elastic local buckling stress for web, flange and lip. Thus, critical local buckling load, P_{crl} is obtained by product of the critical local buckling stress, f_{crl} and the gross area of the section, A_g .

$$\text{Local buckling load,} \quad P_{crl} = f_{crl} A_g \quad \text{Eq. H-62}$$

where

Critical elastic local buckling stress, $f_{crl} = \min \{ f_{crl,web}, f_{crl,flange}, f_{crl,lip} \}$

$$f_{crl,web} = k \frac{\pi^2 E}{12(1-\nu^2)} \left(\frac{t}{a} \right)^2 \quad \text{Eq. H-63}$$

$$f_{crl,flange} = k \frac{\pi^2 E}{12(1-\nu^2)} \left(\frac{t}{b} \right)^2 \quad \text{Eq. H-64}$$

$$f_{crl,lip} = k \frac{\pi^2 E}{12(1-\nu^2)} \left(\frac{t}{c} \right)^2 \quad \text{Eq. H-65}$$

where

k = Plate buckling coefficient. Determined using either elemental approach or semi empirical approach. For DSM, ignoring the interaction between web/flanges and lips/flanges may be too conservative for predicting the local buckling stress, thus, semi empirical approach is recommended (AISI 2004a).

$\nu =$ Poisson's ratio (Taken as 0.3 for steel)

For Elemental Approach, the plate buckling coefficients are:

$$k_{web} = 4$$

$$k_{lip} = 0.43$$

$$k_{flange} = 4$$

For Semi-empirical Approach, the plate buckling coefficients are:

$$\text{For } \frac{\bar{a}}{\bar{b}} \geq 1, \quad k_{flange/web} = 4 \left(\frac{\bar{b}}{\bar{a}} \right)^2 \left[2 - \left(\frac{\bar{b}}{\bar{a}} \right)^{0.4} \right] \quad \text{Eq. H-66}$$

$$\text{For } \frac{\bar{a}}{\bar{b}} < 1, \quad k_{flange/web} = 4 \left[2 - \left(\frac{\bar{a}}{\bar{b}} \right)^{0.2} \right] \quad \text{Eq. H-67}$$

$$\left(\frac{\bar{c}}{\bar{b}} \right) < 0.6 \quad k_{flange/lip} = -11.07 \left(\frac{\bar{c}}{\bar{b}} \right)^2 + 3.95 \left(\frac{\bar{c}}{\bar{b}} \right) + 4 \quad \text{Eq. H-68}$$

The critical distortional buckling stress is obtained from the product of the critical local buckling stress and the gross area of the section.

$$P_{crd} = A_g \times f_{crd} \quad \text{Eq. H-69}$$

According to Schafer (2002, 289-299), distortional buckling stress mainly deals with the rotational stiffness at the corner of the flange and web and is expressed as summation of elastic stiffness $(k_{\phi e} + k_{\phi v})$ and stress dependent geometric stiffness $(k_{\phi g} + k_{\phi w})$ with contribution from both web and flange.

$$k_{\phi} = (k_{\phi e} + k_{\phi v}) - (k_{\phi g} + k_{\phi w})$$

Buckling occurs when the elastic stiffness is countered by the geometric stiffness (i.e. $k_{\phi} = 0$). Mathematically, k_{ϕ} is:

$$k_{\phi} = (k_{\phi e} + k_{\phi v}) - f (k_{\phi g} + k_{\phi w}) = 0$$

Thus, if the stress dependent portion which is the geometric stiffness is linearised and is expressing the stress (f_{crd}) explicitly, the distortional buckling stress is expressed as:

$$f_{crd} = \frac{k_{\phi e} + k_{\phi v}}{k_{\phi g} + k_{\phi w}} \quad \text{Eq. H-70}$$

Flange rotational stiffness

$$k_{\phi fe} = \left(\frac{\pi}{L_{cr}} \right)^4 \left[EI_{xf} \left(\frac{h_x}{2} \right)^2 + EC_{wf} - E \frac{I_{xyf}^2}{I_{yf}} \left(\frac{h_x}{2} \right)^2 \right] + \left(\frac{\pi}{L_{cr}} \right)^2 GJ_f \quad \text{Eq. H-71}$$

$$\bar{k}_{\phi fg} = \left(\frac{\pi}{L} \right)^2 \left\{ A_f \left[\left(\frac{h_x}{2} \right)^2 \left(\frac{I_{xyf}}{I_{yf}} \right)^2 - 2y_0 \left(\frac{h_x}{2} \right) \left(\frac{I_{xyf}}{I_{yf}} \right) + h_x^2 + y_0^2 \right] + I_{xf} + I_{yf} \right\} \quad \text{Eq. H-72}$$

Web rotational stiffness

$$k_{\phi we} = \frac{Et^3}{6A'(1-\nu^2)} \quad \text{Eq. H-73}$$

$$\bar{k}_{\phi wfg} = \left(\frac{\pi}{L_{cr}} \right)^2 \frac{tA'^3}{60} \quad \text{Eq. H-74}$$

Critical elastic global buckling load, P_{cre} is determined as the product of elastic global buckling stress, f_{cre} and the gross cross sectional area, A_g .

$$P_{cre} = A_g \times f_{cre} \quad \text{Eq. H-75}$$

Elastic global buckling stress used for direct strength method is computed as the minimum elastic buckling stress determined from clause C4.1 – C4.4 according to the AISI specifications (AISI 2002c, 97-98). The elastic flexural buckling stress is determined as:

$$f_{cre} = \min \left(f_{cre1}, f_{cre2} \right) \quad \text{Eq. H-76}$$

$$f_{cre1} = \frac{\pi^2 E}{(KL/r)^2} \quad (\text{As per Eq. 7-20})$$

$$f_{cre2} = \frac{1}{2\beta} \left[\left(\sigma_{ex} + \sigma_t \right) + \sqrt{\left(\sigma_{ex} + \sigma_t \right)^2 - 4\beta\sigma_{ex}\sigma_t} \right]$$

H.1.3 Direct Strength Method by CUFSM (DSM II)

H.1.3.1 Finite Strip Analysis Software – CUFSM

The DSM II uses finite strip software – Cornell University Finite Strip Method (CUFSM) to assist in the determination of the elastic buckling strength. The CUFSM is an open source software for elastic buckling determination of cold formed steel members. It was established by Schafer (2008, 766-778) based on finite strip analysis. The CUFSM provides elastic buckling solutions with minimum time and effort. It is a powerful tool compared to manual calculations which use plate buckling solutions and plate buckling coefficients that only partially account for the stability behaviour of

cold-formed steel members. In this research, the CUFSM version 4 is used. The main step in the CUFSM is to define the model according to the actual properties and cross section.

The CUFSM provides two results for elastic buckling analysis in terms of (i) buckling load ratio and (ii) buckling behaviour as shown in Figure H.4. The CUFSM curve shows the half-wavelength on x-axis and the corresponding load ratio on the y-axis. The minima on the curve are identified as the buckling mode. The first minima indicate local buckling load ratio, the second minima represent distortional buckling load ratio, and the global buckling load ratio is indicated at the physical length of the column.

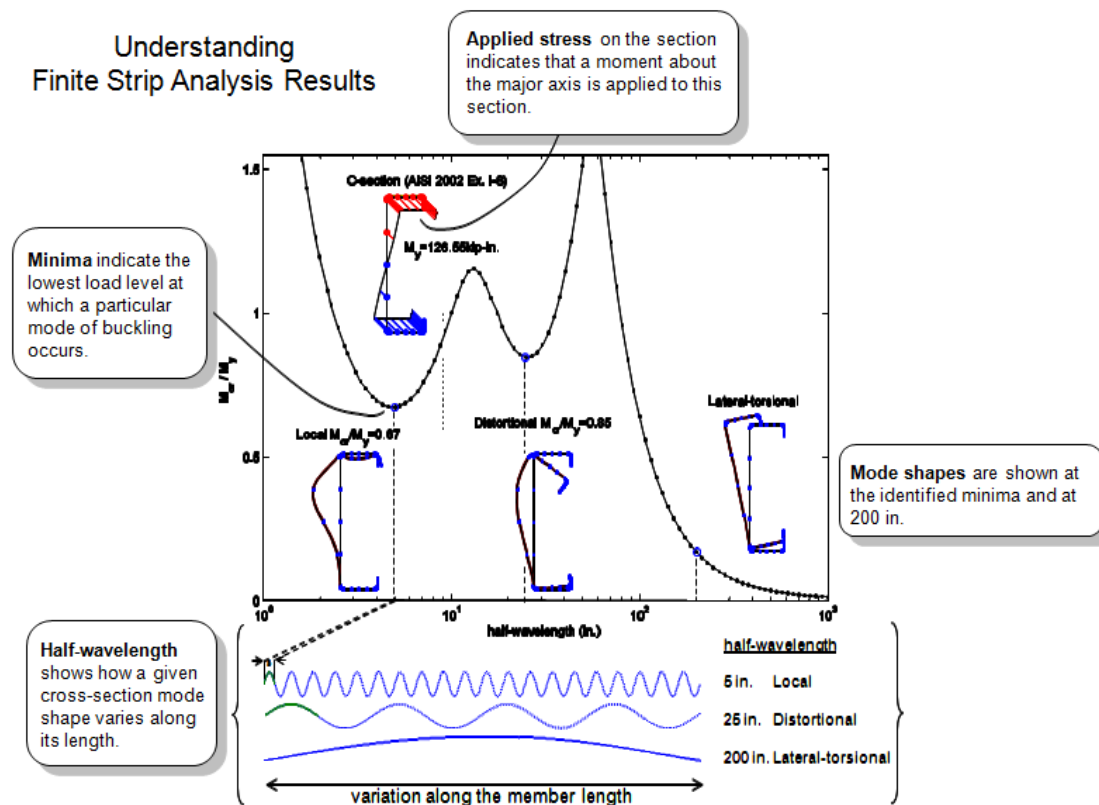


Figure H.4: Interpretation of CUFSM Results (Schafer 2006)

The CUFSM is able to display the buckled shape according to the selected point on the curve. The finite strip method assumes the member buckles as a single half sine wave along the length (AISI 2006, 11). The length of this half sine wave is known as the half-wavelength. Local buckling usually occurs at a half-wavelength at or near the outer dimensions of the member. Distortional buckling occurs between three to nine times the outer dimensions of the cross-section. At longer half-wavelength, global buckling occurs. Global buckling is not easily identifiable from the curve because it is possible to

be any point after the point where distortional buckling occurs. However, it is usually best examined by taking the physical length of the member (AISI 2006, 11).

H.1.3.2 Nominal Axial Strength, P_{n-DSMI}

Nominal axial strength, P_n is the minimum of global buckling strength, P_{ne} , local buckling strength, P_{nl} and distortional buckling strength, P_{nd} . The load ratios are determined from the CUFSM curve with local (P_{crl}/P_y) from the first minima, distortional (P_{crd}/P_y) from the second minima and global (P_{cre}/P_y) from load ratio at the member's length. The load ratios are then used to determine nominal axial strength, P_n in accordance with the Direct Strength Method as shown in section H.1.2.2.

H.1.4 Beam-column Design

Singly symmetric columns like C-channel columns experience a shift of effective centroid under axial load. The shift causes an additional moment to the column, thus, the strength of the column is better estimated as a beam-column rather than a column. The AISI Specification clause C4.1(b) suggests an additional bending moment as specified in clause C5.2 to be included when designing concentrically loaded angle columns (AISI 2007). These columns need to satisfy the beam-column interaction equation as stated in clause C5.2 of the AISI Specification. Therefore, in this research, the design of C-channel columns for both the Effective Width Method (EWM) and Direct Strength Method (DSM) uses the beam-column equation from the AISI Specification. The beam-column equation taken from Equation C5.2.2-1 of AISI Specification is as shown below:

$$\frac{P_u}{\phi_c P_n} + \frac{C_{mx} M_{ux}}{\phi_b M_{nx} \alpha_x} + \frac{C_{my} M_{uy}}{\phi_b M_{ny} \alpha_y} \leq 1.0$$

where

P_u = Required compressive axial strength

P_n = Nominal axial strength determined in accordance with clause C4 of AISI Specification

M_{ux} , M_{uy} = Required flexural strengths with respect to centroidal axes of effective section determined for required compressive axial strength alone

M_{nx}, M_{ny} = Nominal flexural strengths about centroidal axes determined in accordance with clause C3.1 of the AISI Specification

ϕ_b, ϕ_c = Reduction factors

$$\alpha_x, \alpha_y = 1 - \frac{P_u}{P_{Ex}} > 0, 1 - \frac{P_u}{P_{Ey}} > 0$$

Moment induced by the shift of effective centroid occurs only in the minor axis i.e. the y-axis. Thus, the moment part of the beam-column equation in x-axis is disregarded. For comparison with the experimental results, unfactored design strength was used in the calculation. Therefore, the reduction factors ϕ_b and ϕ_c are taken as 1.0. The interaction equation is then rewritten as follows:

$$\frac{P_u}{P_n} + \frac{C_{my} P_u e_s}{M_{ny} \left(1 - \frac{P_u}{P_{Ey}} \right)} \leq 1.0 \quad \text{Eq. H-77}$$

where

P_u = Required compressive axial strength

P_n = Nominal axial strength determined in accordance with clause C4 of the AISI Specification

C_{my} = Moment gradient factor

e_s = Shift of centroid with respect to centroidal axes of effective section determined at stress level F_n

M_{ny} = Nominal flexural strengths about centroidal axes determined in accordance with clause C3.1 of the AISI Specification

$$P_{Ey} = \frac{\pi^2 EI_y}{L_y^2}$$

Nominal axial strength, P_n is calculated using the procedures documented in this thesis in Section H.1.1.2 for Effective Width Method, Section H.1.2.2 for Direct Strength Method by manual calculation, and Section H.1.3.2 for Direct Strength Method by CUFSM. Moment gradient factor, C_{my} is taken as 1.0 since the C-channel columns are unrestrained at their ends. The shift, e_s is determined as the distance between the

centroid of the unreduced cross-section to the centroid of the effective cross section. As for nominal flexural strength, M_{ny} , it is determined in this thesis in accordance with Section H.1.4.1 for Effective Width Method, Section H.1.4.2 for Direct Strength Method by manual calculation and Section H.1.4.3 for Direct Strength Method by CUFSM.

H.1.4.1 EWM for Beam-column Design

Nominal flexural strength, M_{ny} is determined based on Clause C3.1.1 and Clause C3.1.2 of the AISI Specification (2007). From Clause C3.1.1, the nominal section strength is determined based on initiation of yielding, whereas from Clause C3.1.2, the lateral-torsional buckling strength is determined for open cross-section members.

Yielding

$$M_{ny} = S_e F_y \quad \text{Eq. H-78}$$

Lateral-torsional Buckling

$$M_{ny} = S_c F_c \quad \text{Eq. H-79}$$

where

S_c = Elastic section modulus of effective section calculated relative to extreme compression fiber at F_c .

F_c = Depending on F_e conditioned as follows:

$$\text{Condition 1: } F_e \geq 2.78 F_y \quad M_{ny} = S_e F_y$$

$$\text{Condition 2: } 2.78 F_y > F_e > 0.56 F_y \quad F_c = \frac{10}{9} F_y \left(1 - \frac{10 F_y}{36 F_e} \right)$$

$$\text{Condition 3: } F_e \leq 0.56 F_y \quad F_c = F_e$$

The determination of S_c requires the failure mode of the tested specimens to determine the element in compression. For C-channel column failing in minor axis in the direction of the web, the web is subjected to tension while the lip is subjected to compression. On the other hand, when the C-channel column fails in the direction of the lip, the web is subjected to compression while the lip is subjected to tension.

For Condition 1 with $F_e \geq 2.78F_y$, the members are not subjected to lateral-torsional buckling at bending moments less than or equal to M_y . The flexural strength is determined in accordance with the initiation of yielding. Condition 2 with $2.78F_y > F_e > 0.56F_y$, F_c is determined as follows:

$$F_c = \frac{10}{9} F_y \left(1 - \frac{10F_y}{36F_e} \right) \quad \text{Eq. H-80}$$

For Condition 3, with $F_e \leq 0.56F_y$, F_c is determined as the elastic critical lateral-torsional buckling stress, F_e . For singly symmetric section bending about the centroidal axis perpendicular to the axis of symmetry, F_e is determined as:

$$F_e = \frac{C_s A \sigma_{ex}}{C_{TF} S_f} \left[j + C_s \sqrt{j^2 + r_o^2 \left(\frac{\sigma_t}{\sigma_{ex}} \right)} \right] \quad \text{Eq. H-81}$$

where

$$C_s = \begin{cases} +1 & \text{(compression at web)} \\ -1 & \text{(tension at web)} \end{cases}$$

$$\sigma_{ex} = \frac{\pi^2 E}{\left(\frac{L_x}{r_x} \right)^2} \quad \text{Eq. H-82}$$

$$j = \frac{1}{2I_y} \left[\int_A x^3 dA + \int_A xy^2 dA \right] - x_o \quad \text{Eq. H-83}$$

In determining C_s , the failure mode of the tested specimen is required. As mentioned previously in the determination of S_c , for C-channel column failing in minor axis in the direction of the web, the web is subjected to tension while the lip is subjected to compression. On the other hand, when the C-channel column fails in the direction of the lip, the web is subjected to compression while the lip is subjected to tension.

H.1.4.2 DSM I for Beam-column Design

Nominal flexural strength, M_{ny} is determined based on clause C1.2.2 of the Direct Strength Method (2004) as the minimum of global buckling nominal flexural strength, M_{ne} , local buckling nominal flexural strength M_{nl} , and distortional buckling nominal flexural strength M_{nd} .

In terms of global buckling, there are three conditions with:

- (a) member not subjected to lateral-torsional buckling,

$$M_{cre} \geq 2.78M_y, \quad M_{ne} = M_y$$

- (b) member subjected to lateral-torsional buckling, and

$$M_{cre} \leq 0.56M_y, \quad M_{ne} = M_{cre}$$

- (c) member in between the aforementioned,

$$2.78M_y > M_{cre} > 0.56M_y, \quad M_{ne} = \frac{10}{9}M_y \left(1 - \frac{10M_y}{36M_{cre}} \right)$$

The member is not subjected to lateral-torsional buckling when M_{cre} is greater than $2.78M_y$. The flexural strength is therefore determined in accordance with the initiation of yielding. The effective section modulus at yield in the main specification is equivalent to the bending strength for a fully braced member. The nominal strength of a fully braced member in the Direct Strength Method is obtained by setting the global buckling strength to its full nominal strength, i.e. $M_{ne} = M_y$ (DSM Section 1.2.2.1), and then proceeding normally through the Direct Strength Method expressions. Global buckling strength is at full nominal strength, i.e. $M_{ne} = M_y$, because lateral-torsional buckling does not occur in a fully braced member.

For M_{cre} in between $2.78M_y$ and $0.56M_y$, M_{ne} is determined as:

$$M_{ne} = \frac{10}{9}M_y \left(1 - \frac{10M_y}{36M_{cre}} \right) \quad \text{Eq. H-84}$$

For M_{cre} less than $0.56M_y$, M_{ne} is determined as the elastic critical lateral-torsional buckling stress, M_{cre} . For singly symmetric section bending about the centroidal axis perpendicular to the axis of symmetry, M_{ne} is determined as:

$$M_{ne} = M_{cre} \quad \text{Eq. H-85}$$

In terms of local buckling, when λ_l is less than or equal to 0.776, local-global interaction occurs. Thus, the local buckling strength of a member is limited to a

maximum of the lateral-torsional buckling strength ($M_{nl} = M_{ne}$). For λ_l greater than 0.776, the local buckling strength is calculated as follows:

$$\lambda_l = \sqrt{\frac{M_{ne}}{M_{crl}}} \quad \text{Eq. H-86}$$

$$M_{nl} = \left(1 - 0.15 \left(\frac{M_{crl}}{M_{ne}}\right)^{0.4}\right) \left(\frac{M_{crl}}{M_{ne}}\right)^{0.4} M_{ne} \quad \text{Eq. H-87}$$

In terms of distortional buckling, when λ_d is less than or equal to 0.673, the distortional buckling strength of the member is limited to the yield moment, M_y , instead of the lateral-torsional buckling strength, M_{ne} ($M_{nd} = M_y$). This is because this design method presumes that distortional buckling failures are independent of lateral-torsional buckling behaviour. For λ_d greater than 0.673, the distortional buckling strength is calculated as follows:

$$\lambda_d = \sqrt{\frac{M_y}{M_{crd}}} \quad \text{Eq. H-88}$$

$$M_{nd} = \left(1 - 0.22 \left(\frac{M_{crd}}{M_y}\right)^{0.5}\right) \left(\frac{M_{crd}}{M_y}\right)^{0.5} M_y \quad \text{Eq. H-89}$$

The critical buckling flexural strength for local (M_{crl}), distortional (M_{crd}) and global (M_{cre}) buckling needs to be manually determined in the DSM I.

For local buckling, M_{crl} , is determined for web, flange and lip element as:

$$M_{crl} = S_g f_{crl} \quad \text{Eq. H-90}$$

where,

Gross section modulus to the extreme compression fiber, $S_g = \frac{I_x}{\left(\frac{A'}{2}\right)}$

Local buckling stress at the extreme compression fiber, $f_{crl} = k \frac{\pi^2 E}{12 \left(1 - \nu^2\right) \left(\frac{t}{a}\right)^2}$

The critical local buckling stress, f_{crl} , is as per determined in section H.1.2.2, but the coefficient k for flexural member is used instead. For Elemental Approach, the plate

buckling coefficients are determined from Table C-B2-1 of the commentary for the Direct Strength Method:

$$k_{web} = 23.9$$

$$k_{lip} = 0.43$$

$$k_{flange} = 4$$

For Semi-empirical approach, the plate buckling coefficients are:

$$k_{flange/web} = 1.125 \cdot \min \left[4 \left(0.5 \xi^3 + 4 \xi^2 + 4 \left(\frac{\bar{b}}{a} \right)^2 \right) \right] \quad \text{Eq. H-91}$$

$$k_{flange/lip} = 0.55 \xi - 11.07 \left(\frac{\bar{c}}{\bar{b}} \right)^2 + 0.95 - 1.59 \xi \left(\frac{\bar{c}}{\bar{b}} \right) + 4 \quad \text{Eq. H-92}$$

where,

$$\left(\frac{\bar{c}}{\bar{b}} \right) \leq 0.6 \quad \text{and} \quad \xi < 1.0.$$

For distortional buckling, M_{crd} , is determined as:

$$M_{crd} = S_g f_{crd} \quad \text{Eq. H-93}$$

In this case, the critical length, L_{cr} for bending is different from the critical length, L_{cr} for compression as shown in section H.1.2.1. As detailed in section H.1.2.2, the distortional buckling stress is expressed as:

$$f_{crd} = \frac{k_{\phi_{fe}} + k_{\phi_{we}}}{k_{\phi_{fg}} + k_{\phi_{wg}}}$$

Flange rotational stiffness

$$k_{\phi_{fe}} = \left(\frac{\pi}{L_{cr}} \right)^4 \left[EI_{xf} \left(\bar{c}_0 - h_x \right)^2 + EC_{wf} - E \frac{I_{xyf}^2}{I_{yf}} \left(\bar{c}_0 - h_x \right)^2 \right] + \left(\frac{\pi}{L_{cr}} \right)^2 GJ_f$$

$$\bar{k}_{\phi_{fg}} = \left(\frac{\pi}{L} \right)^2 \left\{ A_f \left[\left(\bar{c}_0 - h_x \right)^2 \left(\frac{I_{xyf}}{I_{yf}} \right)^2 - 2y_0 \left(\bar{c}_0 - h_x \right) \left(\frac{I_{xyf}}{I_{yf}} \right) + h_x^2 + y_0^2 \right] + I_{xf} + I_{yf} \right\}$$

Web rotational stiffness

$$k_{\phi_{we}} = \frac{Et^3}{12(1-\nu^2)} \left[\frac{3}{\bar{a}} + \left(\frac{\pi}{L_{cr}} \right)^2 \times \frac{19\bar{a}}{60} + \left(\frac{\pi}{L_{cr}} \right)^4 \times \frac{\bar{a}^3}{240} \right] \quad \text{Eq. H-94}$$

$$\bar{k}_{\phi wg} = \frac{\bar{a} t \pi^2}{13440} \times \frac{5360 \psi + 62160 \left(\frac{L_{cr}}{\bar{a}} \right)^2 + 448 \pi^2 + \left(\frac{\bar{a}}{L_{cr}} \right)^2 (3 + 3 \psi \pi^4)}{\pi^4 + 28 \pi^2 \left(\frac{L_{cr}}{\bar{a}} \right)^2 + 420 \left(\frac{L_{cr}}{\bar{a}} \right)^4} \quad \text{Eq. H-95}$$

For global buckling, M_{cre} , is determined as:

$$M_{cre} = S_g f_{cre} \quad \text{Eq. H-96}$$

Elastic global buckling stress used for direct strength method is computed for the least elastic buckling stress determined from section C4.1-C4.4 according to the AISI specifications (AISI 2002c, 97-98). The elastic flexural buckling stress is determined as:

$$f_{cre} = \min \{ f_{cre1}, f_{cre2} \}$$

$$f_{cre1} = \frac{\pi^2 E}{(KL/r)^2} \quad (\text{As Eq. 7-20})$$

$$f_{cre2} = \frac{C_b r_o A}{S_g} \sqrt{\sigma_{ey} \sigma_t} \quad \text{Eq. H-97}$$

H.1.4.3 DSM II for Beam-column Design

Nominal flexural strength, M_{ny} is determined as the minimum of global buckling strength, M_{ne} , local buckling strength, M_{nl} , and distortional buckling strength, M_{nd} in accordance with the Direct Strength Method expressions as shown in section H.1.4.2. The load ratio for local $\{M_{cr1}/M_y\}$, distortional $\{M_{crd}/M_y\}$ and global buckling $\{M_{cre}/M_y\}$ is determined from the CUFSM curve. The load ratios are then used to determine nominal flexural strength, M_{ny} . In the finite strip method using the CUFSM, members are loaded with a reference stress distribution generated from pure bending for finding M_{cr} . The determination of load ratio for local $\{M_{cr1}/M_y\}$, distortional $\{M_{crd}/M_y\}$ and global buckling $\{M_{cre}/M_y\}$ is the same as the determination for compression member in section H.1.3.2. The load ratios are determined with local $\{M_{cr1}/M_y\}$ from the first minima, distortional $\{M_{crd}/M_y\}$ from the second minima and global $\{M_{cre}/M_y\}$ from load ratio at the member's length.

H.2 C-channel Column Spreadsheets

H.2.1 Effective Width Method (EWM)

LIPPED C-CHANNEL	Specimen : C75L500-1
	Date : 22.02.2013
C75L500-1 = 24.99 kN	Analysed by : Tina

(Load ratio from CUFSM for DSM II)

$P_{ce}/P_y =$

$P_{ce}/P_y =$

$P_{ce}/P_y =$

(Take flexural-torsional buckling into account)

Torsion = (Y for 'YES', N for 'NO')

Buckle = (Buckle towards the web, "web", Buckle away from the web i.e. towards the lip, "lip")

1. Geometry

A'	=	<input type="text" value="76.85"/>	mm
B'	=	<input type="text" value="19.46"/>	mm
C'	=	<input type="text" value="10.6"/>	mm
t	=	<input type="text" value="1.2"/>	mm
R	=	<input type="text" value="1.5"/>	mm
w	=	<input type="text" value="0"/>	mm
L	=	<input type="text" value="678"/>	mm

K_x	=	<input type="text" value="0.50"/>	($L_x = K_x L$)
K_y	=	<input type="text" value="1.00"/>	($L_y = K_y L$)
K_t	=	<input type="text" value="1.00"/>	($L_t = K_t L$)

2. Material's Properties

θ	=	<input type="text" value="1.57"/>	rad
ν	=	<input type="text" value="0.30"/>	
G	=	<input type="text" value="79630.77"/>	MPa
F_y	=	<input type="text" value="560"/>	MPa
E	=	<input type="text" value="207040"/>	MPa

(A) SECTION PROPERTIES

3. Dimensional Limits & Considerations (Section B1)

A'/t	=	<input type="text" value="64.04"/>	≤	<input type="text" value="260"/>	Web OK!	$K_y L_y / r_y$	=	<input type="text" value="94.22"/>	Intermediate
B'/t	=	<input type="text" value="16.22"/>	≤	<input type="text" value="60"/>	Flange OK!	$20r_y$	=	<input type="text" value="143.92"/>	$L > 20r_y$ (7.1.1), Not Stub
C'/b	=	<input type="text" value="0.75"/>	≤	<input type="text" value="0.8"/>	Lip OK!	$3A'$	=	<input type="text" value="230.55"/>	$L \geq 3A'$ (7.1.2), Stub

4. Gross Section Properties

α	=	<input type="text" value="1"/>		r	=	<input type="text" value="2.10"/>	mm
a	=	<input type="text" value="71.45"/>	mm	a_{bar}	=	<input type="text" value="75.65"/>	mm
b	=	<input type="text" value="14.06"/>	mm	b_{bar}	=	<input type="text" value="18.26"/>	mm
c	=	<input type="text" value="7.90"/>	mm	c_{bar}	=	<input type="text" value="10.00"/>	mm
u	=	<input type="text" value="3.30"/>	mm				
x_c	=	<input type="text" value="5.18"/>	mm	x_{1c}	=	<input type="text" value="5.78"/>	mm
I_{xc}	=	<input type="text" value="125781.64"/>	mm ⁴	I_{1c}	=	<input type="text" value="7989.10"/>	mm ⁴
r_{xc}	=	<input type="text" value="28.55"/>	mm	r_{1c}	=	<input type="text" value="7.20"/>	mm
m	=	<input type="text" value="8.972"/>	mm				
x_o	=	<input type="text" value="-14.15"/>	mm	r_{oc}	=	<input type="text" value="32.67"/>	mm
J_c	=	<input type="text" value="74.05"/>	mm ⁴	C_{wc}	=	<input type="text" value="11080319.88"/>	mm ⁶
b	=	<input type="text" value="0.812"/>					
A_c	=	<input type="text" value="154.28"/>	mm ²				

(B) DETERMINE MEMBER AXIAL CAPACITY (P_n) (Section C4)

5. Buckling Stresses (same as DSM Euler)

5.1 Flexural Buckling about Weak Axis (Section C4.1)

<u>x-axis flexural buckling</u>		<u>y-axis flexural buckling</u>	
$K_x L / r_{yc}$	= 11.87	$K_y L / r_{yc}$	= 94.22
F_{ex}	= 14496.69 MPa	F_{ey}	= 230.19 MPa
F_{e1}	= 230.19 MPa	<i>(Euler buckling about y-axis controls.)</i>	

5.2 Singly Symmetric Sections subjected to Flexural-torsional Buckling (Section C4.2)

σ_{ex}	= 14496.69 MPa
σ_t	= 1232.31 MPa
β	= 0.81
F_{e2}	= 1211.58 MPa

$F_{e2} = 1/2\beta [(\sigma_{ex} + \sigma_t) - \sqrt{(\sigma_{ex} + \sigma_t)^2 - 4\beta\sigma_{ex}\sigma_t}]$

5.3 Determine controlling buckling mode

Note: $F_{e1} < F_{e2}$, Flexural buckling governs.

F_e	= 230.19 MPa	Torsion considered, take minimum of FE1 & FE2.
λ_c	= 1.560	(> 1.5, $F_{ne} = (0.877/\lambda_c^2)F_y$)
F_{ne}	= 201.88 MPa	

6. Compute effective area of Single C at F_{ne}

6.1 Web (Section B2.1)

k_{web}	= 4.00	
$(f_{cr})_{web}$	= 211.13 MPa	
λ_w	= 0.98	(> 0.673, Local Buckling, web not fully effective.)
ρ	= 0.793	
b_w	= 56.63 mm	

6.2 Flange (Section B4.2)

Check flange as a uniformly compressed element with an edge stiffener.

b/t	= 11.72	
S	= 40.99	$S = 1.28 \sqrt{E/F_{ne}}$
$0.328S$	= 13.45	($b/t < 0.3283$, Edge stiffener required.)
		($b/t \leq 0.3283$, Edge stiffener required.)
l_b	= 0.0000	
l_s	= 49.30	$l_s = (c^3 t \sin^2 \theta) / 12$
R_f	= 1.00	$R_f = l_w / l_b \leq 1$ (Note: If $l_b = 0$, $R_f = 1$ because no edge stiffener required)
n	= 0.51	$n = 0.582 - [(b/t)/4S] \geq 1/3$

$0.25 < C'/b \leq 0.8$, $k = (4.82 - 5C'/b)(R_f)^n + 0.43 \leq 4$

k_{flange}	= 1.48	
$(f_{cr})_{flange}$	= 2017.97 MPa	
λ_f	= 0.316	(≤ 0.673 , No Local Buckling, flange fully effective.)
ρ	= 1.000	
b_f	= 14.06 mm	

6.3 Lip (Section B3.1)

k_{lip}	= 0.43	
$(f_{cr})_{lip}$	= 1856.56 MPa	
λ_l	= 0.330	(≤ 0.673 , No Local Buckling, lip fully effective)
ρ	= 1.000	
d_s	= 7.90 mm	$\lambda \leq 0.673 \quad \lambda > 0.673$
R_l	= 1.00	$R_l = l_w / l_b$
$b_l = d_s$	= 7.90 mm	

6.4 Corner

b_c	= 3.30 mm
-------	-----------

6.5 Effective Area

b_1	= 113.74 mm
A_{ec}	= 136.49 mm ²

8. Nominal Axial Capacity, P_n			
A_{cc}	=	136.49	mm ²
F_{ne}	=	201.88	kN
P_{ne}	=	<input type="text" value="27.55"/>	kN
7. Shift in Effective Centroid			
x_{ce}	=	5.85	mm
x_c	=	5.18	mm
e_s	=	0.67	mm
e_{s2}	=	0.45	mm (Taken as 2/3 of e_s since eccentricity varies along the length of the column.)
(C) DETERMINE SECTION AXIAL CAPACITY (P_{no}) (Section C4)			
6. Compute effective area of Single C at F_y			
6.1 Web (Section B2.1)			
k_{web}	=	<input type="text" value="4.00"/>	
$(f_{cr})_{web}$	=	211.13	MPa
λ_w	=	1.63	(> 0.673, Local Buckling, web not fully effective.)
ρ	=	0.531	
b_w	=	<input type="text" value="37.95"/>	mm
6.2 Flange (Section B4.2)			
Check flange as a uniformly compressed element with an edge stiffener.			
b/t	=	11.72	
S	=	24.61	$S = 1.28 \sqrt{E/F_y}$
$0.328S$	=	8.07	($b/t \geq 0.328S$, Check effective width of flange.)
			($b/t > 0.328S$, No edge stiffener required, $l_a = 0$.)
l_b	=	2.6854	
l_b	=	49.30	$l_b = (c^3 t \sin^2 \theta / 12)$
R_l	=	1.00	$R_l = l_w / l_b \leq 1$ (Note: If $l_b = 0$, $R_l = 1$ because no edge stiffener required)
n	=	0.46	$n = 0.582 - [(b/t)/4S] \geq 1/3$
$0.25 < C/b \leq 0.8$, $k = (4.82 - 5C/b)(R_l)^n + 0.43 \leq 4$			
k_{flange}	=	1.48	
$(f_{cr})_{flange}$	=	2017.97	MPa
λ_f	=	0.527	(≤ 0.673 , No Local Buckling, flange fully effective.)
ρ	=	1.000	
b_f	=	<input type="text" value="14.06"/>	mm
6.3 Lip (Section B3.1)			
k_{lip}	=	<input type="text" value="0.43"/>	
$(f_{cr})_{lip}$	=	1856.56	MPa
λ_l	=	0.549	(≤ 0.673 , No Local Buckling, lip fully effective)
ρ	=	1.000	
d_s	=	7.90	mm $\lambda \leq 0.673 \quad \lambda > 0.673$
R_l	=	1.00	$R_l = l_w / l_b$
$b_l = d'_s$	=	<input type="text" value="7.90"/>	mm
6.4 Corner			
b_c	=	<input type="text" value="3.30"/>	mm
6.5 Effective Area			
b_l	=	95.06	mm
A_{ec}	=	<input type="text" value="114.07"/>	mm ²
8. Nominal Axial Capacity, P_{no}			
A_{cc}	=	114.07	mm ²
F_y	=	560.00	MPa
P_{no}	=	<input type="text" value="63.88"/>	kN
7. Shift in Effective Centroid			
x_{ce}	=	7.00	mm
x_c	=	5.18	mm
e_s	=	1.83	mm
e_{s1}	=	1.22	mm (Taken as 2/3 of e_s since eccentricity varies along the length of the column.)

(D) DETERMINE SECTION MOMENT CAPACITY (M_{no}) (Section C3)			
2. Yielding (Section C3.1.1(a))			
* Web is in tension under bending about minor y-axis.			
6.1 Web (Section B2.1)			
k_{web}	=	4.00	
$(f_{cr})_{web}$	=	211.13	MPa
λ_{wv}	=	1.63	(> 0.673, Local Buckling, web not fully effective.)
ρ	=	0.531	
b_w	=	71.45	mm (Tension at Web, no reduction)
6.2 Flange (Section B4.2)			
b/t	=	11.72	
S	=	24.61	$S = 1.28 \sqrt{E/F_y}$
$0.328S$	=	8.07	($b/t \geq 0.328S$, Check effective width of flange.)
			($b/t > 0.328S$, No edge stiffener required, $l_a = 0$.)
l_b	=	2.6854	
l_s	=	49.30	$l_s = (c^2 t \sin^2 \theta / 12)$
R_l	=	1.00	$R_l = l_s / l_b \leq 1$ (Note: If $l_b = 0$, $R_l = 1$ because no edge stiffener required)
n	=	0.46	$n = 0.582 - [(b/t)/4S] \geq 1/3$
$C/b \leq 0.25, k=3.57(R_l)^n n+0.43 \leq 4$			
k_{flange}	=	1.48	
$(f_{cr})_{flange}$	=	2017.97	MPa
λ_f	=	0.527	(≤ 0.673 , No Local Buckling, flange fully effective.)
ρ	=	1.000	
b_f	=	14.06	mm
6.3 Lip (Section B3.1)			
k_{lip}	=	0.43	
$(f_{cr})_{lip}$	=	1856.56	MPa
λ_l	=	0.549	(≤ 0.673 , No Local Buckling, lip fully effective)
ρ	=	1.000	
d_s	=	7.90	mm $\lambda \leq 0.673 \quad \lambda > 0.673$
R_l	=	1.00	$R_l = l_s / l_b$
$b_l = d_s$	=	7.90	mm (Compression at Lip)
6.4 Corner			
b_c	=	3.30	mm
6.5 Effective Area			
b_t	=	128.56	mm
A_{ec}	=	154.28	mm ²
x_{ce}	=	5.18	mm
I_{ye}	=	7989.10	mm ⁴
S_t	=	1382.67	mm ³ (Effective section modulus in tension)
S_c	=	727.47	mm ³ (Effective section modulus in compression)
M_{no}	=	407385.25	Nmm

(E) DETERMINE MEMBER MOMENT CAPACITY (M_{ny}) (Section C3)

1. Lateral Torsional Buckling Strength (Section C3.1.2.1)
(Taken from Section Properties)

x_c	=	5.18	mm	a_{cor}	=	75.65	mm
x_o	=	-14.15	mm	b_{cor}	=	18.26	mm
t	=	1.20	mm	c_{cor}	=	10.00	mm
I_y	=	7989.10	mm ⁴				
j	=	40.61	mm	$j = 1/2 I_y [\int_A x^2 dA + [A xy^2 dA] - x_o$			
C_s	=	-1.00		(Web in tension under bending about minor axis)			
C_{TF}	=	1.00		(Taken as unity because BM at any point within the length is larger than BM at both ends)			
σ_{ex}	=	14496.69	MPa				
S_x	=	610.70	mm ³	(From NA to the extreme compression fiber - LIP)			
M_e	=	2464826.34	Nmm				
F_e	=	4036.10	MPa	$(F_e \geq 2.78F_y, \text{ Member subjected to yielding})$			
$2.78F_y$	=	1556.80	MPa	$(F_e \geq 2.78F_y, F_c = F_y)$			
F_c	=	560.00	MPa				

2. Member Moment Capacity

x_{ce}	=	5.18	mm	(As per determined in M_{no})			
I_{ye}	=	7989.10	mm ⁴	(As per determined in M_{no})			
S_c	=	727.47	mm ³				
M_{ny}	=	407385.25	Nmm				
Final M_{ny}	=	407385.25	Nmm	$(M_{no} \leq M_{ny}, M_{ny} = M_{no})$			

(F) DETERMINE BEAM-COLUMN CAPACITY (P_u) (Section C5.2.2)

Beam Interaction Equation:
$$\frac{P_u}{P_n} + \frac{C_{my} P_u e_{s2}}{M_{ny} \left(1 - \frac{P_u}{P_{ey}} \right)} \leq 1.0$$

(Based on F_{re})		(Based on F_y)					
e_{s2}	=	0.45	mm	e_{s1}	=	1.22	mm
P_n	=	27554.94	N	P_{no}	=	63880.25	N
M_{ny}	=	407385.25	Nmm				
P_{ey}	=	35513.41	N				

Solve beam interaction equation above

Quadratic a	=	11.47	
Quadratic b	=	-735870.29	
Quadratic c	=	1.12E+10	
P_{u1}	=	39.16	kN
P_{u2}	=	24.99	kN
P_{u3}	=	53.65	kN
P_u	=	24.99	kN

H.2.2 Direct Strength Method (DSM I & DSM II)

LIPPED C-CHANNEL	Specimen : C75L500-1
	Date : 22.02.2013
C75L500-1 (DSM I) = 27.79 kN	Analysed by : Tina
C75L500-1 (DSM II) = 26.09 kN	

(Take flexural-torsional buckling into account)

Torsion = Y (Y for 'YES', N for 'NO')

1. Geometry

A'	=	76.85	mm
B'	=	19.46	mm
C'	=	10.6	mm
t	=	1.2	mm
R	=	1.5	mm
w	=	0	mm
L	=	678	mm

K _x	=	0.50	(L _x = K _x L)
K _y	=	1.00	(L _y = K _y L)
K _t	=	1.00	(L _t = K _t L)

2. Material's Properties

θ	=	1.5708	rad
v	=	0.30	
G	=	79631	MPa
F _y	=	560	MPa
E	=	207040	MPa

3. Dimensional Limits & Considerations (Clause B1)

A'/t	=	64.04	≤	260	Web OK!	K _y L _y /r _y	=	94.22	Intermediate
B'/t	=	16.22	≤	60	Flange OK!	20r _y	=	143.92	L > 20r _y (7.1.1), Not Stub
C'/b	=	0.75	≤	0.8	Lip OK!	3A'	=	230.55	L >= 3A' (7.1.2), Stub

(A) SECTION PROPERTIES

4. Gross Section Properties

α	=	1		r	=	2.10	mm
a	=	71.45	mm	a _{bar}	=	75.65	mm
b	=	14.06	mm	b _{bar}	=	18.26	mm
c	=	7.90	mm	c _{bar}	=	10.00	mm
u	=	3.30	mm				
x _c	=	5.18	mm	x _{yc}	=	5.78	mm
I _{yc}	=	125781.64	mm ⁴	I _{yc}	=	7989.10	mm ⁴
r _{yc}	=	28.55	mm	r _{yc}	=	7.20	mm
m	=	8.972	mm				
x _o	=	-14.15	mm	r _o	=	32.67	mm
J _o	=	74.05	mm ⁴	C _{wc}	=	11080319.88	mm ⁶
β	=	0.812					
A _c	=	154.28	mm ²				

(B) DETERMINE MEMBER AXIAL CAPACITY (P _n) (Section C4)			
6. Buckling Stresses (same as DSM Euler)			
P _y	86.40	kN	
6.1 Local Buckling			
Analysis Method (E = Element, S = Semi empirical)			
E / S	S		
6.1.2 Element Method			
(f _{crit}) _{web}	188.34	MPa	k _{web} = 4
(f _{crit}) _{flange}	3232.60	MPa	k _{flange} = 4
(f _{crit}) _{lip}	1145.20	MPa	k _{lip} = 0.425
f _{crit1}	188.34	MPa	
6.1.3 Interaction Method			
(f _{crit}) _{flange/lip}	2297.68	MPa	c'/b' = 0.55
(f _{crit}) _{flange/web}	270.01	MPa	k _{flange/lip} = 2.843
f _{crit2}	270.01	MPa	a'/b' = 4.14
			k _{flange/web} = 0.334
6.2 Distortional Buckling			
A _y	33.91	mm ²	x _o = 5.90 mm
J _y	16.2778	mm ⁴	h _y = y _o = -1.769 mm
I _{yt}	296.472	mm ⁴	h _x = -12.36 mm
I _{yt}	1255.16	mm ⁴	x _o - h _x = 18.26 (Checking: x _o - h _x = b _{over})
I _{xyt}	353.957	mm ⁴	C _{wt} = 0.00
L _{cr}	197.67	mm	
<u>Flange Model</u>		<u>Web Model</u>	
k _{ϕte}	1193.5667	k _{ϕwe}	866.16
k _{ϕtg}	2.11	k _{ϕwg}	2.19
<u>Buckling Stress</u>			
f _{crd}	479.25	MPa	
6.3 Euler Buckling			
6.3.1 Flexural Buckling about Weak Axis (Section C4.1)			
<u>x-axis flexural buckling</u>		<u>y-axis flexural buckling</u>	
K _x L _y /r _x	11.87	K _y L _x /r _y	94.22
F _{ex}	14496.69	F _{ey}	230.19 MPa
F _{e1}	230.19		MPa (Euler buckling about y-axis will control.)
6.3.2 Singly Symmetric Sections subjected to Flexural-torsional Buckling (Section C4.2)			
σ _{ex}	14496.69	MPa	
σ _t	1232.31	MPa	
β	0.81		
F _{e2}	1211.58	MPa	F _{e2} = 1/2β [(σ _{ex} + σ _t) - sqrt((σ _{ex} + σ _t) ² - 4βσ _{ex} σ _t)]
6.3.3 Determine controlling buckling mode			
Note: Fe1 < Fe2, Flexural buckling governs.			
F _e	230.19	MPa	Torsion considered, take minimum of FE1 & FE2.

(C) DETERMINE SECTION AXIAL CAPACITY (P_{no}) (Section C4)	
(At yield, thus determine as a fully braced member. Global buckling P_{ne} is restricted to P_y)	
<p>6.4 Member Axial Capacity</p> <p>6.4.1 DSM I</p> <p>6.3.1 Global Buckling</p> <p>$P_{cre} = 35.51$ kN</p> <p>$P_{cre} / P_y = 0.4111$ -</p> <p>$\lambda_c = 1.560$ - $\lambda_c \leq 1.5, \lambda_c > 1.5$</p> <p>$P_{ne} = 31.15$ kN</p> <p>6.3.1 Local Buckling</p> <p>$P_{cri} = 41.66$ kN</p> <p>$P_{cri} / P_y = 0.482$ -</p> <p>$\lambda_l = 0.86$ - $\lambda_l \leq 0.776, \lambda_l > 0.776$</p> <p>$P_{nl} = 29.09$ kN (Local-global reduction)</p> <p>6.3.1 Distortional Buckling</p> <p>$P_{crid} = 73.94$ kN</p> <p>$P_{crid} / P_y = 0.856$</p> <p>$\lambda_d = 1.08$ - $\lambda_d \leq 0.561, \lambda_d > 0.561$</p> <p>$P_{nd} = 60.77$ kN (Distortional reduction)</p> <p>$P_n = 29.09$ kN (Local-global controls)</p> <p>7. Shift in Effective Centroid</p> <p>$e_{s2} = 0.45$ mm (Same as EWM)</p>	<p>6.4.2 DSM II</p> <p>$P_{cre} = 32.83$ kN</p> <p>$P_{cre} / P_y = 0.3800$ (From CUFSM)</p> <p>$\lambda_c = 1.622$ - $\lambda_c \leq 1.5, \lambda_c > 1.5$</p> <p>$P_{ne} = 28.79$ kN</p> <p>$P_{cri} = 42.33$ kN</p> <p>$P_{cri} / P_y = 0.490$ (From CUFSM)</p> <p>$\lambda_l = 0.82$ - $\lambda_l \leq 0.776, \lambda_l > 0.776$</p> <p>$P_{nl} = 27.71$ kN (Local-global reduction)</p> <p>$P_{crid} = 55.29$ kN</p> <p>$P_{crid} / P_y = 0.640$ (From CUFSM)</p> <p>$\lambda_d = 1.25$ - $\lambda_d \leq 0.561, \lambda_d > 0.561$</p> <p>$P_{nd} = 53.46$ kN (Fully effective for distortional buckling)</p> <p>$P_n = 27.71$ kN (From CUFSM)</p>
<p>6.4.1 DSM I</p> <p>6.3.1 Global Buckling</p> <p>$P_{ne} = 86.40$ kN</p> <p>6.3.1 Local Buckling</p> <p>$P_{cri} = 41.66$</p> <p>$P_{cri} / P_y = 0.4822$</p> <p>$\lambda_l = 1.44$ - $\lambda_l \leq 0.776, \lambda_l > 0.776$</p> <p>$P_{nl} = 57.30$ kN (Local-global reduction)</p> <p>6.3.1 Distortional Buckling</p> <p>$P_{crid} = 73.94$</p> <p>$P_{crid} / P_y = 0.8558$</p> <p>$\lambda_d = 1.08$ - $\lambda_d \leq 0.561, \lambda_d > 0.561$</p> <p>$P_{nd} = 60.77$ kN (Fully effective for distortional buckling)</p> <p>$P_{no} = 57.30$ kN (Local-global controls)</p> <p>7. Shift in Effective Centroid</p> <p>$e_{s1} = 1.22$ mm (Same as EWM)</p>	<p>6.4.2 DSM II</p> <p>$P_{ne} = 86.40$ kN</p> <p>$P_{cri} = 42.33$</p> <p>$P_{cri} / P_y = 0.490$ (Same as for P_n)</p> <p>$\lambda_l = 1.43$ - $\lambda_l \leq 0.776, \lambda_l > 0.776$</p> <p>$P_{nl} = 57.62$ kN (Local-global reduction)</p> <p>$P_{crid} = 55.29$</p> <p>$P_{crid} / P_y = 0.640$ (Same as for P_n)</p> <p>$\lambda_d = 1.25$ - $\lambda_d \leq 0.561, \lambda_d > 0.561$</p> <p>$P_{nd} = 53.46$ kN (Fully effective for distortional buckling)</p> <p>$P_{no} = 53.46$ kN (From CUFSM)</p>

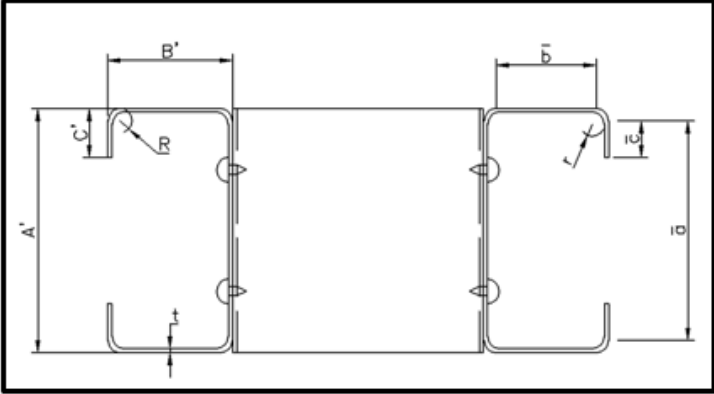
(D) DETERMINE SECTION MOMENT CAPACITY (M_{no})			
S_x	=	207.91	mm ³
M_y	=	116431.88	Nmm
S_x	=	207.91	mm ³
M_y	=	116431.88	Nmm
6.1 Local Buckling			
6.1.2 Element Method			
$(f_{cr})_{web}$	=	1125.31	MPa
$(f_{cr})_{flange}$	=	3232.60	MPa
$(f_{cr})_{lip}$	=	1145.20	MPa
f_{crit}	=	1125.31	MPa
k_{web}	=	23.9	
k_{flange}	=	4	
k_{lip}	=	0.425	
6.1.3 Interaction Method			
f_1	=	560.00	MPa (Extreme fibre)
f_2	=	405.52	MPa (At end of lip)
ξ	=	0.28	(<1.0)
$(f_{cr})_{flange/lip}$	=	2675.23	MPa
c'/b'	=	0.55	(<0.6)
$k_{flange/lip}$	=	3.310	
f_1	=	560.00	MPa (At web compression flange)
f_2	=	-560.00	MPa (At web tension flange)
ξ	=	2.00	(<1.0)
a'/b'	=	4.14	
$(f_{cr})_{flange/web}$	=	1271.28	MPa
$k_{flange/web}$	=	1.573	
f_{crit2}	=	1271.28	MPa
6.2 Distortional Buckling			
(Flange properties previously determined for P_n)			
L_{cr}	=	178.81	mm
<u>Flange Model</u>		<u>Web Model</u>	
$k_{\Phi_{fe}}$	=	1693.7271	
$k_{\Phi_{fw}}$	=	2.58E+00	
$k_{\Phi_{we}}$	=	1547.14	
ψ	=	-1.00	(Stress gradient on web)
$k_{\Phi_{wg}}$	=	4.48E-01	
<u>Buckling Stress</u>			
f_{crd}	=	1070.45	MPa
6.4.1 DSM I		6.4.2 DSM II	
6.3.1 Global Buckling			
(At yield, thus determine as a fully braced member. Global buckling M_{ne} is stricited to M_y)			
M_{ne}	=	116431.88	Nmm
M_{ne}	=	116431.88	Nmm
6.3.1 Local Buckling		6.3.1 Local Buckling	
M_{crit}	=	264316.10	Nmm
M_{crit} / M_y	=	2.2701	
λ_{y1}	=	0.66	- $\lambda_{y1} \leq 0.776, \lambda_{y1} > 0.776$
M_{nl}	=	116431.88	Nmm (Fully effective for local buck)
M_{crit}	=	43.46	
M_{crit} / M_y	=	2.670	
λ_{y1}	=	51.76	- $\lambda_{y1} \leq 0.776, \lambda_{y1} > 0.776$
M_{nl}	=	4921.59	Nmm (Local-global reduction)
6.3.1 Distortional Buckling		6.3.1 Distortional Buckling	
M_{crd}	=	222561.74	Nmm
M_{crd} / M_y	=	1.9115	
λ_{ω}	=	0.72	- $\lambda_{\omega} \leq 0.561, \lambda_{\omega} > 0.561$
M_{rd}	=	108412.64	Nmm (Fully effective for distortional buckling)
M_{crd}	=	34.35	
M_{crd} / M_y	=	2.110	
λ_{ω}	=	0.69	- $\lambda_{\omega} \leq 0.561, \lambda_{\omega} > 0.561$
M_{rd}	=	110928.95	Nmm (Fully effective for distortional buckling)
M_{no}	=	108412.64	Nmm (Distortional controls)
M_{no}	=	4921.59	Nmm (From CUFSM)

(E) DETERMINE MEMBER MOMENT CAPACITY (M_{ny})			
S_y	=	3273.43	mm ³
M_y	=	1833122.18	Nmm
S_y	=	3273.43	mm ³
M_y	=	1833122.18	Nmm
6.3 Global Buckling			
6.3.1 Individual buckling modes (Section C3.1.2.1(a))			
σ_{ey}	=	230.19	MPa
σ_z	=	1232.31	MPa
6.3.2 Lateral-torsional Buckling (Section C3.1.2.1(a))			
C_b	=	1.00	(According to Eq. C3.1.2.1-10, conservatively taken as 1.0.)
F_{cre}	=	820.07	MPa $F_{ez} = C_b F_o A / S_y$ (sqrt($\sigma_{ey} \sigma_z$))
6.1 Local Buckling			
$(f_{cr})_{web}$	=	1125.31	MPa
$(f_{cr})_{flange}$	=	3232.60	MPa
$(f_{cr})_{lip}$	=	1145.20	MPa
f_{crit}	=	1125.31	MPa
k_{web}	=	23.9	
k_{flange}	=	4	
k_{lip}	=	0.425	
6.1.3 Interaction Method			
f_1	=	560.00	MPa (Extreme fibre)
f_2	=	405.52	MPa (At end of lip)
ξ	=	0.28	(<1.0)
$(f_{cr})_{flange/lip}$	=	2675.23	MPa
c'/b'	=	0.55	(<0.6)
$k_{flange/lip}$	=	3.310	
f_1	=	560.00	MPa (At web compression flange)
f_2	=	-560.00	MPa (At web tension flange)
ξ	=	2.00	(<1.0)
$(f_{cr})_{flange/web}$	=	1271.28	MPa
a'/b'	=	4.14	
$k_{flange/web}$	=	1.573	
f_{crit}	=	1271.28	MPa
6.2 Distortional Buckling			
(Flange properties previously determined for P_n)			
L_{cr}	=	178.81	mm
<u>Flange Model</u>		<u>Web Model</u>	
k_{flange}	=	1693.7271	N
k_{web}	=	1547.14	N
k_{lip}	=	2.58E+00	mm ²
		ψ	= -1.00 (Stress gradient on web)
		k_{web}	= 4.48E-01 mm ²
Buckling Stress			
f_{crd}	=	1070.45	MPa

DSM I	DSM II
6.1 Global Buckling	
$M_{cre} = 2684439.70$ Nmm	$M_{cre} = 1319847.97$ Nmm
$M_{cre} / M_y = 1.4644$	$M_{cre} / M_y = 0.7200$ (From CUFSM)
$\lambda_c = 0.826$ - $\lambda_c \leq 1.5, \lambda_c > 1.5$	$\lambda_c = 1.179$ - $\lambda_c \leq 1.5, \lambda_c > 1.5$
$M_{ne} = 1377410.56$ Nmm	$M_{ne} = 1025008.28$ Nmm
6.3.1 Local Buckling	
$M_{crl} = 4161435.26$ Nmm	$M_{crl} = 4894436.22$ Nmm
$M_{crl} / M_y = 2.2701$	$M_{crl} / M_y = 2.670$ (From CUFSM)
$\lambda_l = 0.58$ - $\lambda_l \leq 0.776, \lambda_l > 0.776$	$\lambda_l = 0.46$ - $\lambda_l \leq 0.776, \lambda_l > 0.776$
$M_{nl} = 1377410.56$ Nmm (Fully effective for local buckling)	$M_{nl} = 1025008.28$ Nmm (Fully effective for local buckling)
6.3.1 Distortional Buckling	
$M_{cd} = 3504047.86$ Nmm	$M_{cd} = 3867887.80$ Nmm
$M_{cd} / M_y = 1.9115$	$M_{cd} / M_y = 2.110$ (From CUFSM)
$\lambda_d = 0.72$ - $\lambda_d \leq 0.561, \lambda_d > 0.561$	$\lambda_d = 0.69$ - $\lambda_d \leq 0.561, \lambda_d > 0.561$
$M_{nd} = 1282541.52$ Nmm (Distortional reduction)	$M_{nd} = 976563.27$ Nmm (Distortional reduction)
$M_{ny} = 1282541.52$ Nmm (Distortional controls)	$M_{ny} = 976563.27$ Nmm (From CUFSM)
(F) DETERMINE BEAM-COLUMN CAPACITY (P_u) (Section C5.2.2)	
Beam Interaction Equation: $\frac{P_u}{P_n} + \frac{C_{my} P_u e_{s2}}{M_{ny} \left(1 - \frac{P_u}{P_{Ey}}\right)} \leq 1.0$	
DSM I	DSM II
(Based on F_{ne})	(Based on F_{ne})
$e_{s2} = 0.45$ mm	$e_{s2} = 0.45$ mm
$P_n = 29091.75$ N	$P_n = 27713.37$ N
(Based on F_y)	(Based on F_y)
$e_{s1} = 1.22$ mm	$e_{s1} = 1.22$ mm
$P_{no} = 57301.06$ N	$P_{no} = 53456.71$ N
$M_{ny} = 1282541.52$ Nmm	$M_{ny} = 976563.27$ Nmm
$P_{Ey} = 35513.41$ N	$P_{Ey} = P_{cre} = 32830.28$ N
Solve beam interaction equation above	
Quadratic a = 36.11	Quadratic a = 29.75
Quadratic b = -2346254.32	Quadratic b = -1813385.10
Quadratic c = 3.73E+10	Quadratic c = 2.71E+10
$P_{u1} = 37.18$ kN	$P_{u1} = 34.87$ kN
$P_{u2} = 27.79$ kN	$P_{u2} = 26.09$ kN
$P_{u3} = 54.35$ kN	$P_{u3} = 50.12$ kN
$P_u = 27.79$ kN	$P_u = 26.09$ kN

H.3 Plain Built-up Back-to-back Channels Column Spreadsheets

H.3.1 Effective Width Method (EWM)

BUILT-UP BACK-TO-BACK CHANNELS		Specimen :	BU75S100L500-1
BU75S100L500-1 82.37 kN		Date :	13.10.2011
		Analysed by :	Tina
<i>(Load ratio from CUFSM for DSM II)</i>			
P_{crit}/P_y	=	0.0000	
P_{crit}/P_y	=	0.0000	
P_{crit}/P_y	=	0.0000	
<i>(Take flexural-torsional buckling into account)</i>			
Torsion	=	Y	(Y for 'YES', N for 'NO')
1. Geometry			
A'	=	73.61	mm
B'	=	19.79	mm
C'	=	11.23	mm
t	=	1.2	mm
R	=	1.5	mm
w	=	0	mm
L	=	655	mm
s	=	100.00	mm
K _x	=	0.50	(L _y = K _x L)
K _y	=	1.00	(L _y = K _y L)
K _t	=	1.00	(L _t = K _t L)
			
2. Material's Properties			
θ	=	1.57	rad
v	=	0.30	
G	=	79630.77	MPa
F _y	=	560	MPa
E	=	207040	MPa
3. Dimensional Limits & Considerations (Section B1)			
A'/t	=	61.34	≤ 260 Web OK!
B'/t	=	16.49	≤ 60 Flange OK!
C'/b	=	0.78	≤ 0.8 Lip OK!
K _y L _y /r _y	=	67.79	Intermediate
20r _y	=	193.25	L > 20r_y (7.1.1), Not Stub
3A'	=	220.83	L >= 3A' (7.1.2), Stub
4.2 Gross Section Properties for Built-up			
α	=	1	
a	=	68.21	mm
b	=	14.39	mm
c	=	8.53	mm
u	=	3.30	mm
x _c	=	2.78	mm
I _{xBU}	=	230560.24	mm ⁴
r _{xBU}	=	27.48	mm
r	=	2.10	mm
a _{0BU}	=	72.41	mm
b _{0BU}	=	18.59	mm
c _{0BU}	=	10.63	mm
x _{1BU}	=	6.16	mm
I _{yBU}	=	28511.05	mm ⁴
r _{yBU}	=	9.66	mm
r _{0BU}	=	29.13	mm
C _{wBU}	=	22283069.21	mm ⁶
J _{BU}	=	146.59	mm ⁴
A ₀	=	305.39	mm ²

5. Buckling Stresses (same as DSM Euler)

5.1 Flexural Buckling about Weak Axis (Section C4.1)

x-axis flexural buckling

$K_x L_x / r_{x, BU} = 11.92$

$F_{ex} = 14383.51 \text{ MPa}$

$F_{e1} = 427.87 \text{ MPa}$ (Euler Buckling about y-axis controls.)

y-axis flexural buckling (Section C4.5)

$(KL/r)_m = 69.11$

$s/r_{yc} = 13.43$ ($(KL/r)_m = \text{sqrt}[(KL/r_{x, BU})^2 + (s/r_{yc})^2]$
 $(s/r_{yc} \leq 0.5(KL/r)_m \text{ satisfied.})$)

$F_{ey} = 427.87 \text{ MPa}$

5.2 Doubly Symmetric Sections subjected to Flexural-torsional Buckling (Section C4.2)

$$\sigma_t = \frac{1}{A r_c^2} \left[GJ + \frac{\pi^2 E C_w}{(K_t L_t)^2} \right]$$

$\sigma_t = F_{e2} = 454.72 \text{ MPa}$

5.3 Determine controlling buckling mode

Note: $F_{e1} < F_{e2}$, Flexural buckling governs.

$F_e = 427.87 \text{ MPa}$ Torsion considered, take minimum of FE1 & FE2.

$\lambda_c = 1.144$ (≤ 1.5 , $F_{ne} = [0.658^{(\lambda_c^2)}] F_y$)

$F_{ne} = 323.80 \text{ kN}$

6. Compute effective area of Single C at F_{ne}

6.1 Web (Section B2.1)

$k_{web} = 4.00$

$(f_{cr})_{web} = 231.66 \text{ MPa}$

$\lambda_w = 1.18$ (> 0.673 , Local Buckling, web not fully effective.)

$\rho = 0.688$

$b_w = 46.96 \text{ mm}$

6.2 Flange (Section B4.2)

Check flange as a uniformly compressed element with an edge stiffener.

$b/t = 11.99$

$S = 32.37$ $S = 1.28 \text{ sqrt}(E/F_{ne})$

$0.328S = 10.62$ ($b/t \geq 0.328S$, Check effective width of flange.)
($b/t > 0.328S$, No edge stiffener required, $l_a = 0$.)

$l_b = 0.0635$

$l_s = 62.07$ $l_s = (c^3 t \sin^2 \theta) / 12$

$R_l = 1.00$ $R_l = l_y / l_b \leq 1$ (Note: if $l_b = 0$, $R_l = 1$ because no edge stiffener required)

$n = 0.49$ $n = 0.582 - [(b/t) / 4S] \geq 1/3$

$0.25 < C/b \leq 0.8$, $k = (4.82 - 5C/b)(R_l)^n + 0.43 \leq 4$

$k_{flange} = 1.35$

$(f_{cr})_{flange} = 1754.11 \text{ MPa}$

$\lambda_f = 0.430$ (≤ 0.673 , No Local Buckling, flange fully effective.)

$\rho = 1.000$

$b_f = 14.39 \text{ mm}$

6.3 Lip (Section B3.1)	
k_{lip}	= 0.43
$(f_{cr})_{lip}$	= 1592.44 MPa
λ_1	= 0.451 (≤ 0.673 , No Local Buckling, lip fully effective)
ρ	= 1.000
d_s	= 8.53 mm $\lambda \leq 0.673 \quad \lambda > 0.673$
R_1	= 1.00 $R_1 = L_y/L_x \leq 1$
$b_l = d'_s$	= 8.53 mm
6.4 Corner	
b_c	= 3.30 mm
6.5 Effective Area	
b_t	= 105.99 mm
A_{eBU}	= 254.38 mm ²
7. Shift in Effective Centroid	
No shift in effective centroid for Doubly Symmetric Sections.	
8. Member Axial Capacity	
A_{eBU}	= 254.38 mm ²
F_{ne}	= 323.80 kN
P_{EWM-BU}	= 82.37 kN

H.3.2 Direct Strength Method (DSM I & DSM II)

BUILT-UP BACK-TO-BACK CHANNELS		Specimen :	BU75S100L500-1
		Date :	13.10.2011
BU75S100L500-1	81.21	kN	Analysed by : Tina
BU75S100L500-1	82.17	kN	

(Load ratio from CUFSM for DSM II)

$P_{crz}/P_y =$
 $P_{crot}/P_y =$
 $P_{crt}/P_y =$

(Take flexural-torsional buckling into account)

Torsion = Y (Y for 'YES', N for 'NO')

1. Geometry

A'	=	73.61	mm
B'	=	19.79	mm
C'	=	11.23	mm
t	=	1.20	mm
R	=	1.50	mm
w	=	0.00	mm
L	=	655.00	mm
s	=	100.00	mm
K_x	=	0.50	($L_x = K_x L$)
K_y	=	1.00	($L_y = K_y L$)
K_t	=	1.00	($L_t = K_t L$)

2. Material's Properties

θ	=	1.5708	rad
ν	=	0.3	
G	=	79631	MPa
F_y	=	560	MPa
E	=	207040	MPa

3. Dimensional Limits & Considerations (Clause B1)

A'/t	=	61.34	≤	260	Web OK!	$K_y L_y / r_y$	=	87.98	Intermediate
B'/t	=	16.49	≤	60	Flange OK!	$20r_y$	=	148.91	$L > 20r_y$ (7.1.1), Not Stub
C'/b	=	0.78	≤	0.8	Lip OK!	$3A'$	=	220.83	$L \geq 3A'$ (7.1.2), Stub

4. Gross Section Properties

α	=	1		r	=	2.10	mm
a	=	68.21	mm	a_{bar}	=	72.41	mm
b	=	14.39	mm	b_{bar}	=	18.59	mm
c	=	8.53	mm	c_{bar}	=	10.63	mm
u	=	3.30	mm	x_{BU}	=	6.16	mm
x_c	=	5.56	mm	I_{yBU}	=	28511.05	mm ⁴
I_{xBU}	=	230560.24	mm ⁴	r_{yBU}	=	9.66	mm
r_{xBU}	=	27.48	mm	r_{oBU}	=	29.13	mm
J_{BU}	=	146.59	mm ⁴	C_{wBU}	=	22283069.21	mm ⁶
A_o	=	305.39	mm ²				

5. Buckling Stresses (same as DSM Euler)			
P_y	171.02	kN	
5.1 Local Buckling			
5.1.2 Element Method			
$(f_{crit})_{web}$	= 205.57	MPa	k_{web} = 4
$(f_{crit})_{flange}$	= 3118.85	MPa	k_{flange} = 4
$(f_{crit})_{lip}$	= 1025.41	MPa	k_{lip} = 0.43
f_{crit}	= 205.57	MPa	
5.1.3 Interaction Method			
$(f_{crit})_{flange/lip}$	= 2057.75	MPa	c'/b' = 0.57
			$k_{flange/lip}$ = 2.639
			a'/b' = 3.90
$(f_{crit})_{flange/web}$	= 291.81	MPa	$k_{flange/web}$ = 0.374
f_{crit}	= 291.81	MPa	
<u>Analysis Method (E = Element, S = Semi empirical)</u>			
E / S	=	S	
P_{crit}	=	89.11	kN
P_{crit} / P_y	=	0.521	-
P_{crit}	=	92.35	kN
P_{crit} / P_y	=	0.540	(From CUFSM)
5.2 Distortional Buckling			
A_f	= 35.06	mm ²	x_o = 5.91 mm
J_f	= 16.8307	mm ⁴	$h_y = y_o$ = -1.93 mm
I_{yf}	= 352.05	mm ⁴	h_x = -12.68 mm
I_{xf}	= 1343.60	mm ⁴	$x_o - h_x$ = 18.59 (Checking: $x_o - h_x = b_{over}$)
I_{yxf}	= 400.93	mm ⁴	C_{wtf} = 0.00
L_{cr}	= 205.69	mm	
<u>Flange Model</u>		<u>Web Model</u>	
$k_{\Phi te}$	= 1217.56	$k_{\Phi we}$	= 904.91
$k_{\Phi tg}$	= 2.17	$k_{\Phi wg}$	= 1.77
<u>Buckling Stress</u>			
f_{crit}	= 538.84	MPa	
P_{crit}	=	164.55	kN
P_{crit} / P_y	=	0.962	
P_{crit}	=	123.13	kN
P_{crit} / P_y	=	0.720	(From CUFSM)
5.3 Euler Buckling			
5.3.1 Flexural Buckling about Weak Axis (Section C4.1)			
<u>x-axis flexural buckling</u>		<u>y-axis flexural buckling</u>	
$K_x L_x / r_x$	= 11.92	$K_y L_y / r_y$	= 69.11
			$(KL/r)_m = \text{sqrt}[(KL/r_{yEU})^2 + (s/r_{yc})^2]$
F_{ex}	= 14383.51	MPa	$s/r_{yc} = 13.43$
			($s/r_{yc} \leq 0.5(KL/r)_m$ satisfied.)
		F_{ey}	= 427.87
F_{e1}	=	427.87	MPa (Euler buckling about y-axis will control.)

5.3.2 Doubly Symmetric Sections subjected to Flexural-torsional Buckling (Section C4.2)

$$\sigma_t = \frac{1}{Ar_o^2} \left[GJ + \frac{\pi^2 EC_w}{(K_t L_t)^2} \right]$$

$F_{e2} = 454.72$ MPa

5.3.3 Determine controlling buckling mode
 Note: $F_{e1} < F_{e2}$, Flexural buckling governs.

$F_e = 427.87$ MPa Torsion considered, take minimum of FE1 & FE2.

5.3.4 Euler Load Ratio

$P_{cre} = 130.67$ kN	$P_{cre} = 130.67$ kN
$P_{cre} / P_y = 0.7641$ -	$P_{cre} / P_y = 0.7641$ (From manual calculation)

5.4 Member Axial Capacity

5.4.1 DSM I		5.4.2 DSM II	
$\lambda_1 = 1.05$ - $\lambda_1 \leq 0.776, \lambda_1 > 0.776$	$\lambda_1 = 1.03$ - $\lambda_1 \leq 0.776, \lambda_1 > 0.776$		
$P_{nl} = 81.21$ kN (Local-global reduction)	$P_{nl} = 82.17$ kN (Local-global reduction)		
$\lambda_d = 1.02$ - $\lambda_d \leq 0.561, \lambda_d > 0.561$	$\lambda_d = 1.18$ - $\lambda_d \leq 0.561, \lambda_d > 0.561$		
$P_{nd} = 126.29$ kN (Distortional reduction)	$P_{nd} = 111.60$ kN (Fully effective for distortional buckling)		
$\lambda_c = 1.144$ - $\lambda_c \leq 1.5, \lambda_c > 1.5$	$\lambda_c = 1.144$ - $\lambda_c \leq 1.5, \lambda_c > 1.5$		
$P_{ne} = 98.89$ kN	$P_{ne} = 98.89$ kN		
$P_{DSM I-BU} = 81.21$ kN (Local-global controls)	$P_{DSM II-BU} = 82.17$ kN (From CUFSM)		

H.4 Gapped Built-up Back-to-back Channels Column Spreadsheet

H.4.1 Thickness Reduction Method (TRem)

GAPPED BUILT-UP BACK-TO-BACK CHANNELS		Specimen :	GBU75S100L500-1
		Date :	22.02.2013
		Analysed by :	Tina
GBU75S100L500-1 = 99.16 kN			
<i>(Take flexural-torsional buckling into account)</i>			
Torsion	=	Y	(Y for 'YES', N for 'NO')
1. Geometry			
A'	=	73.57	mm
B'	=	19.84	mm
C'	=	11.25	mm
t	=	1.2	mm
R	=	1.5	mm
w	=	73.57	mm
L	=	678	mm
s	=	100.22	mm
K _x	=	0.50	(L _x = K _x L)
K _y	=	1.00	(L _y = K _y L)
K _t	=	1.00	(L _t = K _t L)
2. Material's Properties			
θ	=	1.57	rad
v	=	0.30	
G	=	79630.77	MPa
F _y	=	560	MPa
E	=	207040	MPa
3. Dimensional Limits & Considerations (Section B1)			
A'/t	=	61.31	≤ 260 Web OK!
B'/t	=	16.53	≤ 60 Flange OK!
C'/b	=	0.78	≤ 0.8 Lip OK!
K _y L/r _y	=	69.94	Intermediate
20r _y	=	193.89	L > 20r_y (7.1.1), Not Stub
3A'	=	220.71	L >= 3A' (7.1.2), Stub
4. Gross Section Properties for Built-up			
α	=	1	
a	=	68.17	mm
b	=	14.44	mm
c	=	8.55	mm
u	=	3.30	mm
x _c	=	2.79	mm
I _{xBU}	=	230631.71	mm ⁴
r _{xBU}	=	27.47	mm
r	=	2.10	mm
a _{oer}	=	72.37	mm
b _{oer}	=	18.64	mm
c _{oer}	=	10.65	mm
x _{xBU}	=	6.18	mm
I _{yBU}	=	28724.74	mm ⁴
r _{yBU}	=	9.69	mm
r _{oBU}	=	29.13	mm
C _{wBU}	=	22426230.84	mm ⁶
J _{BU}	=	146.70	mm ⁴
A _o	=	305.63	mm ²

1. Buckling Stresses

1.1 Flexural Buckling about Weak Axis (Section C4.1)

x-axis flexural buckling

$K_x L_x / r_{x, \text{BU}} = 12.34$

$F_{\text{ex}} = 13417.81 \text{ MPa}$

$F_{\text{e1}} = 402.95 \text{ MPa}$ (Euler Buckling about y-axis controls.)

y-axis flexural buckling (Section C4.5)

$(KL/r)_m = 71.21$ $(KL/r)_m = \text{sqrt}[(KL_x/r_{x, \text{BU}})^2 + (s/r_{yc})^2]$

$s/r_{yc} = 13.42$ (s/r_{yc} <= 0.5(KL/r)_m satisfied.)

$F_{\text{ey}} = 402.95 \text{ MPa}$

1.2 Doubly Symmetric Sections subjected to Flexural-torsional Buckling (Section C4.2)

$$\sigma_t = \frac{1}{Ar_o^2} \left[GJ + \frac{\pi^2 E C_w}{(K_t L_t)^2} \right]$$

$\sigma_t = F_{\text{e2}} = 429.42 \text{ MPa}$

1.3 Determine controlling buckling mode

Note: Fe1 < Fe2, Flexural buckling governs.

$F_e = 402.95 \text{ MPa}$ Torsion considered, take minimum of FE1 & FE2.

$\lambda_c = 1.179$ (<= 1.5, Fne = [0.658^(lambda_c^2)]*Fy)

$F_{\text{ne}} = 313.02 \text{ MPa}$

2. Reduced Web Thickness, t_{rw}

$k_{\text{web}} = 4.00$

$(f_{\text{cr}})_{\text{web}} = 231.94 \text{ MPa}$

$\lambda_w = 1.16$ (> 0.673, Local Buckling, web not fully effective.)

$\rho = 0.698$

$t_{\text{rw}} = 1.67 \text{ mm}$ (Web thickness to be used in CUFSM)

3. Recalculated Section Properties with Reduced Cross-sectional Area

$A_{\text{rw}} = 305.63 \text{ mm}$	$x_c = 5.58 \text{ mm}$
$I_{yc} = 115315.85 \text{ mm}^4$	$x_{\text{cNEW}} = 6.18 \text{ mm}$
$r_{\text{xcNEW}} = 27.47 \text{ mm}$	$I_{\text{cNEW}} = 8521.65 \text{ mm}^4$
$(K_x L_x / r_x)_{\text{NEW}} = 12.34$	$r_{\text{ycNEW}} = 7.47 \text{ mm}$
	$(K_x L_x / r_x)_{\text{NEW}} = 90.79$
$I_{\text{yBU}} = 230631.71 \text{ mm}^4$	$x_{\text{yBU}} = 42.97 \text{ mm}$
$r_{\text{yBUNEW}} = 27.47 \text{ mm}$	$I_{\text{yBU}} = 581289.73 \text{ mm}^4$
$(K_x L_x / r_x)_{\text{BUNEW}} = 12.34$	$r_{\text{yBU}} = 43.61 \text{ mm}$
	$(K_x L_x / r_x)_{\text{yBU}} = 15.55$
	$I_{\text{yBU}} = 28724.74 \text{ mm}^4$
	$r_{\text{yBUNEW}} = 9.69 \text{ mm}$
	$(K_x L_x / r_x)_{\text{NEW}} = 69.94$
	$r_{\text{cNEW}} = 29.13 \text{ mm}$

6. Buckling Stresses (same as DSM Euler)	
P_y	171.15 kN
P_{crit}	167.73 kN
P_{crit} / P_y	0.980 (From CUFSM)
P_{cnd}	193.40 kN
P_{cnd} / P_y	1.130 (From CUFSM)
6.3 Euler Buckling	
6.3.1 Flexural Buckling about Weak Axis (Section C4.1)	
<u>x-axis flexural buckling</u>	
$(K_x L_x / r_x)_{BUNEUV}$	12.34
s/r_{yc}	($s/r_{yc} \leq 0.5(KL/r)_m$ satisfied.)
$(K_y L_y / r_y)_m$	12.34 ($(KL/r)_m = \text{sqrt}[(KL_x/r_{yBU})^2 + (s/r_{yc})^2]$)
F_{ex}	13417.81 MPa
F_{e1}	4844.44 MPa (Euler buckling about y-axis will control.)
<u>y-axis flexural buckling</u>	
$(K_y L_y / r_y)_{BBU}$	15.55
s/r_{yc}	($s/r_{yc} \leq 0.5(KL/r)_m$ not satisfied.)
$(K_y L_y / r_y)_m$	20.54 ($(KL/r)_m = \text{sqrt}[(KL_x/r_{yBU})^2 + (s/r_{yc})^2]$)
F_{ey}	4844.44 MPa
6.3.2 Doubly Symmetric Sections subjected to Flexural-torsional Buckling (Section C4.2)	
$\sigma_t = \frac{1}{A r_o^2} \left[GJ + \frac{\pi^2 E C_w}{(K_t L_t)^2} \right]$	
F_{e2}	429.42 MPa
6.3.3 Determine controlling buckling mode	
Note: $F_{e2} < F_{e1}$, Flexural-torsional buckling governs.	
F_e	429.42 MPa Torsion considered, take minimum of FE1 & FE2.
6.3.4 Euler Load Ratio	
P_{cre}	131.24 kN
P_{cre} / P_y	0.7668
P_{cre}	131.24 kN
P_{cre} / P_y	0.7668 (From manual calculation)
6.4 Member Axial Capacity	
λ_1	0.77 - $\lambda_1 \leq 0.776, \lambda_1 > 0.776$
P_{nl}	99.16 kN (Fully effective for local)
λ_d	0.94 - $\lambda_d \leq 0.561, \lambda_d > 0.561$
P_{nd}	134.63 kN (Fully effective for distortional)
λ_c	1.142 - $\lambda_c \leq 1.5, \lambda_c > 1.5$
P_{ne}	99.16 kN
$P_{ODSM II-BU}$	99.16 kN (From CUFSM)